TERDENTATE IRON COMPLEXES: CATALYTIC HYDROSILYLATION ACTIVITY AND THE DETERMINATION OF ELECTRONIC STRUCTURE OF REDOX-ACTIVE BIS(IMINO)PYRIDINE IRON COMPLEXES.

A Dissertation

Presented to the Faculty of the Graduate School

of Cornell University

In Partial Fulfillment of the Requirements for the Degree of

Doctor of Philosophy

by

Aaron Maurice Tondreau

May 2011

TERDENTATE IRON COMPLEXES: CATALYTIC HYDROSILYLATION ACTIVITY AND THE DETERMINATION OF ELECTRONIC STRUCTURE OF REDOX-ACTIVE BIS(IMINO)PYRIDINE IRON COMPLEXES.

Aaron Maurice Tondreau, Ph. D.

Cornell University 2011

A three-electron series of four-coordinate bis(imino)pyridine iron nitrosyl complexes was synthesized. The electronic structure of this series of compounds was determined by the use of X-ray crystallography, Mössbauer, IR, NMR, and EPR spectroscopies, and corroborated by DFT calculations. (^{iPr}PDI)Fe(NO) was determined to be an intermediate-spin ferric complex with a triplet two electron reduced bis(imino)pyridine chelate and a triplet NO^-. The overall spin state of (^{iPr}PDI)Fe(NO) is $S = ½$. The oxidation of (^{iPr}PDI)Fe(NO) occurs at the bis(imino)pyridine chelate, and the electronic structure of the iron nucleus remains intermediate-spin ferric. The reduction of (^{iPr}PDI)Fe(NO) also is bis(imino)pyridine chelate centered. This yields a three-electron reduced chelate, leaving the iron intermediate-spin ferric and the nitrosyl as NO^-. The reduction and oxidation of compounds was carried out to yield two other three-electron series. The synthesis and characterization of $[Li(OEt_2)_3]$-$[(^{iPr}PDI)Fe(CH_2CMe_3)(N_2)]$, (^{iPr}PDI)Fe($CH_2CMe_3$), and $[(^{iPr}PDI)Fe(CH_2CMe_3)][BPh_4]$ allowed for the determination of the degree of chelate participation over a three-electron series pertinent to olefin polymerization. The redox events were shown to occur at the bis(imino)pyridine chelate, leaving the iron nucleus Fe(II) throughout the series. [Na-15-Crown-5]$[(^{iPr}PDI)Fe(CO)_2]$, (^{iPr}PDI)Fe$(CO)_2$, and $[(^{iPr}PDI)Fe(CO)_2][BArF_{24}]$ were also synthesized. Analysis of $[(^{iPr}PDI)Fe(CO)_2][BArF_{24}]$ indicates that oxidation of the

formally Fe(0) complex (^{iPr}PDI)Fe(CO)$_2$ results in the oxidation of the bis(imino)pyridine chelate to a neutral ligand, giving a formally Fe(I) species. [Na-15-Crown-5][(^{iPr}PDI)Fe(CO)$_2$] was not structurally characterized, but EPR spectroscopy indicates that the reduction occurred at the ligand, and the iron is low spin Fe(II). Bis(imino)pyridine iron complexes also were utilized as catalysts for the hydrosilylation of ketones, aldehydes, and olefins. The hydrosilylation of ketones and aldehydes was performed with primary and secondary silanes using bis(imino)pyridine iron dialkyl complexes and pybox iron dialkyls. The hydrosilylation of olefins was performed with tertiary silanes utilizing several reduced bis(imino)pyridine iron complexes. The result was reactivity that proved to be competitive with platinum based catalysis. In several instances iron outperformed platinum in terms of selectivity and fewer side-products.

BIOGRAPHICAL SKETCH

Aaron Maurice Tondreau was born in 1981 in Santa Monica, California. He grew up in a small town in southern California that goes by the name of Pine Mountain Club, surrounded by pine trees and fresh mountain air. After graduating high school, a member of the first four-year graduating class at Frazier Mountain High School in 1999, Aaron moved north to the Monterey Bay area, where he attended Hartnell College and Monterey Peninsula College for the next four years. Aaron moved yet again, this time to Bakersfield where he attended California State University of Bakersfield and worked as an undergraduate researcher for Dr. Karl Kemnitz working on the photolysis of aryl epoxides. Finally, six years after his undergraduate studies began, he obtained his B.S. degree in Chemistry, graduating *Magna cum Laude*. After taking a year off from school, time he spent trying his hand in the stock market, Aaron made the cross-country move to Cornell University to attend graduate school. After joining Paul Chirik's lab in the winter of 2006, he quickly grew to appreciate the art of organometallic synthesis. Over the course of the next four years, Aaron spent his time honing his synthetic skills and trying to gain an understanding of the complexes he was able to make. After his departure from the Chirik lab, Aaron plans on making the biggest, distance-wise, move of his life to the brisk Alpine air of Zürich, Switzerland, where he plans on joining Dr. Grützmacher's lab and continuing his chemical education and putting his synthetic skills to good use.

For My Family:

Mom and Dad,

Brother and Sister,

Niece and Nephews.

ACKNOWLEDGEMENTS

First and foremost, this work would not have been possible without the guidance, mentorship, and patience of my advisor Paul Chirik. Without his labs to call home for the past four years of my life, none of this work would exist. I am indebted for being allowed to work and (hopefully) prove my worth as a chemist. The immense quantity of knowledge and experience I have amassed in your group is going to serve me well for the rest of my life, and I am grateful.

I have had the great fortune of meeting and working besides a large number of terrific scientists during my tenure in the Chirik group. Pete Wolczanski and Dave Collum are giants in the field of chemistry, and in life, and I was fortunate enough to have both as members of my committee. On a weekly basis Pete would inspire me to learn as many facts as I possibly could, for at the very least to not appear an idiot. I was honored to present my work to Prof. Dr. Karl Wieghardt and Dr. Ekhard Bill in Germany, even more so when we sat and discussed the chemistry, doodling on napkins when necessary, drinking coffee all the while. I am eternally grateful for the amount of interest and enthusiasm Prof. Wieghardt expressed in my work.

While working in collaboration with Momentive Performance Materials, I was part of a team of very talented chemists. Keith Weller, Ken Lewis, Susan Nye, and Jos Delis, on a biweekly basis, would help me overcome the limitations of iron catalysis. The patience and understanding they showed to me was exceedingly generous, and I thank them especially for sitting through more than one terrible presentation over the last 2 years. I have learned a great deal about a subset of chemistry far removed from the other work I was performing in the lab.

My coworkers in the Chirik group, past and present, are what kept me going when I didn't care to. For the members past, Kevin Sylvester, the other half of the Brain

Trust, in particular, kept my head above water when I was sinking. Doris Pun was the world's most wonderful box mate and friend, and she served as a chemist to emulate when I felt lost. Ignacio Fernandez was present to teach me how to make compounds in my early days, and the skills I learned from him are the foundation my work is built on. David Benito Garagorri was my mate for celebrations throughout his days in the group. I would like to thank Amanda Bowman for becoming a friend over her last several months in the group. Hiding in the back of the office with David and Mandy allowed me to escape lab when I needed it the most.

The current batch of member is owed many thanks as well. Jon Darmon has made himself useful to me for the past three years, and for that he gets thanks. Crisita Atienza is the hope for the future, mostly because she can make me laugh, but she is pretty good at chemistry, too. I have to thank Dr. Carsten Milsmann as well, for all of his BS calculations he ran on my compounds, and for not strangling me when I sent him CIF after CIF requesting said calculations. The two others in my year, Don Knobloch and Sarah Russell, are amazing people. Don is skilled to the nines and helped keep the tone from ever getting too heavy in lab. Sarah is my friend without whom graduate school would have been a completely different experience.

My family is the only reason I was able to get this far, or wanted to. My Mom and Dad worked tirelessly to raise Adam, Amy, and me. Without their encouragement to succeed, I would have given up on school a long time ago. Arrti Tondreau is deserving of more thanks than I can give, and it's safe to say I would not have tried to do as well in life without her. Thank you all for being so supportive and giving me reasons to do something with my life.

TABLE OF CONTENTS

Chapter 2: Oxygen Atom Transfer and Attempted Nitrogen Atom Transfer from Molybdenum Complexes to Bis(imino)pyridine Iron

Chapter 3: The Synthesis and Electronic Structure of Cationic and Anionic Bis(imino)pyridine Iron Alkyl Complexes

Chapter 4: Synthesis, Characterization, and Ketone and Aldehyde Hydrosilylation Activity of N,N,N-Chelate Iron Dialkyl Compounds

Chapter 5: Industrially Relevant Hydrosilylation Activity of Olefins and Tertiary Silanes with Bis(imino)pyridine and Terpyridine Iron Complexes

Chapter 6: The Oxidation and Reduction of Bis(imino)pyridine Iron($L)_2$: Investigating the Behavior of the Redox Active Ligand

LIST OF FIGURES

LIST OF TABLES

LIST OF ABBREVIATIONS

EPR = Electron paramagnetic resonance

SQUID = Superconducting quantum interference device

NMR = Nuclear magnetic resonance

IR = infra-red

COSY = Correlated spectroscopy

THF = Tetrahydrofuran

Py = Pyridine

Cy = cyclohexyl

^{n}Hex = *n*-hexyl

Ph = Phenyl

NO = Nitric oxide

CHAPTER 1

SYNTHESIS AND ELECTRONIC STRUCTURE OF FOUR- AND FIVE - COORDINATE, NEUTRAL, CATIONIC, AND ANIONIC, BIS(IMINO)PYRIDINE IRON NITROSYL COMPOUNDS

1.1 Abstract

A series of bis(imino)pyridine iron nitrosyl complexes was synthesized and characterized. The planar (^{iPr}PDI)Fe(NO) compound was prepared from the addition of one equivalent of nitric oxide to (^{iPr}PDI)Fe(N_2)$_2$. Full characterization of the compound indicates that the electronic structure is best described as an intermediate-spin ferric compound with a triplet di-anionic bis(imino)pyridine chelate and a triplet NO^-. This compound represents an unprecedented class of four-coordinate, non-heme iron nitrosyl complexes. Chemical reduction and oxidation was conducted on (^{iPr}PDI)Fe(NO) to determine the degree of chelate participation as opposed to the {Fe(NO)} unit participation during the redox processes. Redox chemistry occurs at the ligand, leaving the $\{Fe(NO)\}^7$ fragment intact in all cases ; the iron is best described as an intermediate ferric compound and the nitrosyl as an anionic ligand antiferromagnetically coupled. This rare three electron series, retaining coordination number and geometry, was synthesized and crystallographically characterized. The five coordinate, with pyridine in the fifth coordination site, neutral nitrosyl complex was synthesized and is best described as a high-spin ferrous compound, where the bis(imino)pyridine and the nitrosyl are both considered anionic ligands. Dinitrosyl complexes were synthesized in order to compare with the mono nitrosyl compound. Additionally, a variety of neutral, mono nitrosyl iron complexes were subsequently synthesized to determine what effects the sterics of the PDI ligand alterations had on the overall electronic structure of the {Fe(NO)} unit.

1.2 Introduction

The chemistry of iron nitrosyl complexes has a rich and varied history. Sodium nitroprusside was one of the first identified iron nitrosyl complexes, synthesized in the mid-1900's by Playfair.[1,2] Work with iron nitrosyl complexes has continued to expand since that time, including both heme and non-heme type iron nitrosyls, and there are a multitude of reviews on each subgroup of compounds.[3,4] Upon the discovery of the biosynthesis of NO,[5] the research into biologically relevant nitrosyl compounds has increased dramatically and led to nitric oxide being named molecule of the year in 1992.[6] One of the initial reasons for the interest in these compounds is the flexible coordination of the nitrosyl ligand. The two extremes are the linear NO^+ where the Fe-N-O angle is 180º, and the other is the NO^- and the Fe-N-O angle reaches 120º, as presented in Figure 1.1.

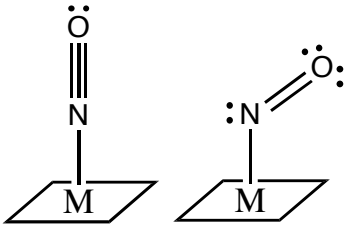

Figure 1.1 The two limiting cases of nitric oxide binding to a metal.

Enemark and Feltham have used molecular orbital correlation theory to construct a generalized description of metal nitrosyl complexes.[7,8] The notation used, $\{MNO\}^n$, attempts to justify and predict the bonding mode of the nitrosyl ligand. Treating the MNO fragment as an 'inorganic functional group', the remaining ligands coordinated to the metal dictate the geometry and modify the coordination mode of the nitrosyl. Importantly, the *n* term arises from the number of d electrons in conjunction with the number of electrons in the π^* system of the nitrosyl. This *n*-count, when

taken into consideration with the geometry of the molecule, predicts the binding mode of the nitrosyl ligand to the metal.

The two limiting cases in geometry of linear and bent were originally thought to have the limiting electronic descriptions of NO^+ and NO^-, respectively. [9,10] The bent binding mode of NO can generally be thought of as the nitrosyl acting as an X-type ligand with the metal undergoing a concurrent 1-electron oxidation, though resonance structures can be drawn to further reduce the nitrosyl and oxidize the metal (Figure 1.2). The linear bonding mode is best thought of as one of several bonding modes that arise from resonance structures.

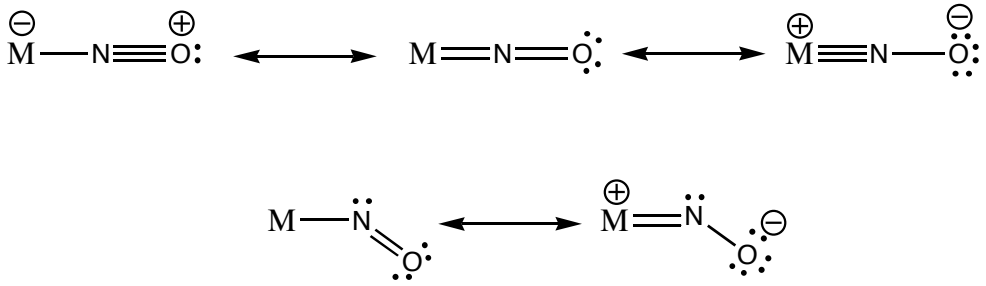

Figure 1.2 Resonance structures that explain the high degree of covalency in metal nitrosyl complexes.

Of particular interest to this work are compounds containing a single linear nitrosyl ligand bound to an overall four coordinate iron center. The earliest structurally characterized examples of this structural motif were of the type $\{MNO\}^{10}$, such as $Ni(NO)(N_3)(PPh_3)_2$[11] or $Co(NO)(CO)_2(PPh_3)$ and $Co(NO)(CO)(PPh_3)_2$.[12] For iron complexes, $Fe(NO)(CO)_3^-$ and $Fe(NO)_2(CO)_2$ are both known and isolable compounds, isoelectronic to $Ni(CO)_4$.[13] Connelly[14] and Cummins[15] have both reported tetrahedral $\{Fe(NO)\}^7$ complexes bearing linear nitrosyl units. In both cases, the nitrosyl ligand has been designated as an NO^+ fragment. Interestingly, Lippard reported an

isoelectronic tri-thiolate tetrahedral iron compound bearing a linear nitrosyl, although Lippard proposes an electronic structure of Fe(III) and a reduced nitrosyl.[16] These complexes are presented in Figure 1.3.

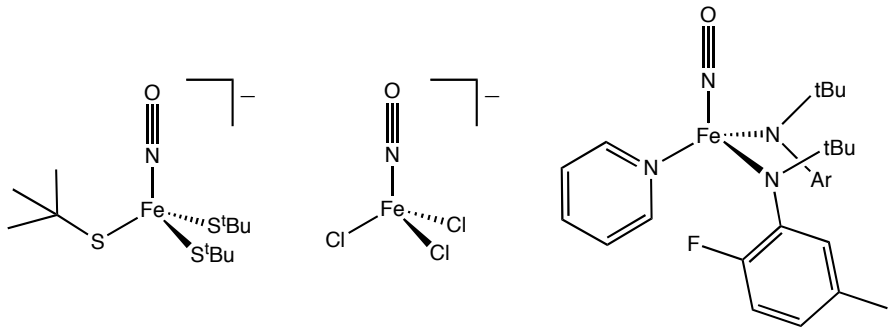

Figure 1.3 Tetrahedral $\{Fe(NO)\}^7$ iron complexes with linear nitrosyl ligands reported by, from left to right, Lippard, Connelly, and Cummins.

In order to attain a greater discussion of electronic structure of the [Fe(NO)] fragment in the literature, one needs to find compounds of more interesting architecture or utility. Unfortunately, iron nitrosyl compounds that have any sort of detailed electronic structure work or description are of coordination number five or six. Solomon has reported several examples of in depth electronic investigations of iron nitrosyl complexes. This group was able to show a new binding type of NO with six-coordinate high-spin ferrous centers, where the $S = 5/2$ iron is antiferromagnetically coupled to a nitrosyl anion of $S = 1$, giving an overall $S = 3/2$ molecule. [17,18] Borovik was able to show that the same bonding mode can be achieved with five-coordinate, anionic ferrous compounds. Lippard has also reported a five coordinate neutral iron complex bearing a proposed reduced linear nitrosyl. The complexes of Borovik and Lippard are presented in Figure 1.4.

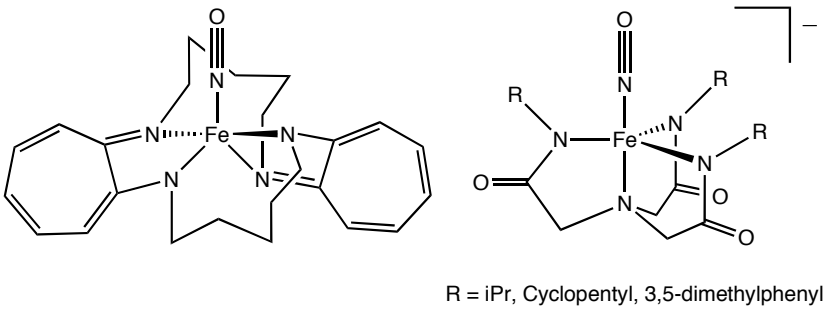

Figure 1.4 Two reported compounds with proposed linear NO^- by Lippard (Left) and Borovik (Right).

This work also investigated the role of sterics surrounding the nitrosyl ligand and the role steric demand plays on the coordination geometry and electronics of the nitrosyl ligand.[19,20] Another investigation conducted by Weighardt[21] investigated a 3 electron redox series of octahedral cyclam iron complexes, $LFeCl(NO)^{2+,+,0}$ giving $\{Fe(NO)\}^{6,7,8}$, respectively. This leads to a similar result as Solomon and Lippard in that the iron reduces the nitrosyl ligand to NO^-. The $\{Fe(NO)\}^6$ is an $S = 1$ Fe(IV) antiferromagnetically coupled to a triplet nitrosyl anion to yield a diamagnetic molecule and for the $\{Fe(NO)\}^7$ species, an intermediate-spin ferric ($S = 3/2$) antiferromagnetically coupled to a triplet NO to yield an overall $S = 1/2$ complex. This concept of NO reduction is taken further in the case of the neutral $\{Fe(NO)\}^8$ complex, where it is proposed that the nitrosyl is yet again reduced to the dianionic radical NO^{2-} of $S = 1/2$ and the iron is then a low-spin ferric ($S = 1/2$) center, giving rise to an overall $S = 0$ complex.

For the amount of attention, in both biology and fundamental coordination chemistry, that iron nitrosyls have been furnished for more than 100 years, there is still continuing interest in both heme and non-heme iron nitrosyls and dinitrosyl iron

complexes.[22,23] For this reason, an investigation into the chemistry between nitric oxide and the reduced iron dinitrogen complex (^{iPr}PDI)Fe(N_2)$_2$ (PDI = 2,6-(*R*N=CMe)$_2$$C_5H_3N$, R = 2,6R-$C_6H_3$). Bis(imino)pyridines are also well-established redox-active ligands[24,25,26,27,28,29] and are able to promote reversible transfer of 1-3 electrons between the chelate and the transition metal. Nitrosyl ligands are also redox-active ligands, and therefore complicated electronic structures are anticipated. The complexes that have been synthesized allow for a fundamental study of both the (PDIFe) unit as well as the {Fe(NO)} unit. And due to the paucity of four-coordinate iron nitrosyl compounds, the synthesis could also yield bonding types of an {Fe(NO)} unit that have yet to be observed in over 150 years of iron nitrosyl investigations.

1.3 Preparation and Electronic structure of (^{iPr}PDI)Fe(NO)

In order to begin the investigation into bis(imino)pyridine iron nitrosyl chemistry, several synthetic routes to the four coordinate nitrosyl complex were developed. Many methods are known in the synthesis of transition metal nitrosyl complexes.[30] The addition of cationic nitric oxide in the form of [NO][BF_4] to the anionic [Na(Et_2O)$_x$][(^{iPr}PDI)Fe(N_2)][31] resulted in metathesis to form $NaBF_4$ and the desired (^{iPr}PDI)Fe(NO). Another route comes from the comproportionation of (^{iPr}PDI)Fe(NO)$_2$ and an equimolar amount of (^{iPr}PDI)Fe(N_2)$_2$ [32]to yield two equivalents of the desired compound. The synthesis and characterization of the dinitrosyl compound will be discussed in more detail later in the chapter. The addition of a stoichiometric quantity of nitric oxide to the dinitrogen compound of the desired ligand set resulted in the formation of the desired product in high yield. This method proved to be the most useful and general route. A general reaction scheme for these routes is presented in Figure 1.5.

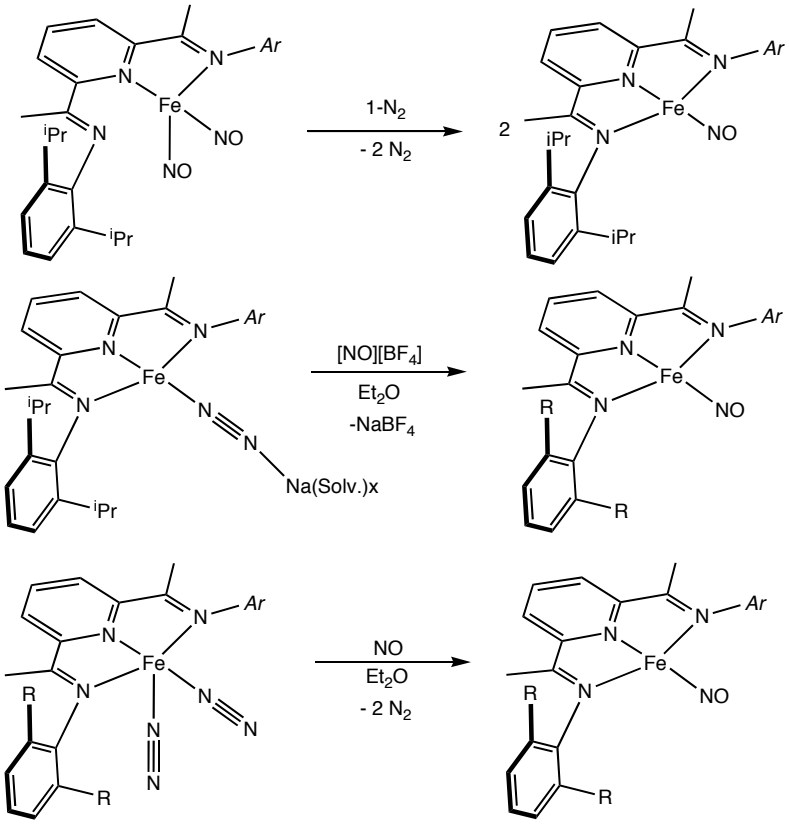

(^{iPr}PDI)Fe(N_2)$_2$ (R = ^{i}Pr)
[(^{Et}PDI)Fe(N_2)]$_2$(N_2) (R = Et)
[(^{Me}PDI)Fe(N_2)]$_2$(N_2) (R = Me)

(^{iPr}PDI)Fe(NO) (R = ^{i}Pr): 95 %
(^{Et}PDI)Fe(NO) (R = Et): 87 %
(^{Me}PDI)Fe(NO) (R = Et): 78 %

Figure 1.5 The reactions forming four coordinate bis(imino)pyridine iron nitrosyl compounds.

The careful addition of one equivalent of nitric oxide to a frozen ether solution of (^{iPr}PDI)Fe(N_2)$_2$ resulted in a color change from green to dark red, signalling the formation of (^{iPr}PDI)Fe(NO). Initially, the thawing solution takes on a bright pink color, indicating the formation of the dinitrosyl complex, (^{iPr}PDI)Fe(NO)$_2$, followed by comproportionation with the unreacted (^{iPr}PDI)Fe(N_2)$_2$ to yield the desired compound. The solution was filtered through Celite, rinsed through with a minimal amount of diethyl ether, and the volatiles removed. Recrystallization of the resultant solid yielded a dark, paramagnetic powder that was identified as (^{iPr}PDI)Fe(NO).

(^{iPr}PDI)Fe(NO) exhibited an $S = 1/2$ ground state with a μ_{eff} of 1.8 μ_B at 290 K in a magnetic susceptibility balance as a solid. NO stretching frequencies of 1726 cm^{-1} in KBr and 1724 cm^{-1} in toluene were observed by IR. The addition of ^{15}NO resulted in a shift of the frequency to 1696 cm^{-1} in KBr and 1693 cm^{-1} in toluene. The benzene-d_6 ^{1}H NMR spectra of (^{iPr}PDI)Fe(NO) at 20 °C establish that this compound exhibits either C_{2v} symmetry in solution. A solid-state structure was obtained for (^{iPr}PDI)Fe(NO) and it is presented in Figure 1.6.

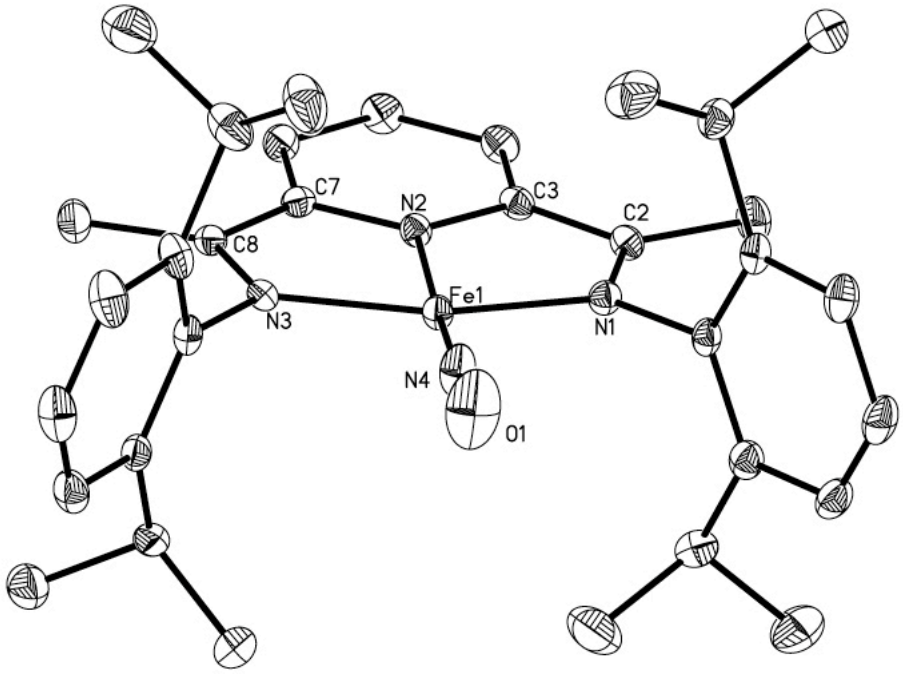

Figure 1.6 Molecular structure **(^{iPr}PDI)Fe(NO)** at 30% probability ellipsoids. Hydrogen atoms omitted for clarity.

The solid-state structure of (^{iPr}PDI)Fe(NO) exhibited a near square planar geometry with an essentially linear iron nitrosyl (Fe(1)-N(4)-O(1) = 178.37(17)) bond and a near linear pyridine-iron-nitrosyl (N(2)-Fe(1)-N(4) = 174.02(7)) bond. The Fe(1)-N(4) bond of 1.6309(15) Å is one of the shortest iron nitrogen bonds reported for a PDI iron complex, indicating a very strong iron-nitrosyl bond. The

bis(imino)pyridine ligand appears to be doubly reduced, as the imine bonds have elongated to 1.3308(19) Å and 1.3375(19) Å for N(1)-C(2) and N(3)-C(8), respectively. The C_{ipso}-C_{imine} bond lengths are contracted to 1.427(2) Å and 1.426(3) Å for C(2)-C(3) and C(7)-C(8), respectively. With the doubly reduced bis(imino)pyridine, this complex can be described in the Enemark Feltham notation as an $\{Fe(NO)\}^7$ complex. This planar geometry of the iron along with the linear nitrosyl ligand is a unique structural motif in iron nitrosyl chemistry.

Mössbauer parameters were obtained for (^{iPr}PDI)Fe(NO), and the spectrum exhibited a quadrupole doublet $\delta = 0.10$ mm/s and $\Delta E_Q = 0.86$ mm/s and the spectrum is presented in Figure 1.7. These values are ambiguous as to the oxidation state of the iron in (^{iPr}PDI)Fe(NO). Previously synthesized PDI iron compounds that exhibit similar parameters are PDI imide compounds[33], (^{iPr}PDI)Fe(NR) or (^{iPr}PDI)Fe(NAr) where R = alkyl and Ar = aryl), and the PDI iron alkyl anion compounds $[Li(OEt_2)_3][(^{iPr}PDI)Fe(R)(N_2)]$,[34,35] both iron centers are highly covalent to the PDI ligand, as well as to the other coordinating ligands. The aryl imide compounds are designated as intermediate-spin ferric, while the alkyl anions have been determined to be low-spin ferrous complexes. This indicates a high degree of covalency for the iron in (^{iPr}PDI)Fe(NO), both to the PDI as well as to the nitrosyl ligand, and that the electronic structure description is not trivial.

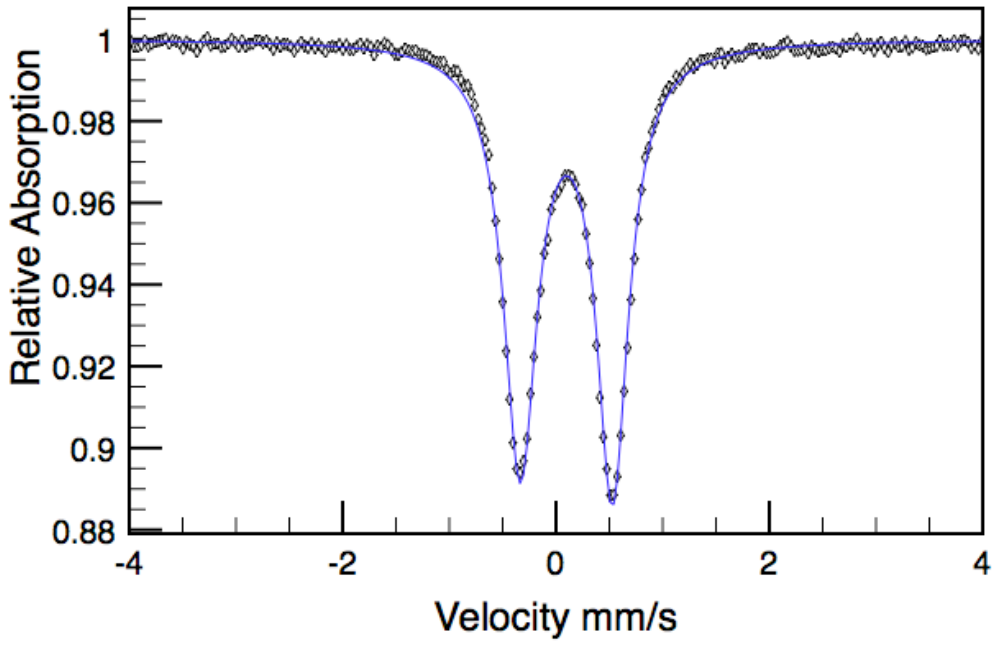

Figure 1.7 The zero-field Mössbauer spectrum of **(^{iPr}PDI)Fe(NO)** recorded at 80 K**.**

The elucidation of the electronic structure of (^{iPr}PDI)Fe(NO) was undertaken utilizing an array of spectroscopic and structural techniques, as well as DFT calculations. To this end, the spectroscopic data is presented along with calculations in order to establish the electronic structure most consistent with the data. The structural data establishes 2 electron reduction at the chelate, along with an exceedingly short Fe(1)-N(4) bond length, indicating a strong interaction between the iron and nitrosyl. This is very likely due to the two π bonds that can arise with the π* orbital of the nitrosyl. The IR stretching frequency of the nitrosyl is inconsistent with NO^+, and although 1724 cm^{-1} seems high for NO^-, precedent in the literature establishes that it is reasonable for an $\{Fe(NO)\}^7$ complex containing a linear, reduced NO ligand.[36, 37] The magnetic susceptibility measurement indicates that the compound contains only one

unpaired electron for a $\mu_{eff} = 1.8\ \mu_B$ at 290 K, so EPR studies were undertaken to try and establish the location of the unpaired spin in the compound is located.

Both toluene glass and powder samples of (^{iPr}PDI)Fe(NO) were prepared and spectra were recorded at 10 K. The powder spectrum is presented in Figure 1.8. The spectra did not change much from a glass to a solid sample, and in each case there was no hyperfine coupling in a near axial signal for an $S = 1/2$ complex. The ^{15}N isotopologue was subjected to EPR as well, and only subtle shifts in the spectrum could be seen, indicating a low amount of spin localized on the nitrosyl ligand.

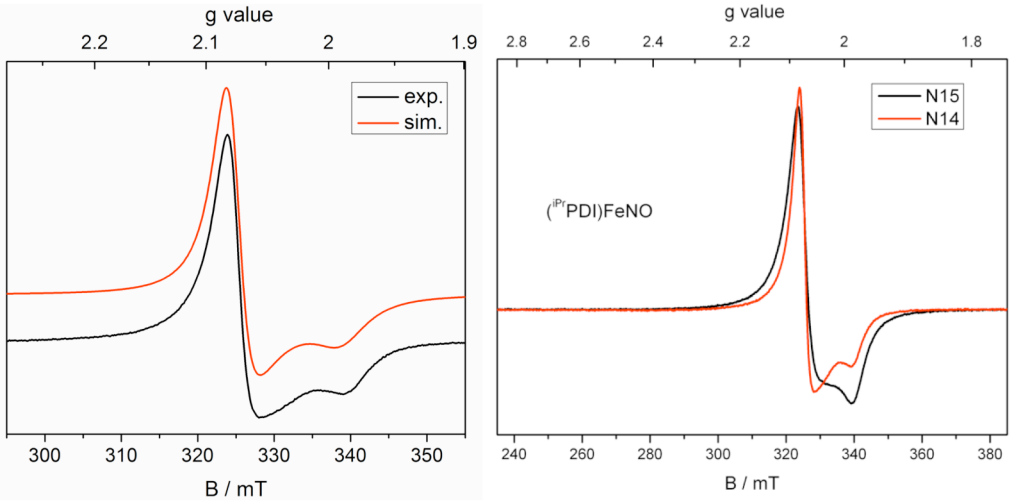

Figure 1.8 The powder EPR spectrum of **(^{iPr}PDI)Fe(NO)** at 10 K.

The g anisotropy of (^{iPr}PDI)Fe(NO) was small, but not small enough to rule out an iron based spin. The three g values, g_y, g_x, and g_z, with values of 2.08, 2.07, and 1.99, respectively, have an anisotropy, g_{max}-g_{min}, of 0.09. This leaves the iron and the PDI as viable options for the unpaired spin. As this complex is paramagnetic, applied field Mössbauer spectroscopy was performed, and the resultant spectra are presented in Figure 1.9.

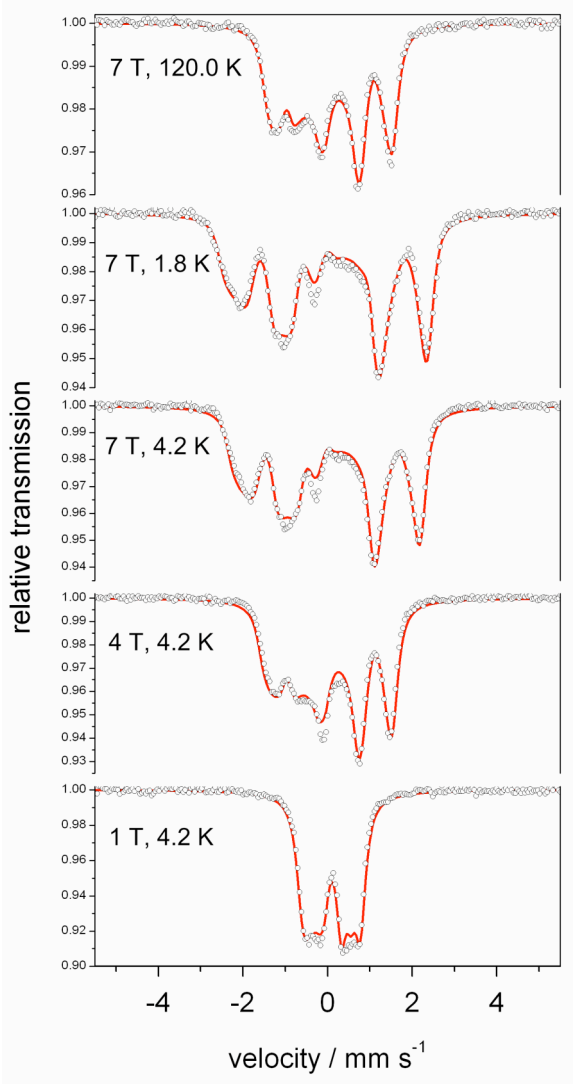

Figure 1.9 The spectra obtained from the applied-field, variable temperature Mössbauer.

This series of spectra provided sufficient data to begin piecing together an electronic structure picture for (^{iPr}PDI)Fe(NO). The quadrupole splitting was determined to be $\Delta E_Q = -0.86$ mm/s. More importantly, however, are the A values gleaned from the fit, the three being $A_{xx} = 125$ kG, $A_{yy} = 115$ kG, and $A_{zz} = 91$ kG. This relatively odd combination of A values, where each one is small and positive, is highly indicating that the majority of the unpaired spin is PDI based. This points to the

SOMO of the compound being PDI π* based, which is in agreement with the EPR data. This information, along with the crystal data, allows one to construct a qualitative d-orbital splitting diagram of the molecule (Figure 1.10).

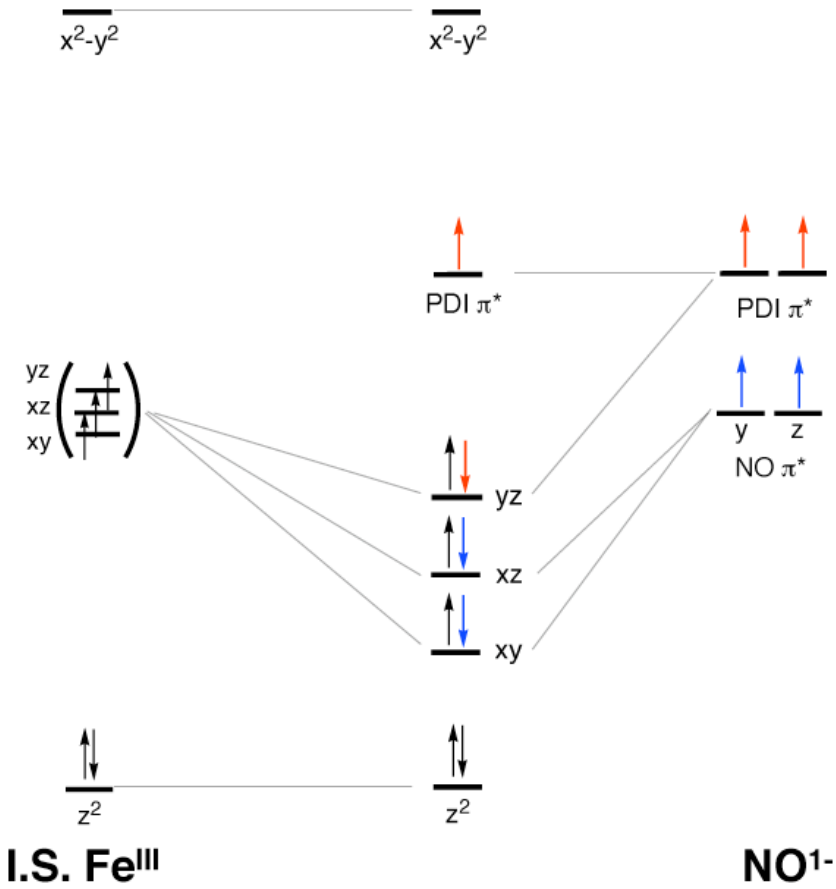

Figure 1.10 Model d-orbital splitting diagram for **(^{iPr}PDI)Fe(NO).**

This diagram qualitatively explains every piece of the data collected for (^{iPr}PDI)Fe(NO). Placing the d-z^2 orbital lowest in energy is nt necessarily rigorously correct, as it is anti-bonding with respect to the ligands in the idealized square plane. However, due to the contracted Fe-ligand bonds as a whole, the anti-bonding nature of this orbital does not seem to perturb the ligand distances to an appreciable extent, and therefore the orbital, in effect, is no longer considered in this discussion. Treating the

nitrosyl as an anion and the iron as a ferric center as the two 'starting' pieces is a stylistic choice to emphasize the fact that the final electronic structure appears to maintain this configuration. The diagram shows that the origin of the short Fe-NO bond length arises from the sigma interaction as well as two π-interactions. Importantly, the SOMO is consistent with the EPR and magnetic Mössbauer data.

Another spectroscopy utilized in this investigation is X-ray absorption spectroscopy (XAS). This method measures the ejection of an 1s electron on the iron center into the 'continuum' and any transitions in between. A forbidden transition of the 1s electron into the 3d orbital set of the iron can be observed, and is called the pre-edge feature. The energy of the 1s electron is directly correlated to the effective charge on the metal nucleus (*i.e.* the oxidation state of the metal). Effectively, the oxidation state of a metal can be assigned utilizing this transition in XAS.[38] The transition of the electron into the 4p set, called the rising edge, also says something about the oxidation of the metal, such that more oxidized metals require more energy make this transition. Caveats exist in the interpretation of the forbidden transition, as the feature is susceptible to changes in coordination number, geometry, field strength of ligands, etc., so care must be taken. A blow-up of the pre-edge s-to-d transition of the XAS spectrum of (^{iPr}PDI)Fe(NO) is presented in Figure 1.11, and the rising edge s-to-p transition is presented in Figure1.12, along with the data for (^{iPr}PDI)$FeCl_2$ and (^{iPr}PDI)FeN(2,6-diisopropylphenyl) (labeled as (^{iPr}PDI)FeN(Dipp) in the spectrum), compounds that have been assigned as Fe(II) and Fe(III), respectively.

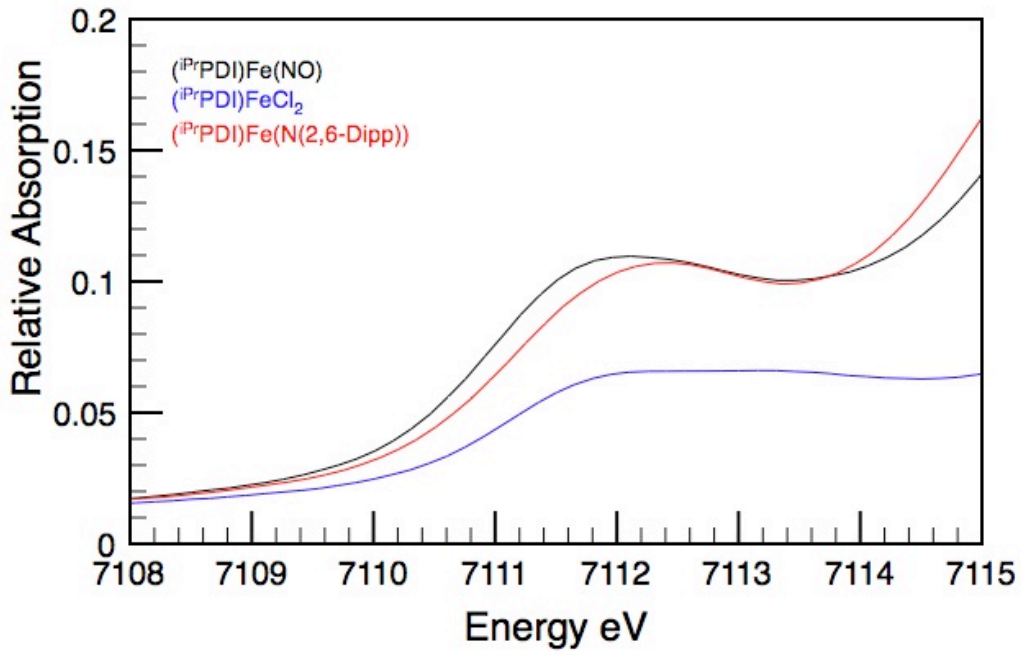

Figure 1.11 XAS pre-edge region of **(^{iPr}PDI)Fe(NO), (^{iPr}PDI)FeCl$_2$,** and **(^{iPr}PDI)FeN(Dipp).**

From the pre-edge region of the XAS, (^{iPr}PDI)Fe(NO) does not appear to be an Fe(III) complex. The peak maximum is more akin to (^{iPr}PDI)FeCl$_2$, a known ferrous species. The peak maximum of (^{iPr}PDI)FeN(Dipp) is nearly 0.5 eV, indicating that (^{iPr}PDI)Fe(NO) is not as oxidized as the previously reported Fe(III) species. However, (^{iPr}PDI)Fe(NO) is a planar, 4-coordinate complex, and (^{iPr}PDI)FeN(Dipp) is not planar; the imide is canted out of the plane of the chelate just over 41º.[39] (^{iPr}PDI)FeCl$_2$ is five coordinate, so the direct comparison with these two compounds to (^{iPr}PDI)Fe(NO) is less than perfect when looking at the pre-edge. Upon examination of the rising edge, however, a different oxidation state picture emerges.

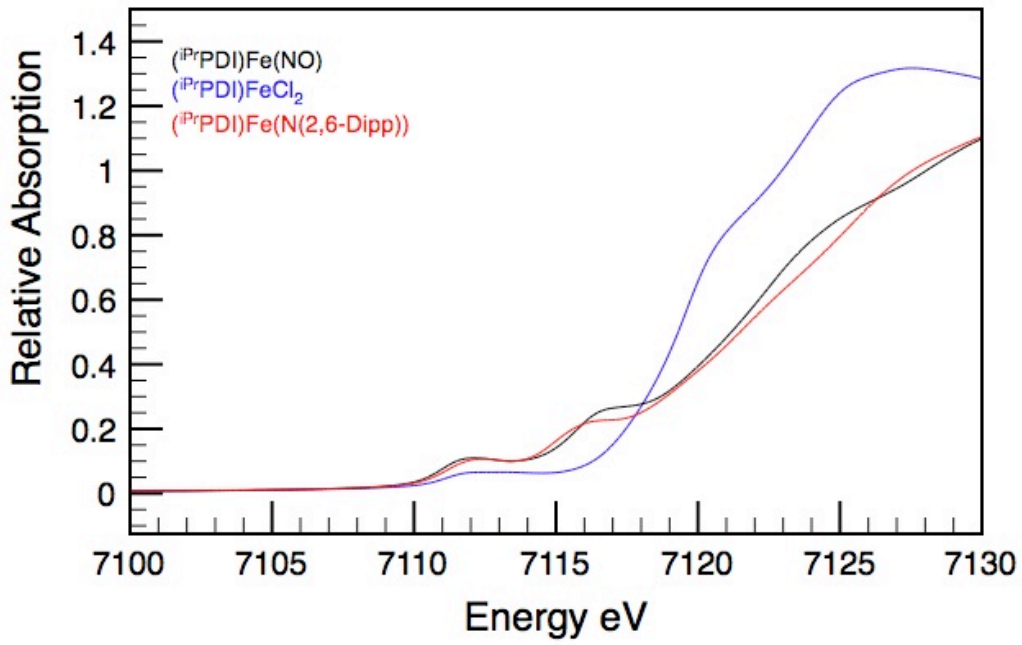

Figure 1.12 XAS rising edge feature of **(^{iPr}PDI)Fe(NO)**.

Upon examination of the rising edge region of the XAS data, the ferrous compound (^{iPr}PDI)$FeCl_2$ is more reduced than the two other compounds. Both (^{iPr}PDI)Fe(NO) and (^{iPr}PDI)FeN(Dipp) have nearly overlapping rising edges, both of which are at a higher energy than (^{iPr}PDI)$FeCl_2$. This data supports the proposed electronic structure of (^{iPr}PDI)Fe(NO) containing a ferric center.

In order to confirm this electronic structure, DFT calculations using the B3LYP functional were performed on (^{iPr}PDI)Fe(NO). The compound was calculated as a spin-unrestricted doublet based on the experimentally determined $S = 1/2$ ground state. A geometry optimization was obtained for (^{iPr}PDI)Fe(NO) and is presented in Table 1.1, and the distances will be referred to in upcoming discussions.

Table 1.1 Select calculated and X-ray parameters of **(^{iPr}PDI)Fe(NO)**.

	(^{iPr}PDI)Fe (NO)	**Calc.**		**(^{iPr}PDI)Fe (NO)**	**Calc.**
Fe(1)-N(1)	1.911(2)	1.938	C(2)-C(3)	1.427(2)	1.432
Fe(1)-N(2)	1.864(1)	1.889	C(7)-C(8)	1.426(3)	1.432
Fe(1)-N(3)	1.910(2)	1.937			
Fe(1)-N(4)	1.631(2)	1.693	N(1)-Fe(1)-N(2)	79.51(5)	80.02
			N(1)-Fe(1)-N(4)	100.69(6)	100.08
N(1)-C(2)	1.331(2)	1.349	N(2)-Fe(1)-N(3)	79.77(5)	80.00
N(3)-C(8)	1.338(2)	1.349	N(3)-Fe(1)-N(4)	99.85(6)	99.91
N(2)-C(3)	1.379(2)	1.368	N(2)-Fe(1)-N(4)	174.02(7)	179.35
N(2)-C(7)	1.376(2)	1.368			
			Fe(1)-N(4)-O(1)	178.37(17)	179.80
N(4)-O(1)	1.185(2)	1.169			

The computed electronic structure corresponds to a broken symmetry (3,4) solution, obtained via spontaneous symmetry breaking during the unrestricted calculation of (^{iPr}PDI)Fe(NO). The BS (*m*, *n*) descriptor refers to a broken symmetry state with *m* unpaired spin up electrons on fragment 1 and *n* unpaired spin down electrons essentially localized on fragment 2. The computed ^{57}Fe Mössbauer parameters of $\delta = 0.07$ mm s^{-1} and $\Delta E_Q = -1.96$ mm s^{-1}, compared to the experimentally determined values ($\delta = 0.10$ mm/s; $\Delta E_Q = -0.86$ mm/s), are in excellent agreement for the isomer shift, but the quadrupole splitting values are very different. The qualitative MO diagram from the calculations is presented in Figure 1.13, and an enlargement up of the SOMO is presented in Figure 1.14.

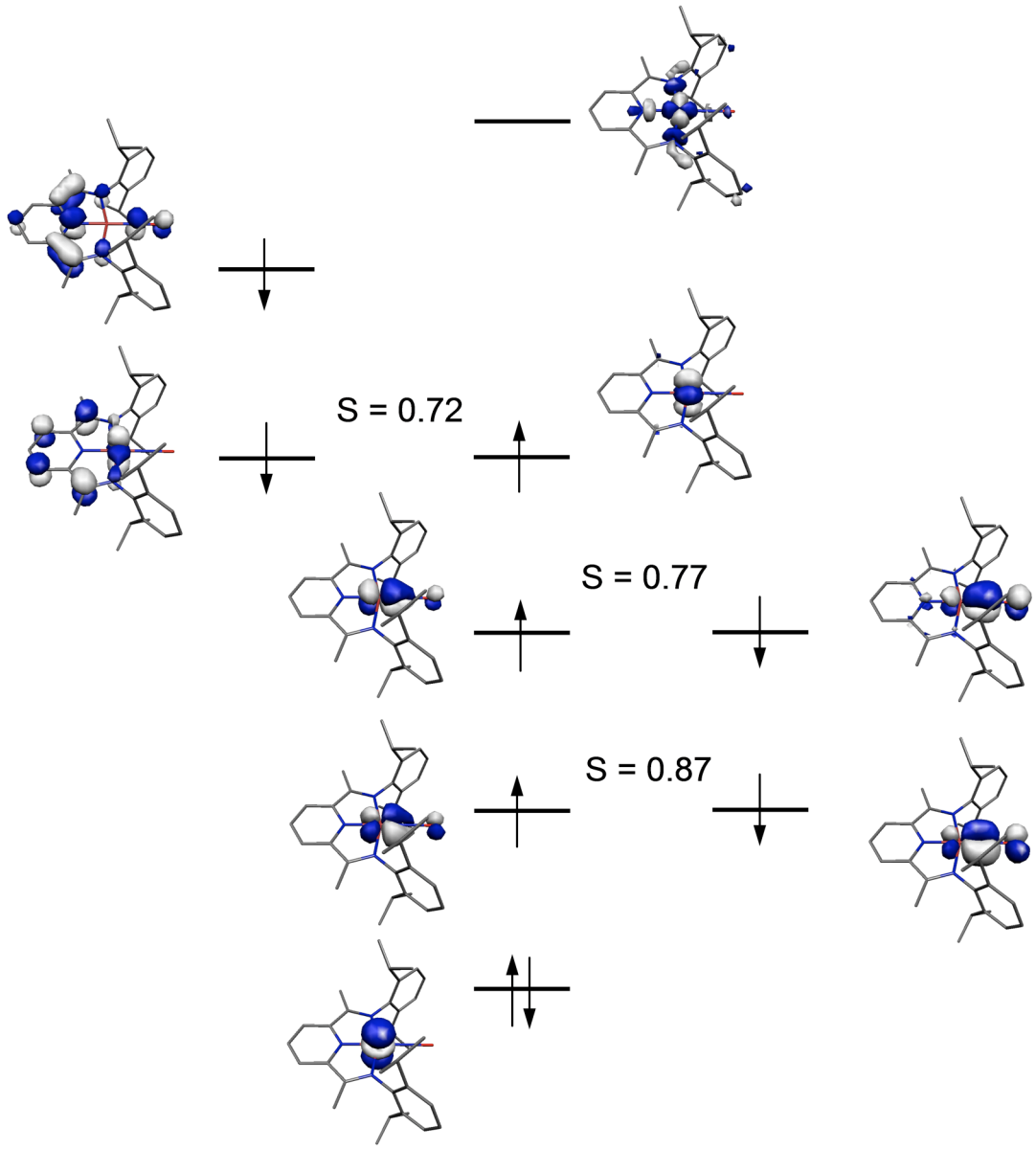

Figure 1.13 D-orbital splitting diagram of (^{iPr}PDI)Fe(NO) obtained from the BS (3,4) calculation.

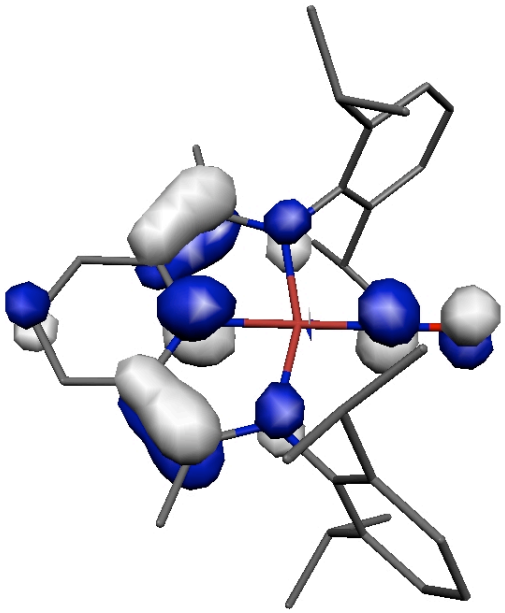

Figure 1.14 The B_2 SOMO of **(^{iPr}PDI)Fe(NO)** showing the lack of iron contribution to the spin and the ~10% contribution of the nitrosyl ligand.

The calculated orbital diagram of (^{iPr}PDI)Fe(NO) is consistent with the 'back of the envelope' bonding description above. The ordering of the orbitals is approximate, as the α and β sets have different energies, but the pairs are chosen based in the corresponding orbital transformation, where the orbitals are matched based on maximum similarity, regardless of the energy ordering.[60] However, the overall meaning of the calculation is upheld in that the orbital scheme provides support for the spectroscopy, and that the electronic picture is rational. If all the data is placed together, than the electronic description of the compound is best thought of as an intermediate ferric center (S = 3/2), antiferromagnetically coupled to an NO^- (S = 1) and to one of the two radicals on the $[PDI]^{2-}$ chelate (S = 1/2), leaving the other radical as the SOMO (S = 1/2) of the molecule, where the total spin of the complex is S = 1/2. The caveat in this case is that the {Fe(NO)} unit is highly covalent, as seen in the high

spatial overlap values in the two π bonds. This does impart ambiguity to the electronic structure assignment, but this remains the description that best fits the evidence, as there is no directly contradicting data. This coordination number and geometry is heretofore unknown in the long history of iron nitrosyl complexes. The derivatives of (^{iPr}PDI)Fe(NO) were investigated next, in part to continue studying this unprecedented type of iron nitrosyl compound, as well as to make sure that there is consistency throughout a series of similar nitrosyl compounds.

1.4 Preparation and Electronic Structure of [(15-Crown-5)Na(THF)$_2$]-[(^{iPr}PDI)Fe(NO)].

Attempted reduction of (^{iPr}PDI)Fe(NO) with cobaltacene or pentamethylcobaltacene produced no reaction in either diethyl ether or THF. These unsuccessful experiments do lend some insight into the stability of (^{iPr}PDI)Fe(NO), however. A stronger reducing agent, 1.0% Na/Hg amalgam, was utilized in both THF and diethyl ether and the reaction furnished a slow color change to pink, in the case of THF, and a precipitated pink solid in the case of diethyl ether. The diethyl ether reaction was decanted off of the amalgam onto a glass frit to yield, in most cases over 80%, the bright pink solid product. In the case of the THF reaction, the solution was filtered through Celite, the volume of THF reduced under vacuum, and an equivalent of pentane was used to precipitate the product. Again, the yield was high, typically near 90%.

Both products displayed similar spectroscopic and physical characteristics. The IR stretching frequency of the two complexes were within error of each other, with the THF product displaying a strong stretch at 1601 cm^{-1} and the diethyl ether product displaying a stretch at 1603 cm^{-1}. The red-shift of 125 wavenumbers in the IR seems reasonable to the addition of 1 electron, as seen with (^{iPr}PDI)Fe(N_2) (ν (N_2) = 2034 cm^{-1}) to [(^{iPr}PDI)Fe(N_2)]$^-$) (ν (N_2) = 1966 cm^{-1}), but most probably the sodium cation is

interacting with the nitrosyl, much as in the case of the sodium in the nitrogen compound. This is presented in Figure 1.15.

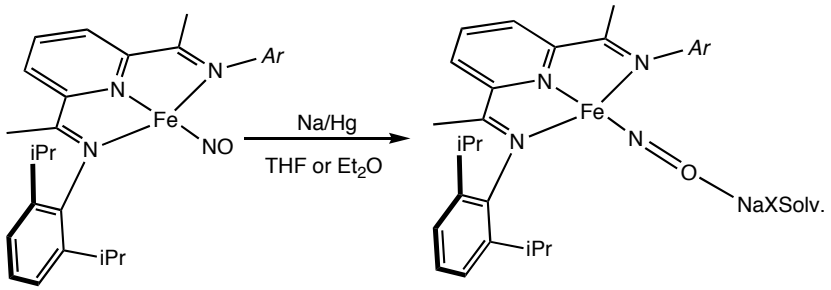

Figure 1.15 The synthesis of **[Na(Solv)$_x$] [(^{iPr}PDI)Fe(NO)]** with an interacting sodium molecule.

Zero-field Mössbauer data were collected at 80 K for both complexes, and the data is nearly indistinguishable. Both complexes display isomer shifts of -0.03 mm/s and a quadrupole splitting of 1.54 mm/s. The spectra of [Na(Solv)$_x$][(^{iPr}PDI)Fe(NO)] and [Crown-Na][(^{iPr}PDI)Fe(NO)] are presented in Figure 1.16. These parameters, upon first inspection, seem to contradict typical Mössbauer rules, in that metal centers with more electron density typically increase in their isomer shifts. This, of course, ignores another feature of Mössbauer in that field strength and covalency both tend to lower the isomer shifts of a compound. With this knowledge, one can predict that either the PDI or NO is somehow interacting stronger with the iron center due to the reduction. The attempts to crystallize either compound, utilizing an array of techniques and solvent, were unsuccessful.

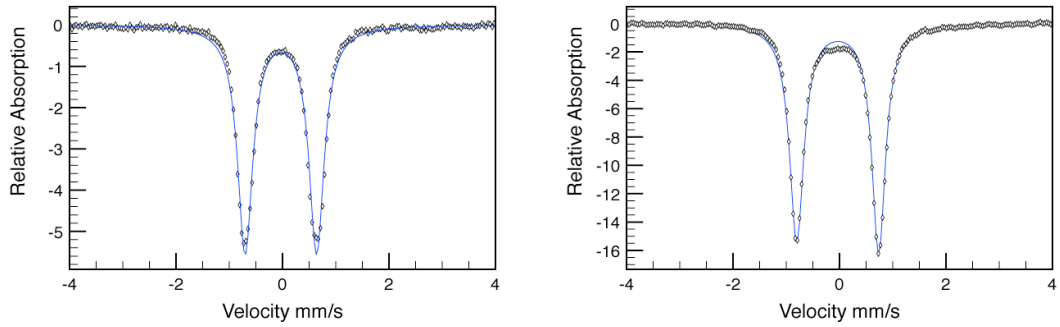

Figure 1.16 The Mössbauer at 80 K of **[Na(Solv)$_x$][(^{iPr}PDI)Fe(NO)]** on the right and **[Crown-Na][(^{iPr}PDI)Fe(NO)]** on the left.

To overcome this problem, as well minimize sodium coordination to [Na(Solv)$_x$][(^{iPr}PDI)Fe(NO)], 15-crown-5 was added to a THF solution of the reduced compound. The synthesis of these compounds is presented in Figure 1.17. Immediately, there was a precipitation of a diamagnetic brick red solid. This cryptand version of the reduced nitrosyl compound, [Crown-Na][(^{iPr}PDI)Fe(NO)], displayed a strong stretch in the IR at 1676 cm^{-1}, a blue-shift of 70 wavenumbers, confirming the sodium-nitrosyl interaction in the compound without the cryptand. The isomer shift remains at -0.03 mm/s, indicating no gross electronic structural changes occurred upon encapsulation of the sodium ion, and the quadrupole splitting only slightly lowered to 1.36 mm/s.

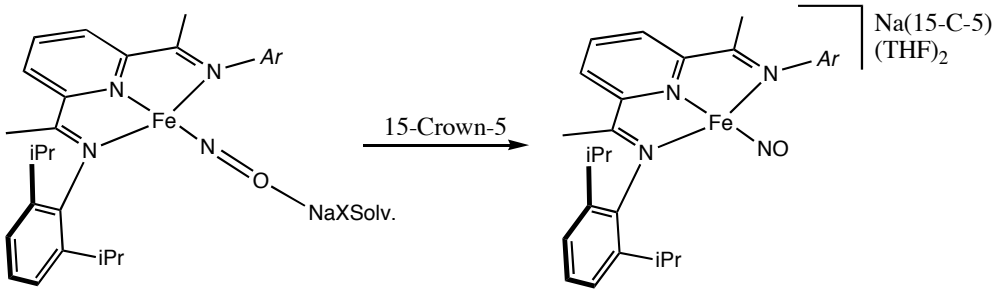

Figure 1.17 The encapsulation of the solvent solvated species of **[Na(Solv)$_x$][(^{iPr}PDI)Fe(NO)]**to yield **[Crown-Na][(^{iPr}PDI)Fe(NO)]**.

To gain an understanding of the more electronic structure of these compounds, the well-understood metrical parameters of the PDI-Fe fragment are necessary, thus, crystals suitable for a solid-state structure were obtained by the cooling of a concentrated THF solution of [Crown-Na][(^{iPr}PDI)Fe(NO)] to -35 ºC. The structure establishes the non-coordinating sodium encapsulated with the cryptand and two THF molecules, one of which is disordered. The iron nitrosyl bond is linear and remains in the plane of the chelate. The structure is presented in Figure 1.18.

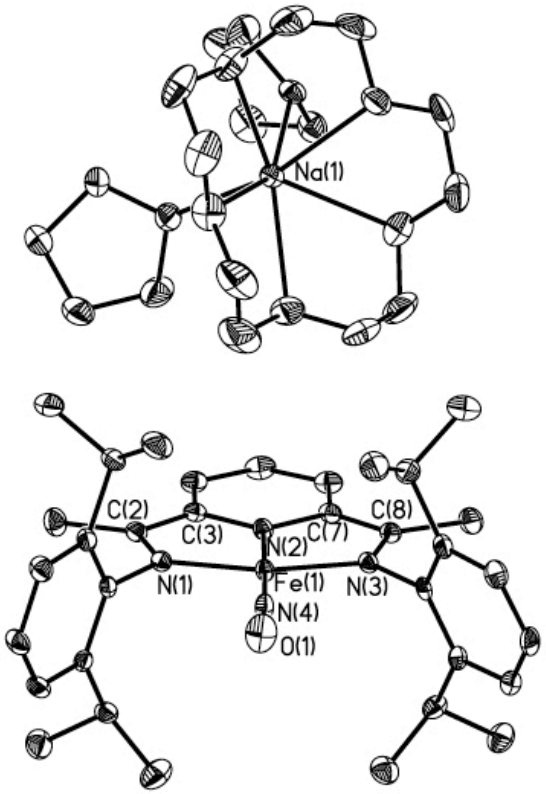

Figure 1.18 A representation of **[Crown-Na][(iPrPDI)Fe(NO)]** in the solid state presented at 30% probability ellipsoids. Hydrogen atoms were removed for clarity.

The metrical parameters of [Crown-Na][(^{iPr}PDI)Fe(NO)] indicate that the chelate are highly reduced. The imine bond distances for N(1)-C(2) and N(3)-C(8) are exceedingly long at 1.365(4) Å and 1.370(4) Å, respectively. Accordingly, C(2)-C(3) and C(7)-C(8) are exceedingly short at 1.399(4) Å and 1.394(4) Å. These highly reduced metrics are indicative of previously reported bis(imino)pyridine iron mono-alkyl anions, where it was determined that a singlet diradical chelate yields similar bond lengths.[35] Another alternative is that the bis(imino)pyridine was actually reduced again, yielding a true $[PDI]^{3-}$ bound to a transition metal center. These two possibilities are presented in Figure 1.19. The metrical parameters of [Crown-

Na][(^{iPr}PDI)Fe(NO)], along with (^{iPr}PDI)Fe(NO) and [(^{iPr}PDI)Fe(NO)][$BArF_{24}$] for comparison, are presented in Table 1.2. Calculations were run to distinguish the two possibilities.

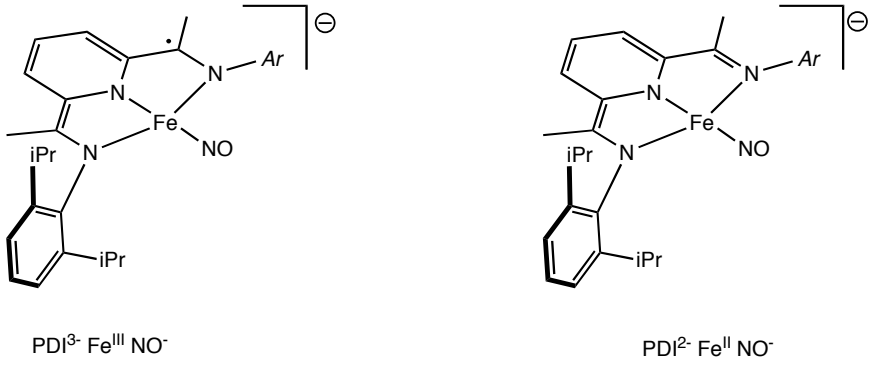

Figure 1.19 The two most likely possibilities for the electronic structure of **[Crown-Na][(^{iPr}PDI)Fe(NO)]**.

Table 1.2 The metrical parameters of the 3-electron series **[[Crown-Na]-[(^{iPr}PDI)Fe(NO)]**, **(^{iPr}PDI)Fe(NO)** and **[(^{iPr}PDI)Fe(NO)][$BArF_{24}$].** Distances in Å, angles in º.

	[Na-$(THF)_2$(15-C-5)][(^{iPr}PDI)Fe(NO)]	**(^{iPr}PDI)Fe(NO)**	**[(^{iPr}PDI)Fe(NO)] [BArF24]**
Fe(1)-N(1)	1.885(2)	1.9107(13)	1.946(3)
Fe(1)-N(2)	1.833(2)	1.8640(12)	1.869(3)
Fe(1)-N(3)	1.893(2)	1.9096(12)	1.950(3)
Fe(1)-N(4)	1.631(3)	1.6309(15)	1.625(4)
N(1)-C(2)	1.365(4)	1.3308(19)	1.302(5)
N(3)-C(8)	1.370(4)	1.3375(19)	1.307(5)
N(2)-C(3)	1.395(4)	1.3794(19)	1.352(5)
N(2)-C(7)	1.399(4)	1.3759(19)	1.359(5)
N(4)-O(1)	1.193(3)	1.185(2)	1.171(5)
C(2)-C(3)	1.399(4)	1.427(2)	1.460(6)
C(7)-C(8)	1.391(4)	1.426(3)	1.453(6)
N(1)-Fe(1)-N(2)	80.00(11)	79.51(5)	79.24(14)
N(1)-Fe(1)-N(4)	98.69(12)	100.69(6)	99.34(17)
N(2)-Fe(1)-N(3)	80.08(11)	79.77(5)	79.49(14)

N(3)-Fe(1)-N(4)	101.24(12)	99.85(6)	99.91(17)
N(2)-Fe(1)-N(4)	178.66(12)	174.02(7)	158.97(18)
Fe(1)-N(4)-O(1)	177.5(2)	178.37(17)	174.6(5)

The compound was calculated as a spin-unrestricted singlet based on the experimentally determined $S = 0$ ground state. The computed electronic structure corresponds to a broken symmetry (3,3) solution, obtained via spontaneous symmetry breaking during the unrestricted calculation. The computed ^{57}Fe Mössbauer parameters of $\delta = 0.00$ mm s^{-1} and $\Delta E_Q = -2.16$ mm s^{-1}, are in agreement with the experimentally determined values ($\delta = -0.03$ mm/s; $\Delta E_Q = |1.54$ mm/s$|$). The qaudrupole splitting values are outside the accepted values. The calculated metrical parameters (Table 1.3) are in good agreement with the experimental data, so the cause of the discrepancy in ΔE_Q remains unknown. The qualitative MO diagram from the calculations is presented in Figure 1.20.

Table 1.3 Select calculated and experimental metrical parameters for **[Crown-Na][(^{iPr}PDI)Fe(NO)]**.

	(^{iPr}PDI)Fe(NO)-	**Calc.**		**(^{iPr}PDI)Fe(NO)-**	**Calc.**
Fe(1)-N(1)	1.885(2)	1.927	C(2)-C(3)	1.399(4)	1.402
Fe(1)-N(2)	1.833(2)	1.859	C(7)-C(8)	1.391(4)	1.402
Fe(1)-N(3)	1.893(2)	1.928			
Fe(1)-N(4)	1.631(3)	1.673	N(1)-Fe(1)-N(2)	80.00(11)	80.47
			N(1)-Fe(1)-N(4)	98.69(12)	99.60
N(1)-C(2)	1.365(4)	1.383	N(2)-Fe(1)-N(3)	80.08(11)	80.44
N(3)-C(8)	1.370(4)	1.382	N(3)-Fe(1)-N(4)	101.24(12)	99.50
N(2)-C(3)	1.395(4)	1.395	N(2)-Fe(1)-N(4)	178.66(12)	179.79
N(2)-C(7)	1.399(4)	1.395			
			Fe(1)-N(4)-O(1)	177.5(2)	179.22
N(4)-O(1)	1.193(3)	1.186			

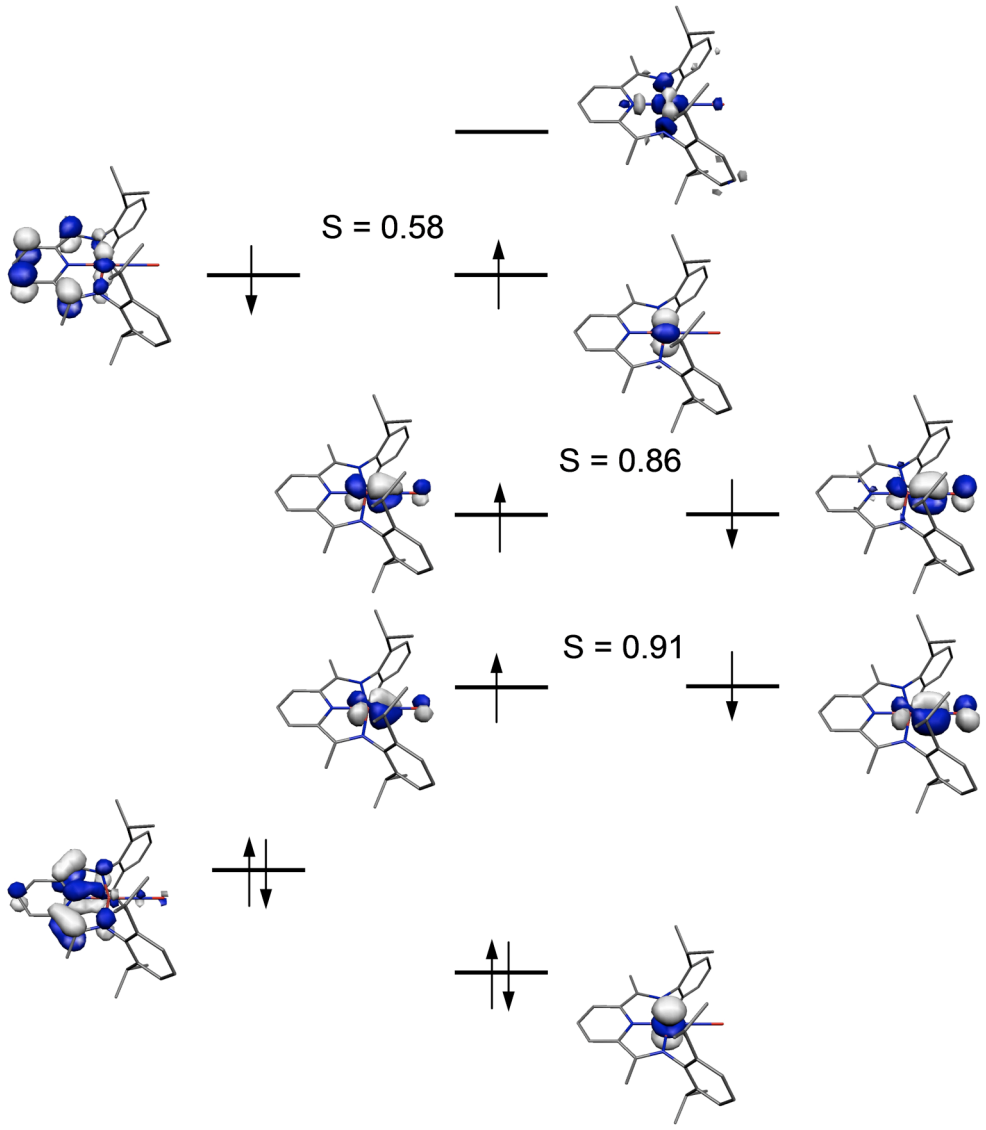

Figure 1.20 Qualitative Molecular orbital picture arising from DFT calculations on **[Crown-Na][(^{iPr}PDI)Fe(NO)]**.

The calculations show a doubly filled b_2 PDI orbital, as well as a singly occupied a_2 orbital that is antiferromagnetically coupling to the iron. This indicates that the PDI is triply reduced, and that the iron center remains intermediate-spin ferric, as in the neutral complex. The [Fe(NO)] subunit has a very high degree of overlap, indicating a high degree of covalency, and remains an $\{Fe(NO)\}^7$. The $[PDI]^{3-}Fe(III)$

center is unexpected and a cause for concern, but the calculations are consistent with experimentally determined parameters. An intermediate-spin ferrous complex with a singlet diradical bis(imino)pyridine chelate has not been ruled out calculationally, however. With the success of the reduction of (^{iPr}PDI)Fe(NO), the oxidation was undertaken in the hopes of completing the three electron series.

1.5 Preparation and Electronic structure of [(^{iPr}PDI)Fe(NO)][BArF$_{24}$]

The use of [Cp_2Fe][BPh_4] to oxidize (^{iPr}PDI)Fe(NO) was ineffective, resulting on the isolation of unreacted starting materials. A more non-coordinating anion in tetrakis(1,3-bistrifluoromethylphenyl)borate ($BArF_{24}$) was utilized. The oxidation was performed in either toluene, in which [(^{iPr}PDI)Fe(NO)][$BArF_{24}$] was only sparingly soluble and precipitated from the reaction mixture. Upon the addition of [Cp_2Fe][$BArF_{24}$] to (^{iPr}PDI)Fe(NO) in a fluorobenzene solution, the color changed immediately to bright purple from a dull red color. The product was precipitated by the addition of pentane and cooling the solution to -35 ºC overnight. The bright purple powder was collected and identified as [(^{iPr}PDI)Fe(NO)][$BArF_{24}$]. The reaction mixture should not contain any compounds coordinating lone-pairs of electrons, such as diethyl ether or THF, because coordinating solvents quickly bind to the cation, resulting in a shift to an apical, bent nitrosyl and the ligand bound in the plane of the chelate to yield [(^{iPr}PDI)Fe(NO)(L)][$BArF_{24}$], a compound class that will be discussed later in the chapter. This reactivity is summed up in Figure 1.21.

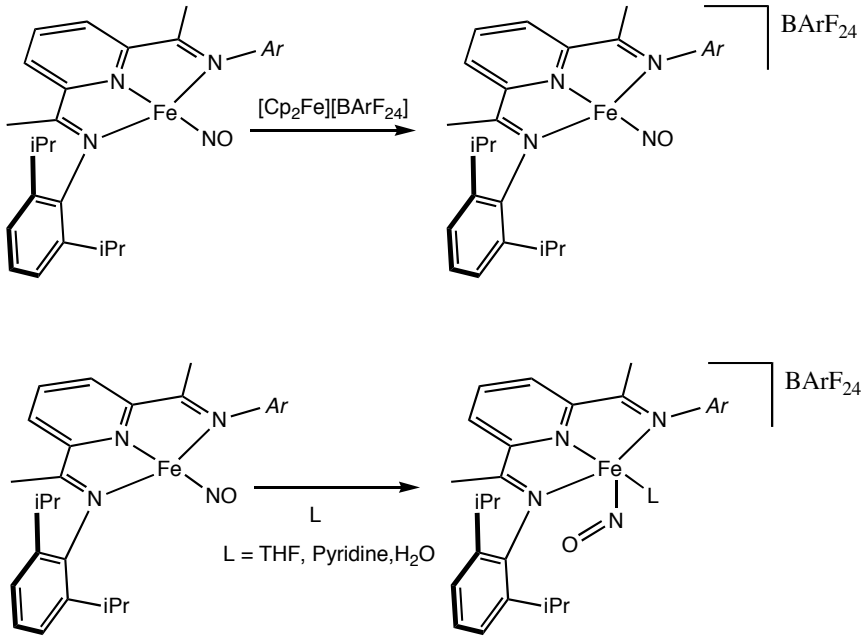

Figure 1.21 The synthesis of the complexes **[(^{iPr}PDI)Fe(NO)][BArF$_{24}$]** and **[(^{iPr}PDI)Fe(NO)(L)][BArF$_{24}$].**

The nitrosyl stretching frequency of [(^{iPr}PDI)Fe(NO)][BArF$_{24}$] in fluorobenzene showed up in the IR at 1809 cm^{-1} and in KBr at 1786 cm^{-1}. The Mössbauer spectrum showed a quadrupole doublet with an isomer shift of 0.22 mm/s and a quadrupole splitting of 0.94 mm/s and is presented in Figure 1.22. This spectrum is consistent with a molecule that has ligands of slightly less field strength and/or a lower degree of covalency than the parent complex. The NMR spectrum was consistent with a C_2 or C_s symmetric compound, and the chemical shift range is on the order of 10 ppm indicative of a diamagnetic compound.

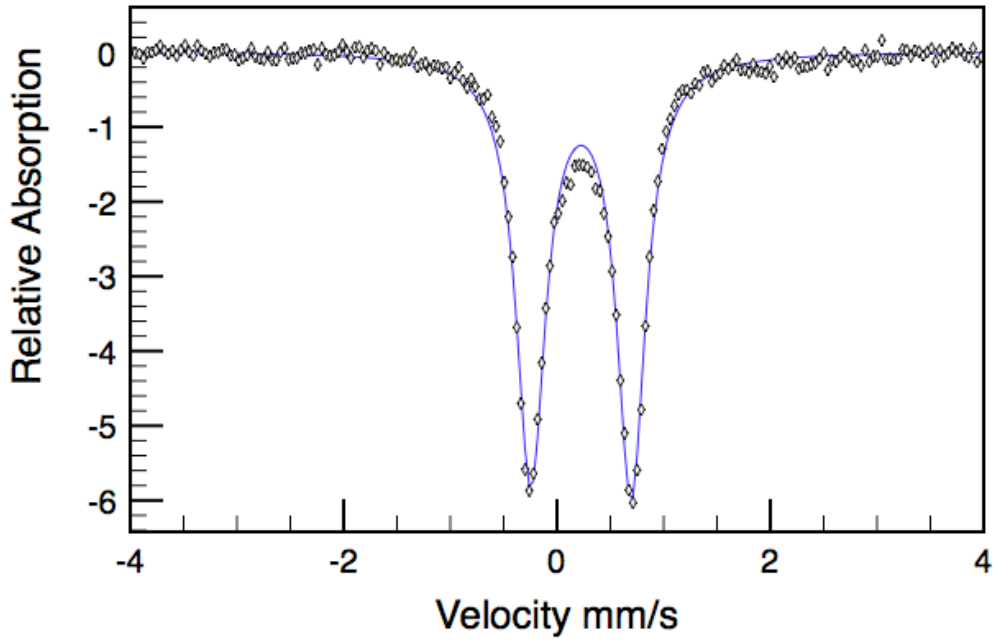

Figure 1.22 Zero-field Mössbauer spectrum of **[(^{iPr}PDI)Fe(NO)][BArF$_{24}$]** obtained at 80 K.

X-ray quality crystals were grown from a concentrated fluorobenzene solution layered with pentane and cooled to -35ºC. The structure revealed a four-coordinate compound bis(imino)pyridine iron nitrosyl complex with a non-coordinating $BArF_{24}$ anion and a disordered fluorobenzene molecule was also contained within in the crystal lattice. The nitrosyl ligand is linear, but is canted out of the metal-chelate plane by 18º. The solid-state structure of [(^{iPr}PDI)Fe(NO)][$BArF_{24}$] is presented in Figure 1.23.

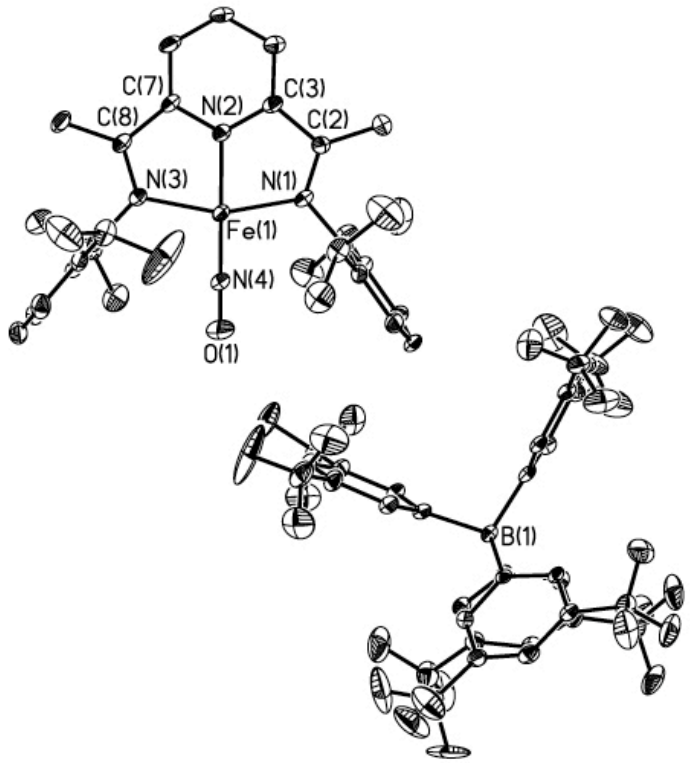

Figure 1.23 A representation of **[(^{iPr}PDI)Fe(NO)][BArF$_{24}$]** in the solid state presented at 30% probability ellipsoids. Disordered -CF3 groups and hydrogens were removed for clarity.

The ligand metrics of obtained from the solid-state structure of [(^{iPr}PDI)Fe(NO)][BArF$_{24}$] indicate that the PDI ligand is mono-reduced. The SOMO of the neutral complex appears to have been oxidized, leaving the rest of the electron distribution unperturbed. The imine bond distances have contracted significantly from the diradical distances at 1.302(5) Å and 1.307(5) Å for N(1)-C(2) and N(3)-C(8), respectively. The bond lengths of the C(2)-C(3) and C(7)-C(8) have lengthened considerably to 1.460(6) Å and 1.453(6) Å, respectively. This oxidation of the PDI leaves the iron-nitrosyl fragment electronically unperturbed as an {Fe(NO)}^{7}.

The oxidation of (^{iPr}PDI)Fe(NO) is, at first glance, the easiest transformation. The SOMO appears to have been oxidized, leaving the rest of the orbitals and couplings intact, producing a diamagnetic compound. The diamagnetism of [(^{iPr}PDI)Fe(NO)][$BArF_{24}$] results again in the loss of several useful spectroscopic methods, such as EPR and applied field Mössbauer. The calculations, aside from previous works in PDI iron oxidation and reduction chemistry,[35] are essentially the sole basis on which to describe the electronic structure.

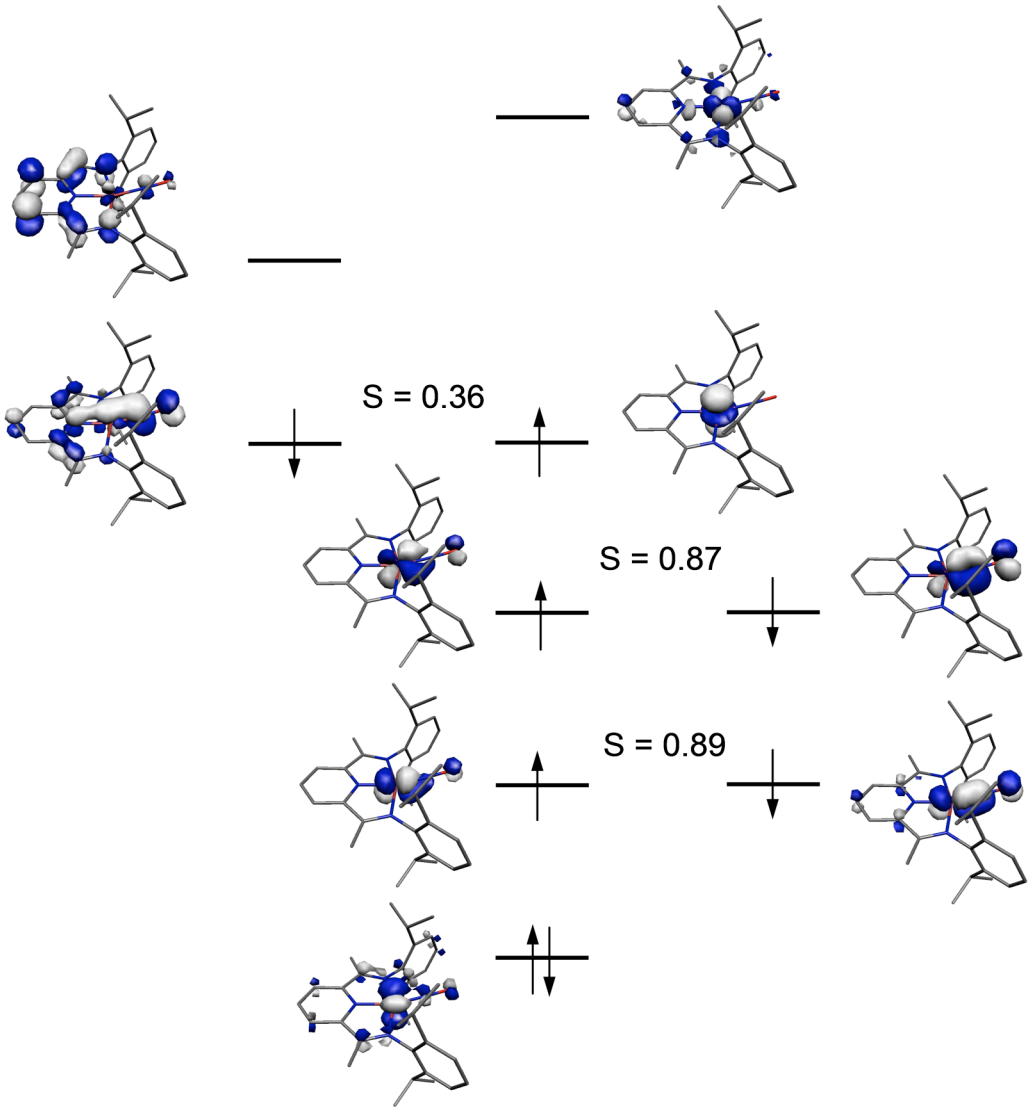

Figure 1.24 Qualitative molecular orbital diagram of **[(^{iPr}PDI)Fe(NO)]-[$BArF_{24}$]** from DFT calculations.

[(^{iPr}PDI)Fe(NO)][$BArF_{24}$] was calculated as a spin-unrestricted singlet based on the experimentally determined $S = 0$ ground state. The computed electronic structure corresponds to a broken symmetry (3,3) solution, obtained via spontaneous symmetry breaking during the unrestricted calculation. The computed ^{57}Fe Mössbauer parameters of $\delta = 0.31$ mm s^{-1} and $\Delta E_Q = -0.63$ mm s^{-1}, are in decent agreement with the experimentally determined values ($\delta = 0.22$ mm/s; $\Delta E_Q = |0.94$ mm/s|). The isomer shift difference can be explained by the calculations overestimating the Fe(1)-N(4) bond length by 0.08 Å, the experimental distance being 1.625(4) Å and the calculations giving 1.713 Å. This overestimation decreases the covalency of the iron-nitrosyl bond in the calculation, giving rise to an increased isomer shift. The qualitative MO diagram from the calculations is presented in Figure 1.24.

The calculations confirm the initial hypothesis of the oxidation of bis(imino)pyridine from the dianion to the monoanion upon formation of [(^{iPr}PDI)Fe(NO)][$BArF_{24}$]. Interestingly, a cloverleaf d-orbital is not involved in the magnetic pair that arises from antiferromagnetic coupling from the iron to the PDI. The cant of the nitrosyl out of the plane of the chelate appears to be partially responsible. The cant allows for the 'dz^2' iron based orbital to tilt sufficiently to couple to the PDI based radical. This orbital has NO π bonding character as well, so it's not a pure orbital to say the least. However, it appears that the {Fe(NO)}^{7} unit remains intact. The electronic structure is best described as an intermediate-spin ferric iron antiferromagnetically coupled to a PDI based radical as well as two NO anion based radicals. Mössbauer data corroborates this description, as the parameters do not greatly change for the oxidation. The increase in isomer shift is explained by the weakened, lower covalent PDI mono radical in the oxidized complex versus the diradical in the neutral complex.

From the spectroscopy and calculations, it appears the {Fe(NO)} unit along this series of complexes is too stable allow for redox changes. Therefore, the redox chemistry is confined to the supporting PDI ligand. A representation of electron flow along the series is outlined in Figure 1.25.

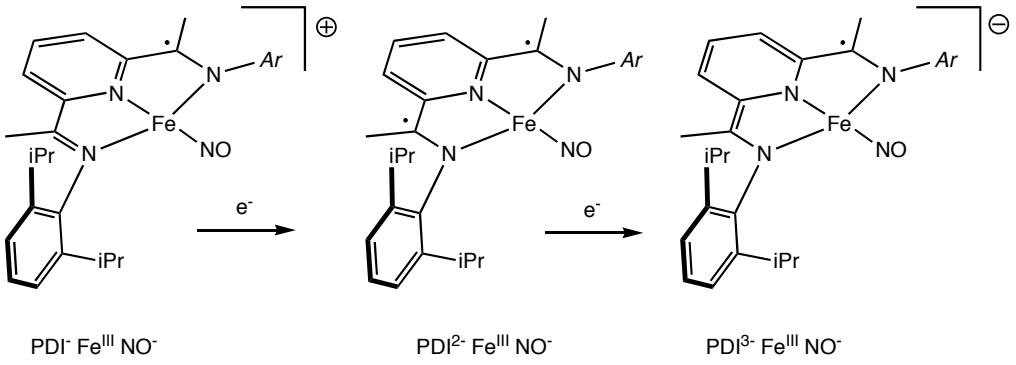

Figure 1.25 Electron movement over the three electron redox series of **[Crown-Na][(^iPrPDI)Fe(NO)]**, **(^iPrPDI)Fe(NO)**, and **[(^iPrPDI)Fe(NO)][BArF$_{24}$]**.

1.6 Preparation and Electronic structure of (^iPrPDI)Fe(NO)(Py)

Addition of a slight excess of pyridine to a diethyl ether solution of (^{iPr}PDI)Fe(NO) resulted in an immediate color change from brown/red to dark green and the precipitation of the product as a dark green powder identified as the pyridine adduct, (^{iPr}PDI)Fe(NO)(Py), as presented in Figure 1.26. This product displayed broad signals between -2 and 12 ppm in the ^{1}H NMR spectrum, and a shift in the IR from 1726 cm^{-1} to 1628 cm^{-1}. The solid-state magnetic susceptibility balance yielded a μ_{eff} of 1.8μB at 290K.

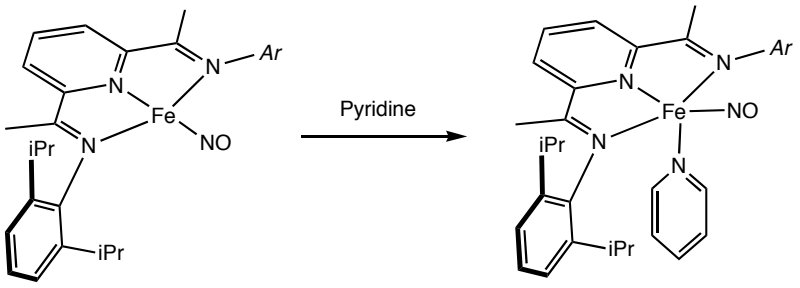

Figure 1.26 The synthetic route to the five-coordinate neutral complex **(^{iPr}PDI)Fe(NO)(Py).**

Zero field Mössbauer measurements yielded a quadrupole doublet with an isomer shift of $\delta = 0.59$ mm/s and a quadrupole splitting $\Delta E_Q = 0.86$ mm/s. This is the most informative spectroscopy as to the effect of adding a fifth ligand on the electronic structure. The Mössbauer parameters are most consistent with a high-spin ferrous center, indicating a spin change at the iron. The structure was determined by X-ray diffraction and is presented in Figure 1.27.

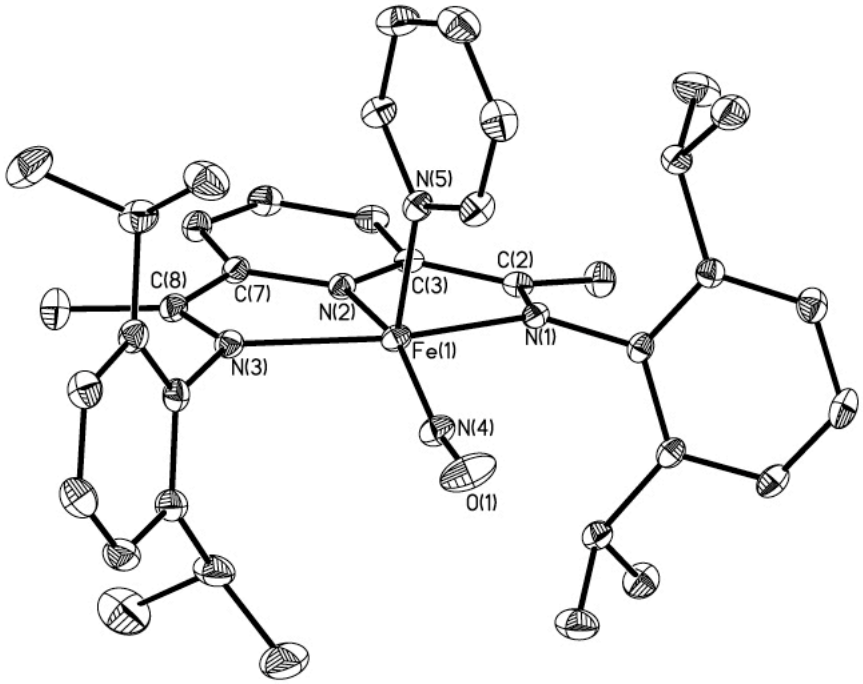

Figure 1.27 Representative structure of **(^{iPr}PDI)Fe(NO)(Py)** at 30% probability ellipsoids. Hydrogen atoms and a distorted fluorobenzene molecule are removed for clarity.

The pyridine coordinates in the apical position of (^{iPr}PDI)Fe(NO) of the distorted square pyramidal structure. The nitrosyl drops out of the plane of the chelate, with an N(2)-Fe(1)-N(4) angle of 154.76(10)º. The nitrosyl ligand has bent nearly 20º, giving an Fe(1)-N(4)-O(1) angle of 162.5(2) º. This angle is odd in that it falls nearly perfectly between the two limiting cases of 120 º and 180 º. The reduction metrics of the chelate indicate a single reduction of the PDI as opposed to the doubly reduced (^{iPr}PDI)Fe(NO). The N(1)-C(2) and the N(3)-C(8) bond distances are typical distances for single reduction at, 1.303(3) Å and 1.310(3) Å, respectively. The Fe(1)-N(1) and Fe(1)-N(3) distances are also much long than the other PDI iron compounds, at 2.176 (2) Å and 2.131(2) Å, respectively, indication population of the dx^2-y^2 orbital.

The electronic structure of (^{iPr}PDI)Fe(NO)(Py) was elucidated utilizing standard spectroscopic techniques and DFT calculations. (^{iPr}PDI)Fe(NO)(Py), based on the Mössbauer and crystal structure data, appears to be the only complex with an {Fe(NO)}^{8} fragment. In order to verify this, (^{iPr}PDI)Fe(NO)(Py) was subjected to the same spectroscopic techniques as the four-coordinate neutral complex. EPR spectroscopy was performed in a toluene glass at 77 K. The spectrum is presented in Figure 1.28.

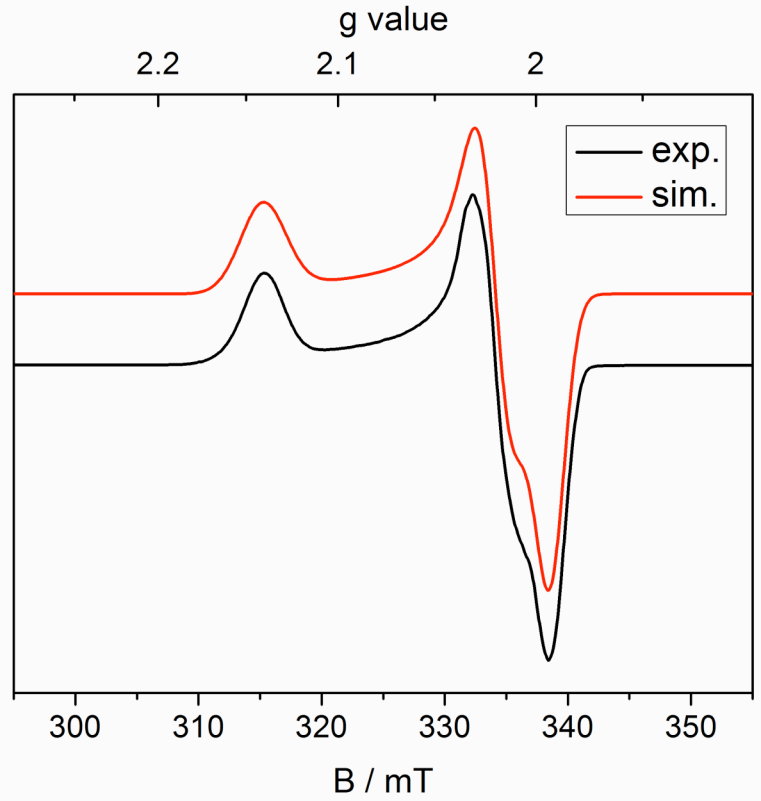

Figure 1.28 The EPR spectrum of **(^{iPr}PDI)Fe(NO)(Py)** at 77 K in toluene glass.

The rhombic symbol is slightly more anisotropic than (^{iPr}PDI)Fe(NO), with three g values of 2.14, 2.02, and 1.99, for g_z, g_y, and g_x, respectively, have a Δ g of 0.15, higher than the Δ g value of (^{iPr}PDI)Fe(NO) by nearly twice the magnitude. This is encouraging for the molecule containing a higher percentage of the spin on the iron center. (^{iPr}PDI)Fe(^{15}NO)(Py) was obtained as well, but there were only subtle changes

in the EPR spectrum. More data, however, is needed. Applied field Mössbauer data was performed on (^{iPr}PDI)Fe(NO)(Py) and the applied field spectra are presented in Figure 1.29.

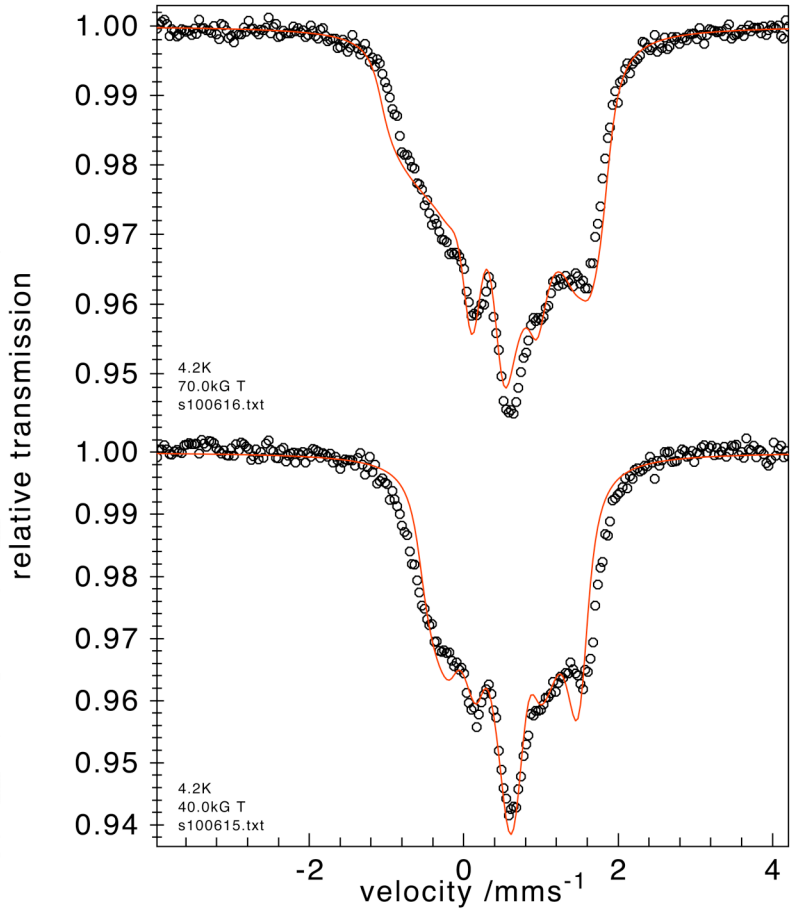

Figure 1.29 The applied field Mössbauer spectrum of **(^{iPr}PDI)Fe(NO)(Py)**.

These spectra provided sufficient data to begin piecing together an electronic structure picture. The sign of the qaudrupole splitting was determined to be ΔE_Q = -0.86 mm/s, identical to the four-coordinate complex. The A values of A_{xx} = -166.77 kG, A_{yy} = -269.92 kG, and A_{zz} = 25.72 kG, with two of the three values being large and negative, are indicative of the majority spin being iron based. This points to the

SOMO of (^{iPr}PDI)Fe(NO)(Py) being iron based, which is in agreement with the EPR spectrum. The Euler angle obtained from the fit of 28 º is in good agreement with the corresponding Fe-NO vector that has an angle of 25 º, indicating again the strength of the interaction of the iron nitrosyl fragment. From the Mössbauer, EPR, and crystal structure data, this compound is best described as high-spin ferrous center with a singly reduced PDI, and an iron nitrosyl bond that is both X-type and L-type. Calculations were performed in order to try and support the interpretations of the spectroscopy. Geometry optimized bond angles and distances for both (^{iPr}PDI)Fe(NO)(Py) are presented in Table 1.4.

Table 1.4 The calculated and experimentally determined structural parameters of **(^{iPr}PDI)Fe(NO)(Py)**.

Bond Distance Å **Bond Angle º**	**Calc.**	**(^{iPr}PDI)Fe(NO)(Py)**
Fe(1)-N(1)	2.314	2.176(2)
Fe(1)-N(2)	2.036	1.972(2)
Fe(1)-N(3)	2.312	2.131(2)
Fe(1)-N(4)	1.782	1.683(2)
Fe(1)-N(5)	2.160	2.056(2)
Fe(1)-O(2)		
N(1)-C(2)	1.304	1.303(3)
N(3)-C(8)	1.305	1.310(3)
N(2)-C(3)	1.379	1.375(3)
N(2)-C(7)	1.379	1.374(3)
N(4)-O(1)	1.193	1.159(3)
C(2)-C(3)	1.461	1.444(3)
C(7)-C(8)	1.460	1.445(3)
N(1)-Fe(1)-N(2)	73.97	75.09(8)
N(1)-Fe(1)-N(4)	102.75	101.90(9)
N(2)-Fe(1)-N(3)	74.08	75.47(8)
N(3)-Fe(1)-N(4)	102.81	102.72(9)
N(2)-Fe(1)-N(4)	154.40	154.76(10)
N(2)-Fe(1)-N(5)	103.54	105.59(8)
Fe(1)-N(4)-O(1)	174.81	162.5(2)

DFT calculations using the B3LYP functional were performed on (^{iPr}PDI)Fe(NO)(Py). The compound was calculated as a spin-unrestricted doublet based on the experimentally determined $S = 1/2$ ground state. The computed electronic structure corresponds to a broken symmetry (4,3) solution, obtained via spontaneous symmetry breaking during the unrestricted calculation. The computed ^{57}Fe Mössbauer parameters of $\delta = 0.78$ mm s^{-1} and $\Delta E_Q = 1.13$ mm s^{-1}, are in poor agreement with the experimentally determined values ($\delta = 0.56$ mm/s; $\Delta E_Q = -0.86$ mm/s). The calculated bond lengths are overestimated by nearly 0.1 Å for all Fe-N bonds. This could explain why the isomer shift is calculated so high; the chelate and NO are less covalent and therefore the iron has a greater effective charge, increasing the isomer shift. The qualitative MO diagram from the calculations is presented in Figure 1.30.

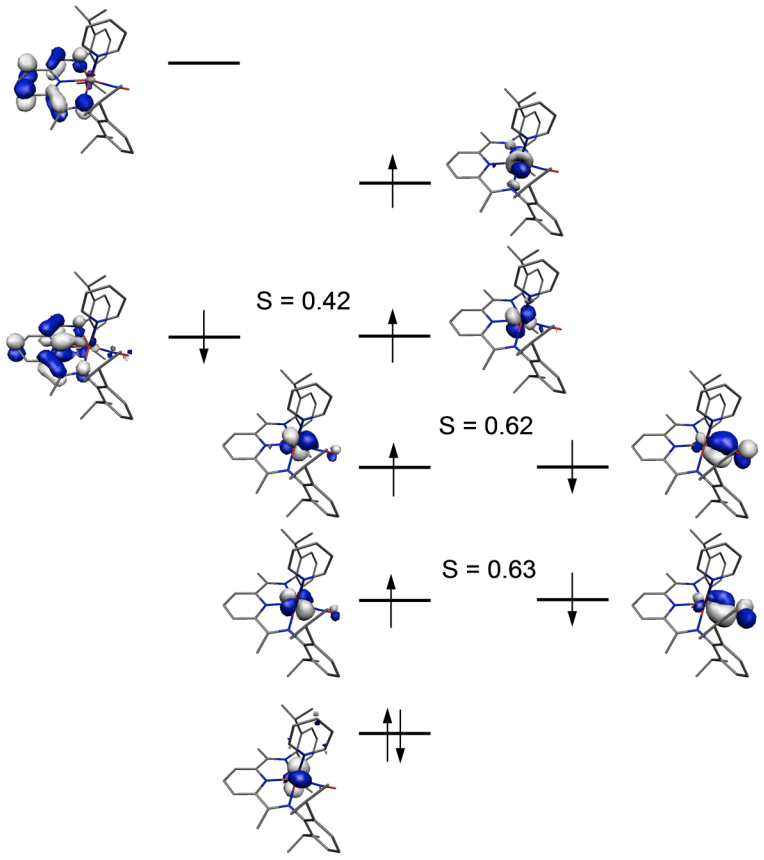

Figure 1.30 Molecular orbital picture arising from DFT calculations on **(^{iPr}PDI)Fe(NO)(Py)**.

The calculated MO diagram supports the experimental data. The addition of the fifth ligand raises the z^2 orbital in energy and drops the x^2-y^2 orbital energy sufficiently that it is accessible. One thing to notice as well is that the spatial overlap between the iron and the nitrosyl ligand has dropped significantly. This indicates a lower degree of covalency overall in the molecule and comes about, most likely, due to the increase in the Fe-NO bond length. This is also the case in the overlap with the PDI ligand, again, most likely arising from the increased bond length due to the molecule being in a high-spin manifold.

1.7 Preparation and Electronic structure of [(^{iPr}PDI)Fe(NO)(L)][BArF$_{24}$]

Additional variations of [(^{iPr}PDI)Fe(NO)][BArF$_{24}$] can be achieved by performing the oxidation of (^{iPr}PDI)Fe(NO) in coordinating solvents, or by adding coordinating solvents to [(^{iPr}PDI)Fe(NO)][BArF$_{24}$]**.** The oxidation of (^{iPr}PDI)Fe(NO) in THF with [Cp_2Fe][BArF$_{24}$] results in a color change to blue from red, and the product was isolated by the addition of pentane and cooling to -35 ºC overnight to yield [(^{iPr}PDI)Fe(NO)(THF)][BArF$_{24}$]. The teal colored powder is diamagnetic and exhibits an NMR spectrum consistent with a *C*s symmetric compound. The IR stretch at 1656 cm^{-1} is consistently blue shifted from (^{iPr}PDI)Fe(NO)(Py), the other five-coordinate nitrosyl complex.

The zero-field Mössbauer spectrum of [(^{iPr}PDI)Fe(NO)(THF)][BArF$_{24}$] at 80 K yields a quadrupole doublet with an isomer shift of 0.32 mm/s and a narrow quadrupole splitting of 0.51 mm/s. These parameters in and of themselves do not lend to an easily assigned electronic structure picture. However, the lowering of the isomer shift from 0.56 mm/s in the high-spin ferrous five coordinate compound to 0.32 mm/s in the five coordinate cation shows, at minimum, a spin state change from the neutral five-coordinate complex

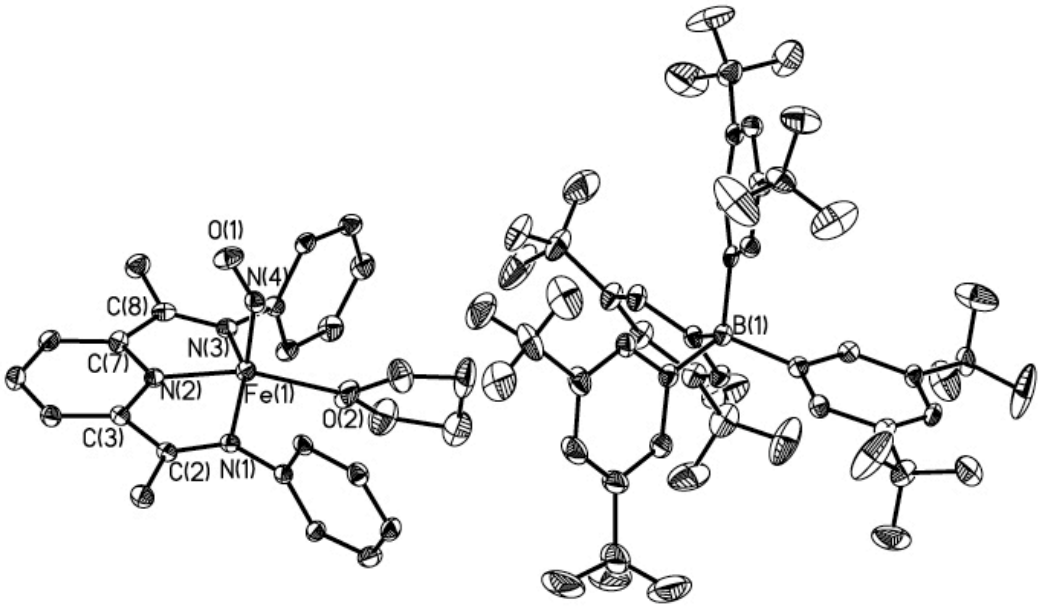

Figure 1.31 A representation of **[(^{iPr}PDI)Fe(NO)(THF)][BArF$_{24}$]** in the solid state presented at 30% probability ellipsoids. Disordered -CF3 groups, isopropyl substituents, and hydrogens were removed for clarity.

Crystals suitable for X-ray diffraction were obtained from a concentrated solution of [(^{iPr}PDI)Fe(NO)(THF)][BArF$_{24}$] in diethyl ether cooled to -35 ºC. The solid-state structure is presented in Figure 1.31. The nitrosyl ligand of [(^{iPr}PDI)Fe(NO)(THF)][BArF$_{24}$] is found in the apical position of a distorted square pyramid, with a THF molecule in the basal plane of the chelate. The borate is non-binding, and an ether molecule is present in the crystal lattice. Bis(imino)pyridine metrical parameters of [(^{iPr}PDI)Fe(NO)(THF)][BArF$_{24}$] are presented along with (^{iPr}PDI)Fe(NO)(Py) in Table 1.5. for comparison.

Table 1.5 Acomparison of the experimentally determined structural parameters of **(^{iPr}PDI)Fe(NO)(Py)** and the cation **[(^{iPr}PDI)Fe(NO)(THF)][BArF$_{24}$]**.

	(^{iPr}PDI)Fe(NO)(Py)	**[(^{iPr}PDI)Fe(NO)(THF)][BArF$_{24}$]**
Fe(1)-N(1)	2.176(2)	1.998(3)
Fe(1)-N(2)	1.972(2)	1.828(3)
Fe(1)-N(3)	2.131(2)	2.005(3)
Fe(1)-N(4)	1.683(2)	1.692(3)
Fe(1)-N(5)	2.056(2)	
Fe(1)-O(2)		2.076(3)
N(1)-C(2)	1.303(3)	1.312(4)
N(3)-C(8)	1.310(3)	1.303(4)
N(2)-C(3)	1.375(3)	1.369(4)
N(2)-C(7)	1.374(3)	1.372(4)
N(4)-O(1)	1.159(3)	1.176(4)
C(2)-C(3)	1.444(3)	1.438(5)
C(7)-C(8)	1.445(3)	1.447(5)
N(1)-Fe(1)-N(2)	75.09(8)	79.13(12)
N(1)-Fe(1)-N(4)	101.90(9)	102.12(13)
N(2)-Fe(1)-N(3)	75.47(8)	79.37(13)
N(3)-Fe(1)-N(4)	102.72(9)	100.70(13)
N(2)-Fe(1)-N(4)	154.76(10)	100.56(13)
N(2)-Fe(1)-N(5)	105.59(8)	
N(2)-Fe(1)-O(2)		160.61(12)
Fe(1)-N(4)-O(1)	162.5(2)	147.4(3)

Drawing a comparison of [(^{iPr}PDI)Fe(NO)(THF)][BArF$_{24}$] to the five-coordinate neutral complex, (^{iPr}PDI)Fe(NO)(Py), allows for the comparison of the difference of 1 electron in the 5-coordinate species. The bis(imino)pyridine reduction metrics for each compound is very similar, indicating 1 electron in each case. The cation is also not a high-spin complex, as seen from magnetic measurements, and corroborated by the relatively (to the neutral) short iron-imine bond distances, with Fe(1)-N(1) and Fe(1)-N(3) at 1.998(3) Å and 2.006(3) Å, respectively, much shorter

than the two distances of the neutral complex at 2.1763(19) Å and 2.131(2) Å. With the nitrosyl acting as a pseudo-halide, the PDI being mono-reduced, and an overall cationic charge on the iron fragment, the iron is Fe(III). The metrical parameters of the chelate indicate an intermediate or low-spin iron complex.

Two other variations of [(^{iPr}PDI)Fe(NO)(L)][$BArF_{24}$]were synthesized in order to gain further understanding into influence of the coordinated ligand. The water adduct, as well as the pyridine derivative were synthesized. The water compound was synthesized by performing the oxidation of (^{iPr}PDI)Fe(NO) in toluene that contained degassed H_2O to yield [(^{iPr}PDI)Fe(NO)(H_2O)][$BArF_{24}$]. [(^{iPr}PDI)Fe(NO)(Py)][$BArF_{24}$] was synthesized upon the oxidation of (^{iPr}PDI)Fe(NO)(Py) with [Cp_2Fe][$BArF_{24}$].

Zero-field Mössbauer parameters were obtained for each complex. The spectra were highly reminiscent of the THF adduct, with isomer shifts of ~ 0.3 mm/s and a small quadrupole splitting. Table 1.6 summarizes the Mössbauer parameters and IR stretching frequencies of this series of compounds.

Table 1.6. Mössbauer parameters and IR data are presented for the three derivatives of **(^{iPr}PDI)Fe(NO)(L)$^+$**.

'L'	δ mm/s	ΔE_Q mm/s	ν(NO) cm^{-1} (KBr)
THF	0.32	0.51	1656
H_2O	0.28	0.32	1656
Pyridine	0.26	0.36	1658

The final compound to be computed in the ^{iPr}PDI series of compounds is the five coordinate [(^{iPr}PDI)Fe(NO)(THF)][$BArF_{24}$]. This compound is of interest in that the nitrosyl is bound bent and in the apical position. The degree of any π bonding between the nitrosyl and iron center is unknown. The PDI is mono reduced, and to

maintain the overall diamagnetism of the molecule, there needs to be at least one cloverleaf of the iron only half-filled. This can be achieved in either a low-spin or intermediate-spin manifold. This being a diamagnetic compound, the loss of spectroscopy impedes the electronic structure assignment. XAS was performed on [(^{iPr}PDI)Fe(NO)(THF)][$BArF_{24}$], and the pre-edge region is presented in Figure 1.32.

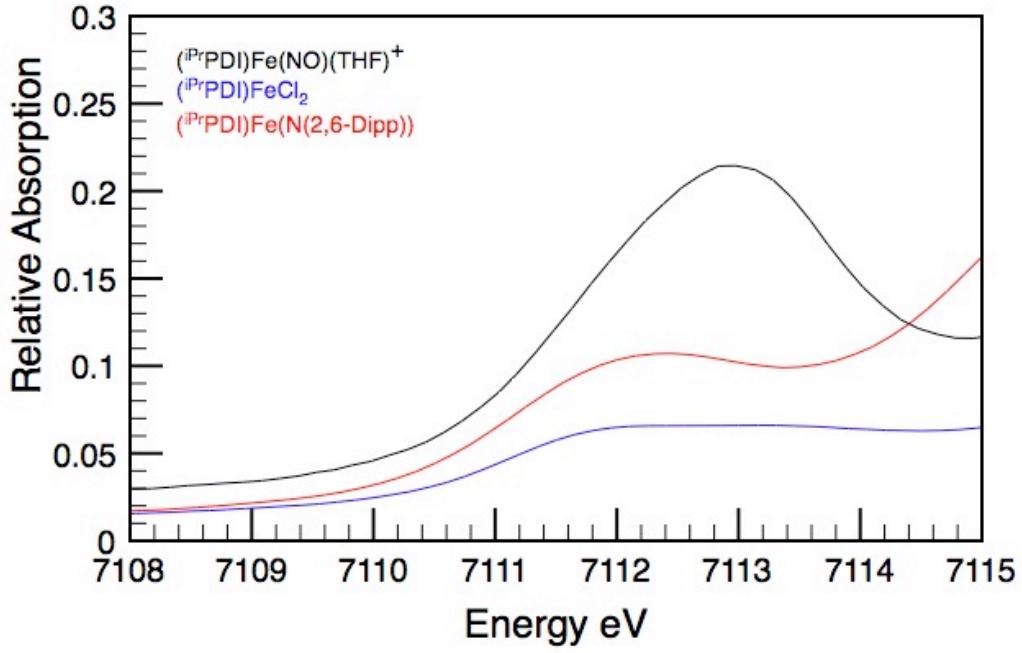

Figure 1.32 XAS pre-edge region of **[(^{iPr}PDI)Fe(NO)(THF)][$BArF_{24}$].**

The pre-edge indicates that [(^{iPr}PDI)Fe(NO)(THF)][$BArF_{24}$] is more oxidized than the reference compounds. Compared to (^{iPr}PDI)$FeCl_2$, the pre-edge feature is approximately 1 eV higher in energy, indicating that the iron is one-electron more oxidized. This is a valid direct comparison because both complexes have the same coordination number and roughly the same geometry. The rising edge is presented in Figure 1.33.

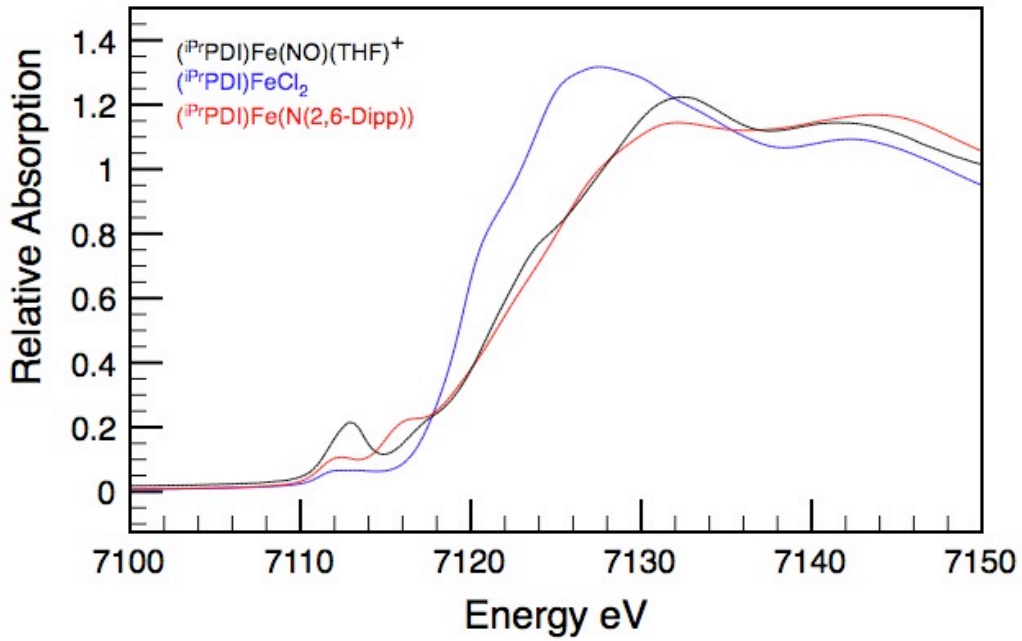

Figure 1.33 XAS data for **[(^{iPr}PDI)Fe(NO)(THF)][$BArF_{24}$].**

The rising edge supports the pre-edge in that [(^{iPr}PDI)Fe(NO)(THF)][$BArF_{24}$] in that the s-to-p transition occurs at a higher energy than (^{iPr}PDI)$FeCl_2$, and at roughly the same energy as the Fe(III) complex(^{iPr}PDI)FeN(Dipp). This data provides further evidence that [(^{iPr}PDI)Fe(NO)(THF)][$BArF_{24}$] contains an Fe(III) nucleus.

DFT calculations using the B3LYP functional were performed on [(^{iPr}PDI)Fe(NO)(THF)][$BArF_{24}$]. The compound was calculated as a spin-unrestricted singlet based on the experimentally determined $S = 0$ ground state. The computed electronic structure corresponds to a broken symmetry (3,3) solution, obtained via spontaneous symmetry breaking during the unrestricted calculation. The calculated structural parameters of [(^{iPr}PDI)Fe(NO)(THF)][$BArF_{24}$] are presented in Table 1.7. The computed ^{57}Fe Mössbauer parameters of $\delta = 0.40$ mm s^{-1} and $\Delta E_Q = 0.42$ mm s^{-1}, are in good agreement with the experimentally determined values ($\delta = 0.32$ mm/s;

ΔE_Q = |0.51 mm/s|). The bond distances of the calculations are only slightly overestimated, but may still account for the high isomer shift in the calculations. The qualitative MO diagram from the calculations is presented in Figure 1.34.

Table 1.7 The experimentally determined and calculated structural parameters of the cation **[(^{iPr}PDI)Fe(NO)(THF)][$BArF_{24}$]**.

	Calc.	**[(^{iPr}PDI)Fe(NO)(THF)][$BArF_{24}$]**		**Calc.**	**[(^{iPr}PDI)Fe(NO)(THF)][$BArF_{24}$]**
Fe(1)-N(1)	2.056	1.998(3)	C(2)-C(3)	1.456	1.438(5)
Fe(1)-N(2)	1.842	1.828(3)	C(7)-C(8)	1.455	1.447(5)
Fe(1)-N(3)	2.064	2.005(3)			
Fe(1)-N(4)	1.764	1.692(3)	N(1)-Fe(1)-N(2)	79.54	79.13(12)
			N(1)-Fe(1)-N(4)	99.57	102.12(13)
Fe(1)-O(2)	2.118	2.076(3)	N(2)-Fe(1)-N(3)	79.31	79.37(13)
			N(3)-Fe(1)-N(4)	96.24	100.70(13)
N(1)-C(2)	1.310	1.312(4)	N(2)-Fe(1)-N(4)	98.00	100.56(13)
N(3)-C(8)	1.311	1.303(4)	N(2)-Fe(1)-O(2)	166.06	160.61(12)
N(2)-C(3)	1.365	1.369(4)			
N(2)-C(7)	1.364	1.372(4)	Fe(1)-N(4)-O(1)	140.50	147.4(3)
N(4)-O(1)	1.177	1.176(4)			

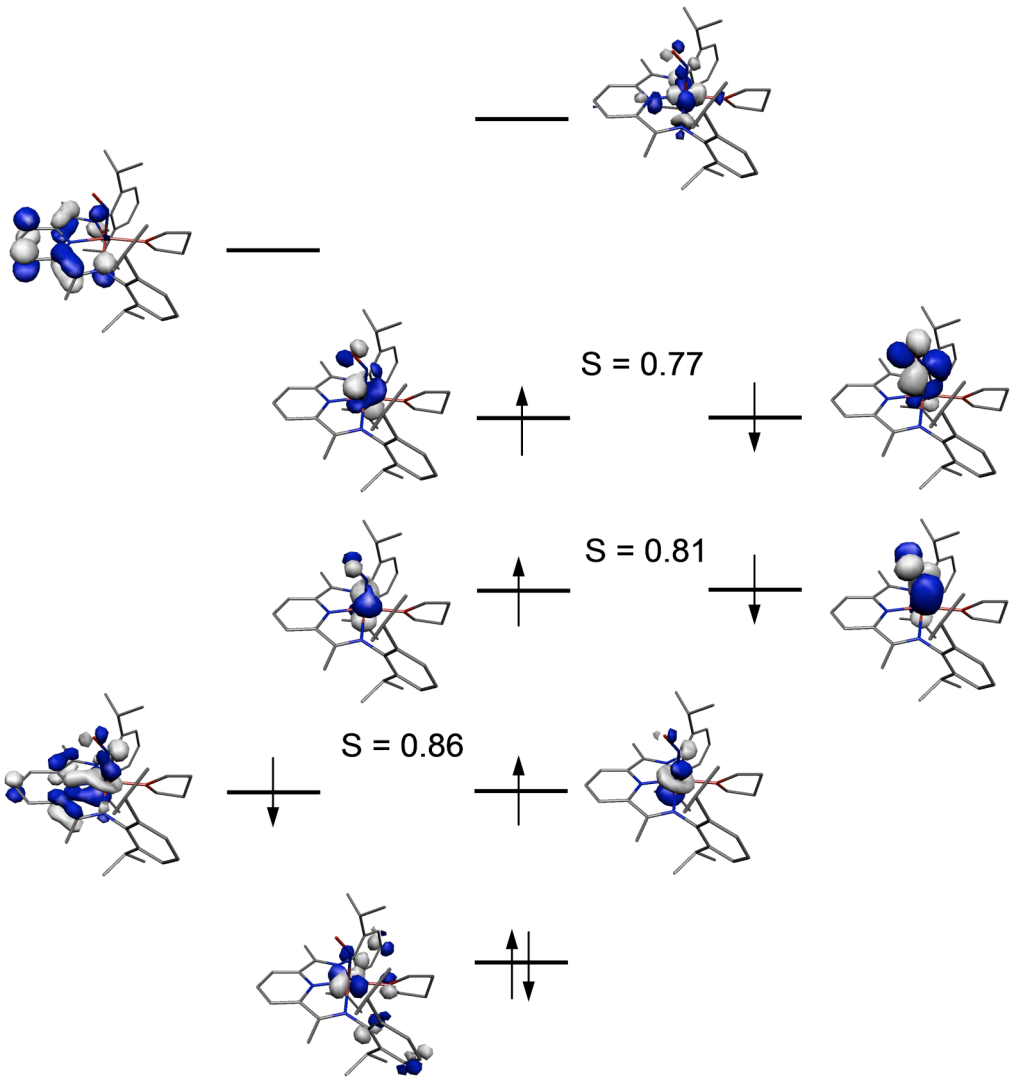

Figure 1.34 Qualitative molecular orbital diagram of **[(^{iPr}PDI)Fe(NO)(THF)][BArF$_{24}$]** that arises from DFT calculations.

The calculations confirm the iron remains an intermediate Fe(III) center. The surprising result is that the nitrosyl ligand, although bent, still looks as if it forming two π bonds with the iron. The z^2 orbital appears to have canted in order to take on a π-type symmetry with respect to either the PDI or NO. The spatial overlap of the iron and nitrosyl is still high although the iron nitrosyl bond distance in this case is the

longest out of any of this series of compounds. Although this compound has a different coordination number and geometry, the electronic structure appears to be the same as the four-coordinate cation, an intermediate ferric iron antiferromagnetically coupled to a PDI based radical as well as to two NO anion based radicals.

The series of calculations yielded good support for the interpretation of the various spectroscopies used in the electronic structure determination of the ^{iPr}PDI series of complexes. The electronic structures of five various ^{iPr}PDI based compounds were presented along with the supporting spectroscopic and calculational evidence.

1.8 Preparation and Electronic structure of (^{iPr}PDI)Fe(NO)$_2$

The addition of one equivalent of nitric oxide to (^{iPr}PDI)Fe(NO) or two equivalents to (^{iPr}PDI)Fe(N$_2$)$_2$, in toluene, led to the formation of the dinitrosyl iron compound, (^{iPr}PDI)Fe(NO)$_2$. Seen in small quantities in the formation of the mono-nitrosyl, this compound was synthesized in part to garner a better understanding of PDI iron nitrosyl chemistry in the context of a multitude of other DNICs recently reported. [40,41] The isolation of the compound, by washing with copious amounts of diethyl ether then drying under reduced pressure, led to a brick red powder identified as (^{iPr}PDI)Fe(NO)$_2$ in greater than 90% yield.

The benzene-d_6 ^{1}H NMR spectrum of (^{iPr}PDI)Fe(NO)$_2$ was consistent with a diamagnetic, C_s or C_2 symmetric molecule, as seen in Figure 1.35. The IR spectrum consisted of two bands, 1709 cm^{-1} and 1682 cm^{-1}, in KBr. X-ray quality crystals were grown from a dichloromethane solution of (^{iPr}PDI)Fe(NO)$_2$ layered with diethyl ether and the solutions were allowed to diffuse gradually at -35 ºC.

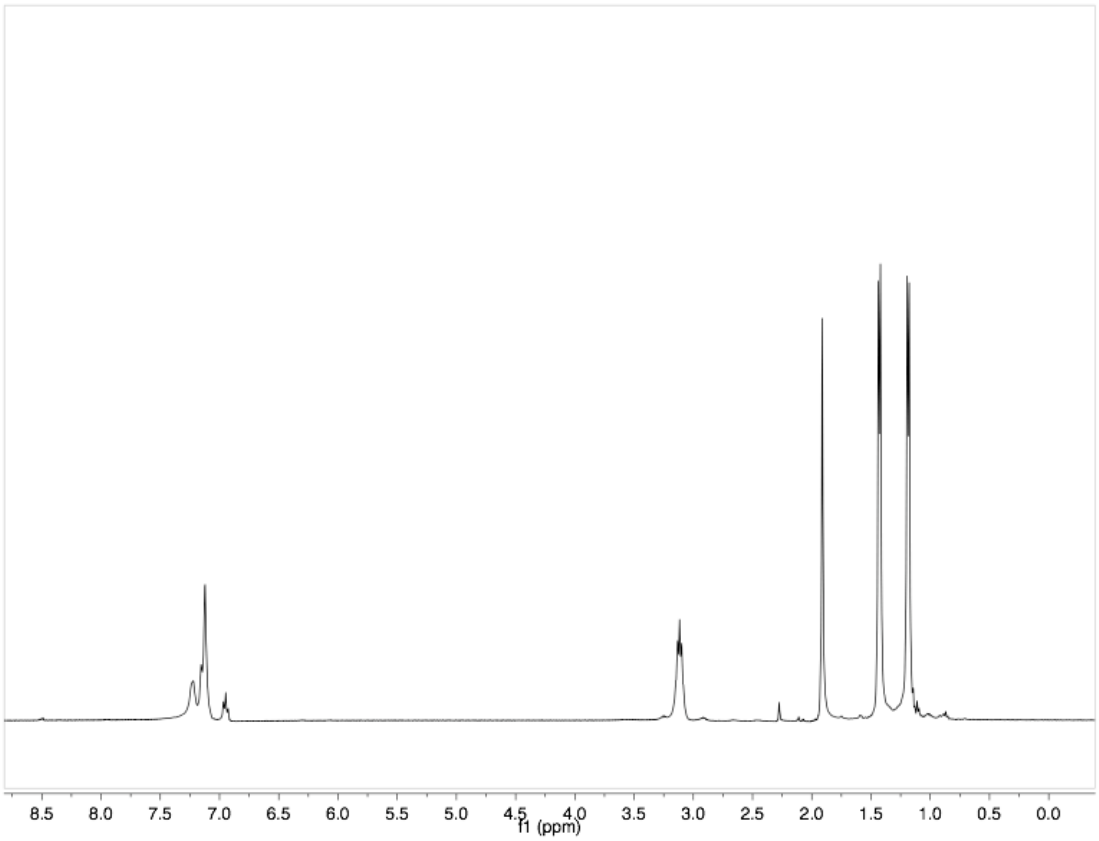

Figure 1.35 ^{1}H NMR spectrum of **(^{iPr}PDI)Fe(NO)$_2$** in benzene-d_6 at 23 ºC indicating the high symmetry of the molecule in solution.

The solid-state structure of (^{iPr}PDI)Fe(NO)$_2$, presented in Figure 1.36, is of a C_1 symmetric, κ-2 PDI tetrahedral iron center. One of the nitrosyl units is disordered, and both remain linear at nitrogen, with bond angles Fe(1)-N(4)-O(1) and Fe(1)-N(5)-O(2) at 171.4(5)º and 170.1(2)º . The solid-state structure is inconsistent with the NMR data, and may be indicative of rapid fluxionality of the imine dissociation/association in solution. Zero field Mössbauer parameters of the solid powder yield a quadrupole doublet centered at 0.26 mm/s with a quadrupole splitting of 0.59 mm/s.

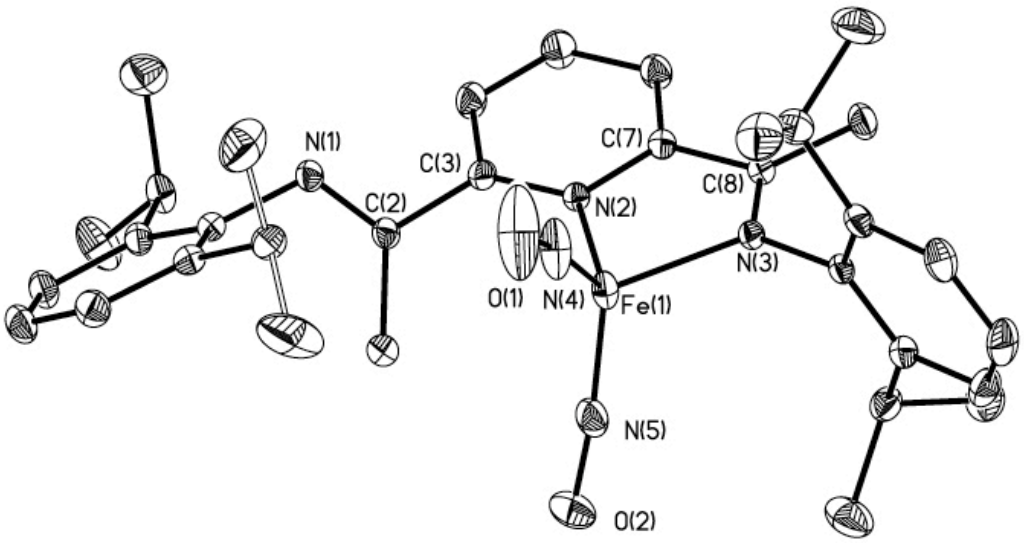

Figure 1.36 A representation of **(^{iPr}PDI)Fe(NO)$_2$** in the solid state presented at 30% probability ellipsoids. A disordered NO group and hydrogen atoms were removed for clarity.

The pyridine imine bidentate ligand is non-reduced according to the metrics of pyridine imine ligands. The C-N bond length of 1.283(2) Å is short, and the C-C bond of 1.474(2) Å is long, both consistent with a non-reduced chelate. The compound is clearly κ-2, with one imine arm fully rotated away from the iron center. The iron nitrosyl distances, Fe(1)-N(4) and Fe(1)-N(5), at 1.637(2) Å and 1.645(3) Å, respectively, are nearly as short as the bond in (^{iPr}PDI)Fe(NO), indicating a strong interaction between the nitrosyl ligands and the iron center.

This data, along with the IR stretching frequencies, show that (^{iPr}PDI)Fe(NO)$_2$ is analogous to the (Fe(NO)$_2$)[10] compound reported by Lippard and calculated by Neese to be a high-spin ferrous center. To help confirm this assignment, XAS was

performed on (^{iPr}PDI)Fe(NO)$_2$, and a blow up of the s-to-d transition region is presented in Figure 1.37, along with the reference compounds (^{iPr}PDI)FeCl$_2$ and (^{iPr}PDI)FeN(2,6-diisopropylphenyl) (labeled as (^{iPr}PDI)FeN(Dipp) in the spectrum).

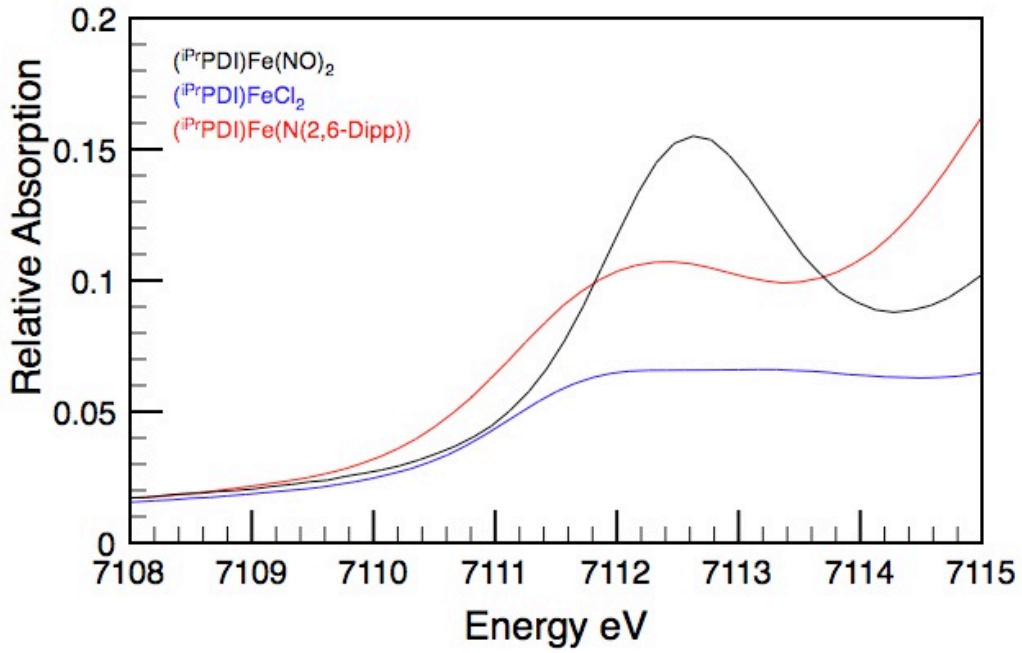

Figure 1.37 The pre-edge region of the XAS data of **(^{iPr}PDI)Fe(NO)$_2$**.

The data indicates that (^{iPr}PDI)Fe(NO)$_2$ is the most oxidized species out of the three presented. The intensity of the peak for (^{iPr}PDI)Fe(NO)$_2$ is large due to the tetrahedral geometry allowing p-d mixing, making for a more allowed s-to-d transition. The geometry difference may cause subtle variations in this region of the spectrum, so the rising edge was analyzed for consistency, and it is presented in Figure 1.38.

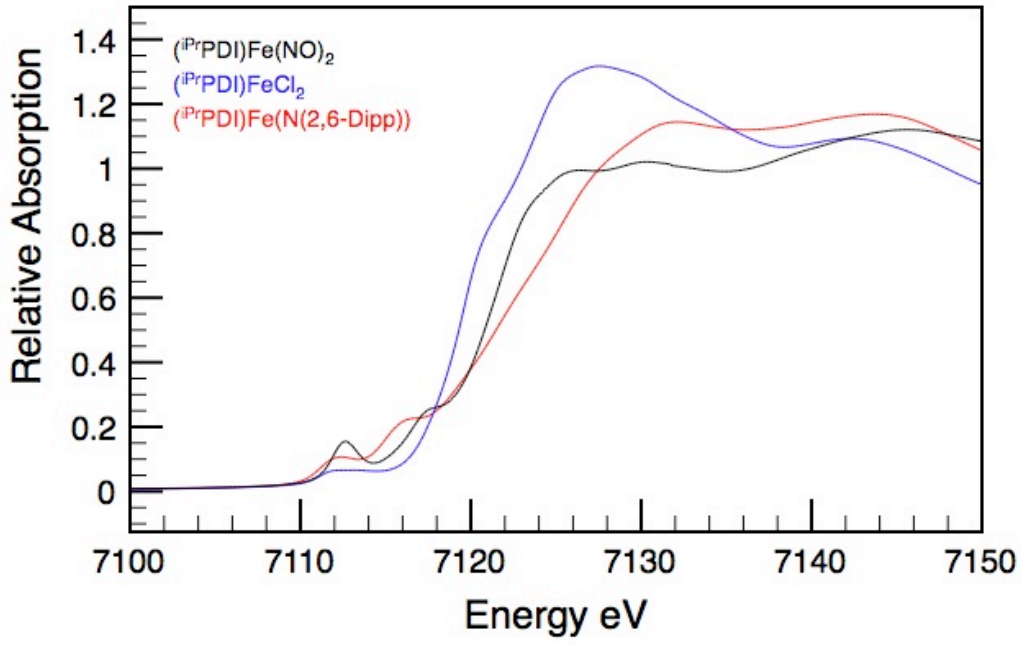

Figure 1.38 The rising edge is the of the XAS for **(^{iPr}PDI)Fe(NO)$_2$**.

Along the rising edge, (^{iPr}PDI)Fe(NO)$_2$ appears somewhere in between the reference compounds (^{iPr}PDI)FeCl$_2$ and (^{iPr}PDI)FeN(2,6-Dipp). The assignment of the iron nucleus in (^{iPr}PDI)Fe(NO)$_2$ as Fe(II) is reasonable, although by XAS the iron is more oxidized than the iron in (^{iPr}PDI)FeCl$_2$.

1.9 Preparation and Electronic structure of (^{Et}PDI)Fe(NO) and other derivatives

The bridging dinitrogen compounds [(^{Et}PDI)FeN$_2$]$_2$(μ-N$_2$)[42] and [(^{Me}PDI)FeN$_2$]$_2$(μ-N$_2$)[42] were subjected to the same reaction conditions using two equivalents of nitric oxide added per dimer, and the reactions yielded (^{Et}PDI)Fe(NO) and (^{Me}PDI)Fe(NO), respectively. Again, the nitrosyl compounds (^{Et}PDI)Fe(NO) and (^{Me}PDI)Fe(NO) were $S = 1/2$ (both had a $\mu_{eff} = 1.8\ \mu_B$ as solids at 290 K) in the ground

state, but the IR stretching frequencies were much more reduced than (^{iPr}PDI)Fe(NO). In KBr, (^{Et}PDI)Fe(NO) exhibited a stretch at 1685 cm^{-1} and (^{Me}PDI)Fe(NO) exhibited a stretch at 1663 cm^{-1}. In toluene, the stretching frequencies split into two, one at 1724 cm^{-1} and the other at 1685 cm^{-1} for the ethyl PDI and 1724 cm^{-1} and the other at 1685 cm^{-1} for the methyl PDI complex.

The benzene-d_6 ^{1}H NMR spectra of (^{iPr}PDI)Fe(NO), (^{Et}PDI)Fe(NO), (^{Me}PDIFe)(NO) at 20 °C establish that these compounds exhibit either C_2 or C_s symmetry in solution, as presented in Figure 1.39. As the steric demand decreases, the back-bone methyl groups move in from 274 ppm in (^{iPr}PDI)Fe(NO)to 134 ppm in (^{Me}PDIFe)(NO), and the resonances become sharper. The *p*-pyridine resonance also shifts in from -158 to -58 ppm.

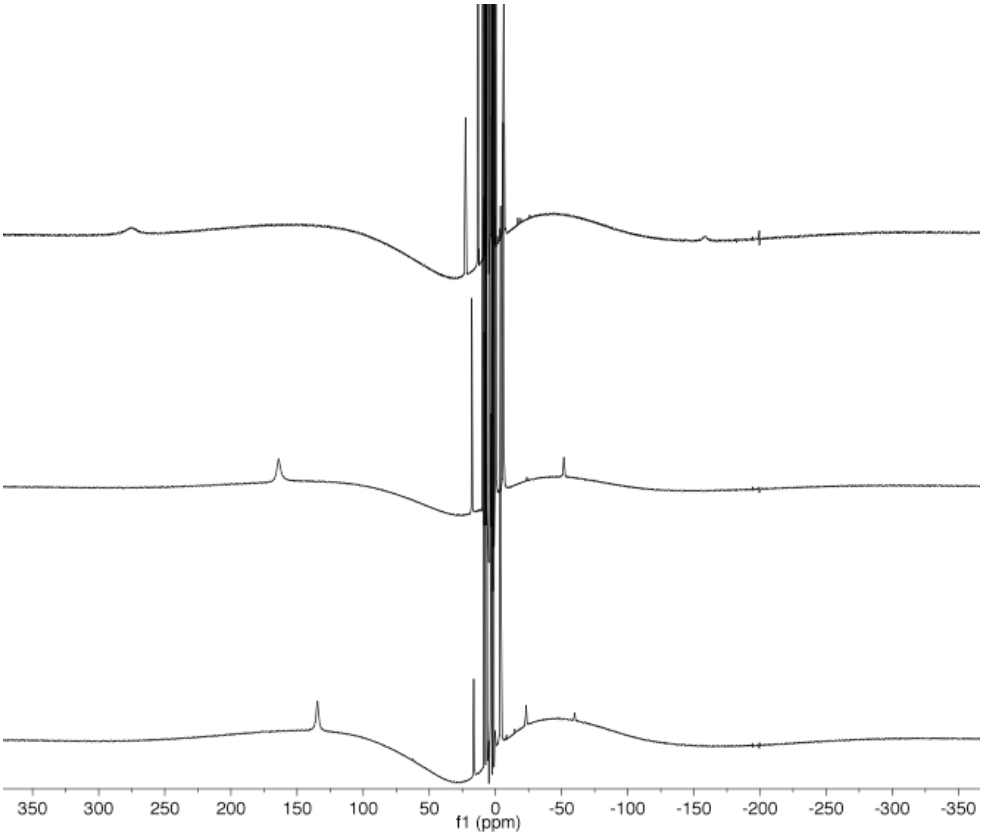

Figure 1.39 Comparative 1H NMR spectra of : Top = **(^{iPr}PDI)Fe(NO)**, Middle = **(^{Et}PDI)Fe(NO)**, and Bottom = **(^{Me}PDIFe)(NO).**

A crystal structure was obtained of (^{Et}PDI)Fe(NO) and it is presented in Figure 1.40. The solid state structure of (^{Et}PDI)Fe(NO) confirms a molecular geometry for this compound that is distinct from the isopropyl-substituted derivative. Unfortunately, the crystal structure has two inequivalent PDI iron compounds in the unit cell. While a linear nitrosyl is maintained with an Fe(1)-N(4)-O(1) of 176.4(4)º and Fe'(1)-N'(4)-O'(1) of 178.5(4)º, the NO ligand is lifted out of the idealized square plane and the N(2)-Fe(1)-N(4) angle is contracted to 140.80(16)º and the second molecule has an N'(2)-Fe'(1)-N'(4) angle of 144.99(17)º. The deviation does not result in a significant perturbation of the Fe(1)-N(4) and Fe'(1)-N'(4)bond lengths as the value of 1.650(4) Å and 1.643(3) Å are only slightly elongated from the distance of 1.6309(15)) Å in (^{iPr}PDI)Fe(NO). The ligand reduction metrical parameters of this compound are slightly more ambiguous than the isopropyl case, being nearer to the singly reduced/double reduced cutoff, but still best described as an $\{Fe(NO)\}^7$molecule. There is also concern regarding the nitrosyl; if the ligand is really canted out of the plane or if there is enough thermal motion to cause two species in the unit cell.

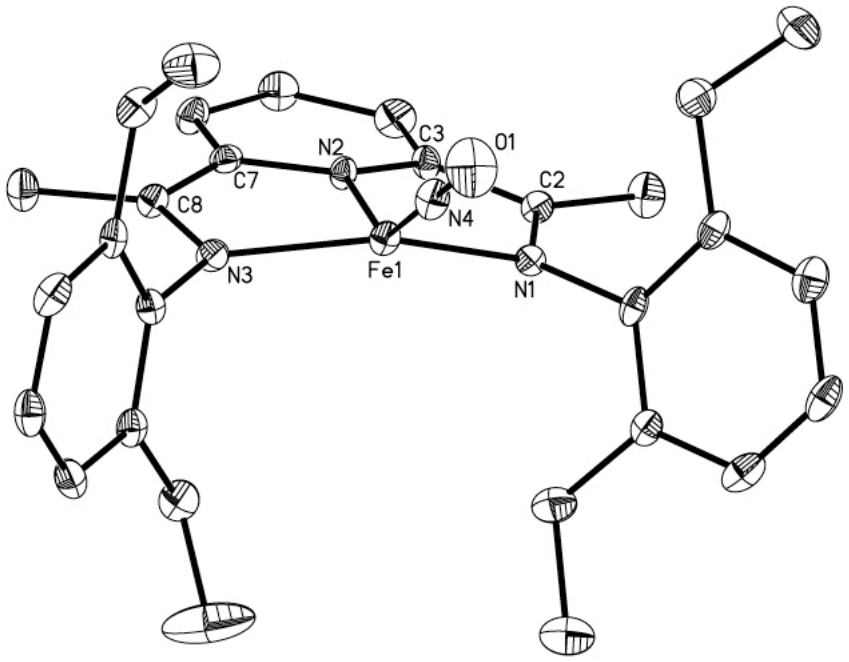

Figure 1.40 Molecular structure of one of two structures of **(^{Et}PDI)Fe(NO)** at 30% probability ellipsoids. Hydrogen atoms omitted for clarity.

Zero field Mössbauer parameters of (^{Et}PDI)Fe(NO) were determined at 80K, and the spectrum displayed a clean quadrupole doublet with an isomer shift of 0.33 mm/s and the quadrupole splitting of 0.86 mm/s. The rise in the isomer shift is most likely due to the weakening of one of the two π-bonds to the nitrosyl ligand, as the PDI metrics are similar to (^{iPr}PDI)Fe(NO). Again, though, the electronic structure determination is not going to be trivial, and there is the added complication of fluxionality in the in the complex. A comparison of the Mössbauer spectra of (^{Et}PDI)Fe(NO) and (^{iPr}PDI)Fe(NO) is presented in Figure 1.41.

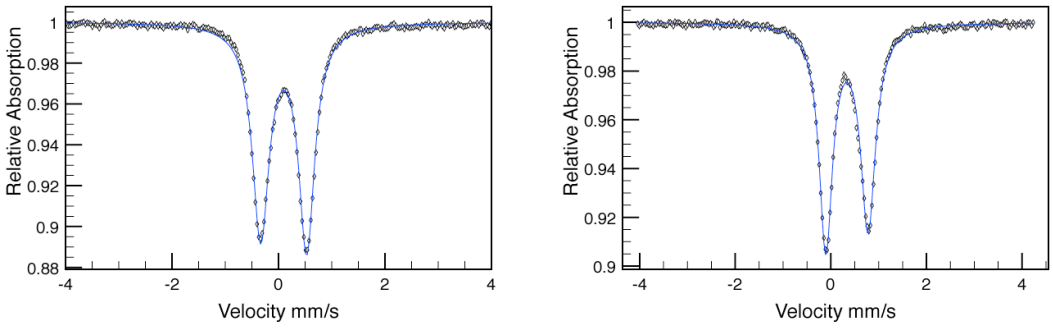

Figure 1.41 **(^{iPr}PDI)Fe(NO)** (left) and **(^{Et}PDI)Fe(NO)** (right) Mössbauer spectra taken at 80 K.

To counter any concerns regarding (^{Et}PDI)Fe(NO), a substitution at the para position of the pyridine ring of PDI was performed, replacing the *p*-hydrogen with a *tert*-butyl group. This will change the way the compound crystallizes, but won't interfere with the sterics around the iron-nitrosyl fragment. The addition of nitric oxide to the bridging dinitrogen compound resulted in the formation of the desired four coordinate (^{Et}(p-^{t}Bu)PDI)Fe(NO).

The solid-state structure of (^{Et}(p-^{t}Bu)PDI)Fe(NO), presented in Figure 1.42, retains the 'canted' geometry of the parent ethyl compound, with a slightly more contracted N(2)-Fe(1)-N(4) angle of 135.42(7)º. The nitrosyl, although slightly more bent, remains linear, with an Fe(1)-N(4)-O(1) angle of 173.02(15). In KBr, (^{Et}(*p*-^{t}Butyl)PDI)Fe(NO) exhibits a stretch at 1685 cm^{-1}, but in toluene, the stretching frequencies split into two, one at 1724 cm^{-1} and the other at 1685 cm^{-1} maintaining the odd vibrational spectrum exhibited by (^{Et}PDI)Fe(NO).

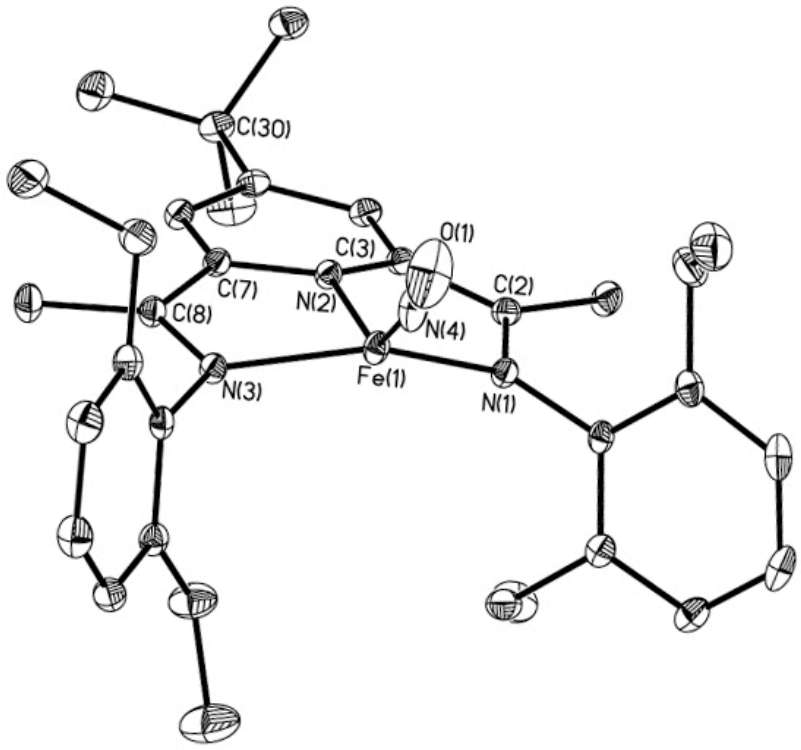

Figure 1.42 Molecular structure of **(^{Et}(p-^{t}Bu)PDI)Fe(NO)** at 30% probability ellipsoids. Hydrogen atoms omitted for clarity.

The contracting of the N(2)-Fe(1)-N(4) angle supports the structure of (^{Et}PDI)Fe(NO) as being correct and not arising from crystal effects. The cant out of the plane of the nitrosyl is a real effect and the electronic effects this has on the iron center will be discussed in the electronic structure section. Geometric effects ligand substitutions, as well as metrical parameters of the PDI, are presented in Table 1.8.

Table 1.8 Selected bond distances and angles from the 4-coordinate **(^{iPr}PDI)Fe(NO), (^{Et}PDI)Fe(NO)** (both molecules in the unit cell)**,** and **(^{Et}(p-^{t}Bu)PDI)Fe(NO).**

	(^{Et}PDI)Fe (NO) (Molecule 1)	(^{Et}PDI)Fe (NO) (Molecule 2)	(^{Et}(p-^{t}Bu)PDI)Fe (NO)	(^{iPr}PDI)Fe (NO)
Fe(1)-N(1)	1.968(3)	1.975(3)	1.9975(14)	1.9107(13)
Fe(1)-N(2)	1.866(3)	1.876(3)	1.8907(13)	1.8640(12)
Fe(1)-N(3)	1.971(3)	1.989(3)	1.9798(13)	1.9096(12)
Fe(1)-N(4)	1.650(4)	1.643(3)	1.6502(15)	1.6309(15)
N(1)-C(2)	1.315(5)	1.338(5)	1.325(2)	1.3308(19)
N(3)-C(8)	1.330(5)	1.325(5)	1.3229(19)	1.3375(19)
N(2)-C(3)	1.375(5)	1.371(5)	1.370(2)	1.3794(19)
N(2)-C(7)	1.381(5)	1.384(5)	1.369(2)	1.3759(19)
N(4)-O(1)	1.188(4)	1.194(5)	1.187(2)	1.185(2)
C(2)-C(3)	1.431(5)	1.422(6)	1.434(2)	1.427(2)
C(7)-C(8)	1.424(6)	1.433(5)	1.426(2)	1.426(3)
N(1)-Fe(1)-N(2)	78.52(13)	78.83(14)	77.93(5)	79.51(5)
N(1)-Fe(1)-N(4)	103.70(15)	104.27(16)	113.72(7)	100.69(6)
N(2)-Fe(1)-N(3)	78.86(14)	78.62(14)	78.51(5)	79.77(5)
N(3)-Fe(1)-N(4)	109.30(15)	105.61(15)	104.70(7)	99.85(6)
N(2)-Fe(1)-N(4)	140.80(16)	144.99(17)	135.42(7)	174.02(7)
Fe(1)-N(4)-O(1)	176.4(4)	178.5(4)	173.02(15)	178.37(17)

The PDI chelate in all three cases appears to be doubly reduced, as the imine bonds elongate from the non-reduced ligand, and the C-C bonds contract accordingly. Canting the nitrosyl out of the plane of the chelate results in a lengthening of the Fe(1)-N(4) bond from 1.6309(15) in (^{iPr}PDI)Fe(NO) to 1.650(4) and 1.643(3) in (^{Et}PDI)Fe(NO) and 1.6502(15) in (^{Et}(p-^{t}Bu)PDI)Fe(NO)**,** most likely as a result of the weakening of the in-plane π bond. Whatever subtle differences there are in the

geometry of the compounds, the molecules all retain an $S = 1/2$ ground state, with a $[PDI]^{2-}$ supporting ligand, yielding an $\{Fe(NO)\}^7$ complex.

The synthesis of the p-tert-butyl bis(imino)pyridine iron nitrosyl compounds (^{iPr}(p-tBu)PDI)Fe(NO) and the (^{Me}(p-tBu)PDIFe)(NO) was achieved in order to complete the two series of compounds so that comparisons can be drawn. The IR stretching frequencies and Mössbauer parameters of these six compounds are presented in Table 1.9.

Table 1.9 Mössbauer parameters of the two sesries of nitrosyl complexes.

Compound	**δ**	**ΔE_Q**	**IR (KBr) cm^{-1}**	**IR (Toluene) cm^{-1}**
(^{iPr}PDI)Fe(NO)	0.1	0.86	1724	1724
(^{Et}PDI)Fe(NO)	0.33	0.86	1686	1686, 1724
(^{Me}PDIFe)(NO)	0.40	1.23	1663	1668, 1724
(^{iPr}(p-tBu)PDI)Fe(NO)	0.1	0.86	1724	1729
(^{Et}(p-tBu)PDI)Fe(NO)	0.28	0.80	1690	1686, 1724
(^{Me}(p-tBu)PDIFe)(NO)	0.33	0.82	1668	1668, 1724

The isomer shifts of the isopropyl substituted ligands have isomer shifts that are routinely lower than the isomer shifts of the smaller aryl groups, about 0.1 mm/s versus 0.3 mm/s. The *para*-pyridine substitution to the *tert*-butyl group does not change the electronics of any of the compounds appreciably. The IR stretching frequencies of the nitrosyl groups of the smaller groups indicate, roundly, that there is more electron density in the π* system of the nitrosyl group.

Another para-substituted nitrosyl complex was synthesized via oxidative addition of the pyridine C-H bond by a Ta(III) reagent. Cummins has shown that the deoxygenation of the nitrosyl ligand by a metal center was a viable route to form a terminal metal nitride.[43] In an attempt to generate an iron nitride, the potent deoxygenating agent $(Silox)_3Ta$ was used (Silox = $-OSi(tBu)_3$).[44] The result of this reaction was an iron center that retained the nitrosyl (via IR) and developed a peak in

the IR that is consistent with a tantalum hydride at 1852 cm^{-1}.[31] The crystal structure showed the C-H activation at the p-pyridine position, much akin to the seminal work of C-H activation on 2,6-Lutidine using the same tantalum reagent.[45] The product retained the same geometry and electronic structure as (^{iPr}PDI)Fe(NO), but with a Ta^{V} substituent in the para-position of the pyridine. The molecular structure is presented in Figure 1.43.

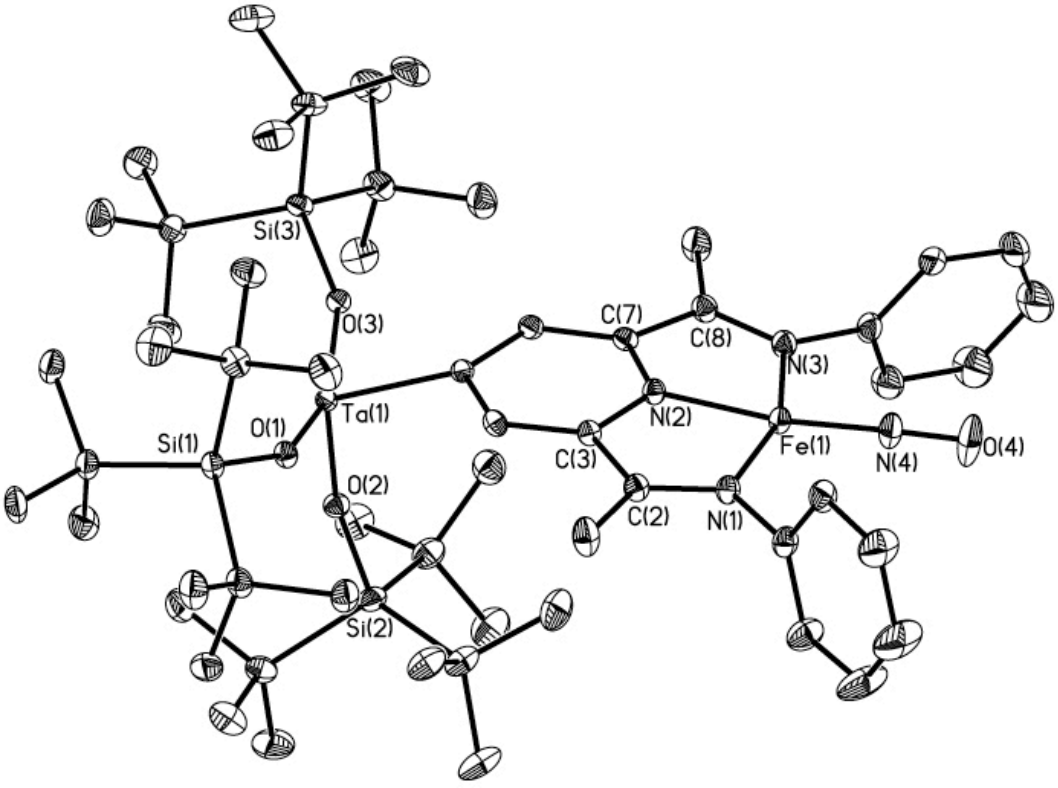

Figure 1.43 Molecular structure of **^{Ta}(^{iPr}PDI)Fe(NO)** at 30% probability ellipsoids. Hydrogen atoms and iso-propyl groups omitted for clarity.

Unfortunately, the tantalum hydride could not be crystallographically refined, and thus the geometry that the tantalum adopts is speculative, but without the hydride, it appears to be distorted tetrahedral. With the consideration of the hydride, the

tantalum could either adopt a pseudo trigonal bipyramidal structure or distorted square planar, depending on the position of the hydride. Table 1.10 provides selected bond distances and angles for $^{Ta}(^{iPr}PDI)Fe(NO)$.

Table 1.10 Metrics for both the iron and tantalum parts of **$^{Ta}(^{iPr}PDI)Fe(NO)$**.

	((p-silox3TaH) ^{iPr}PDI)Fe(NO) (Regarding Fe)		**((p-silox3TaH) ^{iPr}PDI)Fe(NO) (Regarding Ta)**
Fe(1)-N(1)	1.912(2)	Ta(1)-O(2)	1.870(1)
Fe(1)-N(2)	1.859(2)	Ta(1)-O(3)	1.921(1)
Fe(1)-N(3)	1.918(2)	Ta(1)-O(1)	1.922(1)
Fe(1)-N(4)	1.636(2)	Ta(1)-C(5)	2.165(2)
N(1)-C(2)	1.324(2)	C(5)-Ta(1)-O(1)	90.67(6)
N(3)-C(8)	1.323(3)	C(5)-Ta(1)-O(2)	108.53(6)
N(2)-C(3)	1.377(2)	C(5)-Ta(1)-O(3)	92.26(6)
N(2)-C(7)	1.368(2)	O(1)-Ta(1)-O(2)	101.69(5)
		O(1)-Ta(1)-O(3)	154.63(5)
N(4)-O(1)	1.183(2)	O(2)-Ta(1)-O(3)	101.23(5)
C(2)-C(3)	1.436(3)		
C(7)-C(8)	1.428(3)		
N(1)-Fe(1)-N(2)	79.59(7)		
N(1)-Fe(1)-N(4)	98.94(8)		
N(2)-Fe(1)-N(3)	79.52(7)		
N(3)-Fe(1)-N(4)	102.02(8)		
N(2)-Fe(1)-N(4)	169.71(7)		
Fe(1)-N(4)-O(1)	177.60(17)		

The PDI iron fragment in $^{Ta}(^{iPr}PDI)Fe(NO)$ appears to be consistent electronically to $(^{iPr}PDI)Fe(NO)$. The nitrosyl is slightly more lifted out of the plane of the chelate, but there is negligible change in the IR, the stretch coming at 1724 cm^{-1}, just slightly red shifted. The substitution of the *para* position of the pyridine of the

PDI chelate does not seem to have too great of an effect on the electronic structure of the compound.

(^{Et}PDI)Fe(NO) was derivatized to [(^{Et}PDI)Fe(NO)(THF)][$BArF_{24}$], [Na]-[(^{Et}PDI)Fe(NO)], and (^{Et}PDI)Fe(NO)(Py) in order to establish that it is indeed a single species with fluxional IR behavior as opposed to two different complexes. The oxidation was carried out in the same manner as (^{iPr}PDI)Fe(NO). An IR spectrum obtained of [(^{Et}PDI)Fe(NO)(THF)][$BArF_{24}$] showed a sharp peak at 1675 cm^{-1} in KBr, attributed to the nitrosyl of the complex. A solid state structure, shown in Figure 1.44, was obtained and the complex revealed a geometry very similar to [(^{iPr}PDI)Fe(NO)(THF)][$BArF_{24}$] with an apical bent nitrosyl and a THF coordinated in the basal plane.

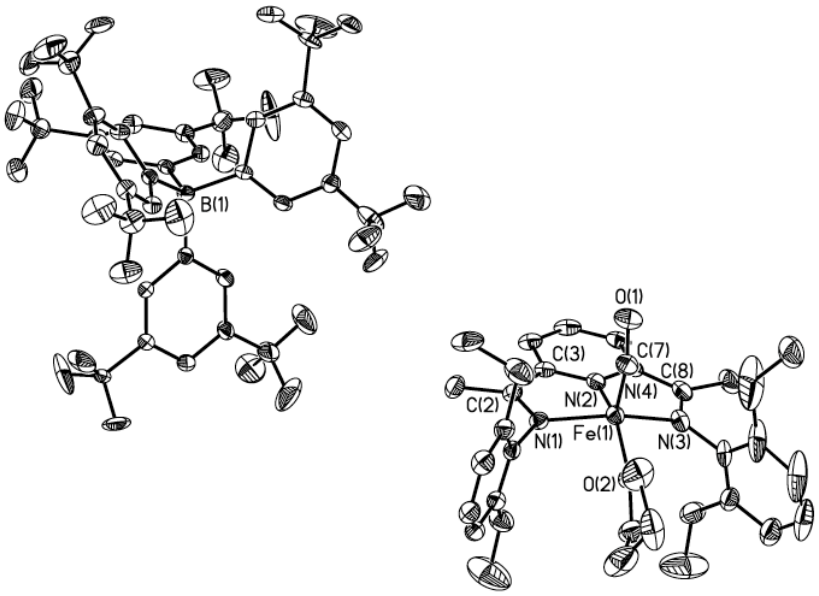

Figure 1.44 Molecular structure of **[(^{Et}PDI)Fe(NO)(THF)]$^{+}$** at 30% probability ellipsoids. Hydrogen atoms and disorder -CF_3 groups omitted for clarity.

The single stretch observed by IR indicates that [(^{Et}PDI)Fe(NO)(THF)]$^{+}$ is not fluxional like (^{Et}PDI)Fe(NO), which makes sense with the geometry and coordination number. The anions were synthesized as well, giving (^{Et}PDI)Fe(NO)$^{-}$ and [Na-Crown][(^{Et}PDI)Fe(NO)].

Finally, the pyridine adduct was synthesized in order to obtain an EPR spectrum in solution in order to compare (^{Et}PDI)Fe(NO)(Py) with (^{iPr}PDI)Fe(NO)(Py). The EPR data indicates that (^{Et}PDI)Fe(NO)(Py) is a single species and is electronically very similar to (^{iPr}PDI)Fe(NO)(Py). The g values obtained from the fit of 2.12, 2.00, and 1.98, for g_z, g_y, and g_x, respectively, are very similar to the values for (^{iPr}PDI)Fe(NO)(Py). The EPR spectrum of (^{Et}PDI)Fe(NO)(Py) is shown in Figure 1.45.

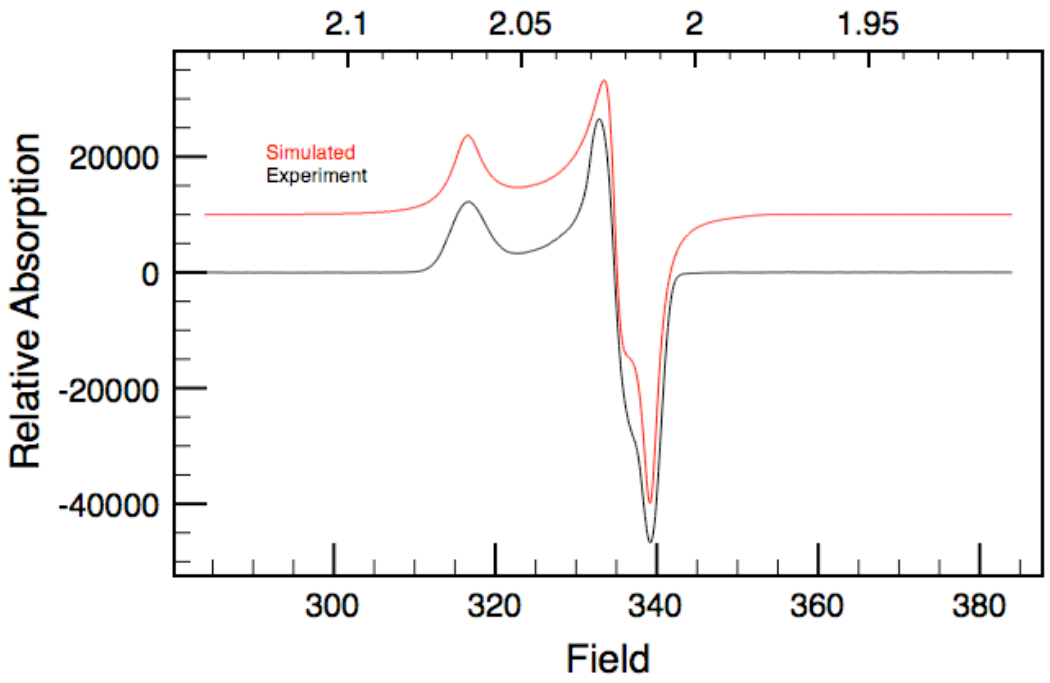

Figure 1.45 The EPR spectrum of **(^{Et}PDI)Fe(NO)(Py)** at 77 K.

The determination of the electronic structure of (^{Et}PDI)Fe(NO) will be undertaken to bring the electronic structure discussion to a close. The fluxional observed in the IR spectrum for the complex is the reason why this compound is not ascribed as having the same electronic structure as (^{iPr}PDI)Fe(NO). The two stretches, as seen in toluene at 1724 cm^{-1} and 1689 cm^{-1}, shift in intensity as the temperature is changed, with the lower energy band being more prevalent at cold temperatures, and seemingly the only band in the solid-state. The stretch at 1724 cm^{-1} is most likely a planar complex akin to (^{iPr}PDI)Fe(NO), as small variations in the bonding mode of the nitrosyl have yielded large shifts in the IR spectrum. The solid state IR spectrum (KBr) has only one shift located at 1685 cm^{-1}, so it stands to reason that the solid state structure, where the NO is canted out of the plane of the chelate, would correspond to that stretch. So it is postulated that the fluxionality involves the interconversion of the planar nitrosyl to the canted nitrosyl in solution, as presented in Figure 1.46.

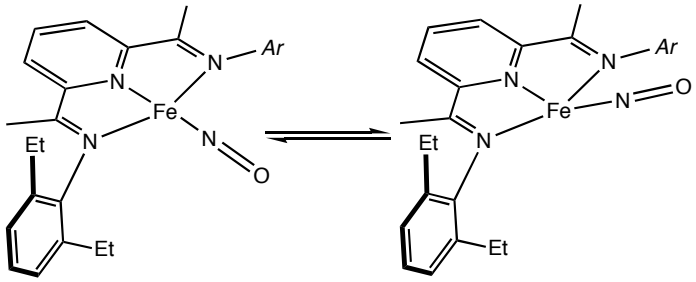

Figure 1.46 Fluxional nature of the nitrosyl in the case of **(^{Et}PDI)Fe(NO)**.

Two different sets of EPR experiments were performed, one set was performed in solution in toluene glass and the other EPR spectrum obtained on a solid sample. The Powder EPR spectrum taken reveals a single species present at 10. The EPR data obtained of (^{Et}PDI)Fe(NO) displays a spectrum that contains a higher g anisotropy in a

rhombic spectrum, which would therefore be the canted nitrosyl. The large g-anisotropy, with g values obtained from the fit of 2.31, 2.25, and 1.99, for g_y, g_x, and g_z, would lead one to believe that the canted nitrosyl could contain the majority of it's unpaired spin on a metal-based d-orbital, as was the case for (^{iPr}PDI)Fe(NO)(Py). The EPR spectrum of (^{Et}PDI)Fe(^{15}NO) contains shoulder peaks indicating unpaired spin on the nitrosyl. This EPR spectrum is presented in Figure 1.47.

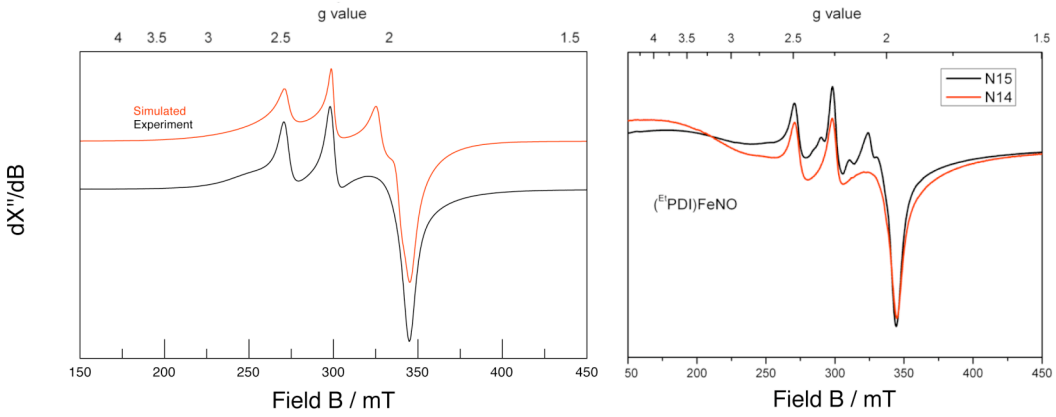

Figure 1.47 The powder EPR spectrum and computed fits of **(^{Et}PDI)Fe(NO)** and **(^{Et}PDI)Fe(^{15}NO)** at 10 K.

The EPR sample of (^{Et}PDI)Fe(NO) collected in toluene glass at 10 K reveals a signal much more similar to (^{iPr}PDI)Fe(NO) (Figure 1.48). Although the two spectra do not overlay precisely, the similarity between the two spectra is much closer than in the solid state.

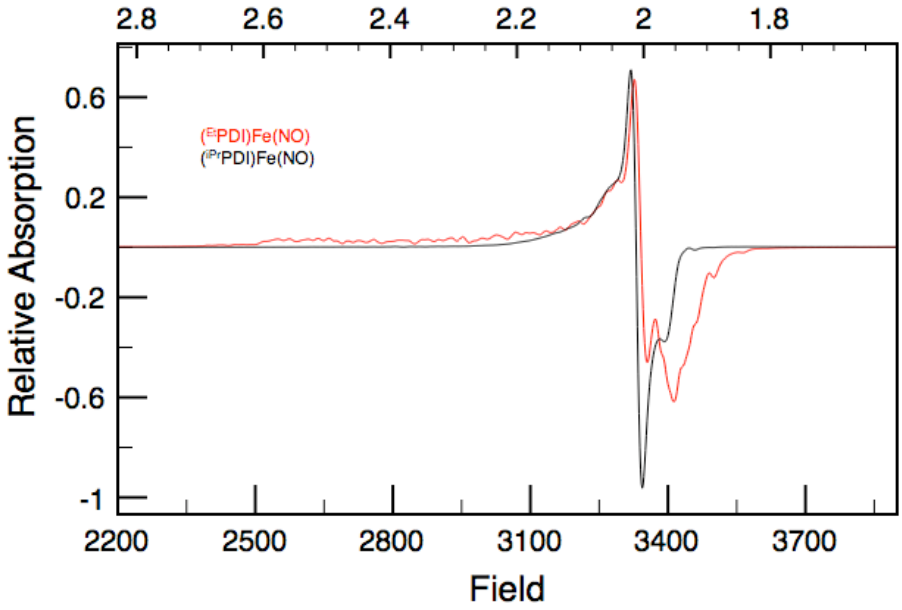

Figure 1.48 The toluene glass EPR spectra of **(^{Et}PDI)Fe(NO)** and **(^{iPr}PDI)Fe(NO)** obtained at 10 K.

This EPR data supports the hypothesis that (^{Et}PDI)Fe(NO) contains a fluxional nitrosyl ligand. This fluxionality between planar and canted is present only in solution, and in the solid state the nitrosyl ligand remains canted out of the plane of the chelate. This can be seen by comparing the solid-state EPR signals of (^{Et}PDI)Fe(NO) and (^{iPr}PDI)Fe(NO), where the spectra are exceedingly different. In a toluene glass, (^{Et}PDI)Fe(NO) and (^{iPr}PDI)Fe(NO) display spectra that are far more similar. The differences arise because (^{Et}PDI)Fe(NO) exists as both isomers, causing the signal to broaden and become more anisotropic.

Applied field Mössbauer spectroscopy was performed on (^{Et}PDI)Fe(NO) and a comparison to (^{iPr}PDI)Fe(NO) again shows a difference in the electronic structures between the two compounds. The spectrum (Figure 1.49) is best simulated with the

quadrupole splitting having a value of $\Delta E_Q = +0.86$ mm/s, the same magnitude as the value for (^{iPr}PDI)Fe(NO) but having the opposite sign. This indicates that the ordering of the orbitals is different for (^{Et}PDI)Fe(NO) than for (^{iPr}PDI)Fe(NO), most likely due to the canting of the Fe-NO bond in the solid-state. The A values A_{xx}, A_{yy}, and A_{zz} were best simulated as having values of -42 kG, 83 kG, and 327 kG, respectively. The large difference from the values of $A_{xx} = 125$ kG, $A_{yy} = 115$ kG, and $A_{zz} = 91$ kG for (^{iPr}PDI)Fe(NO) indicate that the SOMO is not bis(imino)pyridine based, but rather on the [Fe(NO)] fragment. This is consistent with a different ordering of orbitals in the molecule.

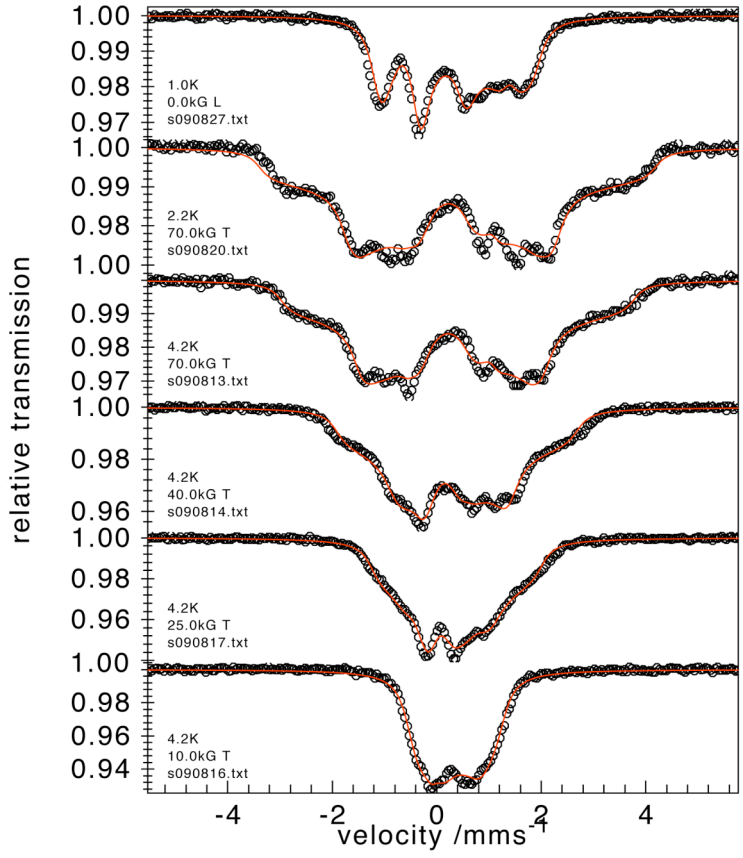

Figure 1.49 Applied field Mössbauer spectrum of **(^{Et}PDI)Fe(NO)**.

XAS data was collected on a solid sample of (^{Et}PDI)Fe(NO) in order to determine whether or not the shift in geometry has an effect on the oxidation state of the iron nucleus. The pre-edge feature of the spectrum is presented along with the reference compounds (^{iPr}PDI)FeCl$_2$ and (^{iPr}PDI)FeN(2,6-Dipp) in Figure 1.50.

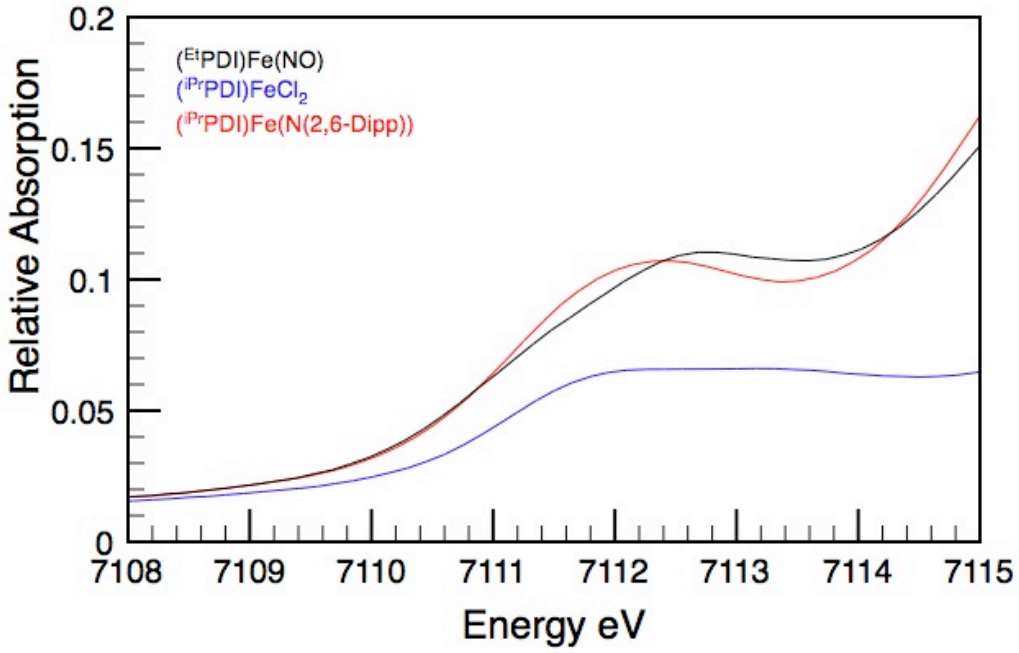

Figure 1.50 XAS pre-edge region of **(^{Et}PDI)Fe(NO).**

Unlike the data for (^{iPr}PDI)Fe(NO), the s-to-d transition of (^{Et}PDI)Fe(NO) appears slightly more oxidized than the Fe(III) reference complex (^{iPr}PDI)FeN(2,6-Dipp). This comparison may be more valid as the fourth ligand in both cases is canted out of the plane significantly. This similar geometry, along with the similar XAS data allow for the assignment of the Fe(III) nucleus in (^{Et}PDI)Fe(NO). Comparing the XAS data of (^{Et}PDI)Fe(NO) to (^{iPr}PDI)Fe(NO), as presented in Figure 1.51, also shows that the two iron centers of the complexes have very similar oxidation states even with the different geometries.

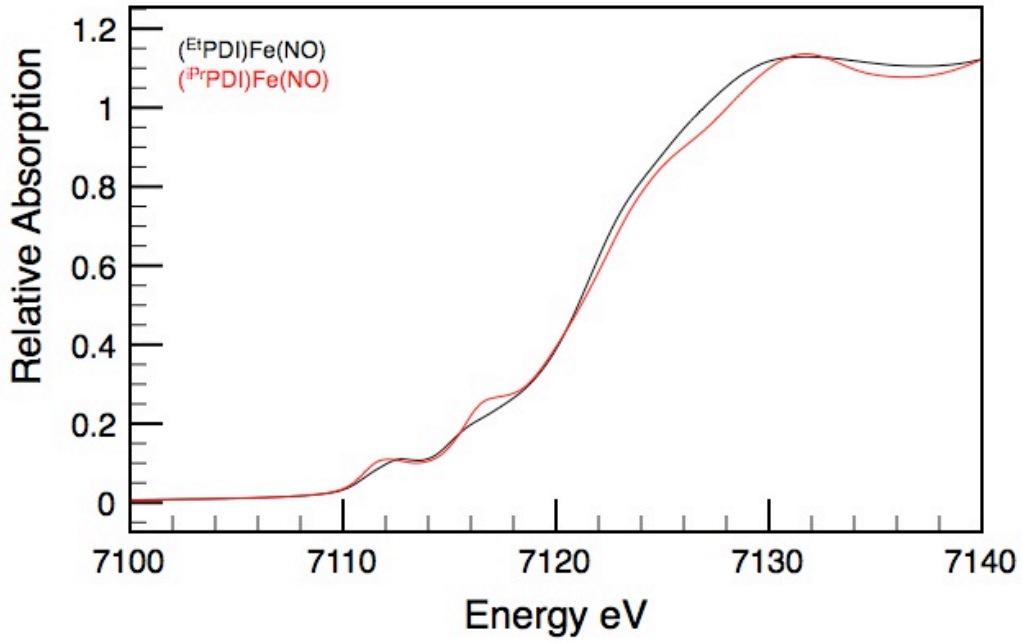

Figure 1.51 XAS data for **(^{Et}PDI)Fe(NO)** and **(^{iPr}PDI)Fe(NO).**

The EPR data is consistent with most of the unpaired spin of the system being localized on the [Fe(NO)] fragment. This is in contrast to (^{iPr}PDI)Fe(NO), where the majority spin is localized on the bis(imino)pyridine chelate. The XAS data confirms a similar oxidation state to (^{iPr}PDI)Fe(NO) although the geometries of the two compounds are different. This data allows the assignment of an intermediate-spin ferric center with a triplet 2 electron reduced chelate and a triplet NO^-. The chelate in (^{Et}PDI)Fe(NO) contains a minority of the unpaired spin, indicating that both radicals are antiferromagnetically coupled to the iron nucleus. This leaves an unpaired spin on either the NO ligand or the iron. A qualitative d-orbital splitting diagram (Figure 5.52) is presented based upon conclusions drawn from the spectroscopy

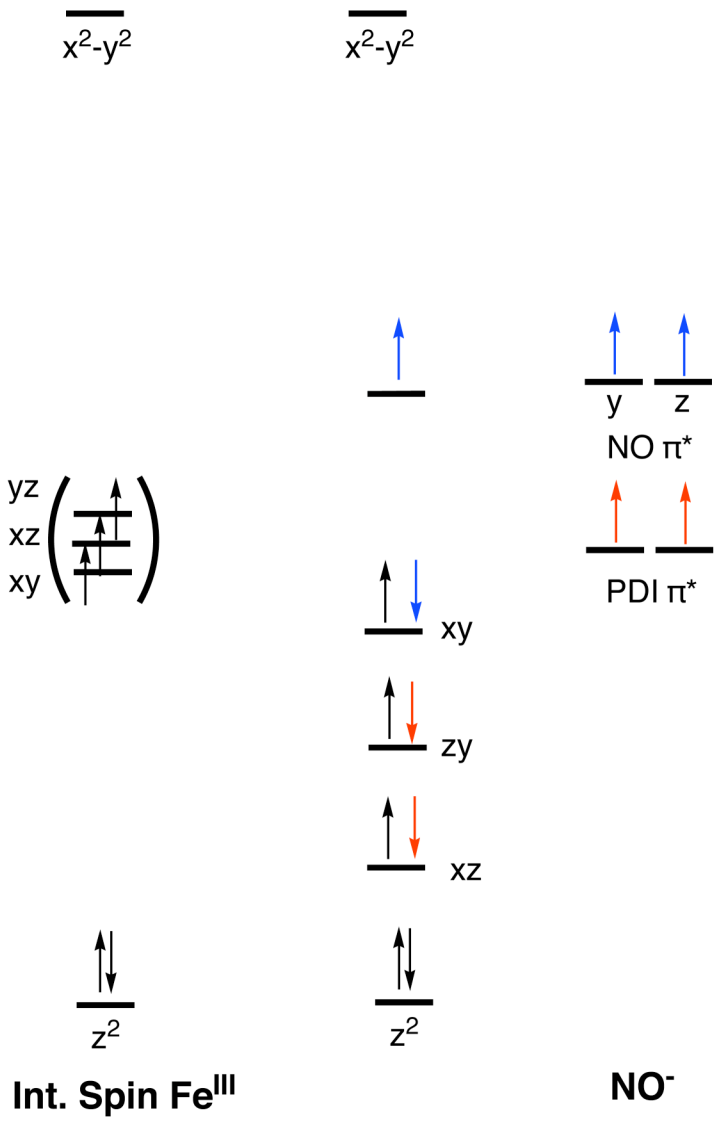

Figure 1.52 A qualitative molecular orbital diagram of **(^{Et}PDI)Fe(NO)**.

(^{Et}PDI)Fe(NO) and (^{iPr}PDI)Fe(NO) have been shown to have the same oxidation state at the iron, bis(imino)pyridine chelate, and nitrosyl ligand. The only difference electronically between the two complexes is the ordering of the d-orbital electrons which arises from the canting of the nitrosyl ligand in the less sterically demanding environment in the (^{Et}PDI)Fe(NO). This difference is highlighted in the EPR and applied field Mössbauer spectra, where the parameters are significantly different than the parameters for (^{iPr}PDI)Fe(NO).

1.10 Conclusions

The synthesis of a four coordinate planar, intermediate-spin Fe(III) nitrosyl complex (^{iPr}PDI)FeNO was achieved by the careful addition of one equivalent of nitric oxide to (^{iPr}PDI)Fe(N_2)$_2$. Sterically smaller versions of the complex were synthesized by the addition of two equivalents of nitric oxide to the smaller bridging dinitrogen complexes. Substitution of the isopropyl aryl groups for ethyl or methyl groups resulted in a four coordinate complex that showed fluxional behavior at the nitrosyl group in solution. Para-substitutions of the PDI ligand did not alter the complexes substantially. These four coordinate complexes undergo a spin transition and ligand oxidation to form high-spin Fe (II) five coordinate complexes. The four coordinate neutral complexes can also be oxidized with one equivalent of [Cp_2Fe][$BArF_{24}$] or reduced with in an excess sodium amalgam to produce the corresponding four coordinate anionic or cationic complexes. The five-coordinate cation can be prepared by oxidation in THF to form a complex with a bent nitrosyl in the apical position and a THF adduct in the plane of the chelate. The five-coordinate anion did not form. Also prepared in this study was the tetrahedral iron dinitrosyl complex by the addition of two equivalents of nitric oxide to the starting dinitrogen complex. The kappa-2 ligand is not reduced, giving a formally Fe^{2-} complex (from two linear "NO^+" ligands), but spectroscopically the compound exhibits what is best described as a high-spin ferrous center with two anionic NO compounds.

The electronic structure of this series of compounds was determined by the use of X-ray crystallography, Mössbauer, IR, NMR, and EPR spectroscopies, and corroborated by DFT calculations. The data were analyzed to yield electronic structures of each compound type, yielding a nice correlation of PDI reduction to overall compound reduction. Another result of this work has been the elucidation of a new coordination type of {Fe(NO)}^{7}. After over 150 years of iron nitrosyl compounds,

there is still plenty of room for new discoveries and fundamental investigations in this area.

1.11 Experimental Procedures

General Considerations. All air- and moisture-sensitive manipulations were carried out using standard vacuum line, Schlenk, and cannula techniques or in an MBraun inert atmosphere dry box containing an atmosphere of purified nitrogen. Solvents for air- and moisture-sensitive manipulations were initially dried and deoxygenated using literature procedures.[46] Benzene-d_6 and fluorobenzene-d_5 were purchased from Cambridge Isotope Laboratories and CDN Isotopes, respectively, and dried over 4 Å molecular sieves or calcium hydride, respectively. The complexes $[(^{Me}PDI)FeN_2]_2(\mu\text{-}N_2)$,[41] $[(^{Et}PDI)FeN_2]_2(\mu\text{-}N_2)$,[41] and $(^{iPr}PDI)Fe(N_2)_2$[32] were prepared according to literature procedures. Nitric oxide was purchased from Sigma-Aldrich and was dried by freezing the gas in liquid nitrogen and slowly allowing it to warm to above the freezing point.

^1H NMR spectra were recorded on Varian Mercury 300, Inova 400, 500, and 600 spectrometers operating at 299.76, 399.78, 500.62, and 599.78 MHz, respectively. ^{13}C NMR spectra were recorded on an Inova 500 spectrometer operating at 125.893 MHz. All ^1H and ^{13}C NMR chemical shifts are reported relative to $SiMe_4$ using the ^1H (residual) and ^{13}C chemical shifts of the solvent as a secondary standard. For diamagnetic complexes, many assignments were made based on COSY and HSQC NMR experiments. Solution magnetic moments were determined by Evans method[47] using a ferrocene standard and are the average value of at least two independent measurements. Magnetic susceptibility balance measurements were performed with a Johnson Matthey instrument that was calibrated with $HgCo(SCN)_4$. Peak widths at half heights are reported for paramagnetically broadened and shifted resonances.

Infrared spectra were collected on a Thermo Nicolet spectrometer. Elemental analyses were performed at Robertson Microlit Laboratories, Inc., in Madison, NJ.

Single crystals suitable for X-ray diffraction were coated with polyisobutylene oil in a drybox, transferred to a nylon loop and then quickly transferred to the goniometer head of a Bruker X8 APEX2 diffractometer equipped with a molybdenum X-ray tube (l = 0.71073 Å). Preliminary data revealed the crystal system. A hemisphere routine was used for data collection and determination of lattice constants. The space group was identified and the data were processed using the Bruker SAINT+ program and corrected for absorption using SADABS. The structures were solved using direct methods (SHELXS) completed by subsequent Fourier synthesis and refined by full-matrix least-squares procedures.

Mössbauer data were collected on an alternating constant-acceleration spectrometer. The minimum experimental line width was 0.24 mm s^{-1} (full width at half height). A constant sample temperature was maintained with an Oxford Instruments Variox or an Oxford Instruments Mössbauer-Spectromag 2000 cryostat. Reported isomer shifts (δ) are referenced to iron metal at 293 K.

Quantum-chemical calculations. All DFT calculations were performed with the ORCA program package.[48] The geometry optimizations of the complexes and single-point calculations on the optimized geometries were carried out at the B3LYP level[49,50,51] of DFT. This hybrid functional often yields better results for transition metal compounds than pure gradient-corrected functionals, especially with regard to metal-ligand covalency.[52] The all-electron Gaussian basis sets were those developed by the Ahlrichs group.[53,54] Triple-ζ quality basis sets TZVP with one set of polarization functions on the metal and on the atoms directly coordinated to the metal center were used.[73] For the carbon and hydrogen atoms, slightly smaller polarized

split-valence SV(P) basis sets were used, that were of double-ζ quality in the valence region and contained a polarizing set of d-functions on the non-hydrogen atoms.[72] Auxiliary basis sets used to expand the electron density in the resolution-of-the-identity (RI) approach were chosen,[55,56] to match the orbital basis.

The SCF calculations were tightly converged (1×10^{-8} E_h in energy, 1×10^{-7} E_h in the density change and 1×10^{-7} in maximum element of the DIIS error vector). The geometry optimizations for all complexes were carried out in redundant internal coordinates without imposing symmetry constraints. In all cases the geometries were considered converged after the energy change was less than 5×10^{-6} E_h, the gradient norm and maximum gradient element were smaller than 1×10^{-4} E_h $Bohr^{-1}$ and 3×10^{-4} E_h $Bohr^{-1}$, respectively, and the root-mean square and maximum displacements of all atoms were smaller than 2×10^{-3} Bohr and 4×10^{-3} Bohr, respectively.

Throughout this paper we describe our computational results by using the broken-symmetry (BS) approach by Ginsberg[57] and Noodleman.[58] Because several broken symmetry solutions to the spin-unrestricted Kohn-Sham equations may be obtained, the general notation BS(*m,n*)[59,16] has been adopted, where *m* (*n*) denotes the number of spin-up (spin-down) electrons at the two interacting fragments. Canonical and corresponding[60] orbitals, as well as spin density plots were generated with the program Molekel.[61] Frequency calculations were performed at the BP86[62,63] level of theory using the same basis sets as described above. The differences in the obtained geometries were negligible compared to those of the B3LYP optimizations.

Nonrelativistic single-point calculations on the optimized geometries were carried out to predict Mössbauer spectral parameters (isomer shifts and quadrupole splittings). These calculations employed the CP(PPP) basis set[64] for iron. The Mössbauer isomer shifts were calculated from the computed electron densities at the iron centers as previously described.[65]

Preparation of (^{iPr}PDI)Fe(NO). A thick walled glass vessel was charged with 0.35 g (0.59 mmol) of (^{iPr}PDI)Fe(N_2)$_2$ and 50 mL diethyl ether. The vessel was placed in a liquid nitrogen bath and degassed on a high vacuum line. A calibrated glass bulb (0.1001 L) was used to transfer 0.59 mmol of nitric oxide to the frozen iron solution. The reaction vessel was thawed with vigorous shaking under running tap water. The solution changed from green to dark red as the solution thawed. The reaction was placed on a dry ice/acetone bath and degassed. The ether solution was filtered through Celite and the volatiles were removed leaving 0.32 g (95%)of a dark red/brown powder identified as (^{iPr}PDI)Fe(NO). X-Ray quality crystals were grown from a dilute ether solution at -35 °C. Analysis for $C_{33}H_{43}N_4FeO$: Calcd C, 69.83; H, 7.64; N, 9.87. Found: C, 69.96; H, 7.63; N, 9.31. Magnetic susceptibility: μ_{eff} = 1.8 μ_B (Magnetic Susceptibility Balance). IR (KBr): ν NO 1724 cm^{-1}. ^{1}H NMR (benzene-d_6): δ -158.54 (1174 Hz, 1H, p-*pyH*), -6.23 (120 Hz, 4H, C*H*(CH_3)$_2$), 1.42 (34 Hz, 12H, CH(C*H*$_3$)$_2$), 3.10 (13 Hz, 12H, CH(C*H*$_3$)$_2$), 6.70 (16 Hz, 2H, p-*ArH*), 13.32 (17 Hz, 4H, m-*ArH*), 22.67 (95 Hz, 2H, m-*pyH*), 274.74 (2775 Hz, 6H, CN-*CH*$_3$).

Preparation of (^{2,6Et}PDI)Fe(NO). A procedure similar to that used for (^{iPr}PDI)Fe(NO) was followed. To an ether solution containing 0.40 g (0.38 mmol) of [(^{2,6Et}PDI)Fe(N_2)]$_2$(μ-N_2) was added with 0.76 mmol of nitric oxide via calibrated gas bulb. The same work-up yielded 0.34 g (87%) of a red powder identified as (^{2,6Et}PDI)Fe(NO). X-Ray quality crystals were grown from a dilute ether solution at -35 °C. Analysis for $C_{29}H_{35}N_4FeO$: Calcd C, 68.10; H, 6.90; N, 10.95. Found: C, 68.04; H, 6.63; N, 10.40. Magnetic susceptibility: μ_{eff} = 1.9 μ_B (Magnetic Susceptibility Balance). IR (KBr): ν NO 1685 cm^{-1}, ^{1}H NMR (benzene-d_6): δ -51.70 (294 Hz, 1H, p-*pyH*), -5.87 (139 Hz, 8H, *CH*$_2$CH$_3$), 0.56 (29 Hz, 12H, CH$_2$C*H*$_3$), 4.88

(16 Hz, 2H, p-*ArH*), 9.56 (17 Hz, 4H, m-*ArH*), 17.92 (95 Hz, 2H, m-*pyH*), 163.96 (1235 Hz, 6H, CN-CH_3).

Preparation of (^{2,6Me}PDI)Fe(NO). A procedure similar to that used for (^{iPr}PDI)Fe(NO) was followed. To an ether solution containing 0.20 g (0.21 mmol) of [(^{2,6Me}PDI)Fe(N_2)]$_2$(μ-N_2) was added with 0.42 mmol of nitric oxide via calibrated gas bulb. The same work-up yielded 0.34 g (87%) of a red powder identified as (^{2,6Me}PDI)Fe(NO). Analysis for $C_{29}H_{35}N_4FeO$: Calcd C, 65.94; H, 5.98; N, 12.30. Found: C, 64.42; H, 6.45; N, 10.73. Magnetic susceptibility: μ_{eff} =1.8 μ_B (Magnetic Susceptibility Balance). IR (KBr): ν NO 1663 cm^{-1}. ^{1}H NMR (benzene-d_6): δ -59.79 (112 Hz, 1H, p-*pyH*), -23.14 (530 Hz, 2H, p-*ArH*), -3.83 (96 Hz, 12H, CH_3), 8.49 (17 Hz, 4H, m-*ArH*), 16.39 (88 Hz, 2H, m-*pyH*), 134.55 (805 Hz, 6H, CN-CH_3).

Preparation of [(^{iPr}PDI)Fe(NO)][B-((3,5-(CF_3)$_2$)C_6H_3)$_4$]. A 100 mL round bottom flask was charged with 0.150 g (0.262 mmol) of (^{iPr}PDI)Fe(NO) and 0.275 g (0.261 mmol) of ferrocenium tetrakis[3,5-bis(trifluoromethyl)phenyl]borate and was fitted with a needle valve and moved onto a high vacuum line. The flask was evacuated and the reagents were pumped on to remove traces of ether. Toluene was vacuum transferred into the flask at -78 °C, warmed to room temperature, and a violet precipitate was formed. The reaction was stirred overnight. The flask was transferred into a dry-box and the reaction mixture was filtered and the precipitate was collected on a glass frit and dried under reduced pressure to yield 0.290 g (77%) of a violet powder identified as [(^{iPr}PDI)Fe(NO)][B-((3,5-(CF3)2)C6H3)4]. Analysis for $C_{61}H_{63}BF_{24}FeN_4O_2$: Calcd C, 52.08; H, 4.51; N, 3.98. Found: C, 53.83; H, 3.83; N, 3.69. IR (KBr): ν NO 1809 cm^{-1}. ^{19}F NMR (benzene-d_6): -62.35. ^{1}H NMR

(fluorobenzene-d_5): -4.88 (4H, C*H*$(CH_3)_2$), 0.59-0.52 (24H, CH(C*H*$_3)_2$), 3.84 (6H, C*H*$_3$), 7.85 (4H, B-(m-*ArH)*), 8.00 (1H, *p-pyH*), 8.60 (8H, o-*ArH*), 9.72 (1H, *p-pyH)*

Preparation of [(^{iPr}PDI)Fe(NO)(THF)][B-((3,5-$(CF_3)_2$)$C_6H_3)_4$]. A scintillation vial was charged with 0.150 g (0.262 mmol) of (^{iPr}PDI)Fe(NO) and 0.275 g (0.261 mmol) of ferrocenium tetrakis[3,5-bis(trifluoromethyl)phenyl]borate. With stirring, 3 mL of THF was added to the vial. After 10 minutes of stirring, 10 mL of pentane was added and the reaction mixture was cooled to -35 °C and the dark blue precipitate was collected on a glass frit, washed with ~ 20 mL of pentane, and dried under reduced pressure to yield 0.345 g (93%) of a blue green powder identified as [(^{iPr}PDI)Fe(NO)(THF)][B-((3,5-(CF3)2)C6H3)4]. X-ray quality crystals were grown from a concentrated ether solution at -35 °C overnight. Analysis for $C_{61}H_{63}BF_{24}FeN_4O_2$: Calcd C, 52.08; H, 4.51; N, 3.98. Found: C, 53.83; H, 3.83; N, 3.69. IR (KBr): ν NO 1656 cm^{-1}. ^{19}F NMR (benzene-d_6): -63.16. ^{1}H NMR (benzene-d_6): 0.80-1.20 (24H, CH(C*H*$_3)_2$), 1.40 (s, 8H, *THF*), 1.50 (6H, *CH*$_3$), 2.28 (8H, *o* B-*Ar*), 3.55 (8H, *THF*), 6.63 (1H, *p* Py), 6.83 (2H, *p-Ar*),6.89 (2H, *m-Ar*), 7.03 (2H, *m-Ar*), 7.22 (4H, m-*Py*), 7.65 (4H, B-*ArH*), 8.39 (8H, B-ArH).

Preparation of [(^{iPr}PDI)Fe(NO)(H_2O)][B-((3,5-$(CF_3)_2$)$C_6H_3)_4$]. A scintillation vial was charged with 0.150 g (0.262 mmol) of (^{iPr}PDI)Fe(NO) and 0.275 g (0.261 mmol) of ferrocenium tetrakis[3,5-bis(trifluoromethyl)phenyl]borate. With stirring, 3 mL of THF was added to the vial. After 10 minutes of stirring, 10 mL of pentane was added and the reaction mixture was cooled to -35 °C and the dark blue precipitate was collected on a glass frit, washed with ~ 20 mL of pentane, and dried under reduced pressure to yield 0.345 g (93%) of a blue green powder identified as [(^{iPr}PDI)Fe(NO)(THF)][B-((3,5-(CF3)2)C6H3)4]. X-ray quality crystals were grown

from a concentrated ether solution at -35 °C overnight. Analysis for $C_{61}H_{63}BF_{24}FeN_4O_2$: Calcd C, 52.08; H, 4.51; N, 3.98. Found: C, 53.83; H, 3.83; N, 3.69. IR (KBr): ν NO 1656 cm^{-1}.

Preparation of [(^{iPr}PDI)Fe(NO)(Pyridine)][B-((3,5-$(CF_3)_2$)C_6H_3)$_4$]. A scintillation vial was charged with 0.150 g (0.262 mmol) of (^{iPr}PDI)Fe(NO) and 0.275 g (0.261 mmol) of ferrocenium tetrakis[3,5-bis(trifluoromethyl)phenyl]borate. With stirring, 3 mL of THF was added to the vial. After 10 minutes of stirring, 10 mL of pentane was added and the reaction mixture was cooled to -35 °C and the dark blue precipitate was collected on a glass frit, washed with ~ 20 mL of pentane, and dried under reduced pressure to yield 0.345 g (93%) of a blue green powder identified as [(^{iPr}PDI)Fe(NO)(THF)][B-((3,5-(CF3)2)C6H3)4]. X-ray quality crystals were grown from a concentrated ether solution at -35 °C overnight. Analysis for $C_{61}H_{63}BF_{24}FeN_4O_2$: Calcd C, 52.08; H, 4.51; N, 3.98. Found: C, 53.83; H, 3.83; N, 3.69. IR (KBr): ν NO 1658 cm^{-1}.

Preparation of [(^{2,6Et}PDI)Fe(NO)(THF)][B-((3,5-$(CF_3)_2$)C_6H_3)$_4$]. A procedure similar to that of [(^{iPr}PDI)Fe(NO)(THF)][B-((3,5-(CF3)2)C6H3)4] was used with 0.100 g (0.196 mmol) of (^{2,6Et}PDI)Fe(NO) and 0.205 g (0.196 mmol) of ferrocenium tetrakis[3,5-bis(trifluoromethyl)phenyl]borate to yield 0.345 g (93%) of a blue green powder identified as [(^{2,6Et}PDI)Fe(NO)(THF)][B-((3,5-(CF3)2)C6H3)4]. X-ray quality crystals were grown from a concentrated ether solution at -35 °C overnight. Analysis for $C_{65}H_{55}BF_{24}FeN_4O_2$: Calcd C, 53.96; H, 3.83; N, 3.87. IR (KBr): ν NO 1654 cm^{-1}.

Preparation of [(^{iPr}4-[(Silox)$_3$TaH]PDI)Fe(NO)]. A scintillation vial was charged with 0.024 g of (^{iPr}PDI)Fe(NO) and 5 mL of ether. To the stirring iron solution was

added 0.035 mg of $(Silox)_3Ta$ in 5 mL of ether. The solution was stirred overnight, over the course of the reaction time the solution turned from dark red to purple. Analysis for $C_{69}H_{124}N_4FeO_4Si_3Ta$: Magnetic susceptibility: $\mu_{eff} = 1.8\ \mu_B$ (Gouy Balance). IR (KBr): ν NO 1719 cm^{-1}, ν Ta-H 1844 cm^{-1}. ^1H NMR (benzene-d_6): -14.58 , -6.23 (120 Hz, 4H, C*H*$(CH_3)_2$), 2.20 (Si(C*Me*$_3$), 3.10 (13 Hz, 12H, CH(C*H*$_3)_2$), 6.69 (16 Hz, 2H, p-*ArH*), 13.32 (95 Hz, 2H, m-*pyH*), 18.54 (1H, Ta-H), 127.10 (95 Hz, 4H, m-*pyH*), 195.11 (2775 Hz, 6H, CN-*CH*$_3$).

Preparation of (^{iPr}(4-^{t}Bu)PDI)Fe(NO). A procedure similar to that used for (^{iPr}PDI)Fe(NO) was followed. To an ether solution containing 0.40 g (0.38 mmol) of (^{iPr}(4-^{t}Bu)PDI)Fe(N_2) was added with 0.38 mmol of nitric oxide. The same work-up yielded 0.34 g (87%) of a red powder identified as (^{iPr}4-^{t}BuPDI)Fe(NO). Analysis for $C_{37}H_{51}N_4FeO$: Calcd C, 71.25; H, 8.24; N, 8.98. Found: C, 71.17; H, 8.49; N, 8.56. Magnetic susceptibility: $\mu_{eff} = 1.8\ \mu_B$ (Gouy Balance). IR (KBr): ν NO 1728 cm^{-1}. ^1H NMR (benzene-d_6): δ = -4.05 (164 Hz), 1.18 (333 Hz), 6.85 (39 Hz), 14.19 (54.66 Hz), 24.43 (178 Hz)

Preparation of (^{2,6Et}(4-^{t}Bu)PDI)Fe(NO). A procedure similar to that used for (^{iPr}PDI)Fe(NO) was followed. To an ether solution containing 0.40 g (0.38 mmol) of [(^{2,6Et}4-^{t}BuPDI)Fe(N_2)]$_2$(μ-N_2) was added with 0.76 mmol of nitric oxide. The same work-up yielded 0.34 g (87%) of a red powder identified as (^{iPr}4-^{t}BuPDI)Fe(NO). X-ray quality crystals were grown from a concentrated ether solution cooled to -35 °C overnight. Analysis for $C_{33}H_{43}N_4FeO$: Calcd C, 69.83; H, 7.64; N, 9.87. Magnetic susceptibility: $\mu_{eff} = 1.8\ \mu_B$ (Gouy Balance). IR (KBr): ν NO 1690 cm^{-1}. ^1H NMR (benzene-d_6): δ = -4.48 (174 Hz, 2H, CH_2CH$_3$), -4.24 (120 Hz, 2H, CH_2CH$_3$), 0.48 (34

Hz, 9H, CH_2CH_3), 4.92 (13 Hz, 2H, *p-Ar*), 5.73 (16 Hz, 6H, CH_2CH_3), 10.51 (17 Hz, 4H, m-*ArH*), 19.60 (95 Hz, 4H, m-*pyH*), 194.40 (2775 Hz, 6H, CN-CH_3).

Preparation of (^{2,6Me}4-^{t}BuPDI)Fe(NO). A procedure similar to that used for (^{iPr}PDI)Fe(NO) was followed. To an ether solution containing 0.100 g (0.102 mmol) of [(^{2,6Me}4-^{t}BuPDI)Fe(N_2)]$_2$(μ-N_2) was added with 0.204 mmol of nitric oxide. The same work-up yielded 0.34 g (87%) of a red powder identified as (^{iPr}4-^{t}BuPDI)Fe(NO). Analysis for $C_{33}H_{43}N_4FeO$: Calcd C, 69.83; H, 7.64; N, 9.87. Found C, 69.40; H, 7.83; N, 9.70. Magnetic susceptibility: μ_{eff} = 1.8 μ_B (Gouy Balance). IR (KBr): ν NO 1690 cm^{-1}. δ = -3.08 (34 Hz, 9H, CH_2CH_3), 3.49 (13 Hz, 2H, *p-Ar*), 5.48 (16 Hz, 6H, CH_2CH_3), 9.15 (17 Hz, 4H, m-*ArH*), 17.83 (95 Hz, 4H, m-*pyH*), 154.49 (2775 Hz, 6H, CN-CH_3).

Preparation of [Na(THF)$_{xx}$][(^{iPr}PDI)Fe(NO)]. A scintillation vial was charged with 0.200 g (0.352 mmol) of (^{iPr}PDI)Fe(NO) and the solid was dissolved in 10 mL of THF. To this stirring solution was added freshly prepared 1.0% sodium amalgam (2eq., 0.016 g of sodium in 1.6 g Hg). The solution was stirred for 12 hours, gradually changing color from a dark red/brown to a bright pink solution. The solution was decanted from the amalgam, passed through Celite into a 20 mL scintillation vial, and concentrated to approximately 1/3 the volume, at which time 5 mL of pentane was layered on top and the vial was placed at -35 °C for an hour. The solid that formed was collected on a glass frit and washed with pentane, yielding 0.232 g of a dark pink powder. Analysis for [Na(THF)$_{xx}$] [(^{iPr}PDI)Fe(NO)]. IR (KBr): ν NO 1602 cm^{-1}.

Preparation of [Na(THF)$_2$(15-Crown-5)] [(^{iPr}PDI)Fe(NO)]. A procedure similar to that of [Na(THF)$_{xx}$] [(^{iPr}PDI)Fe(NO)] was used in the preparation with one additional

step. The dark pink powder was dissolved in THF and 0.097 g (1.25 eq. to the starting material, 0.441 mmol) of 15-crown-5 was added, causing the precipitation of a pink solid. Pentane was added to the solution, which was subsequently cooled to -35 °C for an hour, and the pink solid was collected on a glass frit, washed with pentane, and dried under reduced pressure to yield 0.280 g (83% overall) of $[Na(THF)_2(15\text{-Crown-}5)]$ [(^{iPr}PDI)Fe(NO)]. X-ray quality crystals were grown by layering a saturated THF solution of the compound with pentane and allowing the solutions to diffuse slowly at -35 °C overnight. Analysis for $C_{51}H_{79}FeN_4NaO_8$: Calcd C, 64.14; H, 8.34; N, 5.87. Found: C, 53.20; H, 6.62; N, 5.70. IR (KBr): ν NO 1676 cm^{-1}.

Preparation of $[Na(THF)_{xx}]$[(^{Et}PDI)Fe(NO)]. A procedure similar to that of $[Na(THF)_{xx}]$ [(^{iPr}PDI)Fe(NO)] was used but with 0.150 g (0.293 mmol) of (^{2,6Et}PDI)Fe(NO) and 0.013 g (2 eq., 0.586 mmol) of sodium in 1.3 g of mercury. Analysis for $[Na(THF)_{xx}]$ [(^{2,6Et}PDI)Fe(NO)]. IR (KBr): ν NO 1602 cm^{-1}.

Preparation of $[Na(THF)_2$(15-Crown-5)][(^{Et}PDI)Fe(NO)]. A procedure similar to that of $[Na(15\text{-crown-}5)(THF)_2]$ [(^{iPr}PDI)Fe(NO)] was used with 0.150 g (0.293 mmol) of (^{2,6Et}PDI)Fe(NO), 0.013 g (2 eq., 0.586 mmol), and 0.081 g of 15-crown-5, yielding 0.200 g (76%) of a bright pink solid identified as $[Na(THF)_2$ (15-Crown-5)] [(^{2,6t}PDI)Fe(NO)]. Analysis for $C_{47}H_{71}FeN_4NaO_8$: Calcd C, 62.80; H, 7.96; N, 6.23. Found: IR (KBr): ν NO 1658 cm^{-1}.

Preparation of (^{iPr}PDI)Fe(NO)(pyridine). To a stirring ether (10 mL) solution of 0.150 g (0.265 mmol) (^{iPr}PDI)Fe(NO) in a scintillation vial was added 0.050 g (0.660 mmol) of pyridine. The solution became green and thick with precipitate, and stirring was continued for 30 minutes before the vial was cooled to -35 °C. The solid was

collected via filtration and dried under reduced pressure to yield 0.138 g (80%) of a dark green powder identified as (^{iPr}PDI)Fe(NO)(pyridine). Analysis for $C_{38}H_{48}FeN_5O$: Calcd C, 70.58; H, 7.48; N, 10.83. Found: C, 70.18; H, 7.24; N, 10.54. IR (KBr): ν(NO) = 1626 cm^{-1}. ^{1}H NMR (benzene-d_6): 8.64 (96 Hz), 7.67 (204 Hz), 0.73 (278 Hz).

Preparation of (κ-2-^{iPr}PDI)Fe(NO)$_2$. A thick walled glass vessel was charged with 0.35 g (0.59 mmol) of (^{iPr}PDI)Fe(N_2)$_2$ and 50 mL toluene. The vessel was placed in a liquid nitrogen bath and degassed on a high vacuum line. A calibrated glass bulb (0.1001 L) was used to transfer 0.110 mmol of nitric oxide to the frozen iron solution. The reaction vessel was thawed with vigorous shaking under running tap water. The solution changed from green to bright red/pink as the solution thawed. The reaction was placed on a dry ice/acetone bath and degassed. The toluene solution was filtered through Celite and the volatiles were removed leaving 0.32 g (95%)of a red/salmon powder identified as (^{iPr}PDI)Fe$(NO)_2$. X-Ray quality crystals were grown from a concentrated methylene chloride solution layered with ether and held at -35 °C overnight. Analysis for $C_{33}H_{43}FeN_5O_2$: Calcd C, 66.33; H, 7.25; N, 11.72. Found: C, 66.61; H, 7.29; N, 11.48. IR (KBr): ν NO 1706, 1664 cm^{-1}. ^{1}H NMR (benzene-d_6): 1.18(d, 12H, CH_3), 1.43(d, 12H, CH_3), 1.91 (s, 6H, CH_3), 3.12 (sep, 4H, C*H*CH_3), 6.95 (t, 1H, p-*pyH*), 7.12-7.40 (m, 8H, *Ar-H and m-PyH*).

REFERENCES

[1] Playfair, L. *Annolen* **1850**, 74, 317.

[2] Swinehart, J. H. *Coord. Chem. Rev.* **1967**, 2, 385.

[3] a) McCleverty, J. A. *Chem. Rev.* **2004**, 104, 403. b) Hayton, T. W.; Legzdins, P.; Sharp, B. W. *Chem. Rev.* **2002**, 102, 935. Richter-Addo, G. B.; Legzdins, P. *Chem. Rev.* **1988**, 88, 991.

[4] a) Scheidt, W. R.; Barabanschhikov, A.; Pavlik, J. W.; Silvernail, N. J.; Sage, T.J. *Inorg. Chem.* **2010**, 49, 6240. b) Goodrich, L.E.; Paulat, F.; Praneeth, V. K. K.; Lehnert, N. *Inorg. Chem*. **2010**, 49, 6293.

[5] Moncada, S.; Palmer, R. M.; Higgs, E. A.; *Pharmacol. Rev.* **1991**, 43, 109.

[6] Culotta, E.; Koshland, D. E., Jr. *Science*, **1992**, 258, 1862.

[7] Enemark, J. H.; Feltham, R, D. *Coord. Chem. Rev.* **1974**, 13, 339.

[8] Enemark, J. H.; Feltham, R, D. *Proc. Nat. Acad. Sci.* **1972**, 69, 3534.

[9] Sidgwick, N. V.; Bailey, R.W. *Proc. Roy. Soc. London*, A144, **1934**, 1523.

[10] McCleverty, J. A. Chem. Rev. 2004, 104, 403.

[11] Brock, C.P.; lbcas, J.A. *Inorg Chem,* **1972**, 11, 2812.

[12] Hieber, W. and Ellermann, J. *Chem. Ber.* **1963**, 96, 16431.

[13] Heibner, W.; Beutner, H. Z. Anorg. Allg. Chem. **1963**, 320, 101.

[14] Connelly, N. G. *J. Chem. Soc. Dalton Trans.* **1976**, 1525.

[15] Stokes, S. L.; Davis, W. M.; Odom, A. L.; Cummins, C. C. *Organometallics*, **1996**, 4521.

[16] Harrop, C. T.; Song, D.; Lippard, S. J.; *J. Am. Chem. Soc.*, **2006**, 128, pp 3528.

[17] Zhang, Y.; Pavlosky, M. A.; Brown, C. A.; Westre, T. E.; Hedman, B.; Hodgson, K.O.; Solomon, E.I. *J. Am. Chem. Soc.*, **1992**, 114, 9189-9191.

[18] Brown, C. A.; Pavlosky, M. A.; Westre, T. E.; Zhang, Y.; Hedman, B.; Hodgson, K.O.; Solomon, E.I. *J. Am. Chem. Soc.*, **1995**, 117, 715-732.

[19] Hammes, B. S.; Ramos-Maldonado, D.; Yap, G. P. A.; Liable- Sands, L.; Rheingold, A. L.; Young, V. G.; Borovik, A. S. *Inorg. Chem*. **1997**, 36, 3210.

[20] Hammes, B. S.; Ramos-Maldonado, D.; Yap, G. P. A.; Liable- Sands, L.; Rheingold, A. L.; Young, V. G.; Borovik, A. S. *Inorg. Chem*. **1999**, 38, 3110.

[21] Hauser, C.; Glaser, T.; Bill,E.; Weyhermüller, T.; Wieghardt, K. *J. Am. Chem. Soc.*, **2000**, 122 (18), pp 4352.

[22] a)Xu, N.; Yi, Y.; Richter-Addo, *Inorg. Chem.* **2010**, 49, 6253. b) Wang, J.; Schopfer, M. P.; Puiu, C. S.; Sarjeant, A. A. N.; Karlin, K. D. *Inorg. Chem.* **2010**, 49, 1404.

[23] a)Tonzetich, Z. J.; McQuade, L. E.; Lippard, S. J. *Inorg. Chem.* **2010**, 49, 6338. b) Tonzetich, Z. J.; Wang, H.; Mitra, D.; Tinberg, C. E.; Do, L. H.; Jenny Jr., F. E.; Adams, M. W. W.; Cramer, S. P.; Lippard, S. J. *J. Am. Chem. Soc.* **2010**, 132, 6914.

[24] a) Knijnenburg, Q.; Gambarotta, S.; Budzelaar, P. H. M. *Dalton Trans.* **2006**, 5442. b) Bart, S. C.; Chlopek, K.; Bill, E.; Bouwkamp, M. W.; Lobkovsky, E.; Neese, F.; Wieghardt, K.; Chirik, P. J. *J. Am. Chem. Soc.* **2006**, *128*, 13901.

[25] Butin, K. P.; Beloglazkina, E. K.; Zyk, N. V. *Russ. Chem. Rev*. **2005**, *74*, 531.

[26] Kuwabara, I. H.; Comninos, F. C. M.; Pardini, V. L.; Viertler, H.; Toma, H. E. *Electrochim. Acta* **1994**, *39*, 2401.

[27] Toma, H. E.; Chavez-Gil, T. E. *Inorg. Chim. Acta* **1997**, *257*, 197.

[28] de Bruin, B.; Bill, E.; Bothe, E.; Weyermüller, T.; Wieghardt, K. *Inorg. Chem.* **2000**, *39*, 2936.

[29] Budzelaar, P. H. M.; de Bruin, B.; Gal, A. W.; Wieghardt, K.; van Lenthe, J. H. *Inorg. Chem.* **2001**, *40*, 4649.

[30] Caulton, K. G. *Coord. Chem. Rev.* **1975**, 14, 317-355

[31] See Chapter 6 of this thesis

[32] Bart, S. C.; Lobkovsky,E.; Chirik, P.J., *J. of the Am. Chem. Soc.* **2004,** *126* (42), 13794.

[33] Bowman, A. C. PhD. Dissertation, Cornell University, **2009**.

[34] Fernández, I.; Trovitch, R. J.; Lobkovsky, E.; Chirik, P. J.; *Organometallics*, **2008**, 27, 109–118

[35] Tondreau, A. M.; Milsmann, C.; Patrick, A. D.; Hoyt, H. M.; Lobkovsky, E.; Wieghardt, K.; Chirik, P. J. *J. Am. Chem. Soc.* **2010***,* 132, 15046.

[36] Franz, K. J.; Lippard, S. J. *J. Am. Chem. Soc.* **1999**, 121, 10504.

[37] Tangen, E.; Conradie, J.; Ghosh, A. *Inorg. Chem.* **2005**, 44, 8699.

[38] Westre, T. E.; Kennepohl, P.; DeWitt, J. G.; Hedmon, B.; Hodgson, K. O.; Soloman, E. I. *J. Am. Chem. Soc.* **1997,** 119, 6297.

[39] Bart, S. C.; Lobkovsky, E.; Bill, E.; Chirik, P.J. *J. Am. Chem. Soc.* **2006,** 128, 5302.

[40] Tonzetich, Z. J.; Do, L. H.; Lippard, S. J. *J. Am. Chem. Soc.* **2009,** 131, 7964.

[41] Ye, S.; Neese, F. *J. Am. Chem. Soc.* **2010,** 132, 3646.

[42] Russell, S. K.; Darmon, J. M.; Lobkovsky, E.; Chirik P. J. *Inorg. Chem.* **2010,** *49*, 2782.

[43] Odom, A. L.; Protasiewicz. J. D.; Cummins. C. C. *J. Am. Chem. Soc.* **1995**, 117*,* 6613.

[44] LaPointe, R. E.; Wolczanski, P. T.; Mitchell, J. F. *J. Am. Chem. Soc.*, **1986**, 108, 6382.

[45] Covert, K. J.; Neithamer, D. R.; Zonnevylle, M. C.; LaPointe, R. E.; Schaller, C. P.; Wolczanski, P. T. *Inorg. Chem.* **1991**, 30, 2494.

[46] Pangborn, A. B.; Giardello, M. A.; Grubbs, R. H.; Rosen, R. K.; Timmers, F. J. *Organometallics* **1996**, *15*, 1518.

[47] Sur, S. K. *J. Magn. Reson.* **1989**, *82*, 169.

[48] F. Neese, Orca – an ab initio, DFT and Semiempirical Electronic Structure Package, Version 2.7, Revision 0; Institut für Physikalische und Theoretische Chemie, Universität Bonn, Bonn (Germany), August **2009**.

[49] Becke, A. D. *J. Chem. Phys.* **1986**, *84*, 4524.

[50] Becke, A. D. *J. Chem. Phys.* **1993**, *98*, 5648.

[51] Lee, C. T.; Yang, W. T.; Parr, R. G. *Phys. Rev. B* **1988**, *37*, 785.

[52] F. Neese, E. I. Solomon, In *Magnetism: From Molecules to Materials*; Miller, J. S., Drillon, M., Eds.; Wiley: New York, **2002**; Vol. 4, p 345.

[53] Schäfer, A.; Horn, H.; Ahlrichs, R. *J. Chem. Phys.* **1992**, *97*, 257.

[54] Schäfer, A.; Huber, C.; Ahlrichs, R. *J. Chem. Phys.* **1994**, *100*, 5829.

[55] Eichkorn, K.; Weigend, F.; Treutler, O.; Ahlrichs, R. *Theor. Chem. Acc.* **1997**, *97*, 119.

[56] Eichkorn, K.; Treutler, O.; Öhm, H.; Häser, M.; Ahlrichs, R. *Chem. Phys. Lett.* **1995**, *240*, 283.

[57] Ginsberg, A. P. *J. Am. Chem. Soc.* **1980**, *102*, 111.

[58] Noodleman, L.; Peng, C. Y.; Case, D. A.; Mouesca, J. M. *Coord. Chem. Rev.* **1995**, *144*, 199.

[59] Kirchner, B.; Wennmohs, F.; Ye, S.; Neese, F. *Curr. Opin. Chem. Biol.* **2007**, *11*, 134.

[60] Neese, F. *J. Phys. Chem. Solids* **2004**, *65*, 781.

[61] *Molekel*, Advanced Interactive 3D-Graphics for Molecular Sciences, available under http://www.cscs.ch/molekel/.

[62] Perdew, J. P.; Yue, W. *Phys. Rev. B* **1986**, *33*, 8800.

[63] Perdew, J. P. *Phys. Rev. B* **1986**, *33*, 8822.

[64] Neese, F. *Inorg. Chim. Acta* **2002**, *337*, 181.

[65] Sinnecker, S.; Slep, L. D.; Bill, E.; Neese, F. *Inorg. Chem.* **2005**, *44*, 2245.

CHAPTER 2

OXYGEN ATOM TRANSFER AND ATTEMPTED NITROGEN ATOM TRANSFER FROM MOLYBDENUM COMPLEXES TO BIS(IMINO)PRYIDINE IRON

2.1 Abstract

The transfer of an oxygen atom from (^{t}Bu(Ar)N)$_3$MoNO to one equivalent of [(^{Me}PDI)FeN$_2$]$_2$(μ-N$_2$) or [(^{Et}PDI)FeN$_2$]$_2$(μ-N$_2$) was accomplished at room temperature, yielding one equivalent of (^{t}Bu(Ar)N)$_3$MoN and [(^{Me}PDI)Fe]$_2$(μ-O) or [(^{Et}PDI)Fe]$_2$(μ-O), respectively. (^{iPr}PDI)Fe(N$_2$)$_2$ was ineffective for this reaction. An oxygen atom was also transferred from (Me)$_3$NO and N$_2$O to (^{iPr}PDI)Fe(N$_2$)$_2$ to give the bridging [(^{iPr}PDI)Fe]$_2$(μ-O), albeit in low yields. The metrical parameters from two crystal structures of [(^{iPr}PDI)Fe]$_2$(μ-O) and [(^{Et}PDI)Fe]$_2$(μ-O) indicate a high-spin ferrous center, with a bis(imino)pyridine radical anion. Nitrogen atom transfer was attempted from adding (^{t}Bu(Ar)N)$_3$MoNNNa to the compounds of the type (^{R}PDI)FeCl (^{R}PDI = 2,6-(2,6-R-C$_6$H$_3$N=CMe)$_2$C$_5$H$_3$N; R = Me, Et or ^{i}Pr). The bridging dinitrogen complexes [(^{t}Bu(Ar)N)$_3$Mo](μ-N$_2$)[(^{R}PDI)Fe] were isolated. The yields of the bridging compounds increased with decreased steric demand of R. A crystal structure of [(^{t}Bu(Ar)N)$_3$Mo](μ-N$_2$)[(^{Me}PDI)Fe] was obtained and the compound is best described as a Mo(IV), $(N_2)^{2-}$ and a high-spin Fe(II) center supported by a bis(imino)pyridine radical anion, yielding an overall S = 3/2 complex.

2.2 Introduction

Isolable bridging oxo compounds of ferrous ions are rare. Only one other isolable example has appeared in the literature, although evidence exists for

electrochemically-generated species.[1] Holland and co-workers reported the bridging oxo diketiminate iron complex L-Fe-O-Fe-L, where L is the anionic ArNC(tBu)CHC(tBu)Ar$^-$ and Ar is the bulky 2,6-diisopropylphenyl.[2] This compound was prepared by the addition of an equivalent of water to the bridging hydride complex (Figure 2.1).

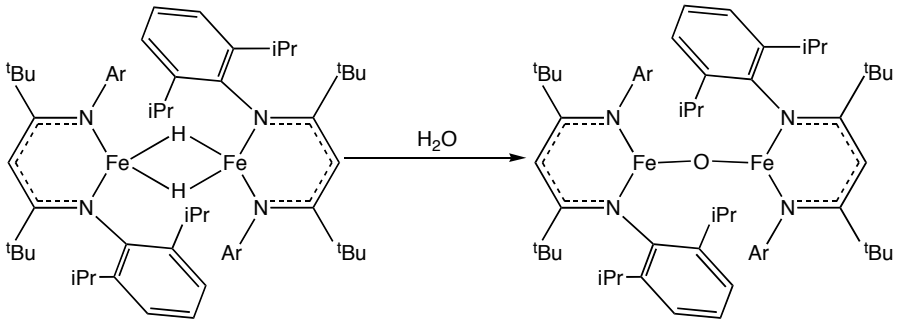

Figure 2.1 Holland's synthesis of the first diferrous bridging oxo complex.

Iron nitride species have been implicated in a number of important reactions. Ertl has demonstrated that an iron-nitrido species is a key intermediate in the Haber-Bosch process. [3] Iron-nitrido species have also been implicated as intermediates in the formation of ammonia from molecular nitrogen in biology.[4] Several isolable iron nitrido species are known, and all crystallographically characterized complexes have been synthesized from the iron azide precurser,[5,6,7] although spectroscopically characterized species have been generated from nitrogen atom transfer from Li-2,3:5,6-dibenzo-7-azabicyclo[2.2.1]hept a-2,5-diene (Lidbabh).[8]

The formation of (^{t}Bu(Ar)N)$_3$MoN is a highly energetically favored process,[9] with the three coordinate (^{t}Bu(Ar)N)$_3$Mo complex able to cleave molecular nitrogen at cold temperatures.[10] The use of (^{t}Bu(Ar)N)$_3$MoN as a leaving group has been performed to transfer both atoms of oxygen and nitrogen. Oxygen has been transferred from analogous chromium nitrosyl complexes to 2 equivalents of V(III)

(Mesityl)$_3$V(THF) starting material to yield the V(IV) bridging oxo and Mo(VI) complexes.[11] The molybdenum congener has been theoretically shown to be a more favored process (Figure 2.2).[8]

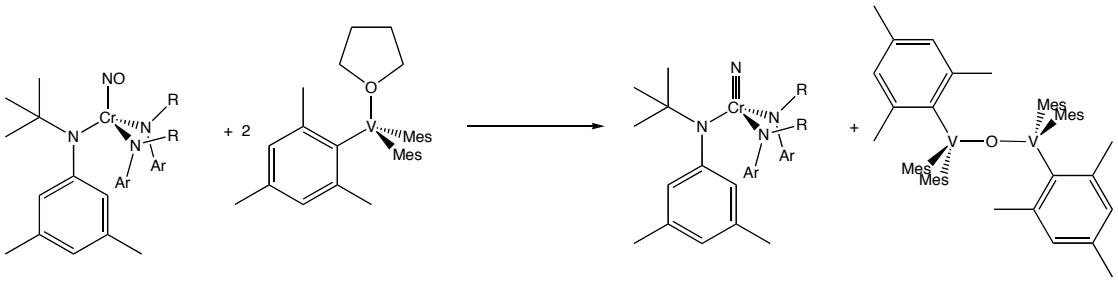

Figure 2.2 O-atom transfer from **(NO)Cr(NR(Ar)$_3$** to **(Mes)$_3$V(THF)**.

A nitrogen atom derived from N_2 in the complex (^{t}Bu(Ar)N)$_3$MoNNNa has been successfully transferred to Nb via the bridging compound (^{t}Bu(Ar)N)$_3$Mo(NN)Nb(^{t}Bu(Ar)N)$_3$ followed by reduction with KC_8 (Figure 2.3).[12]

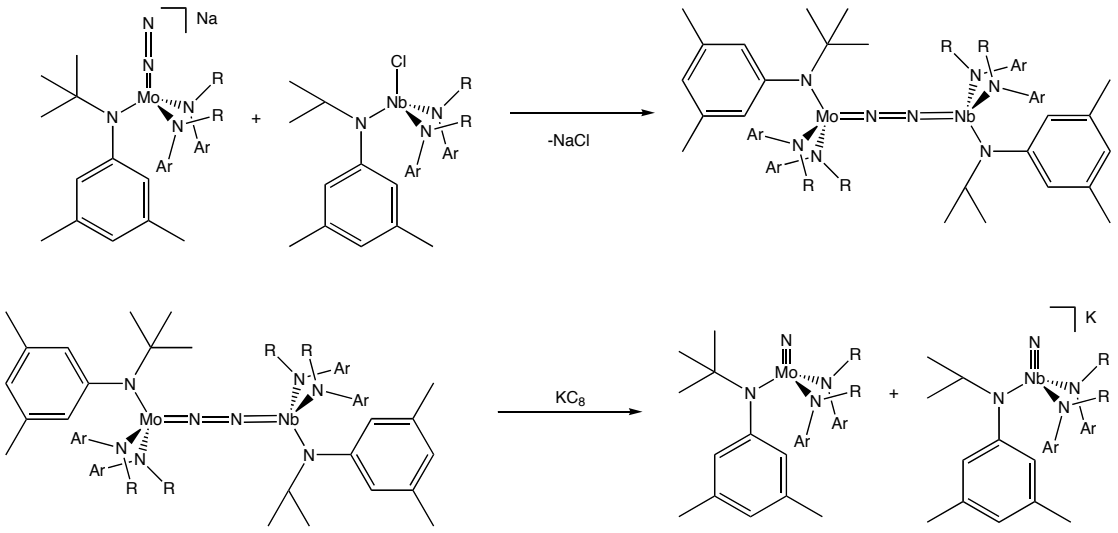

Figure 2.3 The cleavage of dinitrogen via a bridging Mo-NN-Nb intermediate.

Reactions with aryl and alkyl azide compounds with (^{iPr}PDI)Fe(N_2)$_2$ yield the imide compounds that contain heteroatom multiple bonds. In the case of certain aryl imides, the catalytic hydrogenation of the imide is possible. This rare metal-nitrogen hydrogenation/cleavage reaction highlights the unique reactivity imposed by the redox active ligand/iron cooperation in [PDIFe] complexes. [13,14,15,16,17,18] Here we attempt to extend this concept and generate multiply bonded heteroatoms (N or O) to [PDIFe] fragments through the use of molybdenum based atom tranfer reagents. Terminal functionality was not observed; bridging compounds were isolated instead

2.3 Preparation of μ-Oxo Complexes

Addition of (^{iPr}PDI)Fe(N_2)$_2$[19] to the molybdenum nitrosyl, (^{t}Bu(Ar)N)$_3$MoNO, complex in diethyl ether produced no reaction. In this case, the steric demand of the reactants is too large to allow reactivity. Stirring the smaller, bridging dinitrogen complex [(^{Et}PDI)FeN_2]$_2$(μ-N_2)[20] with (^{t}Bu(Ar)N)$_3$MoNO in diethyl ether overnight resulted in the quantitative conversion to (^{t}Bu(Ar)N)$_3$MoN and [(^{Et}PDI)Fe]$_2$(μ-O). Utilizing the methyl variant, [(^{Me}PDI)FeN_2]$_2$(μ-N_2), the bridging [(^{Me}PDI)Fe]$_2$(μ-O) was formed. The various methods of the synthesis of bridging PDI iron oxo-complexes is shown in Figure 2.4.

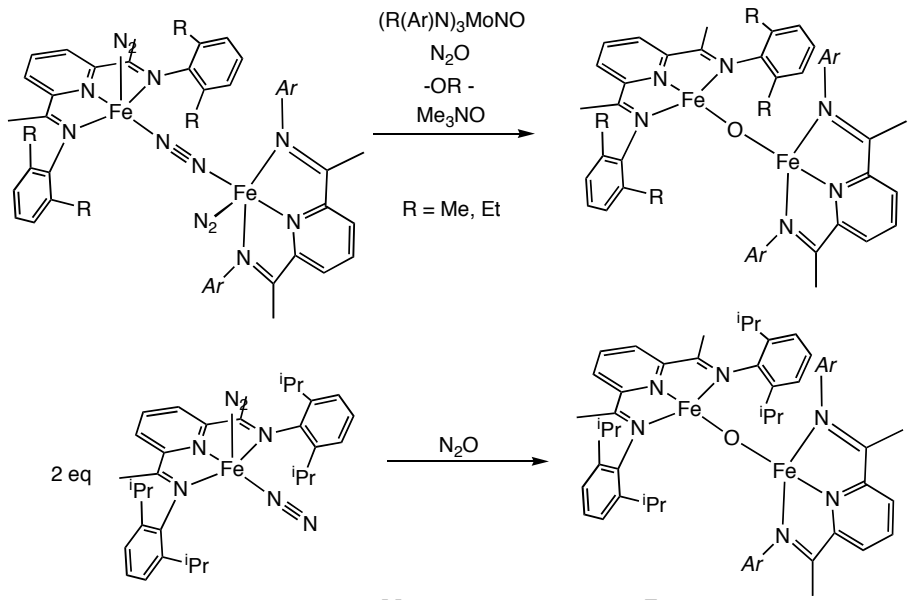

Figure 2.4 Syntheses of **[(^{Me}PDI)Fe]$_2$(μ-O)**, **[(^{Et}PDI)Fe]$_2$(μ-O)**, and **[(^{iPr}PDI)Fe]$_2$(μ-O)**.

An alternative route to these bridging oxo complexes was sought due to the stoichiometric molybdenum byproduct formed in the reaction. To this end, nitrous oxide was utilized as an oxygen atom source. The addition of one equivalent of nitrous oxide was added to a stirring solution of [(^{Me}PDI)FeN$_2$]$_2$(μ-N$_2$) via calibrated gas bulb addition. The resulting solution turned from red/purple to bronze as the reaction proceeded. Filtration through Celite and recrystallization from diethyl ether yielded [(^{Me}PDI)Fe]$_2$(μ-O) as a dark brown powder. Due to difficulty in growing crystals of [(^{Me}PDI)Fe]$_2$(μ-O), [(^{Et}PDI)Fe]$_2$(μ-O) was synthesized by the same method from [(^{Me}PDI)FeN$_2$]$_2$(μ-N$_2$). An X-ray quality crystal of [(^{Et}PDI)Fe]$_2$(μ-O) was obtained and the solid-state structure is shown in Figure 2.5.

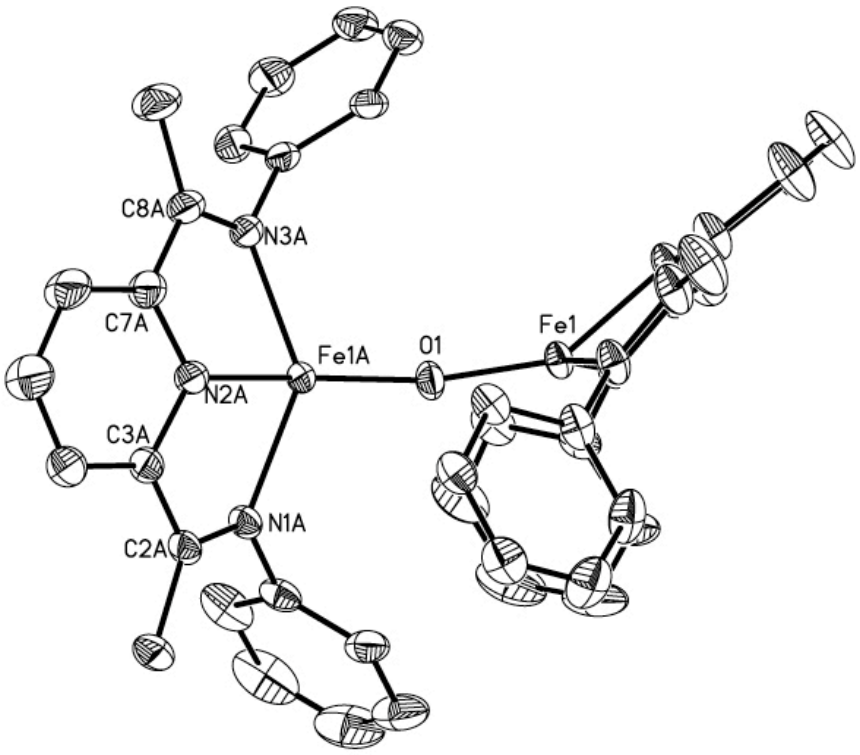

Figure 2.5 Solid-state structure of **[(^{Et}PDI)Fe]$_2$(μ-O)** shown at 30% probability ellipsoids. Ethyl groups and hydrogen omitted for clarity.

The metrical parameters of [(^{Et}PDI)Fe]$_2$(μ-O), presented in Table 2.1, are consistent with a high-spin ferrous center antiferromagnetically coupled to a bis(imino)pyridine radical anion. The structure has a crystallographically imposed C_2 axis, making the two iron centers equal. This description of the electronic structure can be confirmed by Mössbauer spectroscopy, as high-spin ferrous compounds supported by bis(imino)pyridine chelates are well characterized. [13] The Fe-N_{imine} bonds are rather long, at 2.097(2) Å and 2.110(2) Å for Fe(1)-N(1) and Fe(1)-N(3), respectively, indicating population of dx^2-y^2. The imine bond lengths have elongated to 1.313(3) Å and 1.318(4) Å for N(1)-C(2) and N(3)-C(8), respectively. The C_{ipso}-C_{imine} bond lengths have contracted to 1.444(4) Å and 1.436(4) Å for C(2)-C(3) and C(7)-C(8), respectively. This is in the well-established range of $[PDI]^{-1}$.

Table 2.1 Metrical parameters of **[(^{Et}PDI)Fe]$_2$(μ-O)** in the solid-state.

	[(^{Et}PDI)Fe]$_2$(μ-O)
Fe(1)-N(1)	2.097(2)
Fe(1)-N(2)	1.975(2)
Fe(1)-N(3)	2.110(2)
Fe(1)-O(1)	1.7721(5)
N(1)-C(2)	1.313(3)
N(3)-C(8)	1.318(4)
N(2)-C(3)	1.370(3)
N(2)-C(7)	1.373(4)
C(2)-C(3)	1.444(4)
C(7)-C(8)	1.436(4)
N(1)-Fe(1)-N(2)	76.15(9)
N(1)-Fe(1)-N(3)	138.00(9)
N(3)-Fe(1)-N(2)	75.98(9)
N(1)-Fe(1)-O(1)	109.20(9)
N(2)-Fe(1)-O(1)	147.63(9)
N(3)-Fe(1)-O(1)	111.22(8)
Fe(1)-O(1)-Fe(1)	165.72(17)

[(^{Me}PDI)Fe]$_2$(μ-O) is paramagnetic with an ^{1}H NMR spectrum that spans 80 ppm and has a number of peaks consistent with two equivalent iron centers with C_{2v} symmetry at 293 K. The NMR data are more contracted when compared to the analogous silanolate complex, (^{Me}PDI)Fe(OSiMe$_3$), a compound that exhibits a chemical shift range of over 400 ppm. The analogous [(^{Et}PDI)Fe]$_2$(μ-O) compound was synthesized in the same fashion, and the compound exhibits very similar spectral properties. Both compounds decomposed in the solid state at -35 ºC over the course of weeks. The ^{1}H NMR spectra of [(^{Me}PDI)Fe]$_2$(μ-O) and [(^{Et}PDI)Fe]$_2$(μ-O) are presented in Figure 2.6.

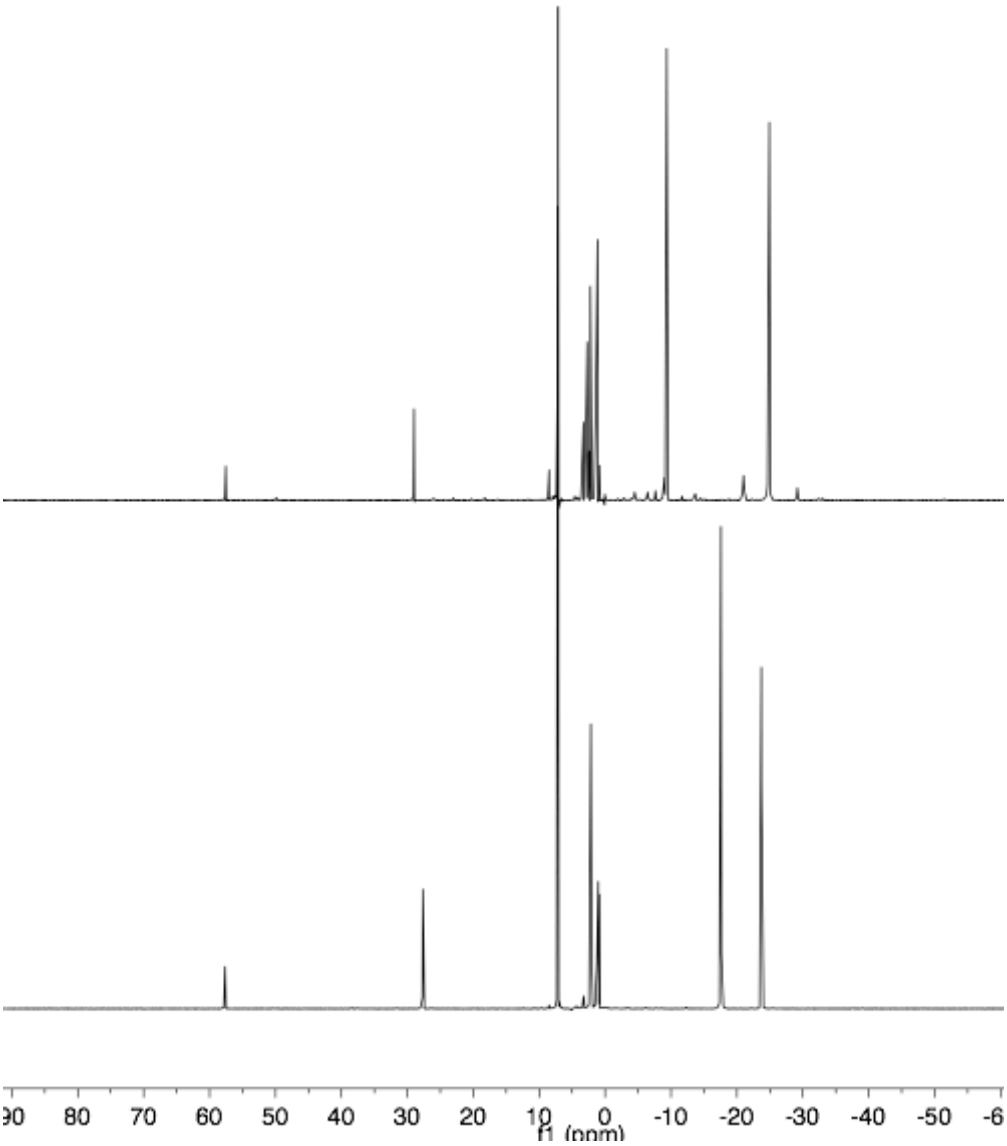

Figure 2.6 ^{1}H NMR spectrum of **[(^{Me}PDI)Fe]$_2$(μ-O)** and **[(^{Et}PDI)Fe]$_2$(μ-O)** in benzene-d_6 at room temperature.

The zero-field Mössbauer parameters were obtained for both [(^{Me}PDI)Fe]$_2$(μ-O) and [(^{Et}PDI)Fe]$_2$(μ-O). The spectra for both compounds exhibited multiple species at 80 K. When warmed to 293 K, a single quadrupole doublet was observed for both compounds; [(^{Me}PDI)Fe]$_2$(μ-O) yielded parameters of δ = 0.59 mm/s and ΔE_Q = 1.09 mm/s, while those for [(^{Et}PDI)Fe]$_2$(μ-O) were δ = 0.56 mm/s and ΔE_Q = 0.76 mm/s.

When the temperature was lowered to 80 K, however, two species were observed for both [(^{Me}PDI)Fe]$_2$(μ-O) and [(^{Et}PDI)Fe]$_2$(μ-O). The two species for [(^{Me}PDI)Fe]$_2$(μ-O had parameters of of $\delta = 0.72$ mm/s and $\Delta E_Q = 1.78$ mm/s for the species in 78 % and $\delta = 0.70$ mm/s and $\Delta E_Q = 1.20$ mm/s for the minor species in 22 %. The two species of [(^{Et}PDI)Fe]$_2$(μ-O) had parameters of $\delta = 0.67$ mm/s and $\Delta E_Q = 0.74$ mm/s for the species in 63 % and $\delta = 0.63$ mm/s and $\Delta E_Q = 1.05$ mm/s for the minor species in 37 %. Lowering the temperature further to 15 K resulted in the observation of two species for[(^{Me}PDI)Fe]$_2$(μ-O) and only one species for [(^{Et}PDI)Fe]$_2$(μ-O). The two species for [(^{Me}PDI)Fe]$_2$(μ-O) had parameters of of $\delta = 0.70$ mm/s and $\Delta E_Q = 1.24$ mm/s for the species in 68 % and $\delta = 0.73$ mm/s and $\Delta E_Q = 1.72$ mm/s for the minor species in 32 %. The species observed for [(^{Et}PDI)Fe]$_2$(μ-O) had parameters of of $\delta = 0.63$ mm/s and $\Delta E_Q = 1.01$ mm/s. These Mössbauer spectra are presented in Figure 2.7.

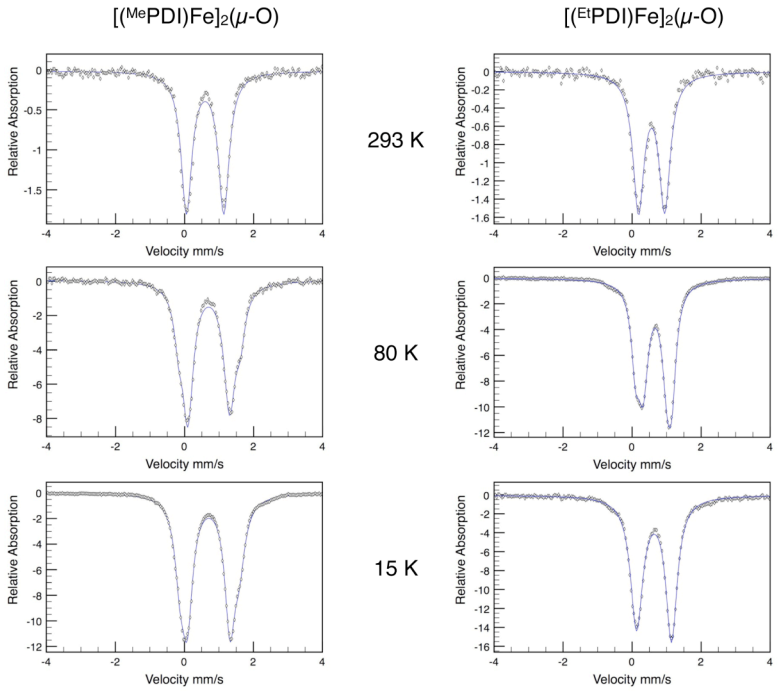

Figure 2.7 Variable temperature Mössbauer spectra for **[(^{Me}PDI)Fe]$_2$(μ-O)** and **[(^{Et}PDI)Fe]$_2$(μ-O)**.

The isomer shifts in the Mössbauer spectra are consistent with high-spin Fe(II) compounds. The temperature dependence indicates that there is fluxionality, either electronic or physical, in the solid-state. This unusual behavior has made the investigation into the magnetic behavior of [(^{Me}PDI)Fe]$_2$(μ-O) and [(^{Et}PDI)Fe]$_2$(μ-O) difficult. Solid state moments obtained at 290 K on a magnetic susceptibility balance yielded a μ_{eff} of 3.9 μB for [(^{Me}PDI)Fe]$_2$(μ-O) and 3.8 μB for [(^{Et}PDI)Fe]$_2$(μ-O). These numbers are consistent with overall S = 3/2 complexes, an unreasonable number of unpaired electrons. SQUID data obtained for [(^{Me}PDI)Fe]$_2$(μ-O) and [(^{Et}PDI)Fe]$_2$(μ-O) corroborate the 290 K magnetic moments, but attempts to fit the SQUID data to obtain D values were unsuccessful. The SQUID traces are presented in Figure 2.8.

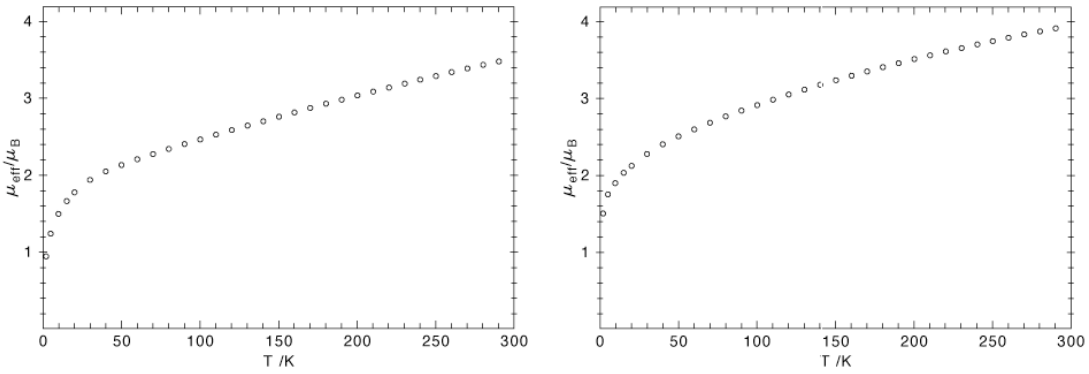

Figure 2.8 SQUID data for **[(^{Me}PDI)Fe]$_2$(μ-O)** on the left and **[(^{Et}PDI)Fe]$_2$(μ-O)** on the right.

The addition of nitrous oxide to (^{iPr}PDI)Fe(N_2)$_2$ yielded the bridging oxo complex, [(^{iPr}PDI)Fe]$_2$(μ-O). The compound was not isolated cleanly due to the copious amount of free ligand formed in the reaction. The steric bulk imposed by two (^{iPr}PDI)Fe fragments resulted in low yields. A crystal of the bridging compound was grown and picked from crystals of the free ligand. The solid-state structure of [(^{iPr}PDI)Fe]$_2$(μ-O) is presented in Figure 2.9.

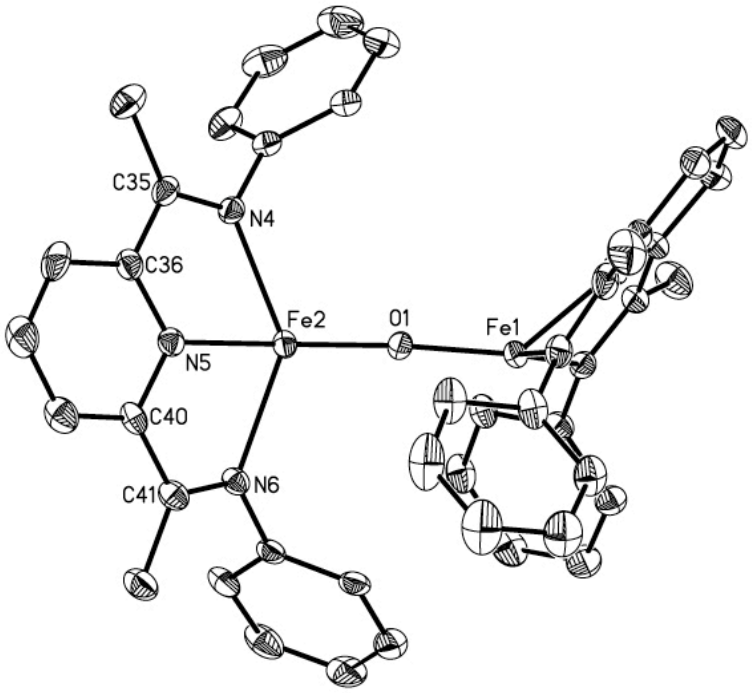

Figure 2.9 Solid-state structure of **[(^{iPr}PDI)Fe]$_2$(μ-O)** shown at 30% probability ellipsoids. Hydrogen atoms and isopropyl groups removed for clarity.

Much like the case of [(^{Et}PDI)Fe]$_2$(μ-O), [(^{iPr}PDI)Fe]$_2$(μ-O) has metrical parameters consistent with a high-spin ferrous complex anti-ferromagnetically coupled to a [PDI]$^{-}$. The largest difference in the two structures is the Fe(1)-O(1)-(Fe) angle, where [(^{iPr}PDI)Fe]$_2$(μ-O) has a more linear bond at 175.29(11)º compared to [(^{Et}PDI)Fe]$_2$(μ-O) that has an angle of 165.72(17)º. The Fe-N$_{imine}$ bonds are rather long, at 2.097(2) Å and 2.110(2) Å for Fe(1)-N(1) and Fe(1)-N(3), respectively, indicating population of dx^2-y^2 if the plane of the chelate is taken to be in the xy plane. The imine bond lengths have elongated to 1.313(3) Å and 1.318(4) Å for N(1)-C(2) and N(3)-C(8), respectively. The C$_{ipso}$-C$_{imine}$ bond lengths have contracted to 1.444(4) Å and 1.436(4) Å for C(2)-C(3) and C(7)-C(8), respectively. This is in the well-established range of [PDI]$^{-1}$. Important metrical parameters are reported in Table 2.2.

Table 2.2 Metrical parameters for **[(^{iPr}PDI)Fe]$_2$(μ-O)**.

	[(^{iPr}PDI)Fe]$_2$(μ-O)		[(^{iPr}PDI)Fe]$_2$(μ-O)
Fe(1)-N(1)	2.097(2)	Fe(2)-N(4)	2.226(2)
Fe(1)-N(2)	1.975(2)	Fe(2)-N(5)	2.000(2)
Fe(1)-N(3)	2.110(2)	Fe(2)-N(6)	2.228(2)
Fe(1)-O(1)	1.7721(5)	Fe(2)-O(1)	1.7994(16)
N(1)-C(2)	1.313(3)	N(4)-C(35)	1.322(3)
N(3)-C(8)	1.318(4)	N(6)-C(41)	1.306(3)
N(2)-C(3)	1.370(3)	N(5)-C(36)	1.365(3)
N(2)-C(7)	1.373(4)	N(5)-C(40)	1.378(3)
C(2)-C(3)	1.444(4)	C(35)-C(36)	1.446(4)
C(7)-C(8)	1.436(4)	C(40)-C(41)	1.433(4)
N(1)-Fe(1)-N(2)	76.15(9)	N(4)-Fe(2)-N(5)	74.34(8)
N(1)-Fe(1)-N(3)	138.00(9)	N(4)-Fe(2)-N(6)	137.85(8)
N(3)-Fe(1)-N(2)	75.98(9)	N(5)-Fe(2)-N(6)	73.37(8)
N(1)-Fe(1)-O(1)	109.20(9)	N(4)-Fe(2)-O(1)	113.41(8)
N(2)-Fe(1)-O(1)	147.63(9)	N(5)-Fe(2)-O(1)	141.36(8)
N(3)-Fe(1)-O(1)	111.22(8)	N(6)-Fe(2)-O(1)	108.74(8)
Fe(1)-O(1)-Fe(2)	175.29(11)	Fe(2)-O(1)-Fe(1)	175.29(11)

2.4 Preparation of μ-N_2 Complexes

The addition of [Na][(^{t}Bu(Ar)N)$_3$MoNN] to a stirring diethyl ether solution of (^{iPr}PDI)FeCl resulted in a near quantitative conversion to (^{t}Bu(Ar)N)$_3$Mo and (^{iPr}PDI)Fe(N_2)$_2$ resulting from reduction of the iron complex concurrent with oxidation of the molybdenum. Again, the steric demand of the two metal compounds was too great to yield fruitful reactivity. Present in the reaction mixture, however, was a new paramagnetic compound in *ca* 5-10 %. Smaller PDI ligands were next explored for this chemistry.

When the reaction was run with (^{Et}PDI)FeCl [21] in place of (^{iPr}PDI)FeCl, the addition of [Na][(^{t}Bu(Ar)N)$_3$MoNN] yielded primarily a new paramagnetic complex with only small quantities of products derived from reduction. Using less sterically demanding complex, (^{Me}PDI)FeCl, produced an even cleaner reaction. Removing the diethyl ether from the reaction mixture, and then dissolving and filtering the residue in pentane, followed by recrystallization, yielded dark green crystals that were identified as [(^{Me}PDI)Fe](μ-N$_2$)[Mo(N(Ar)^{t}Bu)$_3$].

The IR spectrum of [(^{Me}PDI)Fe](μ-N$_2$)[Mo(N(Ar)^{t}Bu)$_3$] in KBr had a sharp absorption at ν = 1685 cm^{-1}. This was assigned as the bridging dinitrogen stretching frequency. The NMR spectrum at 293 K displayed the right number of peaks for a *C*s symmetric compound, and the chemical shift range of over 500 ppm is reminiscent of many other PDIFe(X) type compounds. An X-ray quality crystal was grown from a pentane solution, and the structure is presented in Figure 2.10.

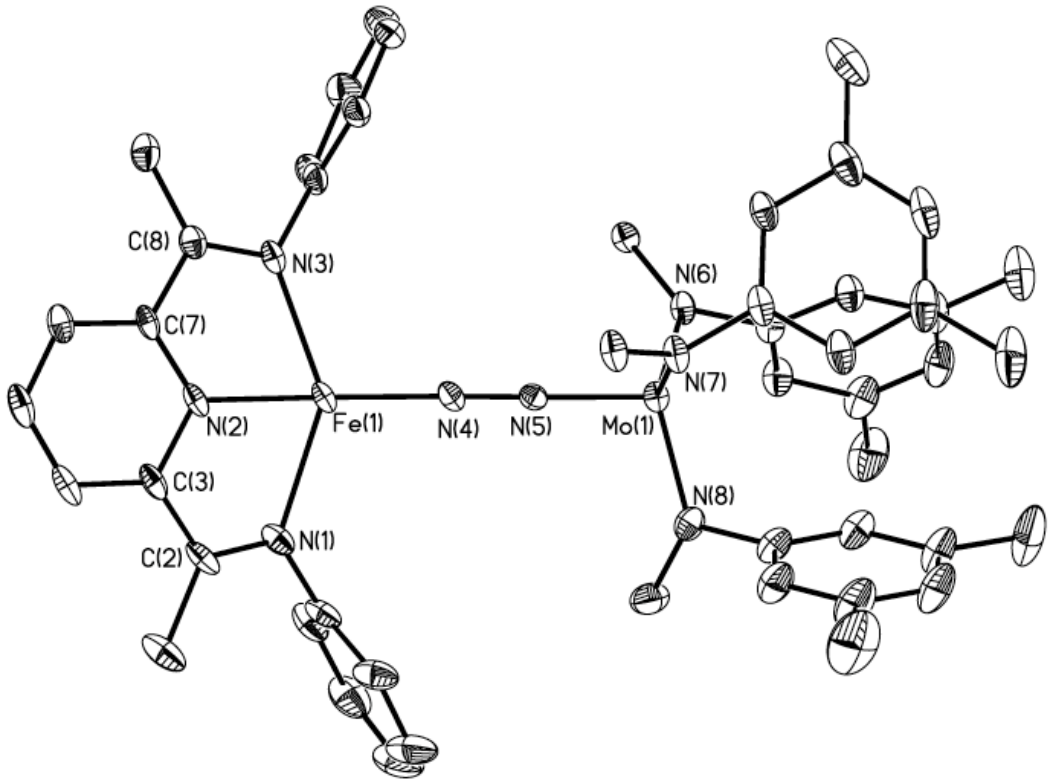

Figure 2.10 Solid-state structure of **[(^{Me}PDI)Fe](μ-N_2)[Mo(N(Ar)^{t}Bu)$_3$]** at 30% probability ellipsoids. Hydrogen atoms, PDI aryl methyl groups, and ^{t}butyl groups removed for clarity.

The metrical parameters of the bis(imino)pyridine chelate indicate a single electron reduction of the ligand, with the imine bonds lengthened to distances of 1.308(5) Å and 1.318(5) Å for N(1)-C(2) and N(3)-C(8), respectively. The bonds of C(2)-C(3) and C(7)-C(8) have contracted to 1.425(6) Å 1.442(5) Å, respectively. The Fe-N_{imine} bond distances are long and indicate the population of dx^2-y^2 in a high-spin iron environment with Fe(1)-N(1) at 2.208(3) Å and Fe(1)-N(3) at 2.194(3) Å. The dinitrogen bridge has an N(4)-N(5) bond length of 1.202(4) Å, indicating double reduction of the bridging dinitrogen. This configuration indicates that the iron contributes one electron to the dinitrogen and the molybdenum contributes the other, giving a Mo(IV) center. The dinitrogen is not activated enough to produce useful

functionalization when either H_2 or CO is added to [(^{Me}PDI)Fe](μ-N_2)[Mo(N(Ar)^{t}Bu)$_3$]. Hydrogen fails to react and CO displaces the nitrogen ligand, giving (^{Me}PDI)Fe(CO)$_2$ and (N(Ar)^{t}Bu)$_3$MoCO, both of which are previously characterized complexes. The important metrical parameters are presented in Table 2.3.

Table 2.3 Metrical parameters for **[(^{Me}PDI)Fe](μ-N_2)[Mo(N(Ar)^{t}Bu)$_3$]**.

	(^{Me}PDI)Fe(μ-N_2) Mo(N(Ar)R)$_3$
Fe(1)-N(1)	2.208(3)
Fe(1)-N(2)	1.998(3)
Fe(1)-N(3)	2.194(3)
Fe(1)-N(4)	1.866(3)
N(1)-C(2)	1.308(5)
N(3)-C(8)	1.318(5)
N(2)-C(3)	1.363(5)
N(2)-C(7)	1.350(5)
C(2)-C(3)	1.425(6)
C(7)-C(8)	1.442(5)
N(4)-N(5)	1.202(4)
N(1)-Fe(1)-N(2)	74.60(13)
N(1)-Fe(1)-N(3)	140.19(13)
N(3)-Fe(1)-N(2)	74.61(13)
N(1)-Fe(1)-N(4)	108.27(14)
N(2)-Fe(1)-N(4)	159.23(14)
N(3)-Fe(1)-N(4)	109.51(13)
Fe(1)-N(4)-N(5)	177.8(3)

Zero-field Mössbauer parameters were obtained for [(^{Me}PDI)Fe](μ-N_2)[Mo(N(Ar)^{t}Bu)$_3$], and the parameters were consistent with a high-spin Fe(II) center with an isomer shift of 0.86 mm/s and quadrupole splitting of 0.99 mm/s. This data is

consistent with both the ^{1}H NMR data and the crystal structure in that the iron is ferrous and the PDI is anti-ferromagnetically coupling to a mono-reduced chelate, very much a similar electronic structure as a number of mono-X type compounds of PDI iron. The Mössbauer spectrum is presented in Figure 2.11.

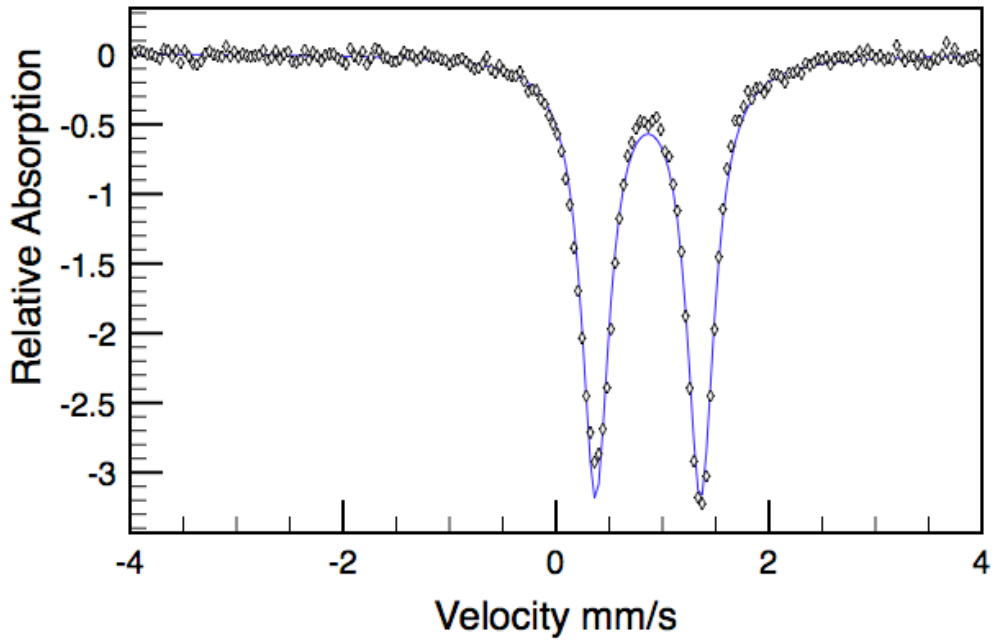

Figure 2.11 Zero-field Mössbauer spectrum of **[(^{Me}PDI)Fe](μ-N$_2$)[Mo(N(Ar)^{t}Bu)$_3$]** obtained at 80 K.

Magnetic data obtained on a magnetic susceptibility balance of [(^{Me}PDI)Fe](μ-N$_2$)[Mo(N(Ar)^{t}Bu)$_3$] at 290 K furnished a μ_{eff} = 3.8 μB, indicating an overall magnetic moment of S=3/2. Variable temperature SQUID data collected on the complex indicates unusual magnetic behavior, but the room temperature moment was consistent between the two methods. The SQUID data was fit with three paramagnetic centers, the iron containing 3 unpaired electrons, the doubly reduced nitrogen with two unpaired electrons, and the molybdenum center with two unpaired electrons also. This

data rules out an alternative electronic structure description that would have a singlet molybdenum and a singlet bridging dinitrogen, and the contribution of magnetism comes only from the $S = 3/2$ iron center. The SQUID trace is presented in Figure 2.12.

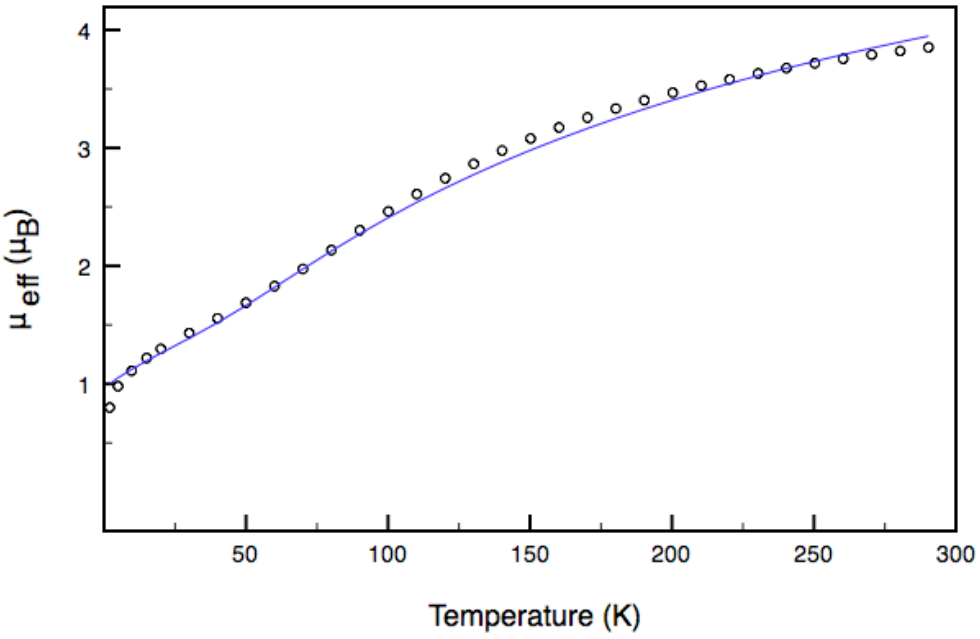

Figure 2.12 SQUID data for **[(^{Me}PDI)Fe](μ-N_2)[Mo(N(Ar)^{t}Bu)$_3$]**.

The fit from the SQUID trace revealed a complicated coupling scheme between the three spin systems. The effective moment at 290 K is consistent with the moment obtained by magnetic susceptibility balance. The low temperature behavior is difficult to model and requires large D values from both the molybdenum and iron centers.

The EPR spectrum of [(^{Me}PDI)Fe](μ-N_2)[Mo(N(Ar)^{t}Bu)$_3$] corroborates the proposed electronic structure for the iron center. The spectrum was obtained in toluene glass at 10 K. The spectrum is rhombic with a large g-anisotropy and is consistent

with an *S*=3/2 compound. There is impurity from the three-coordinate molybdenum compound, as well as some decomposition of the material. The spectrum is shown in Figure 2.13.

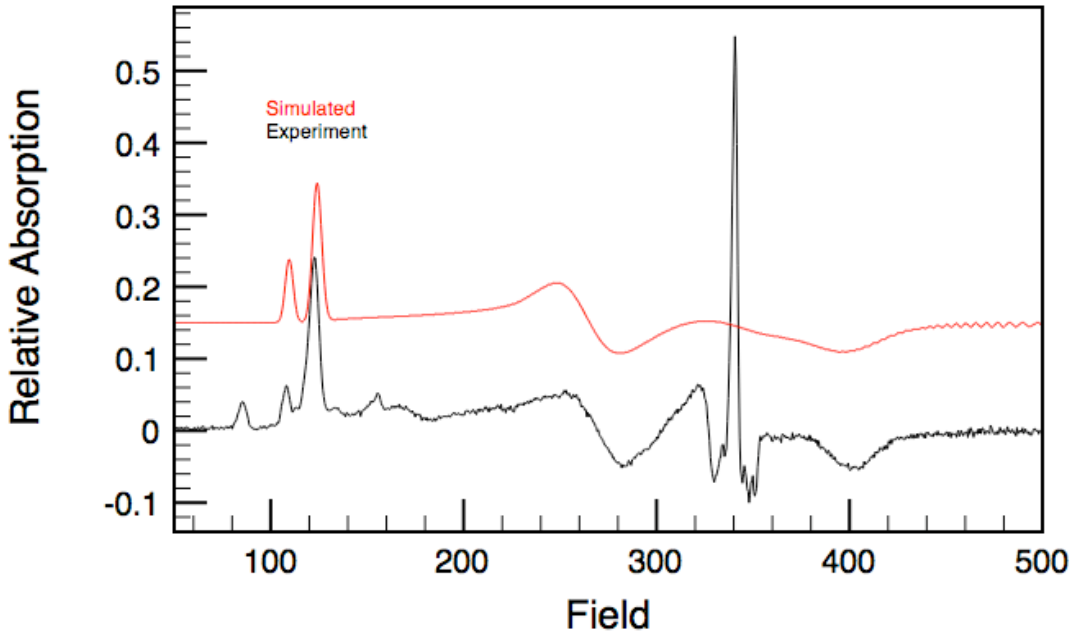

Figure 2.13 10 K EPR spectrum of **[(^{Me}PDI)Fe](μ-N_2)[Mo(N(Ar)^{t}Bu)$_3$]** in toluene glass.

The large spike in the spectrum is due to an impurity. The fit of the spectrum gives g values of g_{min} = 2.05, g_{mid} = 2.20 and g_{max} = 2.23. A D value of 0.84 was obtained and value of E/D of 0.28 is indicative of a large anisotropy, which is also consistent with the large values obtained from the SQUID fit. These data, along with the SQUID and Mössbauer data, suggest that [(^{Me}PDI)Fe](μ-N_2)[Mo(N(Ar)^{t}Bu)$_3$] behaves as a simple PDIFe-X type complex, although the electronic details are far from simple.

The fact that cleavage of the bridging dinitrogen ligand in [(^{Me}PDI)Fe](μ-N_2)[Mo(N(Ar)^{t}Bu)$_3$] does not occur can be attributed to the redox activity of the bis(imino)pyridine chelate. Electron density from the iron center needed to cleave the N_2 bond is instead found in the π^* system of the chelate. Another route, therefore, is needed in order to synthesize the desired planar, 4-coordinate bis(imino)pyridine iron nitride.

2.5 Conclusion

Two new classes of bridging, paramagnetic bis(imino)pyridine iron complexes were synthesized and studied. The homo bridging oxo dimmers [(^{Me}PDI)Fe]$_2$(μ-O), [(^{Et}PDI)Fe]$_2$(μ-O), and [(^{iPr}PDI)Fe]$_2$(μ-O) were all synthesized from nitrous oxide. [(^{Me}PDI)Fe]$_2$(μ-O) and [(^{Et}PDI)Fe]$_2$(μ-O) could also be synthesized from one equivalent of (^{t}Bu(Ar)N)$_3$MoNO added to one equivalent of either [(^{Me}PDI)FeN$_2$]$_2$(μ-N_2) or [(^{Et}PDI)FeN$_2$]$_2$(μ-N_2). These complexes showed temperature dependant conformations, either electronic or geometric, that made a full characterization of their electronic structures difficult, but each iron center appears to be high-spin ferrous, and there is some degree of coupling through the bridging oxo ligand to lower the magnetic moment to ~3.8 μB. Heter bridging dinitrogen dimer of [(^{Me}PDI)Fe](μ-N_2)[Mo(N(Ar)^{t}Bu)$_3$] also contains a high-spin ferrous center. The magnetism of the complex is consists of an $S = 3/2$ iron and a triplet dinitrogen and Mo(IV) centers. The coupling from these spin-centers yields the observed SQUID data. The redox activity of the bis(imino)pyridine iron unit in this instance is detrimental to the desired reactivity of cleavage of the N_2 unit.

2.6 Experimental Procedures

General Considerations. All air- and moisture-sensitive manipulations were carried out using standard vacuum line, Schlenk, and cannula techniques or in an MBraun inert atmosphere dry box containing an atmosphere of purified nitrogen. Solvents for air- and moisture-sensitive manipulations were initially dried and deoxygenated using literature procedures.[22] Benzene-d_6 was purchased from Cambridge Isotope Laboratories and dried over 4 Å molecular. The complexes $[(^{Me}PDI)FeN_2]_2(\mu\text{-}N_2)$,[19] $[(^{Et}PDI)FeN_2]_2(\mu\text{-}N_2)$,[19] ($^{Et}PDI)FeCl$, ($^{iPr}PDI)Fe(N_2)_2$,[18] ($^{t}Bu(Ar)N)_3MoNO$, and ($^{t}Bu(Ar)N)_3MoNNNa$ were prepared according to literature procedures.

^1H NMR spectra were recorded on Varian Mercury 300 and Inova 400, spectrometers operating at 299.76, 399.78 MHz, respectively. All ^1H chemical shifts are reported relative to $SiMe_4$ using the ^1H (residual). For diamagnetic complexes, many assignments were made based on COSY and HSQC NMR experiments. Solution magnetic moments were determined by Evans method[23] using a ferrocene standard and are the average value of at least two independent measurements. Magnetic susceptibility balance measurements were performed with a Johnson Matthey instrument that was calibrated with $HgCo(SCN)_4$. Peak widths at half heights are reported for paramagnetically broadened and shifted resonances. Infrared spectra were collected on a Thermo Nicolet spectrometer. Elemental analyses were performed at Robertson Microlit Laboratories, Inc., in Madison, NJ.

Single crystals suitable for X-ray diffraction were coated with polyisobutylene oil in a drybox, transferred to a nylon loop and then quickly transferred to the goniometer head of a Bruker X8 APEX2 diffractometer equipped with a molybdenum X-ray tube (l = 0.71073 Å). Preliminary data revealed the crystal system. A hemisphere routine was used for data collection and determination of lattice constants. The space group was identified and the data were processed using the Bruker SAINT+

program and corrected for absorption using SADABS. The structures were solved using direct methods (SHELXS) completed by subsequent Fourier synthesis and refined by full-matrix least-squares procedures.

Mössbauer data were collected on an alternating constant-acceleration spectrometer. The minimum experimental line width was 0.24 mm s^{-1} (full width at half height). A constant sample temperature was maintained with an Oxford Instruments Variox or an Oxford Instruments Mössbauer-Spectromag 2000 cryostat. Reported isomer shifts (δ) are referenced to iron metal at 293 K.

Preparation of [(^{iPr}PDI)Fe]$_2$(μ-O). A thick walled glass vessel was charged with 0.300 g (0.50 mmol) of 1-N_2 and 50 mL toluene. The vessel was placed in a dry-ice/acetone bath and degassed on a high vacuum line. A calibrated glass bulb (0.1001 L) was used to transfer 0.25 mmol of nitrous oxide to the frozen iron solution. The high pressure vessel was thawed with vigorous shaking under running tap water. The solution changed from green to dark red as the solution thawed. The reaction was placed on a dry ice/acetone bath and degassed. The toluene solution was filtered through Celite and the volatiles were removed. The residue was taken up in a minimum amount of diethyl ether and placed in a freezer at-35 °C for 12 hours. NMR spectroscopy of the solid indicated a high percentage of free ligand. Filtration yielded a dark red/brown powder identified as [(^{iPr}PDI)Fe]$_2$(μ-O). X-Ray quality crystals were grown from a dilute ether solution at -35 °C. ^{1}H NMR (benzene-d_6): δ -250.66 (62 Hz, 6H, C(CH_3)), -24.48 (308 Hz, 2H, CH_2CH$_3$), -66.10 (257 Hz, 2H, CH_2CH$_3$),), -27.70 (68 Hz, 12H, CH$_2$CH_3), -16.09 (31 Hz, 2H, *p-aryl*), -11.90 (37 Hz, 4H, *m-aryl*), 67.38 (87 Hz, 2H, *m-pyr*), 91.06 (443 Hz, 9H, C(CH_3)$_3$), 347.84 (235 Hz, 1H, *p-pyr*), Fe-CH_2C(CH$_3$)$_3$.

Preparation of [(^{Et}PDI)Fe]$_2$(μ-O). This complex was prepared in a manner similar to **[(^{iPr}PDI)Fe]$_2$(μ-O)** with 0.525 g (0.502 mmol) of **[(^{Et}PDI)Fe(N$_2$)]$_2$(μ-N$_2$)** to yield 0.330 g (67%) of a dark red/brown brown powder identified as **[(^{Et}PDI)Fe]$_2$(μ-O)**. X-Ray quality crystals were grown from a dilute ether solution at -35 °C. Analysis for $C_{58}H_{70}N_6FeO$: Calcd C, 75.47; H, 7.64; N, 9.10. Found: C, 69.36; H,7.99; N, 8.26. Magnetic susceptibility: $\mu_{eff} = 3.8\ \mu_B$ (benzene-*d*$_6$). ^{1}H NMR (benzene-*d*$_6$): δ -24.90 (14 Hz, 6H, C(C*H*$_3$)), -21.03 (20 Hz, 8H, Ar-*Me*), -9.36 (20 Hz, 12H, Ar-*Me*), 1.45 (18 Hz, 2H, *p-Ar*), 2.75 (14 Hz, 4H, *m-Ar*), 27.65 (15 Hz, 2H, *m-Py*), 57.68 (12 Hz, 1H, *p-Py)*.

Alternative Preparation of [(^{Et}PDI)Fe]$_2$(μ-O). To a stirring diethyl ether solution of 0.100 g (0.095 mmol) of **[(^{Et}PDI)Fe(N$_2$)]$_2$(μ-N$_2$)** was added 0.007 g (0.095 mmol) of Me_3NO. The reaction mixture was stirred for 1 hour, over which time the color changed from maroon to bronze. The solution was filtered, concentrated, cooled to -35 ºC overnight, and the solid filtered to yield 0.075 g of **[(^{Et}PDI)Fe]$_2$(μ-O)**.

O-Atom Transfer in the Synthesis of [(^{Et}PDI)Fe]$_2$(μ-O). To a stirring diethyl ether solution of 0.100 g (0.095 mmol) of **[(^{Et}PDI)Fe(N$_2$)]$_2$(μ-N$_2$)** was added 0.062 g (0.095 mmol) of **(^{t}Bu(Ar)N)$_3$MoNO**. The reaction mixture was stirred for 1 hour, over which time the color changed from maroon to bronze. The solution was filtered through Celite, and the volatiles were removed. Analysis of the residue showed conversion to **[(^{Et}PDI)Fe]$_2$(μ-O)** and **(^{t}Bu(Ar)N)$_3$MoN.**

Preparation of [(^{Me}PDI)Fe]$_2$(μ-O). This complex was prepared in a manner similar to **[(^{iPr}PDI)Fe]$_2$(μ-O)** with 0.400 g (0.428 mmol) of **[(^{Me}PDI)Fe(N$_2$)]$_2$(μ-N$_2$)** to yield 0.270 g (72%) of a dark red brown powder identified as **[(^{Me}PDI)Fe]$_2$(μ-O)**. Analysis

for $C_{50}H_{54}N_6FeO$: Calcd C, 74.06; H, 6.71; N, 10.36. Found: C, 69.61; H, 7.31; N, 8.22. Magnetic susceptibility: μ_{eff} = 3.8 μ_B (benzene-d_6). ^{1}H NMR (benzene-d_6): δ -23.71 (14 Hz, 6H, C(C*H*$_3$)), -17.56 (20 Hz, 12H, Ar-*Me*), 1.03 (21 Hz, 2H, *p-Ar*), 2.16 (13 Hz, 4H, *m-Ar*), 27.65 (15 Hz, 2H, *m-Py*), 57.68 (12 Hz, 1H, *p-Py)*.

Alternative Preparation of [(^{Me}PDI)Fe]$_2$(μ-O). To a stirring diethyl ether solution of 0.100 g (0.107 mmol) of **[(^{Me}PDI)Fe(N$_2$)]$_2$(μ-N$_2$)** was added 0.008 g (0.107 mmol) of Me_3NO. The reaction mixture was stirred for 1 hour, over which time the color changed from maroon to bronze. The solution was filtered, concentrated, cooled to -35 ºC overnight, and the solid filtered to yield 0.055 g of **[(^{Me}PDI)Fe]$_2$(μ-O)**.

O-Atom Transfer in the Synthesis of [(^{Me}PDI)Fe]$_2$(μ-O). To a stirring diethyl ether solution of 0.100 g (0.107 mmol) of **[(^{Me}PDI)Fe(N$_2$)]$_2$(μ-N$_2$)** was added 0.070 g (0.107 mmol) of **(^{t}Bu(Ar)N)$_3$MoNO**. The reaction mixture was stirred for 1 hour, over which time the color changed from maroon to bronze. The solution was filtered through Celite, The solution was filtered through Celite, and the volatiles were removed. Analysis of the residue showed conversion to **[(^{Me}PDI)Fe]$_2$(μ-O)** and **(^{t}Bu(Ar)N)$_3$MoN.**

Preparation of [(^{Me}PDI)Fe](μ-N$_2$)[Mo(N(Ar)^{t}Bu)$_3$]. To a stirring diethyl ether solution of 0.147 g (0.218 mmol) **(N(Ar)^{t}Bu)$_3$MoNNNa** was added a diethyl ether solution of 0.100 g (0.218 mmol) **(^{Me}PDI)FeCl**. The solution took on a dark, forest green color and a precipitate belived to be NaCl was formed. The solution was filtered through Celite and the volatiles were removed. The residue was taken into pentane, filtered through Celite, and cooled to -35 ºC overnight. The crystals were collected in a glass frit and dried under reduced pressure giving 0.130 g (55%) **[(^{Me}PDI)Fe](μ-**

N_2)[Mo(N(Ar)^{t}Bu)$_3$]. Analysis for $C_{50}H_{54}N_6FeO$: Calcd C, 69.29; H, 6.28; N, 9.70. Magnetic susceptibility: $\mu_{eff} = 3.7\ \mu_B$ (benzene-d_6). ^{1}H NMR (benzene-d_6): δ -216.16 (280 Hz, 6H, C(C*H*$_3$)), -55.39 (240 Hz, 12H, Ar-*Me*), -13.49 (45 Hz, 6H, *o-Ar*), -13.26 (36 Hz, 4H, *m-Ar*), 6.00 (153 Hz, 18H, *m-Ar CH*$_3$), 9.31 (22 Hz, 3H, *p-Ar)* 19.22 (350 Hz ,27 H, tBu), 55.98 (105 Hz, 2H, *m-Py*), 348.66 (12 Hz, 1H, *p-Py*).

Preparation of (^{Me}PDI)FeCl. To a stirring 1% sodium amalgam in 50 mL toluene was added 2.000 g (4.030 mmol) of (^{Me}PDI)FeCl$_2$ and 50 mL of diethyl ether. The reaction was stirred overnight at room temperature, at which time the stirring was stopped and the amalgam settled. The solution was filtered through Celite and the volatiles were removed. The residue was slurried with pentane, and filtered to yield 1.300 g (70%) of a green powder identified as (^{Me}PDI)FeCl.

REFERENCES

[1] Musie, G.; Lai, C.; Reibenspies, J. H.; Sumner, L. W.; Darensbourg, M. Y. *Inorg. Chem.* **1998**, *37*, 4086.

[2] Eckert, N. A.; Stoin, S.; Smith, J. M.; Bominaar, E. L.; Münck, E.; Holland, P. L. *J. Am. Chem. Soc.* **2005**, 127, 9344.

[3] G. Ertl, *Chem. Rec*. **2001**, 1, 33.

[4] J. B. Howard, D. C. Rees, *Chem. Rev*. **1996**, 96, 2965.

[5] Scepaniak, J. J.; Young, J. A.; Bontchev, R. P.; Smith, J. M. *Angew. Chem.* **2009,** 121, 3204-3206.

[6] Vogel, C.; Heinemann, F. W.; Sutter, J.; Anthon, C.; Meyer, K. *Angew. Chem.* **2008,** 47, 1-5.

[7] Meyer, K.; Bill, E.; Mienert, B.; Weyhermüller, T.; Wieghardt*,* K. *J. Am. Chem. Soc*. **1999**, 121, 4859 – 4876.

[8] Betley, T. A. and Peters, J. C. . *J. Am.* Chem. Soc., **2004**, 26*,* 6252.

[9] Musaev, D. G. ; Cui, Q.; Svensson, M.; Morokuma, K. *Transition State Modeling for Catalysis.* **April 8, 1999**, 198-207.

[10] a) Laplaza, C. E.; Cummins, C. C. *Science*, **1995**, 268, 861 b) Laplaza, C. E.; Johnson, M. J. A.; Peters, J. C.; Odom, A. L.; Kim, E.; Cummins, C. C.; George, G. N.; Pickering I. J. *J. Am. Chem. Soc.* **1996,** *118*, 8623.

[11] Odom, A.L. and Cummins, C. C. *J. Am.* Chem. Soc., **1995**, 117*,* 6613.

[12] Figueroa, J. S.; Piro, N. A.; Clough, C. R.; Cummins, C. C.;*J. Am. Chem. Soc.* **2006,** *128*, 940.

[13] a) Knijnenburg, Q.; Gambarotta, S.; Budzelaar, P. H. M. *Dalton Trans.* **2006**, 5442. b) Bart, S. C.; Chlopek, K.; Bill, E.; Bouwkamp, M. W.; Lobkovsky, E.; Neese, F.; Wieghardt, K.; Chirik, P. J. *J. Am. Chem. Soc.* **2006**, *128*, 13901.

[14] Butin, K. P.; Beloglazkina, E. K.; Zyk, N. V. *Russ. Chem. Rev*. **2005**, *74*, 53.

[15] Kuwabara, I. H.; Comninos, F. C. M.; Pardini, V. L.; Viertler, H.; Toma, H. E. *Electrochim. Acta* **1994**, *39*, 2401.

[16] Toma, H. E.; Chavez-Gil, T. E. *Inorg. Chim. Acta* **1997**, *257*, 197.

[17] de Bruin, B.; Bill, E.; Bothe, E.; Weyermüller, T.; Wieghardt, K. *Inorg. Chem.* **2000**, *39*, 2936.

[18] Budzelaar, P. H. M.; de Bruin, B.; Gal, A. W.; Wieghardt, K.; van Lenthe, J. H. *Inorg. Chem.* **2001**, *40*, 4649.

[19] Bart, S. C.; Lobkovsky,E.; Chirik, P.J., *J. of the Am. Chem. Soc.* **2004,** *126* (42), 13794.

[20] Russell, S. K.; Darmon, J. M.; Lobkovsky, E.; Chirik P. J. *Inorg. Chem.* **2010,** *49*, 2782.

[21] M. A. Bouwkamp , S. C. Bart , E. J. Hawrelak , R. J. Trovitch , E. P. Lobkovsky , J. Chirik , *Chem. Commun.* **2005**, 3406.

[22] Pangborn, A. B.; Giardello, M. A.; Grubbs, R. H.; Rosen, R. K.; Timmers, F. J. *Organometallics* **1996**, *15*, 1518.

[23] Sur, S. K. *J. Magn. Reson.* **1989**, *82*, 169.

CHAPTER 3

THE SYNTHESIS AND ELECTRONIC STRUCTURE OF CATIONIC AND ANIONIC BIS(IMINO)PYRIDINE IRON ALKYL COMPLEXES*

3.1 Abstract

A new, more generalized synthetic route to the catalytically relevant, 14 electron compounds of the type $[(^{iPr}PDI)Fe\text{-}R][BPh_4]$ (^{iPr}PDI = 2,6-(2,6-$^{i}Pr_2$-$C_6H_3N{=}CMe)_2C_5H_3N$; R = CH_2SiMe_3, CH_2CMe_3 or CH_3) has been developed. This new method allows for a variety of catalytically active PDI iron alkyl complexes to be made easily from PDI iron mono alkyl complexes. The resultant mono alkyl cationic compounds have been characterized as high-spin Fe(II) compounds supported by an neutral bis(imino)pyridine. $[Li(Et_2O)_3][(^{iPr}PDI)Fe(CH_2CMe_3)N_2]$ was synthesized to determine the degree of PDI participation in the overall electronic structure of these compounds over three oxidation states: anionic, neutral, and cationic. $[Li(Et_2O)_3][(^{iPr}PDI)Fe(R)N_2]$ were characterized as low-spin Fe(II) compounds supprted by a singlet diradical PDI chelate. The electronic structures of the charged compounds were determined utilizing a combination of magnetic data, crystallography, NMR and Mössbauer spectroscopies, and DFT calculations. The conclusions drawn highlight the importance of electronic structure and its relevance to single component olefin polymerization catalysis.

3.2 Introduction

Formally 14-electron bis(imino)pyridine iron alkyl cations, $[(^{Ar}PDI)Fe\text{-}R]^+$, have been long-standing targets for single component iron polymerization catalysts.[1] The synthesis of the bis(imino)pyridine iron alkyl cation was accomplished by

* Parts of this chapter have been taken from (a) Tondreau, A. M.; Milsmann, C.; Patrick, A. D.; Hoyt, H. M.; Lobkovsky, E.; Wieghardt, K.; Chirik, P. J. *J. Am. Chem. Soc.* **2010***,* 132, 15046. Copyright 2010 American Chemical Society.

protonation of (^{iPr}PDI)Fe(CH_2SiMe_3)$_2$ with [$PhNMe_2H$][BPh_4] to yield [(^{iPr}PDI)Fe(CH_2SiMe_3)][BPh_4]. When $B(C_6F_5)_3$ is added to (^{iPr}PDI)Fe(CH_2SiMe_3)$_2$, a silicon methide was abstraction and yielded [(^{iPr}PDI)Fe($CH_2SiMe_2CH_2SiMe_3$)]-[$MeB(C_6F_5)_3$] following alkyl migration. Crystalline compounds were obtained upon addition Et_2O and THF and both [(^{iPr}PDI)Fe(CH_2SiMe_3)L][BPh_4] (L = Et_2O, THF) have been structurally characterized, as has[(^{iPr}PDI)Fe($CH_2SiMe_2CH_2SiMe_3$)]-[$MeB(C_6F_5)_3$].[2] Upon exposure to ethylene, all three iron compounds serve as single component polymerization catalysts and yield linear polyethylene terminated by olefin end groups arising from α-hydrogen elimination. This reactivity is shown in Figure 3.1.

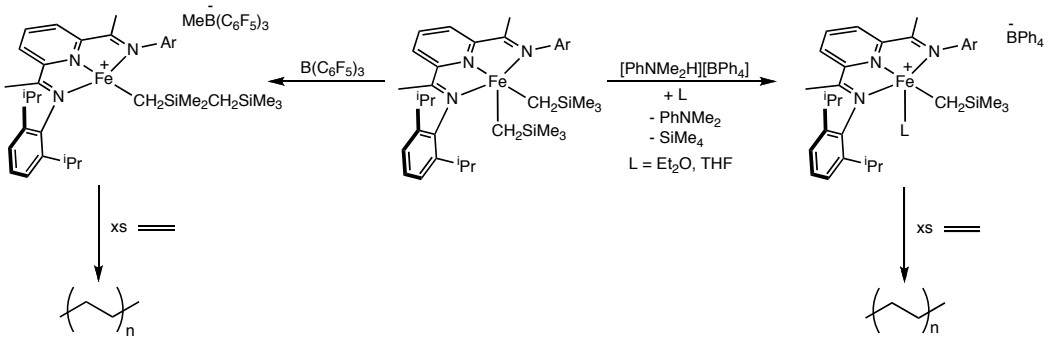

Figure 3.1 The generation of the catalytically active species **[(^{iPr}PDI)Fe(CH_2SiMe_3)L][BPh_4]** and **[(^{iPr}PDI)Fe($CH_2SiMe_2CH_2SiMe_3$)]-[$MeB(C_6F_5)_3$]**.

The generation of the catalytically active species for both types of complexes require the use of (^{iPr}PDI)Fe(CH_2SiMe_3)$_2$, a complex that remained elusive for iron, although known for cobalt,[3,4,5] until 2005 when several groups independently reported methods for their preparation. Our laboratory reported direct alkylation of (^{iPr}PDI)$FeCl_2$ with $LiCH_2SiMe_3$ to yield (^{iPr}PDI)Fe(CH_2SiMe_3)$_2$, following recrystallization.[6] Cámpora and coworkers have described an alternative route to (^{R}PDI)Fe(CH_2SiMe_3)$_2$ compounds where the free chelate is added to independently or

in situ prepared (pyridine)$_2$Fe(CH$_2$SiMe$_3$)$_2$.[7] This method has proven versatile for the introduction of various bis(imino)pyridine chelates[8,9] and enantiopure pyridine bis(oxazoline) ligands.[10] However, simply substituting (pyridine)$_2$Fe(CH$_2$SiMe$_3$)$_2$ with the neopentyl analog resulted in competing alkyl migration and iron alkyl homolysis.[9] In order to synthesize bis(imino)pyridine iron alkyl cation complexes with alkyls other than neosilyl, a new method needed to be developed. The synthetic methods used to generate (^{iPr}PDI)Fe(CH$_2$SiMe$_3$)$_2$ are shown in Figure 3.2.

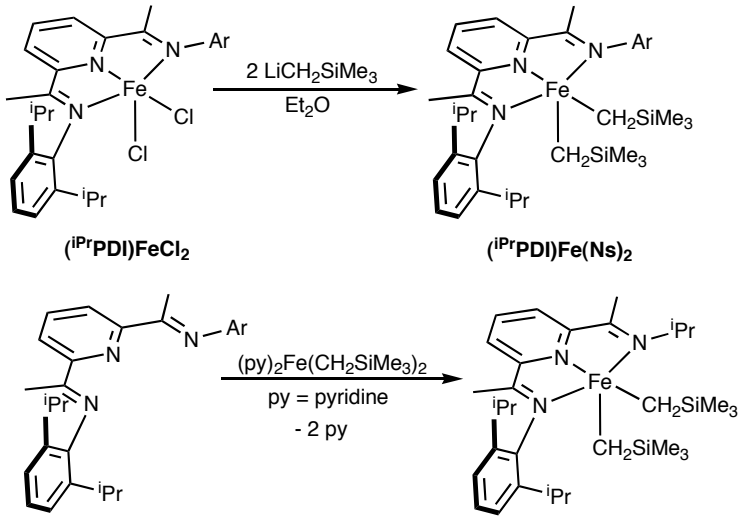

Figure 3.2 The synthetic routes to **(^{iPr}PDI)Fe(CH$_2$SiMe$_3$)$_2$**.

Bis(imino)pyridine iron monoalkyl complexes have also been reported and been prepared by direct alkylation of the corresponding monohalide precursor.[7,9] In this manner, several β-hydrogen stabilized iron alkyl complexes such as (^{iPr}PDI)FeCH$_3$, (^{iPr}PDI)FeCH$_2$SiMe$_3$ and (^{iPr}PDI)FeCH$_2$CMe$_3$, have been synthesized. A route to kinetically unstable β-hydrogen-containing neutral iron alkyls such as (^{iPr}PDI)FeCH$_2$CH$_3$ has also been reported by our laboratory by treatment of the iron bis(dinitrogen) compound, (^{iPr}PDI)Fe(N$_2$)$_2$,[11] with the appropriate alkyl halide.[12] This method unfortunately yields an equimolar mixture of the desired monoalkyl complex

along with the iron monobromide compound, (^{iPr}PDI)FeBr. These (^{iPr}PDI)FeR complexes could prove to be useful synthons in the generation of new [(^{iPr}PDI)FeR]$^+$ complexes. These synthetic routes are shown in Figure 3.3.

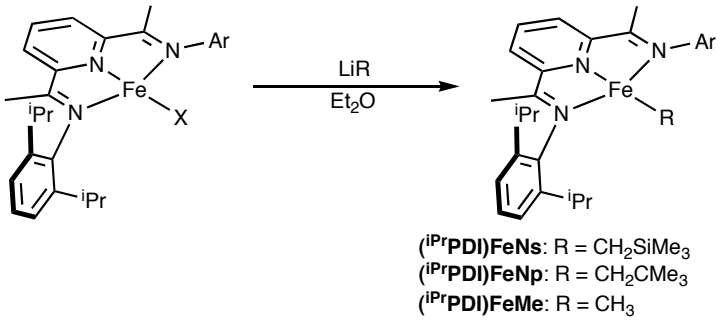

Figure 3.3 The synthesis of **(^{iPr}PDI)FeR**.

Anionic, paramagnetic bis(imino)pyridine iron alkyl complexes have also been synthesized[30] and in one case, [Li(THF)$_4$][(^{iPr}PDI)FeMe], have been shown to be active for ethylene polymerization upon treatment with excess MAO.[13] These complexes were not thoroughly studied, nor were their electronic structures presented.

Many advances in bis(imino)pyridine iron dihalide olefin polymerization have been made since the independent reports in 1998 by Brookhart[14] and Gibson,[15,16] many of which have focused on alteration of the modular bis(imino)pyridine ligand framework[17,18] to establish structure-reactivity relationships. The ambiguity as to the active species upon treatment of (^{iPr}PDI)FeCl$_2$ with MAO in recent years has been somewhat deconvoluted by Talsi and[19,20,21] Gibson,[22] giving a better understanding of the (^{iPr}PDI)FeCl$_2$ / MAO system. Kinetic data has shown that two different active species are present and account for the low and high molecular weight polyethylene generated.

With reported complexes of anionic, cationic, and neutral bis(imino)pyridine iron monoalkyl complexes, an opportunity exists to examine the electronic structures of a series of compounds that vary by one electron. However, the electronic structures

of have not been systematically or thoroughly studied. As bis(imino)pyridines are also well-established redox-active ligands, [23,24,25,26,27,28] determining the three electron series' electronic structures could prove useful to understanding the active species in the (^{iPr}PDI)$FeCl_2$ / MAO system. Chelate participation in the olefin polymerization catalysis is key for understanding the reactivity of the active species. The results of such an investigation, a new route to cationic bis(imino)pyridine iron alkyls and the determination of the degree of bis(imino)pyridine participation over iron compounds with three different formal oxidation states, is presented.

3.3 Preparation of Cationic Iron Alkyl Complexes

The previous preparation of (^{iPr}PDI)Fe(CH_2SiMe_3)$^+$ was limited by the fact that (^{iPr}PDI)Fe(CH_2SiMe_3)$_2$ remains the only readily isolable dialkyl complex. With other variations such as neopentyl and more importantly methyl being synthetically inaccessible, [29,30] a new synthetic route into the chemistry proved necessary. Although characterized by NMR spectroscopy, the base free neosilyl cation was not isolated. The target, then, was the synthesis and isolation of the compound [(^{iPr}PDI)Fe(CH_2SiMe_3)][BPh_4].

The mono alkyl complexes of the type (^{iPr}PDI)FeR, where R is a β-hydrogen stabilized alkyl group, are readily accessible from the salt metathesis of the alkyl lithium salt with (^{iPr}PDI)FeCl. The one electron oxidant [Cp_2Fe][BPh_4] was added as a solid to a vigorously stirring benzene solution of (^{iPr}PDI)Fe(CH_2SiMe_3). Within five minutes, the solution had become viscous with product, and precipitation was completed by the addition of pentane. [(^{iPr}PDI)Fe(CH_2SiMe_3)][BPh_4] was collected on a glass frit as a dull grey/red solid after being washed with copious amounts of pentane to remove ferrocene and then drying under reduced pressure with an average yield of

~90%. The two synthetic methods to the neosilyl variants of the alkyl anions are presented in Figure 3.4.

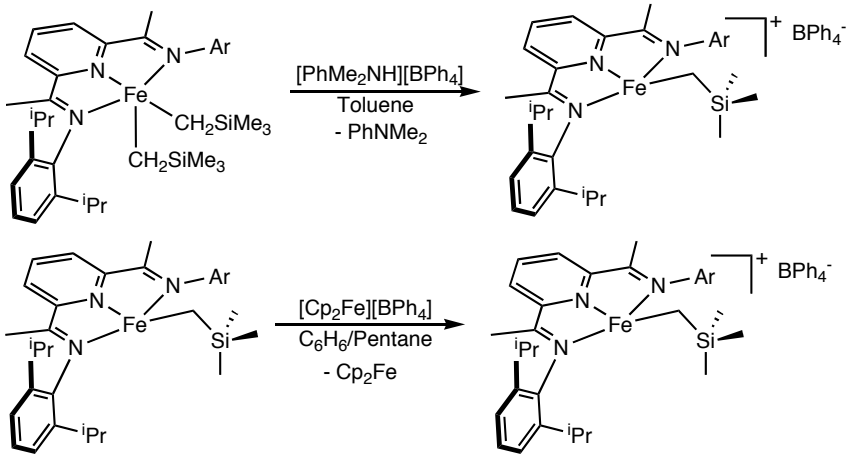

Figure 3.4 Synthetic routes to **[(^{iPr}PDI)Fe(CH_2SiMe_3)][BPh_4]**.

A solid-state magnetic measurement of [(^{iPr}PDI)Fe(CH_2SiMe_3)][BPh_4] gave a μ_{eff} of 4.8 μB (magnetic susceptibility balance), indicative of an $S = 2$ complex. The Mössbauer spectrum exhibited a quadrupole doublet with an isomer shift of 0.64 mm/s and a quadrupole splitting of 1.35 mm/s, parameters that are most consistent with a high-spin iron (II) complex. The slight change from the neutral complex, with parameters of $\delta = 0.54$ mm/s and $\Delta E_Q = 1.55$ mm/s, indicate that the oxidation is ligand, rather than iron, based and the electronics about the iron nucleus of [(^{iPr}PDI)Fe(CH_2SiMe_3)][BPh_4] remains relatively unchanged from the neutral complex. The ^{1}H NMR spectrum was obtained from performing the oxidation in C_6D_6 and filtering through Celite followed by immediately taking the NMR spectrum, or by dissolving the isolated complex in C_6D_5F. The NMR spectrum was identical to the previously reported spectrum. All spectroscopic indications were that this method of oxidation of the mono alkyl complex resulted in the desired complex cleanly and in high yield.

The conversion of this complex to the five coordinate compounds [(^{iPr}PDI)Fe(CH_2SiMe_3)(L)][BPh_4], where L = diethyl ether or THF, was performed. The addition of an excess of diethyl ether to [(^{iPr}PDI)Fe(CH_2SiMe_3)][BPh_4], followed by cooling to -35ºC for an hour followed by filtration led to the formation of a dull blue colored powder identified as [(^{iPr}PDI)Fe(CH_2SiMe_3)(Et_2O)][BPh_4]. This complex gave a solid-state magnetic measurement of μ_{eff} of 4.8 μB, similar [(^{iPr}PDI)Fe(CH_2SiMe_3)][BPh_4]. The addition of THF to the 4-coordinate alkyl cation resulted in the formation of a blue solution. [(^{iPr}PDI)Fe(CH_2SiMe_3)(THF)][BPh_4] could be precipitated by the addition of pentane followed by cooling at -35ºC for an hour. Again, this compound was identical to the previously reported five-coordinate cation.

The zero-field Mössbauer spectra of [(^{iPr}PDI)Fe(CH_2SiMe_3)(L)][BPh_4] vary significantly from the four coordinate complexes. Upon ligation of diethyl ether or THF, the isomer shifts increase to 0.88 mm/s for both [(^{iPr}PDI)Fe(CH_2SiMe_3)(Et_2O)]-[BPh_4] and [(^{iPr}PDI)Fe(CH_2SiMe_3)(THF)][BPh_4], and the quadrupole splittings increase to 2.20 mm/s and 2.29 mm/s, respectively. This phenomenon is consistent for each alkyl cation and can be attributed to the overall increase in the metal-ligand bond distances as the coordination number increases from four to five, resulting in an overall weaker ligand field and hence a decrease in charge density at the iron nucleus. The isomer shifts for the three different alkyl complexes, as well as the four and five coordinate cationic complexes, are presented in Table 3.1.

Table 3.1 Zero-field Mössbauer parameters of mono alkyl and mono alkyl cations of PDI iron.

Compound	**δ = (mm/s)**	**ΔE_Q = (mm/s)**

(^{iPr}PDI)Fe(CH_3)	0.24	3.27
(^{iPr}PDI)Fe(CH_2CMe_3)	0.56	1.13
(^{iPr}PDI)Fe(CH_2SiMe_3)	0.54	1.55
[(^{iPr}PDI)Fe(CH_2SiMe_3)][BPh_4]	0.64	1.35
[(^{iPr}PDI)Fe(CH_2SiMe_3)(Et_2O)][BPh_4]	0.88	2.20
[(^{iPr}PDI)Fe(CH_2SiMe_3)(THF)][BPh_4]	0.88	2.29
[(^{iPr}PDI)Fe(CH_2CMe_3)][BPh_4]	0.57	1.30
[(^{iPr}PDI)Fe(CH_2CMe_3)(Et_2O)][BPh_4]	0.84	2.18
[(^{iPr}PDI)Fe(CH_2CMe_3)(THF)][BPh_4]	0.84	2.18
[(^{iPr}PDI)FeCH_3][BPh_4]	0.53	1.53
[(^{iPr}PDI)Fe(CH_3)(THF)][BPh_4]	0.73	2.98

The neopentyl version of the alkyl cation, $[(^{iPr}PDI)Fe(CH_2CMe_3)]^+$, was next targeted. Again, this compound was inaccessible due to the inability to synthesize the bis neopentyl complex (^{iPr}PDI)Fe(CH_2CMe_3)$_2$. The same method of oxidation was used in this instance with (^{iPr}PDI)Fe(CH_2CMe_3) as above, with benzene as the solvent followed by precipitation of the oxidized [(^{iPr}PDI)Fe(CH_2CMe_3)][BPh_4] with an excess of pentane. [(^{iPr}PDI)Fe(CH_2CMe_3)][BPh_4] was isolated as a dull red powder and had properties consistent with the 4-coordinate neosilyl cation. A solid-state magnetic susceptibility reading gave a μeff of 4.8 μB, indicative of an $S = 2$ compound.

The Mössbauer spectrum revealed a quadrupole doublet with an isomer shift of 0.57 mm/s and a quadrupole splitting of 1.30 mm/s, parameters that are most consistent with a high-spin iron (II) complex. The slight change from the neutral complex, with parameters of δ = 0.54 mm/s and ΔE_Q =1.15 mm/s, is reminiscent of the changes for the neosilyl derivative, and again indicate that the oxidation is ligand, rather than iron, based. The Mössbauer spectrum of the two compounds is shown in Figure 3.5.

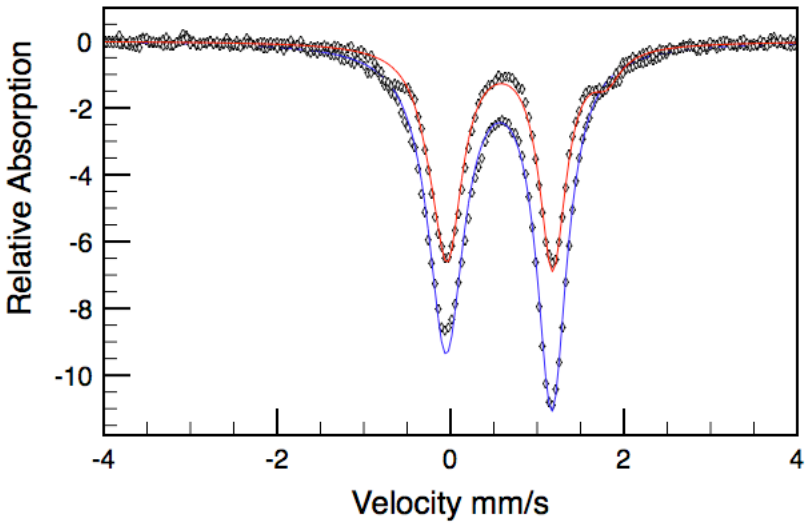

Figure 3.5 Overlaying Mössbauer spectra of **(^{iPr}PDI)Fe(CH_2CMe_3)** (blue) and **[(^{iPr}PDI)Fe(CH_2CMe_3)][BPh_4]** (red).

Variable temperature SQUID magnetic data were collected for [(^{iPr}PDI)Fe(CH_2CMe_3)][BPh_4], but the decomposition of the compound was rapid enough to prove the data unreliable, thus the data was collected for the base stabilized bis(imino)pyridine iron cation, [(^{iPr}PDI)Fe(CH_2CMe_3)(THF)][BPh_4], and are presented in Figure 3.6. Between 40 and 300 K, an essentially temperature independent magnetic moment of 4.7 μB was measured, slightly lower than the expected spin only value for

four unpaired electrons but remains most consistent with an $S = 2$ ground state. Modeling the data established a g value of 1.906 and D value of 6.6 cm^{-1}.

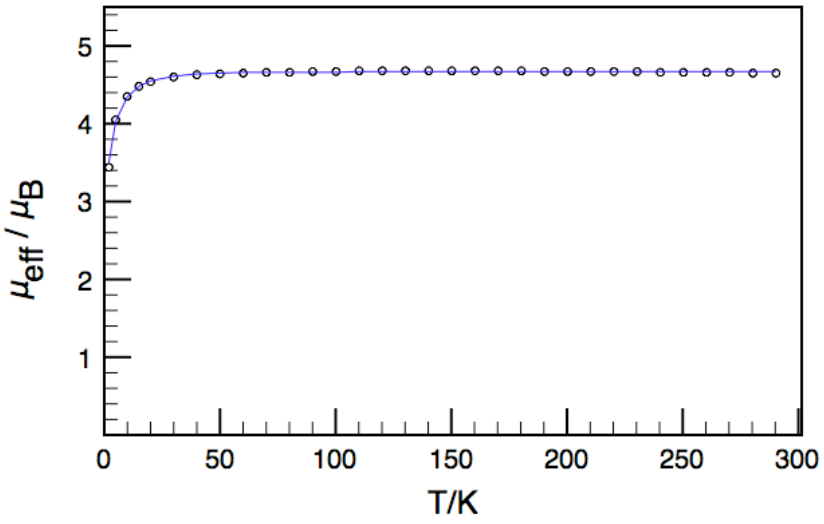

Figure 3.6 SQUID trace of **[(^{iPr}PDI)Fe(CH_2CMe_3)(THF)][BPh_4]** indicating an S=2 species at nearly all temperatures.

The ^{1}H NMR spectrum was obtained from performing the oxidation in benzene-d_6 and filtering through Celite followed by immediately recording the NMR spectrum, but the spectrum contained a huge ferrocene peak as well as small amounts of impurities that made integration and peak assignment difficult. Thus, fluorobenzene d_5 was used to obtain acceptable NMR data. The NMR spectrum consists of paramagnetically broadened resonances spread over nearly 300 ppm. A ^{1}H NMR spectrum of [(^{iPr}PDI)Fe(CH_2CMe_3)][BPh_4] in fluorobenzene *d-5* is shown in Figure 3.7.

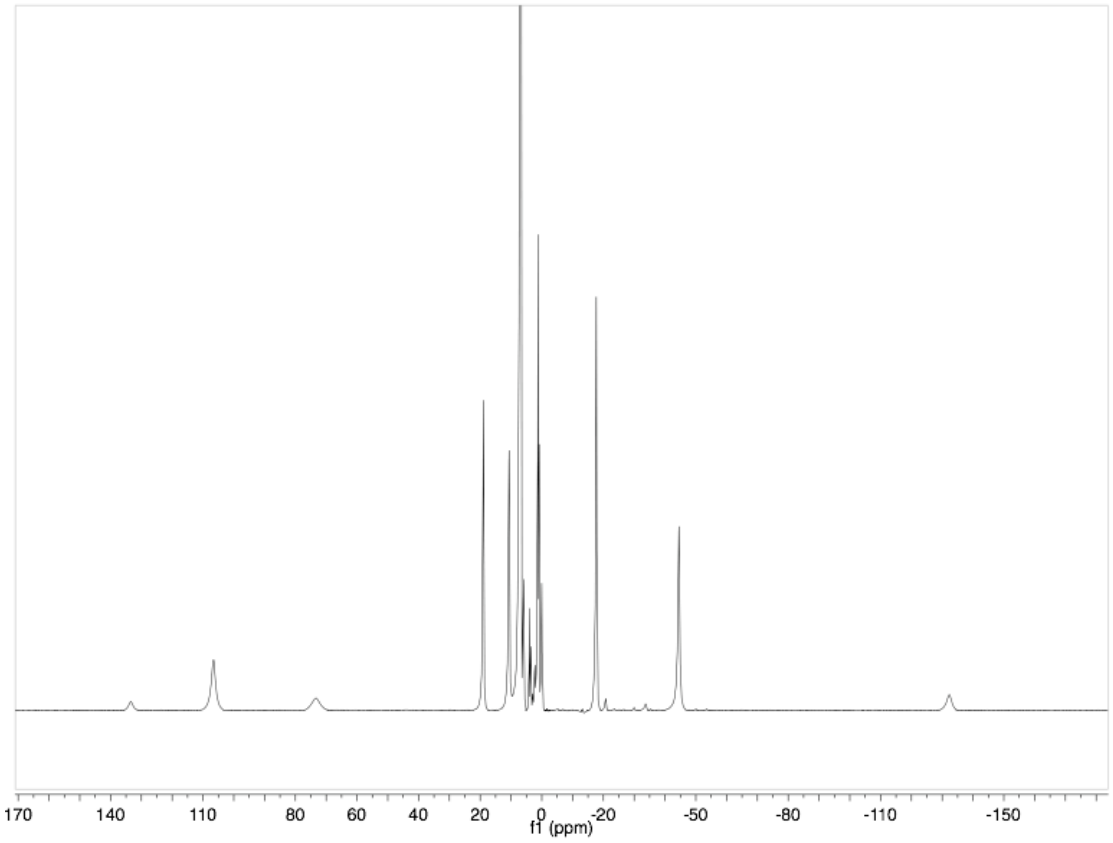

Figure 3.7 1H NMR spectrum of **[(^{iPr}PDI)Fe(CH_2CMe_3)][BPh_4]** in fluorobenzene-d_5.

X-ray quality crystals were grown by dissolving the solid in fluorobenzene, carefully layering the solution with pentane, and allowing the layers to slowly diffuse at -35ºC overnight. The solid-state structure, presented in Figure 3.8, thus obtained showed a distorted square planar iron with the non-interacting tetraphenylborate anion co-crystallized with a molecule of fluorobenzene. There is disorder in one of the isopropyl groups as well as the neopentyl group.

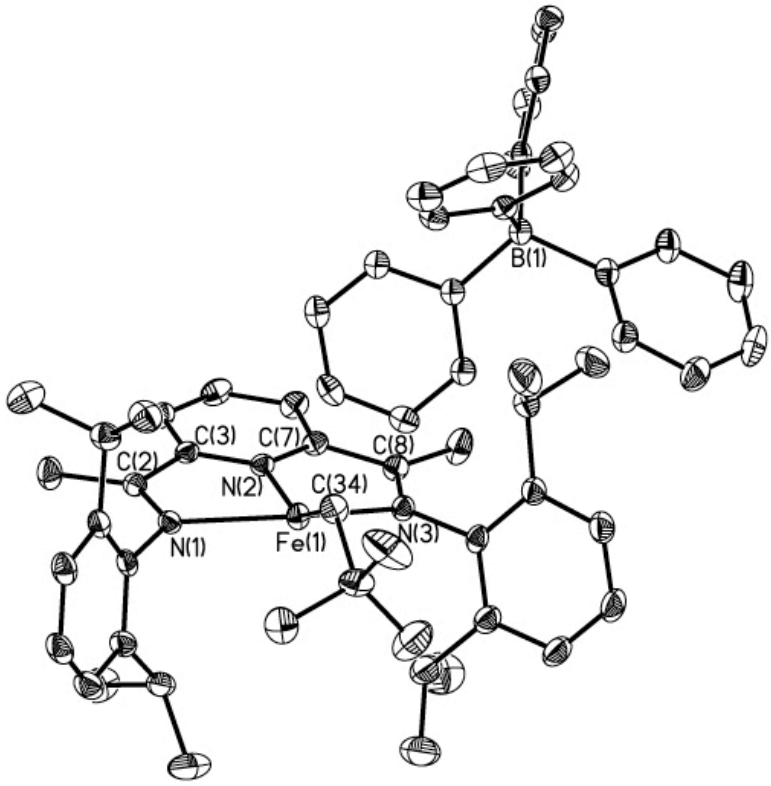

Figure 3.8 Representation of the solid state structure of **[(^{iPr}PDI)Fe(CH_2CMe_3)]-[BPh_4]** at 30 % probability ellipsoids. Hydrogen atoms omitted for clarity.

The metrical parameters of the bis(imino)pyridine indicate a non-reduced, neutral ligand. The N_{imine}-C_{imine} bond lengths of 1.284(2) Å and 1.288(2) Å are most consistent with a neutral bis(imino)pyridine ligand, as well as the long C_{Py}-C_{Imine} bond lengths of 1.490(3) Å and 1.486(3) Å. The Fe-N_{pyr} distance of 2.1103(15) Å and the Fe-N_{imine} distances for Fe(1)-N(1) and Fe(1)-N(3) of 2.2128(15)Å and 2.2415(16) Å, respectively, are notably long, generally indicating population of the d_{x2-y2} orbital of the high-spin ferrous complex. Of note, too, is the bend of the alkyl group out of the plane of the chelate; the N(2)-Fe(1)-C(34) angle of 151.61(8) º exhibits less pronounced distortion than the neutral complex (142.24(14)º), but still lifted

significantly. This is most likely to reduce steric interactions between the isopropyl groups of the PDI and the tert-butyl group of the alkyl.

The conversion of [(^{iPr}PDI)Fe(CH_2CMe_3)][BPh_4] to the five coordinate compounds with an L-type ligand apically coordinated, [(^{iPr}PDI)Fe(CH_2CMe_3)(L)]-[BPh_4], was performed similarly to the neosilyl variant. The addition of an excess of diethyl ether to [(^{iPr}PDI)Fe(CH_2CMe_3)][BPh_4], followed by cooling to -35ºC for an hour followed by filtration led to the formation of [(^{iPr}PDI)Fe(CH_2CMe_3)(Et_2O][BPh_4]. The addition of THF to the 4-coordinate alkyl cation resulted in the formation of a blue solution and [(^{iPr}PDI)Fe(CH_2CMe_3)(THF][BPh_4] could be precipitated by the addition of pentane followed by cooling at -35ºC for an hour. Upon addition of diethyl ether or THF to the fifth coordination site, the isomer shifts increase to 0.84 mm/s and the quadrupole splittings increase to 2.18 mm/s for both complexes. Mössbauer data for the base free compound, as well as the THF adduct, are shown overlaid in figure 3.9.

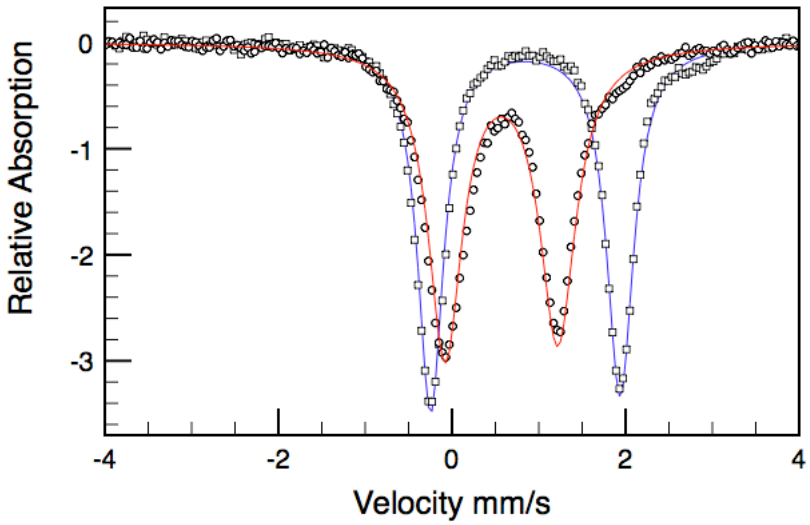

Figure 3.9 Overlapping Mössbauer spectra of **[(^{iPr}PDI)Fe(CH_2CMe_3)(THF)][BPh_4]** (blue) and **[(^{iPr}PDI)Fe(CH_2CMe_3)]-[BPh_4]** (red).

The most relevant synthetic target is the bis(imino)pyridine iron mono methyl cation, as this is the species that has been proposed as a possibility to be the active species of olefin polymerization in the $PDIFeCl_2$/MAO systems. To this end, the previously synthesized and characterized (^{iPr}PDI)Fe(CH_3) was subjected to the same oxidation conditions as (^{iPr}PDI)Fe(CH_2SiMe_3) and (^{iPr}PDI)Fe(CH_2CMe_3). Upon stirring [Cp_2Fe][BPh_4] with (^{iPr}PDI)Fe(CH_3) for 15 to 20 minutes in benzene, followed by precipitation with pentane afforded [(^{iPr}PDI)FeCH_3][BPh_4] as a dull grey/red compound in approximately 85% yield. The magnetic moment was slightly higher than the other complexes with a μeff of 5.2 μB. Mössbauer data is similar to the other alkyl compounds with an isomer shift of 0.53 mm/s and a qaudrupole splitting of 1.53 mm/s, again, parameters that best describe a high-spin ferrous center. A summary of the magnetic data for the cationic compounds and their neutral counterparts are presented in Table 3.2.

Table 3.2 Magnetic moments of neutral and cationic species.

Compound	μ_{eff} (μ_B, 23 °C)
(^{iPr}PDI)Fe(CH_2CMe_3)	4.0[a,c]
(^{iPr}PDI)Fe(CH_2SiMe_3)	3.8[a,c]
(^{iPr}PDI)Fe(CH_3)	
[(^{iPr}PDI)Fe(CH_2SiMe_3)][BPh_4]	4.8[b]
[(^{iPr}PDI)Fe(CH_2CMe_3)][BPh_4]	4.8[b]
[(^{iPr}PDI)Fe(CH_2CMe_3)(Et_2O)][BPh_4]	4.8[b]
[(^{iPr}PDI)Fe(CH_2CMe_3)(THF)][BPh_4]	4.9[b]
[(^{iPr}PDI)FeCH_3][BPh_4]	5.2[b]

[(^{iPr}PDI)FeCH$_3$][BPh$_4$] was not soluble enough in fluorobenzene to grow crystals. If, though, the reaction was performed in fluorobenzene, filtered, and the filtrate layered with pentane, x-ray quality crystals could be grown. The solid-state structure is shown in Figure 3.10.

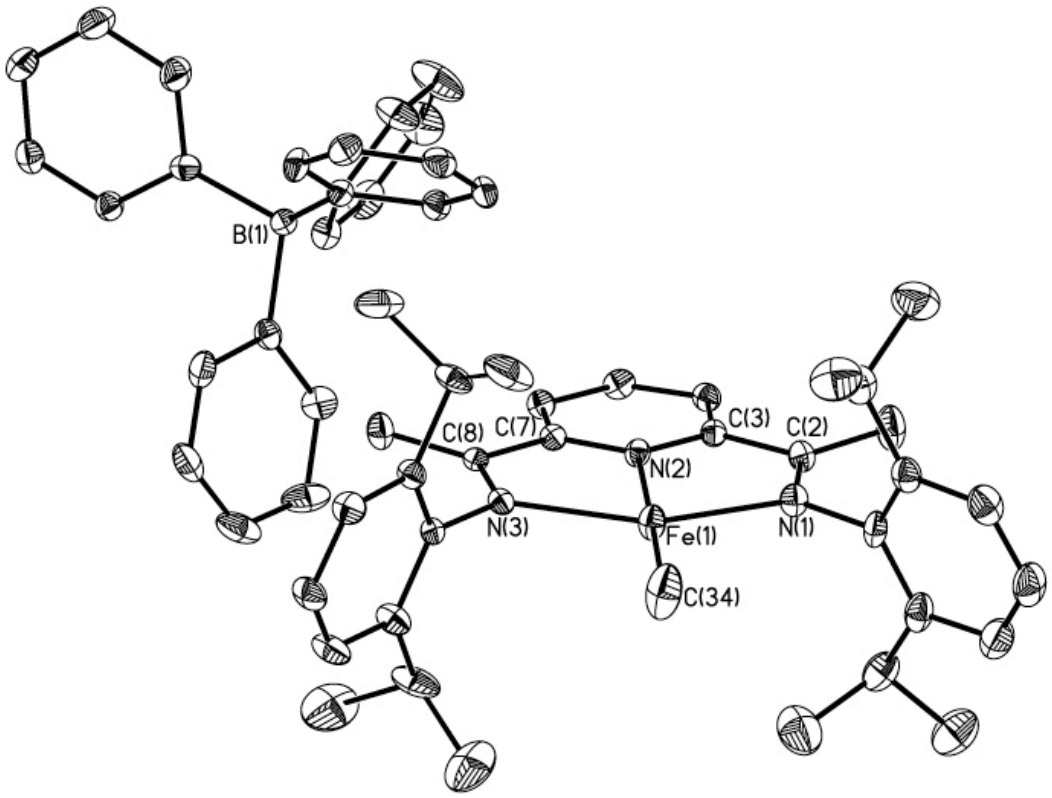

Figure 3.10 Representation of the solid state structure of **[(^{iPr}PDI)Fe(CH$_3$)][BPh$_4$]** at 30% probability ellipsoids. Hydrogen atoms omitted for clarity.

The PDI chelate in [(^{iPr}PDI)Fe(CH_3)][BPh_4] appears non-reduced, much as in [(^{iPr}PDI)Fe(CH_2SiMe_3)][BPh_4] and [(^{iPr}PDI)Fe(CH_2CMe_3)][BPh_4]. The N_{imine}-C_{imine} bond lengths of 1.284(2) Å and 1.288(2) Å for N(1)-C(2) and N(3)-C(8), respectively, are most consistent with a neutral bis(imino)pyridine ligand, as well as the long C_{Py}-C_{Imine} bond lengths of 1.490(3) Å and 1.486(3) Å. The Fe-N_{pyr} distance of 2.117(3) Å and the Fe-N_{imine} distances for Fe(1)-N(1) and Fe(1)-N(3) of 1.293(4) Å and 1.286(4) Å, respectively, are indicative of a high-spin complex. Again, the alkyl ligand retains the geometric configuration of the neutral mono alkyl complex, the methyl group remaining in the plane of the chelate for the two compounds.

The five coordinate derivatives of the mono methyl compound proved more difficult to synthesize. Diethyl ether did not coordinate; even with ether as a solvent at cold temperatures there was no color change indicating coordination of a fifth ligand. Dissolving the methyl cation in THF produced a blue solution that undergoes a color change over the course of minutes to a green solution. A blue powder consistent with [(^{iPr}PDI)Fe(CH_3)(THF)][BPh_4] was isolated if the initial blue solution was treated with an excess of pentane to cause immediate precipitation. [(^{iPr}PDI)Fe(CH_3)(THF)][BPh_4] exhibits a higher isomer shift, 0.73 mm/s, and quadrupole splitting, 2.98 mm/s, than [(^{iPr}PDI)Fe(CH_3)][BPh_4], a change similarly observed in the other complexes. The cause in the difference in reactivity among the alkyl compounds is unknown, but the methyl cation is kinetically inert to diethyl ether coordination and instable when excess THF is present. A summary of the synthesis of five-coordinate alkyl cations is shown in Figure 3.11.

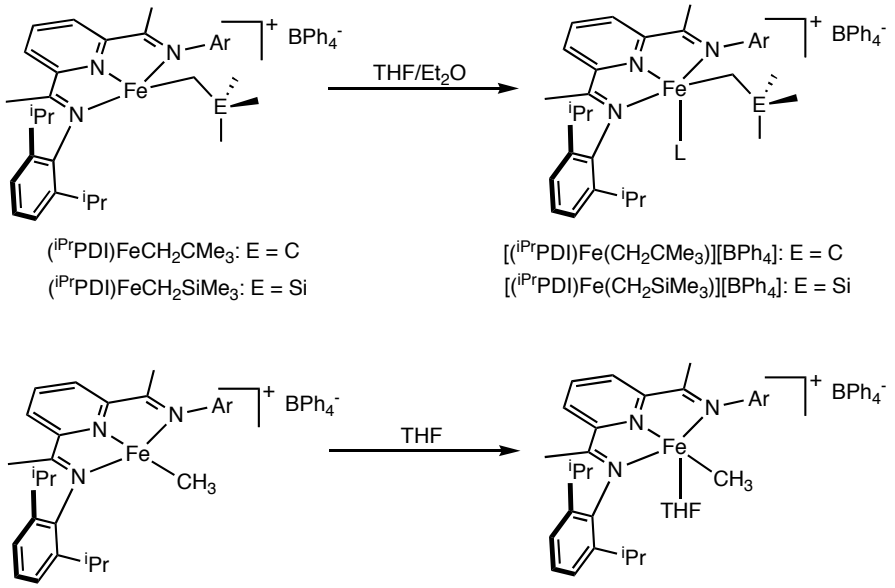

(^{iPr}PDI)FeCH$_2$CMe$_3$: E = C
(^{iPr}PDI)FeCH$_2$SiMe$_3$: E = Si

[(^{iPr}PDI)Fe(CH$_2$CMe$_3$)][BPh$_4$]: E = C
[(^{iPr}PDI)Fe(CH$_2$SiMe$_3$)][BPh$_4$]: E = Si

Figure 3.11 Synthetic routes to the five-coordinate alkyl cations.

This new method for the generation of catalytically competent mono alkyl cationic compounds has allowed for the isolation of previously synthesized, as well as new, compounds in high yields. The generated alkyl cations retain the geometry of the neutral compounds, with the neosilyl and neopentyl variants bent out of the plane of the chelate, and the methyl complexes remaining planar.

3.4 Synthesis of Anionic PDI Iron Alkyl Complexes

Formally zero valent alkyl anions have been synthesized previously. Gambarotta has reported the four-coordinate planar methyl anion, [Li(THF)$_4$][(^{iPr}PDI)FeMe], resulting from the addition of three equivalents of methyl lithium to (^{iPr}PDI)FeCl$_2$. This compound was shown to polymerize ethylene with MAO activation. Our group has also reported the isolation of a five coordinate tolyl anion with a bridging dinitrogen to the lithium counterion, [Li(Et$_2$O)$_3$][(^{iPr}PDI)Fe(C$_6$H$_4$-4-Me)N$_2$], though a detailed electronic structure

description was not presented. In order to attain a three electron series of bis(imino)pyridine iron alkyls for comparison, attempts to form anionic compounds bearing the neosilyl and neopentyl groups were targeted. Gambarotta's $[Li(THF)_4][(^{iPr}PDI)FeMe]$ was synthesized and the Mössbauer parameters were obtained to complete a second three electron redox series.

The initial attempt at synthesizing an alkyl anion was centered around the neosilyl anion, $[Li(Et_2O)_3][(^{iPr}PDI)Fe(CH_2SiMe_3)N_2]$, as this was the initial alkyl group investigated in the oxidation chemistry. The addition of one equivalent of neosilyl lithium to the $(^{iPr}PDI)Fe(N_2)_2$ in diethyl ether afforded a color change from green to purple. As the reaction continued stirring, another color change occurred to a less intense brown/red color. The removal of volatiles afforded a dark powder. The infra-red spectrum of the powder indicated a dinitrogen molecule was coordinated, as there was a fairly intense peak centered at 1934 cm^{-1}. The benzene-d_6 ^1H NMR experiment showed the presence of broadened ether peaks, as well as resonances consistant with $(^{iPr}PDI)Fe(CH_2SiMe_3)$. As the two previously characterized PDI alkyl anions were reported to be NMR silent, this data was consistent with the desired compound. The IR spectra of the synthesized alkyl anions are reported in Table 3.3.

Table 3.3 Dinitrogen stretching frequencies of various alkyl anions. The mono-dinitrogen compound is presented for comparison.

Compound	**ν(N≡N) (cm^{-1})**
$[Li(OEt_2)_3][(^{iPr}PDI)Fe(CH_2CMe_3)N_2]$	1948
$[Li(OEt_2)_3][(^{iPr}PDI)Fe(CH_2SiMe_3)N_2]$	1934
$[Li(Et_2O)_3][(^{iPr}PDI)Fe(C_6H_4\text{-}4\text{-}Me)(N_2)]$	1948
$[Li(12\text{-crown-}4)][(^{iPr}PDI)Fe(CH_2CMe_3)N_2]$	1996
$(^{iPr}PDI)FeN_2$	2046

Mössbauer data was collected on the powder to confirm the synthesis of $[Li(Et_2O)_3][(^{iPr}PDI)Fe(CH_2SiMe_3)N_2]$. The spectrum consisted of 2 pairs of quadrupole doublets in approximately a 95:5 ratio. The major component had parameters that were consistent with $(^{iPr}PDI)Fe(CH_2SiMe_3)$, and the minor component had an isomer shift = 0.04 mm/s and a qaudrupole splitting of 0.86 mm/s, consistent with previously reported compound $[Li(Et_2O)_3][(^{iPr}PDI)Fe(C_6H_4\text{-}4\text{-}Me)N_2]$. The tolyl anion seems to have a greater stability to decomposition, as the complex is isolated pure with a Mössbauer spectrum with parameters isomer shift = 0.02 mm/s and a qaudrupole splitting of 0.93 mm/s. Although the neosilyl anion could not be isolated, spectral parameters were still obtained and are presented. The Mössbauer data for the alkyl anionic compounds are presented in Table 3.4.

Table 3.4 Zero-field Mössbauer parameters of the various alkyl anion compounds collected at 80 K.

Compound	δ = (mm/s)	ΔE_Q = (mm/s)
$[(^{iPr}PDI)Fe(CH_2CMe_3)N_2]^-$	0.06	0.86
$[(^{iPr}PDI)Fe(CH_2SiMe_3)N_2]^-$	0.04	0.88
$[(^{iPr}PDI)Fe(CH_3)]^-$	0.18	2.96
$[(^{iPr}PDI)Fe(C_6H_4\text{-}4\text{-}Me)N_2]^-$	0.02	0.93

Due to the complications associated with isolation of the iron neosilyl anion, attention was then devoted to the preparation of the corresponding neopentyl complex, $[Li(Et_2O)_3][(^{iPr}PDI)Fe(CH_2SiMe_3)N_2]$. Our laboratory has reported the synthesis of the neutral variant, $(^{iPr}PDI)FeCH_2CMe_3$, by straightforward salt metathesis of $(^{iPr}PDI)FeBr$ with $LiCH_2CMe_3$. Treatment of a diethyl ether solution of $(^{iPr}PDI)Fe(N_2)_2$ with one equivalent of $LiCH_2CMe_3$ followed by recrystallization at -35 ºC furnished red-brown solid identified as $[Li(Et_2O)_3][(^{iPr}PDI)Fe(CH_2CMe_3)N_2]$. This compound was also prepared by addition of two equivalents of $LiCH_2CMe_3$ to a

diethyl ether solution of the bis(imino)pyridine iron bromide, (^{iPr}PDI)FeBr. The crown ether derivative, [Li(12-crown-4)][(^{iPr}PDI)Fe(CH_2CMe_3)(N_2)], was also synthesized by addition of 12-crown-4 to a diethyl ether solution of the initially generated anion. The diethyl ether solvate, [Li(Et_2O)$_3$][(^{iPr}PDI)Fe(CH_2CMe_3)N_2], is an exceedingly reactive compound and undergoes decomposition in the solid state and in solution. For subsequent spectroscopic and crystallographic studies (vide infra), the compound was prepared and used immediately. A summary of the alkyl anions is shown in Figure 3.12 with the respective lifetimes of the compounds.

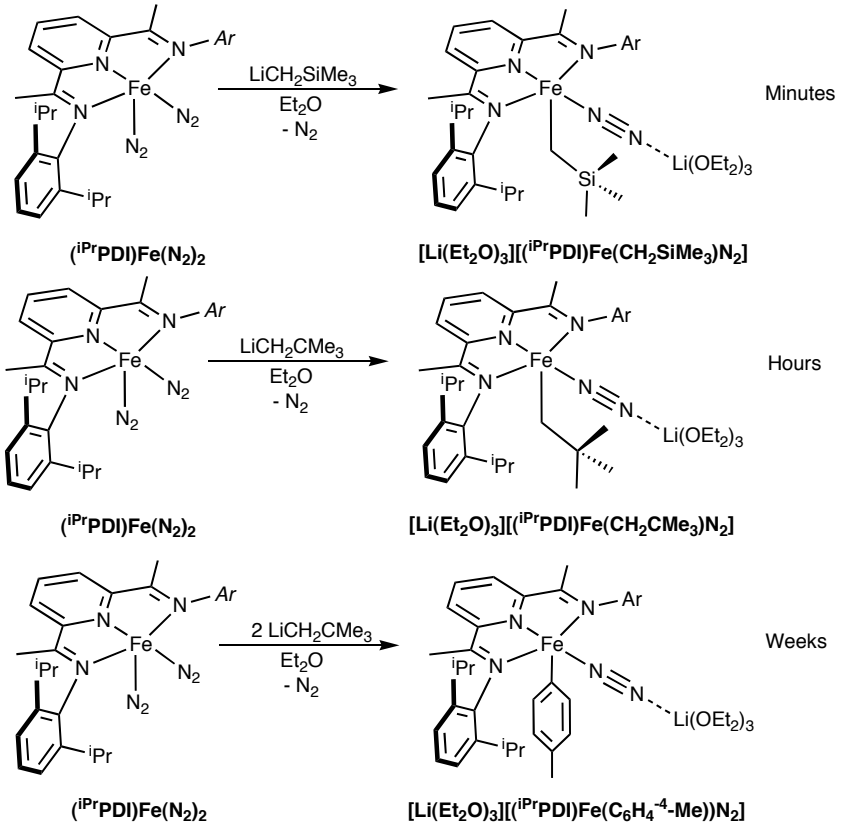

Figure 3.12 The synthesis and relative lifetimes of the alkyl anion complexes is presented.

Spectroscopic characterization, again, proved difficult. The N_2 stretch in the IR was the most convenient handle on the compound but was not a good judge of purity. As was observed for $[Li(THF)_4][(^{iPr}PDI)FeMe]$, $[Li(Et_2O)_3][(^{iPr}PDI)Fe(C_6H_4\text{-}4\text{-}Me)N_2]$, and $[Li(Et_2O)_3][(^{iPr}PDI)Fe(CH_2SiMe_3)N_2]$, $[Li(Et_2O)_3]$-$[(^{iPr}PDI)Fe(CH_2CMe_3)N_2]$ exhibits no observable or assignable ^1H NMR resonances, other than broadened diethyl ether, in benzene-d_6 at 23 ºC. This spectroscopic behavior contrasts the neutral bis(imino)pyridine iron mono- and dialkyl complexes where sharp paramagnetically shifted resonances are observed and readily assigned.[33,35,32]

Single crystals of $[Li(OEt_2)_3][(^{iPr}PDI)Fe(CH_2CMe_3)(N_2)]$ were obtained from a concentrated diethyl ether solution cooled to -35 ºC. The crystals were large and fragile and did not diffract well. Each of the diethyl ether ligands on the $[Li(Et_2O)_3]^+$ cation is severely disordered and were successfully modeled. The asymmetric unit also contained half of either a pentane or diethyl ether molecule that was disordered and was removed by the SQUEEZE routine. The solid-state structure is shown in Figure 3.13.

The overall molecular geometry of $[(^{iPr}PDI)Fe(CH_2CMe_3)(N_2)]^-$ is best described as idealized square pyramidal with the alkyl ligand in the apical position and the dinitrogen molecule and the bis(imino)pyridine chelate defining the basal plane. This arrangement is likely preferred to maximize π-backbonding with the N_2 ligand and is corroborated by the relatively low N_2 stretching frequency observed by infrared spectroscopy. Another factor could be that the alkyl group has a strong trans-influence and the apical position is preferred. The dinitrogen ligand is capped by the $[Li(Et_2O)_3]^+$ cation, which also likely contributes to the reduced infrared stretching frequency. A similar overall molecular geometry was observed in the solid state

structure of the previously characterized bis(imino)pyridine iron tolyl anion, $[Li(Et_2O)_3][(^{iPr}PDI)Fe(C_6H_4\text{-}4\text{-}Me)(N_2)]$.

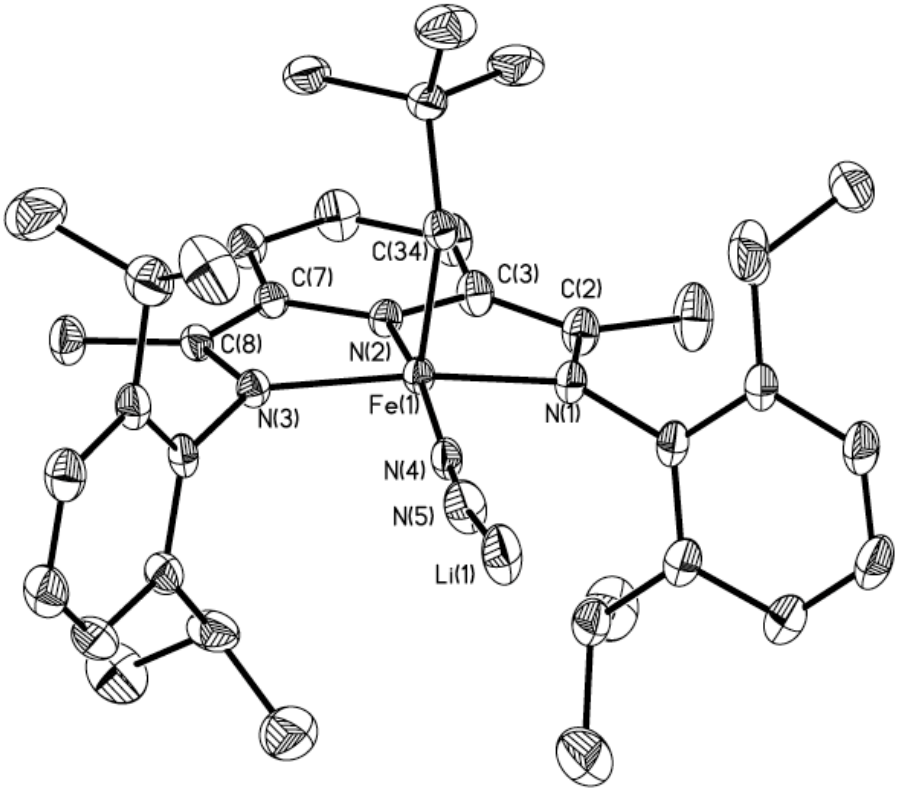

Figure 3.13 Representation of the solid state structure of **$[Li(OEt_2)_3]$ $[(^{iPr}PDI)Fe(CH_2CMe_3)]$** at 30 % probability ellipsoids. Hydrogen, disordered dithyl ether, and isopropyl aryl substituents omitted for clarity.

The metrical parameters of the bis(imino)pyridine chelate in cationic, neutral and anionic iron neopentyl derivatives are reported in Table 3.5 and indicate different ligand rather than metal oxidation states within the series of compounds. $[Li(OEt_2)_3][(^{iPr}PDI)Fe(CH_2CMe_3)(N_2)]$, the N_{imine}-C_{imine} distances of 1.361(3) and 1.355(3) Å are significantly elongated while the C_{imine}-C_{ipso} lengths of 1.394(3) and 1.398(3) Å are the most contracted of any bis(imino)pyridine iron compound crystallographically characterized to date. These values are similar to those reported for both $[(^{iPr}PDI)FeMe]^-$ and $[(^{iPr}PDI)Fe(C_6H_4\text{-}4\text{-}Me)(N_2)]^-$ and suggest either two or

possibly even three[31]-electron reduction of the chelate. A summary of the metrical parameters of the PDI ligand for the members of the three-electron redox series is presented in Table 3.5.

Table 3.5 Metrical parameters for the three-electron redox series

	[(^{iPr}PDI)Fe(CH_2CMe_3)][BPh_4]	(^{Et}PDI)Fe(CH_2CMe_3)	[(^{iPr}PDI)Fe(CH_2CMe_3)]$^-$
Fe(1)-N(1)	2.213(2)	2.158(3)	1.931(2)
Fe(1)-N(2)	2.110(2)	1.986(3)	1.832(2)
Fe(1)-N(3)	2.242(2)	2.126(3)	1.919(2)
Fe(1)-N(4)			1.746(2)
Fe(1)-C(34)[a]	2.035(2)	2.036(4)	2.079(2)
N(1)-C(2)	1.284(2)	1.314(4)	1.361(3)
N(3)-C(8)	1.288(2)	1.329(4)	1.355(3)
N(2)-C(3)	1.333(2)	1.390(4)	1.386(3)
N(2)-C(7)	1.336(2)	1.366(4)	1.386(3)
C(2)-C(3)	1.490(3)	1.446(5)	1.394(3)
C(7)-C(8)	1.486(3)	1.428(5)	1.398(3)
N(4)-N(5)			1.138(3)
N(1)-Fe(1)-N(2)	73.14(6)	75.08(10)	80.17(8)
N(1)-Fe(1)-N(3)	142.87(6)	136.68(11)	154.90(8)
N(2)-Fe(1)-N(3)	72.83(6)	75.19(10)	79.85(8)
N(2)-Fe(1)-N(4)			167.76(9)
N(1)-Fe(1)-N(4)			98.45(9)
N(4)-Fe(1)-C(34)[b]			87.41(9)
N(2)-Fe(1)-C(34)[b]	151.61(8)	142.24(14)	104.82(9)

Following the addition of electrons to the mono-alkyl cation, the metrical parameters of the PDI ligand clearly indicate that the reduction of the compound

occurs on the PDI ligand. The N_{imine}-C_{imine} bond distances elongate by roughly 0.03 Å per electron and the C_{imine}-C_{ipso} bond lengths contract by roughly 0.04 Å per electron. The Mössbauer spectra are nearly identical for the cationic and neutral complexes, but change dramatically upon further reduction. This indicates either an oxidation state change or spin change at the metal center. The spectroscopy gathered thus far is unable to distinguish these two possibilities, so calculations were performed to provide evidence for one or the other possibility.

3.5 Calculations and Electronic Structure Discussion

DFT calculations using the B3LYP functional were performed to gain additional insight into the electronic structure of the bis(imino)pyridine iron alkyl compounds. The series of cationic, neutral and anionic bis(imino)pyridine iron neopentyl compounds was examined. For consistency within the computed series, all calculations were performed using the ^{iPr}PDI ligand without truncation.

For the base free cation, $[(^{iPr}PDI)Fe(CH_2CMe_3)]^+$, a calculation assuming a simple quintet ground state successfully reproduced the metrical parameters determined by X-ray diffraction including the deviation of the neopentyl group from idealized square planar geometry. The computed structure slightly overestimates the metal-ligand bond distances, a typical occurrence for the B3LYP functional.[32] A qualitative molecular orbital (MO) diagram and a spin density plot derived from these results are shown in Figure 3.14. This solution clearly establishes a high-spin iron(II) (S_{Fe} = 2) configuration with a neutral, redox innocent bis(imino)pyridine ligand, consistent with the metrical parameters of the chelate determined from X-ray diffraction. From this electronic structure description, computed ^{57}Fe Mössbauer parameters of δ = 0.58 mm/s and ΔE_Q = -1.81 mm/s were obtained that are in excellent agreement with the experimentally determined values (δ = 0.57 mm/s; ΔE_Q = |1.30 mm/s |).

Table 3.6 Computed and experimental bond distances (Å) and angles (deg) for cationic and neutral bis(imino)pyridine iron neopentyl complexes.

	$[(^{iPr}PDI)Fe(CH_2CMe_3)]^+$		$(^{Et}PDI)Fe(CH_2CMe_3)$		$(^{iPr}PDI)Fe(CH_2CMe_3)$
	Exp.	Calc.	Exp.	Calc.	Calc.
Fe(1)-N(1)	2.213(2)	2.302	2.158(3)	2.286	2.334
Fe(1)-N(2)	2.110(2)	2.145	1.986(3)	2.033	2.040
Fe(1)-N(3)	2.242(2)	2.331	2.126(3)	2.226	2.281
Fe(1)-C(34)	2.035(2)	2.034	2.036(4)	2.073	2.070
N(1)-C(2)	1.284(2)	1.286	1.314(4)	1.308	1.306
N(3)-C(8)	1.288(2)	1.285	1.329(4)	1.317	1.312
N(2)-C(3)	1.333(2)	1.340	1.390(4)	1.370	1.377
N(2)-C(7)	1.336(2)	1.340	1.366(4)	1.374	1.374
C(2)-C(3)	1.490(3)	1.497	1.446(5)	1.462	1.461
C(7)-C(8)	1.486(3)	1.498	1.428(5)	1.452	1.455
N(1)-Fe(1)-N(2)	73.14(6)	72.68	75.08(10)	73.28	74.08
N(1)-Fe(1)-N(3)	142.87(6)	140.68	136.68(11)	137.79	140.85
N(2)-Fe(1)-N(3)	72.83(6)	72.21	75.19(10)	74.38	73.17
N(2)-Fe(1)-C(34)	151.61(8)	138.03	142.24(14)	138.88	145.25

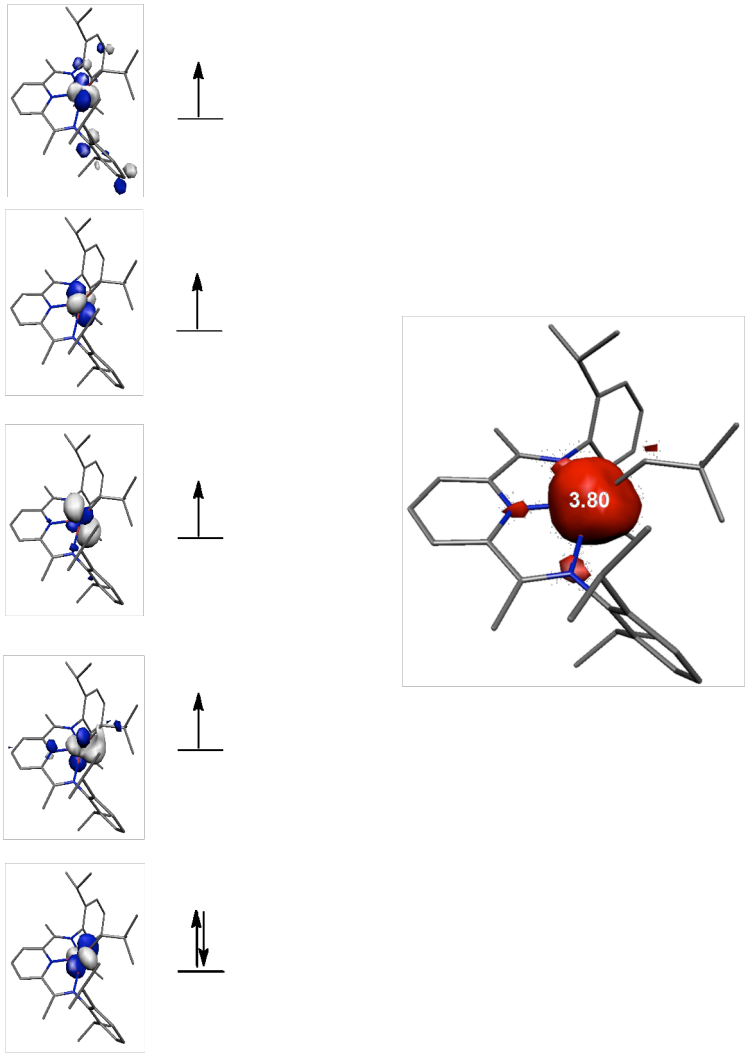

Figure 3.14 Qualitative molecular orbital diagram for $S = 2$ **[(^{iPr}PDI)Fe(CH_2CMe_3)]$^+$** from a B3LYP DFT calculation and the spin density plot obtained from a Mulliken population analysis (red: positive spin density, yellow: negative spin density).

The neutral bis(imino)pyridine iron neopentyl compound, (^{iPr}PDI)FeCH_2CMe_3, was calculated as a spin-unrestricted quartet based on the experimentally determined $S = 3/2$ ground state. Generally, the optimized geometry is in good agreement with the

structural parameters obtained from X-ray crystallography for (^{Et}PDI)FeCH$_2$CMe$_3$. However, the imine-metal bond lengths are exceedingly overestimated by up to 0.17 Å. This is most likely due to the increased steric demand of the 2,6-diisopropyl aryl in the computational model rather than the ethyl substituents in the experimentally determined X-ray crystal structure. Consistent with previous proposals,[36,47b] the computed electronic structure corresponds to a broken symmetry (4,1) solution, obtained via spontaneous symmetry breaking during the unrestricted quartet calculation. A qualitative MO diagram and spin density plot are shown in Figure 3.15. Antiferromagnetic coupling between a singly occupied orbital of the high-spin iron(II) ion and the bis(imino)pyridine radical, similar to the previously computed structure of (^{iPr}PDI)FeCl,[47b] accounts for the $S = 3/2$ ground state. The computed ^{57}Fe Mössbauer parameters of $\delta = 0.57$ mm/s and $\Delta E_Q = +1.78$ mm/s, are in excellent agreement with the experimentally determined values ($\delta = 0.57$ mm/s; $\Delta E_Q = |1.16$ mm/s$|$).

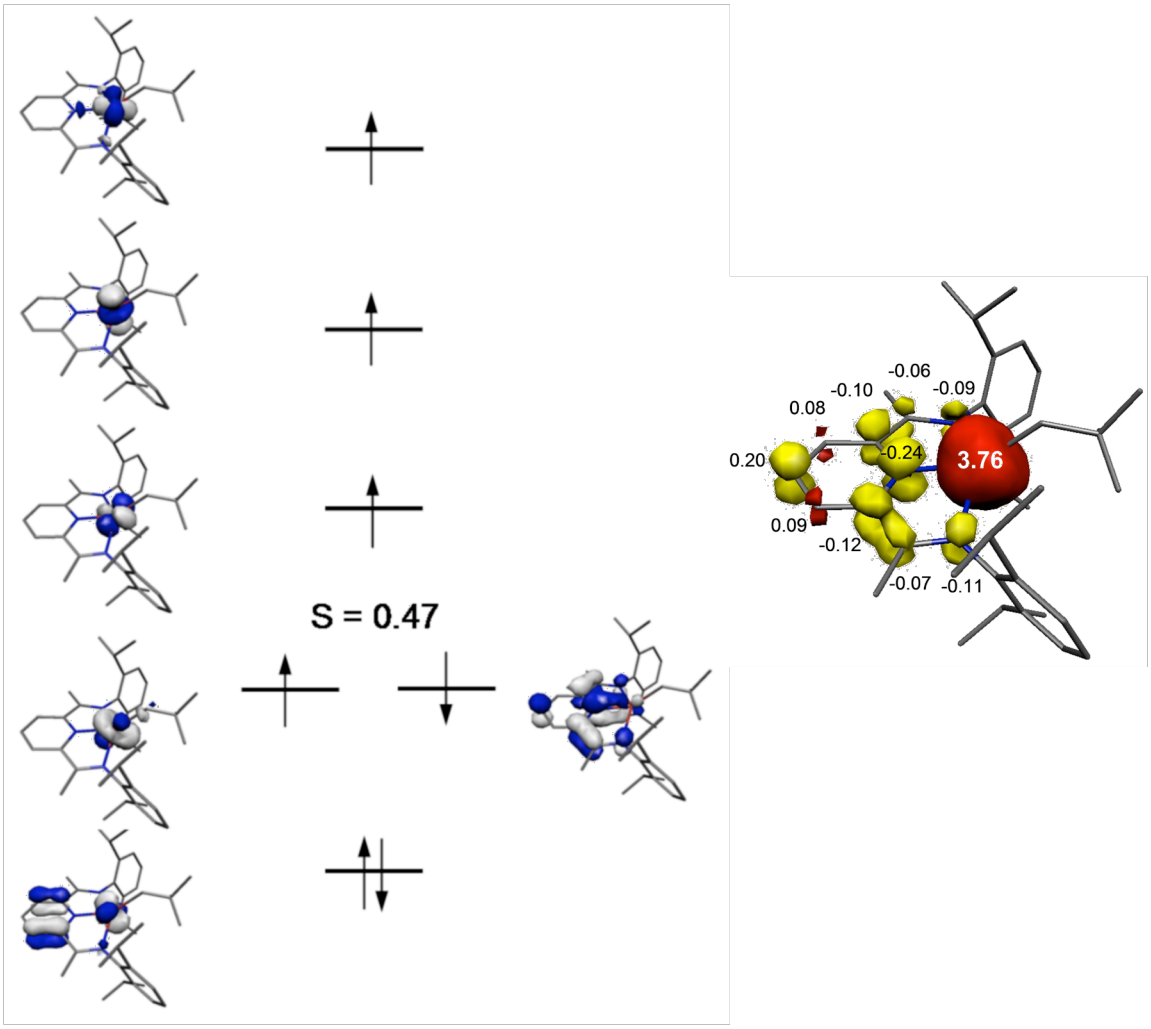

Figure 3.15 Qualitative molecular orbital diagram for $S = 3/2$ **(^{iPr}PDI)Fe(CH_2CMe_3)** from a B3LYP DFT calculation and the spin density plot obtained from a Mulliken population analysis (red: positive spin density, yellow: negative spin density).

The final compound in the series, diamagnetic [(^{iPr}PDI)Fe(CH_2CMe_3)N_2]$^-$, was also examined computationally. Initial studies were performed on the anionic component, [(^{iPr}PDI)Fe(CH_2CMe_3)N_2]$^-$, without the lithium cation, but with application of a COSMO solvation (THF) model. Two electronic structure descriptions were explored; a spin-restricted closed-shell structure and an open-shell BS(2,2) singlet alternative. Analysis of the computed electronic structures revealed

that the closed-shell solution corresponds to a low-spin Fe(II) ion coordinated by a closed-shell dianionic PDI^{2-} ligand with a doubly filled b_2 orbital, while the open-shell solution corresponds to an intermediate spin Fe(II) ion antiferromagnetically coupled to triplet PDI^{2-} ligand. The energy difference between the two solutions was essentially indistinguishable, with the open-shell being more stable by only 3.5 kcal/mol. The structural parameters of both solutions are in reasonable agreement with the experimental values (see Table 3.7). The most significant differences were found for the Fe(1)-C(34) bond length, which is significantly overestimated by almost 0.07 Å in the BS(2,2) approach but underestimated by only 0.1 Å in the closed-shell calculation. Similarly, the N(1)-C(2) and N(3)-C(8) distances are more accurately matched by the closed-shell singlet.

Table 3.7. Computed and Experimental Bond Distances (Å) and Angles (deg) for the anionic bis(imino)pyridine iron neopentyl complex.

	$[(^{iPr}PDI)FeN_2(CH_2CMe_3)]^-$			$[Li(Et_2O)_3][(^{iPr}PDI)FeN_2(CH_2CMe_3)]$	
	Exp.	Calc. BS(2,2)	Calc. RKS	Exp.	Calc.
Fe(1)-N(1)	1.9306(19)	2.023	2.029	1.9306(19)	2.043
Fe(1)-N(2)	1.8316(19)	1.875	1.849	1.8316(19)	1.851
Fe(1)-N(3)	1.9192(19)	2.015	2.000	1.9192(19)	2.033
Fe(1)-N(4)	1.746(2)	1.823	1.794	1.746(2)	1.756
Fe(1)-C(34)	2.079(2)	2.147	2.069	2.079(2)	2.076
N(1)-C(2)	1.361(3)	1.371	1.348	1.361(3)	1.353
N(3)-C(8)	1.355(3)	1.372	1.361	1.355(3)	1.349
N(2)-C(3)	1.386(3)	1.377	1.388	1.386(3)	1.390

N(2)-C(7)	1.386(3)	1.377	1.396	1.386(3)	1.387
C(2)-C(3)	1.394(3)	1.414	1.430	1.394(3)	1.421
C(7)-C(8)	1.398(3)	1.415	1.418	1.398(3)	1.425
N(4)-N(5)	1.138(3)	1.117	1.124	1.138(3)	1.137
N(1)-Fe(1)-N(2)	80.17(8)	80.17	79.79	80.17(8)	79.15
N(1)-Fe(1)-N(3)	154.90(8)	147.73	154.78	154.90(8)	154.11
N(2)-Fe(1)-N(3)	79.85(8)	80.03	79.93	79.85(8)	79.44
N(2)-Fe(1)-N(4)	167.76(9)	167.81	163.53	167.76(9)	165.44
N(1)-Fe(1)-N(4)	98.45(9)	96.69	97.58	98.45(9)	98.33
N(4)-Fe(1)-C(34)	87.41(9)	88.39	89.68	87.41(9)	88.79
N(2)-Fe(1)-C(34)	104.82(9)	103.80	106.79	104.82(9)	105.77

The ^{57}Fe Mössbauer parameters were calculated for both electronic structures to further substantiate the ground state of the molecule. Based on the broken-symmetry solution, values of δ = 0.29 mm/s and ΔE_Q = +1.63 mm/s were computed, which are in agreement with the data obtained for previously reported intermediate spin Fe(II) complexes with PDI ligands (*e.g.* (^{iPr}PDI)Fe(DMAP),[47b] but disagree with the experimental parameters of δ = 0.06 mm/s; ΔE_Q = |0.86 mm/s|. By contrast, the closed-shell calculation reproduces the small quadrupole splitting with a computed value of ΔE_Q = +1.09 mm/s, but still overestimates the isomer shift significantly (δ = 0.25 mm/s).

To investigate the influence of the terminal $Li(Et_2O)_3^+$ ion coordinated to the dinitrogen ligand, the molecule was calculated as $[Li(Et_2O)_3]$-[(^{iPr}PDI)Fe(CH_2CMe_3)N_2] without any truncations. Surprisingly, all attempts to obtain

an open-shell singlet broken-symmetry solution for this compound failed and converged back to the closed-shell solution. The structural parameters obtained from the geometry optimization of the full molecule are in excellent agreement with the experimental values. One notable exception is the significant overestimation of the iron-imine bonds, which is slightly more pronounced than usually observed at the B3LYP level of theory. The calculated Mössbauer parameters of $\delta = 0.21$ mm/s and $\Delta E_Q = +1.12$ mm/s match the experimental values more closely than the values obtained for the truncated molecule. However, the isomer shift is still notably overestimated, which is due to the elongated iron-imine bonds in the obtimized geometry. Consequently, a spin-restricted closed-shell calculation yielded Mössbauer parameters of $\delta = 0.11$ mm/s and $\Delta E_Q = -0.96$ mm/s in good agreement with experiment.

Based on these results, the electronic structure of $[Li(Et_2O)_3]$-$[(^{iPr}PDI)Fe(CH_2CMe_3)N_2]$ is best described as a singlet with a low-spin Fe(II) ion and a closed-shell $^{iPr}PDI^{2-}$ dianion. An important feature of this model is the strong covalent interaction of the axial neopentyl substituent with the d_{z2} orbital of the Fe center, which is most likely the reason for the spin state change from high-spin to low-spin upon reduction of the neutral compound to the anion. The corresponding MO diagram is shown in Figure 3.16. This description is in agreement with the structural data, which shows very short metal-ligand bonds expected for low-spin Fe(II) complexes and indicates a two-electron reduced ligand.

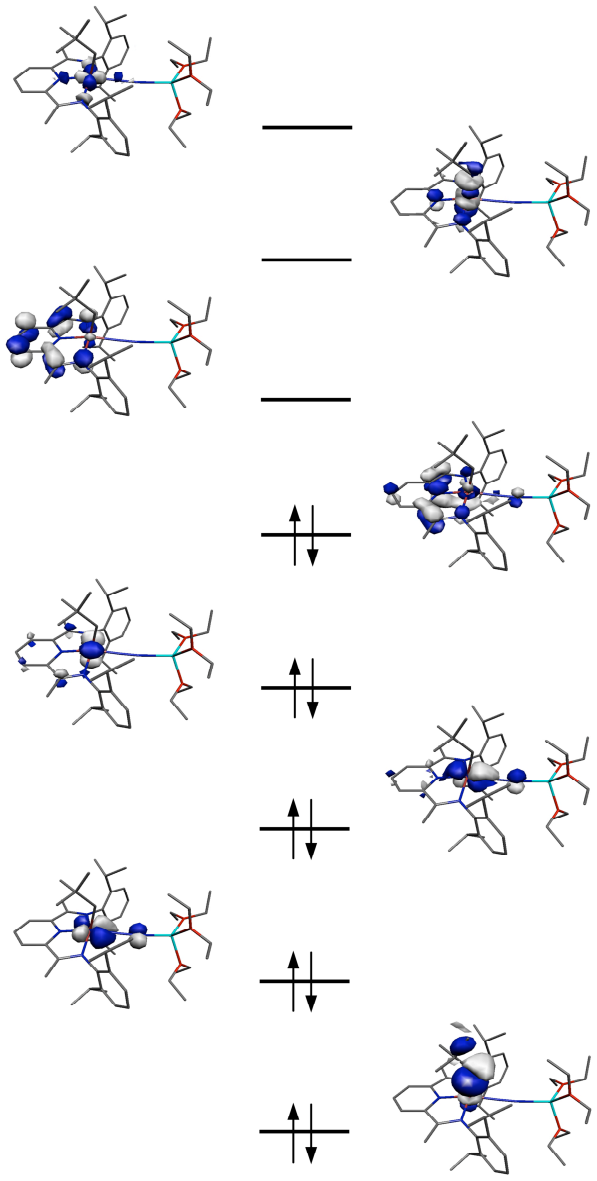

Figure 3.16 Qualitative molecular orbital diagram for $S = 0$ **[(^{iPr}PDI)Fe-(CH_2CMe_3)N_2]$^-$** from a B3LYP DFT calculation. The lowest energy orbital shown highlights the strong covalent interaction of the iron with the apical carbon donor of the alkyl.

With the three electron series completed, a summary of the electronic structure descriptions are provided. The neutral four coordinate iron monoalkyls, (^{iPr}PDI^{1-})Fe^{II}CH$_2$EMe$_3$ (E = C, Si), are used as the reference point. These compounds are best

described as high-spin ferrous derivatives antiferromagnetically coupled to a bis(imino)pyridine radical anion chelate. This configuration avoids formation of relatively rare Fe(I) alkyl species.[33] One electron oxidation of the neutral iron monoalkyl compounds to the corresponding alkyl cations, $[(^{iPr}PDI^{0})Fe^{II}(CH_2EMe_3)]^{+}$ (E = C, Si) is ligand based as both the experimental and computational data support high-spin ferrous complexes with a redox-innocent neutral bis(imino)pyridine chelate. $[(^{iPr}PDI^{0})Fe^{II}(Me)]^{+}$, although having a different geometry, also has the same electronic structure description. Given the single component ethylene polymerization activity previously demonstrated for certain members of this series,[2] redox-activity, at least in the initiating species, is not required for polymerization activity.

The final member of the series is the monoalkyl anion, $[(^{iPr}PDI^{2-})Fe^{II}$-$(CH_2CMe_3)(N_2)]^{-}$. The experimental and computational data establish that the electronic structure of $[(^{iPr}PDI^{2-})Fe^{II}$-$(CH_2CMe_3)(N_2)]^{-}$ is best described as a low-spin ferrous compound ($S_{Fe} = 0$) with a closed-shell PDI^{2-} dianion. The low Mössbauer isomer shift and the extreme distortions to the chelate are consistent with this description. The electron movement throughout the series is presented in Figure 3.17.

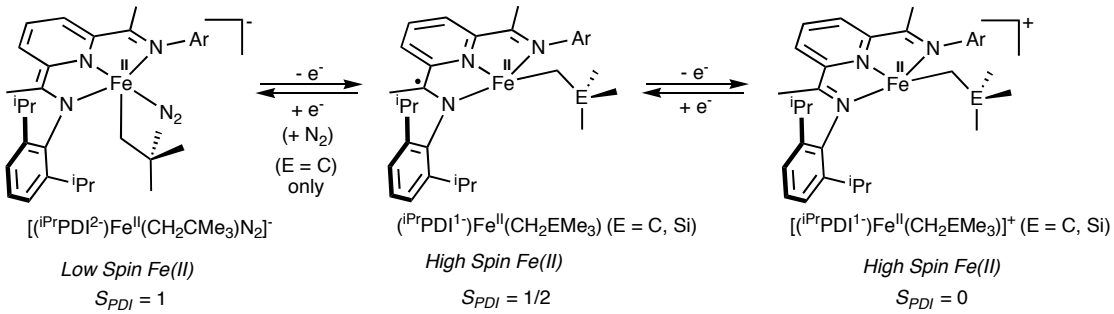

Figure 3.17 Redox-chemistry of the three electron mono-alkyl series highlighting the involvement of the PDI ligand.

One electron reduction of (^{iPr}PDI^{1-})Fe^{II}(CH_2CMe_3) is ligand-based and is also accompanied by a change in spin state at the metal from high- to low-spin. As previous studies have shown, reduction of the bis(imino)pyridine ligand changes its field strength such that neutral and monoanionic forms are relatively weak field while two electron reduced forms (either singlet or triplet) are stronger field.[47] Additionally, the shift of the strongly σ-donating neopentyl group from a more apical position in the distorted square-planar neutral complex to the axial position in the square-pyramidal anion facilitates the change to the low-spin configuration. For the neopentyl, tolyl and phenyl derivatives prepared by our laboratory, the d^6 electron configuration of the low-spin ferrous center is well established for π-backbonding and formation of dinitrogen complexes.

This completed characterization now allows for the conjecture of the electronic structures of isolated intermediates in the iron species proposed to form upon treatment of (^{iPr}PDI)$FeCl_2$ with MAO or $AlMe_3$ (Figure 10).[21] Recently Bryliakov, Talsi and coworkers reported observation of (^{iPr}PDI)Fe(μ-X)(μ-CH_3)Al(CH_3)$_2$ (X = Cl, CH_3) and [(^{iPr}PDI)Fe(μ-X)(μ-CH_3)Al(CH_3)$_2$]$^+$ by ^{1}H NMR and EPR spectroscopies.[21] The identity of "X" was determined by the relative ratio of MAO or $AlMe_3$ to the iron dihalide. For both the neutral and cationic complexes, these species were only observed in situ and we not isolated and hence no crystallographic, magnetic or Mössbauer data are available. However, based on analogy to compounds prepared and studied in this work, electronic structures for both classes of compounds are proposed and shown in Figure 3.18.

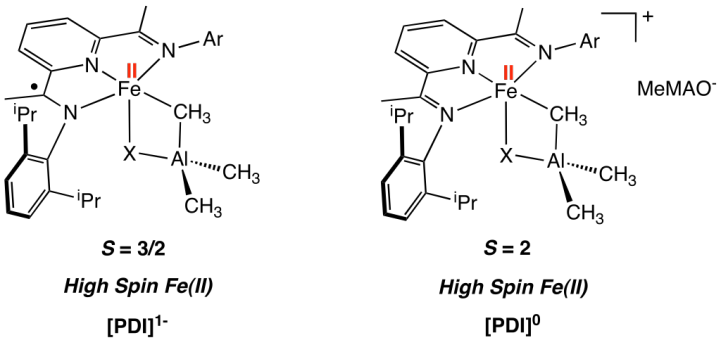

Figure 3.18 Proposed electronic structures of for intermediates detected from treatment of (^{iPr}PDI)$FeCl_2$ with MAO and $AlMe_3$

The neutral compound, ($^{iPr}PDI^{1-}$)Fe^{II}(μ-X)(μ-CH_3)$Al(CH_3)_2$, is best described as a ferrous compound with a bis(imino)pyridine radical anion. The cationic complex, [($^{iPr}PDI^{0}$)Fe^{II}(μ-X)(μ-CH_3)$Al(CH_3)_2$]$^+$, is likely a high-spin ferrous compound (S_{Fe} = 2) with a redox-innocent, neutral bis(imino)pyridine chelate. Notably, our data suggest that treatment of (^{iPr}PDI)$FeCl_2$ with MAO or trialkylaluminums does not result in redox change at the iron center – all oxidation/reduction events occur at the bis(imino)pyridine ligand.

3.6 Conclusions

A new method of generating PDI iron mono-alkyl cationic compounds was discovered. This, along with the synthesis of the five-coordinate [(^{iPr}PDI)Fe(CH_2CMe_3)(N_2)]$^-$, allowed for the isolation and study of three similar compounds that vary by one electron. This study established that bis(imino)pyridine iron monoalkyl complexes that differ by three formal oxidation states (cation, neutral, and anion) all contain ferrous centers and the redox chemistry is confined to the chelate. For neopentyl and neosilyl derivatives, the neutral and monoanionic forms of the bis(imino)pyridine are sufficiently weak field such that high-spin ferrous compounds result. In the case of the anion, the field strength increases sufficiently

such that a low-spin, d^6 compound results and dinitrogen coordination results. These studies imply that the ferrous oxidation state is maintained during treatment of (^{iPr}PDI)$FeCl_2$ with MAO and that redox events are confined to the bis(imino)pyridine chelate.

3.7 Experimental Procedures

General Considerations. All air- and moisture-sensitive manipulations were carried out using standard vacuum line, Schlenk, and cannula techniques or in an MBraun inert atmosphere dry box containing an atmosphere of purified nitrogen. Solvents for air- and moisture-sensitive manipulations were initially dried and deoxygenated using literature procedures.[34] Benzene-d_6 and toluene-d_8 were purchased from Cambridge Isotope Laboratories and dried over 4 Å molecular sieves or titanocene, respectively. The complex (^{iPr}PDI)$Fe(N_2)_2$ was prepared according to literature procedure.[11] (^{iPr}PDI)$Fe(CH_2SiMe_3)$,[8] (^{iPr}PDI)$Fe(CH_2CMe_3)$,[8] (^{iPr}PDI)$FeCH_3$,[6] [(^{iPr}PDI)$Fe(CH_2SiMe_3)(Et_2O)$][BPh_4],[2] [(^{iPr}PDI)$Fe(CH_2SiMe_3)$(THF)][BPh_4],[2] [(^{iPr}PDI)$Fe(CH_2SiMe_2CH_2SiMe_3)$][$MeB(C_6F_5)_3$],[2] [$Li(Et_2O)_3$][(^{iPr}PDI)$Fe(C_6H_4$-4-R)(N_2)][8] were prepared according to literature procedures.

^{1}H NMR spectra were recorded on Varian Mercury 300, Inova 400, 500, and 600 spectrometers operating at 299.76, 399.78, 500.62, and 599.78 MHz, respectively. ^{13}C NMR spectra were recorded on an Inova 500 spectrometer operating at 125.893 MHz. All ^{1}H chemical shifts are reported relative to $SiMe_4$ using the ^{1}H (residual) and shifts of the solvent as a secondary standard. For diamagnetic complexes, many assignments were made based on COSY and HSQC NMR experiments. Solution magnetic moments were determined by Evans method[35] using a ferrocene standard and are the average value of at least two independent measurements. Magnetic susceptibility balance measurements were performed with a Johnson Matthey

instrument that was calibrated with $HgCo(SCN)_4$. Peak widths at half heights are reported for paramagnetically broadened and shifted resonances. Infrared spectra were collected on a Thermo Nicolet spectrometer. Elemental analyses were performed at Robertson Microlit Laboratories, Inc., in Madison, NJ.

Single crystals suitable for X-ray diffraction were coated with polyisobutylene oil in a drybox, transferred to a nylon loop and then quickly transferred to the goniometer head of a Bruker X8 APEX2 diffractometer equipped with a molybdenum X-ray tube (l = 0.71073 Å). Preliminary data revealed the crystal system. A hemisphere routine was used for data collection and determination of lattice constants. The space group was identified and the data were processed using the Bruker SAINT+ program and corrected for absorption using SADABS. The structures were solved using direct methods (SHELXS) completed by subsequent Fourier synthesis and refined by full-matrix least-squares procedures.

Mössbauer data were collected on an alternating constant-acceleration spectrometer. The minimum experimental line width was 0.24 mm/s (full width at half height). A constant sample temperature was maintained with an Oxford Instruments Variox or an Oxford Instruments Mössbauer-Spectromag 2000 cryostat. Reported isomer shifts (δ) are referenced to iron metal at 293 K.

Quantum-chemical calculations. All DFT calculations were performed with the ORCA program package.[36] The geometry optimizations of the complexes and single-point calculations on the optimized geometries were carried out at the B3LYP level[37,38,39] of DFT. This hybrid functional often gives better results for transition metal compounds than pure gradient-corrected functionals, especially with regard to metal-ligand covalency.[40] The all-electron Gaussian basis sets were those developed by the Ahlrichs group.[41,42] Triple-ζ quality basis sets TZVP with one set of polarization

functions on the metal and on the atoms directly coordinated to the metal center were used.[73] For the carbon and hydrogen atoms, slightly smaller polarized split-valence SV(P) basis sets were used, that were of double-ζ quality in the valence region and contained a polarizing set of d-functions on the non-hydrogen atoms.[72] Auxiliary basis sets used to expand the electron density in the resolution-of-the-identity (RI) approach were chosen,[43,44,45] to match the orbital basis.

The SCF calculations were tightly converged (1×10^{-8} E_h in energy, 1×10^{-7} E_h in the density change and 1×10^{-7} in maximum element of the DIIS error vector). The geometry optimizations for all complexes were carried out in redundant internal coordinates without imposing symmetry constraints. In all cases the geometries were considered converged after the energy change was less than 5×10^{-6} E_h, the gradient norm and maximum gradient element were smaller than 1×10^{-4} E_h $Bohr^{-1}$ and 3×10^{-4} E_h $Bohr^{-1}$, respectively, and the root-mean square and maximum displacements of all atoms were smaller than 2×10^{-3} Bohr and 4×10^{-3} Bohr, respectively.

Throughout this paper we describe our computational results by using the broken-symmetry (BS) approach by Ginsberg[46] and Noodleman.[47] Because several broken symmetry solutions to the spin-unrestricted Kohn-Sham equations may be obtained, the general notation BS(*m,n*)[48],[16] has been adopted, where *m* (*n*) denotes the number of spin-up (spin-down) electrons at the two interacting fragments. Canonical and corresponding[49] orbitals, as well as spin density plots were generated with the program Molekel.[50] Frequency calculations were performed at the BP86[51,52] level of theory using the same basis sets as described above. The differences in the obtained geometries were negligible compared to those of the B3LYP optimizations. Nonrelativistic single-point calculations on the optimized geometries were carried out to predict Mössbauer spectral parameters (isomer shifts and quadrupole splittings). These calculations employed the CP(PPP) basis set[53] for iron. The Mössbauer isomer

shifts were calculated from the computed electron densities at the iron centers as previously described.[54]

Preparation of $[Li(Et_2O)_3][(^{iPr}PDI)Fe(CH_2CMe_3)N_2]$. A 50 mL round bottom flask was charged with 0.150 g (0.25 mmol) of $(^{iPr}PDI)Fe(N_2)_2$ and approximately 20 mL of diethyl ether. The contents of the flask were cooled to -35 °C. A scintillation vial was charged with 0.020 g (0.25 mmol) of neopentyl lithium and approximately 10 mL of diethyl ether and the resulting solution was cooled to -35 °C. The flask containing the iron compound was stirred and the neopentyl lithium solution was added dropwise over the course of five minutes. The reaction was warmed to room temperature and stirred. After 0.5 hours, the reaction mixture was filtered through Celite. The filtrate was collected and the volatiles were removed. The resulting residue was dissolved in a minimal amount of diethyl ether and the resulting solution was placed in a scintillation vial and cooled overnight at -35 °C for recrystallization. The resulting solid was collected on a glass frit and yielded 0.078 g (34 %) of $[Li(Et_2O)_3][(^{iPr}PDI)Fe(CH_2CMe_3)(N_2)]$. Analysis for $C_{50}H_{84}N_5FeO_3Li$: Calcd C, 69.34; H, 9.78; N, 8.09. Found: C, 69.73; H, 8.92; N, 8.84. Magnetic susceptibility (benzene-d_6, 23 ºC): $\mu_{eff} = 0\ \mu_B$. IR (KBr): $\nu(N_2) = 1948\ cm^{-1}$.

Alternative Preparation of $[Li(Et_2O)_3][(^{iPr}PDI)Fe(CH_2CMe_3)(N_2)]$. This molecule was prepared using an identical procedure to that described above with the exception that 0.100 g (0.14 mmol) of $(^{iPr}PDI)FeBr$ and 0.022 g (0.28 mmol) of neopentyl lithium were used as the reagents. Recrystallization from diethyl ether at -35 ºC furnished 0.052 g (41 %) of $[Li(Et_2O)_3][(^{iPr}PDI)Fe(CH_2CMe_3)(N_2)]$.

Preparation of [Li(12-Crown-4)][(^{iPr}PDI)Fe(CH_2CMe_3)(N_2)]. A scintillation vial was charged with 0.05 g (0.06 mmol) of [Li(Et_2O)$_3$][(^{iPr}PDI)Fe(CH_2SiMe_3)(N_2)] and approximately 5 mL of diethyl ether. A solution containing 0.02 g (0.12 mmol) of 12-crown-4 in diethyl ether was added to the stirring solution of iron compound. The volume of the solution was reduced to approximately 5 mL and the vial was placed in a -35 ºC freezer. The solvent was decanted and the solid was dried under reduced pressure to yield 0.030 g (64 %) of a dark red/brown solid identified as [Li(12-Crown-4)][(^{iPr}PDI)Fe(CH_2CMe_3)(N_2)]. Analysis for $C_{46}H_{70}N_5FeO_4Li$: Calcd C, 67.39; H, 8.61; N, 8.54. Found: C, 67.06; H, 8.42; N, 8.34. Magnetic susceptibility: $\mu_{eff} = 0\ \mu_B$. IR (KBr): $\nu(N_2) = 1996\ cm^{-1}$.

Attempted Preparation of [Li(Et_2O)$_3$][(^{iPr}PDI)Fe(CH_2SiMe_3)(N_2)]. Attempts to synthesize this compound were carried out using the methods to successfully prepare [Li(Et_2O)$_3$] [(^{iPr}PDI)Fe(CH_2CMe_3)(N_2)]. In a typical experiment, 0.300 g (0.50 mmol) of (^{iPr}PDI)Fe(N_2)$_2$ and 0.047 g (0.53 mmol) of $LiCH_2SiMe_3$ were used. Recrystallization from diethyl ether at -35 ºC furnished 0.24 g (51 %) of red crystals identified as (^{iPr}PDI)Fe(CH_2SiMe_3), containing about 5% (as judged by Mössbauer spectroscopy) of the desired [Li(Et_2O)$_3$][(^{iPr}PDI)Fe(CH_2SiMe_3)(N_2)]. IR (KBr): $\nu(N_2) = 1938\ cm^{-1}$.

Preparation of [(^{iPr}PDI)Fe(CH_2CMe_3)][BPh_4]. A 20 mL scintillation vial was charged with 0.100 g (0.164 mmol) of (^{iPr}PDI)Fe(CH_2CMe_3), 0.083 g (0.164 mmol) of [Cp_2Fe][BPh_4], and a stir bar. Approximately 7 mL of benzene were added to the mixture of solids with stirring. The stirring rate was increased as the reaction mixture thickened and a precipitate formed. After 5 minutes, an equal volume of pentane was added and the stirring was continued for another ten minutes. The solid was collected

on a glass frit and washed with 4 x ~ 20mL of pentane. The solid was dried under vacuum and yielded 0.143 g (93%) of a dull gray red powder identified as [(^{iPr}PDI)Fe(CH_2CMe_3)][BPh_4]. Analysis for $C_{62}H_{74}N_3FeB$: Calcd C, 80.25; H, 8.04; N, 4.53. Found: C, 80.41; H, 7.84; N, 4.21. Magnetic susceptibility (MSB, 23 ºC): μ_{eff} = 4.8 μ_B. ^{1}H NMR (benzene-d_6): δ -124.31 (569 Hz, 2H), -43.32 (470 Hz, 12H), -17.35 (258 Hz, 12H,), -0.70 (316 Hz, 4H), 4.61 (64 Hz, 4H), 12.33 (101 Hz, 8H), 23.25 (64 Hz, 8H), 101.95 (1042 Hz, 6H). (Fluorobenzene-d_5): δ -132.53 (588 Hz, 2H), -44.57 (237 Hz, 12H), -17.84 (116 Hz, 12H,), -0.01 (115 Hz, 4H), 5.89 (158 Hz, 4H), 10.60 (158 Hz, 8H), 28.98 (98 Hz, 8H), 73.41 (1138 Hz, 2H), 106.58 (528 Hz, 6H), 133.40 (611 Hz, 1H).

Preparation of [(^{iPr}PDI)Fe(CH_2CMe_3)(THF)][BPh_4]. A 20 mL scintillation vial was charged with 0.050 g (0.054 mmol) of [(^{iPr}PDI)Fe(CH_2CMe_3)][BPh_4]. A minimum amount of THF was added to dissolve the solid, forming a blue solution. The blue solution was layered with approximately 1.5 mL of pentane and the vial was placed in a -35 °C freezer. Over the course of 8 hours, a blue solid formed. The mother liquor was decanted and the solid was dried at room temperature under vacuum yielding 0.045 g (84%) of light blue solid identified as [(^{iPr}PDI)Fe(CH_2CMe_3)(THF)][BPh_4]. Analysis for $C_{66}H_{82}N_3OFeB$: Calcd C, 79.27; H, 8.26; N, 4.20. Found: C, 78.78; H, 7.96; N, 3.94. Magnetic susceptibility (MSB, 23 ºC): μ_{eff} = 4.9 μ_B.

Preparation of [(^{iPr}PDI)Fe(CH_2CMe_3)(OEt_2)][BPh_4]. This compound was prepared in a manner similar to [(^{iPr}PDI)Fe(CH_2CMe_3)(THF)][BPh_4] by dissolving 0.050 g (0.054 mmol) of [(^{iPr}PDI)Fe(CH_2CMe_3)][BPh_4] and approximately 5 mL of diethyl ether. Recrystallization from diethyl ether at -35 ºC furnished 0.045 g (84%) of light blue solid identified as [(^{iPr}PDI)Fe(CH_2CMe_3)(OEt_2)][BPh_4]. Analysis for

$C_{66}H_{84}N_3OFeB$: Calcd C, 79.11; H, 8.45; N, 4.19. Found: C, 78.78; H, 7.96; N, 3.94. Magnetic susceptibility (MSB, 23 ºC): $\mu_{eff} = 4.8\ \mu_B$.

Alternative Preparation of [(^{iPr}PDI)Fe(CH_2SiMe_3)][BPh_4]. This molecule was prepared in a similar manner to [(^{iPr}PDI)Fe(CH_2CMe_3)][BPh_4] with 0.150 g (0.240 mmol) of (^{iPr}PDI)Fe(CH_2SiMe_3) and 0.121 g (0.240 mmol) of [Cp_2Fe][BPh_4] and yielded 0.199 g (88%) of a dull gray-red powder identified as [(^{iPr}PDI)Fe(CH_2SiMe_3)][BPh_4] as reported previously.[40]

Alternative Preparation of [(^{iPr}PDI)Fe(CH_2SiMe_3)(THF)][BPh_4]. This molecule was prepared in a similar manner to [(^{iPr}PDI)Fe(CH_2CMe_3)(THF)][BPh_4] with 0.050 g (0.240 mmol) of [(^{iPr}PDI)Fe(CH_2SiMe_3)][BPh_4] and yielded 0.049 g (96%) of a light blue powder that was identified as [(^{iPr}PDI)Fe(CH_2SiMe_3)(THF)][BPh_4] as reported previously.[40]

Alternative Preparation of [(^{iPr}PDI)Fe(CH_2SiMe_3)(OEt_2)][BPh_4]. This molecule was prepared in a similar manner to [(^{iPr}PDI)Fe(CH_2CMe_3)(OEt_2)][BPh_4] with 0.050 g (0.240 mmol) of [(^{iPr}PDI)Fe(CH_2SiMe_3)][BPh_4]. The addition of ether resulted in an immediate color change of the solid to blue and yielded 0.050 g (98%) of a light blue powder identified as [(^{iPr}PDI)Fe(CH_2SiMe_3)(OEt_2)][BPh_4] as reported previously.[40]

Preparation of [(^{iPr}PDI)FeCH_3][BPh_4]. This molecule was prepared in a similar manner to [(^{iPr}PDI)Fe(CH_2CMe_3)][BPh_4], but with 0.112 g (0.202 mmol) of (^{iPr}PDI)FeCH_3, and 0.100 g (0.200 mmol) of [Cp_2Fe][BPh_4]. The light red solid was collected on a glass frit and washed with 4 x ~ 20mL of pentane. The solid was dried under vacuum and yielded 0.153 g (89%) of a dull gray red powder identified as

[(^{iPr}PDI)FeCH$_3$][BPh$_4$]. Single crystals suitable for X-ray diffraction were grown by dissolving 0.020 g (0.036 mmol) of (^{iPr}PDI)FeCH$_3$ in 1 mL C_6H_5F and adding 0.016 g (0.032 mmol) [Cp_2Fe][BPh$_4$]. After mixing for 1 min with a glass pipette, the resulting solution was filtered through a glass frit into an NMR tube and layered with *n*-hexane. The layers were allowed to diffuse together over the course of 36 hr at room temperature yielding translucent blocks with a reddish-brown hue. Analysis for $C_{58}H_{66}N_3FeB$: Calcd C, 79.90; H, 7.63; N, 4.82. Found: C, 79.62; H, 7.86; N, 4.57. Magnetic susceptibility (MSB, 23 ºC): μ_{eff} = 5.2 μ_B. ^{1}H NMR (benzene-d_6): δ = -115.45 (1715 Hz), -49.31 (1665 Hz), -17.53 (216 Hz), -8.15 (380 Hz), 1.95 (102 Hz), 8.40 (114 Hz), 9.31 (455 Hz), 20.40 (102 Hz), 81.49 (1850 Hz), 131.31 (1053 Hz). (Fluorobenzene-d_5): δ -117.93 (985 Hz, 2H), -46.66 (873 Hz, 12H), -18.36 (454 Hz, 12H,), -0.71 (284 Hz, 4H), 3.73 (186 Hz, 4H), 8.73 (198 Hz, 8H), 12.21 (221 Hz, 8H), 68.61 (730 Hz, 2H), 185.38 (855 Hz, 6H), 128.03 (513 Hz, 1H).

REFERENCES

[1] Britovsek, G. J. P.; Gibson, V. C.; Spitzmesser, S. K.; Tellman, K. P.; White, A. J. P.; Williams, D. *J. Chem. Soc., Dalton Trans.* **2002**, *3*, 207.

[2] Bouwkamp, M. W.; Lobkovsky, E.; Chirik, P. J. *J. Am. Chem. Soc.* **2005**, *127*, 9660.

[3] Kooistra, T. M.; Knijnenburg, Q.; Smits, J. M. M.; Horton, A. D.; Budzelaar, P. H. M.; Gal, A. W. *Angew. Chem. Int. Ed.* **2001**, *40*, 4719.

[4] Gibson, V. C.; Tellmann, K. P.; Humphries, M. J.; Wass, D. F. *Chem. Commun.* **2002**, 2316.

[5] Tellmann, K. P.; Humphries, M. J.; Rzepa, H. S.; Gibson, V. C. *Organometallics* **2004**, *23*, 5503.

[6] Bouwkamp, M. W.; Bart, S. C.; Hawrelak, E. J.; Trovitch, R. J.; Lobkovsky, E.; Chirik, P. J. *Chem. Commun.* **2005**, 3406.

[7] Campora, J.; Naz, A. M.; Palma, P.; Alvarez, E.; Reyes, M. L. *Organometallics* **2005**, *24*, 4878.

[8] Fernández, I.; Trovitch, R. J.; Lobkovsky, E.; Chirik, P. J. *Organometallics* **2008**, *27*, 109.

[9] Tondreau, A. M.; Lobkovsky, E; Chirik, P. J. *Org. Lett.* **2008**, 10 (13), 2789.

[10] Tondreau, A. M.; Darmon, J. M.; Wile, B. M.; Floyd, S. K.; Lobkovsky, E.; Chirik, P. J. *Organometallics* **2009**, *28*, 3928.

[11] Bart, S. C.; Lobkovsky, E.; Chirik, P. J. *J. Am. Chem. Soc.* **2004**, *126*, 13794.

[12] Trovitch, R. J.; Lobkovsky, E.; Chirik, P. J. *J. Am. Chem. Soc.* **2008**, *130*, 11631.

[13] Scott, J.; Gambarotta, S.; Korobkov, I.; Budzelaar, P. H. M. *Organometallics* **2005**, *24*, 6298.

[14] a) Small, B. M.; Brookhart, M. *J. Am. Chem. Soc.* **1998**, *120*, 7143. b) Small, B. L.; Brookhart, M.; Bennett, A. M. A. *J. Am. Chem. Soc.* **1998**, *120*, 4049.

[15] Britovsek, G. J. P.; Gibson, V. C.; Kimberley, B. S.; Maddox, S. J.; Solan, G. A.; White, A. J. P.; Williams, D. J. *Chem. Commun.* **1998**, 849.

[16] Britovsek, G. J. P.; Bruce, M.; Gibson, V. C.; Kimberely, B. S.; Maddox, P. J.; Mastroianni, S.; McTavish, S. J.; Redshaw, C.; Solan, G. A.; Strömberg, S.; White, A. J. P.; Williams, D. J. *J. Am. Soc.* **1999**, *121*, 8728.

[17] Gibson, V C.; Redshaw, C.; Solan, G. A. *Chem. Rev.* **2007**, *107*, 1745.

[18] Matsugi, T.; Fujita, T. *Chem. Soc. Rev.* **2008**, *37*, 1264.

[19] Talsi, E. P.; Babushkin, D. E.; Semikolenova, N. V.; Zudin, V. N.; Panchenko, V. N.; Zakharov, V. A. *Macromol. Chem. Phys.* **2001**, *202*, 2046.

[20] Bryliakov, K. P.; Semikolvenova, N. V.; Zudin, V. N.; Zakharov, V. A.; Talsi, E. P. *Chem. Commun.* **2004**, *5*, 45.

[21] Bryliakov, K. P.; Semikolvenova, N. V.; Zudin, V. N.; Zakharov, V. A.; Talsi, E. P. *Organometallics* **2004**, *23*, 5375.

[22] Britovsek, G. J. P.; Clentsmith, G. K. B.; Gibson, V. C.; Goodgame, D. M. L.; McTavish, S. J.; Pankhurst, Q. A. *Catal. Commun.* **2002**, *3*, 207.

[23] a) Knijnenburg, Q.; Gambarotta, S.; Budzelaar, P. H. M. *Dalton Trans.* **2006**, 5442. b) Bart, S. C.; Chlopek, K.; Bill, E.; Bouwkamp, M. W.; Lobkovsky, E.; Neese, F.; Wieghardt, K.; Chirik, P. J. *J. Am. Chem. Soc.* **2006**, *128*, 13901.

[24] Butin, K. P.; Beloglazkina, E. K.; Zyk, N. V. *Russ. Chem. Rev*. **2005**, *74*, 531.

[25] Kuwabara, I. H.; Comninos, F. C. M.; Pardini, V. L.; Viertler, H.; Toma, H. E. *Electrochim. Acta* **1994**, *39*, 2401.

[26] Toma, H. E.; Chavez-Gil, T. E. *Inorg. Chim. Acta* **1997**, *257*, 197.

[27] de Bruin, B.; Bill, E.; Bothe, E.; Weyermüller, T.; Wieghardt, K. *Inorg. Chem.* **2000**, *39*, 2936.

[28] Budzelaar, P. H. M.; de Bruin, B.; Gal, A. W.; Wieghardt, K.; van Lenthe, J. H. *Inorg. Chem.* **2001**, *40*, 4649.

[29] Scott, J.; Gambarotta, S.; Korobkov, I.; Budzelaar, P. H. M. J. Am. Chem. Soc. 2006, 128, 9660.

[30] Fernández, I.; Trovitch, R. J.; Lobkovsky, E.; Chirik, P. J. Organometallics 2008, 27, 109.

[31] Enright, D.; Gambarotta, S.; Yap, G. P. A.; Budzelaar, P. H. M. *Angew. Chem. Int. Ed.* **2002**, *41*, 3873.
[32] Neese, F., J. Biol. Inorg. Chem. 2006, 11, 702.

[33] Holland, P. L. *Acc. Chem. Res.* **2008**, *41*, 905.

[34] Pangborn, A. B.; Giardello, M. A.; Grubbs, R. H.; Rosen, R. K.; Timmers, F. J. *Organometallics* **1996**, *15*, 1518.

[35] Sur, S. K. *J. Magn. Reson.* **1989**, *82*, 169.

[36] F. Neese, Orca – an ab initio, DFT and Semiempirical Electronic Structure Package, Version 2.7, Revision 0; Institut für Physikalische und Theoretische Chemie, Universität Bonn, Bonn (Germany), August **2009**.

[37] Becke, A. D. *J. Chem. Phys.* **1986**, *84*, 4524.

[38] Becke, A. D. *J. Chem. Phys.* **1993**, *98*, 5648.

[39] Lee, C. T.; Yang, W. T.; Parr, R. G. *Phys. Rev. B* **1988**, *37*, 785.

[40] F. Neese, E. I. Solomon, In *Magnetism: From Molecules to Materials*; Miller, J. S., Drillon, M., Eds.; Wiley: New York, **2002**; Vol. 4, p 345.

[41] Schäfer, A.; Horn, H.; Ahlrichs, R. *J. Chem. Phys.* **1992**, *97*, 2571.

[42] Schäfer, A.; Huber, C.; Ahlrichs, R. *J. Chem. Phys.* **1994**, *100*, 5829.

[43] Eichkorn, K.; Weigend, F.; Treutler, O.; Ahlrichs, R. *Theor. Chem. Acc.* **1997**, *97*, 119.

[44] Eichkorn, K.; Treutler, O.; Öhm, H.; Häser, M.; Ahlrichs, R. *Chem. Phys. Lett.* **1995**, *240*, 283.

[45] Eichkorn, K.; Treutler, O.; Öhm, H.; Häser, M.; R. Ahlrichs, *Chem. Phys. Lett.* **1995**, *242*, 652.

[46] Ginsberg, A. P. *J. Am. Chem. Soc.* **1980**, *102*, 111.

[47] Noodleman, L.; Peng, C. Y.; Case, D. A.; Mouesca, J. M. *Coord. Chem. Rev.* **1995**, *144*, 199.

[48] Kirchner, B.; Wennmohs, F.; Ye, S.; Neese, F. *Curr. Opin. Chem. Biol.* **2007**, *11*, 134.

[49] Neese, F. *J. Phys. Chem. Solids* **2004**, *65*, 781.
[50] *Molekel*, Advanced Interactive 3D-Graphics for Molecular Sciences, available under http://www.cscs.ch/molekel/.

[51] Perdew, J. P.; Yue, W. *Phys. Rev. B* **1986**, *33*, 8800.

[52] Perdew, J. P. *Phys. Rev. B* **1986**, *33*, 8822.

[53] Neese, F. *Inorg. Chim. Acta* **2002**, *337*, 181.

[54] Sinnecker, S.; Slep, L. D.; Bill, E.; Neese, F. *Inorg. Chem.* **2005**, *44*, 2245.

CHAPTER 4

SYNTHESIS, CHARACTERIZATION, AND KETONE AND ALDEHYDE HYDROSILYLATION ACTIVITY OF N,N,N-CHELATE IRON DIALKYL COMPOUNDS*

4.1 Abstract

A series of PDI (PDI = 2,6-(*R*N=CMe)$_2$C$_5$H$_3$N, R = alkyl, aryl) and Pybox (Pybox = 2,6-(*R*-oxazoline)$_2$C$_5$H$_3$N) iron dialkyl compounds were prepared either by salt metathesis of the corresponding iron dichloride with neosilyl lithium, or via chelation to the bis pyridine dialkyl iron (Py)$_2$Fe(CH$_2$SiMe$_3$)$_2$. These series of compounds were characterized using a combination of ^{1}H NMR and Mössbauer spectroscopies, X-ray crystallography and solution and solid-state magnetic measurements. The catalytic activity of these compounds was explored via ketone and aldehyde hydrosilylation. Olefin hydrogenation is also a viable catalytic transformation with these compounds. In the case of the *C$_2$* symmetric Pybox compounds, modest enantioselectivities were found for ketone hydrosilylation. Though the Pybox compounds proved only modest for selectivity, these N,N,N terdentate iron dialkyl compounds have proved to be some of the most active iron based carbonyl hydrosilylation catalysts known.

4.2 Introduction

PDI iron dialkyl compounds remained a synthetic challenge well after the cobalt congeners had been synthesized and characterized. In 2005, there were successive reports on the alkylation of bis(imino)pyridine iron. Chirik and coworkers reported the

* Parts of this chapter have been taken from (a) Wile, B. M.; Trovitch, R. J.; Bart, S. C.; Tondreau, A. M.; Lobkovsky, E.; Milsmann, C.; Bill, E.; Wieghardt, K.; Chirik P. J. *Inorg. Chem.* **2009,** *48* (9), 4190. Copyright 2009 American Chemical Society. b) Tondreau, A. M.; Darmon, J. M.; Wile, B. M.; Floyd, S. K.; Lobkovsky, E.; Chirik, P. J. *Organometallics* **2009**, *28*, 3928. Copyright 2009 American Chemical Society. c) Tondreau, A. M.; Lobkovsky, E; Chirik, P. J. *Org. Lett.* **2008**, 10 (13), 2789. Copyright 2008 American Chemical Society.

isolation and structural characterization of the first example of a bis(imino)pyridine iron dialkyl complex, which was synthesized from salt metathesis of the corresponding iron dichloride compound and two equivalents of (trimethylsilyl)methyl lithium ($LiCH_2TMS$, neosilyl lithium) in diethyl ether followed by recrystallization cleanly gave (^{iPr}PDI)FeR_2.[1] Following this result, Campora and coworkers reported a versatile synthesis involving the ligation of the free chelate to a bis pyridine iron dialkyl compound, which comes from the salt metathesis of the tetrakispyridine iron dihalide compound and two equivalents of $LiCH_2TMS$, to give (^{iPr}PDI)FeR_2 in high yield.[2] The use of neosilyl lithium proved to be necessary in the synthesis of iron dialkyls, as the use of alternative alkyl metals resulted in non-productive chemistry such as reduction and alkyl migration[3,4] and as such, the dialkyl complexes discussed presently pertain only to the neosilyl variant. These two methods of bis(imino)pyridine iron dialkyl preparation are depicted below in Figure 4.1.

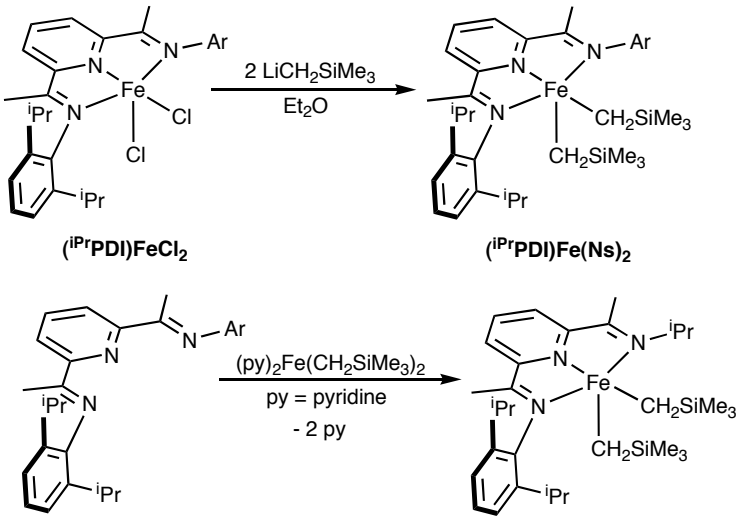

Figure 4.1 Synthetic strategies used in the preparation of dialkyl PDI iron(II) complexes.

Although these compounds' syntheses were finally achieved, the exploration of catalytic transformations utilizing these potential pre-catalysts remains sparse. In the case of (^{iPr}PDI)FeR_2, 14 electron, single component ethylene polymerization catalysts of the type $PDIFeR^+$ were synthesized from the dialkyl complex and were shown to polymerize ethylene at a rate competitive with the $PDIFeCl_2$/MAO systems that had been reported earlier.[5] Reductive catalysis utilizing the bis(imino)pyridine iron system, including hydrogenation and hydrosilylation of alkenes and alkynes, has been reported previously and with turnover frequencies that rival the fastest noble metal catalysts. No direct catalysis using the readily available dialkyl compounds had been attempted, however.

As easily synthesized and as modular as bis(imino)pyridine ligands, C_2 symmetric N,N,N terdentate Pybox ligands may be a route into asymmetric catalysis. These easily accessed chelates have been used in the past as supporting ligands to aid in asymmetric catalysis.[6] Pybox iron dihalide compounds have been synthesized previously, and have been utilized as catalyst precursors.[7,8] Analogous to the bis(imino)pyridine system as an N,N,N terdentate ligand, the corresponding iron dialkyl complexes were targeted for synthesis as precatalysts.

The interest in iron based catalytic systems for the reduction of carbonyl functionalities has seen a steady increase in recent years. The need to replace the heavier noble metals with cheaper, less toxic, and more abundant base metals is driving the research in this area of catalysis. For aldehyde and ketone hydrogenation, highly effective titanium,[9] copper[10] and organocatalytic[11] methods have been developed. Recently, there has been resurgence in iron catalysis and several laboratories have been exploring various carbonyl reduction methods.[12] Beller and Nishiyama have been independently exploring $Fe(OAc)_2$ in combination with various phosphorus-, nitrogen- and thiophene based ligands for the hydrosilylation of various aldehydes and

ketones.[13,14,15,16,17] Typically, tertiary silanes such as PMHS (polymethylhydrosiloxane), $(EtO)_3SiH$ or $(EtO)_2MeSiH$ are used as the stoichiometric reductant followed by straightforward hydrolysis to yield the corresponding alcohols. Using C_2 symmetric phosphines, Beller and coworkers have observed high enantiomeric excesses with select hindered subtrates.[15,17] Gade has also reported a family of bis(pyridylimino)isoindole iron acetate complexes for asymmetric ketone hydrosilylation using $(EtO)_2MeSiH$ as the stoichiometric reductant.

While important and practical advances have been made with $Fe(OAc)_2$ based catalysis, little is known about the nature of the active species or mechanism of action of these compounds. Several groups have been exploring well-defined organometallic and coordination complexes of iron as potential carbonyl reduction catalysts. Inspired by the bifunctional, ionic hydrogenation catalysis known for ruthenium, Casey and Morris have studied related iron complexes. The former group has developed a Shvo-type cyclopentadienyl iron catalyst that efficiently hydrogenates ketones at ambient temperature at 3 atm of H_2.[18] Morris and coworkers have described a family of di-cationic iron(II) compounds with tetradentate diiminophosphine ligands that hydrogenate various acetophenones at 25 atm of H_2 at 50 ºC.[19,20] Using different ligand substituents, transfer hydrogenations of aldehydes, ketones and imines were also observed using ^{i}PrOH as the hydrogen source. Most recently, Morris reported an iron carbonyl complex that catalyzes the asymmetric transfer hydrogenation of ketones with high turnover frequencies (53–4800 hr^{-1}) and enantioselectivities (14– 99%).[21]

Unlike the $Fe(OAc)_2$-catalyzed methods, tertiary silanes are ineffective for carbonyl reduction as the stoichiometric reductants while $PhSiH_3$ and Ph_2SiH_2 produce high turnover frequencies at low (0.1 mol%) catalyst loadings. Hydrosilylation of various substituted acetophenones was observed and substituted enones were also tolerated. The synthesis and characterization of PDI iron dialkyl complexes and enantiopure pyridine

bis(oxazoline) (Pybox) iron dialkyl complexes, the complexes electronic structures, and their application to ketone and aldehyde hydrosilylation are presented.

4.3 Preparation of PDI and Pybox Iron Dialkyl Complexes

This investigation spans three distinct ligand types as support for iron dialkyls: aryl bis(imino)pyridine (PDI), alkyl bis(imino)pyridine (APDI), and C_2 symmetric Pybox ligands were all utilized in the synthesis, mainly via Campora's method. In each case, a high-spin formally iron(II) paramagnetic iron compound was obtained as a purple solid. Comparisons of representative examples from each class of ligand will help highlight the differences and similarities between each type of iron dialkyl compound.

The generality of the synthesis of both PDI and Pybox iron bis neosilyl systems was explored to increase the library of potential precatalysts, as well as try to determine any limitations in the chemistry. Different varieties of PDI were investigated first, with different substitution at the imine position. The use of a viariety of anilines gave rise to the PDI library used in the study. Alkyl amines were also used in the synthesis of ligands to afford alkyl substituted APDI ligands. The Pybox ligands were synthesized from a large number of amino alcohols in order to gain a broader insight into the chemistry. A summation of ligand variety is given in Figure 4.2.

Ligand solubility plays a key role in determining the method used in the synthesis of the desired iron dialkyl complex. The utilization of Campora's method is preferred, with the ability to be carried out in "one pot" and with percent yields of pure compound in the high eighties. With diisopropyl aryl PDI, the method typically gave the dialkyl with high quantities of free ligand present in the product, as well as yields of about 50%, indicating incomplete ligation. The indanyl substituted pybox ligand also performed poorly in this method. The 2-adamantyl substituted APDI ligand is incompatible with

either method for formation of the dialkyl. In these cases, salt metathesis with the corresponding iron dihalide yielded much cleaner compound and in much higher yields.

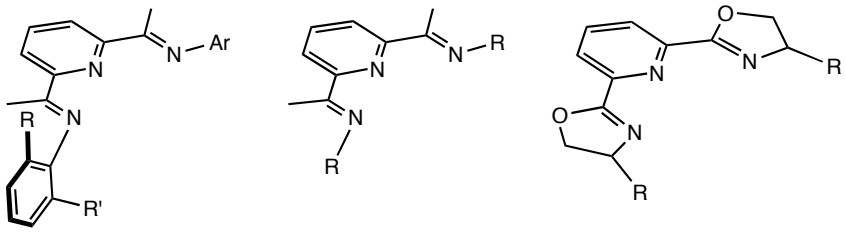

R=R'=iPr
R=R'=Et
R=R'=Me
R=H, R'=iPr
R=H, R'=Me

R=Cy
R=(4-Me)Cy
R=(4-tBu)Cy
R=Adamantyl
R=Myrtanyl

R=iPr
R=iBu
R=Ph
R=Bn
R=tBu

Figure 4.2 The various ligands used in the exploration of N,N,N chelate iron dialkyl chemistry.

The investigation into the PDI iron dialkyl complexes began with the least dramatic change, altering the substituents on the aryl ring. The investigation was performed to determine if there were any steric requirements for the synthesis of these compounds. Since the diisopropyl phenyl had been made and characterized, the symmetric diethyl and dimethyl variants were explored initially. Utilization of Campora's method in both cases yielded dark purple paramagnetic compounds with NMR shifts similar to the previously characterized ^{iPr}PDIFeR$_2$.

Continuing the reasoning, the next anilines utilized were mono substituted at the *ortho* position. The mono isopropyl PDI was synthesized, as was the mono methyl. The synthesis of the dialkyl complexes proceeded without incedent, but the compounds that were synthesized adopted two different conformations, the C_2 and the *Cs* symmetric conformers, or rac and meso, where the alkyl groups on the aryl rings are either *cis* or *trans* around the iron. The NMR spectrum of these molecules clearly distinguishes the two diastereomers. The 2,5-di-^{t}butyl PDI also exhibited two isomers by NMR. The

distinguishing resonances in the ^{1}H NMR spectra of these aryl PDI dialkyl complexes, as well as several APDI complexes, are given in Table 4.1.

The results of the syntheses of various PDI dialkyl complexes indicated that the synthesis of the iron dialkyl complex was not dependant on steric protection from the ligand. The electronics remained roughly constant over the above alterations. In order to change the electronics, as well as to continue to drop the steric demand, smaller alkyl amines were used to synthesize several alkyl substituted PDI, APDI, ligands.

Table 4.1 Distinguishing resonances in the ^{1}H NMR spectra of iron dialkyl complexes

Ar (R)	**B.B Methyl** (Peak Width at ½ Height in Hz)	***m*-Pyridine** (Peak Width at ½ Height in Hz)	***p*-Pyridine** (Peak Width at ½ Height in Hz)
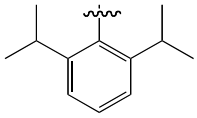	150.52 (673.8)	64.41 (169.8)	281.22 (732.5)
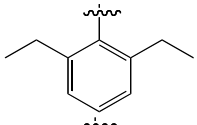	-149.79 (435.5)	59.77 (176.7)	281.22 (732.5)
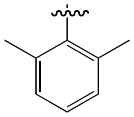	-150.00 (417.5)	58.53 (142.7)	282.52 (276.0)
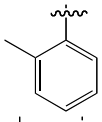	-156.60, -159.67 (737.2, 662.4)	51.74, 48.28 (237.2, 221.3)	326 (1139.6)
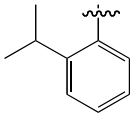	-150.29, -158.31 (791.4, 571.0)	57.59, 49.50 (349.6, 233.1)	321.12, 314.43 (1172.3, 791.0)
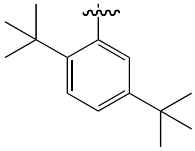	-153.23 (658.0)	50.23 (248.7)	304.57 (474.1)
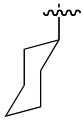	-133.26 (616.5)	40.03 (212.8)	213.92 (2975.9)
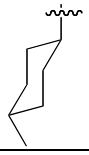	-133.17 (634.4)	39.76 (297.8)	213.36 (947.7)

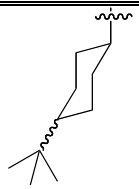	-122.20, -130.45 (778.0, 769.63)	41.38, 40.26 (329.8, 1109.0)	207.93, 195.60 (4722.5, 7193.3)
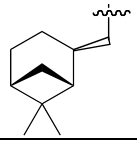	-129.32 (596.6)	43.98 (450.68)	255.27 (1268.5)

The cyclohexyl substituted APDI iron dialkyl was the first non-aryl PDI derivative investigated to compare to the (^{iPr}PDI)FeR_2. The free ligand was synthesized according to published procedure, and Campora's method was utilized for the synthesis of the dialkyl complex. The addition of one equivalent of ligand in diethyl ether to a stirring diethyl ether solution of $(Py)_2Fe(CH_2SiMe_3)_2$ resulted in the immediate color change to deep purple. The pure compound, (^{Cy}APDI)FeR_2, was isolated in over 80% yield as a purple paramagnetic, $\mu_{eff} = 4.7\ \mu_B$, powder. The ^{1}H NMR spectrum exhibited broad peaks in a spectral range of just under 350 ppm. A solid-state x-ray structure was obtained that revealed a molecular geometry most consistent with a distorted trigonal bipyramidal structure, as opposed to the square based pyramid of the (^{iPr}PDI)FeR_2. The trigonal plane consists of the pyridine nitrogen and the two alkyl groups; the summation of these angles around iron is 360.00(21). The axis runs through the iron center and the two imine nitrogens of the chelate; the sum of the angles in this axial plane is 360.00(16). This change in geometry most likely is due to the lowering of the steric demand of the chelate as compared to (^{iPr}PDI)FeR_2.

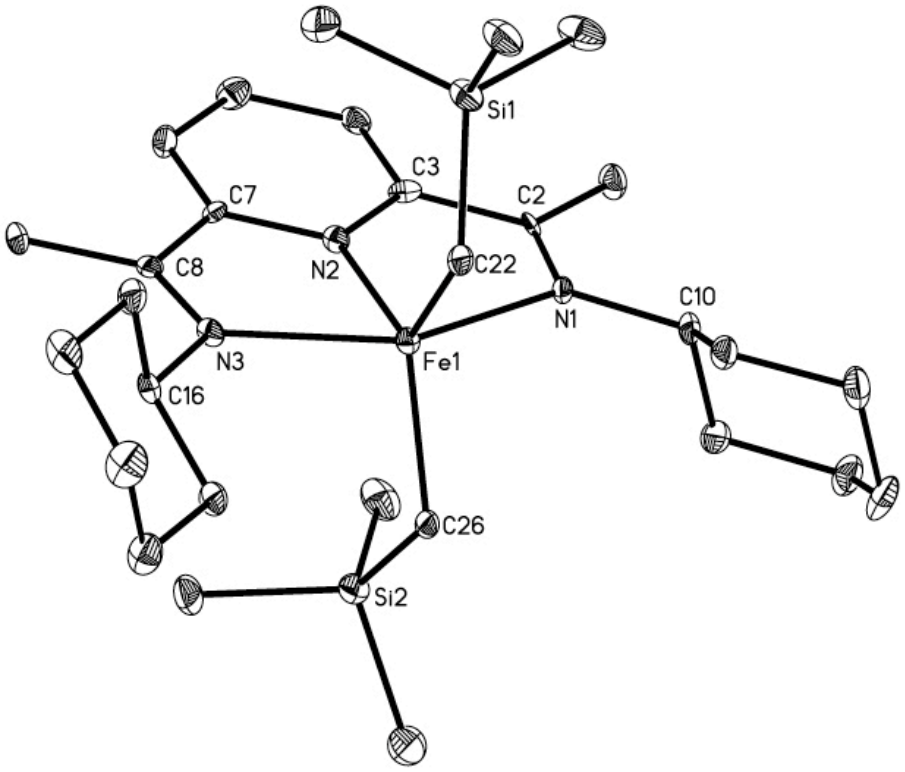

Figure 4.3 Molecular structure of (^{Cy}**APDI)FeR$_2$** at 30% probability ellipsoids. Hydrogen atoms omitted for clarity.

The reduction metrics of APDI ligands aren't as well established as for ^{Ar}PDI iron compounds, but the same general idea would apply to the π* orbitals of the π-acidic imine bonds.[22 23] Upon reduction of the ligand, the imine C=N bond should elongate and the C_{py}-C_{imine} bonds should contract. At first glance, in the case of (^{Cy}APDI)FeR_2, the chelate is unreduced. The N_{imine}-C_{imine} bond lengths of 1.288(4) Å and 1.283(4) Å are most consistent with a neutral bis(imino)pyridine ligand. However the C_{py}-C_{imine} bond lengths of 1.455(4) Å and 1.456(4) Å are significantly shorter than (^{Cy}APDI)$ZnCl_2$, indicating some degree of electron density from the iron.[24] If this is indeed an indication of ligand reduction, it would mean the electron density is not as prevalent in the imine bonds, but rather localized in the pyridine center. The Fe-N_{py} distance of 1.966(2) Å and the Fe-N_{imine} distances of 2.257(2) Å and 2.265(3) Å are notably long, generally

indicating population of the d_{x2-y2} orbital as one would expect from a high-spin iron center. The iron remains in the plane of the chelate, and the iron alkyl bond lengths are in accordance with what was observed for (^{iPr}PDI)FeR_2 at 2.080(4) Å and 2.084(3) Å. The parameters from the crystal structure are slightly ambiguous, but do allow for the assignment of a high-spin formally iron(II) compound.

Table 4.2 Selected crystallographic parameters for **(^{Cy}APDI)FeR_2**.

Bond or Angle	Å or º	Bond or Angle	Å or º
Fe(1)-N(1)	2.265(3)	C(7)-C(8)	1.456(4)
Fe(1)-N(2)	1.966(2)	N(2)-Fe(1)-C(22)	118.44(12)
Fe(1)-N(3)	2.257(2)	N(2)-Fe(1)-C(26)	118.39(12)
Fe(1)-C(22)	2.080(2)	C(22)-Fe(1)-C(26)	123.17(12)
Fe(1)-C(26)	2.084(3)	N(1)-Fe(1)-N(2)	75.06(9)
N(1)-C(2)	1.288(4)	N(2)-Fe(1)-N(3)	75.02(10)
N(3)-C(8)	1.283(4)	N(1)-Fe(1)-N(3)	209.92(9)
C(2)-C(3)	1.455(4)		

The success in the synthesis of a non-aryl substituted PDI compound led to the exploration of other alkyl PDI ligands and their corresponding iron dialkyl complexes. The initial substitutions were trivial, beginning with para substition of the cyclohexyl ring with both a trans methyl group and a *cis/trans* (mixture of isomers) *tert*-butyl group. The chemistry proceeded as readily and cleanly as the parent cyclohexyl compound. An optically active amine, myrtanylamine, was used to synthesize an optically active bis(imino)pyridine chelate. The dialkyl that was formed from the optically active chelate was very greasy and, although the benzene-d_6 ^{1}H NMR spectrum contained peaks consistent with a single compound, is the only dialkyl that could not be isolated as a

solid. Only when the steric demand of the ligand became too great does the chemistry begin to deviate from the expected.

The synthesis of the 2-adamantyl substituted APDI, $^{2\text{-Ad}}$APDI, was easily achieved from the condensation of two equivalents of 2-adamantyl amine, derived from the reductive amination of adamantanone, with 2,6-diacetyl pyridine. Campora's method of chelation to the dialkyl precursor proved ineffective, resulting in the isolation of free ligand. $^{2\text{-Ad}}$APDI was added to $FeCl_2$ and stirred overnight in THF, and the product was precipitated by the addition of pentane, yielding ($^{2\text{-Ad}}$APDI)$FeCl_2$ as a light, light blue solid. A cold diethyl ether slurry of ($^{2\text{-Ad}}$APDI)$FeCl_2$ was treated with 2 equivalents of neosilyl lithium in diethyl ether, which initially gave a dark purple solution, but upon warming to room temperature gave a red solution and brown red/powder. This compound was identified as ($^{2\text{-Ad}}$PDI)FeR, which came about by ejection of an alkyl radical due to the large steric demands of the adamantyl groups. As the dialkyl synthesis was no longer a viable option for this ligand set, the neopentyl (-CH_2CMe_3) version, ($^{2\text{-Ad}}$PDI)FeR'**,** was synthesized and characterized for comparison to other mono alkyls of ^{iPr}PDI iron. The resultant compound has a crystal structure that warrants a deeper consideration.

The ($^{2\text{-Ad}}$PDI)FeR' mono alkyl isolated was the only isolable iron mono-X compound of an alkyl substituted PDI, or Pybox compound, at the time. The dark red ($^{2\text{-Ad}}$PDI)FeR' exhibited a proton NMR spectrum in benzene-d_6 that is consistent with a paramagnetic molecule, the spectrum consisting of broad singlets over a spectral width of nearly 500 ppm. The molecule itself is highly distorted square planar, with the alkyl group bent out of the chelate plane by ~ 54 °. The iron is also lifted out of the plane of the chelate by ~ 0.8 Å. The compound's metrics indicate a high-spin iron, as the Fe-N_{py} distance of 1.9453(17) Å and the Fe-N_{imine} distances of 2.1530(18) Å and 2.2434(17) Å are particularly long, indicating population of the d_{x2-y2} orbital. The C_{imine}-C_{ipso} bond

lengths of 1.459(3) Å and 1.435(3) Å are shorter than in the ^{Cy}APDI zinc dichloride complex and the N_{imine}-C_{imine} bond lengths of 1.312(3) Å and 1.324(3) Å are notably longer than the distances of (^{Cy}APDI)FeR_2, and are more consistent with a singly reduced bis(imino)pyridine ligand. This indicates that the electron density is in the imine π* orbitals, much as in the aryl PDI cases. The solid-state structure is depicted in Figure 4.4.

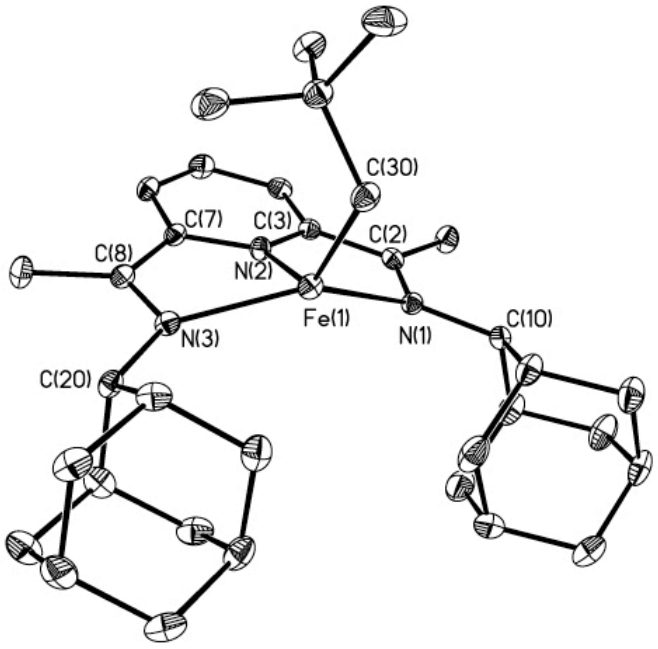

Figure 4.4 Solid-state structure of (**$^{2\text{-Ad}}$APDI)FeR** at 30% probability ellipsoids. Hydrogen atoms are omitted for clarity.

The success in synthesizing a variety of small, sterically forgiving alkyl substituted PDI iron dialkyl complexes prompted further investigation into C_2 symmetric N,N,N terdentate Pybox ligands. Reductive chemistry for this class of iron compound, specifically (*S*,*S*)-(^{iPr}Pybox)$FeCl_2$, results immediately in the paramagnetic bis-chelate iron (0) comound. (*S*,*S*)-(^{iPr}Pybox)$_2$Fe. The benzene-d_6 solution magnetic moment (Evans

method) of 3.0 μB along with the measured solid-state susceptibility of 3.1 μB is consistent with an $S = 1$ complex. The benzene-d_6 solution NMR spectrum of (*S*, *S*)-(^{iPr}Pybox)$_2$Fe at 23 ºC displays 7 peaks over a 350 ppm chemical shift range. The observation of an $S = 1$ ground state is similar to recently reported bis-chelate iron complexes with bis(imino)pyridine ligands where spectroscopic and computational studies supported a high-spin iron(II) center antiferromagnetically coupled to two ligand-centered radical anions. [25] Formally Fe(0) complexes supported by Pybox ligands could be synthesized by reducing the compounds under 4 atmospheres of CO. The resultant dicarbonyl compounds of both (*S*,*S*)-^{ipr}Pybox and (*R*,*R*)-^{indanyl}Pybox were synthesized and characterized as diamagnetic molecules containing CO stretching frequencies that are red shifted compared to (^{iPr}PDI)Fe(CO)$_2$ and more in line with the more electron rich (^{Cy}APDI)Fe(CO)$_2$. In pentane, (*S,S*)-(^{iPr}Pybox)Fe(CO)$_2$ exhibits two bands centered at 1956 and 1852 cm^{-1}, as expected for a C_2 symmetric iron dicarbonyl derivative. However, collecting the spectrum of the same material in KBr revealed four bands, suggesting the presence of two dicarbonyl compounds.

Similar spectroscopic behavior was recently been reported by Goldman and coworkers for the pincer-ligated iron dicarbonyl, (^{tBu}PNP)Fe(CO)$_2$ (^{tBu}PNP = 2,6-*bis*(di-*tert*-butyl-phosphinomethyl)pyridine).[26] For this compound, the four bands were attributed to the presence of both trigonal bipyramidal (TBP) (ν_{CO} = 1846, 1797 cm^{-1}) and square pyramidal (SQP) (ν_{CO} = 1870, 1819 cm^{-1}) isomers in the sample. This behavior is dependent on the phosphine substituents as only the TBP isomer of (^{iPr}PNP)Fe(CO)$_2$ was observed in both the solid-state and in solution.[27] Based on this precedent, the observation of four bands in the solid-state infrared spectrum of (*S,S*)-(^{iPr}Pybox)Fe(CO)$_2$ is likely due to the presence of both TBP and SQP geometries in the solid-state. Interestingly, only one of these isomers was observed in pentane solution (or

the bands are not resolved). It is also noteworthy that (*R*,*R*)-(^{inadanyl}Pybox)Fe(CO)$_2$ exhibits only two bands and hence one geometric isomer in the solid-state.

Table 4.3 Carbonyl stretching frequencies of various dicarbonyl complexes.

Compound	ν_{CO} (cm^{-1})		
			Average
(^{iPr}PDI)Fe(CO)$_2$	1974	1914	1944
(^{Ad}APDI)Fe(CO)$_2$	1951	1882	1916
(^{Cy}APDI)Fe(CO)$_2$	1955	1888	1922
(*S, S*)-(^{iPr}Pybox)Fe(CO)$_2$	1956	1852	1904
(*S, S*)- (^{iPr}Pybox)Fe(CO)$_2$[a]	1954	1878	1916
	1930	1856	1893
(*R, R*)- (^{Ind}Pybox)Fe(CO)$_2$[a]	1938	1868	1903

[a.] Recorded in KBr.

Both the bis-chelate and dicarbonyl complexes are catalytically inert. Another method of introducing an optically active ligand into iron based catalysis proved necessary. Should the dialkyl complexes demonstrate utility in catalysis, then the PyboxFeR$_2$ class of compounds would be a facile route into asymmetric catalysis.

The initial synthesis of the PyboxFeR$_2$ compounds began with ^{iPr}Pybox utilizing Campora's method of synthesis. The Pybox ligand was added to a stirring solution of the dialkyl precursor (Py)Fe(CH$_2$SiMe$_3$)$_2$, resulting in an immediate color change to purple, a reliable indicator of the synthesis of the desired dialkyl complex. (^{iPr}Pybox)FeR$_2$ was isolated as a dark purple powder that displayed an effective magnetic moment of 4.6 μ_B in the solid-state at 290 K, consistent with an S=2, high-spin formally iron(II) compound. The ^{1}H NMR spectrum consists of broad singlets spanning nearly 400 ppm. Comparative ^{1}H NMR spectra from the three classes of the dialkyl compounds, aryl PDI, APDI, and Pybox, are displayed in Figure 4.5.

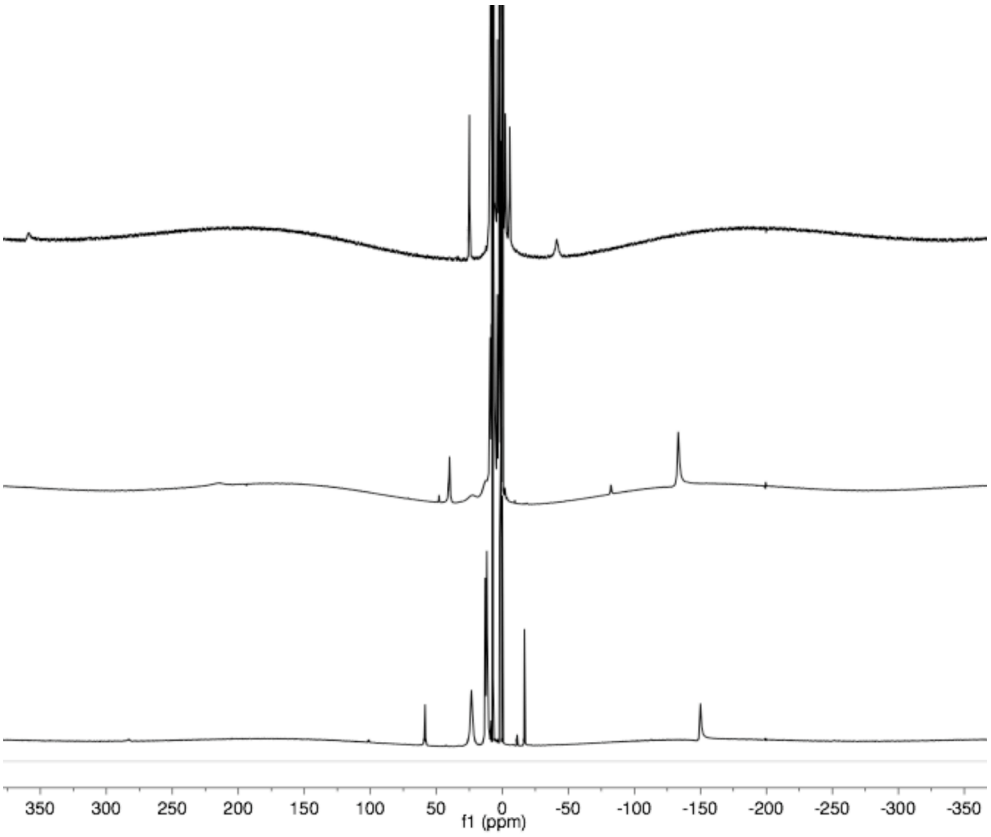

Figure 4.5 Benzene-d_6 spectra, from bottom to top, of (**^{2,6Me}APDI)FeR$_2$**, (**^{cy}APDI)FeR$_2$**, and (**^{iPr}Pybox)FeR$_2$**.

The ^{indanyl}Pybox was subjected to the same synthetic method as the ^{iPr}Pybox, but the ligation of the chelate did not proceed cleanly, yielding mainly free ligand. The dichloride was therefore synthesized, yielding high-spin Fe(II) (^{indanyl}Pybox)FeCl$_2$. This compound was treated with two equivalents of neosilyl lithium, resulting in a color change to dark purple. A dark purple powder was isolated that had characteristic spectroscopy and magnetism for (^{indanyl}Pybox)FeR$_2$, with an effective magnetic moment of 4.6 μ_B, consistent with an $S = 2$, high-spin, formally iron(II) compound.

X-ray diffraction was accomplished for both compounds, yielding structures much more similar to the (^{Cy}APDI)FeR$_2$ than to (^{iPr}PDI)FeR$_2$. Both compounds are trigonal bipyramidal, with the equatorial plane running through the central pyridine ring

and the alkyl groups. The oxazoline nitrogens through the iron center form the axial plane. The metrics of the crystals will be discussed individually.

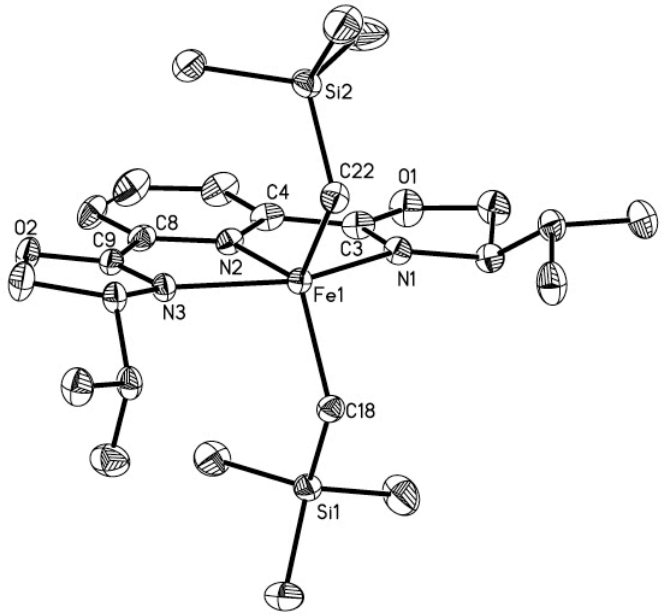

Figure 4.6 X-ray structure of (^{iPr}Pybox)FeR_2 at 30% probability ellipsoids. Hydrogen atoms are omitted for clarity.

The solid-state structure of (^{iPr}Pybox)FeR_2 is in a distorted trigonal bipyriamidal geometry. The isopropyl substituents on the oxazoline ring create the chiral 'pocket' around the iron center along the C_2 axis. Pybox ligands have been previously reported to be redox inactive. A comparison to the zinc(II) chloride adduct will give some indication to the veracity of those previous claims. The $N{=}C_{oxazoline}$ bond lengths of 1.2729(19) Å and 1.2831(19) Å are most consistent with an unreduced Pybox chelate found in (^{iPr}Pybox)$ZnCl_2$[28] that has bond lengths of 1.271(4) Å and 1.271(4) Å. Again, the C-C bond lengths do indicate some degree of back donation to the ligand from the iron center. The $C_{oxazoline}$-C_{ipso} bond lengths of 1.436(2) Å and 1.425(2) Å are significantly shorter than in the zinc dichloride adduct, 1.477(4) Åand 1.476(4) Å, indicating some degree of

electron density on the chelate.[28] The Fe-N_{py} distance of 1.9975(11) Å and the Fe-N_{imine} distances of 2.2859(11) Å and 2.2214(12) Å are similar to those of the high-spin PDI compounds, indicating population of the d_{x2-y2} orbital.

(^{indanyl}Pybox)FeR_2 (Figure 4.7) is structurally very similar to (^{iPr}Pybox)FeR_2 and (^{Cy}APDI)FeR_2. Again, the chiral pocket is very clear, even more so with the size of the indanyl groups. The N=$C_{oxazoline}$ bond lengths of 1.2729(19) Å and 1.2831(19) Å are very similar to the unreduced values of 1.29(1) Å and 1.28(1) Å for the corresponding bonds in (^{indanyl}Pybox)$ZnCl_2$.[29] The $C_{oxazoline}$-C_{ipso} bond lengths, unfortunately, are not significantly shorter than the non-reduced bond lengths of 1.45(1) Å and 1.44(1) Å found in (^{indanyl}Pybox)$ZnCl_2$. The $C_{oxazoline}$-C_{ipso} bond lengths of 1.436(2) Å and 1.425(2) Å may indicate some degree of backbonding from the iron, but the indanyl rings are aromatic and the electron density is more diffuse than the case of (^{iPr}Pybox)FeR_2. The Fe-N_{pyr} distance of 1.9975(11) Å and the Fe-N_{imine} distances of 2.2859(11) Å and 2.2214(12) Å indicate population of the d_{x2-y2} orbital.

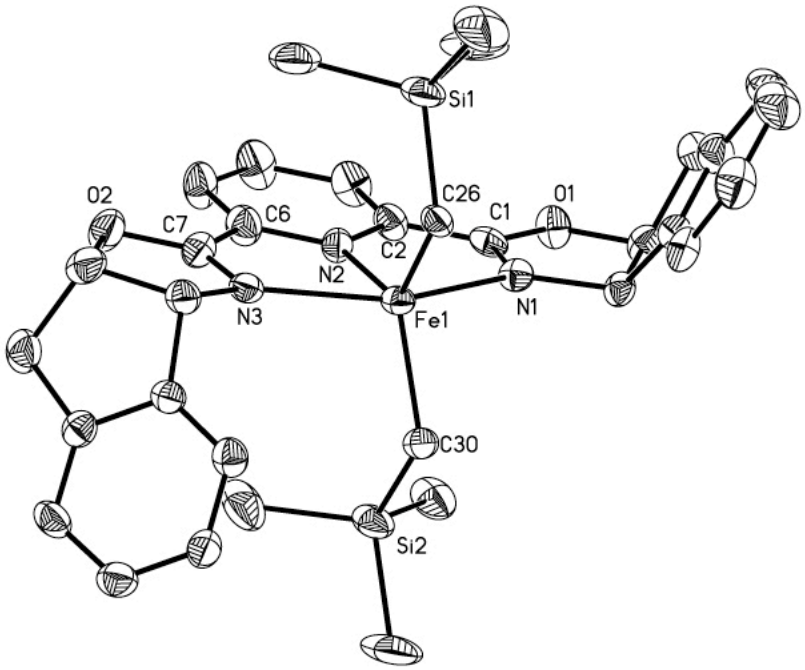

Figure 4.7 X-ray structure of (^{indanyl}**Pybox)FeR$_2$** at 30% probability ellipsoids. Hydrogen atoms are omitted for clarity.

The synthesis of PDI and Pybox bis-neosilyl iron compounds proved to be general and facile. With a large number of compounds synthesized and characterized, comparisons of these compounds' electronic structures and the catalytic competency could be analyzed.

4.4 Determination of the Electronic Structure of Iron Dialkyl Complexes

With the synthesis of three distinct types of iron dialkyl complexes in hand, with each class characterized crystallographically, giving some idea of the degree of chelate participation in each case, a comparison of the electronic structures of these compounds is in order. Each iron dialkyl complex has effectively the same magnetic moment, in the range of 4.6 μ_B to 4.9 μ_B, indicating a ground state of S=2 with a high-spin iron center. In the case of (^{iPr}PDI)FeR$_2$, the metrics of the chelate reduction do indeed indicate that the PDI is one electron reduced, yielding a high-spin ferric center. Another indication of high-spin ferric versus high-spin ferrous is the Mössbauer spectrum. The isomer shift of

0.28 mm/s is too low for a typical high-spin ferrous compound, compounds that have isomer shifts typically of at least 0.6 mm/s.[30] Mössbauer spectroscopy was performed on (^{Cy}APDI)FeR$_2$ and (^{iPr}Pybox)FeR$_2$ as well, and they have low isomer shifts, at 0.27 mm/s for the APDI and 0.28 mm/s for the Pybox compound. This indicates the same electron density at the iron center in each case. Figure 4.8 gives side-by-side comparisons of the Mössbauer spectra.

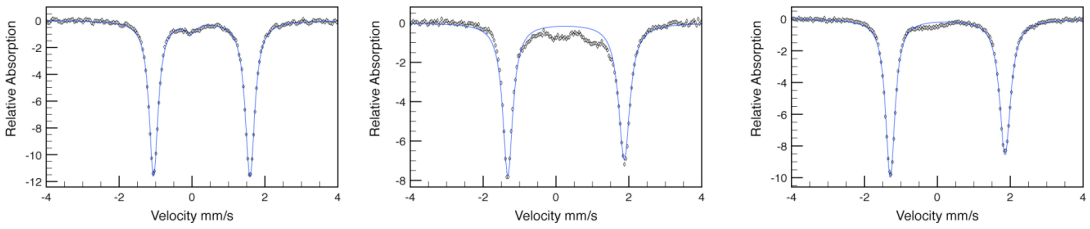

Figure 4.8 Mössbauer spectra of **(^{iPr}PDI)FeR$_2$**, **(^{Cy}APDI)FeR$_2$**, and **(^{iPr}Pybox)FeR$_2$** obtained at 80 K.

The Mössbauer parameters are too similar among the compounds to assign the (^{iPr}Pybox)FeR$_2$ as a ferric center (due to the PDI ligand parameters indicating mono-reduction,) and the other two, less obvious cases as ferrous centers. The imine bond lengths hardly change in both the (^{Cy}APDI)FeR$_2$ and (^{iPr}Pybox)FeR$_2$ cases, but the C$_{imine}$-C$_{ipso}$ bonds in both cases shorten significantly. This could be an indication of radical character more in the pyridine ring of the ligand rather than being delocalized throughout the entire π-system. To determine the electron distribution in these molecules, DFT calculations were performed.

The compounds were each fully geometry optimized at the B3LYP level of theory. The crystal structures were used as starting points in the calculations. Bond lengths and distances for both the crystal structures as well as the computed parameters are given in Table 4.4.

Table 4.4 Selected structural parameters, both computed and experimental, for three different classes of dialkyl complex.

	(^{iPr}Pybox)Fe($CH_2TMS)_2$ X-ray*	Calc.	(^{Et}PDI)Fe($CH_2TMS)_2$ X-ray	Calc.	(^{Cy}APDI)Fe($CH_2TMS)_2$ X-ray	Calc.
Fe(1)-$C_{Alkyl-1}$	2.0610(15)	2.097	2.054(3)	2.095	2.080(4)	2.110
Fe(1)-$C_{Alkyl-2}$	2.0605(16)	2.103	2.062(3)	2.102	2.084(3)	2.111
Fe(1)-N(1)	2.2859(11)	2.284	2.2030(19)	2.295	2.265(3)	2.315
Fe(1)-N(2)	1.9975(11)	2.042	2.0133(19)	2.059	1.966(2)	2.015
Fe(1)-N(3)	2.2214(12)	2.339	2.263(2)	2.322	2.257(2)	2.322
N(1)-C(2)	1.2838(19)	1.290	1.302(3)	1.305	1.288(4)	1.301
N(2)-C(3)	1.3815(17)	1.373	1.368(3)	1.371	1.388(4)	1.372
N(2)-C(7)	1.3691(19)	1.370	1.369(3)	1.370	1.385(4)	1.371
N(3)-C(8)	1.2729(19)	1.292	1.301(3)	1.303	1.283(4)	1.300
C(2)-C(3)	1.425(2)	1.446	1.448(3)	1.458	1.455(4)	1.466
C(7)-C(8)	1.436(2)	1.449	1.454(3)	1.461	1.456(4)	1.466
C(1)-Fe(1)-C(2)	117.07(6)	118.5	112.00(11)	112.7	123.17(12)	121.7
N(2)-Fe(1)-C(1)	121.20(6)	120.9	107.93(9)	140.3	118.39(12)	119.3
N(2)-Fe(1)-C(2)	121.54(6)	120.4	140.02(10)	107.0	118.44(12)	119.0
N(1)-Fe(1)-N(3)	149.89(4)	149.4	141.07(7)	139.4	150.08(9)	149.7
N(2)-Fe(1)-N(1)	75.19(5)	74.7	74.03(7)	73.0	75.06(9)	74.9
N(2)-Fe(1)-N(3)	74.70(5)	74.7	72.88(7)	72.5	75.02(10)	74.8

* The numbering scheme is different, but the analogous bonds are shown.

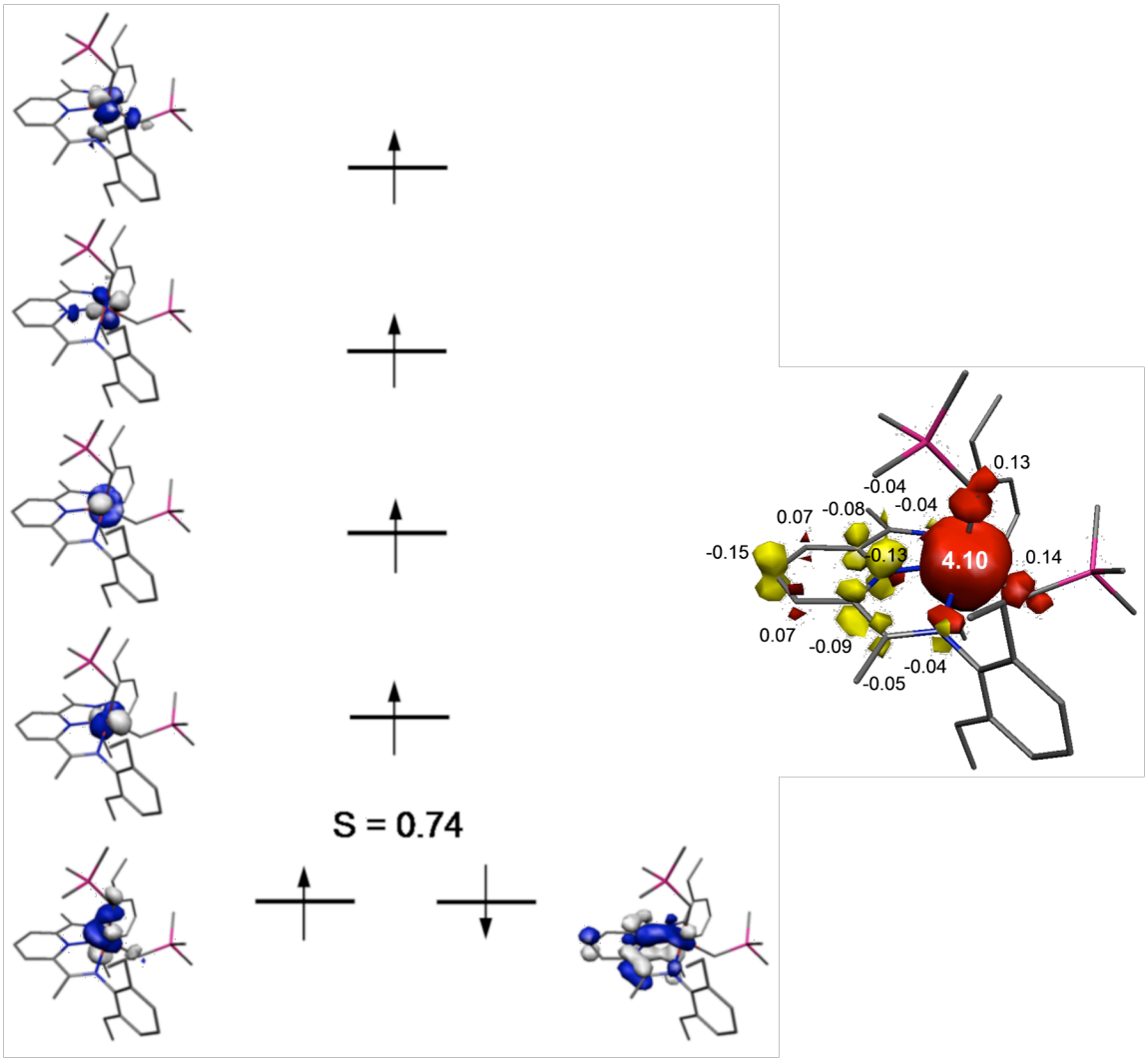

Figure 4.9 A qualitative MO diagram for **(^{Et}PDI)FeR$_2$** and a spin density plot is displayed.

The calculations on (^{Et}PDI)FeR$_2$ were performed, which has Mössbauer parameters identical to the isopropyl compound, and the results confirm the mono-reduction of the PDI ligand, as shown in Figure 4.9, providing further evidence of the high-spin ferric center to help rationalize the low isomer shift in the Mössbauer spectrum. The field strength and covalency of the PDI ligand increases upon reduction

such that the isomer shift tends to lower towards zero the higher the electron density on the PDI.

The molecular orbital of the reduced PDI π* indicates that the imine antibonding orbital contains a large portion of the electron density, explaining the origin of the significant lengthening of the imine bond. The spin density plot yields a total of four unpaired spins on the iron, with the PDI ligand containing a total of one spin of opposite sign.

The antiferromagnetic coupling arises from the b_2 ligand based molecular orbital and a clover-leaf iron based orbital; in the high symmetry limit of C_{2v} for the compound, the d_{yz} orbital is of the proper symmetry and can interact with the PDI orbital. The overlap integral of 0.79 indicates a high degree of covalency between the PDI and the metal center. These calculations help confirm the electronic structure as suggested by the Mössbauer spectrum, crystal structure, and magnetic measurements.

For the APDI iron complexes, the crystal structure is not as helpful in determining chelate participation in the oxidation state of the iron. From the magnetic measurements and with a strong indication from the Mössbauer, the conclusions for the aryl PDI ligands are transferable to the alkyl PDI compounds. The spin density localization of the alkyl PDI ligands ought to be slightly different than that of the aryl PDI compounds based upon the crystal structure data. The DFT calculations were performed and the results are displayed in Figure 4.10.

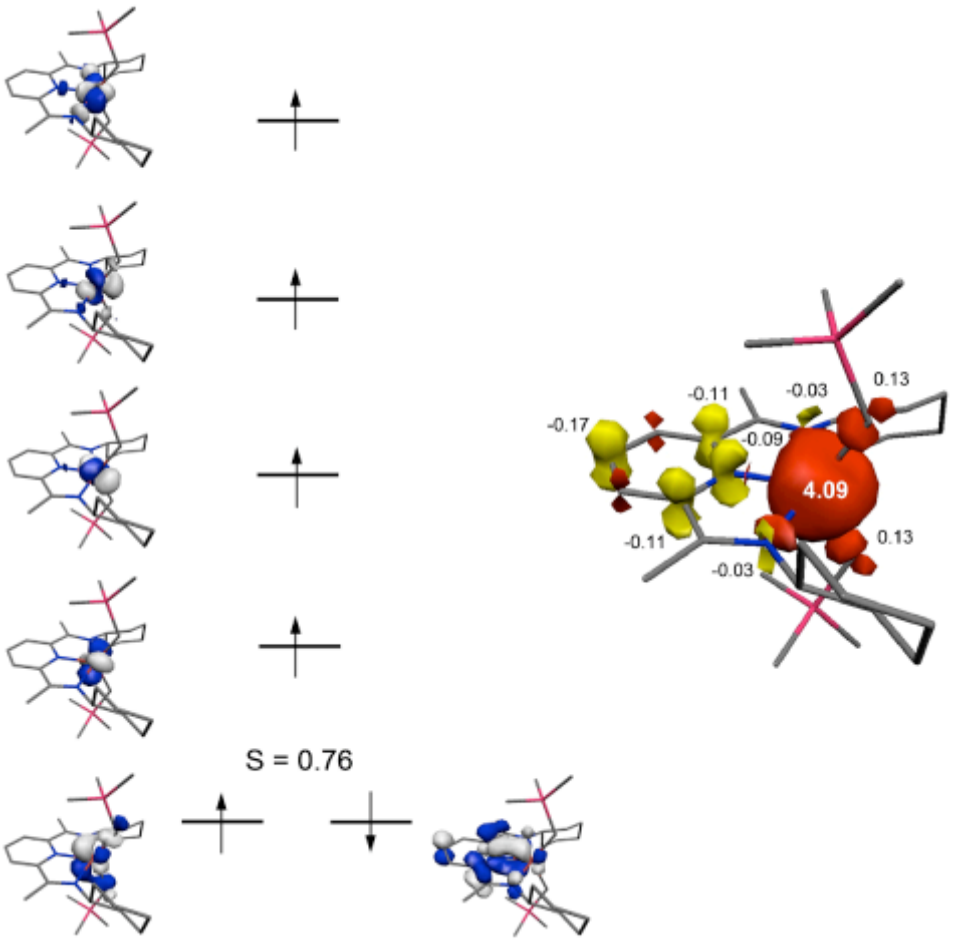

Figure 4.10 A qualitative MO diagram for (^{Cy}**APDI)FeR$_2$** and a spin density plot is given.

The APDI ligand displays a similar amount of electronic character as the PDI complex, confirming the ferric center of the complex. The overlap between the PDI π* b_2 orbital and the corresponding cloverleaf d_{yz} orbital is also similar to the PDI case, indicating a large degree of covalency in the APDI-iron unit. There is also spin density on the alkyl groups in each case. The spin density on the ligand is not evenly distributed throughout the π* system, but is rather localized on the central pyridine ring as well as the C_{imine}-C_{ipso} bond, a result that is supported by the crystal structure. This also helps explain the lack of imine bond elongation in the compound that appears to have the same electronic structure as PDIFeR$_2$.

Finally, (^{iPr}Pybox)FeR_2 was calculated to complete the series. Classically, Pybox ligands have been seen as being non-redox-active. Thus, the similarity to PDI dialkyl systems by Mössbauer spectroscopy was unexpected. The indication is that the iron center has essentially the same electron distribution across the series. Spin unrestricted calculations for a quintet ground state at the B3LYP level of theory were conducted to verify this claim, and the broken symmetry results are given in Figure 4.11.

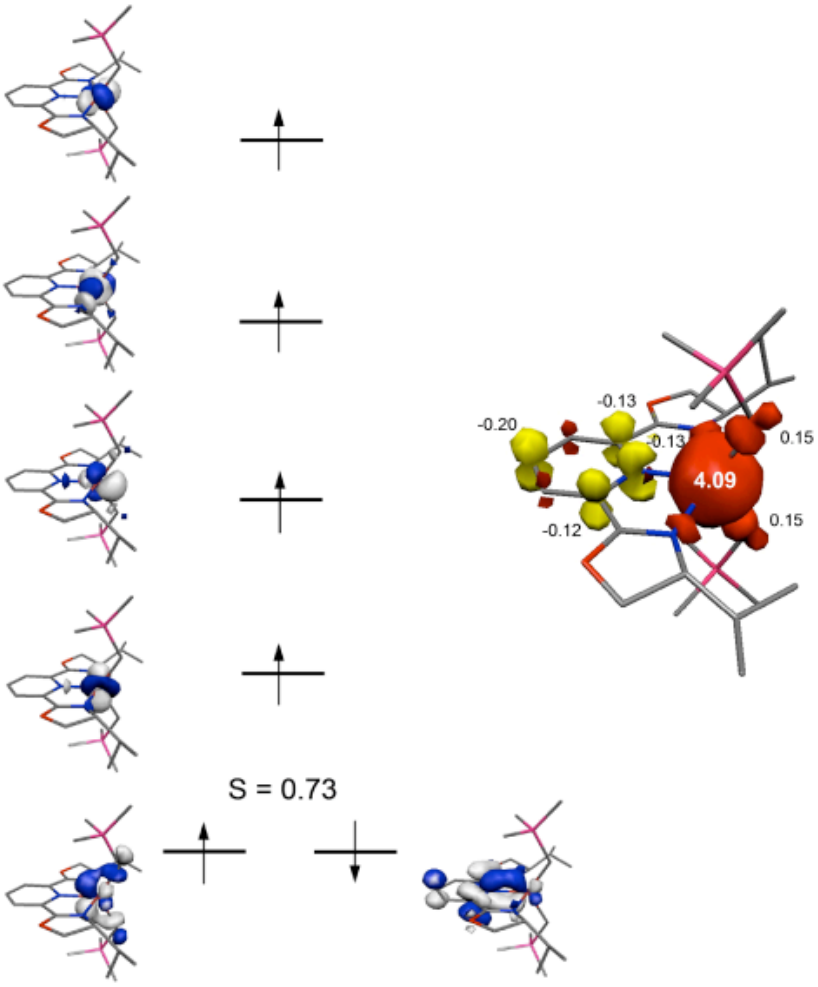

Figure 4.11 A qualitative MO diagram for (^{iPr}**Pybox**)$\mathbf{FeR_2}$ and a spin density plot is displayed.

The pybox ligand is one electron reduced as shown in the spin density plot, with a total spin of 0.6 located on the ligand and a total of four spins on the iron center of opposite sign. The reduced ligand molecular orbital has the significant amount of spin density localized on the pyridine ring of the ligand and almost zero density located on the oxazoline rings. The $C_{oxazoline}$-C_{ipso} bond does contain significant density and accounts for the significant shortening of that bond in the solidstate structure. Given that the oxazoline itself does not contain a large amount of electron density is due in part to the electron-rich oxazoline rings' π^* system being energetically inaccessible.

The results of the electronic structure study indicate that the metal center from all three classes of iron dialkyl is best described as being in a high-spin Fe (III) oxidation state. The electron distribution is slightly different in each case, but the supporting ligand is indeed reduced in for each system. The Mössbauer spectra do not make sense for high-spin ferrous centers, but are compatible with the assignment of high-spin iron (III) anti-ferromagnetically coupled to a mono reduced ligand. The DFT gives further credence to this assignment for each class of compound.

4.5 Catalytic activity of PDI and Pybox Iron Dialkyl Complexes

The initial target for catalysis of the dialkyl compounds was olefin hydrogenation. The comparison of hydrogenation activity to (^{iPr}PDI)Fe(N_2)$_2$ would prove useful. (^{iPr}PDI)FeR_2 was used initially to prove that the PDI supported dialkyl could affect the same catalytic transformation. Both limonene and cyclohexene were successfully hydrogenated under similar conditions to the dinitrogen compound. This result proved that the PDI dialkyl complexes were indeed precatalysts. The other aryl PDI compounds were used in this hydrogenation as well, and each dialkyl complex gave full conversion of the two substrates under 4 atmospheres of H_2 at 1 mol% after one hour. The limonene results are summarized in Table 4.5.

Table 4.5 Limonene hydrogenation results utilizing a variety of dialkyl complexes.

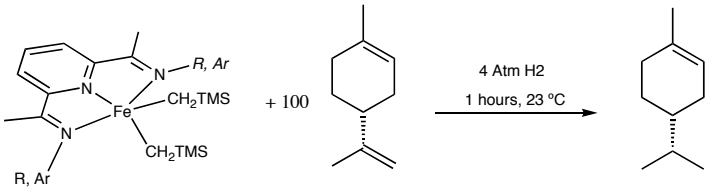

R, Ar	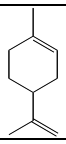		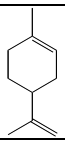
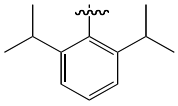	> 95%	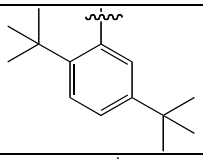	0%
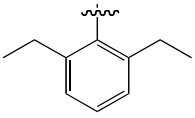	> 95%	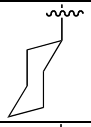	6%
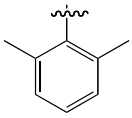	> 95%	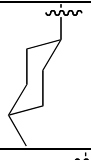	15%
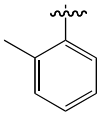	> 95%	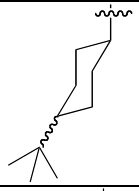	12%
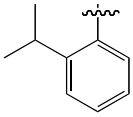	> 95%	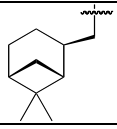	0%

When the less sterically demanding (^{Cy}APDI)FeR_2 compounds were used in the catalytic transformation, the results were less successful. The cyclohexene reduction would not complete, even with extended reaction times, and the limonene reduction

would only proceed to roughly 10%. In order to establish what was happening to the iron under hydrogenative conditions, H_2 was added to (^{Cy}APDI)FeR_2 without substrate, and the product of the reaction analyzed. The resulting iron compound was the bis chelate, (^{Cy}APDI)$_2$Fe, the same product one yielded from amalgam reduction of (^{Cy}APDI)FeX_2 (X = Cl, Br).[25] This identified the formation of the bis chelate as a prevalent catalyst deactivation pathway. The compound displayed an $S = 1$ ground state, and computational studies support a high-spin Fe(II) center antiferromagnetically coupled to two ligand-centered radical anions. The solid-state structure contained a high amount of disorder in the cyclohexyl substituents, but the bond lengths in the core of the molecule were precise enough to compare the oxidation state of the ligands to the dialkyl complex. The solid-state structure is displayed in Figure 4.12.

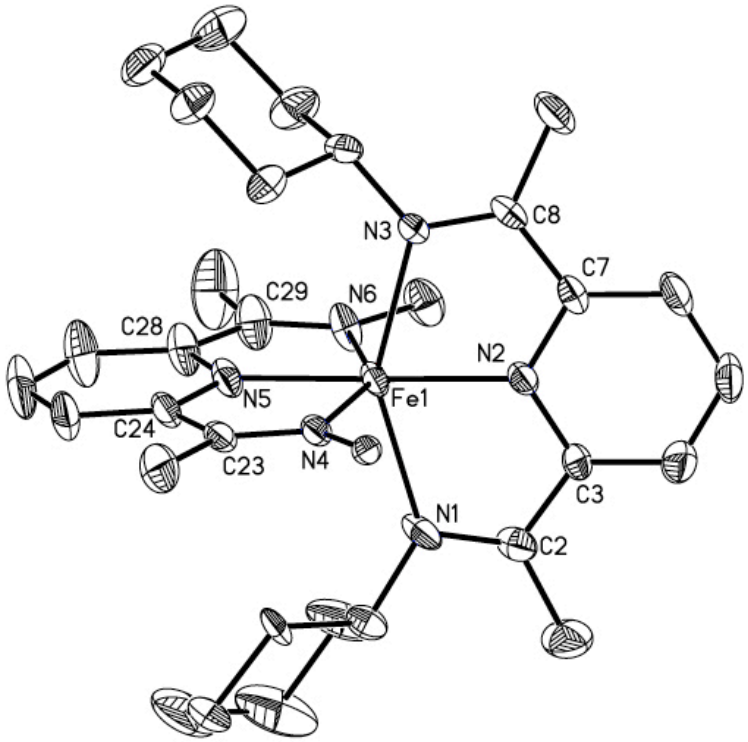

Figure 4.12 Molecular structure of (^{Cy}**APDI)$_2$Fe** at 30% probability ellipsoids. Two cyclohexyl rings and hydrogens omitted for clarity.

The above hydrogenation results indicate that dialkyl complexes with PDI supporting ligands do affect catalytic transformations. The hydrogenation reactions with aryl substituted PDI ligands were qualitatively as effective as the dinitrogen compound in the reduction of geminal and internal alkenes. The alkyl substituted PDI compounds did perform catalysis, but to a much lower extent due to the facile formation of the bis-chelate under reductive conditions. The proof of principle reaction was successful, however, in that the dialkyl complexes proved catalytically competent.

Although it is one of the most active olefin hydrogenation catalysts known, the PDI iron bis dinitrogen compound does not catalytically reduce ketones or aldehydes under hydrogenative conditions. The addition of this substrate class to the scope of viable substrates for reduction would, in effect, double the scope of functionality that this iron system is competent to reduce. This, paired with the ease of synthesis of the starting dialkyl complexes, made the hydrosilylation of ketones and aldehydes a desirable target.

(^{Cy}APDI)FeR_2 was chosen for the initial catalyst screen due to its ready availability, sterics, and the fact that APDI ligands had yet to prove useful for catalysis. The iron dialkyl was added to 20 equivalents of a 1:1 ratio of benzaldehyde and phenylsilane in a stirring solution of diethyl ether for one hour. The purple color of the dialkyl persisted throughout the reaction. After the work-up, the ^{1}H NMR contained no indication of the aldehydic proton and only traces of phenyl silane, but new Si-H resonances were also present. A GC/MS of the product mixture indicated mainly the 1:1 product of hydrosilylation, but also the addition of two and three aldehydes per phenyl silane. After hydrolysis with acidic water, 1M HCl, the product was cleanly benzyl alcohol.

The use of a more sterically hindered silane, diphenylsilane, yielded cleanly the 1:1 hydrosilylation product. Tertiary silanes such as triethylsilane, triethoxysilane, and phenyldimethylsilane were inactive for hydrosilylation, even at elevated temperatures.

The diphenylsilane adduct was more stable to protonolysis and the deprotection of the silylether was carried out more effectively with basic water, 1M KOH, and the deprotection time was on the order of hours, not minutes. The initial discoveries are summed up in Figure 4.13.

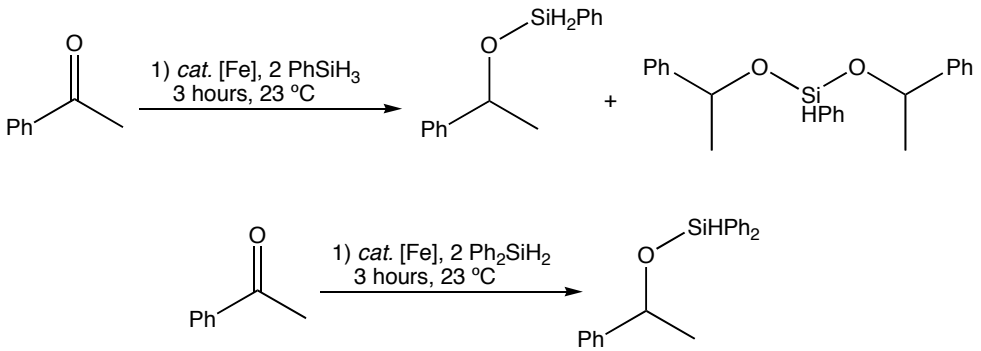

Figure 4.13 General hydrosilylation activity of (^{Cy}**APDI)FeR$_2$** without deprotection.

To further the chemistry, ketones, specifically acetophenones, were targeted next. These carbonyls are slightly more challenging to reduce, but more importantly contain a stereogenic carbon center, allowing for asymmetric reduction. Following the results of multiple insertions using phenylsilane, diphenylsilane was used to simplify the reaction mixture and allow for mechanistic investigations. The silylethers are readily characterized by NMR, GC/MS and IR spectroscopy. Various acetophenones and alkyl ketones were subjected to the same hydrosilylation procedures as benzaldehyde, and for comparison, the previously reported (^{iPr}PDI)FeR$_2$ was used as a precatalyst under the same reaction conditions. The scope of the ketonic substrates is given in Table 4.6.

Table 4.6 Conversion percentage of substrate to alcohol for two dialkyl complexes.

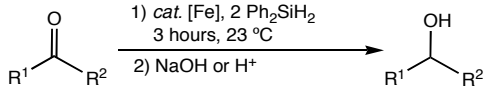

Substrate	^{iPr}PDIFeR_2[a]	^{Cy}APDIFeR_2[b]	Substrate	^{iPr}PDIFeR_2[a]	^{Cy}APDIFeR_2[b]
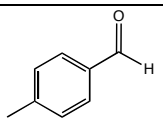	> 99	> 99	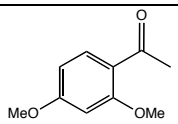	57	94
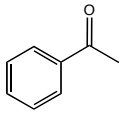	> 99	> 99	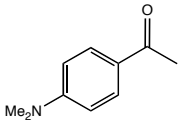	27	95
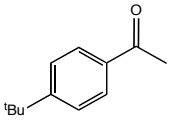	> 99	> 99	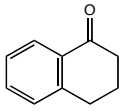	27	82
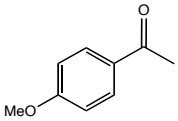	> 99	> 99	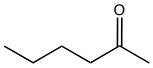	> 99	58
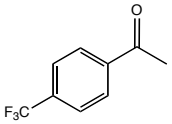	> 99	> 99	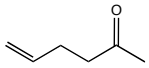	75	54
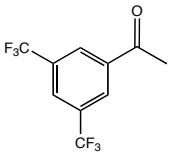	21	68			

[a] 1 mol% ^{iPr}**PDIFeR$_2$**. [b] 0.1 mol% ^{Cy}**APDIFeR$_2$**.

The competition experiment showed that (^{Cy}APDI)FeR_2 was a faster catalyst than (^{iPr}PDI)FeR_2, and was less sensitive to substrate impurities/moisture than the PDI compound. Alkyl ketones such as 2-hexanone were generally slower than the acetophenones, although for extended reaction times the catalysis would complete. There also appeared to be an electronic effect if the aryl group was substituted with either

strongly electron withdrawing or donating groups. This electronic effect was investigated next.

A series of competition experiments were undertaken to determine the electronic effect of the substrate on the rate of hydrosilylation. Two different para-substituted acetophenones were reacted with half an equivalent of silyl-hydride and the relative rate of hydrosilylation was measured to determine the electronic effects of the substrate. The results of this study demonstrate that electron-withdrawing substrates react faster than electron donating substrates, indicating a negative charge build up on the carbonyl carbon in the transition structure of the rate determining step. This electronic effect was consistent throughout each class of dialkyl iron complex.

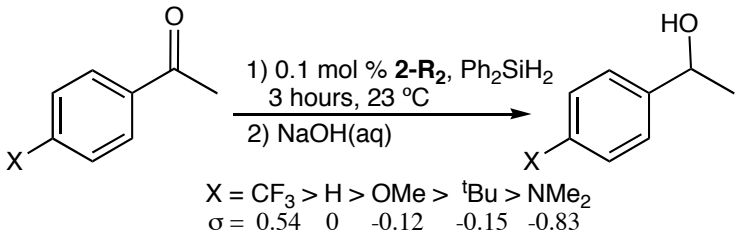

Figure 4.14 Results of the investigation of electronic effects on catalysis

Conjugated α,β unsaturated 'enones' were next considered as substrates in the catalytic transformations to determine chemoselectivity of 1,4- or 1,2- additions of the conjugated bonds. Casey reported little to no chemoselectivity in the use of the iron containing, Schvo type catalyst in the hydrosilylation of enones.[31] The results of these catalyses are given in Figure 4.15. In a constrained, cyclic enone where the single bond is forced *s-trans,* the reduction occurs solely in a 1,2 fashion. Where a rotable single bond is allowed, as in the case of chalcone or benzylidene acetone, and the enone can enter the *s-cis* conformation, the chemoselectivity drops and 1,4 addition begins to be

competitive with 1,2 addition. Deuteration of the silane confirmed the regioselectivity of the reaction.

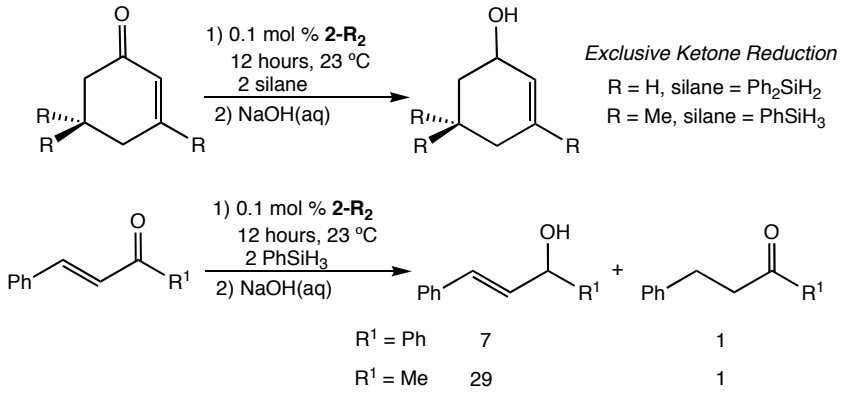

Figure 4.15 Hydrosilylation activity of (^{Cy}**APDI)FeR$_2$ (=2-R$_2$)**with α,β-unsaturated substrates.

The Pybox supported iron complexes were next utilized in catalysis to determine if the reduction of acetophenones could be carried out selectively. Utilizing the same reaction conditions as above, a 1:1 ratio of diphenylsilane to substrate, and with (^{iPr}Pybox)FeR$_2$, the catalysis plateaus at 30% enantiomeric excess (ee). Steps were taken to try and increase the selectivity. The conditions that yielded the highest ee's happened to also be the conditions to give the fastest turnover. Utilizing two equivalents of phenylsilane per substrate, in a 0.4M diethyl ether solution for an hour increased the selectivity, after hydrolysis, to 60% ee. The results from the variety of substrates with turnover frequencies and ee's from a variety of Pybox ligands are located in Table 4.7.

Table 4.7 Hydrosilylation activity of Pybox compounds with substrates. Yields are the top number and ee's are in parenthesis

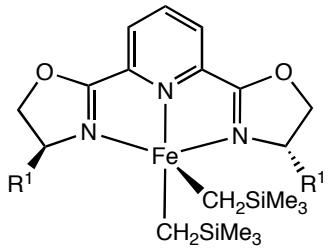

Substrate	R^1 = ^{i}Pr	^{t}Bu	Ind	Bz	^{i}Bu
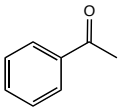	80 (49)	99 (30)	99 (19)	99 (18)	99 (8)
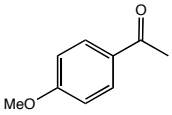	99 (5)	99 (3)	84 (<1)	99 (29)	97 (5)
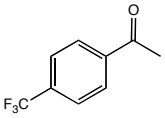	99 (20)	99 (12)	99 (19)	99 (21)	99 (12)
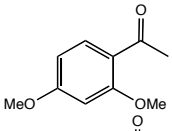	99 (32)	99 (50)	99 (32)	99 (32)	99 (22)
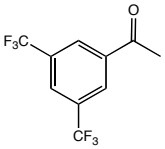	99 (6)	72 (12)	99 (6)	99 (6)	99 (4)
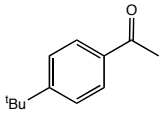	99 (23)	99 (25)	99 (10)	99 (25)	99 (11)
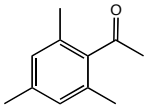	< 1 -	2 (5)	1 (30)	4 (44)	2 (26)
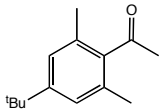	<1 -	1 (30)	1 (33)	<1 -	<1 -
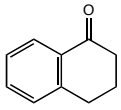	99 (32)	60 (2)	99 (11)	93 (22)	25 (7)

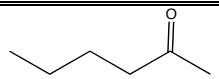	58 (10)	99 (25)	99 (11)	46 (17)	46 (17)

The conversions of substrate to alcohol were good to complete in all cases except when the acetophenone substrate was substituted in the 2 and 6 position, then the catalysis became negligible. The ee in each case was poor, with the best selectivity coming from the parent acetophenone and the isopropyl Pybox compound at 49% ee and the typical selectivity being below 20%.

Comparing (^{Cy}APDI)FeR_2 with the Pybox iron dialkyls indicates that the bis(imino)pyridine compound is more active for catalysis. For example, the hydrosilylation of 2-hexanone with (^{Cy}APDI)FeR_2 proceeds with a turnover frequency of 193 hr^{-1} at 23 ºC, with (^{iPr}Pybox)FeR_2 the value is reduced to 78 hr^{-1}. These comparisons were made with 0.1 mol% catalyst loadings.

In an attempt to improve the enantioselectivity of the iron-catalyzed hydrosilylation reactions, each of the (^{iPr}Pybox)FeR_2-promoted reactions were conducted in the presence of one equivalent (per iron) of $B(C_6F_5)_3$. It was hoped that treatment of the pyridine bis(oxazoline) and bis(oxazoline) iron dialkyls with neutral borane would generate the corresponding iron alkyl cation and may increase activity,[32] prevent bis chelate formation and improve the observed enantioselectivities. The results of these experiments are reported in Table 4.8.

Table 4.8 The conversions and (ee) of the addition of one equivalent of borane to reaction mixture in the hydrosilylation catalysis.

Substrate	(^{iPr}Pybox)FeR_2 + $B(C_6F_5)_3$	Substrate	(^{iPr}Pybox)FeR_2 + $B(C_6F_5)_3$
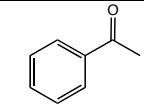	99 (54)	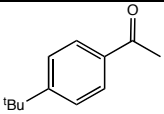	99 (13)
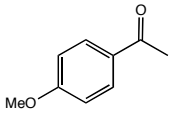	55 (25)	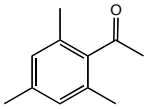	1 (30)
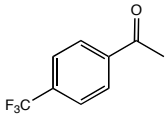	99 (20)	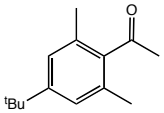	< 1
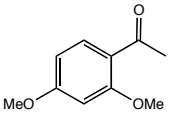	99 (32)	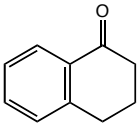	99 (41)
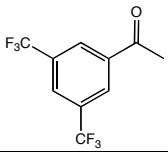	99 (6)	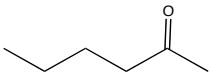	99 (11)

For the (^{iPr}Pybox)FeR_2 catalysis, only modest improvements resulted. Certain substrates such as acetophenone and 2-hexanone were reduced with higher productivity while others such as *p*-methoxyacetophenone were slower. One possibility is that the in situ generated iron alkyl cation may be more sensitive to impurities and undergoes more rapid decomposition. The enantioselectivity for acetophenone and alpha-tetralone was improved to 54% and 41%, respectively.

The results of the catalytic reduction of ketones and aldehydes were encouraging in the sense that a new substrate type could be catalytically reduced utilizing a pre-catalyst that was made without the use of mercury. The number of precatalysts that can be made is much greater than the number of dinitrogen compounds that are available, due to the fact that there are not nearly as many limitations for dialkyl chemistry as there are for dinitrogen chemistry. The catalysis was performed under mild conditions and was fast and with few side-products. One downside is that asymmetric catalysis from the

Pybox series did not yield useful selectivities. For racemic formation of silyl ethers or the deprotected alcohol, the use of PDI and Pybox supported iron dialkyl compounds is a faster and milder method than other known iron based reduction systems.

4.6 Conclusion

The synthesis, electronic structure, and catalytic activity of a series of bis(imino)pyridine iron dialkyl and 2,6-(*R*-oxazoline)$_2$C$_5$H$_3$N iron dialkyl complexes was investigated. These compounds were synthesized either by addition of two equivalents of neosilyllithium to the chelate iron dichloride or by ligation of the chelate to a generated bis pyridine iron (II) dialkyl. The resulting purple compounds were each $S = 2$, with magnetic moments between 4.5 and 4.9 μ_B. These compounds are best described as high-spin iron (III) compounds, with the chelate mono-reduced and antiferromagnetically coupled to the iron center. This is corroborated by X-ray crystallography, Mössbauer spectroscopy, and DFT calculations. In contrast to the popular belief of Pybox ligands being redox innocent, the above studies indeed indicate that the ligand can accept at least one electron, which accounts for the similar isomer shifts in the Mössbauer spectra seen among these iron compounds. The hydrosilylation activity of the compounds was explored and, although enantioselectivity was poor, proved to be among the most active of any other iron system to date.

4.7 Experimental Procedures

General Considerations. All air- and moisture-sensitive manipulations were carried out using standard vacuum line, Schlenk and cannula techniques or in an MBraun inert atmosphere dry box containing an atmosphere of purified nitrogen. Solvents for air- and moisture-sensitive manipulations were initially dried and deoxygenated using literature

procedures.[33] Hydrogen and deuterium gas were passed through a column containing manganese oxide supported on vermiculite and 4 Å molecular sieves before admission to the high vacuum line. Benzene-d_6 and toluene-d_8 were purchased from Cambridge Isotope Laboratories and dried over 4 Å molecular sieves or titanocene, respectively. 2,6-pyridine dicarbonitrile was prepared using slighlty modified literature procedures. **($^{2,6\text{-iPr}}$PDI)Fe(R)$_2$**, **($^{2,6\text{-Et}}$PDI)Fe(R)$_2$**, Pyridinebis(oxazoline) ligands,[34] **(^{iPr}Pybox)FeCl$_2$**,[35] 2-aminoadamantane,[36] were prepared according to literature procedures. Pyridine bis(oxazoline) ligands were purchased from Aldrich and dried overnight on a high vacuum line before use. All aldehydes and ketones were purchased from commercial sources, and were vacuum distilled from CaH_2 before use.

^{1}H NMR spectra were recorded on Varian Mercury 300, Inova 400 and 500 spectrometers operating at 299.76, 399.78 and 500.62 MHz, respectively. ^{2}H NMR spectra were recorded at 20 ºC on Inova 400 and 500 spectrometers operating at 61.37 and 76.85 MHz, respectively. ^{13}C NMR spectra were recorded on the same spectrometers operating at 101.535 or 125.893 MHz, respectively. All ^{1}H and ^{13}C NMR chemical shifts are reported relative to $SiMe_4$ using ^{1}H (residual) and ^{13}C chemical shifts of the solvent as a secondary standard. Solution magnetic moments were determined by Evans method[37] using a ferrocene standard and are the average value of at least two independent measurements. ^{1}H NMR multiplicity and coupling constants are reported where applicable. Peak width at half height is given for paramagnetically broadened resonances. Elemental analyses were performed at Robertson Microlit Laboratories, Inc., in Madison, NJ.

Single crystals suitable for X-ray diffraction were coated with polyisobutylene oil in a drybox, transferred to a nylon loop and then quickly transferred to the goniometer head of a Bruker X8 APEX2 diffractometer equipped with a molybdenum X-ray tube (λ = 0.71073 Å). Preliminary data revealed the crystal system. A hemisphere routine was

used for data collection and determination of lattice constants. The space group was identified and the data were processed using the Bruker SAINT+ program and corrected for absorption using SADABS. The structures were solved using direct methods (SHELXS) completed by subsequent Fourier synthesis and refined by full-matrix least-squares procedures.

Preparation of 2,6-Pyridinedicarboxylic acid dimethyl ester. To a 500 mL round bottom flask was added 50 g (0.299 mol) of 2,6-pyridinedicarboxylic acid, followed by 150 mL of anhydrous methanol, 50 mL of toluene, and 5 mL of sulfuric acid. The reaction was refluxed overnight, cooled on an ice bath, and neutralized with concentrated sodium bicarbonate. The mother liquer was placed on a rotary vaporator until an oil remained. To this oil was added 100 mL of water, and the reaction was extracted with 3 X 50 mL of dichloromethane. The organic layers were combined, dried with magnesium sulfate, and the dichloromethane was removed yielding 55 g (94%) of an analytically pure white powder. The NMR spectrum matched that of a previously reported sample.[38]

Preparation of 2,6-Pyridinedicarboxamide. To a 250 mL round bottom flask was added 55 g (0.281 mol) of 2,6-pyridinedicarboxylic acid dimethyl ester, followed by 100 mL of saturated ammonium hydroxide. The reaction was stirred vigorously and gently warmed (~35 ºC) for one hour. The reaction was cooled on an ice bath and filtered, and the white solid was washed with 2 X 25 mL of water. The solid was dried on a high vacuum line, yielding 46 g (99%) of a white powder that matched a previously characterized sample. [39]

Preparation of 2,6-Pyridinedicarbonitrile. To a 100 mL round bottom flask was added 5 g (0.030 mol) of 2,6-pyridinediamide, 6.7 g (0.066 mol) of triethylamine, and

approximately 30 mL of anhydrous THF. The mixture was cooled on an ice bath, and 14 g (0.066 mol) of trifluoroacetic anhydride was added dropwise to the stirring solution. The reaction was allowed to warm to room temperature and stir for an additional 3 hours. The reaction was quenched on an ice bath with saturated sodium bicarbonate. A precipitate formed upon addition of the sodium bicarbonate, and the precipitate was gather on a glass frit via vacuum filtration, yielding 3 g (78%) of pearlescent white sheets that matched a previously reported sample. [40]

Preparation of (^{Cy}APDI)Fe(CH_2SiMe_3)$_2$. A 20 mL scintillation vial was charged with 0.443 g (1.00 mmol) of $(py)_4FeCl_2$ and approximately 3-5 mL pentane were added. The resulting slurry was cooled to -35 ºC for approximately 30 minutes after which time a pentane solution of $LiCH_2SiMe_3$ (0.188 g, 2.00 mmol) was added dropwise. The yellow slurry turned dark purple as it was warmed. The reaction mixture was stirred for 1-2 hours at ambient temperature. After this time, the reaction mixture was filtered through Celite and the filtrate was transferred to a fresh scintillation vial. A pentane slurry of ^{Cy}APDI ligand (0.326 g, 1.00 mmol) was added dropwise to the stirring solution. The purple solution immediately turned dark violet. This mixture was stirred for 1-2 hours at ambient temperature. The mixture was then cooled to -35 °C and filtered to afford 0.460 g (83%) of **(^{Cy}APDI)Fe(CH_2SiMe_3)$_2$** as a dark purple crystalline solid. Crystals suitable for X-ray diffraction were grown from a solution of pentane at -35 ºC. Analysis for $C_{29}H_{53}N_3FeSi_2$: Calcd C, 62.67; H, 9.54; N, 7.56. Found: C, 62.43; H, 9.26; N, 7.83. Magnetic susceptibility: μ_{eff} = 4.7 μ_B (benzene-d_6, 23 ºC). ^{1}H NMR (benzene-d_6), δ = 212.90 (1192 Hz, 1H, *p-pyr*), 47.89 (64 Hz, 1H imine-cyclohexyl ipso C*H*), 39.79 (147 Hz, 2H, *m-pyr*), 9.05 (295 Hz), 2.48-0.79 (cyclohexyl CH's), -81.83 (100 Hz, imine-cyclohexyl ipso C*H*), -133.16 (737 Hz, 6H, $C(CH_3)$).

Preparation of ($^{2,6\text{-Me}}$PDI)Fe(CH_2SiMe_3)$_2$. A procedure similar to that of ^{Cy}**APDIFeR$_2$** was used, but with 0.443 g (1.00 mmol) of $(py)_4FeCl_2$, 0.188 g $LiCH_2SiMe_3$ (2.00 mmol), and ^{2,6Me}PDI ligand (0.326 g, 1.00 mmol). The reaction afforded 0.460 g (83%) of (**$^{2,6\text{-Me}}$PDI)Fe(R)$_2$** as a dark purple crystalline solid. Analysis for $C_{29}H_{53}N_3FeSi_2$: Calcd C, 50.06; H, 4.54; N, 7.01. Found: C, 62.43; H, 9.26; N, 7.83. Magnetic susceptibility: μ_{eff} = 4.7 μ_B (benzene-d_6, 23 ºC). ^{1}H NMR (benzene-d_6), δ = 282.71 (609 Hz, 1H, *p-pyr*), 58.58 (133 Hz, 2H, *m-pyr*), 23.35 (630 Hz, 2H), 13.01 (96 Hz), 11.79 (18 H, 341 Hz), -16.74 (H, 43 Hz,), -150.22 (420 Hz, 6H, C(CH_3)).

Preparation of ($^{(trans\text{-}4\text{-}Me)Cy}$APDI)Fe($CH_2SiMe_3$)$_2$. A procedure similar to that of ^{Cy}**APDIFeR$_2$** was used, but with 0.221 g (0.50 mmol) of $(py)_4FeCl_2$, 0.094 g $LiCH_2SiMe_3$ (1.00 mmol), and $^{(trans\text{-}4\text{-}Me)Cy}$APDI ligand (0.177 g, 0.50 mmol). The reaction afforded 0.215 g (74%) of (**$^{(trans\text{-}4\text{-}Me)Cy}$APDI)Fe(R)$_2$** as a dark purple crystalline solid. Analysis for $C_{31}H_{57}N_3FeSi_2$: Calcd C, 62.67; H, 9.84; N, 7.20. Found: C, 62.43; H, 9.26; N, 7.83. Magnetic susceptibility: μ_{eff} = 4.7 μ_B (benzene-d_6, 23 ºC). ^{1}H NMR (benzene-d_6), δ = 214.95 (1192 Hz, 1H, *p-pyr*), 47.96 (64 Hz, 1H), 39.81 (276 Hz, 2H, *m-pyr*), 9.05 (295 Hz), 2.48-0.79 (cyclohexyl CH's), -81.84 (100 Hz, imine-cyclohexyl ipso C*H*), -133.74 (737 Hz, 6H, C(CH_3)).

Preparation of ($^{2\text{-Me}}$PDI)Fe(CH_2SiMe_3)$_2$. A procedure similar to that of ^{Cy}**APDIFeR$_2$** was used, but with 0.443 g (1.00 mmol) of $(py)_4FeCl_2$, 0.188 g $LiCH_2SiMe_3$ (2.00 mmol), and ^{2,6Me}PDI ligand (0.341 g, 1.00 mmol). The reaction afforded 0.445 g (78%) of (**$^{2\text{-Me}}$PDI)Fe(R)$_2$** as a dark purple crystalline solid. Analysis for $C_{31}H_{45}N_3FeSi_2$: Calcd C, 62.67; H, 7.93; N, 7.56. Found: C, 62.43; H, 9.26; N, 7.83. Magnetic susceptibility: μ_{eff} = 4.7 μ_B (benzene-d_6, 23 ºC). ^{1}H NMR (benzene-d_6), δ = 326.83 (1H, *p-py*), 51.71 (147 Hz, 2H, *m-pyr*), 48.28 (1192 Hz, 1H, *m-pyr*), 27.56 (64 Hz, 1H), 17.74 (147 Hz, 2H, *m-*

pyr), 13.50 (295 Hz), 10.52( ), -18.64 (100 Hz), -156.91 (737 Hz, 6H, $C(CH_3)$)-159.93 (737 Hz, 6H, $C(CH_3)$).

Preparation of ($^{2\text{-}iPr}$PDI)Fe(CH_2SiMe_3)$_2$. A procedure similar to that of ^{Cy}**APDIFeR$_2$** was used, but with 0.443 g (1.00 mmol) of $(py)_4FeCl_2$, 0.188 g $LiCH_2SiMe_3$ (2.00 mmol), and $^{2\text{-}iPr}$PDI ligand (0.397 g, 1.00 mmol). The reaction afforded 0.400 g (65%) of (**$^{2\text{-}iPr}$PDI)Fe(R)$_2$** as a dark purple crystalline solid. Analysis for $C_{35}H_{53}N_3FeSi_2$: Calcd C, 662.96; H, 8.51; N, 6.69. Found: C, 62.43; H, 9.26; N, 7.83. Magnetic susceptibility: μ_{eff} = 4.7 μ_B (benzene-d_6, 23 ºC). ^{1}H NMR (benzene-d_6), δ = 323.97 (1H, *p-py*), 317.10 (1H, *p-py*), 51.65 (147 Hz, 2H, *m-pyr*), 49.73 (147 Hz, 2H, *m-pyr*), 17.52 (1192 Hz, 1H, *m-pyr*), 14.97 (64 Hz, 1H), 13.64 (147 Hz, 2H, *m-pyr*), 11.35 (295 Hz), 17.56( ), -18.77 (100 Hz), -151.50 (737 Hz, 6H, $C(CH_3)$)-159.46 (737 Hz, 6H, $C(CH_3)$).

Preparation of ($^{3,5\text{-}Me}$PDI)Fe(CH_2SiMe_3)$_2$. A procedure similar to that of ^{Cy}**APDIFeR$_2$** was used, but with 0.443 g (1.00 mmol) of $(py)_4FeCl_2$, 0.188 g $LiCH_2SiMe_3$ (2.00 mmol), and ^{2,6Me}PDI ligand (0.326 g, 1.00 mmol). The reaction afforded 0.460 g (83%) of (**$^{3,5\text{-}Me}$PDI)Fe(R)$_2$** as a dark purple crystalline solid. Analysis for $C_{29}H_{53}N_3FeSi_2$: Calcd C, 62.67; H, 9.54; N, 7.56. Found: C, 62.43; H, 9.26; N, 7.83. Magnetic susceptibility: μ_{eff} = 4.7 μ_B (benzene-d_6, 23 ºC). ^{1}H NMR (benzene-d_6), δ = 212.90 (1192 Hz, 1H, *p-pyr*), 47.89 (64 Hz, 1H imine-cyclohexyl ipso C*H*), 39.79 (147 Hz, 2H, *m-pyr*), 9.05 (295 Hz), 2.48-0.79 (cyclohexyl CH's), -81.83 (100 Hz, imine-cyclohexyl ipso C*H*), -133.16 (737 Hz, 6H, $C(CH_3)$).

Preparation of ($^{2,5\text{-}tBu}$PDI)Fe(CH_2SiMe_3)$_2$. A procedure similar to that of ^{Cy}**APDIFeR$_2$** was used, but with 0.443 g (1.00 mmol) of $(py)_4FeCl_2$, 0.188 g $LiCH_2SiMe_3$ (2.00 mmol), and ^{2,6Me}PDI ligand (0.537 g, 1.00 mmol). The reaction afforded 0.460 g (83%) of (**$^{2,5\text{-}}$**

^{tBu}PDI)Fe(R)$_2$ as a dark purple crystalline solid. Analysis for $C_{45}H_{73}N_3FeSi_2$: Calcd C, 70.37; H, 9.58; N, 5.47. Found: C, 62.43; H, 9.26; N, 7.83. Magnetic susceptibility: μ_{eff} = 4.7 μ_B (benzene-d_6, 23 ºC). ^{1}H NMR (benzene-d_6), δ = 212.90 (1192 Hz, 1H, *p-pyr*), 47.89 (64 Hz, 1H imine-cyclohexyl ipso C*H*), 39.79 (147 Hz, 2H, *m-pyr*), 9.05 (295 Hz), 2.48-0.79 (cyclohexyl CH's), -81.83 (100 Hz, imine-cyclohexyl ipso C*H*), -133.16 (737 Hz, 6H, C(CH_3)).

Preparation of [(^{iPr}Pybox)Fe]$_2$. To a 50 mL round bottom flask was added 20.0 g of mercury and approximately 20 mL of toluene. With stirring, 0.048 g (2.1 mmol) of sodium followed by 0.225 g (0.52 mmol) of (^{iPr}Pybox)$FeCl_2$ was added to the slurry. The resulting reaction mixture was stirred for 1 hour after which time the reaction solution was filtered through Celite and the volatiles were removed, yielding 0.80 g (23%) of (^{iPr}Pybox)$_2$Fe as a dark green powder. For $C_{34}H_{46}N_6FeO_4$: Calcd C, 62.00; H, 7.04; N, 12.76. Found: C, 61.90 H, 7.11; N, 12.55. Magnetic susceptibility: μ_{eff} =2.95 μ_B (C_6D_6), 3.1 (Gouy Balance). ^{1}H NMR (C_6D_6). δ 283.54 (1600 Hz), 66.26 (215 Hz), -0.33 to -5.07. (2 peaks, 600 Hz),-11.65 (95 Hz), -16.98 (95 Hz), -66.42(740 Hz).

Preparation of (^{iPr}Pybox)Fe(CO)$_2$. A thick walled glass vessel was charged with 23.0 g of mercury and approximately 10 mL of toluene. To this stirring solution is added 0.048 g (2.1 mmol) of sodium, followed by 0.225 g (0.52 mmol) of (^{iPr}Pybox)$FeCl_2$. The reaction vessel was then transferred to a high vacuum line, where 1 atm of CO was added. The reaction was stirred for one hour after which time the excess CO and all volatiles were removed. The reaction was transferred into a nitrogen filled drybox. The residue was taken up in pentane and filtered through Celite. Volatiles were again removed, yielding 0.189 g (87%) of a red/brown powder identified as (^{iPr}Pybox)Fe($CO)_2$. For $C_{19}H_{23}N_3FeO_4$: Calcd C, 55.22; H, 5.61; N, 10.17. Found: C, 51.96; H, 5.59; N, 9.88.

IR, ν(CO): Pentane, 1956 and 1852 cm^{-1}, KBr, 1954, 1930, 1878 and 1856 ^{1}H NMR (C_6D_6). δ 7.63 (d, 2H, *m-py-H*), 6.72 (t, 1H, *p-py-H*), 4.02-4.15 (m, 4H, O-CH*H*-C*H*-), 3.89 (t, 2H, O-C*H*H-), 2.69 (m, 2H, C*H*Me_2), 0.62 (d, 6H, CH*Me*Me), 0.54 (d, 6H, CH*Me*Me). ^{13}C NMR (C_6D_6). 216.4, 159.3, 131.2, 121.3, 114.1, 71.7, 71.5, 31.6, 19.5, 14.1.

Preparation of (^{Ind}Pybox)$FeCl_2$ (3-Cl_2). A 50 mL round bottom flask was charged with 0.100 g (0.254 mmol.)of 2,6-Bis[(3aR,8aS)-(+)-8H-indeno[1,2-d]oxazolin-2-yl)pyridine and 0.032 g of $FeCl_2$. To the stirring solution was added approximately 15 mL of THF, immediately eliciting a color change to a red tinted blue. The reaction was stirred overnight, after which pentane was added to precipitate the product. The resulting violet solid was collected by vacuum filtration and yielded 0.113 g (85.6%) of **3-Cl_2**. Analysis for $C_{31}H_{37}N_3FeO_2Si_2$: Calcd C, 57.72; H, 3.68; N, 8.08. Found: C, 57.92; H, 3.40; N, 7.64. Magnetic susceptibility: μ_{eff} =4.8 μ_B (CD_2Cl_2). ^{1}H NMR ($CDCl_3$). δ 62.58 (165.2 Hz), 58.97 (28.4 Hz), 19.99 (35.6 Hz), 9.06 (35.1 Hz), 6.72 (31.3 Hz), 4.09 (14.8 Hz), 2.78 (17.3 Hz), -1.10 (20.3 Hz), -5.15 (21.2 Hz), -14.77 (116.5 Hz).

Preparation of (^{Ind}Pybox)Fe(CH_2SiMe_3)$_2$. A 20 mL scintillation vial was charged with 0.050 g (0.096 mmol) of **(^{Ind}Pybox)$FeCl_2$** and approximately 5 mL of pentane was added forming a slurry. The solution was cooled to -35 ºC for approximately 30 minutes after which time a pentane solution containing 0.015 g (2.00 mmol) of $LiCH_2SiMe_3$ was added dropwise. The blue slurry turned red-brown almost immediately after addition of the alkyl lithium and eventually formed a dark purple reaction mixture after reaching ambient temperature. The reaction mixture was stirred for 2 hours. The mixture was filtered through Celite and the solvent was removed from the filtrate. The purple solid was recrystallized from pentane at –35 ºC and to yield 0.014 g (23%) of

(^{Ind}Pybox)Fe(CH_2SiMe_3)$_2$. X-ray quality crystals of the solid were grown from a dilute solution of pentane at -35 ºC. Analysis for $C_{31}H_{37}N_3FeO_2Si_2$: Calcd C, 63.55; H, 6.63; N, 6.74. Found: C, 63.34; H, 6.43; N, 6.45. Magnetic susceptibility: μ_{eff} =4.5 μ_B (benzene-d_6). ^{1}H NMR (benzene-d_6). δ 22.07 (140.6 Hz), 14.49 (129.3 Hz), 11.39 (86.5 Hz), 7.9 (560 Hz), 6.69 (160 Hz), -4.09 (211.7 Hz), -37.82 (53.24 Hz), -333.87 (116.42 Hz).

Preparation of (^{Ind}Pybox)Fe(CO)$_2$. A thick walled glass vessel was charged with 0.150 g (6.2 mmol) of magnesium powder, followed by 0.150 g (0.29 mol) of (^{Ind}Pybox)$FeCl_2$. The reaction vessel was then transferred to a high vacuum line, where THF was vacuum transferred from sodium benzophenone ketyl into the reaction vessel, followed by 1 atm of CO. The reaction was stirred overnight, during that time the color changed from purple to red. All volatiles were then removed on a high vacuum line and the reaction was transferred into a drybox. The residue was taken up in pentane and filtered through celite. Volatiles were again removed, yielding 0.137 g (94%) of a red/brown powder. For $C_{27}H_{19}N_3FeO_4$: Calcd (%) C, 64.18; H, 3.79; N, 8.32. Found(%): C, 64.55; H, 4.24; N, 7.94. IR (KBr, ν(CO): 1938 and 1868 cm^{-1}. ^{1}H NMR (benzene-d_6). δ 8.48 (d, 2H, Ar-*H*), 7.60 (d, 2H, m-py-*H*), 7.36 (t, 2H, Ar-*H*), 7.10 (t, 2H, Ar-*H*), 6.82 (t, 2H, Ar-*H*), 6.73 (t, 1H, p-py-*H*), 5.31 (d, 2H, =N-C*H*-), 4.94 (d of t, 2H, -O-C*H*-), 2.90-2.70 (m, 4H, -CH_2-). ^{13}C NMR (C_6D_6). 217.1, 158.7, 140.8, 140.6, 129.7, 125.2, 121.4, 114.2, 88.3, 76.5, 39.8

Preparation of (^{iPr}Pybox)Fe(CH_2SiMe_3)$_2$. A 20 mL scintillation vial was charged with 0.050 g (0.14 mmol) of **(^{iPr}Pybox)$FeCl_2$** and approximately 5 mL pentane were added. The solution was cooled to -35 °C for approximately 30 minutes after which time a pentane solution containing 0.022 g (0.23 mmol) of $LiCH_2SiMe_3$ was added dropwise. The reaction was stirred at room temperature for 2 hours after which time the solution was then filtered through celite and excess solvent was removed. The resulting purple

powder was recrystallized from pentane at –35 ºC to yield 0.16 g (26%) of **(^{iPr}Pybox)Fe(CH_2SiMe_3)$_2$.** Analysis for $C_{25}H_{45}N_3FeO_2Si_2$: Calcd C, 56.48; H, 8.53; N, 7.90. Found: C, 56.08; H, 8.27; N, 7.88. Magnetic susceptibility: μ_{eff} = 4.6 μ_B (benzene-d_6). ^{1}H NMR (benzene-d_6). δ 359.56 (427.8 Hz), 240.01 (216.0 Hz), 24.99 (96.6 Hz), 19.49 (140.1 Hz), 8.71 (345.7 Hz), 3.35 (33.4 Hz), -2.23 (158.5 Hz), -5.09 (53.5 Hz), -25.49 (35.4 Hz), -41.87 (546.3 Hz), -72.37 (49.09 Hz).

Alternative Procedure for the Preparation of (^{iPr}Pybox)Fe(CH_2SiMe_3)$_2$. A 20 mL scintillation vial was charged with 0.080 g (0.18 mmol) of $(py)_4FeCl_2$ and pentane was added forming a slurry. The solution was cooled to -35 °C for approximately 30 minutes after which time a pentane solution of $LiCH_2SiMe_3$ (0.034 g, 0.36 mmol) was added dropwise. The yellow slurry turned dark purple as it warmed. The reaction was stirred for 1-2 hours at room temperature. Then it was filtered through Celite and the solution transferred into a new 20 mL scintillation vial. A pentane slurry of ^{iPr}Pybox ligand (0.054 g, 0.18 mmol) was added dropwise to the stirring solution. The purple solution immediately turned dark violet. This mixture was stirred for 1-2 hours at room temperature. The mixture was then cooled to -35 °C and filtered to afford 0.068 g (71%) of (^{iPr}Pybox)Fe(CH_2SiMe_3)$_2$ as a dark purple crystalline solid.

Preparation of (^{tBu}Pybox)Fe(CH_2SiMe_3)$_2$. A 20 mL scintillation vial was charged with 0.080 g (0.18 mmol) of $(py)_4FeCl_2$ and pentane was added forming a slurry. The solution was cooled to -35 °C for approximately 30 minutes after which time a pentane solution of $LiCH_2SiMe_3$ (0.034 g, 0.36 mmol) was added dropwise. The yellow slurry turned dark purple as it warmed. The reaction was stirred for 1-2 hours at room temperature. Then it was filtered through Celite and the solution transferred into a new 20 mL scintillation vial. A pentane slurry of ^{tBu}Pybox ligand (0.059 g, 0.18 mmol) was added dropwise to the

stirring solution. The purple solution immediately turned dark violet. This mixture was stirred for 1-2 hours at room temperature. The mixture was then filtered through celite and cooled to -35 °C to afford 0.010 g (10%) of ^{tBu}PyboxFe(CH_2SiMe_3)$_2$ as a dark purple crystalline solid. The solid quickly decomposes in solution and decomposes as a solid at -35°C. Analysis for $C_{27}H_{49}N_3FeO_2Si_2$. ^{1}H NMR (benzene-d_6). δ 145.40 (415 Hz), 37.41 (65 Hz), 10.72 (190 Hz), 6.55 (120 Hz), -0.36(120 Hz), -5.08 (241 Hz), -35.64 (389 Hz).

Preparation of (^{Bn}Pybox)Fe(CH_2SiMe_3)$_2$. A 20 mL scintillation vial was charged with 0.115 g (0.25 mmol) of $(py)_4FeCl_2$ and pentane was added forming a slurry. The solution was chilled to -35 °C for approximately 30 minutes in the dry box freezer after which time a pentane solution of $LiCH_2SiMe_3$ (0.048 g, 0.51 mmol) was added dropwise. The yellow slurry turned dark purple as it warmed to ambient temperature. The reaction was stirred for 1-2 hours and then filtered through Celite. The filtrate was collected and transferred into a new 20 mL scintillation vial. A pentane slurry of ^{Bn}Pybox ligand (0.1 g, 0.25 mmol) was added dropwise to the stirring solution. The purple solution immediately turned dark violet. This mixture was stirred for 1-2 hours at room temperature. The mixture was then cooled to -35 °C and filtered to yield 0.098 g (61%) of ^{Bn}PyboxFe(CH_2SiMe_3)$_2$ as a dark purple crystalline solid. Analysis for $C_{33}H_{45}N_3FeO_2Si_2$: Calcd C, 63.14; H, 7.23; N, 6.69. Found: C, 63.33; H, 6.95; N, 6.48. Magnetic susceptibility: $\mu_{eff} = 4.4\ \mu_B$ (benzene-d_6). ^{1}H NMR (benzene-d_6). ^{1}H NMR (benzene-d_6). δ δ 22.97 (210 Hz), 8.61 (630 Hz), 7.41 (30 Hz), 7.28 (28 Hz), -3.58 (170 Hz), -7.20 (170 Hz), -41.03 (540 Hz), -345.87 (650 Hz). There are four peaks that weren't located.

Preparation of (^{iBu}Pybox)Fe(CH_2SiMe_3)$_2$. A 20 mL scintillation vial was charged with 0.027 g (0.18 mmol) of $(py)_4FeCl_2$ and pentane was added forming a slurry. The solution was cooled to -35 °C for approximately 30 minutes after which time a pentane solution

of $LiCH_2SiMe_3$ (0.012 g, 0.36 mmol) was added dropwise. The yellow slurry turned dark purple as it warmed. The reaction was stirred for 1-2 hours at room temperature. Then it was filtered through Celite and the solution transferred into a new 20 mL scintillation vial. A pentane slurry of ^{iBu}Pybox ligand (0.020 g, 0.18 mmol) was added dropwise to the stirring solution. The purple solution immediately turned dark violet. This mixture was stirred for 1-2 hours at room temperature. The mixture was then cooled to -35 °C and filtered to afford 0.014 g (41%) of $^{iBu}PyboxFe(CH_2SiMe_3)_2$ as a dark purple crystalline solid. Analysis for $C_{27}H_{49}N_3FeO_2Si_2$: Calcd C, 57.94; H, 8.82; N, 7.51. Found: C, 57.64; H, 8.48; N, 7.64. Magnetic susceptibility: μ_{eff} =4.6 μ_B (benzene-d_6). ^{1}H NMR (benzene-d_6). δ 22.00 (269 Hz), 8.10 (540 Hz), 3.38 (118 Hz), 1.26 (95 Hz), -11.54 (330 Hz), -53.40 (1150 Hz), -342.97 (701 Hz).

Preparation of Diphenyl(1-phenylethoxy)silane. A general hydrosilylation in pentane was performed. The solvent was removed and the product exhibited an ^{1}H NMR spectrum that matched the literature values. The retention time on the Restek RTX-5 column with the indicated temperature profile is 19.06 min. ^{1}H NMR (chloroform-*d*). δ = 7.72-7.52 (dd, J = 7, 28 Hz, 4H, SiAr*H*), 7.36-7.27 (m, 10H), 5.45 (s, 1H, Si*H*), 4.99 (q, 6Hz, 1H, C*H*), 1.49 (d, 6 Hz, 3H, CH_3), 1.33, (s, 9H, C(CH_3)$_3$). ^{13}C {^{1}H} NMR (chloroform-*d*). δ = 150.13, 142.34, 134.92, 134.90, 134.54, 134.33,

Preparation of (1-(4-*tert*-butylphenyl)ethoxy)diphenylsilane. A general hydrosilylation in pentane was performed. The solvent was removed and the product was characterized by GC and ^{1}H NMR. The retention time on the Restek RTX-5 column with the indicated temperature profile is 21.36 min. ^{1}H NMR (chloroform-*d*). δ = 7.72-7.52 (dd, J = 7, 28 Hz, 4H, SiAr*H*), 7.36-7.27 (m, 10H), 5.45 (s, 1H, Si*H*), 4.99 (q, 6Hz, 1H, C*H*), 1.49 (d, 6 Hz, 3H, CH_3), 1.33, (s, 9H, C(CH_3)$_3$). ^{13}C {^{1}H} NMR (chloroform-*d*). δ =

150.13, 142.34, 134.92, 134.90, 134.54, 134.33, 130.46, 130.39, 128.16, 128.10, 125.48, 125.28, 72.68, 34.67, 31.61, 26.23. MS (%) m/z 360 (M+, 3), 344 (16), 225 (23), 199 (100), 183 (64)130.46, 130.39, 128.16, 128.10, 125.48, 125.28, 72.68, 34.67, 31.61, 26.23. ^{13}C {^{1}H} NMR (chloroform-*d*). δ = 145.52, 134.97, 134.93, 134.50, 134.30, 130.59, 130.53, 128.49, 128.27, 128.20, 127.39, 125.81, 72.93, 26.52.

Preparation of (1-(4-methoxyphenyl)ethoxy)diphenylsilane. A general hydrosilylation in pentane was performed. The solvent was removed and the product was characterized by GC and ^{1}H NMR. The retention time on the Restek RTX-5 column with the indicated temperature profile is 21.07 min. ^{1}H NMR (chloroform-*d*). δ = 7.62-7.56 (dd, 7, 26 Hz, 4H, SiAr*H*), 7.38-7.14 (m, 8H), 6.81 (d, 2H, Ar), 5.41(s, 1H, Si*H*), 4.95 (q, 6, Hz, 1H, C*H*), 3.70 (s, 3H, OCH_3), 1.48 (d, 6 Hz, 3H, CH_3). ^{13}C {^{1}H} NMR (chloroform-*d*). δ = 158.91, 137.62, 134.89, 134.85, 134.49, 134.32, 130.47, 130.39, 128.17, 128.10, 127.02, 113.75, 72.53, 55.45, 26.34.

Preparation of (1-(2,4-dimethoxyphenyl)ethoxy)diphenylsilane. A general hydrosilylation in pentane was performed. The solvent was removed and the product was characterized by GC and ^{1}H NMR. The retention time on the Restek RTX-5 column with the indicated temperature profile is 22.66 min. ^{1}H NMR (chloroform-*d*). δ = 7.70-7.55 (dd, 7, 26 Hz, 4H, SiAr*H*), 7.49 (d, 7 Hz, 1H, Ar), 7.48-7.30 (m, 6H), 6.47 (dd, 2, 8 Hz, 1H, Ar), 6.34 (d, 2 Hz, 1H, Ar), 5.42 (s, 1H, Si*H*), 5.35 (q, 6 Hz, 1H, C*H*), 3.73 (s, 3H, OCH_3), 3.60 (s, 3H, OCH_3), 1.46 (d, 6 Hz, 3H, CH_3). ^{13}C {^{1}H} NMR (chloroform-*d*). δ = 160.00, 156.85, 134.88, 134.83, 134.65, 130.32, 130.25, 129.24, 128.44, 128.08, 128.01, 126.97, 126.43, 125.50, 67.03, 55.53, 55.26, 24.92. MS (%) m/z 364 (M+, 22), 349 (100), 271 (22), 227 (18), 199 (30), 183 (57), 165 (55), 151 (100).

Preparation of (1-(4-(trifluoromethyl)phenyl)ethoxy)diphenylsilane. A general hydrosilylation in pentane was performed. The solvent was removed and the product was characterized by GC and 1H NMR. The retention time on the Restek RTX-5 column with the indicated temperature profile is 18.81 min. 1H NMR (chloroform-d). δ = 7.71-7.66 (d, 8Hz, 2H), 7.64-7.59 (m, 4H, Ar), 7.52-738 (m, 8H), 5.49 (s, 1H, SiH), 5.09 (q, 6 Hz, 1H, CH), 1.56 (d, 6 Hz, 3H, CH3). 13C {1H} NMR (chloroform-d). δ = 149.55, 135.97, 134.90, 134.48, 134.05, 133.88, 130.79, 130.74, 128.38, 128.32, 126.07, 125.52 (q, JCF 4 Hz), 123.45, 72.39, 26.46. MS (%) m/z 372 (M+, 4), 357 (38), 294 (61), 279 (84), 235 (38), 225 (61), 216 (22), 199 (100), 183 (95).

Preparation of (1-(3,5-bis-trifluoromethyl)ethoxy)diphenylsilane. A general hydrosilylation in pentane was performed. The solvent was removed and the product was characterized by GC and 1H NMR. The retention time on the Restek RTX-5 column with the indicated temperature profile is 17.31 min. 1H NMR (chloroform-d). δ = 7.78 (s, 2H, Ar), 7.76 (s, 1H, Ar), 7.65 (d, 7 Hz, 2H), 7.57 (d, 7 Hz, 2H), 7.52-7.34 (m, 6H, Ar), 5.47 (s, 1H, SiH), 5.11 (q, 6 Hz, 1H, CH), 1.56 (d, 6H, CH3). 13C {1H} NMR (chloroform-d). δ = 148.08, 135.90, 134.87, 134.81, 133.42, 133.35, 130.89, 130.86, 128.38, 128.34, 126.02, 124.64, 122.47, 121.32 (q, JCF 3 Hz), 71.95, 26.30. MS (%) m/z 439 (M+, 3), 421 (11), 362 (90), 240 (12), 222 (79), 199 (100), 183 (90).

Preparation of 4-(1-(diphenylsiloxy)ethyl)-N,N-dimethylbenzenamine. A general hydrosilylation in pentane was performed. The solvent was removed and the product was characterized by 1H NMR. The retention time on the Restek RTX-5 column with the indicated temperature profile is 23.21 min. 1H NMR (chloroform-d). δ = 7.73-7.58 (m, 4H, SiArH), 7.52-7.36 (m, 6H), 7.28-7.25 (dd, 1, 9 Hz, 2H), 6.78-6.71 (dd, 1, 9 Hz, 2H), 5.44 (d, 1 Hz, 1H, SiH), 5.03-4.96 (q, 6Hz, 1H, CH), 2.99 (s, 6H, NMe2,) 1.56 (d, 6 Hz,

3H, CH3).13C {1H} NMR (chloroform-d). δ = 150.13, 142.35, 134.92, 134.90, 134.54, 134.33, 130.46, 130.39, 128.16, 128.10, 125.28, 72.68, 34.67, 31.61, 26.23.

Preparation of Diphenyl(1,2,3,4-tetrahydronaphthalen-1-yloxy)silane. A general hydrosilylation in pentane was performed. The solvent was removed and the product was characterized by 1H NMR. The retention time on the Restek RTX-5 column with the indicated temperature profile is 22.14 min. 1H NMR (chloroform-d). δ = 7.67-7.55 (m), 7.13-7.03 (m), 5.59 (s, 1H, SiH), 4.97 (t, 5 Hz, 1H, CH), 2.70 (m, 2H, CH2), 2.00-1.93 (m, 4H), 1.66-1.64 (m, 2H). 13C {1H} NMR (chloroform-d). δ = 138.62, 137.25, 134.96, 134.96, 134.71, 134.59, 130.48, 129.03, 128.83, 128.19, 127.51, 126.00, 71.17, 32.28, 29.26, 19.28. MS (%) m/z 330 (M+, 5), 301 (11), 287 (22), 252 (41), 224 (31), 199 (100), 183 (31).

Preparation of (Hexan-2-yloxy)diphenylsilane. A general hydrosilylation in pentane was performed. The solvent was removed and the product was characterized by 1H NMR.The retention time on the Restek RTX-5 column with the indicated temperature profile is 17.29 min. 1H NMR (chloroform-d). δ = 7.72-7.65 (m, 4H), 7.50-7.38(m, 6H), 5.47 (s, 1H, SiH), 3.96 (m, 1H, CH), 1.57-1.20 (m, 9H). 13C {1H} NMR (chloroform-d). δ = 134.88, 134.86, 130.38, 128.14, 71.22, 39.14, 28.06, 23.47, 22.82, 14.28. MS (%) m/z 283 (M+, 7), 269 (10), 227 (95), 206 (76), 199 (70), 183 (100).
S25

Preparation of (Hex-5-en-2-yloxy)diphenylsilane. A general hydrosilylation in pentane was performed. The solvent was removed and the product was characterized by 1H NMR. The retention time on the Restek RTX-5 column with the indicated temperature

profile is 17.29 min. 1H NMR (chloroform-d). δ = 7.74-7.60 (m, 4H), 7.51-7.32 (m, 6H), 5.87-5.73

(m, 1H), 5.49 (s, 1H, SiH), 5.04-4.91(dd, 21, 7 Hz, 2H), 4.02 (m, 1H, CH), 2.28-2.04 (m, 2H). 1.76-1.64 (m, 2H), 1.23(d, 8 Hz, 3H). 13C {1H} NMR (chloroform-d). δ = 138.80, 135.95, 134.93, 130.49, 128.22, 114.76, 70.66, 38.64, 30.20, 23.49. MS (%) m/z 281 (M+, 2), 227 (26), 204 (40), 199 (23), 183 (100) .

Preparation of 4-methylbenzyloxydiphenylsilane. A general hydrosilylation in pentane was performed. The solvent was removed and the product was characterized by 1H NMR. The retention time on the Restek RTX-5 column with the indicated temperature profile is 20.05 min. H NMR (chloroform-d). δ = 7.79-7.60 (dd, 4H), 7.50-7.30 (m, 6H), 7.26-7.09 (m, 4H), 4.83 (s, 1H, SiH), 4.80 (s, 2H, CH2), 2.35 (s, 3H, CH3). MS (%) m/z 304 (M+, 4), 225 (8), 211 (23), 199 (100), 183 (11).

REFERENCES

[1] Bouwkamp, M. W.; Bart, S. C.; Hawrelak, E. J.; Trovitch, R. J.; Lobkovsky, E.; Chirik, P. J. *Chem. Commun*. **2005**, 3406.

[2] Campora, J.; Naz, A. M.; Palma, P.; Alvarez, E.; Reyes, M. L. *Organometallics* **2005**, 24, 4878.

[3] Scott, J.; Gambarotta, S.; Korobkov, I.; Budzelaar, P. H. M. *J. Am. Chem. Soc.* **2006**, 128, 9660.

[4] Fernández, I.; Trovitch, R. J.; Lobkovsky, E.; Chirik, P. J. *Organometallics*, **2008**, 27, 109.

[5] Bouwkamp, M. W.; Lobkovsky, E.; Chirik, P. J. *J. Am. Chem. Soc.* **2005**, 127, 9660.

[6] Johnson, J. S.; Evans, D. A. *Acc. Chem. Res.* **2003**, 33, 325.

[7] Redlich, Mark; Hossain, M. Mahmun. *Tetrahedron Letters*. **2004**, 45, 8987.

[8] Nomura, Kotohiro; Sidokmai, Warit; Imanishi, Yukio. *Bulletin of the Chemical Society of Japan*. **2000**, 73, 599

[9] Yun, J.; Buchwald, S. L. *J. Am. Chem. Soc.* **1999**, *121*, 5640.

[10] L ipshutz, B. H.; Noson, K.; Chrisman, W.; Lower, A. *J. Am. Chem. Soc.* **2003**, *125*, 8779. (b) Lipshutz, B. H.; Frieman, B. A. *Angew. Chem. Int. Ed.* **2005**, *44*, 6345.

[11] Ouellet, S. G.; Walji, A. M.; MacMillan, D. W. C. *Acc. Chem. Res.* **2007**, *40*, 1327.

[12] Enthaler, S.; Junge, K.; Beller, M. *Iron Catalysis in Organic Chemistry*, B. Plietker, Ed., Wiley-VCH, Weinheim, 2008 pp. 125 – 145.

[13] Nishiyama, H.; Furuta, A. *Chem. Commun.* **2007**, 760.

[14] Furuta, A., Nishiyama, H. *Tett. Lett.* **2008**, *49*, 110.

[15] Shaikh, N. S.; Junge, K.; Beller, M. *Org. Lett.* **2007**, *9*, 5429.

[16] Shaikh, N. S.; Enthaler, S.; Junge, K.; Beller, M. *Angew. Chem. Int. Ed.* **2008**, *47*, 2497.

[17] Addis, D.; Shaikh, N.; Zhou, S.; Das, S.; Junge, K.; Beller, M. *Chemistry--An Asian Journal*, **2010**, 5, 1687-1691.

[18] Casey, C. P.; Guan, H. *J. Am. Chem. Soc.* **2007**, *129*, 5816.

[19] Sui-Seng, C.; Freutel, F.; Lough, A. J.; Morris, R. H. *Angew. Chem. Int. Ed.* **2008**, *47*, 940.

[20] Sui-Seng, C.; Haque, F. N.; Pütz, A.-M.; Reuss, V.; Meyer, N.; Lough, A. J.; Zimmer-De Iuliis, M.; Morris, R. H. *Inorg. Chem.* **2009**, ASAP (DOI: 10.1021/ic801518h).

[21] Mikhailine, A.; Lough, A. J.; Morris, R. H. *J. Am. Chem. Soc.* **2009**, *ASAP* DOI: 10.1021/ja809493h.

[22] Bart, S. C.; Chlopek, K.; Bill, E.; Bouwkamp, M. W.; Lobkovsky, E.; Neese, F.; Wieghardt, K.; Chirik, P. J. *J. Am. Chem. Soc.* **2006**, 128, 13901.

[23] Knijnenburg, Q.; Gambarotta, S.; Budzelaar, P. H. M. *Dalton Trans*. **2006**, 5442.

[24] Davis, R.N.; Tanski, J.M.; Adrian Junior, J.C.; Tyler, L.A.; *Inorg.Chim.Acta*, **2007**, 360, 3061.

[25] Wile, B. M.; Trovitch, R. J.; Bart, S. C.; Tondreau, A. M.; Lobkovsky, E.; Milsmann, C.; Bill, E.; Wieghardt, K.; Chirik P. J. *Inorg. Chem.* **2009,** *48* (9), 4190.

[26] Pelczar, E. M.; Emge, T. J.; Krogh-Jespersen, K.; Goldman, A. S. *Organometallics* **2008**, 27, 5759.

[27] Trovitch, R. J.; Lobkovsky, E.; Chirik, P. J. *Inorg. Chem.* **2006**, *45*, 7252.

[28] Panosyan, F.B.; Lough, A.J.; Chin, J. *Acta Crystallogr.,Sect.E:Struct.Rep.Online* **2003**, 59, 864.

[29] Jiang, M.; Dalgarno, S.; Kilner, C.A.; Halcrow, M.A.; Kee, T.P. *Polyhedron*, **2001**, 20, 2151.

[30] Gonser, U. *Topics in Applied Physics Vol 5*; Springer: New York, 1975; 5, p 68.

[31] Casey, C. P.; Guan, H. *J. Am. Chem. Soc*. 2007, 129, 5816.

[32] Bart, S. C.; Hawrelak, E. J.; Schmisseur, A. K.; Lobkovsky, E.; Chirik, P. J. *Organometallics* **2004**, *23*, 237.

[33] Pangborn, A.B.; Giardello, M.A.; Grubbs, R.H.; Rosen, R.K.; Timmers, F.J. *Organometallics* **1996**, *15*, 1518.

[34] Cornejo, A.; Fraile, J. M.; García, J. I.; Gil, M. J.; Martínez-Merino, V.; Mayoral, J. A.; Pires, E.; Villalba, I. *Synlett* **2005**, *15*, 2321.

[35] Sidokmai, W.; Imanishi, Y. *Bull. Chem. Soc. J.* **2000**, 73, 599-605.

[36] Miriyala, B.; Bhattacharyya, S.; Williamson, J. S. *Tetrahedron*, **2004**, 60, 1463.

[37] Sur, S. K. *J. Magn. Res.* **1989**, *82*, 169.

[38] Alcock, Nathaniel W., et.al. *Dalton Transactions*, **2005**, 3, 518.

[39] Watanabe, Kenichi, and Murayama, Kiyoshi, *Bulletin of the Chemical Society of Japan*, **1974**, 478, 1948.

[40] Sakamoto, T.; Kaneda, S.; Nishimura, S.; Yamanaka, H.; *Chemical and Pharmaceutical Bulletin*, **1985**, 33(2), 565.

CHAPTER 5

INDUSTRIALLY RELEVANT HYDROSILYLATION ACTIVITY OF OLEFINS AND TERTIARY SILANES WITH BIS(IMINO)PYRIDINE AND TERPYRIDINE IRON COMPLEXES[*]

5.1 Abstract

The addition of tertiary silanes to terminal alkenes using iron-based catalysts was achieved. Terpyridine iron bis(neosilyl) complexes were effective for the hydrosilylation of unfunctionalized terminal olefins, as well as the epoxide containing vinyl cyclohexene oxide. The hydrosilylations performed optimally at 60 ºC without the use of solvent. The *in situ* activated catalysis using terpyridine iron dichloride was also achieved using a variety of activating agents. Several precatalysts of PDI were explored for their catalytic activity, including: dinitrogen complexes, dialkyl complexes, olefin adducts, as well as *in situ* activated dihalides. The hydrosilylation activity of these compounds rivals the industrially used platinum based catalysts, and the selectivity is typically improved by the iron compound. For allyl-polyethers,no competing olefin isomerisation was observed with the iron catalysts, a frequent side-reaction observed with Pt based systems. Another substrate that particularly benefits from the selectivity of the iron catalyzed hydrosilylation is 1,2,4-trivinylcyclohexane. With a 1:1 stoichiometry of $(TMSO)_2SiMeH$, the catalysis yields an average of 75 % mono hydrosilylated product, with 90 % addition at the C4 vinyl group. Overall, the catalytic activity of iron based complexes was demostrated to be competitive, and in some instances, superior to platinum based hydrosilylation catalysts.

[*] Parts of this chapter have been taken from (a) Delis, G. P.; Nye, S. A.; Lewis, K. M.; Weller, K, J.; Chirik, P. J.; Tondreau, A. M.; Russell, S. K. 2011, Hydrosilylation Catalysts, United States, Momentive Performance Materials, US 2011/0009573 A1. (b) Delis, G. P.; Chirik, P. J.; Tondreau, A. M. 2011, Hydrosilylation Catalysts, United States, Momentive Performance Materials, US 2011/0009565 A1.

5.2 Introduction

Hydrosilylation chemistry, typically involving a reaction between a silyl-hydride and an unsaturated organic group, is the basis for synthesis routes to produce commercial silicone-based products including surfactants, silicone fluids and silanes, as well as addition or UV cured products that find application as sealants, adhesives, and silicone-based coating products. Heretofore, precious metal catalysts, such as platinum or rhodium complexes, have typically catalyzed hydrosilylation reactions. For example, a dimeric platinum complex containing unsaturated siloxanes as ligands, known as Karstedt's-catalyst, is commonly used in industrial hydrosilylations. [1] Other variants include the olefin supported Ashby's catalyst [2] and hexachloroplatinic acid, known as Speier's catalyst.[3] These prevalent industrially utilized hydrosilylation catalysts are presented in Figure 5.1.

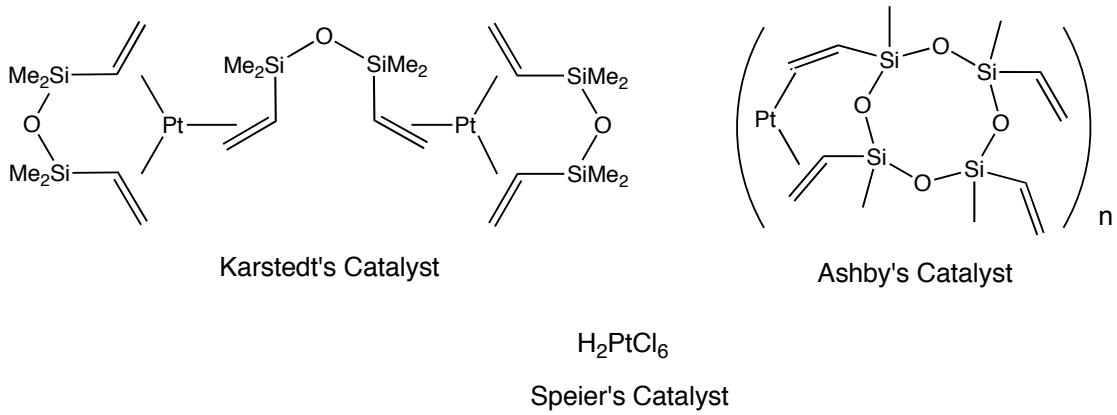

Figure 5.1 Platinum based catalysts used in industrial hydrosilylation applications.

Although these precious metal complex catalysts have enjoyed considerable success as catalysts for hydrosilylation reactions,[4] they have several distinct disadvantages. One is that the precious metal complex catalysts are inefficient in

catalyzing certain reactions. In the precious metal catalyzed hydrosilylation of allyl polyethers with silicone hydrides, up to 30 % excess allyl polyether, relative to the amount of silicone hydride, is required to compensate for the lack of efficiency of the catalyst and to ensure complete conversion to a final product. This increases the costs of starting materials and the final product requires purification. Side reactions can be minimized with the use of designer ligands on the platinum metal, such as N-heterocyclic carbenes.[5,6]

Another disadvantage of the platinum complexes as catalysts is limited scope. It is known that precious metal complex catalysts are susceptible to catalyst poisons such as phosphorous and amine compounds. Accordingly, for a hydrosilylation involving unsaturated amine compounds, the precious metal catalysts known are less effective in promoting the direct reaction between these unsaturated amine compounds with silicon-hydride substrates, and will often lead to the formation of mixtures of undesired isomers. Epoxide-containing olefinic substrates are also problematic, being prone to undesired epoxide ring opening reactions.[5] The discussed undesired side reactions are presented in Figure 5.2.

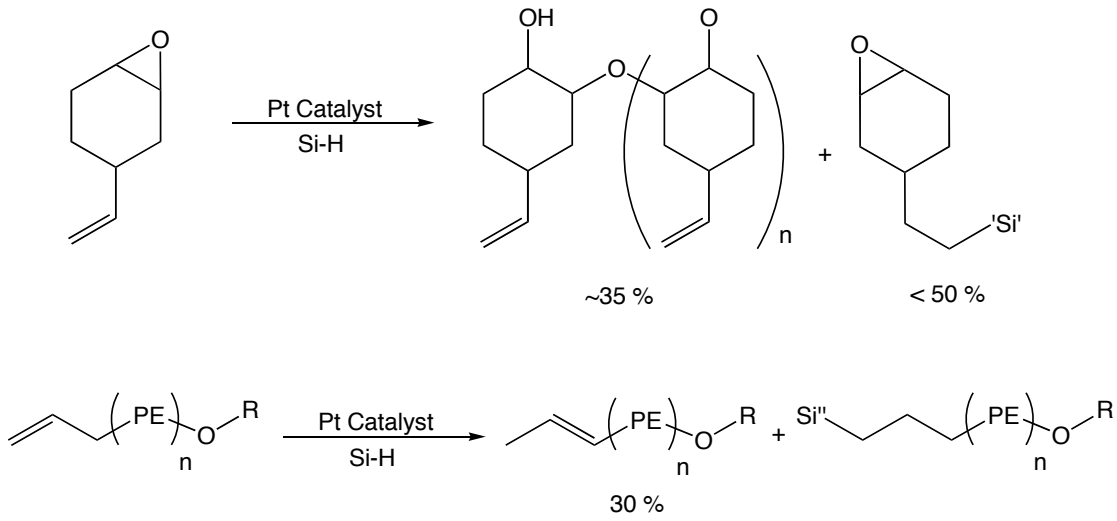

Figure 5.2 Common side reactions of two commercial hydrosilylations with platinum based catalysts.

Due to the high price of precious metals, the platinum and rhodium containing catalysts contribute a significant proportion of the final cost of silicone formulations. Recently, global demand for precious metals, including platinum, has increased, driving prices for platinum to record highs, creating a need for effective, low cost replacement catalysts. As an alternative to precious metals, recently, certain iron complexes have gained attention for use in olefin and ketone hydrosilylation. $Fe(CO)_5$ is known to catalyze hydrosilylation reactions at high temperatures.[7,8,9] However, unwanted by-products such as the unsaturated silyl olefins, which result from dehydrogenative silylation, were formed as well.

Bis(imino)pyridine iron compounds are redox-active complexes that promote many catalytic reactions. [10,11,12,13,14,15,16] Among these is a bis(imino)pyridine iron based hydrosilylation of olefins using primary and secondary silanes.[17] Hydrogenations of functional-group containg olefins have also been reported.[18] Several incompatible functional groups have been reported, such as allyl ether and ester functionalities.[19] The complex used in those studies was (^{iPr}PDI)Fe(N_2)$_2$ (PDI = 2,6-(*R*N=CMe)$_2$$C_5H_3N$),

and the unfortunate result of the sterically encumbering isopropyl groups is that tertiary silanes were unreactive to Si-H addition across double bonds. Other iron based, PDI or Pybox supported complexes have been shown to affect the hydrosilylation of ketones, albeit with primary or secondary silanes.[20,21] Beller and Nishiyama have independently explored $Fe(OAc)_2$ for the hydrosilylation of various aldehydes and ketones, typically using tertiary silanes such as PMHS (polymethylhydrosiloxane), $(EtO)_3SiH$ or $(EtO)_2MeSiH$ as stiochiometric reductants.[22,23,24,25,26] One of the goals is the use of tertiary silanes for the hydrosilylation of olefins.

5.3 Terpyridine-Iron Dialkyl Based Hydrosilylation Reactions

The previous reports of bis(imino)pyridine and bis(oxazoline)pyridine (Pybox) based dialkyl iron complexes as catalysts precursors led to the investigation of the analogous terpyridine supported iron dialkyl complexes as catalyst precursors. Terpyridine iron dichloride, although existing as a salt pair, reacts with two equivalents of neosilyl lithium to yield the terpyridine iron(II) bis neosilyl complex, $(terpy)FeR_2$. The complex was also synthesized via the Campora method, by addition of the free ligand to $(py)FeR_2$, and the conversion is near quantitative to yield $(Terpyridine)Fe(CH_2TMS)_2$, $(terpy)FeR_2$.[27] These two synthetic schemes are outlined in Figure 5.3.

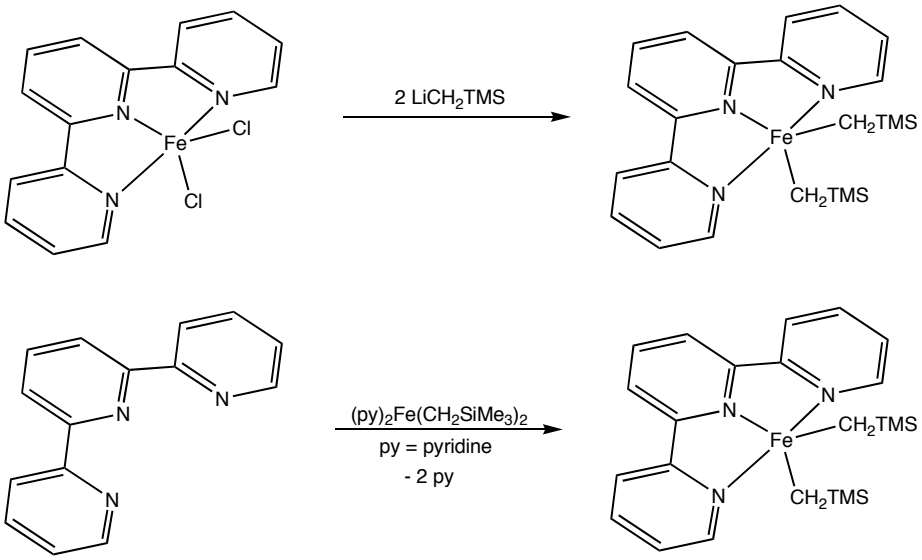

Figure 5.3 Synthetic routes to catalytically relevant **(terpy)FeR_2.**

(Terpy)FeR_2 was obtained as a purple crystalline solid with a magnetic moment of μ_{eff} of 4.6 μB at 290 K in the solid state via a magnetic susceptibility balance. This is low for the spin only value for four unpaired electrons, but is most consistent with an S=2 compound. Mössbauer data obtained the compound show a quadrupole doublet centered at 0.29 mm/s with a quadrupole splitting of 2.37 mm/s. This is consistent with other dialkyl complexes that have been shown to have a mono-reduced chelate and are described as high spin ferric centers containing anti-ferromomagnetic coupling between the iron and the reduced chelate.[28] Recently, terpyridine was shown conclusively to be able to support a one-electron reduction.[29]

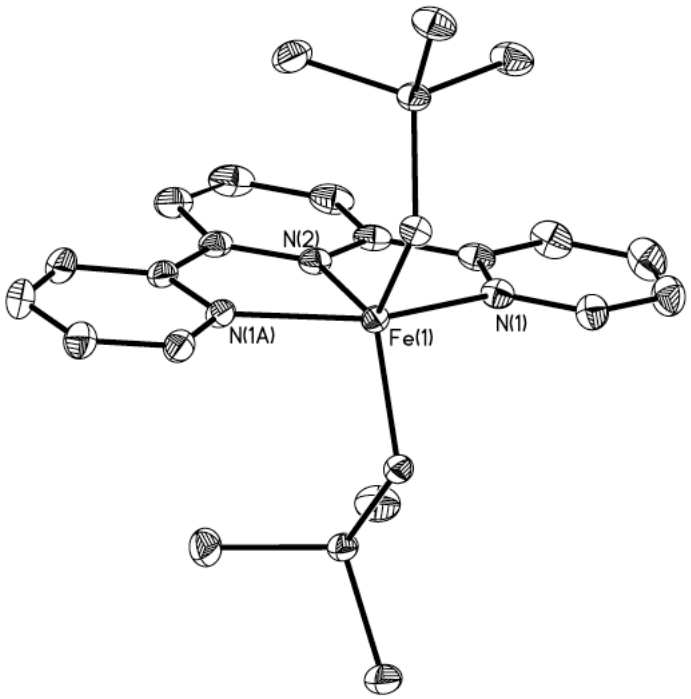

Figure 5.4 The solid-state structure of **(terpy)FeR$_2$** at 30% probability ellipsoids. Hydrogen atoms removed for clarity.

The solid-state structure of (terpy)FeR$_2$ was determined by single crystal X-ray diffraction and is shown in Figure 5.4. In the solid state, the molecule has a crystallographically imposed C_2 axis. The overall geometry is best described as distorted trigonal bipyramidal with the alkyl ligands and central pyridine comprising the equatorial plane, with the N(2)-Fe(1)-C(12) bond angles both being 120.94(4)º and the C(12)-Fe(1)-C(12) bond angle at 118.12(4)º. The constraints of the chelate contract the N(1)-Fe(1)-N(2) to 75.48(4)º, more acute than the optimal 90º for this geometry. The iron carbon bond lengths of 2.073(2) Å is on the order of other N,N,N chelate iron-neosilyl bonds discussed in chapter 4 of this thesis.

Table 1.1 Select distances and angles for (**terpy**)**FeR**$_2$.

(terpy)Fe(CH_2SiMe_3)$_2$	Å or º
Fe(1)-N(1)	2.150(2)
Fe(1)-N(2)	2.014(2)
Fe(1)-C(12)	2.073(2)
N(1)-C(1)	1.350(2)
N(1)-C(5)	1.353(2)
N(2)-C(6)	1.375(2)
C(5)-C(6)	1.457(2)
N(1)-Fe(1)-N(2)	75.48(3)
N(1)-Fe(1)-N(1)	150.96(7)
N(2)-Fe(1)-C(12)	120.94(4)
C(12)-Fe(1)-C(12)	118.12(4)

The catalytic performance of (terpy)FeR_2 was initially assayed in the hydrosilylation of 1-hexene with triethylsilane. The initial reactions were run at 95 ºC with 5 mol % of (terpy)FeR_2, and proceeded to greater than 90 % conversion after 10 hours of stirring. Analysis of the reaction mixture by GC/MS revealed approximately 5 % of dehydrogenative silane coupling. A survey of relevant tertiary silanes was performed in order to assay their performance in the catalysis. Triethoxysilane (**TES**) and bis(trimethylsiloxy)methylsilane (**MD'M**) were subjected to the same reaction conditions, and the results established that **MD'M** was equally competent for the catalysis, but **TES** suffered from disproportionation to tetraethoxysilane, although roughly 5% of the desired product was observed in the reaction mixture. These results are summarized in Figure 5.5.

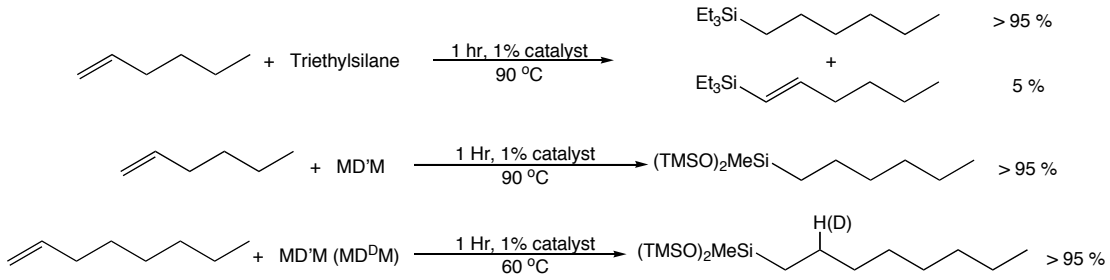

Figure 5.5 The results of the hydrosilylation of 1-hexene and 1-octene with **(terpy)FeR_2**.

Due to the industrial relevance of the product of **MD'M** and 1-octene hydrosilylation,[5,30] this reaction was used to evaluate iron catalysts and establish optimal conditions. The observation of incomplete conversion at 95 ºC, typically converting to no greater than 90 %, with (terpy)FeR_2 suggested that catalyst death was competitive with hydrosilylation. Lowering the temperature to 60 ºC obviated the problem of incomplete reaction times. Although the catalysis was initially slower, the hydrosilylation of 1-octene with **MD'M** was completed within an hour at 60 ºC with (terpy)FeR_2. Deuterium labeling of bis(trimethylsiloxy)methylsilane, **MD^DM**, revealed incorporation of deuterium into the β-position of hydrosilylated 1-octene (Figure 5.5). Many of the top performing Pt catalysts require temperatures greater than 70 ºC, so this elevated temperature is still mild compared to the current industry standard. The catalysis at these two temperatures was monitored by react-IR, measuring the disappearence of the Si-H peak at 2140 cm^{-1}, and the results are presented in Figure 5.6.

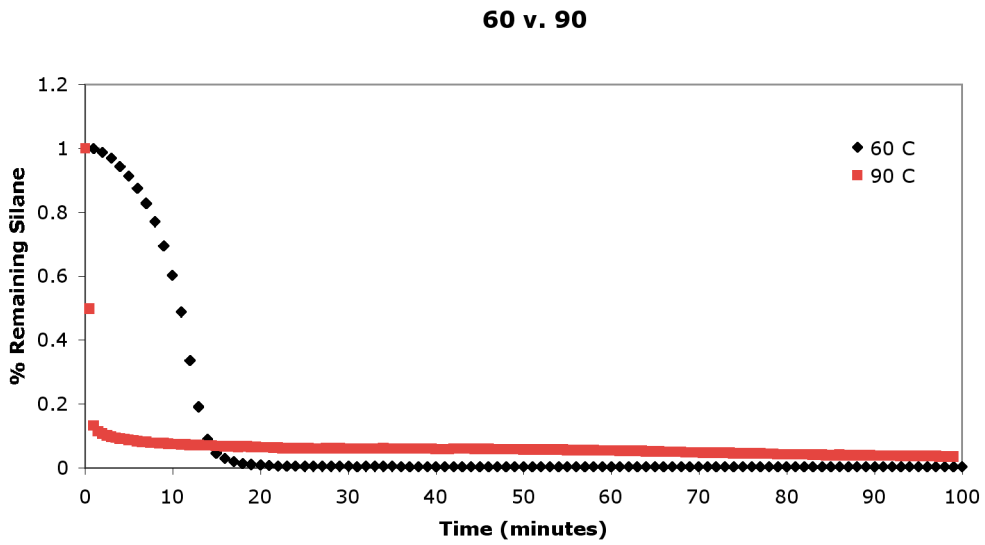

Figure 5.6 The temperature effect on the catalytic reactions with 1.3:1 1-octene to MD'M, 0.5 mol%catalyst to silane, in a neat reaction with **(terpy)FeR_2.**

The single hydrosilylation of 1,2,4-trivinylcyclohexane (**TVCH)** was also explored with (terpy)FeR_2. The selective single addition product is desired in this reaction, as it is a useful bifunctional compound.[31] A 1:1 mixture of **MD'M** and a mixture of isomers of **TVCH** were heated at 60 ºC for one hour with 1.0 mol% of (terpy)FeR_2 in a scintillation vial. Analysis of the product by GC established a distribution that is consistent with a non-selective catalyst, similar to the performance of Karstedt's catalyst. For the iron case 55% of the desired single addition product was observed, as well as 31% of the double addition product, and 14% remaining starting material. There was also no preference for regio- or stereochemistry, as the product distributions were all of near equal intensity. Although the catalysis was viable, the lack of useful selectivity offered no advantage over the current industrial catalyst. This reactivity is shown in Figure 5.7.

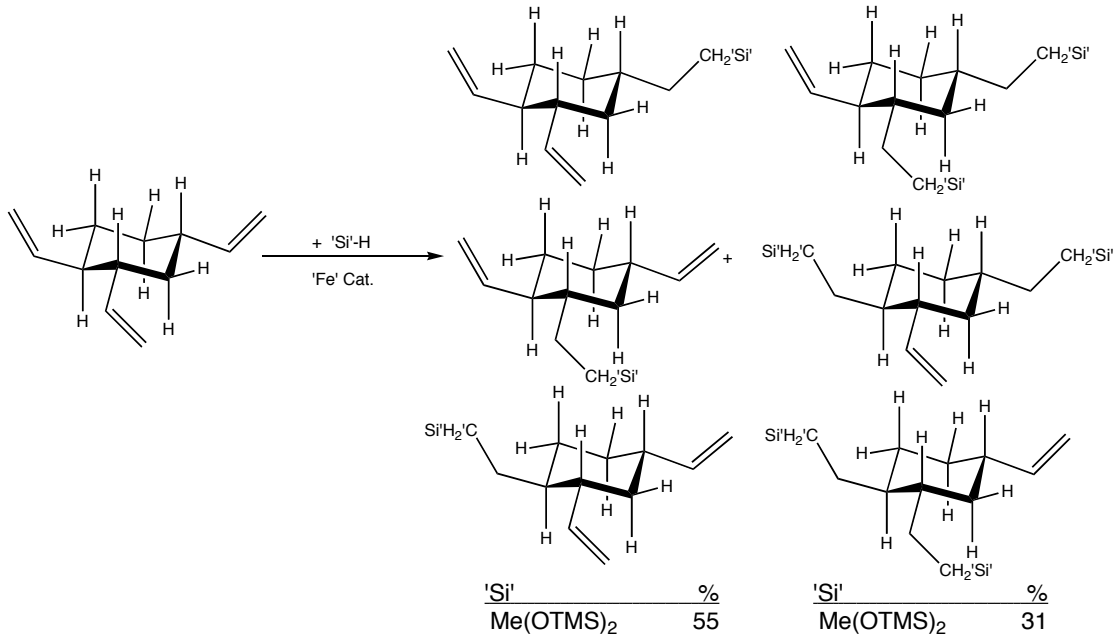

Figure 5.7 The hydrosilylation of 1,2,4-trivinylcyclohexane with **(terpy)FeR_2.**

Epoxide containing substrates such as allyl glycidyl ether (1-allyloxy-2,3-epoxypropane) and vinylcyclohexeneoxide (4-vinyl-1-cyclohexene 1,2-epoxide, **VCHO**) were the next class of olefinic substrates explored with **MD'M** and (terpy)FeR_2 as the pre-catalyst. The allyl glycidyl ether was unreactive with a variety of silanes and temperatures ranging from room temperature to 110 ºC. The reaction with **VCHO** was completed after 12 hours at 60 ºC. The ^{1}H NMR spectrum did not exhibit evidence for epoxide ring opening or polymerization under the reaction conditions. These substrates are reported in Figure 5.8.

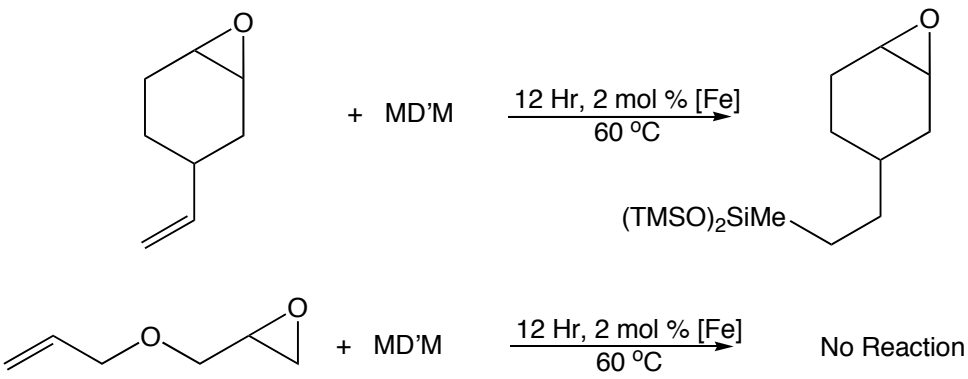

Figure 5.8 The hydrosilylation of epoxide containing olefins with **(terpy)FeR_2.**

The success of **MD'M** with **VCHO** led to the investigation of VCHO using other silanes, including polymeric silanes. Attempts to use **TES** resulted in the disproportionation to tetraethoxysilane and no desired product was detected by GC/MS. The use of more dilute silicon hydrides led to a decrease in reactivity of the reaction. The use of $Me_2HSi(OSiMe_2)_nOSiHMe_2$, where n= 0 (**M'M'**), 3.3, and 24, at 1 mol% catalyst and 60 ºC for one hour provided insight into the concentration dependence of the catalysis. The hydrosilylation activity dropped from 70 % conversion to 15 % conversion when n was changed from 0 to 3.3. There was no appreciable conversion with the higher molecular weight silicon hydride. Diluting the **M'M'** reaction with solvent lowered the yield. The rate of hydrosilylation under dilute conditions is not competitive with the rate of catalyst deactivation in these cases.

One final substrate examined was allylamine. The product of allylamine and **TES**, gamma-aminopropyltriethoxysilane, is a bifunctional coupling agent, used to bind organic compounds to inorganic (glass) surfaces. Unfortunately, as with other hydrosilylation attempts with **TES**, the catalysis with (terpy)FeR_2 was unsuccessful. Using **MD'M** in place of TES resulted in the successful hydrosilylation of the allylamine at 5 mol % catalyst loading at 60 ºC in an hour. The use of 0.5 equivalents

of 1,1,3,3-tetramethyldisoloxane, (**M'M'**) to allylamine with 1 mol % iron complex at 60ºC in this case did result in the hydrosilylation of the olefin. This reactivity is summarized in Figure 5.9.

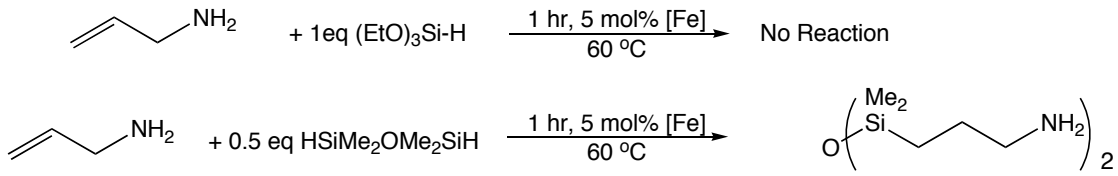

Figure 5.9 The hydrosilylation of allylamine with **(terpy)FeR_2.**

The success of (terpy)FeR_2 in promoting the hydrosilylation of a variety of functional-group containing olefins was encouraging. The investigation into the cross-linking of polymeric silyl-hydrides, SL-6020, or $MD_{15}D'_{30}M$ and vinyl-silanes, SL-6100, or $M^{vi}D_{120}M^{vi}$, in which M^{vi} is vinyl dimethyl Si-O-, was also conducted, and the results were varied. Upon heating the polymers to 60 ºC or 95 ºC with 5 mol % catalyst, some crosslinking of the polymeric materials was observed. Unfortunately, the material was not gelled to the same degree as that obtained with the platinum based Karstedt catalyst. Also, the dark purple color of the reaction mixture is rather persistent after the reaction. The proof of principle reaction did show that polymer crosslinking was possible with iron-based catalysts. This reaction is depicted in Figure 5.10.

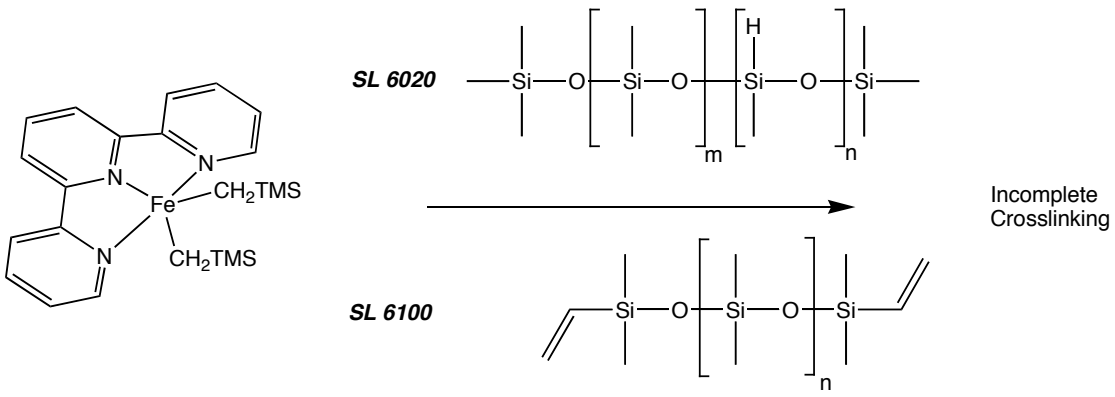

Figure 5.10 The crosslinking of polymeric substrates with **(terpy)FeR_2**.

(Terpy)$FeCl_2$ was explored as a precatalyst, using reducing agents *in situ* to activate the catalyst. This obviates the need to store highly sensitive iron complexes under inert conditions, as well as may lessen the need to use highly purified the substrates. (Terpy)$FeCl_2$ at 1 mol% was added to a stirring solution of 1-octene and **MD'M**, followed by two equivalents of $NaEt_3BH$. The reaction was stirred for 1 hour at room temperature and GC was utilized to evaluate the progress of the reaction, and the reaction mixture was shown to contain 60% of the desired product.

Other reducing agents were evaluated for their utility in the *in situ* activation of (terpy)$FeCl_2$. The reductants such as Mg^o, $LiBH_4$, $NaBH_4$, and Zn^o were all tried but none activated (terpy)$FeCl_2$ to the point of being catalytically active. An easily synthesized reducing reagent that was productive for activation was the polymeric $[(THF)_2Mg(C_4H_6)]_n$. The addition of these compounds to the stirring substrate/precatalyst mixture resulted in an immediate color change, and the reaction was continued for 1 hour at room temperature. Evaluation of the mother liquor showed a similar conversion to that observed with the sodium triethylborohydride reaction.

These *in situ* activations were only successful for the model reaction of **MD'M** and 1-octene. The attempts to perform *in situ* activation in the presence of

functionalized olefins did not yield any catalysis. The limit of *in situ* activation to unactivated olefins is not terribly surprising, as amines and epoxides are reactive. The lower turnover for this method as opposed to using the dialkyl complex may be explained by the temperature difference.

5.4 Hydrosilylation Using PDI Iron Complexes

Bis(imino)pyridine iron complexes bearing the large 2,6-isopropyl substituents on the aryl groups were ineffective for all hydrosilylations attempted with tertiary silanes. This includes attempts using (^{iPr}PDI)FeN_2, (^{iPr}PDI)FeR_2, and (^{iPr}PDI)$Fe(C_4H_6)$. Under a variety of conditions, there was no catalytic activity. In order to accommodate the use of larger silanes, smaller groups on the aryl ring of bis(imino)pyridine were explored. The results of (terpy)FeR_2 a catalyst led to the investigation of the various iron dialkyl complexes, of which many are known.

The use of (^{Me}PDI)FeR_2 in the catalytic reaction of **MD'M** and 1-octene proceeded slowly at room temperature, but the hydrosilylation exhibited complete conversion after 12 hours at 1 mol% of iron. When the reaction was heated to 60 ºC, the catalysis was 70% complete after only 1 hour, with roughly 10% starting 1-octene remained and 20% isomerized olefin. This distribution is not optimal, but does demostrate that the dialkyl complexes can perform the desired catalysis.

For the polymeric vinyl silane SL-6100 and the polymeric silyl-hydride SL-6020, (^{Me}PDI)FeR_2 clearly outperforms (terpy)FeR_2. The product of the crosslinking is a brittle, lightly colored solid much like the product from the use of Pt based systems. The catalysis requires heating at 60 ºC, and the polymer solution slowly gels over time. This result indicates that bis(imino)pyridine based catalyst systems will be able to out perform the terpyridine based systems.

The use of [(^{Me}PDI)FeN_2]$_2$(μ-N_2), [(^{Et}PDI)FeN_2]$_2$(μ-N_2), and [(^{Me,iPr}PDI)FeN_2]$_2$(μ-N_2) were reported as effective catalysts for hydrogenation of

certain tertiary olefins.[32] These compounds proved productive as hydrosilylation catalysts in this study, as well. The model reaction of Si-H addition of **MD'M** to 1-octene was performed at room temperature, and all three iron compounds achieved complete conversion of the olefin within minutes at 1 mol% iron loading. No traces of isomerization or dehydrogenative silane coupling side products were observed in the reaction solution. The initial result was very encouraging. For simplicity, further studies were performed using $[(^{Me}PDI)FeN_2]_2(\mu\text{-}N_2)$, and only when the catalysts vary in reactivity are the other dinitrogen complexes discussed.

The addition of the three model silanes, **MD'M**, **TES**, and triethylsilane was performed with 1-octene with 0.5 mol% $[(^{Me}PDI)FeN_2]_2(\mu\text{-}N_2)$ in order to gauge the relative reactivity of the three silanes. The reaction of **MD'M** and **TES** was completed in under 15 minutes, whereas the reaction of triethylsilane was completed in 1 hour. $[(^{Et}PDI)FeN_2]_2(\mu\text{-}N_2)$ was used, and the reactivity of **MD'M** and **TES** was equivalent to $[(^{Me}PDI)FeN_2]_2(\mu\text{-}N_2)$, but the reaction with triethylsilane was only 40 % complete after one hour.

The hydrosilylation of 1-octene with **MD'M** was optimized to improve catalytic performance, specifically turnover frequency and catalyst loading. The catalysis was performed without the use of solvent. Catalyst loadings were lowered from 0.5 mol% to 0.08 mol% of $[(^{Me}PDI)FeN_2]_2(\mu\text{-}N_2)$ (90 ppm Fe), and this limit is most likely due to impurities in the substrates resulting in catalyst decomposition. On a multigram scale (3 grams of 1-octene), the hydrosilylation was completed within an hour at 290 K, with no evidence for olefin, yielding a minimum turnover frequency of 1250 hr^{-1} (Figure 5.11).

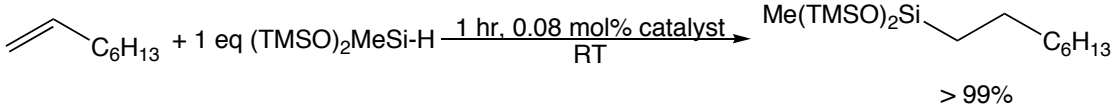

Figure 5.11 The hydrosilylation of 1-octene with **MD'M** and **[(^{Me}PDI)FeN$_2$]$_2$(μ-N$_2$).**

The investigation into the cross-linking of polymeric silyl-hydrides (SL-6020) and vinyl-silanes (SL-6100) was conducted with [(^{Me}PDI)FeN$_2$]$_2$(μ-N$_2$), and the results were encouraging. The addition of [(^{Me}PDI)FeN$_2$]$_2$(μ-N$_2$) to the stirring substrate solution was unsuccessful, as the crystalline iron compound is not readily soluble in the polymers. Addition of diethyl ether or toluene, however, resulted in immediate gelation at a catalyst loading 1000 ppm Fe. The catalyst loading was lowered to 230 ppm of iron, and a hard, gelled product similar to that obtained when using Karstedt's catalyst. Lowering the catalyst loading further resulted in the encapsulation of the catalyst in a shell of crosslinked polymer, inhibiting completion of the reaction. This, however, is likely a mechanical problem, and not due to a deficiency of the catalyst. Pictures depicting the crosslinking of the polymers are shown in Figures 5.12 and 5.13.

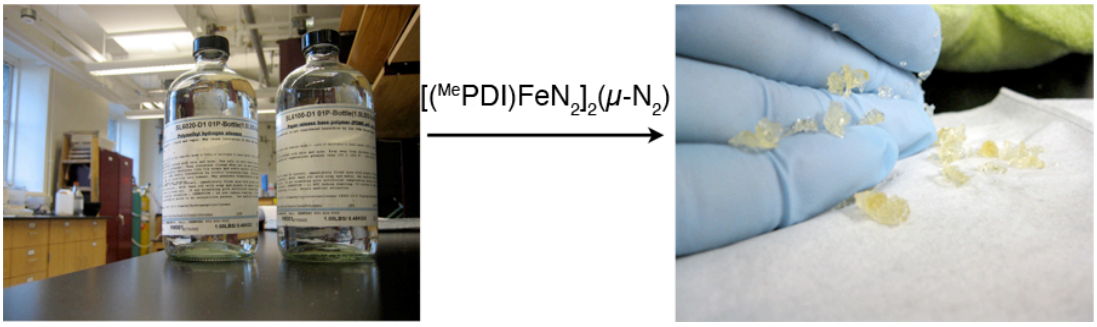

Figure 5.12 A pictorial description of the crosslinking of polymeric substrates.

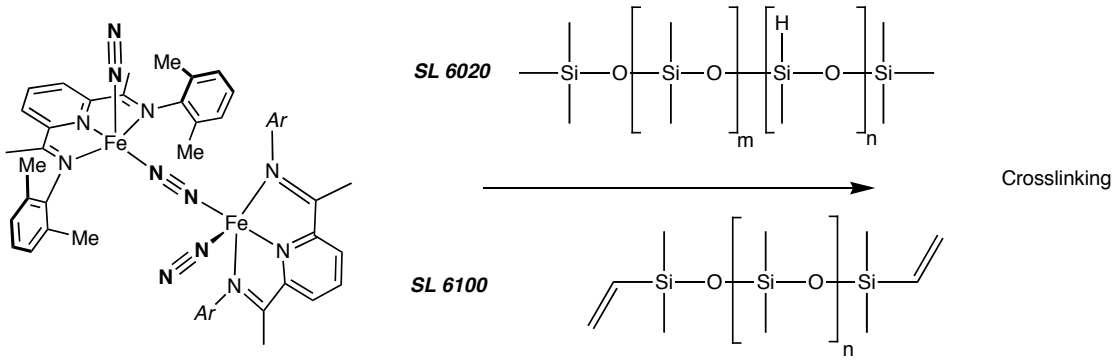

Figure 5.13 The crosslinking of polymeric substrates.

The successful crosslinking of polymeric substrates to form the release-coating product encouraged the investigation of reversible inhibition of the catalyst, as the reaction was completed as the iron compound was added. Several inhibitory substrates were added to the reaction and their effects were noted. The first inhibitor studied was that of the chelating 1,3-divinyl-1,1,3,3-tetramethyldisiloxane, $\mathbf{M^vM^v}$. The addition of this compound did not result in notable inhibition and the addition of excess $\mathbf{M^vM^v}$ resulted in incomplete crosslinking.

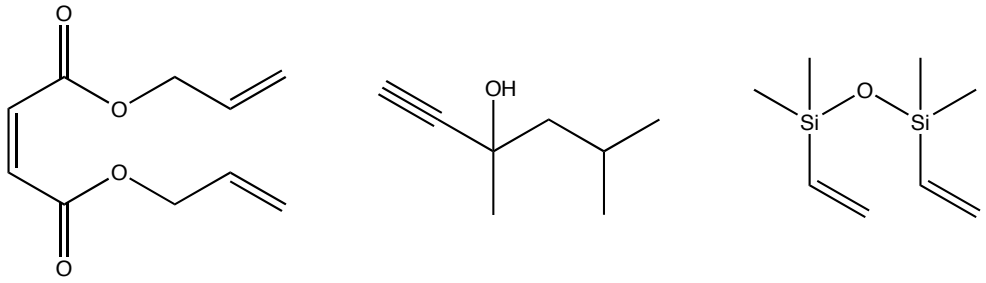

Figure 5.14 Substrates attempted to cause reversible inhibition of catalysis.

The next inhibitor evaluated was diallylmaleate (**DAM**). The use of this inhibitor proved to be irreversible, with no measurable crosslinking occurring even at elevated temperatures. The use of Surfynol 61 as an inhibitor resulted in the same irreversible inhibition. The irreversibility most likely arises from the formation of a non-reactive iron alkoxide. The investigation into reversible inhibitors is an ongoing

effort in the utility of iron compounds as catalysts in the crosslinking of substrates of this type.

The success of $[(^{Me}PDI)FeN_2]_2(\mu\text{-}N_2)$ in the catalytic hydrosilylation of 1-octene under mild conditions prompted the investigations into the reactivity of a variety of functionalized olefins with **MD'M**. The first class of terminal olefin studied were allyl polyethers having general structures $H_2C{=}CHCH_2O(C_2H_4O)_nR$. The end capping (R) of this class of substrates is important, several different end groups, such as hydroxy groups and esters, are incompatible with $[(^{R}PDI)FeN_2]_2(\mu\text{-}N_2)$ catalysts. To this end, $H_2C{=}CHCH_2O(C_2H_4O)_{8.9}CH_3$ was utilized in this investigation, where n was an average of 8.9 repeat units and the methyl end-capping was 100% (the polymer contained no hydroxy terminated chains).

The catalytic hydrosilylation of $H_2C{=}CHCH_2O(C_2H_4O)_{8.9}CH_3$ with **MD'M** using $[(^{Me}PDI)FeN_2]_2(\mu\text{-}N_2)$ was successful. The vigorous stirring of the two substrates, as they are immiscible, with 1 mol% of catalyst for 24 hours resulted in the formation of a new resonance in the ^1H NMR at 0.43 ppm in benzene-d_6 or 0.63 in chloroform-*d*, as well as the disappearance of the Si-H resonance. The solution also becomes homogenized, indicating the slow hydrosilylation of the polymer. As judged by ^1H NMR spectroscopy, no isomerization of the olefin was observed for this reaction. A representative ^1H NMR spectrum of the polymer is shown in Figure 5.15.

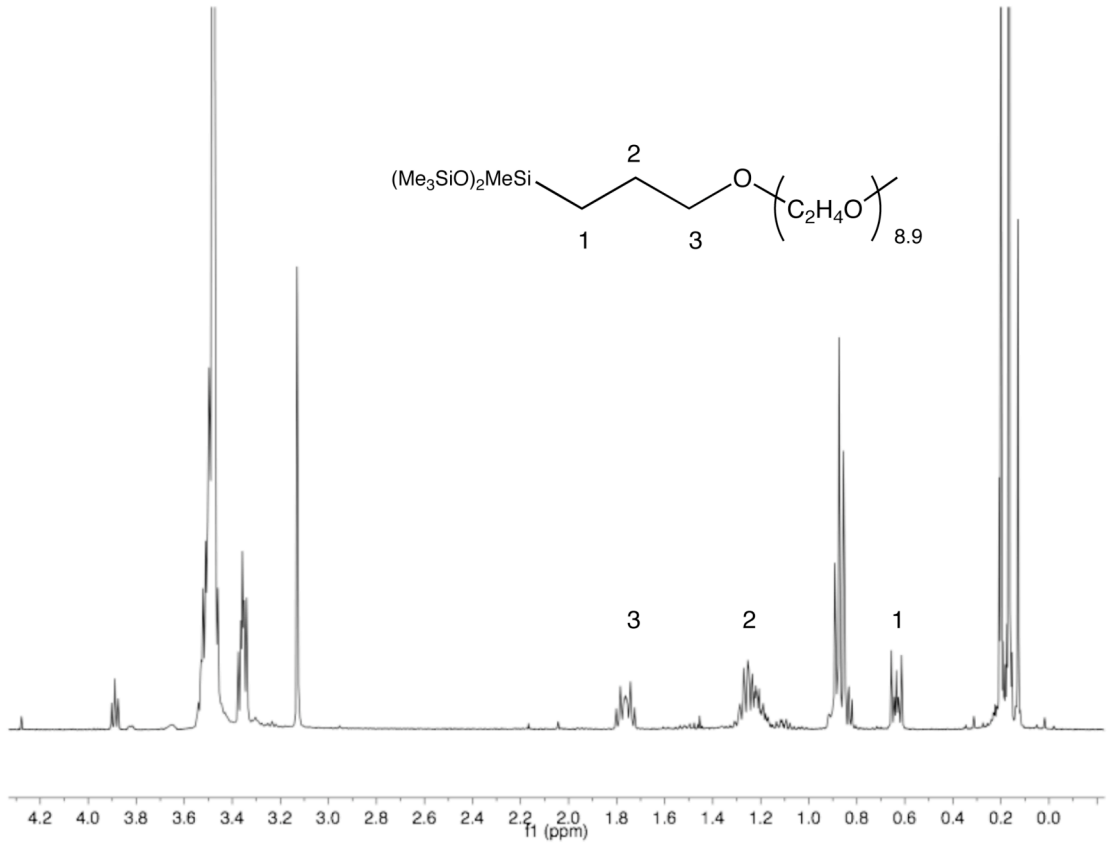

Figure 5.15 ^{1}H NMR spectrum of the hydrosilylated allyl polyether**.**

Optimization of the hydrosilylation of $H_2C{=}CHCH_2O(C_2H_4O)_{8.9}CH_3$ with **MD'M** with $[(^{Me}PDI)FeN_2]_2(\mu\text{-}N_2)$ as the catalyst precurser produced faster reaction times and lower catalyst loadings. Performing the reaction at 60 ºC resulted in complete conversion to the desired polymer after one hour at 1 mol % catalyst loading. Lowering the catalyst loading in this case resulted in a precipitous drop in reactivity, and the lowest loading that still produced complete conversion at 1 hour and 60 ºC was 0.5 mol % (230 ppm Fe). This is likely a result of more 'dilute' conditions of using long chained polymeric materials. However, a turnover frequency of 200 hr^{-1} was achieved at 60 ºC, and the product polymer did not contain any isomerized olefin product.

Epoxide containing substrates such as allyl glycidyl ether (1-allyloxy-2,3-epoxypropane) and vinylcyclohexeneoxide (4-vinyl-1-cyclohexene 1,2-epoxide, **VCHO**) were the next class of olefinic substrates studied for catalytic hydrosilylation with **MD'M** and $[(^{Me}PDI)FeN_2]_2(\mu\text{-}N_2)$ as a catalyst. Both epoxide-containing substrates were not converted to product with a variety of silicon hydrides under various conditions. In most cases, $[(^{Me}PDI)FeN_2]_2(\mu\text{-}N_2)$ appeared to decompose upon the addition of the vinyl epoxide, even when the silanes were added first. This substrate class appears to be incompatible with catalysts of the type $[(^{R}PDI)FeN_2]_2(\mu\text{-}N_2)$.

Another substrate class investigated was allylamine. The hydrosilylation attempts of the substrate with **TES** and $[(^{Me}PDI)FeN_2]_2(\mu\text{-}N_2)$ as the catalyst were modestly successful. The use of **TES** in the catalytic hydrosilylation produced sporadic results, with partial hydrosilylation to the desired gamma-aminopropyltriethoxysilane product, but a majority of the silane disproportionated to tetraethoxysilane. Typically, the hydrosilylation proceeded to 45 % conversion to the desired product after 1 hour with 1 mol % catalyst but the results were inconsistent. Neither longer reaction times nor higher catalyst loadings resulted in higher conversion to the product. Using **MD'M** in place of TES resulted in the slightly less successful hydrosilylation of the allylamine at 1 mol % catalyst loading. The use of 0.5 equivalents of 1,1,3,3-tetramethyldisoloxane, (**M'M'**) to allylamine with 1 mol % iron complex at 60 ºC in this case did result in the hydrosilylation of the olefin. This reactivity is summarized in Figure 5.16.

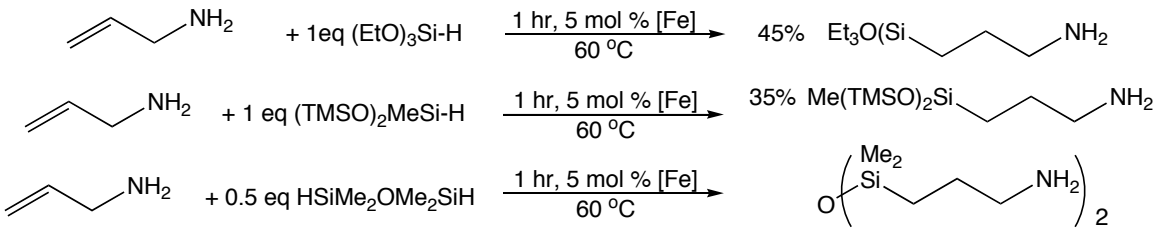

Figure 5.16 The hydrosilylation of allylamine with **[(^{Me}PDI)FeN$_2$]$_2$(μ-N$_2$).**

The use of dimethylallylamine was used to determine the compatibility of the [(^{Me}PDI)FeN$_2$]$_2$(μ-N$_2$) precatalyst with tertiary amines. Previous hydrogenation work utilizing (^{iPr}PDI)Fe(N$_2$)$_2$ and different substitution patterns on allylamines showed tertiary amines to be effective substrates for hydrogenation and showed no inhibition of catalytic activity as compared to terminal alkenes.[18] The use of dimethylallylamine with 1 equivalent of **TES**, triethylsilane, or **MD'M** with 0.5 mol % of [(^{Me}PDI)FeN$_2$]$_2$(μ-N$_2$) at room temperature yielded full conversion to the desired anti-Markovnikov hydrosilylation products (Figure 5.17).

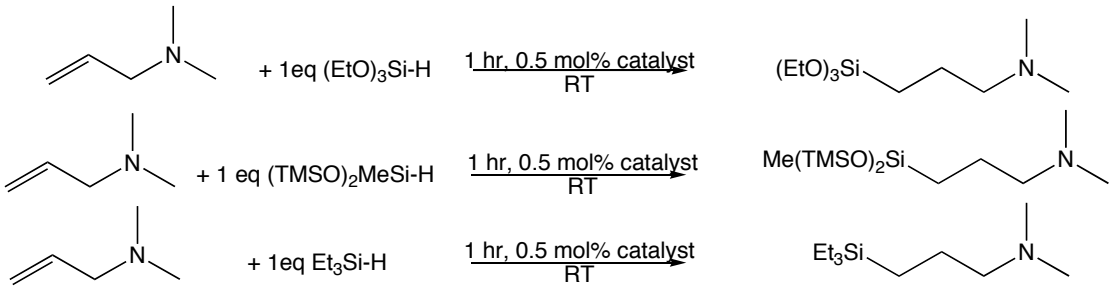

Figure 5.17 The hydrosilylation of dimethylallylamine with **[(^{Me}PDI)FeN$_2$]$_2$(μ-N$_2$)** using **TES**, **MD'M**, and triethylsilane.

[(^{Me}PDI)FeN$_2$]$_2$(μ-N$_2$) proved successful for the hydrosilylation of a multitude of industrially relevant substrates. The lack of isomerization of terminal olefins in these catalyses is a major advantage in the iron-based systems. Functionalized alkenes containing amines were successfully hydrosilylated, as were polymeric allyl polyethers.

Bis(imino)pyridine based dihalides were next investigated as catalyst precursors that were activated *in situ*. (^{Me}PDI)$FeCl_2$ at 1 mol % was added to a stirring solution of 1-octene and **MD'M**, followed by two equivalents of $NaEt_3BH$. The reaction was stirred for 60 minutes at room temperature and the solution was analyzed by GC. At this time, the reaction mixture was converted fully to the desired anti-Markovnikov product. The catalyst loading was further reduced, and full conversion was achieved in an hour with as little as 0.1 mol%iron compound. As with the dinitrogen compounds, (^{Me}PDI)$FeCl_2$, (^{Et}PDI)$FeCl_2$, and (^{Me,iPr}PDI)$FeCl_2$ were indistinguishable in reactivity when used *in situ*. (^{Me}PDI)$FeCl_2$ was mainly used for simplicity.

(^{Me}PDI)$FeCl_2$ was used *in situ* with $NaEt_3BH$ with a variety of substrates. The polymer crosslinking reaction with SL-6100 and SL-6020 worked, but a slight variation of the procedure was necessary. The addition of the reducing agent to a stirring solution of the substrates produced no catalysis. However, (^{Me}PDI)$FeCl_2$ was reduced in a minimal amount of THF with 2 equivalents of $NaEt_3BH$, presumably generating the THF adduct, and then subsequently added to the stirring substrate mixture. This resulted in immediate crosslinking of the polymers. Figure 5.18 presents the reactivity of the in situ generated catalyst.

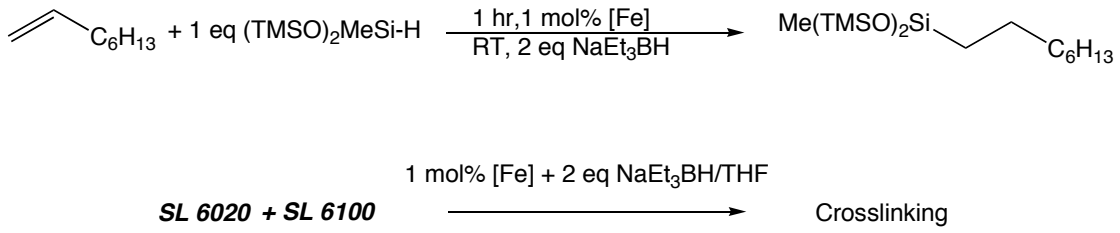

Figure 5.18 The hydrosilylation of substrates using an *in situ* generated catalyst.

The same pre-activation in THF proved necessary in the reaction of $H_2C{=}CHCH_2O(C_2H_4O)_{8.9}CH_3$ with **MD'M** and (^{Me}PDI)$FeCl_2$ as a pre-catalyst. The addition of the activated iron compound to the vigorously stirring solution of substrates, followed by heating at 60 ºC led to the complete hydrosilylation of the allyl polyether in an hour. As with the use of [(^{Et}PDI)FeN_2]$_2$(μ-N_2), there was no evidence of isomerized olefin or any products derived there-from.

The hydrosilylation of **TVCH** was performed with **MD'M** by stirring 1 mol % of (^{Me}PDI)$FeCl_2$, followed by the addition of two equivalents of $NaEt_3BH$. Again, the reaction was complete in less than five minutes, and there was no evidence for a reduction in selectivity of the hydrosilylation compared with [(^{Et}PDI)FeN_2]$_2$(μ-N_2).

One method of pre-activation investigated with PDI iron dihalides was the reduction of the compounds in an olefinic solution, with the hopes of generating the olefin bound complex to use as a catalyst. This method was used on the mono-isopropyl substituted PDI iron dihalide. Two equivalents of sodium was stirred with a catalytic amount of naphthalene and (^{1iPr}PDI)$FeCl_2$. When the sodium was completely dissolved, 1,1,2,2-tetramethyl-1,2-divinyldisiloxane (**M^{v}M^v)** was added to the reaction solution, which was then filtered through Celite and volatiles were removed, leaving a bright red solid residue. This residue, proposed as (^{1iPr}PDI)Fe(M^{v}M^v), was evaluated for catalytic hydrosilylation.

(^{1iPr}PDI)Fe(M^{v}M^v) was added to a stirring solution of 1-octene and **MD'M** at 290 K at an estimated 1 mol %, and stirred for an hour. Analysis of the reaction mixture at this time showed complete conversion to the desired hydrosilylated product. The use of the polymeric substrates SL-6100 and SL-6020 resulted in a gelation of the substrates at a rate indistinguishable from the isolated nitrogen compounds.

5.5 Selective Hydrosilylation of 1,2,4-Trivinylcyclohexane (TVCH) Using PDI Iron Complexes

The singly hydrosilylated product of 1,2,4-trivinylcyclohexane (**TVCH**) is an important bifunctional precursor in the manufacturing of environmentally friendly tires.[33] The current industrial catalyst used for the mono-hydrosilylation of **TVCH** is non-selective, such that an excess of olefin is used and a 3.5-hour slow addition of silane is used, and the percentage of mono-substituted product is only 51%, requiring additional purification.[32] Some reported catalysts overcome the lack of selectivity by hydrosilylating the 1- 2- and 4-vinyl groups three equivalents of Si-H.[34,35] The steric bulk of ^{R}PDIFe complexes may help increase the selectivity of the reaction, driving down the costs in synthesizing the singly hydrosilylated product.

Crude **TVCH** contains four identifiable isomers, two of which, A and B, were isolated pure. The third isomer, isomer C, was contaminated with ~ 10 % of the fourth isomer, isomer D. Isomer D was used as a 50:50 mixture with isomer C. The determination of the stereochemistry for each isomer was achieved using 1D and 2D NMR techniques. The isomers are shown in Figure 5.19. With the isolated isomers, three goals were set: 1) determine the relative rates of hydrosilylation for each isomer, 2) the selectivity of which vinyl group reacts fastest per isomer, 3) and preference for single versus double hydrosilylation.

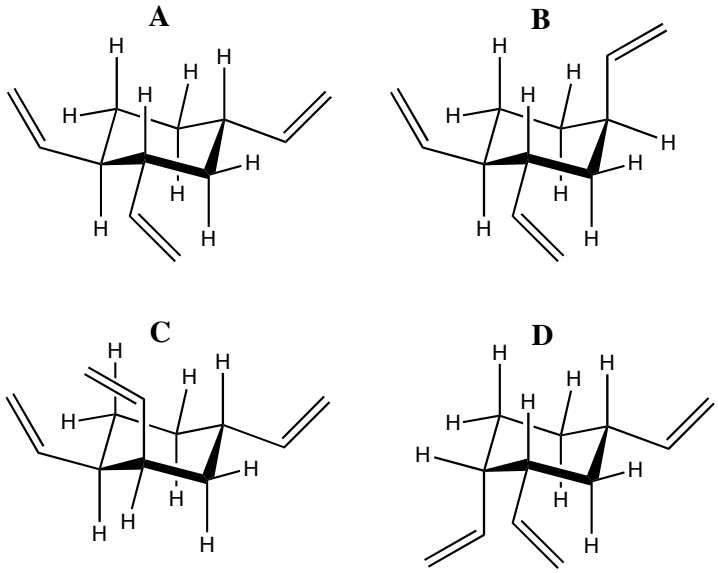

Figure 5.19 The four isomers of **TVCH** investigated.

The thermodynamically most stable isomer, A, was the majority isomer in the crude reaction mixture, and was therefore the first isomer investigated. Each vinyl group is equatorial, so there are no stereochemical (i.e. axial vs. equatorial) issues to consider. Two silanes were used in the investigation, **TES** and **MD'M**. The hydrosilylation of isomer A with **TES,** solvent free, using 0.5 mol% of $[(^{Et}PDI)FeN_2]_2(\mu\text{-}N_2)$ was complete in under 5 min, corresponding to a turnover frequency of at least 4000/hr. Analysis of the product showed 60% mono-hydrosilylation and 24% double hydrosilylation, the remainder being starting **TVCH**. Of the possibilities for the mono-hydrosilylation, one isomer was selectively formed 80% of the time. This result immediately showed promise for the selective catalysis of **TVCH**.

Altering some aspects of the catalytic reaction may increase the percentage of the single-addition product in the reaction mixture. Utilizing 0.8 equivalents of silane, diluting the reaction mixture to 1 M in toluene, and adding the silane dropwise over the course of 1 hour all led to increases in the amount of the desired product. The

increases in selectivity were much more prominent with **TES** as the Si-H source. The reaction was complete in an hour with a 0.5 mol% loading of catalyst and 1M substrate in toluene. Analysis of the mixture by GC showed 73% mono-hydrosilylation and 13% double hydrosilylation, the remainder being starting material. This distribution is similar to that of the catalysis with **MD'M**.

The same reaction was performed with **MD'M** under the same conditions. Again, the catalysis was complete in less than five minutes with a 0.5 mol% loading of catalyst. Analysis of the mixture showed 73% mono-hydrosilylation product and 23% double hydrosilylation product, the remainder being starting material. Of the single addition product, 92% was of a single isomer. The larger substituents on the silane appeared to increase the selectivity of the catalysis, both in terms of single vs double hydrosilylation, but also in terms of regioselectivity. The results of these studies are shown in Figure 5.20.

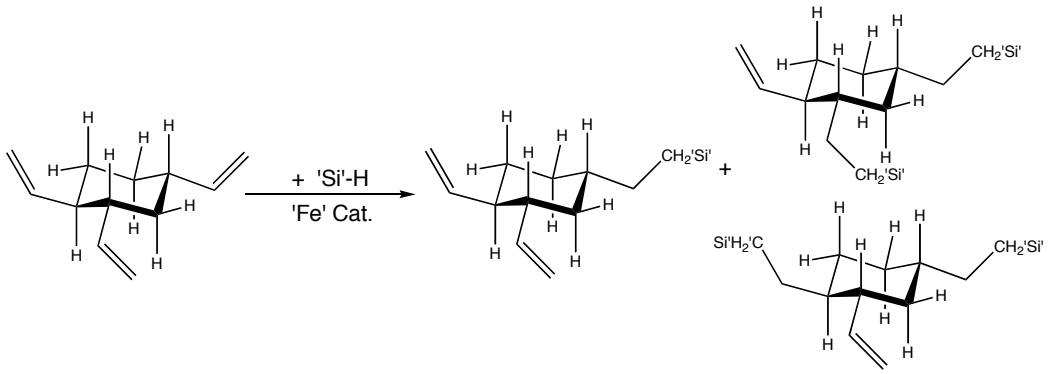

'Si'	%
OEt_3	57
$Me(OTMS)_2$	73

'Si'	%
OEt_3	24
$Me(OTMS)_2$	23

Figure 5.20 The results of hydrosilylation of isomer A with the catalyst **$[(^{Et}PDI)FeN_2]_2(\mu\text{-}N_2)$**.

The above reaction was carried out on a gram scale to attempt to purify the mono-hydrosilylated product and determine the regiochemistry of the product.

Distillation of the crude reaction mixture yielded a product that, by GC, was 90% pure in single addition product. A series of NMR experiments were performed, with the ^{1}H NMR spectrum presented in Figure 5.21, and the product was determined to arise from the hydrosilylation of the C^{4} vinyl group. Thus, the selectivity for vinyl preference, as well as the preference for single addition product, was determined in the hydrosilylation reaction of isomer A of **TVCH** with both **TES** and **MD'M**.

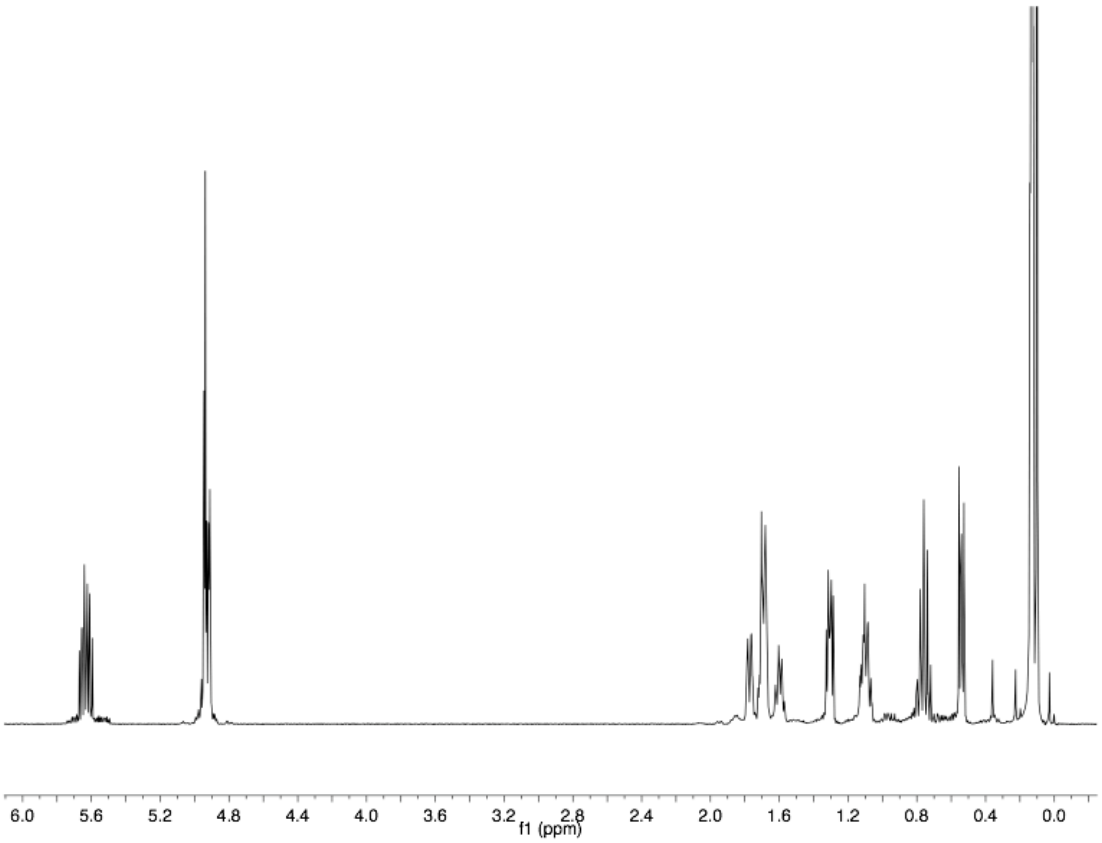

Figure 5.21 ^{1}H NMR spectrum of the hydrosilylation of isomer A with **MD'M**.

The stereochemistry of isomer B of **TVCH** was determined by a series of NMR experiments. The isomer was determined to have a C^{4} vinyl group, while the C^{1} and C^{2} vinyl groups remained equatorial. Isomer B is the second most abundant isomer in crude **TVCH**. The same two silanes were used in the investigation, **TES** and

MD'M. The hydrosilylation of isomer B with **TES,** solvent free, using 0.5 mol% of $[(^{Et}PDI)FeN_2]_2(\mu\text{-}N_2)$, again, was complete in under 5 min, corresponding to a turnover frequency of at least 4000/hr. Analysis of the product established 46% mono-hydrosilylation and 31% double hydrosilylation, the remainder being starting material. Analysis of the mono-hydrosilylation product demonstrates that one isomer was selectively formed over 90% of the time. The double addition products were identified in a near 1:1 ratio. This result immediately showed promise for the selective catalysis of **TVCH**.

The same catalysis was performed with **MD'M** under the same reaction conditions. Again, the catalysis with $[(^{Et}PDI)FeN_2]_2(\mu\text{-}N_2)$ was complete in less than five minutes with a 0.5 mol% loading of catalyst. Analysis of the mixture showed 55% mono-hydrosilylation and 36% double hydrosilylation, the remainder being starting material. Of the single addition product, as judged by NMR, there appeared to be two major products in a ration of 1:3, with the hydrosilylation at the C^4 vinyl the major product. The double addition products are in a near 1:1 ratio. Again, the bulkier silane appeared to increase the selectivity of the catalysis, but isomer B overall shows poorer selectivity. The results of the catalysis are shown in Figure 5.22.

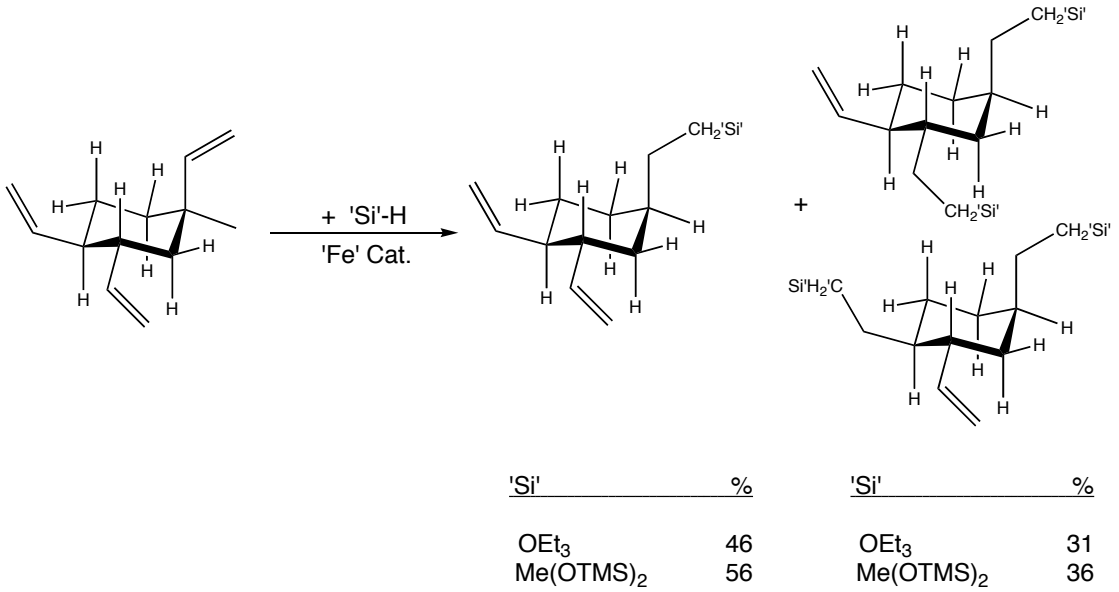

'Si'	%
OEt_3	46
$Me(OTMS)_2$	56

'Si'	%
OEt_3	31
$Me(OTMS)_2$	36

Figure 5.22 The results of hydrosilylation of isomer B with MD'M.

The investigation of isomer C was identical to that of A and B. The stereochemistry was assigned based on a NMR experiments, and the C^2 vinyl group was shown to be axial, while the C^1 and C^4 vinyl groups remain equatorial. The investigation into the reactivity was complicated by the contamination of isomer C with 13% isomer D. Additionally, the two isomers co-elute in gas chromatography. An equimolar mixture of C and D was hydrosilylated with **MD'M** and established that the two isomers had essentially the same reaction rate.

The same two silanes, **TES** and **MD'M,** were used in the investigation of isomer C. As was the case for isomers A and B, isomer C was less selective with the less sterically demanding **TES**. Analysis of the product revealed 56% mono-hydrosilylation and 28% double hydrosilylation, the remainder being starting material. This product distribution is similar to what was seen with isomers A and B with **TES**.

The hydrosilylation of isomer C with **MD'M,** performed solvent free using 0.5 mol% of $[(^{Et}PDI)FeN_2]_2(\mu\text{-}N_2)$, was complete in under 5 min, giving a turnover frequency of at least 4000/hr. Analysis of the product showed 56% mono-

hydrosilylation and 32% double hydrosilylation, the remainder being starting material. The mono-hydrosilylation product shows that two isomers were formed in similar quantities as the >90% majority of the single addition region. The double addition product, however, was >95% one of two possibilities. So although the single addition product makes roughly a 50/50 mixture, the double addition product makes one isomer selectively.

The regioselectivity of the single addition product was determined from a mixture of the two isomers formed. A series of NMR experiments indicated that for both isomers, the hydrosilylation occurred at equatorial vinylic positions, leaving the axial vinyl group in tact. This then carries to the double addition product, where the two hydrosilylations occur on the equatorial vinyl groups, again determined with NMR spectroscopy. A summary of isomer C's reactivity and product distribution from the catalysis is shown below in Figure 5.23.

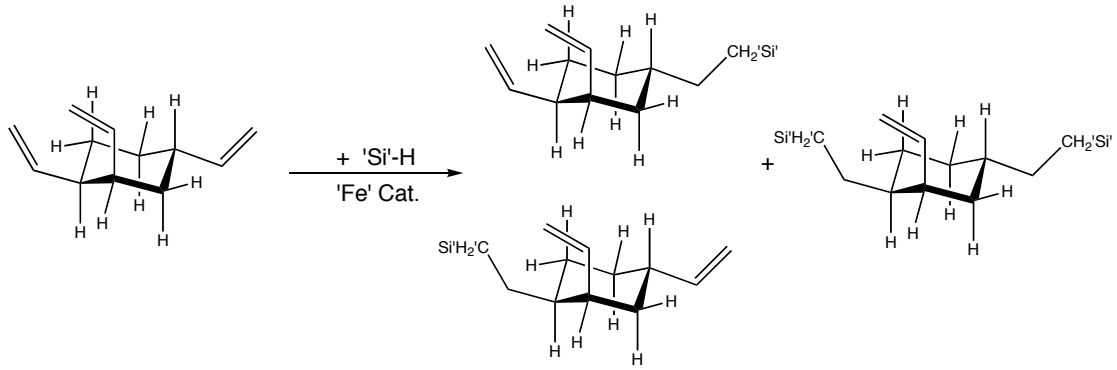

Figure 5.23 The results of hydrosilylation of isomer C with MD'M.

The exploration of isomer D was complicated it's contamination with an equivalent of isomer C, thus all spectroscopy and catalysis were complicated by isomer C and its products. The stereochemistry was determined by NMR

spectroscopoy to have an axial vinyl group on C^1, with the other two vinyl groups equatorial on C^2 and C^4. Much like isomer C, the mono hydrosilylation occurred at one of two vinyl positions nearly equally. The double hydrosilylation product using $[(^{Et}PDI)FeN_2]_2(\mu\text{-}N_2)$ was nearly exclusively one product, the product in which the two equatorial vinyl groups were hydrosilylated. This result is reminiscent of the products of C. This means, then, that the two single addition products are likely where one or the other equatorial groups are hydrosilylated. The product distribution for isomer D and **MD'M** are shown in Figure 5.24, although conversion numbers were not obtained due to high level of contamination by isomer C.

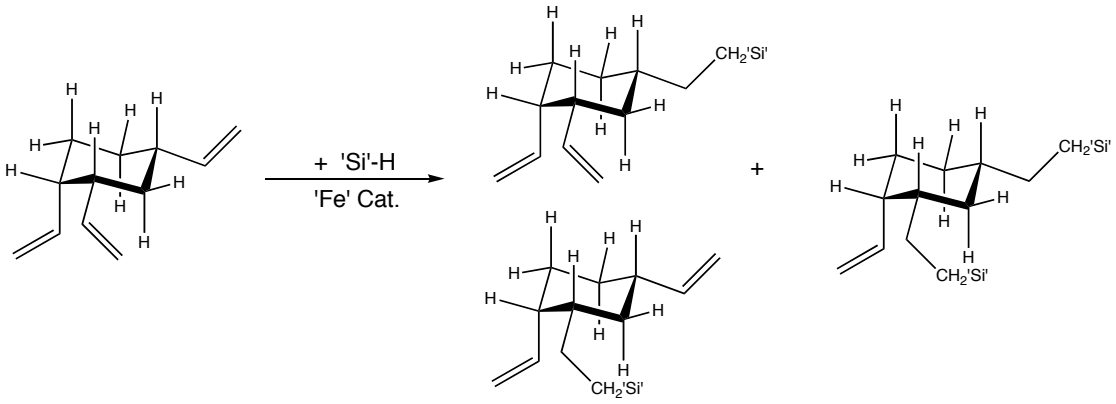

Figure 5.24 The results of hydrosilylation of isomer D with **MD'M.**

The relative reaction rates of A, B, and C were determined, as C and D exhibited similar rates of hydrosilylation. In order to compare the relative rates of A and B, a 47/53 mixture of the two isomers was treated with 0.5 equivalents of **MD'M** using 1 mol % $[(^{Et}PDI)FeN_2]_2(\mu\text{-}N_2)$ as a catalyst. The resultant mixture was analyzed by GC, which clearly separates the two starting materials. The remaining starting isomers were in a 65/35 ration of A to B, indicating clearly that A reacts slower than B in the catalysis. An equimolar mixture of a 1:1:1 mix of A, B, and C was set up with

0.5 equivalents of **MD'M**. Analysis of the reaction mixture yielded the relative rates of hydrosilylation of the isomers, from fastest to slowest, as C~D>B>A.

The investigation into the hydrosilylation of **TVCH** with either **MD'M** or **TES** was very encouraging. The relative rates of reactivity among the four isomers were determined. The product distributions and the preference for axial vs equatorial vinyl group hydrosilylation, as well as the preference for single vs double hydrosilylation, were determined spectroscopically. Most importantly, though, was finding reaction conditions in which the majority of the reaction mixture was the desired single addition hydrosilylation product. This selectivity provides a clear advantage over the current platinum based systems.

5.8 Quinoline, PDI derivatives, Pybox, and Other N,N,N Terdentate Ligand Supported Iron Catalysis

Terpyridine and bis(imino)pyridine complexes were the most successful and the most studied supporting ligands for this iron-based hydrosilylation catalysis. However, many iron complexes bearing a varity of N,N,N terdentate supporting ligands were synthesized that exhibited minimal catalytic activity. This section discusses these alternative complexes and the catalytic activity they displayed.

Many derivatives of bis(imino)pyridine complexes were utilized as catalysts in these hydrosilylation reactions. The most successful of these complexes were mixed PDI ligands, where one imine was 2,6-diisopropylaryl based and the other imine was formed from an alkyl (aliphatic carbon bound) amine. This previously reported class of compounds[36] was successful in the preliminarily screened catalysis. The two complexes are shown in Figure 5.25.

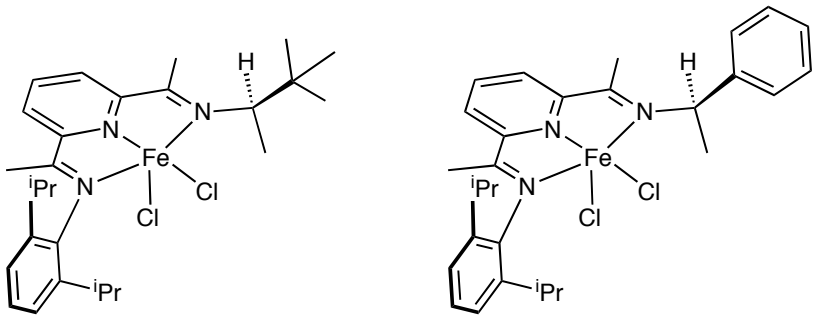

Figure 5.25 Mixed PDI iron compounds used as precatalysts**.**

The *in situ* catalysis performed using the α-methylbenzylamine derived mixed PDI was more effective in the catalysis. The hydrosilylation of 1-octene with **MD'M** was completed after 1 hour at 1 mol % of iron compound and 2 equivalents of $NaEt_3BH$. Utilizing the 2-amino-3,3-dimethylbutane derived complex, with identical reaction conditions, yielded only 40 % of the desired hydrosilylation product. The ^{t}butyl group is most likely prohibitively large to allow the iron to perform the catalysis effectively. The crosslinking of SL-6100 and SL-6020 was readily accomplished with α-methylbenzylamine derived complex, whereas the 2-amino-3,3-dimethylbutane derived complex did not effectively crosslink these polymers. The success of the mixed PDI ligands in the hydrosilylation allows one more area of investigation into the hydrosilylation activity of modular PDI supported iron catalyis.

Changing the backbone methyl groups of bis(imino)pyridine ligands is another way of tuning the sterics and electronics of the ligand framework. Recently, formally Fe(0) derivatives of the aldimine variant of bis(imino)pyridine (^{iPr}PDAI) were reported.[37] The butadiene complex (^{iPr}PDAI)Fe(C_4H_6), was synthesized and hydrosilylation activity was explored. Interestingly, the compound proved effective for the hydrosilylation of terminal olefins although the complex contained the sterically demanding 2,6-diisopropyl groups.

The hydrosilylation of **MD'M** and 1-octene was performed with 1.0 mol% (^{iPr}PDAI)Fe(C_4H_6). Conversions to the desired product at room temperature after an hour were low, but the catalysis was complete after 12 hours. When the catalysis was performed at 60 ºC, the catalysis was approximately 90% complete after an hour, with no indication of isomerized product. The results obtained with (^{iPr}PDAI)Fe(C_4H_6) are summarized in Figure 5.26.

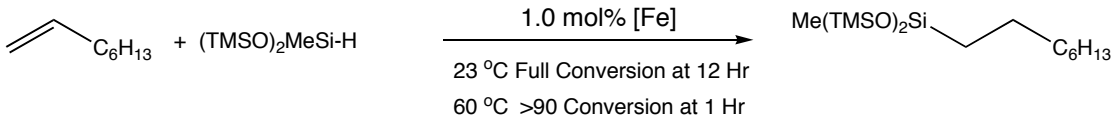

Figure 5.26 Hydrosilylation of 1-octene and **MD'M** using **(^{iPr}PDAI)Fe(C_4H_6)** as a catalyst.

The crosslinking of Sl-6100 and SL-6020 yielded a product similar in properties to the platinum catalyzed reaction. The slow rate of hydrosilylation with (^{iPr}PDAI)Fe(C_4H_6) allowed for the investigation of temperature effects in the crosslinking reaction. At room temperature, with 1.0 mol% (^{iPr}PDAI)Fe(C_4H_6), the polymer solution gelled after 2 hours, gradually thickening over the course of the reaction. When performed at 60 ºC, the reaction mixture gelled at roughly 15 minutes, again, gradually thickening over that time period. When the reaction was brought to 140 ºC, the gellation occurred nearly instantaneously. This curing behavior, summarized in Figure 5.27, was used to premix the catalyst and substrates and gellation was initiated upon the heating of the reaction mixture to 140 ºC, which is preferred to the instantaneous gellation observed when [(^{Et}PDI)FeN_2]$_2$(μ-N_2) is used as a catalyst.

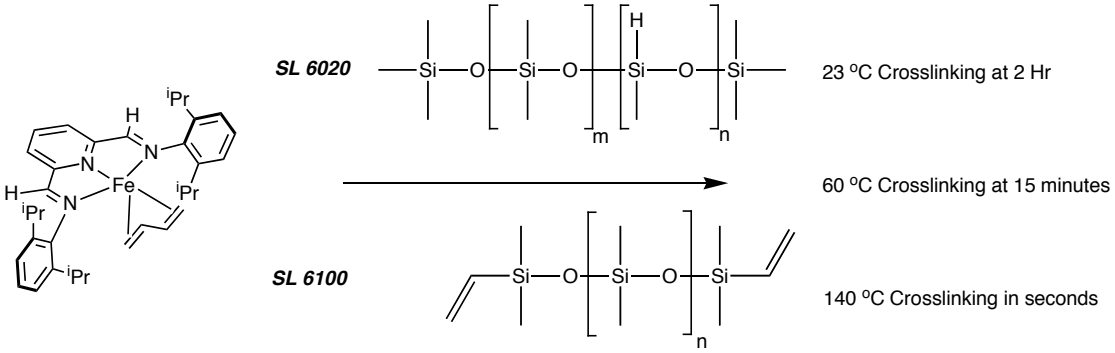

Figure 5.27 Crosslinking of polymeric substrates with (^{iPr}PDAI)Fe(C_4H_6).

A number of other complexes were attempted as hydrosilylation catalysts, including other bis(imino)pyridine derivatives and Pybox complexes. The results of these attempts, using the *in situ* catalysis generation method with 1-octene and **MD'M** are presented in Figure 5.28. These results show that not all N,N,N terdentate ligands are appropriate for this catalysis.

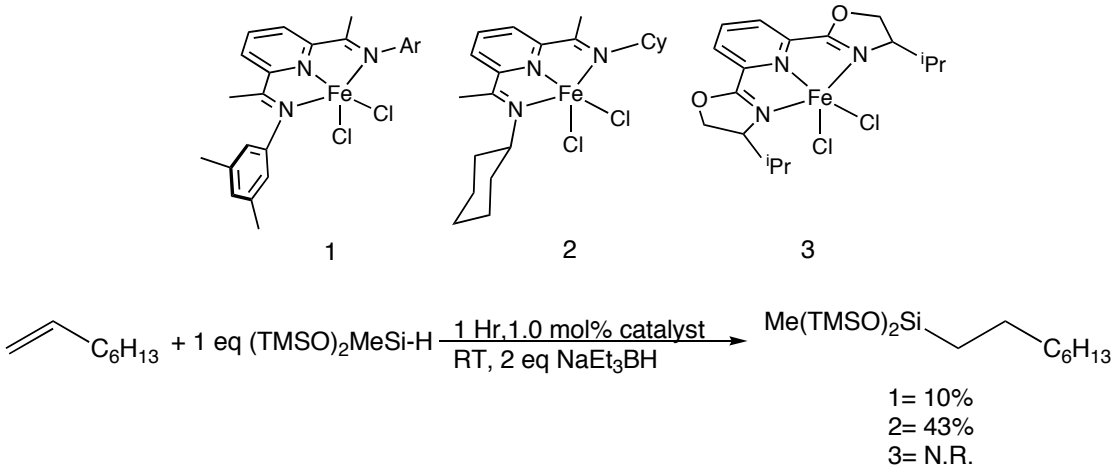

Figure 5.28 *In situ* activation of poorly performing iron complexes.

A quinoline based diimine iron dihalide complex was recently reported. The compound, (^{Me}Quiniline)$FeBr_2$ displayed an increased ethylene polymerization activity, as well as increased thermal stability.[38] (^{Me}Quiniline)$FeBr_2$ was synthesized

according to the published procedure, and the model catalytic reaction of **MD'M** and 1-octene was attempted with the *in situ* activation method. The addition of 2 equivalents of $NaEt_3BH$ to a stirring solution of 1 mol% of (^{Me}Quiniline)$FeBr_2$ in 1-octene and **MD'M** resulted in an immediate color change. After stirring for one hour, the reaction was quenched and analyzed by GC. Analysis showed that there was a 70% conversion to the desired hydrosilylated product, the remainder of the mixture identified as starting material. A summary of the (^{Me}Quiniline)$FeBr_2$ reactivity is shown in Figure 5.29.

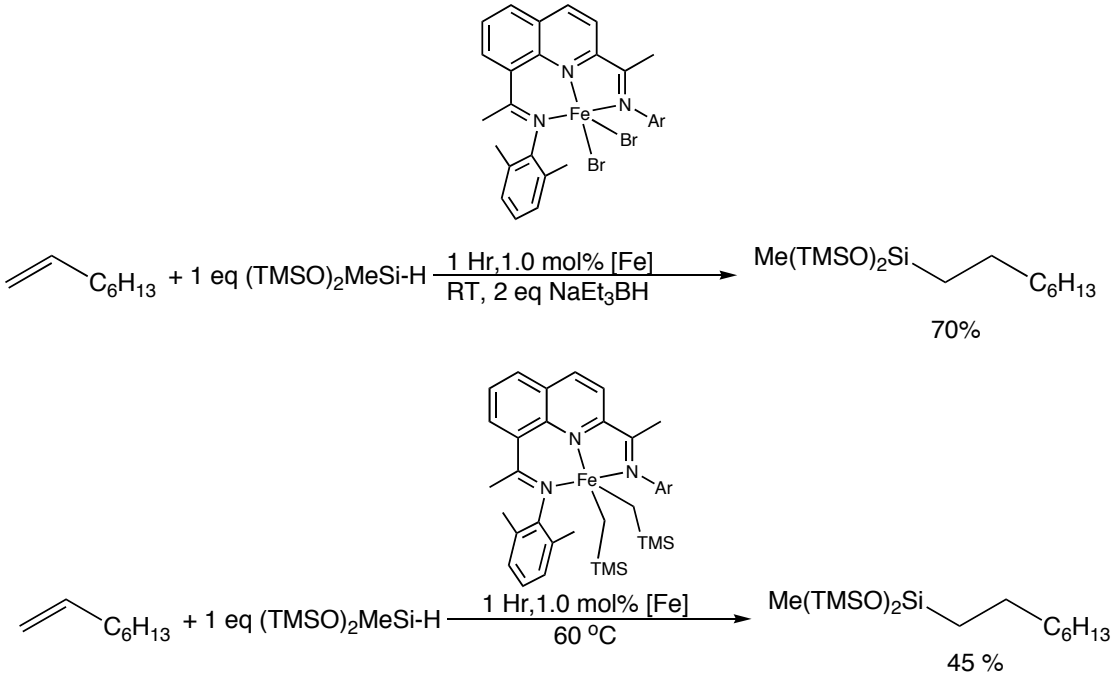

Figure 5.29 Quinoline based catalysis of 1-octene and MD'M **.**

Another potential source of catalytically active N,N,N chelate iron species is the corresponding dialkyl complexes. To this end, the bis-neosilyl complex was synthesized from (^{Me}Quiniline)$FeBr_2$. The resultant dark burgundy complex, (^{Me}Quiniline)FeR_2, was added to a mixture of 1-octene and **MD'M**, and warmed to 60

ºC and reacted for one hour. Analysis by GC indicated a 45% conversion to the desired hydrosilylation product.

The use of (^{Me}Quiniline)$FeBr_2$ or (^{Me}Quiniline)FeR_2 with the polymeric SL-6100 and SL-6020 substrates was unsuccessful. The activation of (^{Me}Quiniline)$FeBr_2$ in THF with two equivalents of $NaEt_3BH$ added to the stirring polymer mixtures did not result in crosslinking or gelation of the polymers, even upon heating. The same holds true for the attempted catalysis with (^{Me}Quiniline)FeR_2. There was no crosslinking of the polymers after heating 1 mol%of the iron compound to 60 ºC. This lack of crosslinking activity, along with the incomplete hydrosilylation of 1-octene, showed there was no benefit of the use of (^{Me}Quiniline)$FeBr_2$ over the bis(imino)pyridine compounds.

5.7 Conclusions.

The hydrosilylation of terminal olefins with tertiary silanes was affected by a number of N,N,N terdentate supported iron complexes. The investigations using (terpy)FeR_2 were successful with a variety of functionalized and unfunctionalized olefins using **MD'M** or triethylsilane as the silicon hydride source. The catalysis of **VCHO** with **MD'M** was only successful with the use of (terpy)FeR_2. The utilization of catalysts of the type [(^{R}PDI)FeN_2]$_2$(μ-N_2) proved to be the most successful for a number of hydrosilylations. The catalytic hydrosilylation without isomerization of the olefin of allyl polyethers gives a large advantage over current platinum based systems. Also, the selective mono-hydrosilylation of trivinylcyclohexane using either **MD'M** or **TES** under dilute conditions is advantageous to current systems that give statistical mixtures of products. The hydrosilylation catalysis presented shows that base-metal catalyzed reactions can offer advantages over noble metal catalysts in terms of selectivity for a number of reactions.

5.8 Experimental Procedures

General Considerations. All air- and moisture-sensitive manipulations were carried out using standard vacuum line, Schlenk, and cannula techniques or in an MBraun inert atmosphere dry box containing an atmosphere of purified nitrogen. Solvents for air- and moisture-sensitive manipulations were initially dried and deoxygenated using literature procedures.[39] Benzene-d_6 was purchased from Cambridge Isotope Laboratories and dried over 4 Å molecular sieves. Dichloromethane-d2 was purchased from Cambridge Isotope Laboratories. The complexes $[(^{Me}PDI)FeN_2]_2(\mu\text{-}N_2)$,[25] $[(^{Et}PDI)FeN_2]_2(\mu\text{-}N_2)$,[25] $[(^{Me,iPr}PDI)FeN_2]_2(\mu\text{-}N_2)$,[25] $(^{iPr}PDI)Fe(N_2)_2$,[17] $(^{iPr}PDAI)Fe(C_4H_6)$,[27] $(^{Me}Quiniline)FeCl_2$,[28] $(terpy)FeCl_2$,[40] and $(^{iPr}Pybox)FeCl_2$[41] were prepared according to literature procedure. **MD'M, M'M', TES,** Triethylsilane, **TVCH**, 1-octene, and 1-Hexene were dried and distilled from lithium aluminum hydride before use. Allylamine was dried on calcium hydride and distilled under reduced pressure before use. Allyl polyethers were dried under vacuum for 12 hours before use. Vinycyclohexeneoxide was passed through dry, neutral alumina before use.

^1H NMR spectra were recorded on Varian Mercury 300, Inova 400, 500, and 600 spectrometers operating at 299.76, 399.78, 500.62, and 599.78 MHz, respectively. ^{13}C NMR spectra were recorded on an Inova 500 spectrometer operating at 125.893 MHz. All ^1H and ^{13}C NMR chemical shifts are reported relative to $SiMe_4$ using the ^1H (residual) and ^{13}C chemical shifts of the solvent as a secondary standard. For diamagnetic complexes, many assignments were made based on COSY and HSQC NMR experiments. Solution magnetic moments were determined by Evans method[42] using a ferrocene standard and are the average value of at least two independent measurements. Magnetic susceptibility balance measurements were performed with a Johnson Matthey instrument that was calibrated with $HgCo(SCN)_4$. Peak widths at

half heights are reported for paramagnetically broadened and shifted resonances. Infrared spectra were collected on a Thermo Nicolet spectrometer. Elemental analyses were performed at Robertson Microlit Laboratories, Inc., in Madison, NJ.

Single crystals suitable for X-ray diffraction were coated with polyisobutylene oil in a drybox, transferred to a nylon loop and then quickly transferred to the goniometer head of a Bruker X8 APEX2 diffractometer equipped with a molybdenum X-ray tube (l = 0.71073 Å). Preliminary data revealed the crystal system. A hemisphere routine was used for data collection and determination of lattice constants. The space group was identified and the data were processed using the Bruker SAINT+ program and corrected for absorption using SADABS. The structures were solved using direct methods (SHELXS) completed by subsequent Fourier synthesis and refined by full-matrix least-squares procedures.

Mössbauer data were collected on an alternating constant-acceleration spectrometer. The minimum experimental line width was 0.24 mm s^{-1} (full width at half height). A constant sample temperature was maintained with an Oxford Instruments Variox or an Oxford Instruments Mössbauer-Spectromag 2000 cryostat. Reported isomer shifts (δ) are referenced to iron metal at 293 K.

Preparation of (terpy)Fe(CH_2SiMe_3)$_2$. A round bottomed flask was charged with 0.360 g (1.0 mmol) of (terpy)$FeCl_2$ and added approximately 10 mL of diethyl ether. The flask was chilled to -35 ºC and a solution containing 0.188 g (2.0 mmol) of $LiCH_2SiMe_3$ and approximately 10 mL of diethyl ether were added. A color change was observed immediately upon addition of the solution and the resulting slurry was stirred and warmed to ambient temperature. After one hour, the reaction mixture was filtered through Celite and the volatiles were removed in vacuo. The resulting purple solid was washed with approximately 5 mL of cold pentane yielding 0.400 g (87 %)

(terpy)FeR_2. Analysis for $C_{23}H_{33}FeN_3Si_2$: Calcd : C, 59.59, H, 7.18, N, 9.06, Found : C, 59.19, H, 6.81, N, 9.10; Magnetic Susceptibility (MSB, 23 ºC): $\mu_{eff} = 4.6\ \mu_B$.^{1}H NMR (benzene-d_6, 20 °C): δ =319.80 (bs, 1H), 194.68 (bs, 2H), 154.65 (bs, 2H), 115.20 (bs, 2H), 59.36 (bs, 2H), 38.56 (bs, 2H), 8.73 (bs, 18H).

Hydrosilylation of 1-octene with Methylbis(trimethylsilyloxy)silane (MD'M) using (terpy)FeR_2.

To a scintillation vial was added 0.150 g (1.33 mmol) of 1-octene and 0.295 g (1.33 mmol) of MD^HM. To this stirring solution was added 0.015 g (2.5 mol%) (terpy)FeR_2. The reaction was sealed and moved to an oil bath, typically held at 60 ^oC for the desired amount of time, typically 1 hour. A resonance upfield at 0.41 ppm was indicative of formation of the desired, previously characterized product. Gas chromatography was performed on a Shimadzu GC- 2010 gas chromatograph. GC analyses were performed using a Supelco 30 m x 0.25 mm BETA DEX 120 capillary column. Temperature program for the reaction of MD'M and 1-octene is as follows: 80 ^oC, 2 min.; 15 ^oC /min to 180 ^oC, 2 min. The retention time of the hydrosilylated product is 7.83 minutes.

Hydrosilylation of Vinylcyclohexene Oxide (VCHO) with MD'M using (terpy)FeR_2.

To a scintillation vial was added 0.150 g (1.33 mmol) of VCHO and 0.295 g (1.33 mmol) of MD^HM. To this stirring solution was added 0.015 g (2.5 mol%) Bis[(trimethylsilyl)methyl]iron(II)terpyridine. The reaction was sealed and run at the desired temperature for the desired amount of time, typically 1 hour. A resonance

upfield at 0.37 ppm was indicative of formation of the desired product, as well as the disappearance of Si-H and olefinic resonances.

(2-(7-oxa-bicyclo[4.1.0]heptan-3-yl)ethyl)bis(trimethylsiloxy)methylsilane (*Cis* and *Trans*). ^{1}H NMR ($CDCl_3$, 22 ºC): 3.16-3.05 (m, 4H), 2.14 (t, 2H, 14.3 Hz), 2.07-1.90 (m, 2H), 1.84-1.72 (m, 1H), 1.72-1.60 (m, 1H), 1.59-1.41 (m, 3H), 1.40-1.20 (m, 5H), 1.19-0.94 (m, 6H), 0.45-0.30 (m, 4H), 0.09 (s, 36H), -0.01 (s, 6H)

Cross linking reaction of $M^{vi}D_{120}M^{vi}$ (SL 6100) and $MD_{15}D'_{30}M$ (SL 6020) with (terpy)FeR_2.

To a scintillation vial in a nitrogen filled drybox was added 3 mg (0.0065 mmol) (terpy)FeR_2. 400 mg of a vinyl end-stopped siloxane polymer of the structure $M^{vi}D_xM^{vi}$ (commercially available from Momentive Preformance Materials Inc. as SL 6100) was then added, followed by 18 mg of a hydride-functional siloxane polymer of the structure $MD_xD^H_yM$ (commercially available from Momentive Performance Materials Inc. as SL 6020). The vial was sealed with a small amount of Krytox grease, electrical tape, removed from the dry box and placed in a 95 ºC oil bath for 12 hours. The reaction was cooled in air and yielded a highly viscous semi-solid. This reaction is 0.7% by mass iron compound and 0.0009% iron by mass.

Hydrosilylation of 1-octene using bis(imino)pyridine iron dinitrogen complexes.

In a nitrogen filled drybox, to a scintillation vial was added 0.100 g (0.891 mmol) of 1-octene and (0.891 mmol) of the desired silane (0.198 g of MD'M, 0.146 g of triethoxy silane, or 0.104 g of triethyl silane). To the stirring substrates was added 0.002 g (0.5 mol % cat) [($^{2,6\text{-Me}}$PDI)Fe(N_2)]$_2$[μ-(N_2)] or [($^{2,6\text{-Et}}$PDI)Fe(N_2)]$_2$[μ-(N_2)] to the stirring solution. The reaction was allowed to proceed for the desired amount of

time and was quenched by opening the reaction vessel to air. The reaction was analyzed by GC or ^{1}H NMR spectroscopy. Gas chromatography was performed on a Shimadzu GC- 2010 gas chromatograph. GC analyses were performed using a Supelco 30 m x 0.25 mm BETA DEX 120 capillary column. Temperature program for the reaction of $MD^{H}M$ and 1-octene was as follows: 80 ^{o}C, 2 min.; 15 ^{o}C /min to 180 ^{o}C, 2 min. The retention time of the hydrosilylated product was 7.83 minutes.

Triethyloctylsilane. ^{1}H NMR (C_6D_6, 22 ºC): 1.39-1.28 (m, 12H), 0.99 (t, 9H, J = 7.9 Hz), 0.93 (t, 3H, 8.6 Hz), 0.97(t, 9H, 8 Hz), 0.59-0.51 (m, 8H). ^{13}C NMR : 34.83, 32.79, 30.21, 30.19, 24.73, 23.53, 14.77, 12.08, 8.16, 4.08.

Tri(ethoxy)octylsilane. ^{1}H NMR (C_6D_6, 22 ºC): 3.82 (dd, 6H, 7.0 Hz, 13.9 Hz) 1.66-1.56 (m, 2H), 1.42-1.22 (m, 10H), 1.19 (t, 9H, 7.0 Hz, 13.9 Hz), 0.97(t, 9H, 8 Hz), 0.89 (t, 3H, 6.6 Hz), 0.76 (m, 2H). ^{13}C NMR : 58.79, 34.00, 32.69, 30.13, 30.08, 23.83, 23.45, 19.00, 14.73, 11.52.

Bis(trimethylsiloxy)methyloctylsilane. ^{1}H NMR (C_6D_6, 22 ºC): 1.48 (dt, 2H, 10.5 Hz, 20.3 Hz) 1.45-1.21 (m, 10H), 0.92 (t, 3H, 6.9 Hz), 1.19 (t, 9H, 7.0 Hz, 13.9 Hz), 0.97(t, 9H, 8 Hz), 0.89 (t, 3H, 6.6 Hz), 0.63 (m, 2H), 0.19 (s, 18H), 0.16 (s, 3H). ^{13}C NMR : 34.11, 32.71, 30.20, 30.12, 24.03, 23.49, 18.49, 14.75, 2.40, 0.42.

Hydrosilylation of N,N-Dimethylallylamine using bis(imino)pyridine iron dinitrogen complexes.

In a nitrogen filled drybox, a scintillation vial was charged with 0.100 g (1.174 mmol) of N,N-Dimethylallylamine and (1.174 mmol) of the desired silane (0.261 g of MD'M, 0.193 g of triethoxy silane, or 0.136 g of triethyl silane). To the stirring

substrates was added 0.003 g (0.5 mol % cat) [($^{2,6\text{-Me}}$PDI)Fe(N_2)]$_2$[μ-(N_2)] or [($^{2,6\text{-Et}}$PDI)Fe(N_2)]$_2$[μ-(N_2)] to the stirring solution. The reaction was allowed to proceed for 15 minutes and was quenched by opening the reaction vessel to air. The reaction was analyzed by ^{1}H NMR spectroscopy.

***N*,*N*-dimethyl-3-(triethylsilyl)propan-1-amine**. ^{1}H NMR (C_6D_6, 22 ºC): 2.21 (t, 2H, J = 7.2 Hz), 2.14 (s, 6H), 1.49 (dt, 2H, 7.2 Hz 19Hz), 0.97(t, 9H, 8 Hz), 0.58 (m, 2H), 0.52 (q, 6H, 8 Hz). ^{13}C NMR : 64.07, 45.99, 22.92, 9.37, 8.13, 4.05.

***N*,*N*-dimethyl-3-(triethoxylsilyl)propan-1-amine**. ^{1}H NMR (C_6D_6, 22 ºC): 3.80 (q, 6H, J = 7.0 Hz), 2.22 (m, 2H), 2.11 (s, 6H), 1.75(dt, 2H, 7.4 Hz, 14.5 Hz), 1.17 (t, 9H, 7H), 0.79 (m, 2H). ^{13}C NMR : 63.15, 58.79, 45.90, 22.00, 18.98, 8.73.

***N*,*N*-dimethyl-3-(bis(trimethylsiloxy)methylsilyl)propan-1-amine**. ^{1}H NMR (C_6D_6, 22 ºC) : 2.23 (t, 2H, J = 7.4 Hz), 2.14 (s, 6H), 1.64 (dt, 2H, 7.7 Hz 15.0Hz), 0.58 (m, 2H), 0.17 (s, 18H), 0.14 (s, 3H). ^{13}C NMR : 63.50, 45.97, 15.80, 9.37, 2.38, 0.37.

Crosslinking of $M^{vi}D_{120}M^{vi}$ (SL 6100) and $MD_{15}D'_{30}M$ (SL 6020).

In an inert atmosphere, to a scintillation vial was added 1.0 g of $M^{vi}D_{120}M^{vi}$, in which M^{vi} is vinyl dimethyl $SiO_{2/2}$, and 44 mg of $MD_{15}D^{H}_{30}M$. Another vial was prepared containing a stock solution of 2 mg of [($^{2,6\text{-Me2}}$PDI)Fe(N_2)]$_2$[μ-(N_2)] dissolved in 200 mg of ether. The catalyst solution was added at once to a stirring solution of 1 gram of 1.0 g of $M^{vi}D_{120}M^{vi}$ and 44 mg of $MD_{15}D^{H}_{30}M$. Almost immediately the solution gelled and became a solid. This gellation was indistinguishable from that observed for the reaction that uses the same silyl hydride and the unsaturated compound but employing a conventional platinum catalyst.

Procedure for the Hydrosilylation of Methyl Capped Allyl Polyether having nominal structure $H_2C=CHCH_2O(C_2H_4O)_8CH_3$ with Methylbis(trimethylsilyloxy)silane (MD^HM)

In a nitrogen filled drybox, a scintillation vial was charged with 1.00 g of methyl capped allyl polyether having nominal structure $H_2C=CHCH_2O(C_2H_4O)_8CH_3$ (2.09 mmol) and 0.465 g (2.09 mmol) of MD^HM, in which $M = (CH_3)_3SiO_{½}$ and $D^H = CH_3SiHO$. To the stirring solution of polyether and silane was added 10 mg (0.01 mmol) of $[(^{2,6Me}PDI)Fe(N_2)][\mu\text{-}(N_2)]$. The scintillation vial was sealed and removed from the drybox and placed in a 60 °C oil bath. The reaction was stirred for 1 hour, at which time the vial was removed from the oil bath and the reaction was quenched by the addition of moist ether. The solution was analyzed by ^1H NMR spectroscopy. The spectra established that the starting material methyl capped allyl polyether resonances were absent and resonances for the hydrosilylated product were present. There was no indication of propenyl resonances formed in the reaction within the detection limits of ^1H NMR spectroscopy. The resonance associated with the Si-H in the ^1H NMR was observed to disappear during the course of the reaction, and a new resonance upfield at 0.41 ppm assignable to methylene attached to silicon appeared, indicating the formation of the desired hydrosilylated product.

General Procedures for Hydrosilylation of 1-octene with Methylbis(trimethylsilyloxy)silane (MD'M) with $NaEt_3BH$ as an activator.

In an inert atmosphere, to a scintillation vial was added 0.100 g (0.89 mmol) of 1-octene and 0.192 g (0.86 mmol, 0.97 eq to olefin) of MD^HM, followed by 0.01 mmol of (N,N,N-Chelate) iron dichloride (or dibromide) (1 mol% to silane). A stir bar was added and a blue slurry was formed, and with stirring 0.02 g (0.02mmol, 2.22 eq.) of a

1M $NaEt_3BH$ solution in toluene was added. The reaction was stirred for the desired amount of time and the reaction was quenched in air and analyzed by GC.

NMR Data for the Isomers of TVCH.

Isomer A : ^{1}H NMR : 5.71(m, 1H), 5.65(m, 1H), 5.64(m, 1H), 4.97(m, 1H), 4.96(m, 1H), 4.95(m, 1H), 1.84(m, 1H), 1.77(m, 1H), 1.75(m, 1H), 1.69(m, 1H), 1.66(m, 1H), 1.58(m, 1H), 1.09(m, 1H), 0.99(m, 1H), 0.95(m, 1H).
^{13}C NMR : 144.51, 143.60, 143.48, 114.15, 114.14, 112.65, 47.25, 47.15, 41.66, 39.10, 32.85, 32.26

Isomer B : ^{1}H NMR : 5.84(m, 1H), 5.72(m, 1H), 5.69(m, 1H), 4.97(m, 1H), 4.96(m, 1H), 4.95(m, 1H), 2.34(m, 1H), 2.09(m, 1H), 1.77(m, 1H), 1.72(m, 1H), 1.59(m, 1H), 1.58(m, 1H), 1.09(m, 1H), 0.99(m, 1H), 0.95(m, 1H).
^{13}C NMR : 144.51, 143.60, 143.48, 114.15, 114.14, 112.65, 47.25, 47.15, 41.66, 39.10, 32.85, 32.26

Isomer C : ^{1}H NMR : 5.91(m, 1H), 5.77(m, 1H), 5.71(m, 1H), 5.03(m, 1H), 4.97(m, 1H), 4.96(m, 1H), 2.38(m, 1H), 2.15(m, 1H), 2.02(m, 1H), 1.79(m, 1H), 1.70(m, 1H), 1.51(m, 1H), 1.33(m, 1H), 1.30(m, 1H), 1.05(m, 1H).
^{13}C NMR : 144.77, 143.20, 138.93, 116.26, 113.71, 112.76, 44.68, 43.54, 38.39, 36.25, 32.38, 26.90

Isomer D : ^{1}H NMR : 5.88(m, 1H), 5.74(m, 1H), 5.73(m, 1H), 5.02(m, 1H), 4.98(m, 1H), 4.97(m, 1H), 2.31(m, 1H), 2.09(m, 1H), 1.89(m, 1H), 1.72(m, 1H), 1.58(m, 1H), 1.45(m, 1H), 1.43(m, 1H), 1.26(m, 1H), 1.19(m, 1H).

^{13}C NMR : 144.62, 143.36, 138.33, 116.34, 113.54, 112.61, 44.86, 43.09, 42.21, 33.17, 32.21, 27.30

Isolation of Majority Hydrosilylation product of 1,2,4-Trivinylcyclohexane (isomer 'A') with Methylbis(trimethylsilyloxy)silane (MD'M).

In an inert atmosphere, a scintillation vial was charged with 0.150 g (6.16 mmol) of 1,2,4-trivinylcyclohexane and 0.002 g (0.002 mmol) of [($^{2,6\text{-Et2}}$PDI)Fe(N_2)]$_2$[μ-(N_2)] (0.5 mol% to silane). To the stirring solution was added 1.370 g (6.16 mmol) of MD'M dropwise over the course of 10 minutes. The reaction was stirred for 20 minutes and the reaction was quenched in air and analyzed by GC, showing the majority product was 75% singly hydrosilylated product, 90% of which was one regioisomer. The crude product was distilled, yielding a >90% purity single hydrosilylation product of 90% single regioisomer. This isomer was determined to be the C_4-vinyl hydrosilylated product. ^{1}H NMR : δ = 5.65-5.74 (m, 2H, $C_1HC\underline{H}CH_2$ and $C_2HC\underline{H}CH_2$), 4.95-5.04 (m, 2H, $C_1HCHC\underline{H_2}$ and $C_2HCHC\underline{H_2}$), 1.84 (ddd, 1H, J= 13 Hz, 3 Hz, 2 Hz , $C_3H_{ax}\underline{H_{eq}}$), 1.72-1.79 (m, 2H, $C_5H_{ax}\underline{H_{eq}}$ and $C_6H_{ax}\underline{H_{eq}}$), 1.65 (m, 1H, $C_1\underline{H}CHCH_2$), 1.37 (m, 2H, $C_4HC\underline{H_2}CH_2Si$), 1.11-1.21 (m, 2H, $C_4\underline{H_{ax}}$ and $C_6\underline{H_{ax}}H_{eq}$), 0.76-0.88 (m, 2H, $C_3\underline{H_{ax}}H_{eq}$ and $C_5\underline{H_{ax}}H_{eq}$), 0.60 (m, 2H, $C_4HCH_2\underline{CH_2}Si$), 0.19 (s, 18H, $Si\underline{Me_3}$), 0.16 (s, 3H, $Si\underline{Me}$). ^{13}C : 143.89, 143.85, 114.04, 113.93, 47.81, 47.76, 40.36, 39.82, 33.31, 32.77, 31.34, 15.44, 2.43, 0.32.

Hydrosilylation of 1,2,4-Trivinylcyclohexane with Triethoxysilane (TES).

In an inert atmosphere, a scintillation vial was charged with 0.150 g (0.92 mmol) of 1,2,4-trivinylcyclohexane and 0.150 g (0.92 mmol, 0.99 eq.) of TES. To the stirring solution was added 0.002 g (0.002 mmol) of [($^{2,6\text{-Et2}}$PDI)Fe(N_2)]$_2$[μ-(N_2)] (0.5 mol% to

silane). The reaction was stirred for typically 60 minutes and the reaction was quenched in air and analyzed by GC and GC/MS.

Hydrosilylation of 1,2,4-Trivinylcyclohexane with Methylbis(trimethylsilyloxy)silane (MD'M).

In an inert atmosphere, a scintillation vial was charged with 0.150 g (0.92 mmol) of 1,2,4-trivinylcyclohexane and 0.205 g (0.92 mmol) of MD'M. To the stirring solution was added 0.002 g (0.002 mmol) of $[(^{2,6\text{-}Et2}PDI)Fe(N_2)]_2[\mu\text{-}(N_2)]$ (0.5 mol% to silane). The reaction was stirred for the desired amount of time and the reaction was quenched in air and analyzed by GC.

REFERENCES

[1] Karstedt, B. D. 1973, Platinum complexes of unsaturated siloxanes and platinum containing organopolysiloxanes, United States, GEN ELECTRIC, US Patent No. 3,775,452

[2] Ashby, B. A. 1964, Platinum-olefin complex catalyzed addition of hydrogen- and alkenyl-substituted siloxanes, United States, GEN ELECTRIC, US Patent No. 3,159,601

[3] Speier, J.L, Webster J.A. and Barnes G.H. *J. Am. Chem. Soc*. **1957**, 79, 974.

[4] Hitchcock, P. B. ; Lappert, M. F.; Warhurst, N. J. W. *Angew. Chem. Int. Ed. Engl.* **1991**, 30, 438.

[5] Marko, I. E.; Sterin, S.; Buisine, O.; Mignani, G.; Branlard, P.; Tinant, B.; Declercq, J. P., *Science*, **2002**, 298, 204.

[6] Marko, I. E.; Sterin, S.; Buisine, O.; Berthon, G.; Michaud, G.; Tinant, B.; Declercq, Jean-Paul. *Advanced Synthesis & Catalysis*, **2004**, 346, 1429.

[7] Nesmeyanov, A.N. et al., *Tetrahedron* **1962**, 17, 61

[8] Corey, J.Y et al., J. *Chem. Rev.* **1999**, 99, 175

[9] C. Randolph, M.S. Wrighton, *J. Am. Chem. Soc.* **1986**, 108, 3366

[10] a) Knijnenburg, Q.; Gambarotta, S.; Budzelaar, P. H. M. *Dalton Trans.* **2006**, 5442. b) Bart, S. C.; Chlopek, K.; Bill, E.; Bouwkamp, M. W.; Lobkovsky, E.; Neese, F.; Wieghardt, K.; Chirik, P. J. *J. Am. Chem. Soc.* **2006**, *128*, 13901.

[11] Butin, K. P.; Beloglazkina, E. K.; Zyk, N. V. *Russ. Chem. Rev*. **2005**, *74*, 531.

[12] Kuwabara, I. H.; Comninos, F. C. M.; Pardini, V. L.; Viertler, H.; Toma, H. E. *Electrochim. Acta* **1994**, *39*, 2401.

[13] Toma, H. E.; Chavez-Gil, T. E. *Inorg. Chim. Acta.* **1997**, *257*, 197.

[14] de Bruin, B.; Bill, E.; Bothe, E.; Weyermüller, T.; Wieghardt, K. *Inorg. Chem.* **2000**, *39*, 2936.

[15] Budzelaar, P. H. M.; de Bruin, B.; Gal, A. W.; Wieghardt, K.; van Lenthe, J. H. *Inorg. Chem.* **2001**, *40*, 4649.

[16] Chirik, P. J.; Wieghardt, K. *Science* **2010**, *327*, 794.

[17] Bart, S. C.; Lobkovsky,E.; Chirik, P.J., *J. Am. Chem. Soc.* **2004,** *126*, 13794.

[18] Trovitch, R. J; Lobkovsky, E.; Bill, E .;Chirik, P. J., *Organometallics,* **2008,** *27*, 1470.

[19] Trovitch, R. J.; Lobkovsky, E.; Bouwkamp, M. W.; Chirik, P. J., *Organometallics,* **2008,** *27* (23), 6264.

[20] Tondreau, A. M.; Lobkovsky, E; Chirik, P. J., *Org. Lett.* **2008**, 10, 2789.

[21] Tondreau, A. M.; Darmon J. M.; Wile B. M., Floyd, S. K.; Lobkovsky, E.; Wieghardt, K.; Chirik, P. J., *Organometallics,* **2009**, 28, 3928.

[22] Nishiyama, H.; Furuta, A. *Chem. Commun.* **2007**, 760.

[23] Furuta, A., Nishiyama, H. *Tett. Lett.* **2008**, *49*, 110.

[24] Shaikh, N. S.; Junge, K.; Beller, M. *Org. Lett.* **2007**, *9*, 5429.

[25] Shaikh, N. S.; Enthaler, S.; Junge, K.; Beller, M. *Angew. Chem. Int. Ed.* **2008**, *47*, 2497.

[26] Addis, D.; Shaikh, N.; Zhou, S.; Das, S.; Junge, K.; Beller, M. *Chemistry--An Asian Journal*, **2010**, 5, 1687-1691.

[27] Campora, J.; Naz, A. M.; Palma, P.; Alvarez, E.; Reyes, M. L. *Organometallics* **2005**, 24, 4878.

[28] See Chapter 4 of this thesis.
[29] Jones, G. D.; Martin, J. L.; McFarland, C.; Allen, O. R.; Hall, R. E.; Haley, A. D.; Brandon, R. J.; Kanovalova, T.; Desrochers, P. J.; Pulay, P.; Vicic, D. A., *J. Am. Chem. Soc*., **2006**, 128, 13175.

[30] Westall, S.; Surgenor, A.; Bunce, T. (Dow Corning Corporation, USA). Hydrosilylation of allyl compounds with silanes or siloxanes in the presence of a noble metal catalyst, Patent NO 7208619, 2004.

[31] Cruse, R.; M. W.; Pohl, E. R.; Prashant, J. Silated core polysulfides, their preparation and use in filled elastomer compositions. United States, Momentive Performance Materials, US Patent NO 7696269, 2010.

[32] Russell S. K.; Darmon J. M.; Lobkovsky, E.; Chirik, P. J., *Inorg. Chem.* **2010** *49*, 2782.

[33] Cruse, Richard W. (Yorktown Heights, NY, US), York, Michael W. (Concord, NC, US), Pohl, Eric R. (Mt. Kisco, NY, US), Joshi, Prashant (Gaithersburg, MD, US) 2010, Silated core polysulfides, their preparation and use in filled elastomer compositions, United States, Momentive Performance Materials Inc. Albany, NY, US, US Patent No. 7696269

[34] Friedmann, Gilbert (Strasbourg, FR), Sperry, Pascal (Blienschwiller, FR), Brossas, Jean (Strasbourg, FR) 1992 Oxygen-permeable transparent polymer compositions for contact lenses of the rigid type, United States, Essilor International, Compagnie Generale d'Optique (Creteil, FR) US Patent No. 5166298

[35] Chen, Grace J. (Fairborn, OH), Snyder Jr., Carl Edgar (Trotwood, OH), Eapen, Kalathil Chandy (Beavercreek, OH) 2001 Polysilahydrocarbons as lubricants for aerospace application United States The University of Dayton, Dayton, OH, US Patent No. 6278011

[36] Bianchini, C.; Mantovani, G.; Meli, A.; Migliacci, F.; Zanobini, F.; Laschi, F.; Sommazzi, A., *Eur. J. Inorg. Chem.* **2003**, 1620.

[37] Russell, S. K.; Milsmann, C.; Lobkovsky, E.; Weyhermüller, T.; Chirik P. J. Submitted to *Inorg. Chem.* **2010.**

[38] Zhang, S.; Sun, W.; Xiao, T.; Hao, X., *Organometallics*, **2010**, 29(5), 1168.

[39] Pangborn, A. B.; Giardello, M. A.; Grubbs, R. H.; Rosen, R. K.; Timmers, F. J. *Organometallics* **1996**, *15*, 1518.

[40] Reiff, W. M.; Erickson, N. E.; Baker, W. A., Jr. *Inorg. Chem.* **1969**, 8, 2019.

[41] Sidokmai, W.; Imanishi, Y. *Bull. Chem. Soc. J.* **2000**, 73, 599.

[42] Sur, S. K. *J. Magn. Reson.* **1989**, *82*, 169.

CHAPTER 6

THE OXIDATION AND REDUCTION OF BIS(IMINO)PYRIDINE IRON(L)$_2$: INVESTIGATING THE BEHAVIOR OF THE REDOX ACTIVE LIGAND

6.1 Abstract

The oxidation and reduction of the formally Fe(0) complexes (^{iPr}PDI)Fe(CO)$_2$ and (^{iPr}PDI)Fe(N$_2$)$_2$ were performed. The oxidation of (^{iPr}PDI)Fe(CO)$_2$ with [Cp$_2$Fe][BArF$_{24}$] yielded low-spin, formally Fe(I) complex with a neutral bis(imino)pyridine chelate identified as [(^{iPr}PDI)Fe(CO)$_2$][BArF$_{24}$]. The reduction of (^{iPr}PDI)Fe(CO)$_2$ in the presence of one equivalent of 15-crown-5, allowed the isolation of [Na-15-Crown-5][(^{iPr}PDI)Fe(CO)$_2$]. Although not structurally characterized, the complex is assigned as low-spin ferrous species, with the reduction of the bis(imino)pyridine chelate to [PDI]$^{3-}$. The oxidation of (^{iPr}PDI)Fe(N$_2$)$_2$ with [Cp$_2$Fe][BArF$_{24}$] in diethyl ether resulted in the loss of dinitrogen and coordination of diethyl ether. [(^{iPr}PDI)Fe(Et$_2$O)][BArF$_{24}$] displayed spectroscopic properties consistent with a high-spin ferrous center antiferromagnetically coupled to a mono reduced chelate. The reduction of (^{iPr}PDI)Fe(N$_2$)$_2$ with sodium naphthalenide led to the loss of one equivalent of dinitrogen and the coordination of the sodium to yield two isomers of [Na][(^{iPr}PDI)Fe(N$_2$)]. The use of 18-crown-6 in the reaction led to the chelation of the sodium, creating the non-interacting salt pair [Na(18-crown-6)(THF$_2$)]-[(^{iPr}PDI)Fe(N$_2$)]. The same reaction methods were applied to the phenylated backbone complexes to yield [Na(18-crown-6)(THF$_2$)][(^{iPr}BPDI)Fe(N$_2$)]. The BPDI complexes could be further reduced to yield the dianionic complexes [Na(18-crown-6)(THF$_2$)]$_2$[(^{iPr}BPDI)Fe(N$_2$)].

6.2 Introduction

Bis(imino)pyridine ligands have garnered increasing attention over the past fifteen years due to their modularity and ease of synthesis. Since the discovery by Brookhart[1] and Gibson[2,3] that aryl substituted bis(imino)pyridine *M* (Fe or Co) dihalides are active for ethylene polymerization upon activation with methylaluminoxane, MAO, and later a variety of other activating agents,[4,5,6,7] much attention has been devoted to the role of this supporting ligand. A single component ethyelene polymerization catalysts of the type [(^{iPr}PDI)Fe(CH_2SiMe3)][BPh_4] were subsequently reported and exhibited activity comparable to the MAO/PDIFeCl_2 system.[8]

As bis(imino)pyridine ligands are redox active and have been shown to accept between 1-3 electrons,[9,10,11,12,13,14,19] the investigation of the reactivity of bis(imino)pyridine iron centers has focused on this phenomenon. In order to gain insight into the reactivity of PDI-Fe systems, an understanding of the redox behavior of the chelate is essential. For single component ethylene polymerization catalysis with [(^{iPr}PDI)Fe(R)][BPh_4] where R = Me, CH_2CMe_3 and CH_2SiMe_3, the activating species has been shown to have a redox neutral chelate, implying that redox activity in the activating species is not required for catalysis.[15]

The understanding of the redox activity of bis(imino)pyridine iron complexes is necessary for assigning the electronic structure. Simply removing a halide from (^{iPr}PDI)FeX_2 (X = Br, Cl) resulting in the formation of the formally Fe(I) complex (^{iPr}PDI)FeX,[16] results in a complicated electronic structure description.[17] Further reduction to form (^{iPr}PDI)Fe$(N_2)_2$ results in further reduction of the chelate.[13] Simple coordination compounds of bis(imin)pyridine iron also require spectroscopy and calculations to assign oxidation states at the iron nucleus. The electronic structure of (^{iPr}PDI)Fe$(CO)_2$ was shown to be much more complicated than the formally Fe(0)

complex suggests.[19,18] Through spectroscopy and computational studies, the proposed electronic structure is proposed as a resonance structure between Fe(II) and Fe(0) species. The contribution of the bis(imino)pyridine in oxidation state of the metal for (^{iPr}PDI)Fe(N_2)$_2$ and (^{iPr}PDI)Fe(CO)$_2$ is presented in Figure 6.1.

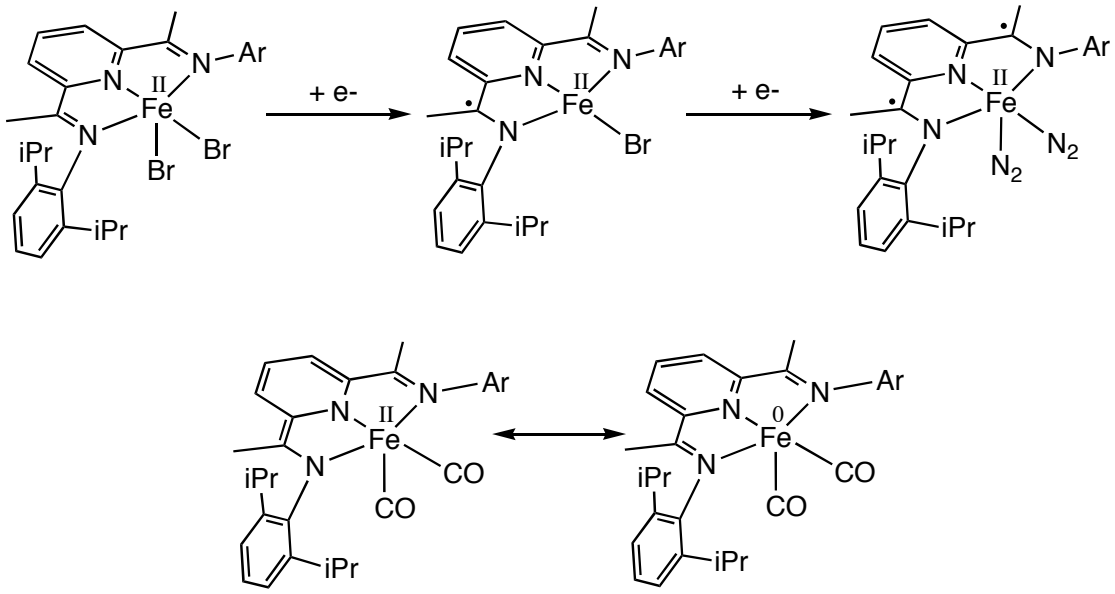

Figure 6.1 Chelate participation in the electronic structures of **(^{iPr}PDI)Fe(N_2)$_2$** and **(^{iPr}PDI)Fe(CO)**.

Redox activity has been implicated in a number of catalytic reactions involving (^{iPr}PDI)Fe(N_2)$_2$. The [2π + 2π] cyclization of α-ω dienes is of particular interest due to the thermally symmetry-disallowed nature of the reaction.[19] Initially reported in 2004, a follow up paper in 2009, focusing on 1,6-enyne reactivity, more thoroughly investigated the role of the bis(imino)pyridine chelate in the catalysis.[20] The report postulates that the iron nucleous remains Fe(II) throughout the catalytic cycle, with the redox events occurring on the ligand (Figure 6.2).

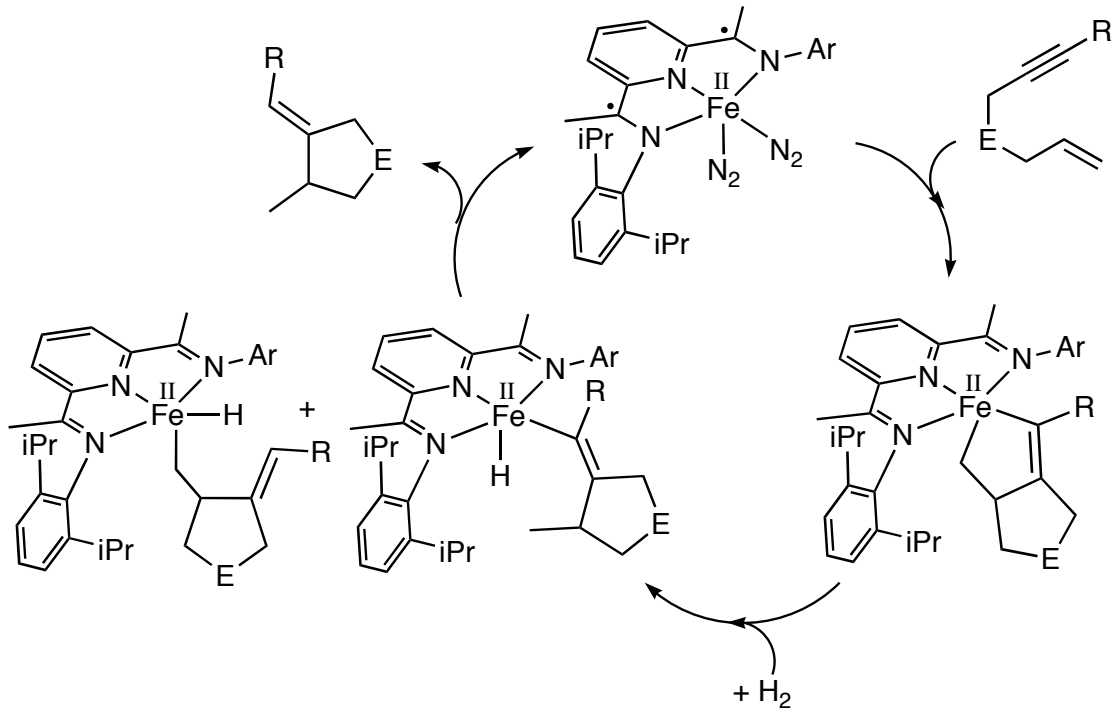

Figure 6.2 Bis(imino)pyridine redox behavior during a catalytic cycle.

The goal of this work is to asses the participation of the bis(imino)pyridine chelate upon the oxidation or reduction of complexes bearing neutral ligands. A greater understanding of the relationship between the iron nucleus and the supporting bis(imino)pyridine ligand. The work also hopes to generate useful synthons for PDI iron chemistry and allow for the exploration of new types of complexes.

6.3 Oxidation and Reduction of Dicarbonyl Complexes

The electronic structure of (^{iPr}PDI)Fe(CO)$_2$ was previously established and a fairly mature understanding of the complex has been reported, and thus was the first compound investigated in redox chemistry. The addition of [Cp$_2$Fe][BPh$_4$] to (^{iPr}PDI)Fe(CO)$_2$ was ineffective for the oxidation and resulted in the recovery of starting material. An oxidizing agent with a more non-coordinating counter-ion, B(3,5-bis-trifluoromethylphenyl)$_4$, BArF$_{24}$, in the form of [Cp$_2$Fe][BArF$_{24}$], was explored as an oxidant. The addition of one equivalent of [Cp$_2$Fe][BArF$_{24}$] to (^{iPr}PDI)Fe(CO)$_2$ in

benzene resulted in the one electron oxidation of (^{iPr}PDI)Fe(CO)$_2$ and the precipitation of a dark powder identified as [(^{iPr}PDI)Fe(CO)$_2$][BArF$_{24}$] after 30 minutes. Magnetic susceptibility measurements on a powder sample of [(^{iPr}PDI)Fe(CO)$_2$][BArF$_{24}$] yielded a magnetic moment of 2.0 μB at 290 K, consistent with the spin only value of an S = ½ species.

The solid-state KBr IR spectrum of [(^{iPr}PDI)Fe(CO)$_2$][BArF$_{24}$] exhibited two CO stretching frequencies at 2028 cm^{-1} and 1981 cm^{-1} . These values are blue-shifted by approximately 80 wavenumbers from the KBr values of 1948 cm^{-1} and 1894 cm^{-1} for (^{iPr}PDI)Fe(CO)$_2$. This is in agreement with the lower amount of electron density at the iron able to back donate into the π* orbitals of the CO ligands. The oxidation of the isotopologue (^{iPr}PDI)Fe(^{13}CO)$_2$ yielded values of 1982 cm^{-1} and 1937 cm^{-1} in KBr, in agreement with calculations for a harmonic oscillator. A table of the comparison of CO stretching frequencies is reported in Table 6.1.

Table 6.1 CO stretching frequencies for **[(^{iPr}PDI)Fe(CO)$_2$][BArF$_{24}$]**.

Compound	ν_{CO} (cm^{-1}) (KBr)	
(^{iPr}PDI)Fe(CO)$_2$	1974	1914
(^{iPr}PDI)Fe(^{13}CO)$_2$	1930	1870
[Na][(^{iPr}PDI)Fe(CO)$_2$]	1935	1863
[Na][(^{iPr}PDI)Fe(^{13}CO)$_2$]	1890	1819
[(^{iPr}PDI)Fe(CO)$_2$][BArF$_{24}$]	2028	1981
[(^{iPr}PDI)Fe(^{13}CO)$_2$][BArF$_{24}$]	1982	1937

The poor solubility of [(^{iPr}PDI)Fe(CO)$_2$][BArF$_{24}$] in solvents such as THF, diethyl ether, and toluene initially made characterization difficult. The use of methylene chloride as a solvent, however, allowed for further spectroscopic

investigations. The ^{1}H NMR spectrum of [(^{iPr}PDI)Fe(CO)$_2$][BArF$_{24}$] in methylene chloride-d_2 exhibited paramagnetically broadened peaks attributed to the complex.

X-ray quality crystals were grown from a concentrated methylene chloride solution of [(^{iPr}PDI)Fe(CO)$_2$][BArF$_{24}$] layered with diethyl ether and cooled to -35 ºC overnight. The structure thus obtained has an idealized square pyramidal iron center with a non-coordinating BArF$_{24}$ anion. The full structure is displayed in Figure 6.3, and the [(^{iPr}PDI)Fe(CO)$_2$] fragment is shown in Figure 6.4.

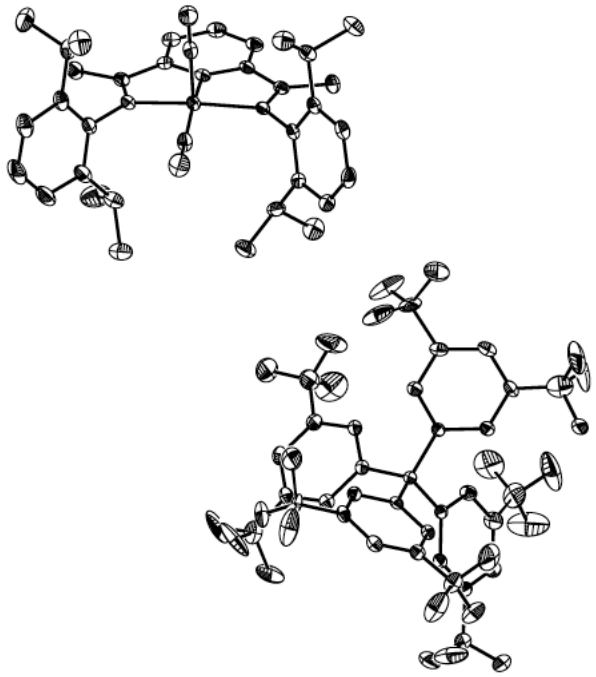

Figure 6.3 Solid-state structure of **[(^{iPr}PDI)Fe(CO)$_2$][BArF$_{24}$]** at 30% probability ellipsoids. Hydrogen atoms and disordered fluorine omitted for clarity.

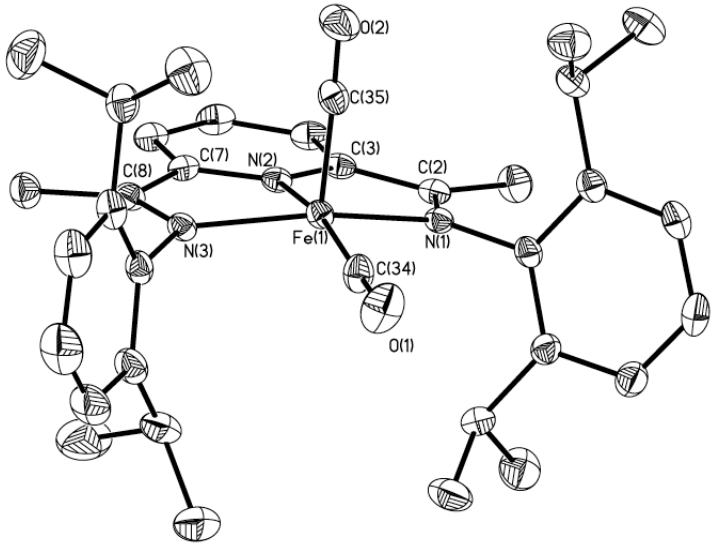

Figure 6.4 Solid-state structure of **[(^{iPr}PDI)Fe(CO)$_2$][BArF$_{24}$]** at 30% probability ellipsoids showing the iron fragment only. Hydrogen atoms removed for clarity.

The metrical parameters of the ligand indicate that the bis(imino)pyridine is in it's neutral form. The imine bond distances of 1.289(4) Å and 1.289(4) Å for N(1)-C(2) and N(3)-C(8), respectively, are consistent with a neutral chelate, as are the long C_{ipso}-C_{imine} bond lengths of 1.462(4) Å and 1.459(4) Å for C(2)-C(3) and C(7)-C(8), respectively. This indicates that the single oxidation of (^{iPr}PDI)Fe(CO)$_2$ resulted in a double oxidation of the ligand, and in turn the resonance of Fe(0)-Fe(II) became an Fe(I) nucleus. A comparison of the metrical parameters of [(^{iPr}PDI)Fe(CO)$_2$][BArF$_{24}$] and (^{iPr}PDI)Fe(CO)$_2$ are shown in Table 6.2.

Table 6.2 Selected metrical parameters comparing **(^{iPr}PDI)Fe(CO)$_2$** and **[(^{iPr}PDI)Fe(CO)$_2$][BArF$_{24}$]**.

	[(^{iPr}PDI)Fe(CO)$_2$][BArF$_{24}$]	(^{iPr}PDI)Fe(CO)$_2$
Fe(1)-N(1)	1.984(4)	1.9500(14)
Fe(1)-N(2)	1.877(2)	1.8488(14)
Fe(1)-N(3)	1.985(4)	1.9622(15)
Fe(1)-C(34)	1.801(4)	1.7823(19)
Fe(1)-C(35)	1.811(4)	1.7809(19)
N(1)-C(2)	1.289(4)	1.335(2)
N(3)-C(8)	1.289(4)	1.330(2)
N(2)-C(3)	1.348(4)	
N(2)-C(7)	1.350(4)	
C(2)-C(3)	1.462(4)	1.423(2)
C(7)-C(8)	1.459(4)	1.425(2)
C(34)-O(1)	1.124(4)	1.147(2)
C(35)-O(2)	1.128(4)	1.148(2)
N(1)-Fe(1)-N(2)	79.49(10)	
N(1)-Fe(1)-N(3)	154.39(10)	
N(2)-Fe(1)-N(3)	78.99(10)	
N(2)-Fe(1)-C(34)	167.36(14)	
N(2)-Fe(1)-C(35)	98.51(13)	
C(34)-Fe(1)-C(35)	94.13(16)	

The zero-field Mössbauer spectrum of [(^{iPr}PDI)Fe(CO)$_2$][BArF$_{24}$] displays parameters slightly shifted from the parameters of the neutral complex, and is shown in Figure 6.5. (^{iPr}PDI)Fe(CO)$_2$ displays an isomer shift of $\delta = 0.03$ mm/s and a quadrupole splitting of $\Delta E_Q = 1.17$ mm/s compared to the isomer shift of $\delta = 0.17$ mm/s and a quadrupole splitting of $\Delta E_Q = 0.62$ mm/s for [(^{iPr}PDI)Fe(CO)$_2$][BArF$_{24}$]. The increase in isomer shift upon oxidation is counter-intuitive, yet is readily explained by the decrease in covalency of the bis(imino)pyridine chelate with the iron.

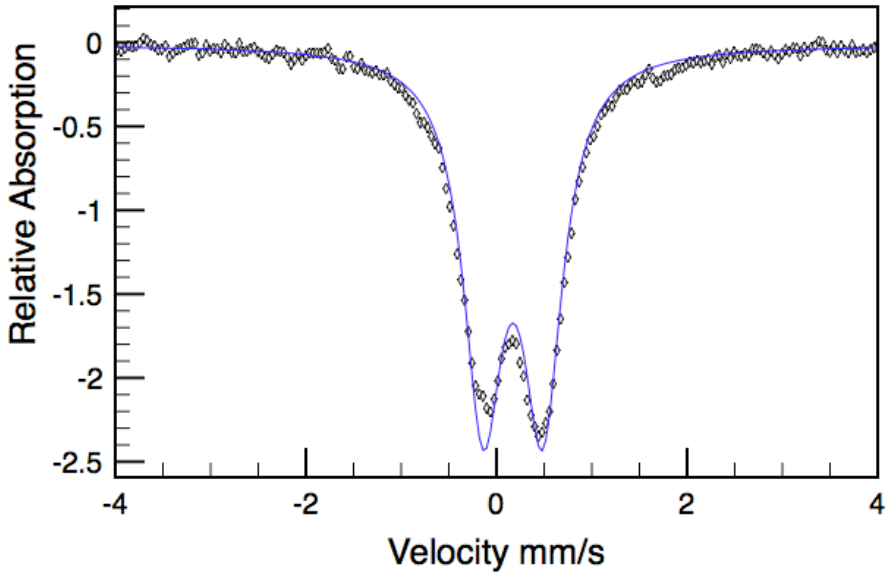

Figure 6.5 Zero-field Mössbauer spectrum of **[(^{iPr}PDI)Fe(CO)$_2$][BArF$_{24}$]** obtained at 80 K.

The 77 K EPR spectrum of [(^{iPr}PDI)Fe(CO)$_2$][BArF$_{24}$] in methylene chloride is consistent with an $S = ½$ compound. Interestingly, the solution turned light green from dark grey upon cooling to 77 K. The fit of the spectrum gives g values of $g_{min} = 1.987$, $g_{mid} = 2.0391$, and $g_{max} = 2.108$. The Δg of 1.2 is larger than what is typically seen for an organic centered radical, indicating the unpaired electron is likely iron-centered. EPR of the ^{13}C labeled complex did not exhibit any differences from the natural abundance complex, indicating that the CO ligands do not contain much of the unpaired spin, consistent with the IR spectrum. The EPR and the fit are shown in Figure 6.6.

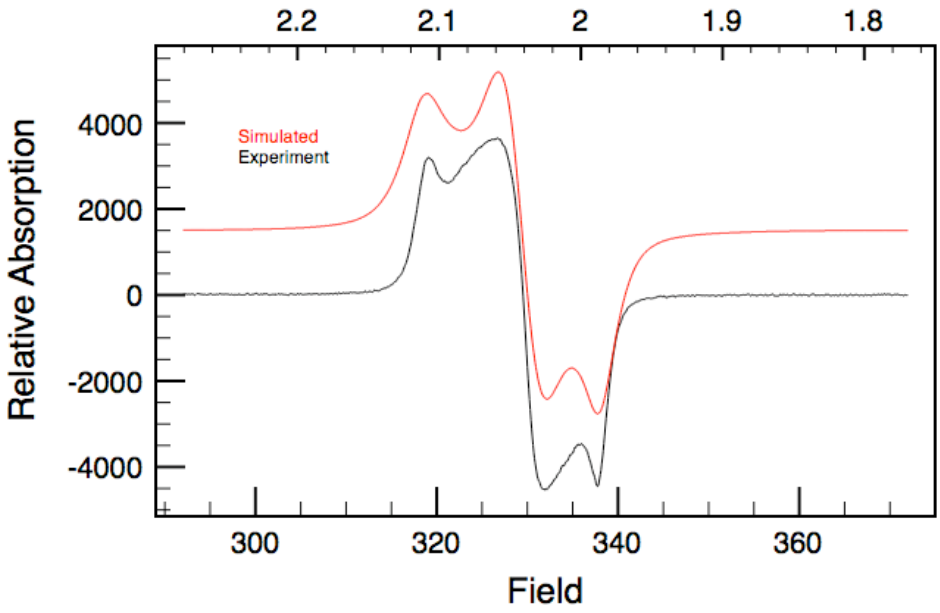

Figure 6.6 EPR spectrum of **[(^{iPr}PDI)Fe(CO)$_2$][BArF$_{24}$]** in methylene chloride at 77 K.

From the spectroscopy, [(^{iPr}PDI)Fe(CO)$_2$][BArF$_{24}$] is best described as a low-spin Fe(I) complex. The unpaired electron likely resides in an iron based orbital. This electronic structure is reasonable based on the electronic structure of the starting material, (^{iPr}PDI)Fe(CO)$_2$. As (^{iPr}PDI)Fe(CO)$_2$ is reported to contain 2 resonance structures, an Fe(0) and an Fe(II) species, the oxidation from Fe(0) to Fe(I) is an expected result. This chemistry is presented in Figure 6.7.

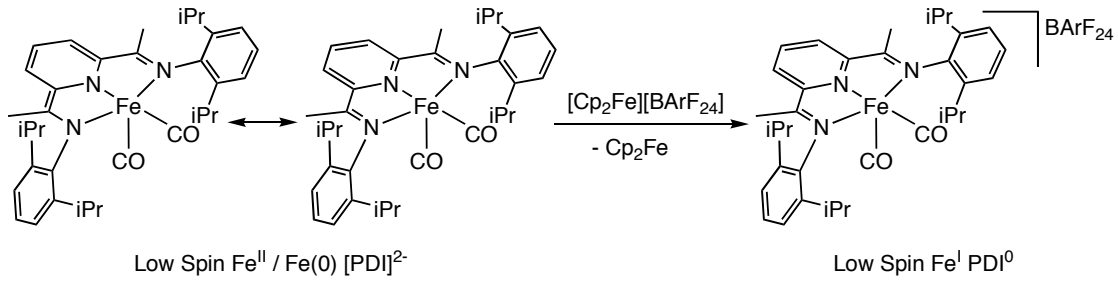

Figure 6.7 The oxidation of **(^{iPr}PDI)Fe(CO)$_2$** with [Cp_2Fe][$BArF_{24}$].

The reduction of (^{iPr}PDI)Fe(CO)$_2$ was slightly more difficult to achieve. The reaction of (^{iPr}PDI)Fe(CO)$_2$ with an excess of sodium amalgam did not provide an isolable compound. The only identified product was of the starting material (^{iPr}PDI)Fe(CO)$_2$. When the reduction was carried out with excess sodium amalgam and 1.2 equivalents of 15-Crown-5 in toluene, a green precipitate was formed that was collected on a glass frit and was identified as [Na-15-Crown-5][(^{iPr}PDI)Fe(CO)$_2$]. The infrared stretching frequencies obtained in KBr show exhibit approximately six stretches, the largest two, attributed to [Na-15-Crown-5][(^{iPr}PDI)Fe(CO)$_2$], are at 1935 cm^{-1} and 1863 cm^{-1}. These values are red-shifted from the values of the neutral complex, the solid-state KBr resonances of (^{iPr}PDI)Fe(CO)$_2$ are at 1948 cm^{-1} and 1894 cm^{-1}. In the IR spectrum, however are several smaller stretches attributed to decomposition products.

As [Na-15-Crown-5][(^{iPr}PDI)Fe(CO)$_2$] is a formally 19 electron complex, it proved to be quite unstable. Decomposition occurred over the course of *ca.* 24 hours at room temperature, and over the course of weeks at -35 ºC in the solid state. [Na-15-Crown-5]-[(^{iPr}PDI)Fe(CO)$_2$] was only sparingly soluble in toluene, THF, or diethyl ether. When methylene chloride was used, the compound decomposed immediately. A zero-field Mössbauer spectrum was obtained by washing [Na-15-Crown-5][(^{iPr}PDI)Fe(CO)$_2$] with copious amounts of toluene followed by pentane and quickly

dried under reduced pressure. The Mössbauer spectrum thus obtained displays an isomer shift of δ = -0.01 mm/s and a quadrupole splitting of ΔE_Q = 1.19 mm/s, values very similar to the neutral complex (δ = 0.03, ΔE_Q = 1.19 mm/s). The Mössbauer spectrum is presented in Figure 6.8.

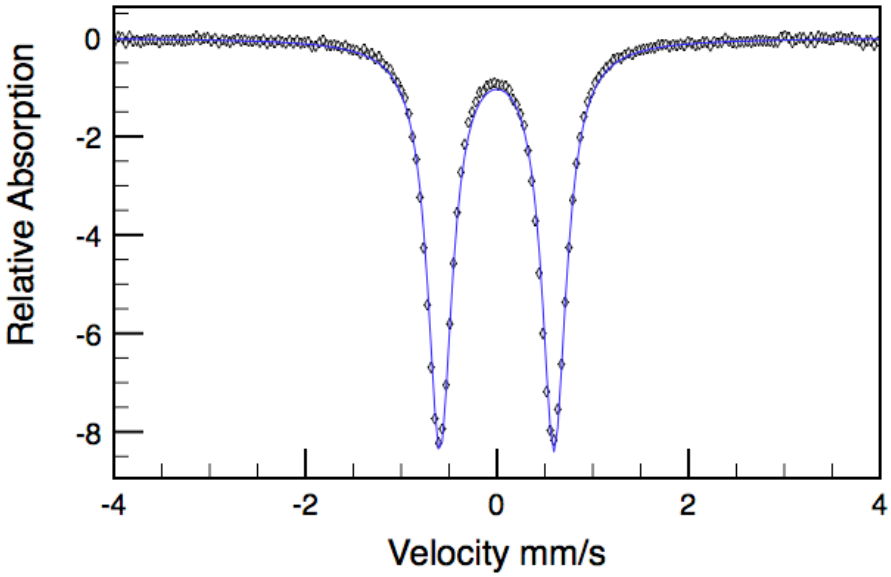

Figure 6.8 Zero-field Mössbauer spectrum of **[Na-15-Crown-5][(^{iPr}PDI)Fe(CO)$_2$]** obtained at 80 K.

EPR spectroscopy was utilized in an attempt to further study the electronic structure of the complex. [Na-15-Crown-5][(^{iPr}PDI)Fe(CO)$_2$] was dissolved in toluene and was frozen in liquid nitrogen to prevent decomposition in order to obtain a spectrum. The spectrum obtained is consistent with an axial signal for an S = ½ complex. Values obtained from the fit are g_z = 1.945, g_y = 1.974, and g_z = 1.976. The Δg value of 0.031 is very low and indicative of a ligand based spin. The spectrum is displayed is Figure 6.9.

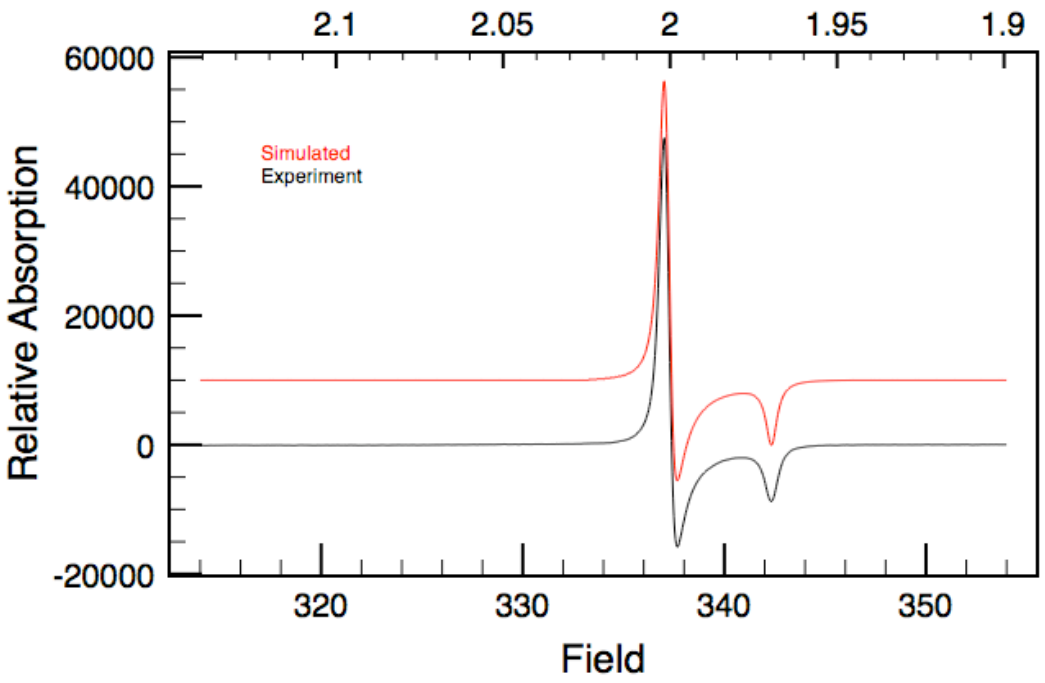

Figure 6.9 EPR spectrum of **[Na-15-Crown-5][(^{iPr}PDI)Fe(CO)$_2$]** in toluene at 77 K.

The ligand based spin indicates that the reduction of the compound most likely occurred at the bis(imino)pyridine ligand, yielding a triplet PDI^{2-} anti-ferromagnetically coupled to an Fe(I) system, giving the overall S = ½ system. The reduction of (^{iPr}PDI)Fe(CO)$_2$, a complex with a doubly reduced chelate, could conceivably occur in this fashion. A greatly simplified model of the three-electron sequence is outlined in Figure 6.10.

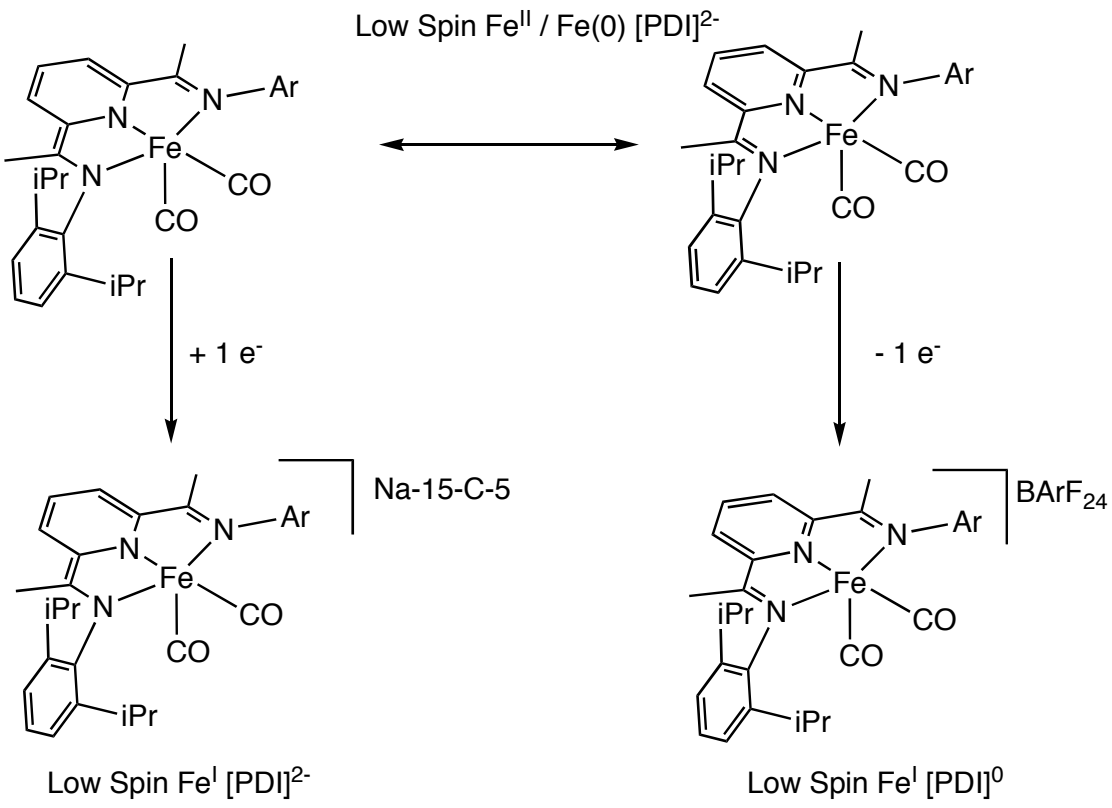

Figure 6.10 A depiction of electron movement over the series **[Na-15-Crown-5]-[(^{iPr}PDI)Fe(CO)$_2$]**, **(^{iPr}PDI)Fe(CO)$_2$**, and **[(^{iPr}PDI)Fe(CO)$_2$][BArF$_{24}$]**.

This depiction is not meant to imply that the resonance structures of (^{iPr}PDI)Fe(CO)$_2$ are discreet complexes that react differently. As electrons are removed from the anionic complex, the bis(imino)pyridine chelate is oxidized from $[PDI]^{2-}$ to $[PDI]^{2-}$ and the iron center is in resonance between low-spin ferrous and Fe(0). The removal of the second electron results in the oxidation of the $[PDI]^{2-}$ to $[PDI]^{0}$, and the iron nucleus is Fe(I). This explanation best suits all of the data gathered on this series of complexes, however, DFT calculations should be performed in order to provide further evidence for the proposed electronic structures.

6.4 Oxidation and Reduction of (^{iPr}PDI)Fe(N_2)$_2$

The oxidation of (^{iPr}PDI)Fe(N_2)$_2$ failed with [Cp_2Fe][BPh_4], much as in the case of (^{iPr}PDI)Fe(CO)$_2$, so [Cp_2Fe][$BArF_{24}$] was evaluated as a potential oxidant. Upon addition of [Cp_2Fe][$BArF_{24}$] to a diethyl ether solution of (^{iPr}PDI)Fe(N_2)$_2$, an evolution of gas (N_2) and a color change from dark green to light green was observed. The addition of pentane and cooling to -35 ºC for 1 hour, followed by filtration and drying of the green powder under reduced pressure yielded [(^{iPr}PDI)Fe(Et_2O)]-[$BArF_{24}$]. Attempts to obtain an ^{1}H NMR spectrum in benzene-d_6 yielded peaks consistent with the [$BArF_{24}$] only; no resonances attributed to the bis(imino)pyridine chelate were observed. ^{19}F NMR displayed a single sharp resonance at 62.30 ppm. A solid-state structure was obtained by dissolving [(^{iPr}PDI)Fe(Et_2O)][$BArF_{24}$] in fluorobenzene and layering the solution with pentane, followed by cooling the solution to -35 ºC for overnight. A representation of the solid-state structure is presented in Figure 6.11.

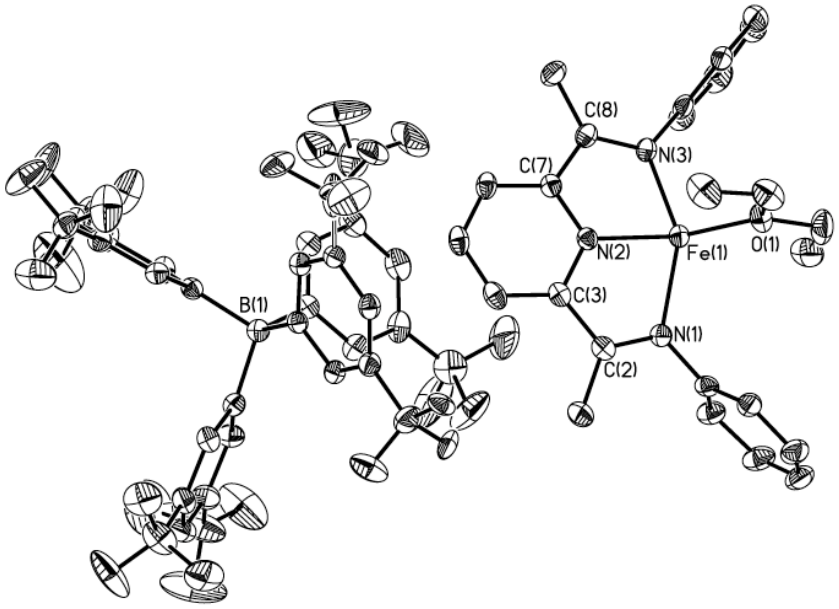

Figure 6.11 Solid state structure of **[(^{iPr}PDI)Fe(Et$_2$O)][BArF$_{24}$]** shown at 30% probability ellipsoids. Hydrogen atoms, iso-propyl groups, and disordered fluorine deleted for clarity.

[(^{iPr}PDI)Fe(Et$_2$O)][BArF$_{24}$] contains a single diethyl ether bound that is canted out of the plane of the chelate 41 º. The bis(imino)pyridine metrics are consistent with mono-reduced chelate where the imine bonds have distances of 1.301(4) Å and 1.316(4) Å for N(1)-C(2) and N(3)-C(8), respectively, consistent with a neutral chelate, as are the elongated C_{ipso}-C_{imine} bond lengths of 1.441(4) Å and 1.448(4) Å for C(2)-C(3) and C(7)-C(8), respectively. The Fe-N_{imine} bond distances, 2.109(2) and 2.106(3) for Fe(1)-N(1) and Fe(1)-N(3) respectively, indicate population of dx^2-y^2. Table 6.2 highlights the important metrical data for [(^{iPr}PDI)Fe(Et$_2$O)][BArF$_{24}$].

Table 6.3 Selected metrical parameters of **[(^{iPr}PDI)Fe(Et$_2$O)][BArF$_{24}$]**.

[(^{iPr}PDI)Fe(Et$_2$O)][BArF$_{24}$]	**Å or º**	**[(^{iPr}PDI)Fe(Et$_2$O)][BArF$_{24}$]**	**Å or º**
Fe(1)-N(1)	2.109(2)	C(2)-C(3)	1.441(4)
Fe(1)-N(2)	1.954(2)	C(7)-C(8)	1.448(4)

Fe(1)-N(3)	2.106(3)		
Fe(1)-O(1)	2.015(2)	N(1)-Fe(1)-N(2)	76.89(10)
		N(1)-Fe(1)-N(3)	145.53(10)
N(1)-C(2)	1.301(4)	N(2)-Fe(1)-N(3)	77.39(10)
N(3)-C(8)	1.316(4)	N(2)-Fe(1)-O(1)	138.12(10)
N(2)-C(3)	1.349(4)		
N(2)-C(7)	1.357(4)		

[(^{iPr}PDI)Fe(Et_2O)][$BArF_{24}$] displayed odd properties by Mössbauer spectroscopy. The 80 K spectrum contained three sets of quadrupole doublets. One explanation is that the complex is a mixture of 4- and 5-coordinate iron, with the mono- and di- ether complexed iron, respectively.[21] Lowering the temperature to 15 K resulted in the splitting of the signal into 6 lines. To obviate the problem of varying coordination number, a solution Mössbauer spectrum was obtained in diethyl ether, resulting in a spectrum consisting of one quadrupole doublet centered at $\delta = 1.16$ mm/s with a quadrupole splitting of $\Delta E_Q = 2.62$ mm/s (Figure 6.12).

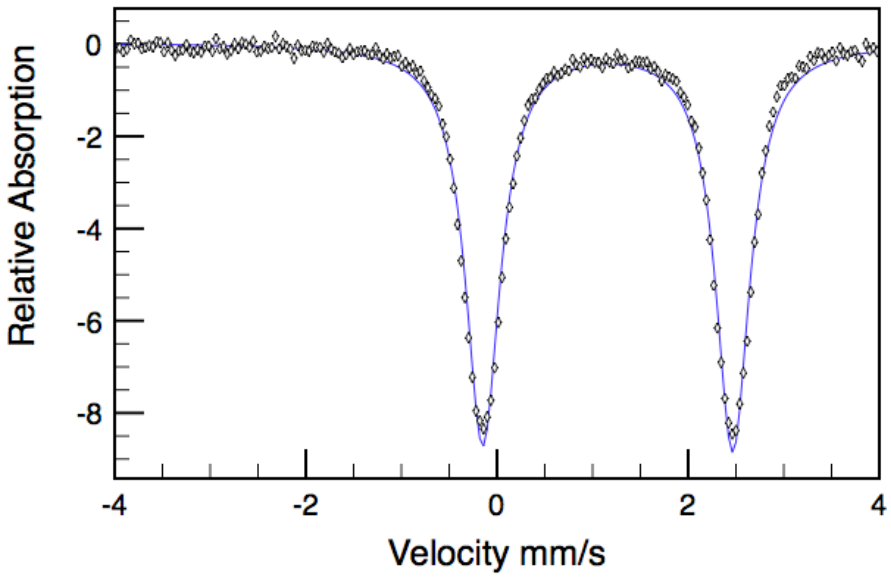

Figure 6.12 Solution Mössbauer spectrum of **[(^{iPr}PDI)Fe(Et_2O)][$BArF_{24}$]** in diethyl ether at 80 K.

Due to the Mössbauer spectra displaying multiple signals as a solid, the EPR spectrum was obtained in diethyl ether. Using diethyl ether as a solvent obviated this problem, and an EPR spectrum consistent with an $S = 3/2$ complex, and it is displayed along with the fit in Figure 6.13. [(^{iPr}PDI)Fe(Et_2O)][$BArF_{24}$] displayed poor solubility in toluene, and cooling the solution to 77 K resulted in precipitation of the iron complex that resulted in a poor EPR spectrum.

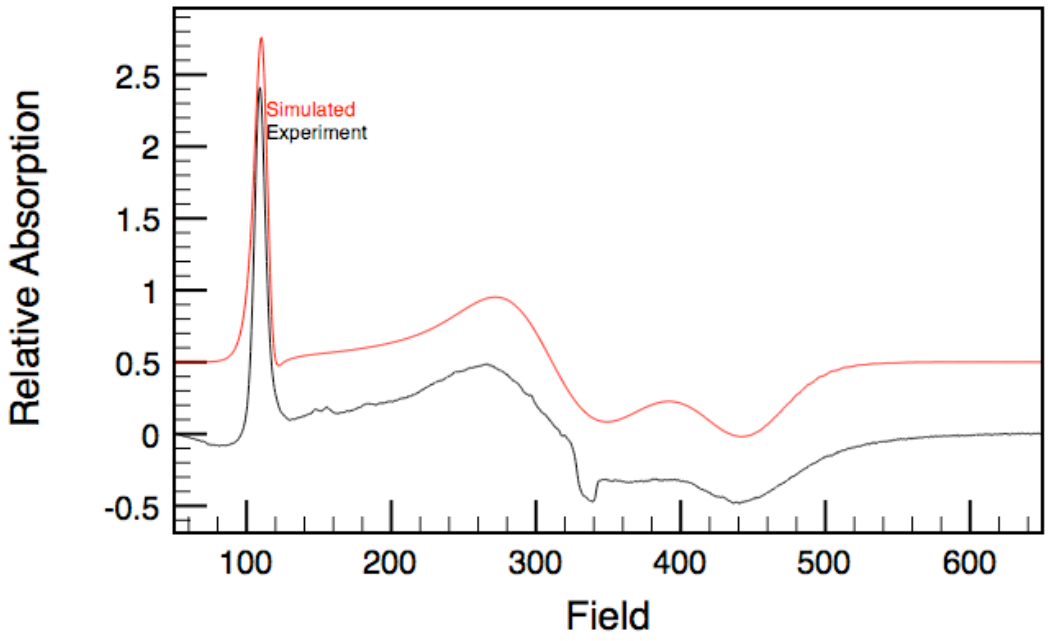

Figure 6.13 EPR spectrum of **[(^{iPr}PDI)Fe(Et_2O)][$BArF_{24}$]** obtained at 10 K in diethyl ether.

The signal contained g values of $g_x = 1.877$, $g_z = 1.918$, and $g_y = 2.333$, giving a $g_{average}$ of 2.042 and the fit yields an E/D value of 0.27 from a D value of 9.01 cm^{-1}. One concern with the data is that the spectrum was obtained in diethyl ether as a solvent, so there is a possibility that the spectrum does not match the solid-state structure in coordination number; often at cold temperatures mono-alkyls and mono-

halides bind a fifth ligand, such as diethyl ether.[21] However, the EPR spectrum does indicate that the complex is isolated cleanly, data the Mössbauer spectrum was unable to provide.

The variable temperature SQUID measurement (Figure 6.14) also was consistent with an $S = 3/2$ complex, although the data is high for the spin only value of an $S = 3/2$ species, topping out at 4.4 μB at roughly 50 K. The magnetic moment obtained for the solid at 290 K on a magnetic susceptibility balance was higher yet, yielding a μ_{eff} of 5.2 μ_B. The origin of the anomalously high magnetic moments remains unknown. The fit if the SQUID gave a D value of 9.559 cm^{-1}, an E/D value of 0.27, with the $g_{average} = 2.352$. These data are close in magnitude to the EPR values obtained in diethyl ether at 10 K. The EPR sample could very well be five-coordinate with a second diethyl ether ligand, which could explain some of the differences in the values.

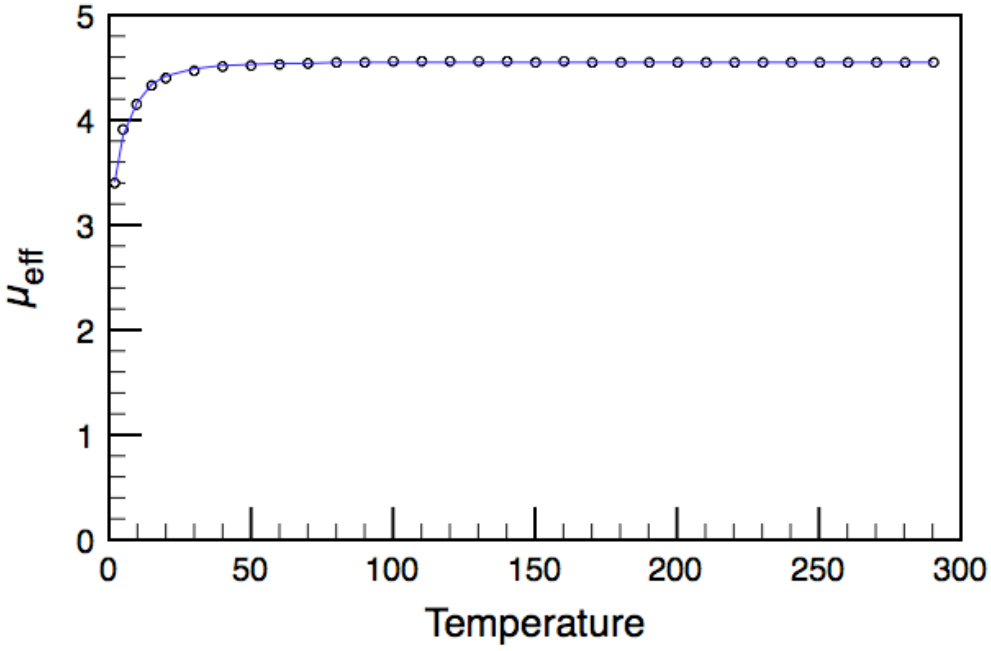

Figure 6.14 SQUID data for **[(^{iPr}PDI)Fe(Et_2O)][$BArF_{24}$]** with a D value of 9.559 cm^{-1}, an E/D = 0.27, and a $g_{average}$ = 2.352.

The data obtained for [(^{iPr}PDI)Fe(Et_2O)][$BArF_{24}$] indicates that the complex is similar to complexes of the type (^{iPr}PDI)Fe(R), where R = to a neopentyl or neosilyl group. In both of those cases, the R group is canted out of the plane of the chelate. This description gives a high-spin ferrous center antiferromagnetically coupled to a mono-reduced bis(imino)pyridine for [(^{iPr}PDI)Fe(Et_2O)][$BArF_{24}$]. The overall transformation of the oxidation of (^{iPr}PDI)Fe(N_2)$_2$ yields the oxidation of the bis(imino)pyridine chelate, retaining the 2+ oxidation state of the iron nucleus, but weakening the field strength of the PDI enough to cause a spin-state change from intermediate-spin to high-spin, as shown in Figure 6.15.

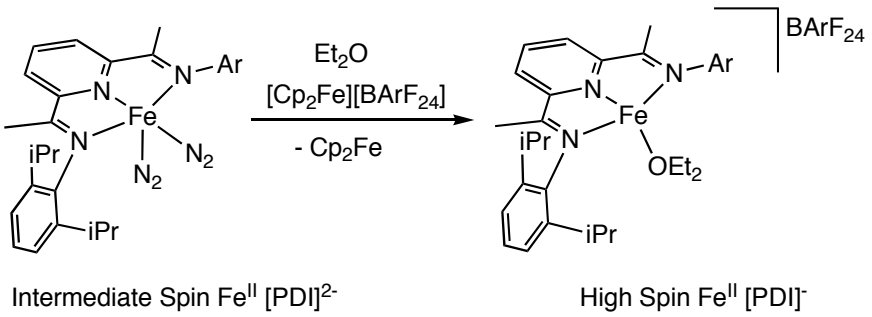

Figure 6.15 Electron movement in the oxidation of **(^{iPr}PDI)Fe(N_2)$_2$**.

The reactivity of [(^{iPr}PDI)Fe(Et_2O)][$BArF_{24}$] is what one would expect for a complex bearing a labile diethyl ether ligand. The addition of one equivalent of nitric oxide, in the presence of a slight excess of THF, yielded the previously characterized complex [(^{iPr}PDI)Fe(NO)(THF)][$BArF_{24}$]. Adding an excess of CO to a diethyl ether solution of this compound yielded [(^{iPr}PDI)Fe($CO)_2$)][$BArF_{24}$]. The utility of [(^{iPr}PDI)Fe(Et_2O)][$BArF_{24}$] as a useful formally iron (I) synthon has yet to be fully explored, but initial results indicate that the diethyl ether ligand can be displaced. The results of these reactions are presented in Figure 6.16.

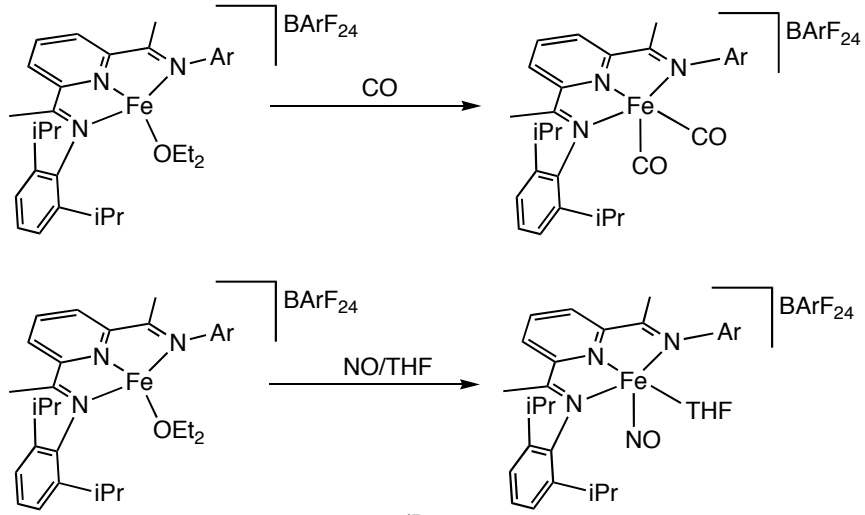

Figure 6.16 The synthesis of **[(^{iPr}PDI)Fe($CO)_2$][$BArF_{24}$]** and **[(^{iPr}PDI)Fe(NO)(THF)][$BArF_{24}$]** from **[(^{iPr}PDI)Fe(Et_2O)][$BArF_{24}$]**.

The reduction of (^{iPr}PDI)Fe(N_2)$_2$ proved more complicated than the oxidation. The formation of [Na][(^{iPr}PDI)Fe(N_2)] was achieved by the addition 1.05 equivalents of sodium naphthalenide to (^{iPr}PDI)Fe(N_2)$_2$ in THF, followed by removal of THF under reduced pressure and the addition of a diethyl ether to mobilize the product, and the powder was collected on a glass frit and identified as [Na][(^{iPr}PDI)Fe(N_2)]. This method was successful in that anionic [Na][(^{iPr}PDI)Fe(N_2)] was formed in the reaction. The unfortunate problem is that there are two isomers present in the reaction mixture. IR stretching frequencies in KBr were seen at 1966 cm^{-1} and 1917 cm^{-1}. These two stretches are similar to those reported for a similar set of complexes synthesized by Gambarotta.[22] These two stretches are attributed to two different sodium-binding modes, which they are outlined in Figure 6.17.

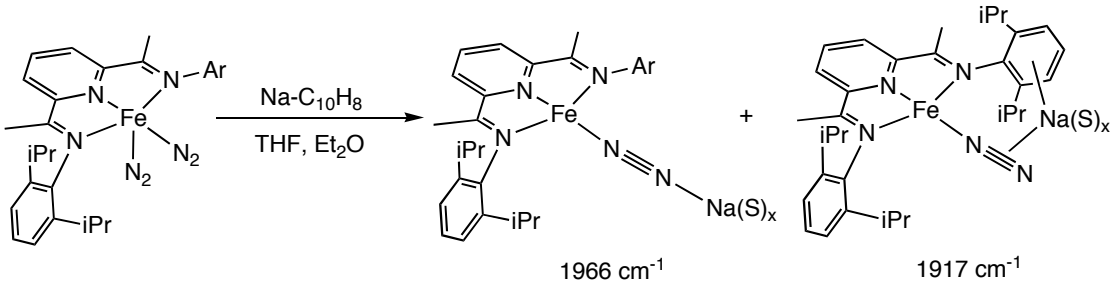

Figure 6.17 The reduction of **(^{iPr}PDI)Fe(N_2)$_2$** with sodium naphthalenide to yield two isomers of **[Na][(^{iPr}PDI)Fe(N_2)]**.

The oxidation of [Na][(^{iPr}PDI)Fe(N_2)] with Me_3SiCl or [Cp_2][BPh_4] resulted in the formation of (^{iPr}PDI)Fe(N_2)$_2$, indicating that the ligand is intact and the anionic complex has generally the right formula. [Na][(^{iPr}PDI)Fe(N_2)] treated with one equivalent of [NO][BF_4] yielded the well characterized complex (^{iPr}PDI)Fe(NO).[23] A solid-state magnetic measurement of the mixture of products yielded a μ_{eff} of 1.7 μB, consistent with the expected value of an S =1/2 compound. Attempts to obtain an EPR

spectrum at 77 K yielded a signal consistent with the independently prepared sodium-reduced bis(imino)pyridine [Na][PDI]. [Na][(^{iPr}PDI)Fe(N_2)] proved to be a useful anionic synthon, although the characterization of the complex was remains incomplete.

A method for generating a single isomer of the product was next developed. The reduction (^{iPr}PDI)Fe(N_2)$_2$ in THF by a stoichiometric amount of sodium naphthalenide was performed, and the reaction mixture was filtered. At this point, one equivalent of 18-crown-6 was added to the filtrate and then the volatiles were removed. The residue was taken up in a minimal amount of THF and the product, [Na-18-Crown-6][(^{iPr}PDI)Fe(N_2)], was precipitated by the addition of pentane. The resulting compound contained a single N_2 stretch by IR in KBr at 1948 cm^{-1}. The magnetic data was similar to the mixture of products, yielding an effective magnetic moment of 1.7 μB at 290 K.

Although full crystallographic characterization of the anionic [Na-18-Crown-6][(^{iPr}PDI)Fe(N_2)] was not obtained, a low-quality structure was collected and connectivity was determined. Each sodium contained two molecules of THF as well as the cryptand, and was non-interacting with the bis(imino)pyridine iron. The iron is 4-coordinate, bound to a single dinitrogen and the bis(imin)pyridine chelate, which is consistent with the IR spectrum. With a clean complex isolated free from other isomers, a zero-field Mössbauer spectrum (Figure 6.18) was obtained at 80 K and an EPR spectrum (Figure 6.19) was taken at 4 K.

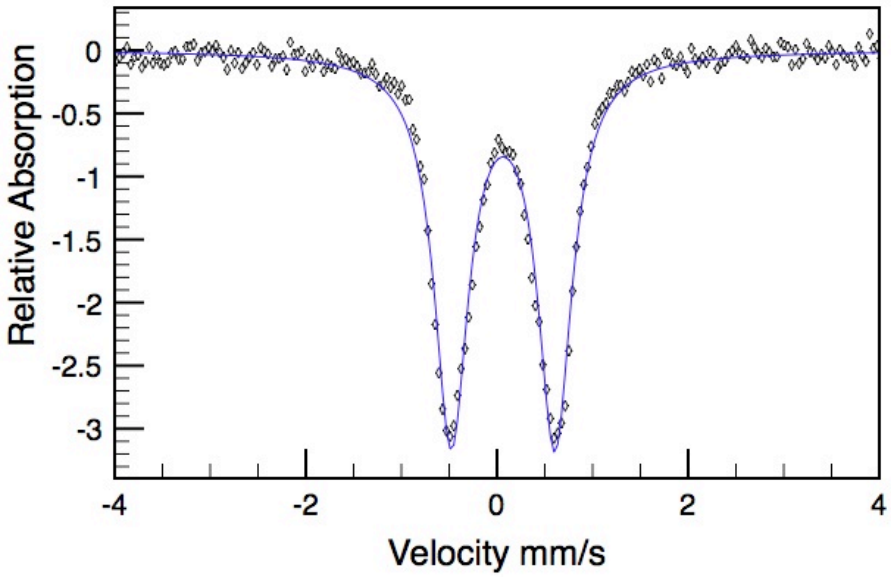

Figure 6.18 Zero-field ^{57}Fe Mössbauer spectrum of **[Na-15-Crown-5][(^{iPr}PDI)Fe(N_2)]** recorded at 80 K.

The isomer shift for [Na-15-Crown-5][(^{iPr}PDI)Fe(N_2)] in the solid state at 80 K was $\delta = 0.06$ mm/s and the quadrupole splitting was $\Delta E_Q = 1.08$ mm/s. The values obtained from the Mössbauer spectrum indicate a stronger ligand-field environment around the iron, with similar effects seen before with bis(imino)pyridine systems. Unfortunately, the data is ambiguous as to the oxidation state of the chelate or the iron center. EPR spectroscopy was thus undertaken to help elucidate the nature of the unpaired spin in the molecule.

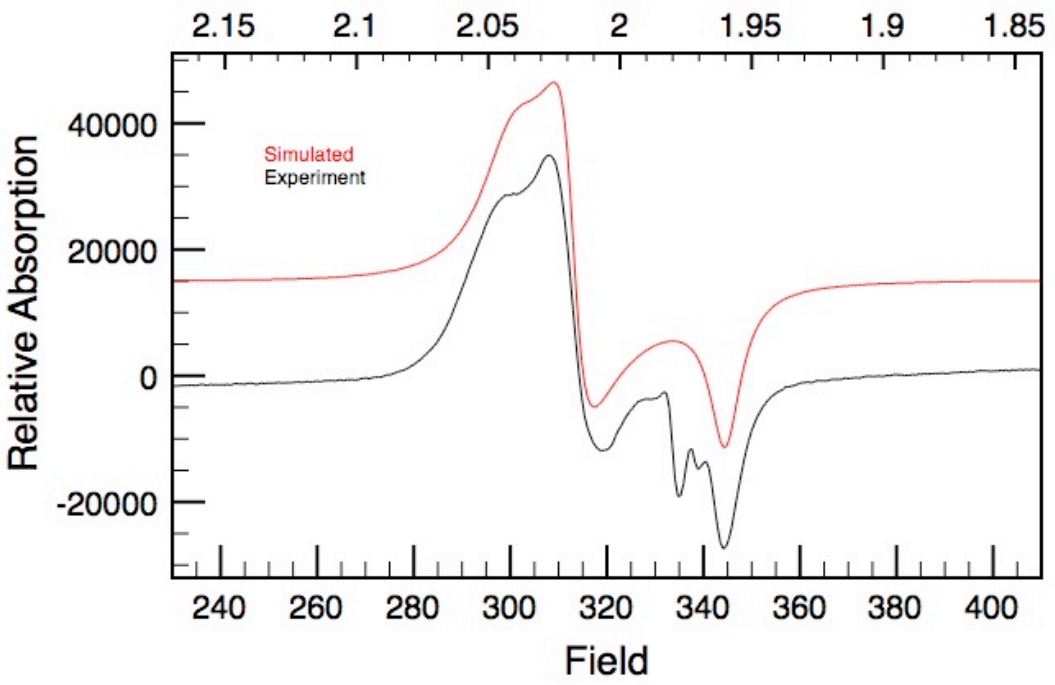

Figure 6.19 The 4 K EPR spectrum of **[Na-18-Crown-6][(^{iPr}PDI)Fe(N_2)]** obtained in a THF glass.

The rhombic signal obtained for [Na-18-Crown-6][(^{iPr}PDI)Fe(N_2)] is consistent with an $S = ½$ species. The g-values obtained from the simulation are higher than what is expected from an organic centered radical, with a $g_{ave} = 2.117$ from values g_x, g_y, and g_z of 1.954, 2.152, and 2.244, respectively. These high g values are more consistent with an iron-centered spin. The data therefore suggests that the reduction is iron based and the final product is a low-spin Fe (I) compound with a singlet PDI^{2-}.

The reductive chemistry of bis(imino)pyridine iron dinitrogen compounds was next explored with the phenyl backbone version of a reduced dinitrogen complex. (^{iPr}(BPDI)Fe(N_2)$_2$ was dissolved in THF and 1.05 equivalents of sodium naphthalenide was added to the stirring iron solution, eliciting a color change from red to pink. The

volatiles were removed under reduced pressure and the residue was taken into diethyl ether and filtered through Celite. The addition of pentane and cooling to -35 ºC caused the product, [Na][(^{iPr}(BPDI)Fe(N_2)] to precipitate was pink/red crystals. The initial product by IR appeared to have the same sodium binding isomers as [Na][(^{iPr}PDI)Fe(N_2)] (Figure 6.20).

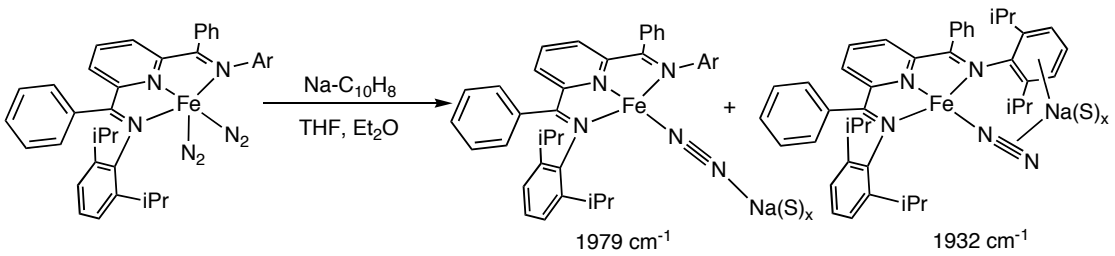

Figure 6.20 The formation of **[Na][(^{iPr}(BPDI)Fe(N_2)]** from **(^{iPr}(BPDI)Fe(N_2)$_2$**.

The IR stretching frequencies for the two isomers are ν(NN) = 1979 cm^{-1} and 1932 cm^{-1}, which are consistent with BPDI being more electron withdrawing than PDI.[24] Attempts to grow an X-ray ray quality crystal of [Na][(^{iPr}(BPDI)Fe(N_2)] were unsuccessful. From the batch of mono-anion crystals, the solid-state structure of the dianionic complex, [Na]$_2$[(^{iPr}(BPDI)Fe(N_2)] was obtained (Figure 6.21). The sodium naphthalenide is in slight excess in the reaction, which accounts for a small quantity of dianion.

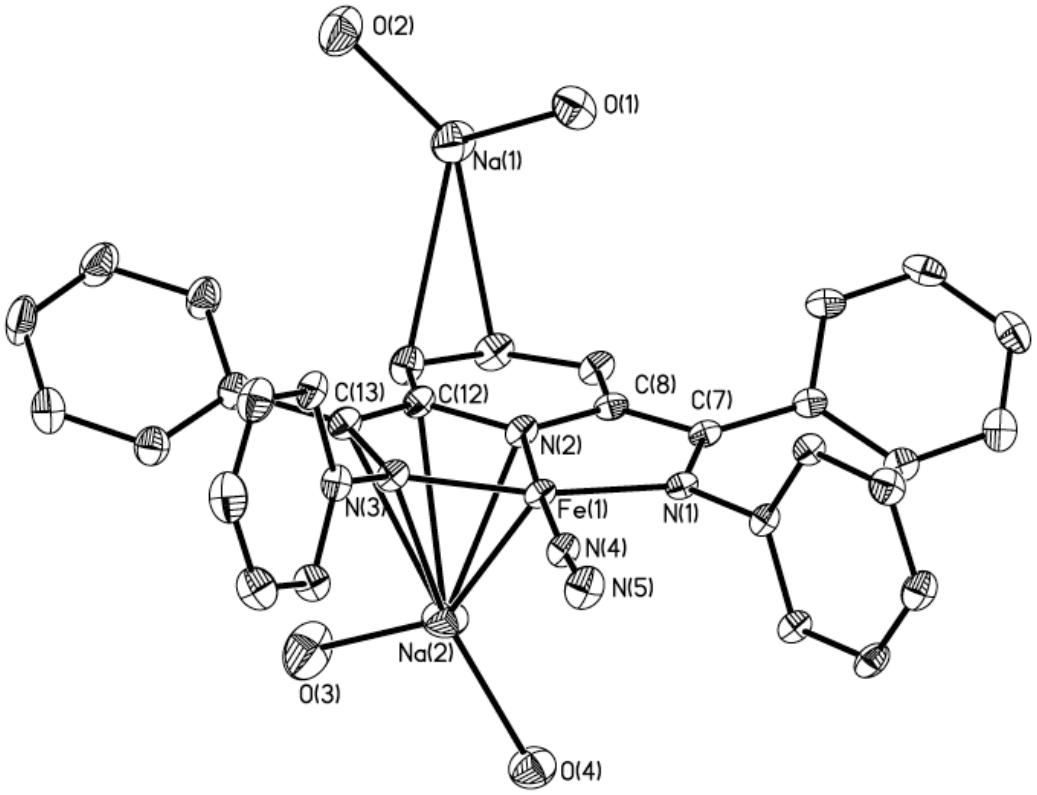

Figure 6.21 The solid-state structure of **$[Na]_2[(^{iPr}(BPDI)Fe(N_2)]$** at 30% probability ellipsoids. Solvent molecules, *iso*-propyl groups, and hydrogen atoms removed for clarity.

A sodium ion is bound to N(5), bridging to another molecule at the pyridine position of the neighboring molecule. The sodium is bound directly to the bis(imino)pyridine chelate in two places, distorting the metrical parameters of the ligand and making the comparison to the parameters of $(^{iPr}(BPDI)Fe(N_2)_2$ difficult. The imine bond bound to the sodium ion, N(3)-C(13), exhibits a C-N bond length of 1.419(2) Å, much longer than the non-sodium bound imine bond length of 1.393(2) Å. Selected metrical parameters of $[Na]_2[(^{iPr}(BPDI)Fe(N_2)]$ are presented in Table 6.4.

Table 6.4 Selected metrical parameters of **$[Na]_2[(^{iPr}(BPDI)Fe(N_2)]$** compared to **$(^{iPr}(BPDI)Fe(N_2)_2$**.

$[Na]_2$-$[(^{iPr}(BPDI)Fe(N_2)]$	**Å or º**	**$(^{iPr}(BPDI)Fe(N_2)_2$**	**Å or º**
Fe(1)-N(1)	1.866(2)	Fe(1)-N(1)	1.945(2)
Fe(1)-N(2)	1.852(2)	Fe(1)-N(2)	1.836(2)
Fe(1)-N(3)	2.106(3)	Fe(1)-N(3)	1.947(2)
Fe(1)-N(4)	1.874(2)	Fe(1)-N(4)	1.834(2)
N(1)-C(7)	1.393(2)	N(1)-C(2)	1.355(7)
N(3)-C(13)	1.419(2)	N(3)-C(8)	1.344(7)
N(2)-C(8)	1.389(2)	N(2)-C(7)	1.379(6)
N(2)-C(12)	1.407(2)	N(2)-C(3)	1.376(7)
C(12)-C(13)	1.402(3)	C(2)-C(3)	1.430(7)
C(7)-C(8)	1.417(2)	C(7)-C(8)	1.429(8)
N(1)-Fe(1)-N(2)	81.23(6)	N(1)-Fe(1)-N(2)	80.9(2)
N(1)-Fe(1)-N(3)	162.20(6)	N(1)-Fe(1)-N(3)	160.2(2)
N(2)-Fe(1)-N(3)	81.23(6)	N(2)-Fe(1)-N(3)	79.3(2)
N(1)-Fe(1)-N(2)	177.38(7)	N(1)-Fe(1)-N(2)	160.9(2)

The dianionic complex was synthesized by the addition of 3 equivalents of sodium naphthalenide to $(^{iPr}(BPDI)Fe(Br)_2$ in THF, followed by removal of the THF. Diethyl ether was added to the residue, and the solution was filtered through Celite, layered with pentane and cooled to -35 ºC to induce precipitation of $[Na]_2[(^{iPr}(BPDI)Fe(N_2)]$. The product contained two stretches in the IR at 1908 cm^{-1} and 1830 cm^{-1} for two different sodium-binding isomers. The first isomer is the one crystallographically characterized with a bridging sodium ion. These two isomers are presented in Figure 6.22.

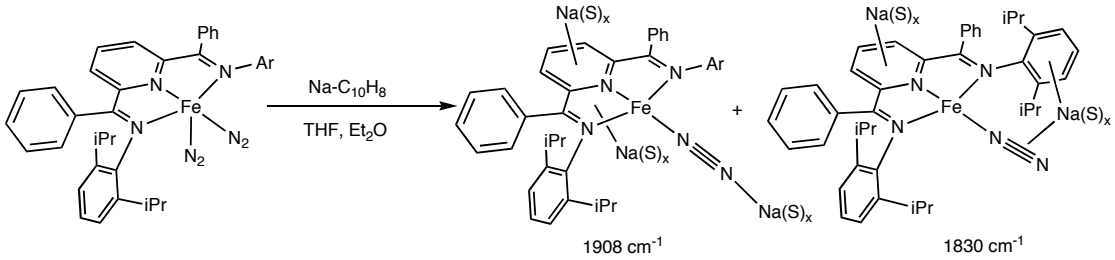

Figure 6.22 Proposed isomers of **$[Na]_2[(^{iPr}(BPDI)Fe(N_2)]$**.

The same synthetic route to form a single isomer of the type $[Na][(^{iPr}(BPDI)Fe(N_2)]$ was used to yield single isomers of $[Na][(^{iPr}(BPDI)Fe(N_2)]$ and $[Na]_2[(^{iPr}(BPDI)Fe(N_2)]$. The addition of 18-crown-6 in the synthesis of both complexes afforded the compounds $[Na(18\text{-crown-6})(THF)_2][(^{iPr}(BPDI)Fe(N_2)]$ and $[Na(18\text{-crown-6})(THF)_2]_2[(^{iPr}(BPDI)Fe(N_2)]$. The IR stretching frequency of $[Na(18\text{-crown-6})(THF)_2][(^{iPr}(BPDI)Fe(N_2)]$ occurs at 1971 cm^{-1}, consistent with the more electron withdrawing chelate as compared to $[Na(18\text{-crown-6})(THF)_2]$-$[(^{iPr}(PDI)Fe(N_2)]$ with a stretching frequency at 1948 cm^{-1}. The Mössbauer spectrum was obtained at 80 K which displayed an isomer shift of $\delta = 0.30$ mm/s and a quadrupole splitting of $\Delta E_Q = 1.08$ mm/s. With a measured solid-state magnetic measurement at 290 K yielding a $\mu_{eff} = 1.7$ μB, the electronic structure of the complex can be assumed to be similar to $[Na\text{-}18\text{-}Crown\text{-}6][(^{iPr}PDI)Fe(N_2)]$, containing an Fe (I) center and a singlet PDI^{2-}, and the higher isomer shift attributed to the more electron-withdrawing nature of BPDI as opposed to PDI.

$[Na(18\text{-crown-6})(THF)_2]_2[(^{iPr}(BPDI)Fe(N_2)]$ contained a single N_2 stretch at 1887 cm^{-1}, consistent with a more reduced complex. The Mössbauer spectrum was obtained at 80 K which displayed an isomer shift of $\delta = 0.15$ mm/s and a quadrupole splitting of $\Delta E_Q = 1.49$ mm/s (Fugure 6.23).

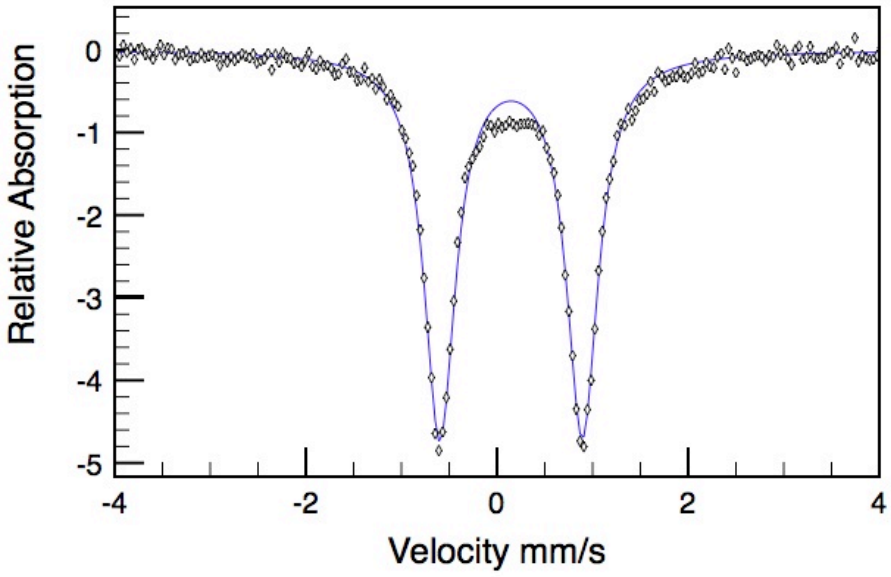

Figure 6.23 Zero-field ^{57}Fe Mössbauer spectrum of **[Na-15-Crown-5]$_2$-[(^{iPr}BPDI)Fe(N$_2$)]** recorded at 80 K.

The Mössbauer isomer shift among the three-electron series starting with (^{iPr}(BPDI)Fe(N$_2$) change by approximately 0.15 mm/s upon the addition of one electron. Given that the electronic structure of [Na(18-crown-6)(THF)$_2$][(^{iPr}(BPDI)Fe(N$_2$)] is similar to [Na(18-crown-6)(THF)$_2$][(^{iPr}(PDI)Fe(N$_2$)] as an iron (I) species with a singlet [PDI]$^{2-}$, [Na(18-crown-6)(THF)$_2$]$_2$[(^{iPr}(BPDI)Fe(N$_2$)] is most likely reduced at the bis(imino)pyridine chelate, yielding an iron (I), [PDI]$^{3-}$ species with antiferromagnetic coupling to yield the overall diamagnetic molecule. The electron withdrawing properties of BPDI allow for this electronic structure, whereas the synthesis of the dianionic (^{iPr}(PDI)Fe(N$_2$) compound remains elusive.

6.5 Conclusion

The oxidation and reduction chemistry of neutral ligand complexes was explored. [(^{iPr}PDI)Fe(CO)$_2$][BArF$_{24}$] was synthesized by the oxidation of

(^{iPr}PDI)Fe(CO)$_2$ with [Cp$_2$Fe][BArF$_{24}$] and was determined to be a low-spin Fe(I) with a neutral bis(imino)pyridine chelate. The anionic complex [Na-15-Crown-5]-[(^{iPr}PDI)Fe(CO)$_2$] was not structurally characterized, but based on EPR spectroscopy, the unpaired electron was determined to be a ligand based spin, indicating reduction of the bis(imino)pyridine ligand to [PDI]$^{2-}$, and the iron center is reduced to a low-spin Fe(I). The oxidation of (^{iPr}PDI)Fe(N$_2$)$_2$ in diethyl ether with [Cp$_2$Fe][BArF$_{24}$] yielded the cationic complex [(^{iPr}PDI)Fe(Et$_2$O)][BArF$_{24}$]. This compound was determined to be high-spin ferrous with a 1 electron reduced bis(imino)pyridine chelate. EPR data and SQUID measurements confirm this assignment. The reduction of (^{iPr}PDI)Fe(N$_2$)$_2$ resulted in the formation of two isomers of the anionic [Na][(^{iPr}PDI)Fe(N$_2$)], yet a single non-interaacting salt pair was formed with the use of 18-crown-6 to yield [Na(18-crown-6)(THF$_2$)][(^{iPr}PDI)Fe(N$_2$)]. [Na(18-crown-6)(THF$_2$)][(^{iPr}PDI)Fe(N$_2$)] was determined to be a low spin iron (I) complex with a [PDI]$^{2-}$ supporting chelate. (^{iPr}BPDI)Fe(N$_2$)$_2$ was reduced to both the anionic and dianionic complexes, although both complexes contained at least two distinguishable isomers. One isomer of the dianionic complex [Na]$_2$[(^{iPr}(BPDI)Fe(N$_2$)] was structurally characterized, and contained two interacting sodium ions. However, the use of a chelating crown ether resulted in the formation of the single species [Na(18-crown-6)(THF)$_2$]-[(^{iPr}(BPDI)Fe(N$_2$)] and [Na(18-crown-6)(THF)$_2$]$_2$[(^{iPr}(BPDI)Fe(N$_2$)] when the single- and di-reductions were employed with the use of the cryptand. [Na(18-crown-6)(THF)$_2$][(^{iPr}(BPDI)Fe(N$_2$)] was determined to contain a low spin iron (I) center supported by a doubly reduced chelate. The reduction to [Na(18-crown-6)(THF)$_2$]$_2$[(^{iPr}(BPDI)Fe(N$_2$)] occurred in bis(imino)pyridine chelate, yielding an Iron (I) center and a [BPDI]$^{3-}$ ligand. Both the cationic [(^{iPr}PDI)Fe(Et$_2$O)][BArF$_{24}$] and the anionic [Na][(^{iPr}PDI)Fe(N$_2$)] proved to be useful starting materials for other reagents.

6.6 Experimental Procedures

General Considerations. All air- and moisture-sensitive manipulations were carried out using standard vacuum line, Schlenk, and cannula techniques or in an MBraun inert atmosphere dry box containing an atmosphere of purified nitrogen. Solvents for air- and moisture-sensitive manipulations were initially dried and deoxygenated using literature procedures.[25] Benzene-d_6 was purchased from Cambridge Isotope Laboratories and dried over 4 Å molecular sieves. The complexes (^{iPr}PDI)Fe(N_2)$_2$,[11] (^{iPr}BPDI)Fe(N_2)$_2$,[24] and (^{iPr}PDI)Fe(CO)$_2$[18] were prepared according to literature procedures.

^{1}H NMR spectra were recorded on Varian Mercury 300, Inova 400, 500, and 600 spectrometers operating at 299.76, 399.78, 500.62, and 599.78 MHz, respectively. ^{13}C NMR spectra were recorded on an Inova 500 spectrometer operating at 125.893 MHz. All ^{1}H and ^{13}C NMR chemical shifts are reported relative to $SiMe_4$ using the ^{1}H (residual) and ^{13}C chemical shifts of the solvent as a secondary standard. For diamagnetic complexes, many assignments were made based on COSY and HSQC NMR experiments. Solution magnetic moments were determined by Evans method[26] using a ferrocene standard and are the average value of at least two independent measurements. Magnetic susceptibility balance measurements were performed with a Johnson Matthey instrument that was calibrated with $HgCo(SCN)_4$. Peak widths at half heights are reported for paramagnetically broadened and shifted resonances. Infrared spectra were collected on a Thermo Nicolet spectrometer. Elemental analyses were performed at Robertson Microlit Laboratories, Inc., in Madison, NJ.

Single crystals suitable for X-ray diffraction were coated with polyisobutylene oil in a drybox, transferred to a nylon loop and then quickly transferred to the goniometer head of a Bruker X8 APEX2 diffractometer equipped with a molybdenum X-ray tube (l = 0.71073 Å). Preliminary data revealed the crystal system. A

hemisphere routine was used for data collection and determination of lattice constants. The space group was identified and the data were processed using the Bruker SAINT+ program and corrected for absorption using SADABS. The structures were solved using direct methods (SHELXS) completed by subsequent Fourier synthesis and refined by full-matrix least-squares procedures.

Mössbauer data were collected on an alternating constant-acceleration spectrometer. The minimum experimental line width was 0.24 mm s^{-1} (full width at half height). A constant sample temperature was maintained with an Oxford Instruments Variox or an Oxford Instruments Mössbauer-Spectromag 2000 cryostat. Reported isomer shifts (δ) are referenced to iron metal at 293 K.

Preparation of [(^{iPr}PDI)Fe(CO)$_2$][BArF$_{24}$]. A 20 mL scintillation vial was charged with 0.110 g (0.185 mmol) of (^{iPr}PDI)Fe(CO)$_2$, and 0.200 g (0.184 mmol) of [Cp_2Fe][$BArF_{24}$], and a stir bar. Approximately 7 mL of benzene were added to the mixture of solids with stirring. The stirring rate was increased as the reaction mixture thickened and a precipitate formed. After 15 minutes, an equal volume of pentane was added and the stirring was continued for another ten minutes. The solid was collected on a glass frit and washed with 4 x ~ 20mL of pentane. The solid was dried under vacuum and yielded 0.260 g (98%) of a dark black/purple powder identified as [(^{iPr}PDI)$FeCO_2$][$BArF_{24}$]. Analysis for $C_{67}H_{55}N_3FeBF_{24}O_2$: Calcd C, 55.24; H, 3.81; N, 2.88. Found: C, 55.33; H, 3.67; N, 2.81. IR (KBr): ν(CO) = 2028 and 1981 cm^{-1} ν(^{13}CO) = 1982 and 1937 cm^{-1}. Magnetic susceptibility (MSB, 23 ºC): μ_{eff} = 2.0 μ_B. ^{1}H NMR (benzene-d_6): δ 1.40 (569 Hz), 4.32 (370 Hz), 7.35 (18 Hz), 7.58 (12 Hz), 7.76 (15 Hz), 9.44 (45 Hz).

Preparation of [Na-15-Crown-5] [(^{iPr}PDI)Fe(CO)$_2$]. A 20 mL scintillation vial was charged with 0.200 g (0.185 mmol) of (^{iPr}PDI)Fe(CO)$_2$ and 10 mL of diethyl ether. A 1 % sodium amalgam (6 eq.) was prepared in a separate vial in pentane. The amalgam was added to the stirring iron solution. After the amalgam was added, 0.080 g of 15-crown-5 was added (1.1 eq.). The solution was stirred for approximately 60 minutes, at which time there was a bright green precipitate that was collected on a glass frit. The green powder was washed with toluene (3 * 10mL) and pentane to yield 0.120 g of a green powder identified as [Na-15-Crown-5] [(^{iPr}PDI)Fe(CO)$_2$]. Analysis for $C_{67}H_{55}N_3FeBF_{24}O_2$: IR (KBr): ν(CO) = 1985 and 1963 cm^{-}. Magnetic susceptibility (MSB, 23 ºC): μ_{eff} = 1.9 μ_B.

Preparation of [(^{iPr}PDI)FeOEt$_2$][BArF$_{24}$]. A 20 mL scintillation vial was charged with 0.140 g (0.236 mmol) of (^{iPr}PDI)Fe(N$_2$)$_2$, and 0.247 g (0.236 mmol) of [Cp$_2$Fe][BArF$_{24}$], and a stir bar. Approximately 7 mL of diethyl ether was added to the mixture of solids with stirring. The reaction evolved nitrogen gas immediately and changed color to light green from dark green. Pentane was added after the evolution of gas ceased, and the scintillation vial was cooled to -35 ºC, precipitating a light green solid. The solid was collected on a glass frit and washed with 4 x ~ 20mL of pentane. The solid was dried under vacuum and yielded 0.250 g (73%) of a light green powder identified as [(^{iPr}PDI)FeOEt$_2$][BArF$_{24}$]. Analysis for $C_{69}H_{65}N_3FeBF_{24}O$: Calcd C, 56.19; H, 4.44; N, 2.85. Found: C, 56.34; H, 4.67; N, 2.81. Magnetic susceptibility 290 K: μ_{eff} = 5.2 μ_B. ^{1}H NMR (benzene-d_6): δ 1.29 (569 Hz, Et$_2$O), 4.12 (370 Hz, Et$_2$O), 8.44 (18 Hz), 9.67 (12 Hz). ^{19}F NMR (benzene-d_6): 62.30.

Synthesis of [Na][(^{iPr}PDI)Fe(N$_2$)].

To a scintillation vial is added 0.004 g (0.174 mmol) of sodium and 0.022 g (0.182 mmol) of naphthalene, followed by 5 mL of THF. This solution was stirred until the sodium was dissolved completely, and then was added to a stirring solution of 0.100 g (0.168 mmol) of (^{iPr}PDI)Fe(N_2)$_2$ in THF. The resultant solution was filtered through Celite and the volatiles were removed. The residue was mobilized by the addition of diethyl ether and the solid was collected on a glass frit and washed with pentane and dried under vacuum, yielding 0.090 g of a product identified as [Na][(^{iPr}PDI)Fe(N_2)]. IR (KBr): $\nu(N_2)$ = 1966 and 1914 cm^{-1}

Preparation of [Na(18-Crown-6)(THF)$_2$][(^{iPr}PDI)Fe(N_2)]. A scintillation vial was charged with 0.012 g (0.522 mmol) of sodium, 0.075 g (0.575 mmol) of naphthalene and approximately 10 mL of THF. The solution was stirred until the sodium was completely dissolved. Once this occurred, the sodium naphthalenide solution was added dropwise to a solution containing 0.310 g (0.522 mmol) of (^{iPr}PDI)Fe(N_2)$_2$ in THF. The resulting reaction mixture was filtered through Celite and 0.140 g (0.530 mmol) of 18-crown-6 was added and the volatiles were removed. The residue was dissolved in THF and the product was precipitated with excess pentane. The resulting dark brown powder was collected on a glass frit and washed with pentane and dried under vacuum, yielding 0.390 g (75 %) of a product identified as [Na(18-Crown-6)(THF)$_2$][(^{iPr}PDI)Fe(N_2)]. Analysis for $C_{53}H_{81}FeN_5NaO_8$: Calcd C, 63.84; H, 8.39; N, 7.02. Found: C, 63.77; H, 7.94; N, 6.71. Solid state magnetic susceptibility (23 ºC): μ_{eff} = 1.8 μ_B. IR (KBr): $\nu(N_2)$ = 1949 cm^{-1}.

Synthesis of [Na][(^{iPr}BPDI)Fe(N_2)]. To a scintillation vial is added 0.004 g (0.174 mmol) of sodium and 0.022 g (0.182 mmol) of naphthalene, followed by 5 mL of THF. This solution was stirred until the sodium was dissolved completely, and then

was added to a stirring solution of 0.120 g (0.168 mmol) of (^{iPr}BPDI)Fe(N_2)$_2$ in THF. The resultant solution was filtered through Celite and the volatiles were removed. The residue taken into diethyl ether and filtered through Celite again, and the volume reduced by roughly ½. An equal volume of pentane was added and the solution was cooled to -35 ºC. The solid was collected on a glass frit and washed with pentane and dried under vacuum, yielding 0.083 g of a product identified as [Na][(^{iPr}BPDI)Fe(N_2)]. IR (KBr): $\nu(N_2)$ = 1979 and 1932 cm^{-1}

Preparation of [Na(18-Crown-6)(THF)$_2$][(^{iPr}BPDI)Fe(N_2)]. This molecule was prepared in a similar manner to [Na(18-Crown-6)(THF)$_2$][(^{iPr}PDI)Fe(N_2)] with 0.012 g (0.522 mmol) of sodium, 0.075 g (0.575 mmol) of naphthalene, 0.140 g (0.174 mmol) of (^{iPr}BPDI)FeBr$_2$ and 0.050 g (0.190 mmol) of 18-crown-6. This procedure yielded 0.139 g (73 %) of a bright pink powder identified as [Na(18-Crown-6)(THF)$_2$][(^{iPr}PDI)Fe(N_2)]. Analysis for $C_{63}H_{87}FeN_5NaO_8$: Calcd C, 67.49; H, 7.82; N, 6.25. Found: C, 67.55; H, 7.80; N, 6.21. Solid state magnetic susceptibility (23 ºC): μ_{eff} = 1.7 μ_B. IR (KBr): $\nu(N_2)$ = 1971 cm^{-1}.

Synthesis of [Na]$_2$[(^{iPr}BPDI)Fe(N_2)]. To a scintillation vial is added 0.008 g (0.348 mmol) of sodium and 0.045 g (0.364 mmol) of naphthalene, followed by 5 mL of THF. This solution was stirred until the sodium was dissolved completely, and then was added to a stirring solution of 0.120 g of (^{iPr}BPDI)Fe(N_2)$_2$ in THF. The resultant solution was filtered through Celite and the volatiles were removed. The residue taken into diethyl ether and filtered through Celite again, and the volume reduced by roughly ½. An equal volume of pentane was added and the solution was cooled to -35 ºC. The solid was collected on a glass frit and washed with pentane and dried under vacuum,

yielding 0.110 g of a product identified as $[Na]_2[(^{iPr}BPDI)Fe(N_2)]$. IR (KBr): $\nu(N_2)$ = 1908 and 1830 cm^{-1}

Preparation of $[Na(18\text{-Crown-6})(THF)_2]_2[(^{iPr}BPDI)Fe(N_2)]$. A scintillation vial was charged with 0.020 g (0.869 mmol) of sodium and 0.125 g (0.958 mmol) of naphthalene followed by approximately 10 mL of THF. The solution was stirred until the sodium was completely dissolved. Once this occurred, the sodium naphthalenide solution was added dropwise to a solution containing 0.175 g (0.216 mmol) of $(^{iPr}BPDI)FeBr_2$ in THF. The resulting reaction mixture was filtered through Celite and 0.115 g (0.435 mmol) of 18-crown-6 was added and the volatiles were removed. The residue was dissolved in THF and the product was precipitated with excess pentane and the dark purple powder was collected on a glass frit and washed with pentane and dried under vacuum, yielding 0.235 g (70 %) of a product identified as $[Na(18\text{-Crown-6})(THF)_2][(^{iPr}PDI)Fe(N_2)]$. Analysis for $C_{83}H_{127}FeN_5Na_2O_{16}$: Calcd C, 64.20; H, 8.24; N, 4.51. Found: C, 63.96; H, 8.08; N, 3.92. IR (KBr): $\nu(N_2)$ = 1887 cm^{-1}.

RFERENCES

[1] a) Small, B. M.; Brookhart, M. *J. Am. Chem. Soc.* **1998**, *120*, 7143. b) Small, B. L.; Brookhart, M.; Bennett, A. M. A. *J. Am. Chem. Soc.* **1998**, *120*, 4049.

[2] Britovsek, G. J. P.; Gibson, V. C.; Kimberley, B. S.; Maddox, S. J.; Solan, G. A.; White, A. J. P.; Williams, D. J. *Chem. Commun.* **1998**, 849.

[3] Britovsek, G. J. P.; Bruce, M.; Gibson, V. C.; Kimberely, B. S.; Maddox, P. J.; Mastroianni, S.; McTavish, S. J.; Redshaw, C.; Solan, G. A.; Strömberg, S.; White, A. J. P.; Williams, D. J. *J. Am. Soc.* **1999**, *121*, 8728.

[4] Brookhart, M.; Grant, B.; Volpe, A. F. Jr. *Organometallics* **1992**, *11*, 3920.

[5] Chen, E. Y. X.; Marks, T. J. *Chem. Rev.* **2000**, *100*, 1391.

[6] Yang, X. M.; Stern, C. L.; Marks, T. J. *J. Am. Chem. Soc.* **1994**, *116*, 10015.

[7] Chien, J. C. W.; Tsai, W.-M.; Rausch, M. D. *J. Am. Chem. Soc.* **1991**, *113*, 8570.

[8] Bouwkamp, M. W.; Lobkovsky, E.; Chirik, P. J. *J. Am. Chem. Soc.* **2005**, *127*, 9660.

[9] Knijnenburg, Q.; Gambarotta, S.; Budzelaar, P. H. M. *Dalton Trans.* **2006**, 5442.

[10] Butin, K. P.; Beloglazkina, E. K.; Zyk, N. V. *Russ. Chem. Rev.* **2005**, *74*, 531.

[11] Kuwabara, I. H.; Comninos, F. C. M.; Pardini, V. L.; Viertler, H.; Toma, H. E. *Electrochim. Acta* **1994**, *39*, 2401.

[12] Toma, H. E.; Chavez-Gil, T. E. *Inorg. Chim. Acta* **1997**, *257*, 197.

[13] de Bruin, B.; Bill, E.; Bothe, E.; Weyermüller, T.; Wieghardt, K. *Inorg. Chem.* **2000**, *39*, 2936.

[14] Budzelaar, P. H. M.; de Bruin, B.; Gal, A. W.; Wieghardt, K.; van Lenthe, J. H. *Inorg. Chem.* **2001**, *40*, 4649.

[15] Tondreau, A. M.; Milsmann, C.; Patrick, A. D.; Hoyt, H. M.; Lobkovsky, E.; Wieghardt, K.; Chirik, P. J. *J. Am. Chem. Soc.* **2010***,* 132, 15046.

[16] Bouwkamp, M. W.; Bart, S. C.; Hawrelak, E. J.; Trovitch, R. J.; Lobkovsky. E.; Chirik, P. J. *Chem. Commun.* **2005**, 3406.

[17] Bart, S. C.; Chlopek, K.; Bill, E.; Bouwkamp, M. W.; Lobkovsky, E.; Neese, F.; Wieghardt, K.; Chirik, P. J. *J. Am. Chem. Soc.* **2006**, *128*, 13901.

[18] Bart, S. C.; Lobkovsky, E.; Chirik, P. J. *J. Am. Chem. Soc*. **2004**, *126*, 13794.

[19] Bouwkamp, M. W.; Bowman, A. C.; Lobkovsky, E.; Chirik, P. J. *J. Am. Chem. Soc.* **2006,** *128*, 41, 13340.

[20] Sylvester, K. T.; Chirik, P. C.; *J. Am. Chem. Soc.* **2009**, *131*, 8772.

[21] Bart, S. C.; Lobkovsky, E.; Bill, E.; Wieghardt, K.; Chirik, P. J.; *Inorg. Chem.* **2007**, 46, 7055.

[22] Scott, J.; Vidyaratne, I.; Korobkov, I.; Gambarotta, S.; Budzelaar, H. M. *Inorg. Chem.* **2008**, 47, 896.

[23] See Chapter 1 of this dissertation.

[24] Archer, A. M.; Bouwkamp, M. W.; Cortez, M. P.; Lobkovsky, E.; Chirik, P. J.; *Organometallics* **2006**, 25, 4269.

[25] Pangborn, A. B.; Giardello, M. A.; Grubbs, R. H.; Rosen, R. K.; Timmers, F. J. *Organometallics* **1996**, *15*, 1518.

[26] Sur, S. K. *J. Magn. Reson.* **1989**, *82*, 169.

APPENDIX A

PRELIMINARY INVESTIGATIONS

A.1 Bis(imino)pyridine Iron Isocyanate Complexes

The addition of a stiochiometric quatity of AgNCO as a solid to a stirring toluene solution of (^{iPr}PDI)Fe(N_2)$_2$ resulted in the generation of N_2 and a color change of the dark green solution to a bright green solution. The green solution was filtered through celite and the volatiles were removed. The residue was slurried in pentane and cooled to -35 ºC before collecting the green solid, identified as (^{iPr}PDI)Fe(NCO),on a glass frit.

(^{iPr}PDI)Fe(NCO) displayed an ^{1}H NMR spectrum consistent with a C_{2v} symmetric molecule. The proton resonances in the ^{1}H NMR spectrum were spread over 400 ppm, similar to complexes (^{iPr}PDI)Fe(Cl) and (^{iPr}PDI)Fe(Br). The solid-state magnetic measurement of the complex yielded an effective magnetic moment at 290 K of 3.8 μ_B. This indicates that (^{iPr}PDI)Fe(NCO) is a electronically similar to the mono halide compounds, with a high-spin ferrous center antiferromagnetically coupled to a mono-reduced bis(imino)pyridine chelate. The compound was structurally characterized using x-ray crystallography (Figure A.1.1).

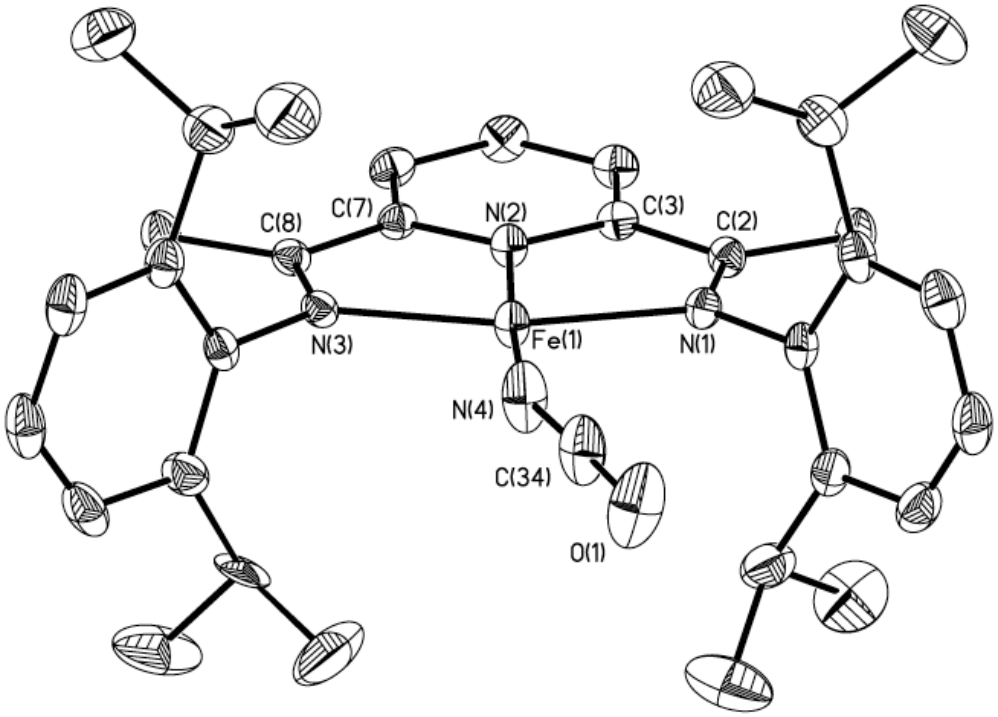

Figure A.1.1 Solid-state structure of **(^{iPr}PDI)Fe(NCO)** shown at 30% probability ellipsoids. Hydrogen atoms removed for clarity.

Mössbauer spectroscopy yielded a temperature dependant isomer shift and quadrupole splitting. At 273 K, the isomer shift was $\delta = 0.57$ and the quadrupole splitting was $\Delta E_Q = 1.30$ mm/s. These parameters are consistent with a high-spin Fe(II) complex similar to (^{iPr}PDI)Fe(Cl). As the temperature was lowered, the quadrupole splitting became much wider and the isomer shift lowered. At 80 K, isomer shift was $\delta = 0.42$ and the quadrupole splitting was $\Delta E_Q = 3.10$ mm/s. Lowering the temperature further to 15 K did not alter the parameters too much much further, with the isomer shift at $\delta = 0.42$ and the quadrupole splitting at $\Delta E_Q = 3.10$ mm/s. As the temperature was lowered, a second species began to grow in, and the peaks became broader. The spectra are shown in Figure A.1.2.

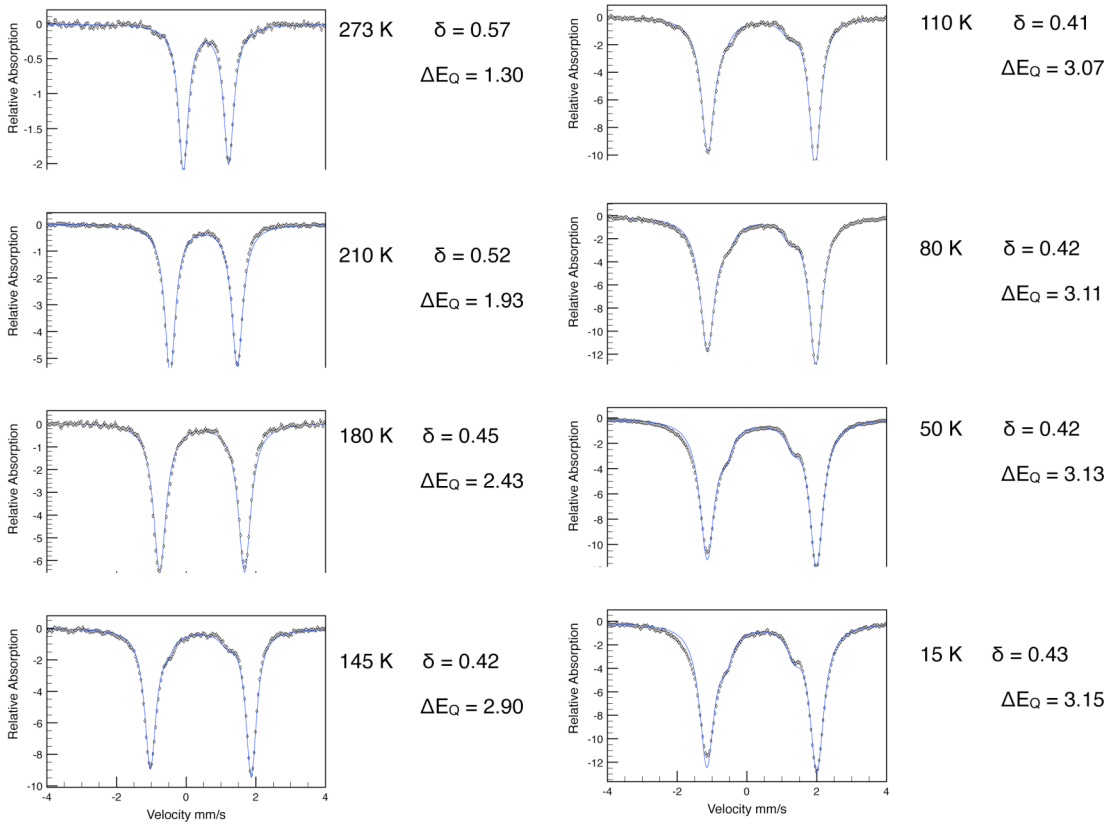

Figure A.1.2 Mössbauer spectra obtained at various temperatures

This dramatic change observed by Mössbauer spectroscopy led to variable temperature SQUID data being collected on (^{iPr}PDI)Fe(NCO). The SQUID data (Figure A.1.3) was consistent with a spin crossover complex, at low temperatures the complex had a μ_{eff} of roughly 1.8 μB, consistent with a spin ½ complex. Upon warming, the μ_{eff} increased to 1.8 μB. This data is consistent with the changes observed by Mössbauer and with (^{iPr}PDI)Fe(NCO) being a spin-crossover complex.

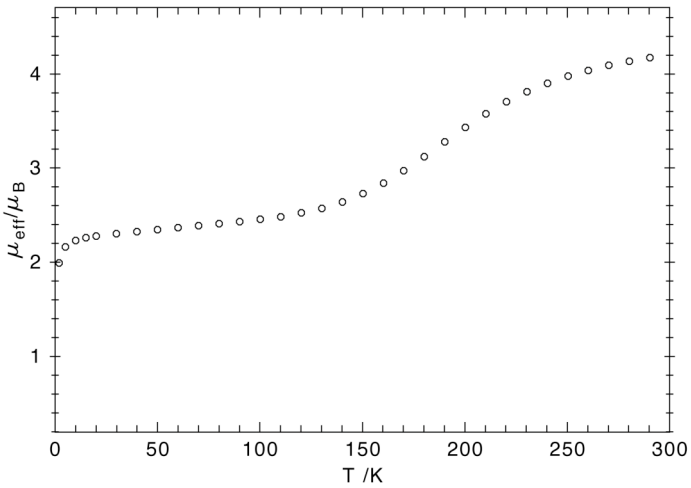

Figure A.1.3 SQUID data of (**^{iPr}PDI)Fe(NCO)** showing the variability if the magnetic moment.

Inconsistent with this data, however, is the EPR. EPR data collected in a toluene glass at 4 K (Figure A.1.4) on (^{iPr}PDI)Fe(NCO) was consistant with an $S = 3/2$ complex. The cause of this contradictory behavior in the EPR versus the SQUID and Mössbauer spectra remains unexplained.

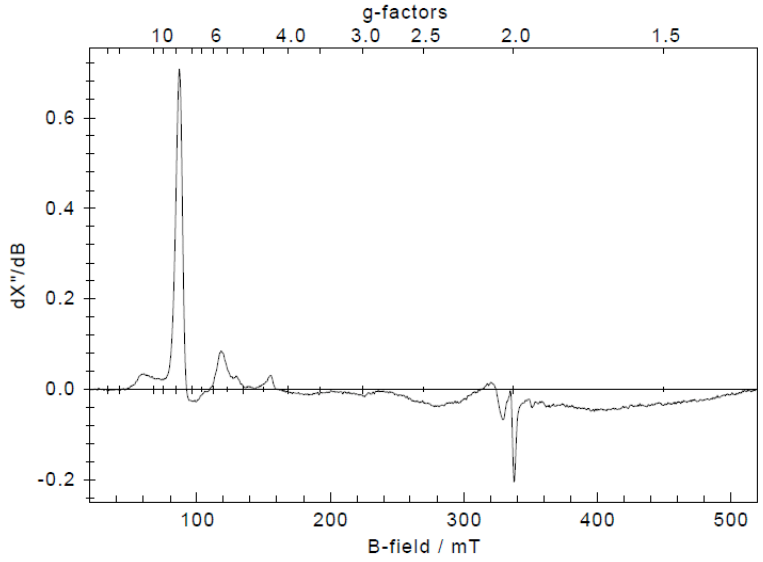

Figure A.1.4 EPR spectrum of **(^{iPr}PDI)Fe(NCO)** in toluene glass at 10 K.

The addition of pyridine to (^{iPr}PDI)Fe(NCO) resulted in the five coordinate complex (^{iPr}PDI)Fe(NCO)(Py). Although not structurally characterized, the geometry is assumed to be similar to other five coordinate complexes of the type (^{iPr}PDI)Fe(X)(L), with the fifth ligand in the apical position of the square based pyramid. The addition of the fifth ligand resulted in a shift of the Mössbauer parameters to isomer shift was $\delta = 0.95$ and the quadrupole splitting was $\Delta E_Q = 1.28$ mm/s. The Mössbauer spectrum is presented in Figure A.1.5

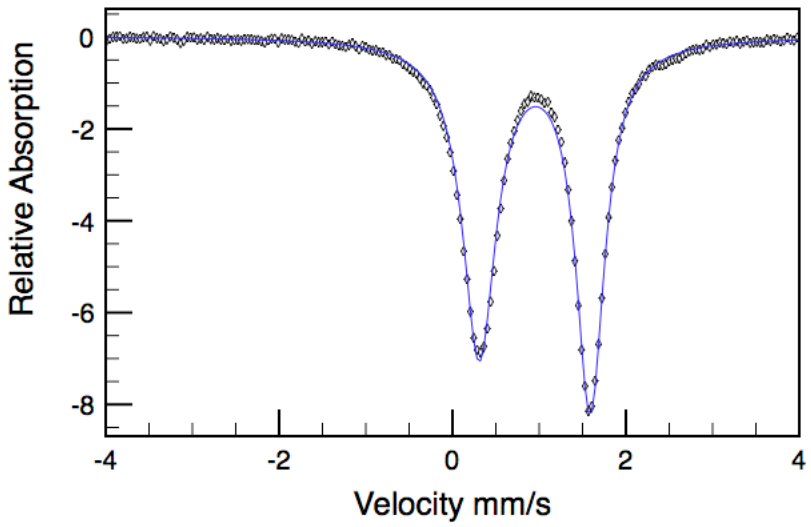

Figure A.1.5 The Mössbauer spectrum of **(^{iPr}PDI)Fe(NCO)** obtained at 80 K.

The parameters of the Mössbauer spectrum are consistent with a high-spin Fe(II) complex. The dramatic shift in the isomer shift from (^{iPr}PDI)Fe(NCO) is due to the lengthening of bonds upon the addition of the fifth ligand in the coordination sphere. This lowers the covalency of the bis(imino)pyridine ligand, increasing the effective charge on the iron nucleus.

Synthesis of (^{iPr}PDI)Fe(NCO). In a 20 mL scintillation vial was added 0.200 grams of (^{iPr}PDI)Fe(N_2)$_2$ and roughly 10 mL of toluene. To the vigorously stirring solution of iron is added X g of AgNCO. Upon addition of the solid, the solution evolves N_2 and a color change to light green. Filtration of the solution through celite and removal of the volatiles gives a light green residue. This residue is slurried with approximately 10 mL of diethyl ether and cooled to -35 ºC. The green solid was collected on a glass frit and dried under vacuum, yielding 0.150 g of (^{iPr}PDI)Fe(NCO). Analysis for $C_{50}H_{54}N_6FeO$: Calcd C, 70.46; H, 7.48; N, 9.67. Found: C, 70.62; H, 7.18; N, 9.79. Magnetic susceptibility: μ_{eff} = 3.8 μ_B (benzene-*d*$_6$). ^{1}H NMR (benzene-*d*$_6$): δ -23.71 (14 Hz, 6H, C(C*H*$_3$)), -17.56 (20 Hz, 12H, Ar-*Me*), 1.03 (21 Hz, 2H, *p-Ar*), 2.16 (13 Hz, 4H, *m-Ar*), 27.65 (15 Hz, 2H, *m-Py*), 57.68 (12 Hz, 1H, *p-Py)*.

Synthesis of (^{iPr}PDI)Fe(NCO)(Py). In a 20 mL scintillation vial was added 0.100 g (0.172 mmol) of (^{iPr}PDI)Fe(NCO) and roughly 10 mL of diethyl ether. To the stirring solution is added 0.025 g (2 eq.) of pyridine. The vial is cooled to -35 ºC, and the dark brown solid was collected on a glass frit and dried under vacuum, yielding 0.060 g of (^{iPr}PDI)Fe(NCO)(Py). Analysis for $C_{50}H_{54}N_6FeO$: Calcd C, 71.11; H, 7.35; N, 10.63. Found: C, 70.84; H, 7.39; N, 10.38. Magnetic susceptibility: μ_{eff} = 3.8 μ_B (benzene-*d*$_6$). ^{1}H NMR (benzene-*d*$_6$): δ -23.71 (14 Hz, 6H, C(C*H*$_3$)), -17.56 (20 Hz, 12H, Ar-*Me*), 1.03 (21 Hz, 2H, *p-Ar*), 2.16 (13 Hz, 4H, *m-Ar*), 27.65 (15 Hz, 2H, *m-Py*), 57.68 (12 Hz, 1H, *p-Py)*.

A.2 Bis(imino)pyridine Iron (Trimethylsilyl)Imide

The addition of one equivalent of (azido)trimethylsilane to a room temperature stirring solution of (^{iPr}PDI)Fe(N_2)$_2$ yielded a bright pink solution. The solution was diluted with an equivalent volume of pentane and filtered through celite, leaving

behind a green, less soluble side product. The volatiles were removed yielding (^{iPr}PDI)Fe(NSiMe$_3$).

(^{iPr}PDI)Fe(NSiMe$_3$) was crystallographically characterized. The unit cell contained two asymmetric units, one of which was disordered in the imide. The non-disordered molecule (Figure A.2.1) contains a linear N(2)-Fe(1)-N(4) bond with and angle of 179.30(11)º, as well as a linear Fe(1)-N(4)-Si(1) bond with an angle of 178.54(17)º. The second molecule in the asymmetric unit is disordered and contains a slightly canted imide, the nitrogen being 7 º out of the plane of the chelate. Selected metrical parameters of the non-disordered molecule are provided in Table A.2.1.

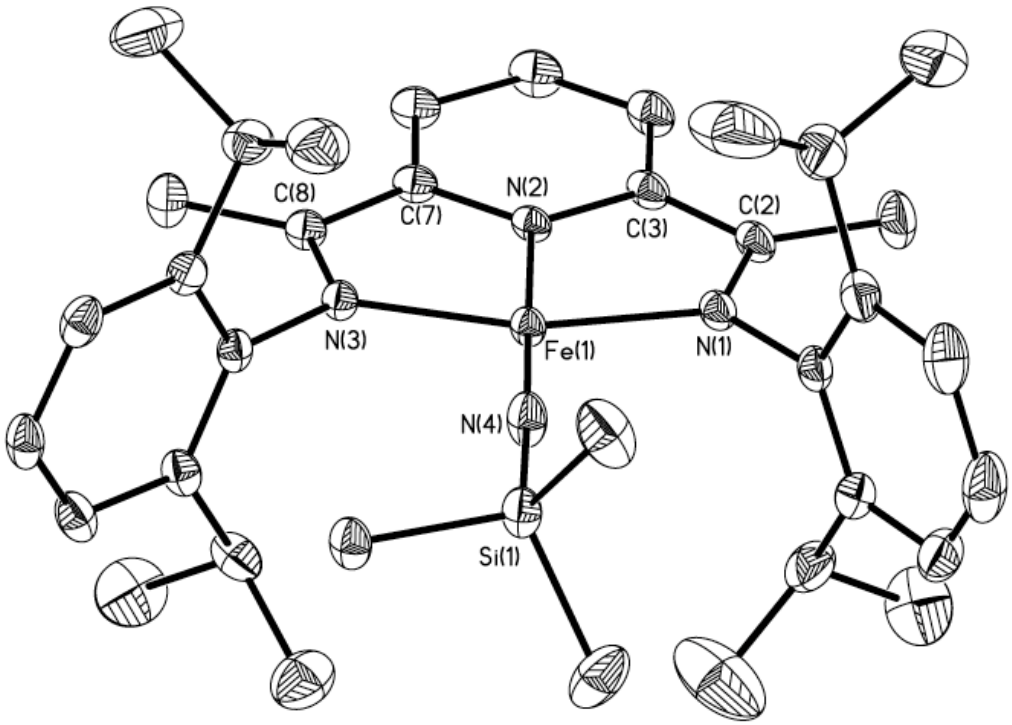

Figure A.2.1 Solid-state structure **(^{iPr}PDI)Fe(NSiMe$_3$)** of shown at 30% probability ellipsoids. Hydrogen atoms removed for clarity.

Table A.2.1 Selected metrical parameters of **(^{iPr}PDI)Fe(NSiMe$_3$)**.

	(^{iPr}PDI)Fe(NSiMe$_3$)		(^{iPr}PDI)Fe(NSiMe$_3$)
Fe(1)-N(1)	1.971(2)	C(2)-C(3)	1.424(4)
Fe(1)-N(2)	1.884(2)	C(7)-C(8)	1.423(4)
Fe(1)-N(3)	1.965(2)		
Fe(1)-N(4)	1.702(2)	N(1)-Fe(1)-N(2)	78.30(9)
		N(1)-Fe(1)-N(4)	101.00(10)
N(1)-C(2)	1.330(3)	N(2)-Fe(1)-N(3)	78.88(9)
N(3)-C(8)	1.328(3)	N(3)-Fe(1)-N(4)	101.82(10)
N(2)-C(3)	1.365(4)	N(2)-Fe(1)-N(4)	179.30(11)
N(2)-C(7)	1.376(3)		
		Fe(1)-N(4)-Si(1)	178.54(17)
N(4)-Si(1)	1.710(2)		

The Mössbauer parameters of (^{iPr}PDI)Fe(NSiMe$_3$) are similar to other bis(imino)pyridine iron imide complexes. The isomer shift was $\delta = 0.20$ and the quadrupole splitting was $\Delta E_Q = 1.44$ mm/s (Figure A.2.2). The solid-state magnetic measurement yielded a μ_{eff} of 3.0 μB, consistent with an $S = 1$ complex.

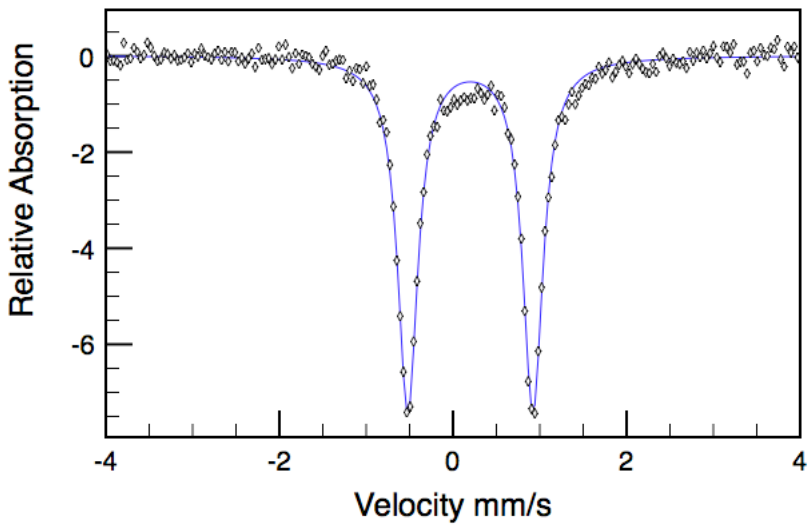

Figure A.2.2 The zero field Mössbauer spectrum of **(^{iPr}PDI)Fe(NSiMe$_3$)**.

The complex (^{iPr}PDI)Fe(NSiMe$_3$) is formally Fe(IV) considering the 2 electron reduced bis(imino)pyridine chelate. The long iron-imide nitrogen bond length of 1.702(2) Å indicates a weaker interaction between the iron nucleus and the imide. This weakened interaction allows for the iron to remain high spin Fe(IV), antiferromagnetically couples to the triplet diradical chelate, yielding an overall triplet spin-state.

Synthesis of (^{iPr}PDI)Fe(NSiMe$_3$). In a 20 mL scintillation vial was added 0.100 grams of (^{iPr}PDI)Fe(N$_2$)$_2$ and roughly 10 mL of diethyl ether. To the stirring solution is added dropwise 0.017 g of (azido)trimethylsilane diluted in 5 mL of diethyl ether. The solution was reduced to in volume by a half, and pentane was added to bring the total volume up to 15 mL. The solution was filtered through celite and the volatiles were removed. yielding 0.080 g of (^{iPr}PDI)Fe(NSiMe$_3$). Analysis for $C_{36}H_{52}N_4FeSi$: Calcd C, 69.21; H, 8.39; N, 8.97. Found: C, 68.80; H, 7.95; N, 8.97. Magnetic susceptibility: μ_{eff} = 3.8 μ_B (benzene-d_6). ^{1}H NMR (benzene-d_6): δ -196.57 (14 Hz, 6H, C(CH_3)), -58.62 (20 Hz, 4H, Ar-*CH*(CH$_3$)$_2$), -13.08 (21 Hz, 12H, Ar-*C*H(CH_3)$_2$), -8.16 (13 Hz, 12H, Ar-*C*H(CH_3)$_2$), -0.84 (15 Hz, 2H, Si*Me*$_3$), 11.18 (15 Hz, 2H, *Ar*), 45.72 (12 Hz, 4H, *m-Ar),* 61.85 (20 Hz, 2H, *m*-Py), 144.17 (12 Hz, 1H, *p-Py).*

A.3 (^{iPr}PDI)Fe(N$_2$)$_2$ Catalyzed *trans*-Addition of Si-H to Terminal Alkynes

The hydrosilylation of 1-hexyne and phenylacetylene with phenylsilane utilizing (^{iPr}PDI)Fe(N$_2$)$_2$ as a catalyst resulted in the *trans* addition of the Si-H bond across the alkyne resulting in the *cis* olefin product. For both 1-hexyne and phenylacetylene, the *cis* olefin products isomerized to the thermodynamically more stable *trans* product under the reaction conditions after 1 hour. In the case of 1-

hexyne, the *cis* product was isolated in > 90 % yield when the reaction mixture was quenched after 2 minutes at 0.4 M substrate in diethyl ether with 2 equivalents of phenylsilane and 5 % (^{iPr}PDI)Fe(N_2)$_2$ loading. Phenylacetylene reacted more slowly than 1-hexyne, and isomerization to the *trans* olefin occurred to approximately 10 % at 95 % conversion. More sterically bulky terminal alkynes such as 3,3-dimethyl-1-propyne and trimethylsilylacetylene yielded only low conversion to the *trans*-product after 12 hours under similar reaction conditions, with no evidence for *trans*-addition of the silane. The reactivity of phenylacetylene and 1-hexyne is shown in Figure A.3.1.

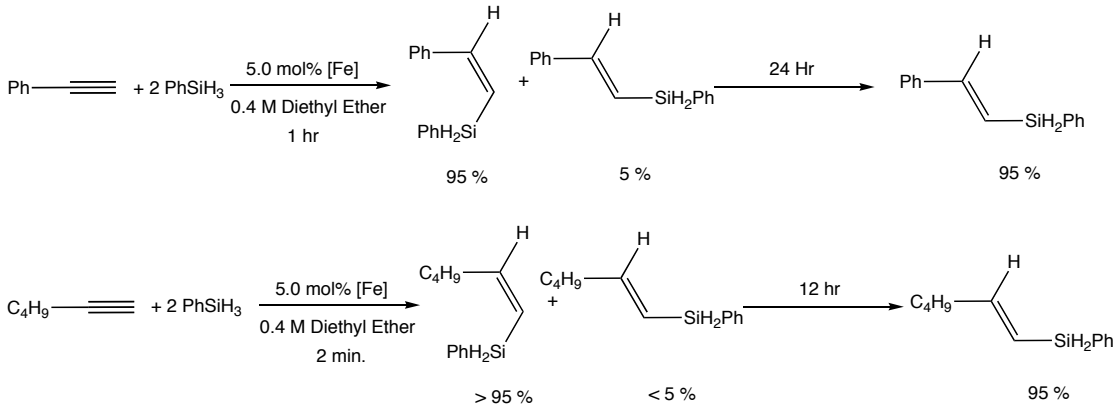

Figure A.3.1 The catalytic *trans* addition of phenylsilane to terminal alkynes, followed by isomerization.

Labeling experiments performed using phenylsilane-*d3* resulted in the formation of the deuterated alkenes in both the α and β positions of the product, indicating reversible C-H activation of the terminal acetylene and exchange with the deuterium atoms of the silane. The converse experiment was performed with the terminal deuterated acetylenes and phenylsilane, and again both positions in the product showed deuterium incorporation, highlighting the exchange of hydrogen atoms (Figure A.3.2).

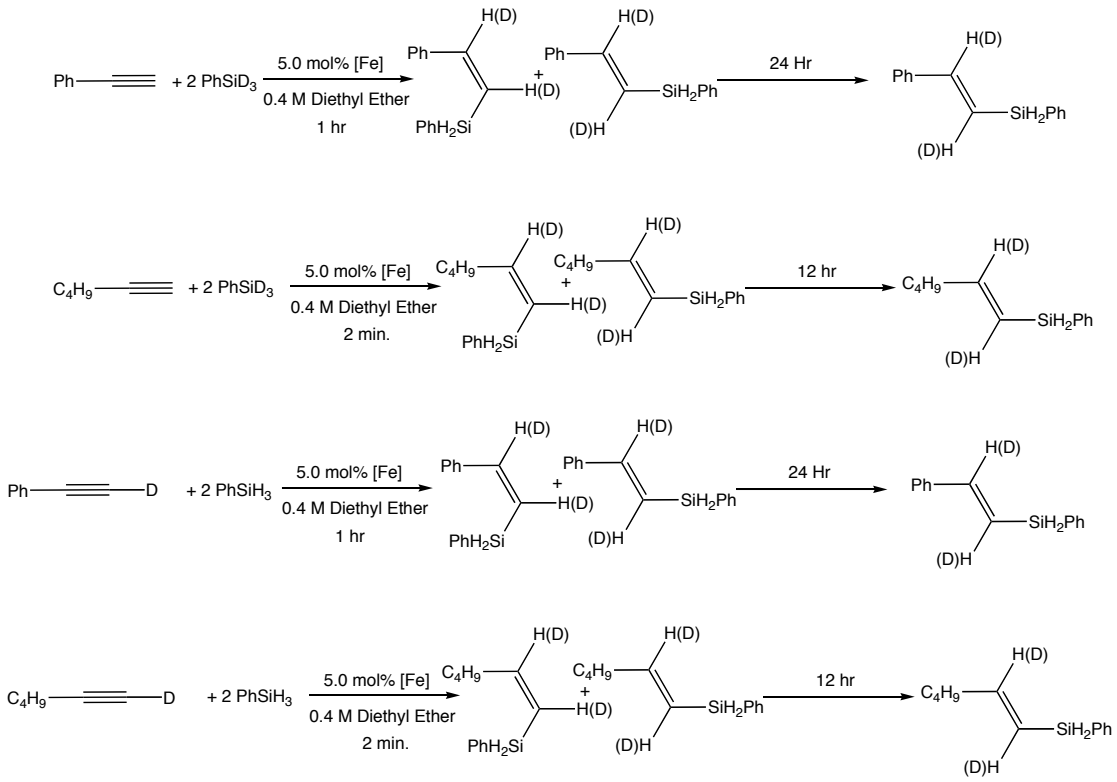

Figure A.3.2 Labelling experiments showing deuterium incorporation into multiple positions during the hydrosilylation reaction.

The hydrosilylation of internal alkynes proceeded according to the *cis* addition of the Si-H across the unsaturated bond, yielding the alkenylsilane. The reactions were performed in a similar manner to the terminal alkynes, in a 0.4 M diethyl ether solution with 2 equivalents of phenylsilane and 5 % (^{iPr}PDI)Fe(N_2)$_2$ loading. The reactions were quenched after an hour and the reactions were analyzed by ^{1}H NMR spectrscopy, GC, and GC/MS. The use of deuterated phenylsilane resulted in incorporation of the deuterium in the product in the expected location, with none of the previously observed scrambling into several positions. Non-symmetric alkynes displayed a slight preference for the silicon to add to the less sterically hindered carbon. The results are displayed in Figure A.3.3.

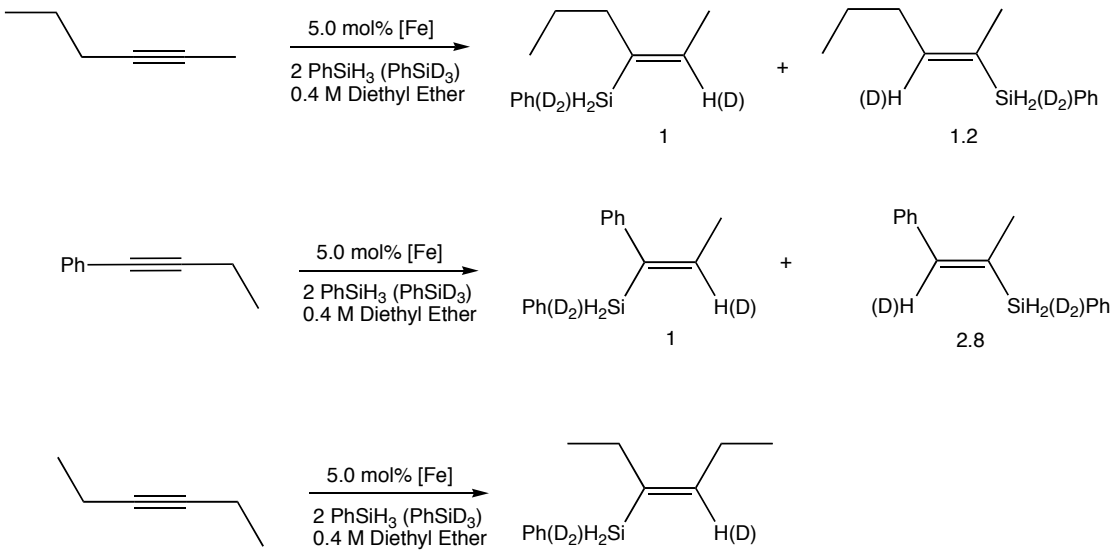

Figure A.3.3 The results of catalyzed hydrosilylation across internal-alkyne bonds.

The results from the hydrosilylation of alkynes with phenylsilane using (^{iPr}PDI)Fe(N_2)$_2$ as a precatalyst were encouraging. Both internal and terminal alkynes were successfully hydrosilylated under mild conditions. The hydrosilylation of terminal alkynes initially yielded the *trans*-addition product, giving a *cis*-olefin. Under reaction conditions, the initial product isomerized to the more thermodynamically stable *trans*-olefin. Internal alkynes exhibited the expected *cis*-addition of the silicon hydride bond.

Characterization of Hydrosilylation Products by Gas Chromatography. Gas chromatography for the silyl alkenes was performed on a Shimadzu GC-2010 gas chromatograph. GC analyses were performed using a Restek 15 m x 0.25 mm RTX-5 5% diphenyl-95% dimethyl polysiloxane column with a film thickness of 0.25 μm. The following temperature program was used: 30 ºC, 3 min; 10 ºC/min to 80 ºC; and 15 ºC/min to 245 ºC, 5 min.

Characterization of Hydrosilylation Products.

Preparation of phenyl(styryl)silane. A general hydrosilylation was performed in diethyl ether. The products were characterized by GC and GCMS. The solvent was removed and the (E) product exhibited a 1H NMR spectrum that matched the literature values. The retention times on the Restek RTX-5 column with the indicated temperature profile are 15.6 min (Z) and 16.1 min (E).

Dash, A.; Gourevich, I.; Wang, J. Q.; Wang, J.; Kapon, M.; Eisen, M.; *Organometallics* **2001**, *20*, 5084

(Z)-phenyl(styryl)silane:

^{1}H NMR (C_6D_6). δ = 7.51 – 7.54 (m, 2H, *p-H*-Ph), 7.02 – 7.21 (m, 8H + 1H, *o*, *m-H*-Ph + *H*CPh), 5.91 (dt, $^3J_{HH}$ = 15 Hz, $^3J_{SiH}$ = 5 Hz, 1H, C*H*SiH_2), 4.93 (d, J_{SiH}= 5 Hz, 2H, SiH_2).

Preparation of hex-1-enyl(phenyl)silane. A general hydrosilylation was performed in diethyl ether. The products were characterized by GC and GCMS. The solvent was removed and the products exhibited 1H NMR spectra that matched the literature values. The retention times on the Restek RTX-5 column with the indicated temperature profile are 13.09 min (Z) and 13.14 min (E).

Dash, A.; Wang, J. Q.; Eisen, M; *Organometallics* **1999**, *18*, 4724

Preparation of (E)-(3,3-dimethylbut-1-enyl)(phenyl)silane. A general hydrosilylation was performed in diethyl ether. The product was characterized by GC and GCMS. The solvent was removed and the product exhibited a 1H NMR spectrum that matched the literature values. The retention time on the Restek RTX-5 column with the indicated temperature profile is 12.1 min.

Dash, A.; Wang, J. Q.; Eisen, M; *Organometallics* **1999**, *18*, 4724

Preparation of (E)-1-((2-(trimethylsilyl)vinyl)silyl)benzene. A general hydrosilylation was performed in diethyl ether. The product was characterized by GC, GCMS, and ^{1}H NMR. The solvent was removed and the product exhibited a 1H NMR spectrum that matched the literature values. The retention time on the Restek RTX-5 column with the indicated temperature profile is 12.3 min. Due to long reaction times (approx. 24 hours for 95% completion), the product was not experimented with further.

Dash, A.; Wang, J. Q.; Eisen, M; *Organometallics* **1999**, *18*, 4724

Preparation of (E)-(1,2-diphenylvinyl)(phenyl)silane. A general hydrosilylation was performed in diethyl ether. The product was characterized by GC and GCMS. The solvent was removed and the product exhibited a 1H NMR spectrum that matched the literature values. The retention time on the Restek RTX-5 column with the indicated temperature profile is 19.3 min.

Bart, S.; Lobkovsky, E.; Chirik, P.; *JACS* **2004**, *126*, 13794

Preparation of (E)-hex-2-en-2-yl(phenyl)silane and (E)-hex-2-en-3-yl(phenyl)silane. A general hydrosilylation was performed in diethyl ether. The products were characterized by GC and GCMS. The retention times on the Restek RTX-5 column with the indicated temperature profile are 13.09 min and 13.14 min, respectively.

(E)-hex-2-en-2-yl(phenyl)silane: ^{1}H NMR (C_6D_6). δ = 6.25 (t, 1H, C*H*CSi), 4.81 (s, 2H, SiH_2), 1.98 (q, J_{HH} = 7, 2H, CH_2CHCSi), 1.69 (s, 3H, CH_3CSi), 1.27 (m, J_{HH} = 8 Hz, 2H, CH_2CH$_2$CH), 0.81 (t, J_{HH} = 7 Hz, 3H, CH_3CH$_2$CH$_2$).

(E)-hex-2-en-3-yl(phenyl)silane: ^{1}H NMR (C_6D_6). δ = 6.25 (q, 1H, C*H*CSi), 4.82 (s, 2H, Si*H*$_2$), 2.17 (t, J_{HH}=8, 2H, C*H*$_2$CSi), 1.53 (d, J_{HH}=7, 3H, C*H*$_3$CHCSi), 1.40 (m, J_{HH} = 7 Hz, 2H, C*H*$_2$CH$_2$CSi), 0.81 (t, J_{HH}= 7 Hz, 3H, C*H*$_3$CH$_2$CH$_2$).

Preparation of (E)-hex-3-en-3-yl(phenyl)silane. A general hydrosilylation was performed in diethyl ether. The product was characterized by GC and GCMS. The retention time on the Restek RTX-5 column with the indicated temperature profile is 12.7 min.

^{1}H NMR (C_6D_6). δ = 6.05 (t, J_{HH}=7, 1H, C*H*CSi), 4.83 (s, 2H, Si*H*$_2$), 2.16 (q, J_{HH}=8, 2H, C*H*$_2$CSi), 1.98 (m, J_{HH}=8, 2H, C*H*$_2$CHCSi), 0.94 (t, J_{HH} = 8 Hz, 3H, C*H*$_3$CH$_2$CSi), 0.84 (t, J_{HH}= 8 Hz, 3H, C*H*$_3$CH$_2$CH).

Preparation of (E)-phenyl(1-phenylpent-1-enyl)silane and (E)-phenyl(1-phenylpent-1-en-2-yl)silane. A general hydrosilylation was performed in diethyl ether. The products were characterized by GC and GCMS. The retention times on the Restek RTX-5 column with the indicated temperature profile are 16.5 min and 17.2 min, respectively.

(E)-phenyl(1-phenylpent-1-enyl)silane: ^{1}H NMR (C_6D_6). δ = 4.89 (s, 2H, Si*H*$_2$), 1.99 (q, J_{HH}=7, 2H, C*H*$_2$CH), 1.20 (m, J_{HH} = 7 Hz, 2H, C*H*$_2$CH$_2$CH), 0.68 (t, J_{HH}= 7 Hz, 3H, C*H*$_3$CH$_2$CH$_2$).

(E)-phenyl(1-phenylpent-1-en-2-yl)silane: ^{1}H NMR (C_6D_6). δ = 6.28 (t, J_{HH}=7, 1H, C*H*CSi), 4.94 (s, 2H, Si*H*$_2$), 2.43 (t, J_{HH}=8, 2H, C*H*$_2$CSi), 1.48 (m, J_{HH} = 8 Hz, 2H, C*H*$_2$CH$_2$CSi), 0.72 (t, J_{HH}= 7 Hz, 3H, C*H*$_3$CH$_2$CH$_2$).

APPENDIX B

CRYSTAL STRUCTURE DATA

Table B.1 Compilation of x-ray data for compounds found in this manuscript.

Compound	Crystal ID	Location
$(^{cy}APDI)FeR_2$	AMT 1	APPENDIX B
$(^{cy}APDI)_2Fe$	AT 1	APPENDIX B
$(^{indanyl}Pybox)FeR_2$	AMT 3	APPENDIX B
$(^{2\text{-}Ad}APDI)FeR$	AMT 4	APPENDIX B
$(^{iPr}Pybox)FeR_2$	AMT 2	APPENDIX B
$[(^{iPr}PDI)FeR(N_2)][LiOEt_2]$	AMT 9	APPENDIX B
$[Na]_2[(^{iPr}BPDI)Fe(N_2)]$	AMT13	APPENDIX B
$(^{iPr}PDI)Fe(NO)$	AMT 14	APPENDIX B
$(^{Et}PDI)Fe(NO)$	AMT 15	APPENDIX B
$^{Ta}(^{iPr}PDI)Fe(NO)$	AMT 16	APPENDIX B
$[(^{iPr}PDI)Fe(NO)(THF)][BArF_{24}]$	AMT 17	APPENDIX B
$[(^{iPr}PDI)]_2Fe(\mu\text{-}O)$	AMT 24	APPENDIX B
$[(^{iPr}PDI)Fe(CH_2CMe_3)][BPh_4]$	AMT 26	APPENDIX B
$(^{iPr}PDI)Fe(NCO)$	AMT 30	APPENDIX B
$[(^{iPr}PDI)Fe(OEt_2)][\ BArF_{24}]$	AMT 31	APPENDIX B
$[(^{iPr}PDI)Fe(CO)_2][\ BArF_{24}]$	AMT 32	APPENDIX B
$(^{Et}(4\text{-}^{t}Bu)PDI)Fe(NO)$	AMT 33	APPENDIX B
$(^{iPr}PDI)Fe(NO)_2$	AMT 34	APPENDIX B
$[(^{Me}PDI)Fe](\mu\text{-}N_2)$	AMT 36	APPENDIX B

$[Mo(N(Ar)^tBu)_3]$		
$[(^{iPr}PDI)Fe(NO)][Na\text{-}C]$	AMT 38	APPENDIX B
$[(^{Et}PDI)Fe(NO)(THF)][BArF_{24}]$	AMT 39	APPENDIX B
$(^{iPr}PDI)Fe(NO)(Py)$	AMT 40	APPENDIX B
$(TRPY)FeR_2$	AMT 42	APPENDIX B
$[(^{iPr}PDI)Fe(NO)][BArF_{24}]$	AMT 44	APPENDIX B
$(^{iPr}PDI)Fe(NTMS)$	AMT 46	APPENDIX B

Table B.2 Crystal data and structure refinement for $(^{cy}APDI)FeR_2$.

Identification code	amt1	
Empirical formula	C29 H53 Fe N3 Si2	
Formula weight	555.77	
Temperature	173(2) K	
Wavelength	0.71073 Å	
Crystal system	Triclinic	
Space group	P-1	
Unit cell dimensions	a = 10.2047(7) Å	α= 70.723(3)°.
	b = 10.8572(7) Å	β= 81.924(3)°.
	c = 15.5304(10) Å	γ = 78.508(2)°.
Volume	1586.45(18) $Å^3$	
Z	2	
Density (calculated)	1.163 Mg/m^3	
Absorption coefficient	0.572 mm^{-1}	
F(000)	604	
Crystal size	0.40 x 0.35 x 0.05 mm^3	
Theta range for data collection	1.39 to 21.99°.	
Index ranges	-10<=h<=10, -9<=k<=11, -16<=l<=16	
Reflections collected	13398	
Independent reflections	3837 [R(int) = 0.0607]	

Completeness to theta = 21.99°	98.8 %
Absorption correction	Semi-empirical from equivalents
Max. and min. transmission	0.9720 and 0.8036
Refinement method	Full-matrix least-squares on F^2
Data / restraints / parameters	3837 / 0 / 324
Goodness-of-fit on F^2	1.166
Final R indices [I>2sigma(I)]	R1 = 0.0661, wR2 = 0.1066
R indices (all data)	R1 = 0.0851, wR2 = 0.1132
Largest diff. peak and hole	0.369 and -0.363 e.Å^{-3}

	x	y	z	U(eq)
Fe(1)	2560(1)	1967(1)	2507(1)	15(1)
Si(1)	4209(1)	3629(1)	3368(1)	23(1)
Si(2)	947(1)	250(1)	1659(1)	23(1)
N(1)	4500(2)	1399(2)	1718(2)	14(1)
N(2)	2558(3)	3379(2)	1325(2)	15(1)
N(3)	618(2)	3362(2)	2588(2)	16(1)
C(1)	5807(3)	2067(3)	204(2)	22(1)
C(2)	4654(3)	2212(3)	906(2)	14(1)
C(3)	3605(3)	3360(3)	652(2)	17(1)
C(4)	3613(3)	4339(3)	-172(2)	20(1)
C(5)	2562(3)	5403(3)	-363(2)	24(1)
C(6)	1516(3)	5422(3)	305(2)	20(1)
C(7)	1518(3)	4440(3)	1125(2)	15(1)
C(8)	465(3)	4372(3)	1868(2)	15(1)
C(9)	-695(3)	5511(3)	1735(2)	21(1)
C(10)	5521(3)	198(3)	2027(2)	20(1)
C(11)	5309(3)	-887(3)	1667(2)	24(1)
C(12)	6382(4)	-2116(3)	1966(2)	32(1)
C(13)	6437(4)	-2602(3)	2994(2)	33(1)
C(14)	6662(4)	-1501(3)	3336(3)	30(1)
C(15)	5564(3)	-291(3)	3051(2)	23(1)
C(16)	-410(3)	3261(3)	3374(2)	18(1)
C(17)	-229(3)	4128(3)	3932(2)	23(1)
C(18)	-1322(4)	4069(4)	4712(2)	31(1)

C(19)	-1364(4)	2655(4)	5324(2)	36(1)
C(20)	-1522(4)	1794(4)	4763(2)	31(1)
C(21)	-430(3)	1848(3)	3981(2)	22(1)
C(22)	3291(3)	2246(3)	3602(2)	19(1)
C(23)	5797(4)	3422(4)	2639(2)	34(1)
C(24)	4666(4)	3821(4)	4435(2)	33(1)
C(25)	3216(4)	5249(3)	2748(3)	38(1)
C(26)	1829(3)	261(3)	2603(2)	18(1)
C(27)	1860(4)	895(4)	507(2)	34(1)
C(28)	-730(3)	1314(4)	1620(3)	33(1)
C(29)	682(4)	-1455(4)	1758(3)	40(1)

Table B.3 Crystal data and structure refinement for (^{iPr}Pybox)FeR_2.

Identification code	amt2	
Empirical formula	C25 H45 Fe N3 O2 Si2	
Formula weight	531.67	
Temperature	203(2) K	
Wavelength	0.71073 Å	
Crystal system	Monoclinic	
Space group	C2	
Unit cell dimensions	a = 16.0297(8) Å	α= 90°.
	b = 12.0347(7) Å	β= 92.797(3)°.
	c = 15.5970(8) Å	γ = 90°.
Volume	3005.3(3) $Å^3$	
Z	4	
Density (calculated)	1.175 Mg/m^3	
Absorption coefficient	0.606 mm^{-1}	
F(000)	1144	
Crystal size	0.60 x 0.30 x 0.15 mm^3	
Theta range for data collection	1.31 to 31.68°.	
Index ranges	-23<=h<=23, -17<=k<=15, -22<=l<=22	
Reflections collected	20601	
Independent reflections	9055 [R(int) = 0.0252]	

Completeness to theta = 31.68°	98.0 %
Absorption correction	Semi-empirical from equivalents
Max. and min. transmission	0.9147 and 0.7127
Refinement method	Full-matrix least-squares on F^2
Data / restraints / parameters	9055 / 1 / 368
Goodness-of-fit on F^2	0.996
Final R indices [I>2sigma(I)]	R1 = 0.0355, wR2 = 0.0795
R indices (all data)	R1 = 0.0493, wR2 = 0.0857
Absolute structure parameter	-0.011(9)
Largest diff. peak and hole	0.551 and -0.353 e.$Å^{-3}$

	x	y	z	U(eq)
Fe(1)	1954(1)	2880(1)	2728(1)	25(1)
Si(1)	4021(1)	3083(1)	2394(1)	36(1)
Si(2)	-75(1)	2978(1)	3195(1)	39(1)
O(1)	1539(1)	2772(1)	-8(1)	44(1)
O(2)	1979(1)	-336(1)	3858(1)	39(1)
N(1)	1730(1)	3449(1)	1337(1)	30(1)
N(2)	1818(1)	1477(1)	2052(1)	28(1)
N(3)	2092(1)	1519(1)	3686(1)	29(1)
C(1)	1737(1)	4433(1)	765(1)	32(1)
C(2)	1391(1)	3951(2)	-92(1)	43(1)
C(3)	1640(1)	2595(1)	849(1)	33(1)
C(4)	1667(1)	1487(1)	1172(1)	34(1)
C(5)	1567(1)	528(2)	699(1)	44(1)
C(6)	1639(1)	-495(2)	1094(1)	50(1)
C(7)	1795(1)	-525(1)	1978(1)	41(1)
C(8)	1874(1)	452(1)	2431(1)	32(1)
C(9)	1999(1)	563(1)	3345(1)	30(1)
C(10)	2104(1)	91(1)	4724(1)	48(1)
C(11)	2110(1)	1362(1)	4628(1)	33(1)
C(12)	1253(1)	5425(1)	1066(1)	37(1)
C(13)	1677(1)	5935(2)	1855(1)	53(1)
C(14)	1154(1)	6295(2)	363(1)	52(1)
C(15)	2835(1)	1943(1)	5103(1)	36(1)

C(16)	2795(1)	1752(2)	6066(1)	48(1)
C(17)	3682(1)	1606(2)	4801(1)	56(1)
C(18)	3111(1)	3604(1)	2943(1)	32(1)
C(19)	3959(1)	1564(2)	2135(1)	51(1)
C(20)	5010(1)	3264(2)	3062(1)	59(1)
C(21)	4115(1)	3825(2)	1353(1)	70(1)
C(22)	967(1)	3593(1)	3323(1)	35(1)
C(23)	-457(1)	3037(3)	2059(1)	95(1)
C(24)	-836(1)	3768(2)	3843(2)	73(1)
C(25)	-101(1)	1510(2)	3553(2)	62(1)

Table B.4 Crystal data and structure refinement for (^{indanyl}Pybox)FeR_2

Empirical formula	C33 H41 Fe N3 O2 Si2	
Formula weight	623.72	
Temperature	173(2) K	
Wavelength	0.71073 Å	
Crystal system	Tetragonal	
Space group	P4(1)	
Unit cell dimensions	a = 19.2130(10) Å	α= 90°.
	b = 19.2130(10) Å	β= 90°.
	c = 11.9944(11) Å	γ = 90°.
Volume	4427.6(5) $Å^3$	
Z	4	
Density (calculated)	0.936 Mg/m^3	
Absorption coefficient	0.419 mm^{-1}	
F(000)	1320	
Crystal size	0.40 x 0.20 x 0.05 mm^3	
Theta range for data collection	2.00 to 23.25°.	
Index ranges	-21<=h<=21, -21<=k<=14, -12<=l<=13	
Reflections collected	16938	
Independent reflections	6287 [R(int) = 0.0615]	
Completeness to theta = 23.25°	99.9 %	
Absorption correction	Semi-empirical from equivalents	
Max. and min. transmission	0.9793 and 0.8503	

Refinement method	Full-matrix least-squares on F^2
Data / restraints / parameters	6287 / 1 / 370
Goodness-of-fit on F^2	0.884
Final R indices [I>2sigma(I)]	R1 = 0.0472, wR2 = 0.0918
R indices (all data)	R1 = 0.0682, wR2 = 0.0997
Absolute structure parameter	-0.01(2)
Largest diff. peak and hole	0.187 and -0.196 e.Å^{-3}

x	y	z	U(eq)	
Fe(1)	2060(1)	3467(1)	1054(1)	35(1)
Si(1)	1983(1)	3866(1)	3751(1)	60(1)
Si(2)	2362(1)	3096(1)	-1620(1)	59(1)
O(1)	104(1)	4362(1)	206(2)	46(1)
O(2)	1920(1)	1367(1)	2126(2)	63(1)
N(1)	1248(1)	4230(1)	587(2)	38(1)
N(2)	1167(1)	2926(1)	1072(2)	39(1)
N(3)	2342(1)	2409(1)	1597(2)	39(1)
C(1)	633(2)	3958(2)	524(2)	39(1)
C(2)	537(2)	3239(2)	792(3)	44(1)
C(3)	-75(2)	2885(2)	809(3)	55(1)
C(4)	-91(2)	2201(2)	1135(4)	69(1)
C(5)	522(2)	1870(2)	1436(3)	61(1)
C(6)	1143(2)	2253(2)	1399(3)	52(1)
C(7)	1824(2)	2011(2)	1701(3)	46(1)
C(8)	381(2)	5066(2)	139(3)	45(1)
C(9)	147(2)	5506(2)	1133(3)	54(1)
C(10)	797(2)	5759(2)	1647(3)	54(1)
C(11)	895(2)	6232(2)	2538(3)	69(1)
C(12)	1545(2)	6393(2)	2875(3)	75(2)
C(13)	2127(2)	6101(2)	2383(3)	68(1)
C(14)	2064(2)	5634(2)	1487(3)	53(1)
C(15)	1389(2)	5468(2)	1147(3)	42(1)
C(16)	1180(2)	4968(2)	249(3)	38(1)
C(17)	2661(2)	1304(2)	2314(3)	58(1)
C(18)	3009(2)	809(2)	1523(3)	60(1)

C(19)	3538(2)	1227(2)	892(3)	44(1)
C(20)	4000(2)	1009(2)	106(3)	53(1)
C(21)	4445(2)	1498(2)	-374(3)	54(1)
C(22)	4427(2)	2171(2)	-53(3)	55(1)
C(23)	3974(2)	2384(2)	755(3)	48(1)
C(24)	3514(2)	1914(2)	1221(3)	40(1)
C(25)	2959(2)	2037(2)	2065(3)	44(1)
C(26)	2483(2)	3916(2)	2447(2)	40(1)
C(27)	1949(2)	2951(2)	4284(3)	80(2)
C(28)	2363(3)	4429(3)	4869(3)	105(2)
C(29)	1057(2)	4138(3)	3534(4)	112(2)
C(30)	2630(2)	3579(2)	-387(2)	44(1)
C(31)	1496(2)	3417(2)	-2112(3)	66(1)
C(32)	2302(2)	2144(2)	-1339(4)	84(1)
C(33)	3004(3)	3203(3)	-2795(3)	104(2)

Table B.5 Crystal data and structure refinement for ($^{2\text{-Ad}}$APDI)FeR

Identification code	amt4	
Empirical formula	C34 H50 Fe N3	
Formula weight	556.62	
Temperature	173(2) K	
Wavelength	0.71073 Å	
Crystal system	Monoclinic	
Space group	P2(1)/n	
Unit cell dimensions	a = 10.4613(5) Å	α= 90°.
	b = 12.1989(7) Å	β= 94.056(2)°.
	c = 22.6392(12) Å	γ = 90°.
Volume	2881.9(3) Å^3	
Z	4	
Density (calculated)	1.283 Mg/m^3	
Absorption coefficient	0.551 mm^{-1}	
F(000)	1204	
Crystal size	0.20 x 0.05 x 0.03 mm^3	
Theta range for data collection	1.80 to 26.44°.	

Index ranges	-13<=h<=8, -15<=k<=15, -26<=l<=28
Reflections collected	19622
Independent reflections	5889 [R(int) = 0.0706]
Completeness to theta = 26.44°	99.3 %
Absorption correction	Semi-empirical from equivalents
Max. and min. transmission	0.9837 and 0.8978
Refinement method	Full-matrix least-squares on F^2
Data / restraints / parameters	5889 / 0 / 348
Goodness-of-fit on F^2	1.004
Final R indices [I>2sigma(I)]	R1 = 0.0478, wR2 = 0.0875
R indices (all data)	R1 = 0.0995, wR2 = 0.1024
Largest diff. peak and hole	0.321 and -0.334 e.$Å^{-3}$

	x	y	z	U(eq)
Fe(1)	376(1)	8618(1)	1491(1)	22(1)
N(1)	-4(2)	9940(1)	2145(1)	20(1)
N(2)	821(2)	7983(1)	2266(1)	21(1)
N(3)	-109(2)	6913(2)	1374(1)	22(1)
C(1)	852(2)	10569(2)	3153(1)	31(1)
C(2)	603(2)	9747(2)	2661(1)	22(1)
C(3)	1067(2)	8627(2)	2750(1)	21(1)
C(4)	1692(2)	8217(2)	3257(1)	26(1)
C(5)	2057(2)	7116(2)	3271(1)	29(1)
C(6)	1708(2)	6449(2)	2800(1)	26(1)
C(7)	1033(2)	6878(2)	2300(1)	21(1)
C(8)	485(2)	6300(2)	1791(1)	23(1)
C(9)	556(2)	5064(2)	1770(1)	30(1)
C(10)	-507(2)	11058(2)	2025(1)	23(1)
C(11)	-794(2)	11245(2)	1363(1)	29(1)
C(12)	-1135(2)	12447(2)	1266(1)	38(1)
C(13)	-2331(2)	12727(2)	1584(1)	37(1)
C(14)	-3442(2)	12027(2)	1341(1)	46(1)
C(15)	-3104(2)	10815(2)	1439(1)	53(1)
C(16)	-2827(2)	10586(2)	2096(1)	53(1)
C(17)	-1722(2)	11303(2)	2341(1)	34(1)

C(18)	-2060(3)	12512(2)	2245(1)	42(1)
C(19)	-1903(2)	10536(2)	1128(1)	45(1)
C(20)	-802(2)	6339(2)	876(1)	22(1)
C(21)	-2208(2)	6147(2)	1007(1)	29(1)
C(22)	-2842(2)	5416(2)	523(1)	38(1)
C(23)	-2805(2)	5985(2)	-77(1)	34(1)
C(24)	-1410(2)	6197(2)	-199(1)	32(1)
C(25)	-771(2)	6938(2)	283(1)	27(1)
C(26)	-1499(2)	8016(2)	281(1)	31(1)
C(27)	-2878(2)	7807(2)	415(1)	33(1)
C(28)	-3525(2)	7067(2)	-65(1)	34(1)
C(29)	-2913(2)	7244(2)	1017(1)	35(1)
C(30)	1657(2)	9232(2)	933(1)	27(1)
C(31)	2983(2)	8698(2)	891(1)	27(1)
C(32)	2834(2)	7544(2)	638(1)	39(1)
C(33)	3813(2)	9387(2)	503(1)	42(1)
C(34)	3680(2)	8618(2)	1509(1)	35(1)

Table B.5 Crystal data and structure refinement for [(^{iPr}PDI)FeR(N_2)][$LiOEt_2$]

Identification code	amt9	
Empirical formula	C50 H84 Fe Li N5 O3	
Formula weight	866.01	
Temperature	173(2) K	
Wavelength	0.71073 Å	
Crystal system	Monoclinic	
Space group	P2(1)/n	
Unit cell dimensions	a = 12.5472(17) Å	α= 90°.
	b = 21.249(3) Å	β= 92.253(4)°.
	c = 20.871(3) Å	γ = 90°.
Volume	5560.0(13) $Å^3$	
Z	4	
Density (calculated)	1.035 Mg/m^3	
Absorption coefficient	0.310 mm^{-1}	
F(000)	1888	

Crystal size	0.60 x 0.55 x 0.45 mm^3
Theta range for data collection	1.86 to 24.71°.
Index ranges	-14<=h<=14, -24<=k<=24, -24<=l<=24
Reflections collected	64320
Independent reflections	9479 [R(int) = 0.0542]
Completeness to theta = 24.71°	100.0 %
Absorption correction	Semi-empirical from equivalents
Max. and min. transmission	0.8729 and 0.8356
Refinement method	Full-matrix least-squares on F^2
Data / restraints / parameters	9479 / 157 / 657
Goodness-of-fit on F^2	1.104
Final R indices [I>2sigma(I)]	R1 = 0.0562, wR2 = 0.1563
R indices (all data)	R1 = 0.0841, wR2 = 0.1693
Largest diff. peak and hole	0.484 and -0.307 e.$Å^{-3}$

	x	y	z	U(eq)
Fe(1)	6192(1)	8232(1)	8407(1)	28(1)
O(1)	2808(2)	6746(2)	7154(2)	62(1)
C(39)	2797(5)	6595(3)	7838(3)	93(2)
C(40)	2514(8)	5966(4)	8175(5)	197(4)
C(41)	1769(4)	6814(3)	6817(3)	79(2)
C(42)	1222(5)	7360(3)	7086(4)	107(3)
O(1')	3024(6)	6476(4)	7324(4)	79(3)
C(39')	2889(15)	6571(8)	7998(6)	144(8)
C(40')	2256(13)	5969(6)	7935(8)	103(5)
C(41')	2031(11)	6368(9)	6914(10)	213(11)
C(42')	1290(30)	6905(14)	6980(30)	390(30)
O(2)	3901(3)	7447(2)	6050(2)	89(2)
C(43)	3795(5)	8113(3)	5779(4)	100(3)
C(44)	3519(6)	8457(4)	6354(3)	102(2)
C(45)	3901(5)	7112(3)	5397(3)	97(2)
C(46)	4924(5)	7186(3)	5069(3)	87(2)
O(2')	3796(13)	7553(5)	6212(6)	174(6)
C(43')	3944(13)	8226(7)	6239(15)	235(15)
C(44')	2815(18)	8350(19)	6410(19)	360(20)

C(45')	3450(12)	7167(7)	5677(6)	118(5)
C(46')	4065(16)	7504(10)	5184(9)	187(9)
O(3)	4927(4)	6216(2)	6572(3)	67(2)
C(47)	6010(5)	6327(4)	6413(3)	87(3)
C(48)	6284(8)	6047(5)	5774(4)	141(4)
C(49)	4553(6)	5591(3)	6674(3)	73(2)
C(50)	4925(8)	5290(5)	7282(4)	110(4)
O(3')	4926(6)	6174(3)	6624(4)	62(3)
C(47')	6058(7)	6258(5)	6565(6)	78(4)
C(48')	6415(10)	5882(5)	6003(5)	77(3)
C(49')	4733(16)	5539(6)	6847(7)	179(11)
C(50')	5309(12)	5419(8)	7465(7)	124(6)
N(1)	5192(2)	8266(1)	9087(1)	33(1)
N(2)	6994(1)	8664(1)	9014(1)	29(1)
N(3)	7579(1)	8152(1)	8060(1)	29(1)
N(4)	5529(2)	7680(1)	7917(1)	34(1)
N(5)	5077(2)	7348(1)	7576(1)	56(1)
C(1)	4788(2)	8771(2)	10147(1)	62(1)
C(2)	5491(2)	8632(1)	9598(1)	39(1)
C(3)	6524(2)	8869(1)	9567(1)	36(1)
C(4)	7102(2)	9250(1)	10000(1)	45(1)
C(5)	8154(2)	9398(1)	9886(1)	46(1)
C(6)	8647(2)	9163(1)	9351(1)	38(1)
C(7)	8061(2)	8783(1)	8916(1)	30(1)
C(8)	8381(2)	8475(1)	8364(1)	30(1)
C(9)	9507(2)	8492(1)	8147(1)	45(1)
C(10)	4218(2)	7906(1)	9152(1)	37(1)
C(11)	4301(2)	7293(1)	9406(2)	54(1)
C(12)	3362(2)	6966(2)	9531(2)	64(1)
C(13)	2378(2)	7231(2)	9397(2)	58(1)
C(14)	2315(2)	7818(1)	9129(1)	51(1)
C(15)	3222(2)	8163(1)	9000(1)	38(1)
C(16)	5391(5)	7034(3)	9648(3)	52(2)
C(17)	5729(5)	7223(4)	10344(3)	78(2)
C(18)	5416(6)	6289(4)	9610(4)	95(3)

C(16')	5327(9)	6896(5)	9399(5)	60(3)
C(17')	5814(11)	7041(7)	10059(7)	95(5)
C(18')	5160(9)	6208(6)	9314(7)	76(4)
C(19)	3087(2)	8804(1)	8696(1)	44(1)
C(20)	2612(2)	8748(2)	8018(2)	63(1)
C(21)	2407(2)	9254(2)	9088(2)	63(1)
C(22)	7896(2)	7719(1)	7568(1)	33(1)
C(23)	8221(2)	7109(1)	7757(1)	41(1)
C(24)	8549(2)	6692(1)	7293(1)	52(1)
C(25)	8554(2)	6855(1)	6657(1)	55(1)
C(26)	8234(2)	7457(1)	6472(1)	49(1)
C(27)	7907(2)	7893(1)	6921(1)	40(1)
C(28)	8255(3)	6896(1)	8452(1)	54(1)
C(29)	9396(3)	6738(2)	8689(2)	79(1)
C(30)	7548(3)	6322(2)	8526(2)	82(1)
C(31)	7586(3)	8540(2)	6698(1)	58(1)
C(32)	8511(3)	8894(2)	6411(2)	85(1)
C(33)	6615(3)	8495(2)	6208(2)	84(1)
C(34)	5532(2)	8924(1)	7809(1)	32(1)
C(35)	5718(2)	9644(1)	7859(1)	39(1)
C(36)	5102(3)	9948(2)	7288(2)	70(1)
C(37)	5304(3)	9921(1)	8468(2)	70(1)
C(38)	6886(2)	9819(1)	7812(2)	53(1)
Li(1)	4142(4)	6945(2)	6838(3)	68(2)

Table B.6 Crystal data and structure refinement for (^{iPr}PDI)Fe(NO)

Identification code	amt14	
Empirical formula	C33 H43 Fe N4 O	
Formula weight	567.56	
Temperature	173(2) K	
Wavelength	0.71073 Å	
Crystal system	Orthorhombic	
Space group	P2(1)2(1)2(1)	
Unit cell dimensions	a = 8.4130(3) Å	□= 90°.

	b = 17.9579(8) Å	□= 90°.
	c = 20.2518(9) Å	□ = 90°.
Volume	3059.6(2) Å^3	
Z	4	
Density (calculated)	1.232 Mg/m^3	
Absorption coefficient	0.524 mm^{-1}	
F(000)	1212	
Crystal size	0.45 x 0.25 x 0.20 mm^3	
Theta range for data collection	2.01 to 28.33°.	
Index ranges	-11<=h<=9, -23<=k<=23, -26<=l<=27	
Reflections collected	40643	
Independent reflections	7625 [R(int) = 0.0507]	
Completeness to theta = 28.33°	100.0 %	
Absorption correction	Semi-empirical from equivalents	
Max. and min. transmission	0.9025 and 0.7984	
Refinement method	Full-matrix least-squares on F^2	
Data / restraints / parameters	7625 / 0 / 414	
Goodness-of-fit on F^2	1.040	
Final R indices [I>2sigma(I)]	R1 = 0.0357, wR2 = 0.0807	
R indices (all data)	R1 = 0.0489, wR2 = 0.0863	
Absolute structure parameter	-0.015(11)	
Largest diff. peak and hole	0.266 and -0.200 e.Å^{-3}	

	x	y	z	U(eq)
Fe(1)	3654(1)	959(1)	1287(1)	22(1)
O(1)	1693(2)	179(1)	2176(1)	78(1)
N(1)	4359(2)	1757(1)	1838(1)	23(1)
N(2)	4744(2)	1540(1)	673(1)	22(1)
N(3)	3330(2)	381(1)	507(1)	22(1)
N(4)	2533(2)	499(1)	1802(1)	38(1)
C(1)	5779(2)	2975(1)	1932(1)	33(1)
C(2)	5214(2)	2299(1)	1565(1)	23(1)
C(3)	5488(2)	2184(1)	878(1)	23(1)
C(4)	6335(2)	2608(1)	422(1)	28(1)
C(5)	6411(2)	2380(1)	-231(1)	31(1)

C(6)	5675(2)	1725(1)	-428(1)	27(1)
C(7)	4839(2)	1304(1)	28(1)	23(1)
C(8)	3985(2)	624(1)	-55(1)	22(1)
C(9)	3860(2)	231(1)	-708(1)	33(1)
C(10)	3895(2)	1808(1)	2524(1)	24(1)
C(11)	4819(2)	1448(1)	3002(1)	29(1)
C(12)	4240(2)	1431(1)	3644(1)	34(1)
C(13)	2801(2)	1752(1)	3809(1)	36(1)
C(14)	1928(2)	2120(1)	3332(1)	33(1)
C(15)	2463(2)	2166(1)	2682(1)	26(1)
C(16)	6390(2)	1083(1)	2835(1)	37(1)
C(17)	7670(2)	1234(1)	3354(1)	52(1)
C(18)	6197(3)	241(1)	2734(1)	68(1)
C(19)	1477(2)	2582(1)	2171(1)	31(1)
C(20)	1026(3)	3363(1)	2404(1)	59(1)
C(21)	12(2)	2145(1)	1979(1)	53(1)
C(22)	2369(2)	-280(1)	507(1)	24(1)
C(23)	3086(2)	-972(1)	600(1)	27(1)
C(24)	2096(2)	-1599(1)	645(1)	36(1)
C(25)	476(2)	-1529(1)	583(1)	40(1)
C(26)	-203(2)	-847(1)	492(1)	42(1)
C(27)	712(2)	-204(1)	456(1)	33(1)
C(28)	4877(2)	-1058(1)	672(1)	36(1)
C(29)	5551(2)	-1620(1)	183(1)	42(1)
C(30)	5306(3)	-1278(1)	1378(1)	62(1)
C(31)	-97(2)	544(1)	347(1)	44(1)
C(32)	-682(3)	617(1)	-367(1)	57(1)
C(33)	-1439(3)	678(1)	834(1)	58(1)

Table B.7 Crystal data and structure refinement for (^{Et}PDI)Fe(NO)

Identification code	amt15
Empirical formula	C29 H35 Fe N4 O
Formula weight	511.46
Temperature	173(2) K

Wavelength	0.71073 Å		
Crystal system	Triclinic		
Space group	P-1		
Unit cell dimensions	a = 8.5349(17) Å	□= 88.37(3)°.	
	b = 11.483(2) Å	□= 89.98(3)°.	
	c = 26.762(5) Å	□ = 77.49(3)°.	
Volume	2559.5(8) $Å^3$		
Z	4		
Density (calculated)	1.327 Mg/m^3		
Absorption coefficient	0.618 mm^{-1}		
F(000)	1084		
Crystal size	0.30 x 0.08 x 0.03 mm^3		
Theta range for data collection	1.82 to 25.49°.		
Index ranges	-10<=h<=10, -13<=k<=13, -32<=l<=0		
Reflections collected	9227		
Independent reflections	9229 [R(int) = 0.0000]		
Completeness to theta = 25.49°	82.1 %		
Absorption correction	Semi-empirical from equivalents		
Max. and min. transmission	0.9847 and 0.8362		
Refinement method	Full-matrix least-squares on F^2		
Data / restraints / parameters	9229 / 0 / 632		
Goodness-of-fit on F^2	1.045		
Final R indices [I>2sigma(I)]	R1 = 0.0554, wR2 = 0.1351		
R indices (all data)	R1 = 0.0795, wR2 = 0.1528		
Largest diff. peak and hole	0.331 and -0.379 e.$Å^{-3}$		

	x	y	z	U(eq)
Fe(1)	4906(1)	6514(1)	3569(1)	23(1)
O(1)	7118(4)	6702(3)	2795(1)	54(1)
N(1)	4923(3)	4797(3)	3590(1)	20(1)
N(2)	2731(4)	6529(3)	3653(1)	21(1)
N(3)	4149(4)	8068(3)	3881(1)	24(1)
N(4)	6210(4)	6650(3)	3127(1)	29(1)
C(1)	3300(5)	3261(3)	3489(2)	34(1)
C(2)	3527(4)	4491(3)	3570(2)	22(1)

C(3)	2210(4)	5477(3)	3645(2)	22(1)
C(4)	607(5)	5471(4)	3726(2)	31(1)
C(5)	-453(5)	6523(4)	3844(2)	31(1)
C(6)	100(5)	7548(4)	3916(2)	28(1)
C(7)	1713(5)	7536(3)	3828(2)	22(1)
C(8)	2568(5)	8442(3)	3924(2)	23(1)
C(9)	1765(5)	9650(3)	4084(2)	32(1)
C(10)	6386(4)	3941(3)	3501(2)	23(1)
C(11)	7407(4)	3553(3)	3906(2)	23(1)
C(12)	8857(5)	2771(4)	3816(2)	33(1)
C(13)	9256(5)	2394(4)	3343(2)	33(1)
C(14)	8258(5)	2784(4)	2948(2)	35(1)
C(15)	6794(5)	3585(3)	3015(2)	26(1)
C(16)	6907(5)	4008(4)	4420(2)	37(1)
C(17)	8120(6)	3639(5)	4837(2)	62(2)
C(18)	5754(5)	4075(4)	2565(2)	38(1)
C(19)	5327(7)	3138(5)	2241(2)	58(2)
C(20)	5178(4)	8862(3)	3987(2)	22(1)
C(21)	5444(5)	9716(3)	3629(2)	26(1)
C(22)	6439(5)	10460(4)	3767(2)	31(1)
C(23)	7142(5)	10366(4)	4230(2)	32(1)
C(24)	6900(5)	9499(4)	4567(2)	30(1)
C(25)	5915(5)	8725(3)	4457(2)	25(1)
C(26)	4645(5)	9831(4)	3122(2)	36(1)
C(27)	5790(6)	9850(5)	2689(2)	54(2)
C(28)	5679(5)	7752(4)	4823(2)	35(1)
C(29)	7020(7)	7285(6)	5168(2)	95(2)
Fe(1A)	-130(1)	1207(1)	1439(1)	24(1)
O(1A)	2146(4)	1591(3)	2153(1)	61(1)
N(1A)	-854(4)	2784(3)	1101(1)	24(1)
N(2A)	-2308(4)	1231(3)	1328(1)	24(1)
N(3A)	-142(4)	-522(3)	1492(1)	21(1)
N(4A)	1202(4)	1416(3)	1850(1)	35(1)
C(1A)	-3245(5)	4376(4)	847(2)	36(1)
C(2A)	-2433(5)	3151(3)	1020(2)	23(1)

C(3A)	-3279(5)	2229(3)	1114(2)	23(1)
C(4A)	-4873(5)	2242(4)	1004(2)	32(1)
C(5A)	-5449(5)	1220(4)	1086(2)	33(1)
C(6A)	-4410(5)	181(4)	1256(2)	28(1)
C(7A)	-2845(5)	178(3)	1360(2)	22(1)
C(8A)	-1559(4)	-817(3)	1482(2)	21(1)
C(9A)	-1850(5)	-2039(3)	1556(2)	32(1)
C(10A)	154(5)	3607(3)	997(2)	26(1)
C(11A)	908(5)	3535(3)	529(2)	27(1)
C(12A)	1857(5)	4342(4)	416(2)	31(1)
C(13A)	2094(5)	5161(4)	761(2)	32(1)
C(14A)	1399(5)	5189(4)	1223(2)	31(1)
C(15A)	420(5)	4422(4)	1355(2)	28(1)
C(16A)	644(5)	2638(4)	160(2)	33(1)
C(17A)	1929(7)	2294(6)	-213(2)	92(2)
C(18A)	-425(5)	4495(4)	1853(2)	35(1)
C(19A)	544(6)	4753(4)	2291(2)	51(2)
C(20A)	1305(5)	-1402(3)	1592(2)	24(1)
C(21A)	1652(5)	-1922(4)	2068(2)	30(1)
C(22A)	3153(5)	-2704(4)	2138(2)	37(1)
C(23A)	4207(5)	-2973(4)	1748(2)	39(1)
C(24A)	3824(5)	-2467(4)	1281(2)	33(1)
C(25A)	2370(5)	-1663(3)	1191(2)	26(1)
C(26A)	525(6)	-1709(4)	2517(2)	38(1)
C(27A)	319(6)	-494(4)	2734(2)	54(2)
C(28A)	1922(5)	-1078(4)	688(2)	32(1)
C(29A)	3126(6)	-1403(5)	271(2)	53(2)

Table B.8 Crystal data and structure refinement for $^{Ta}(^{iPr}PDI)Fe(NO)$

Identification code	amt16
Empirical formula	C69 H123 Fe N4 O4 Si3 Ta
Formula weight	1393.78
Temperature	173(2) K
Wavelength	0.71073 Å

Crystal system	Triclinic	
Space group	P-1	
Unit cell dimensions	a = 15.4155(8) Å	□= 110.845(3)°.
	b = 16.7128(9) Å	□= 92.864(2)°.
	c = 20.2809(16) Å	□ = 114.375(2)°.
Volume	4327.3(5) $Å^3$	
Z	2	
Density (calculated)	1.070 Mg/m^3	
Absorption coefficient	1.511 mm^{-1}	
F(000)	1476	
Crystal size	0.40 x 0.20 x 0.10 mm^3	
Theta range for data collection	1.49 to 28.49°.	
Index ranges	-19<=h<=20, -22<=k<=22, -27<=l<=27	
Reflections collected	65209	
Independent reflections	21269 [R(int) = 0.0372]	
Completeness to theta = 28.49°	96.9 %	
Absorption correction	Semi-empirical from equivalents	
Max. and min. transmission	0.8636 and 0.5832	
Refinement method	Full-matrix least-squares on F^2	
Data / restraints / parameters	21269 / 0 / 739	
Goodness-of-fit on F^2	1.022	
Final R indices [I>2sigma(I)]	R1 = 0.0301, wR2 = 0.0714	
R indices (all data)	R1 = 0.0402, wR2 = 0.0745	
Largest diff. peak and hole	1.261 and -0.581 e.$Å^{-3}$	

	x	y	z	U(eq)
Ta(1)	2907(1)	7845(1)	1199(1)	17(1)
Fe(1)	1704(1)	5011(1)	2992(1)	22(1)
Si(1)	4493(1)	7222(1)	202(1)	22(1)
Si(2)	4254(1)	9729(1)	2908(1)	26(1)
Si(3)	785(1)	7957(1)	667(1)	21(1)
O(1)	3880(1)	7484(1)	835(1)	22(1)
O(2)	3659(1)	8943(1)	2054(1)	23(1)
O(3)	1691(1)	7903(1)	1113(1)	20(1)

O(4)	1314(1)	3880(1)	3796(1)	59(1)
N(1)	2822(1)	4890(1)	2704(1)	23(1)
N(2)	1865(1)	5546(1)	2317(1)	21(1)
N(3)	677(1)	5382(1)	3058(1)	25(1)
N(4)	1459(1)	4355(1)	3459(1)	34(1)
C(1)	4028(1)	5163(1)	1933(1)	38(1)
C(2)	3174(1)	5220(1)	2220(1)	24(1)
C(3)	2650(1)	5653(1)	1998(1)	20(1)
C(4)	2860(1)	6172(1)	1578(1)	21(1)
C(5)	2284(1)	6606(1)	1462(1)	19(1)
C(6)	1468(1)	6452(1)	1780(1)	22(1)
C(7)	1277(1)	5939(1)	2210(1)	21(1)
C(8)	555(1)	5784(1)	2628(1)	25(1)
C(9)	-238(1)	6077(2)	2592(1)	38(1)
C(10)	3270(1)	4438(1)	2984(1)	28(1)
C(11)	2905(1)	3435(1)	2638(1)	32(1)
C(12)	3348(2)	3019(2)	2922(1)	52(1)
C(13)	4099(2)	3564(2)	3529(2)	70(1)
C(14)	4428(2)	4546(2)	3873(2)	66(1)
C(15)	4018(2)	5004(2)	3607(1)	40(1)
C(16)	2056(2)	2812(1)	1979(1)	35(1)
C(17)	1225(2)	2019(2)	2102(2)	62(1)
C(18)	2388(2)	2396(2)	1306(1)	53(1)
C(19)	4363(2)	6085(2)	4002(1)	54(1)
C(20)	4124(3)	6317(3)	4742(2)	118(2)
C(21)	5421(3)	6677(2)	4052(3)	136(2)
C(22)	69(1)	5264(1)	3568(1)	31(1)
C(23)	304(2)	6058(2)	4221(1)	40(1)
C(24)	-276(2)	5914(2)	4720(1)	60(1)
C(25)	-1042(2)	5022(2)	4565(1)	68(1)
C(26)	-1252(2)	4269(2)	3923(1)	51(1)
C(27)	-705(1)	4352(2)	3408(1)	35(1)
C(28)	1163(2)	7044(2)	4398(1)	49(1)
C(29)	904(3)	7871(2)	4701(3)	153(2)
C(30)	2044(2)	7193(2)	4862(2)	120(2)

C(31)	-968(2)	3499(2)	2694(1)	41(1)
C(32)	-1904(2)	3270(2)	2208(1)	60(1)
C(33)	-1093(2)	2601(2)	2791(2)	65(1)
C(34)	3652(1)	5935(1)	-514(1)	29(1)
C(35)	2610(1)	5810(1)	-670(1)	37(1)
C(36)	3566(2)	5141(1)	-266(1)	38(1)
C(37)	3991(2)	5716(2)	-1237(1)	44(1)
C(38)	5661(1)	7299(1)	674(1)	29(1)
C(39)	5428(1)	6779(1)	1179(1)	34(1)
C(40)	6158(1)	6842(2)	126(1)	41(1)
C(41)	6427(1)	8340(2)	1152(1)	38(1)
C(42)	4821(1)	8168(1)	-199(1)	26(1)
C(43)	5651(1)	8214(2)	-601(1)	39(1)
C(44)	5147(2)	9165(1)	411(1)	38(1)
C(45)	3958(1)	7983(1)	-749(1)	33(1)
C(46)	4715(2)	9073(2)	3331(1)	37(1)
C(47)	3887(2)	8324(2)	3510(1)	49(1)
C(48)	5140(2)	8504(2)	2792(1)	44(1)
C(49)	5533(2)	9783(2)	4036(1)	53(1)
C(50)	5273(2)	10807(1)	2822(1)	35(1)
C(51)	6096(2)	10573(2)	2565(1)	51(1)
C(52)	5730(2)	11725(2)	3535(1)	53(1)
C(53)	4885(2)	11052(1)	2245(1)	42(1)
C(54)	3314(2)	10043(1)	3375(1)	34(1)
C(55)	2335(2)	9120(2)	3151(1)	40(1)
C(56)	3101(2)	10739(2)	3147(1)	43(1)
C(57)	3652(2)	10520(2)	4214(1)	51(1)
C(58)	1377(1)	8965(1)	335(1)	29(1)
C(59)	665(2)	9341(1)	166(1)	39(1)
C(60)	1746(2)	8654(2)	-359(1)	41(1)
C(61)	2264(1)	9819(1)	928(1)	39(1)
C(62)	21(1)	8260(1)	1349(1)	31(1)
C(63)	542(2)	9327(2)	1905(1)	42(1)
C(64)	-995(1)	8054(2)	978(1)	45(1)
C(65)	-150(1)	7671(2)	1802(1)	39(1)

C(66)	26(1)	6713(1)	-116(1)	31(1)
C(67)	-653(2)	6738(2)	-688(1)	47(1)
C(68)	-619(2)	5949(1)	138(1)	43(1)
C(69)	710(2)	6348(2)	-497(1)	40(1)

Table B.9 Crystal data and structure refinement for [(^{iPr}PDI)Fe(NO)(THF)][$BArF_{24}$]

Table B.10 Crystal data and structure refinement for [(^{iPr}PDI)]$_2$Fe(μ-O)

Identification code	amt24	
Empirical formula	C70 H96 Fe2 N6 O2	
Formula weight	1165.23	
Temperature	173(2) K	
Wavelength	0.71073 Å	
Crystal system	Monoclinic	
Space group	P2(1)/n	
Unit cell dimensions	a = 13.2449(5) Å	α= 90°.
	b = 24.8769(9) Å	β= 91.9100(10)°.
	c = 20.6717(6) Å	γ = 90°.
Volume	6807.4(4) Å^3	
Z	4	
Density (calculated)	1.137 Mg/m^3	
Absorption coefficient	0.472 mm^{-1}	
F(000)	2504	
Crystal size	0.35 x 0.20 x 0.15 mm^3	
Theta range for data collection	1.28 to 23.26°.	
Index ranges	-14<=h<=14, -27<=k<=27, -22<=l<=21	
Reflections collected	41893	
Independent reflections	9669 [R(int) = 0.0536]	
Completeness to theta = 23.26°	99.0 %	
Absorption correction	Semi-empirical from equivalents	
Max. and min. transmission	0.9326 and 0.8523	
Refinement method	Full-matrix least-squares on F^2	
Data / restraints / parameters	9669 / 0 / 725	
Goodness-of-fit on F^2	1.034	

Final R indices [I>2sigma(I)]		R1 = 0.0473, wR2 = 0.1239		
R indices (all data)		R1 = 0.0727, wR2 = 0.1348		
Largest diff. peak and hole		0.441 and -0.438 e.Å^{-3}		
	x	y	z	U(eq)
Fe(1)	9887(1)	1980(1)	7083(1)	28(1)
Fe(2)	8581(1)	1839(1)	8569(1)	28(1)
O(1)	9192(1)	1925(1)	7812(1)	30(1)
N(1)	9896(2)	2798(1)	6669(1)	36(1)
N(2)	9571(2)	1890(1)	6141(1)	33(1)
N(3)	10541(2)	1190(1)	6804(1)	30(1)
N(4)	6966(2)	1598(1)	8454(1)	30(1)
N(5)	7854(2)	2255(1)	9238(1)	31(1)
N(6)	9701(2)	2000(1)	9374(1)	30(1)
C(1)	9104(3)	3347(1)	5775(2)	64(1)
C(2)	9413(2)	2826(1)	6101(1)	42(1)
C(3)	9230(2)	2319(1)	5783(1)	38(1)
C(4)	8805(2)	2243(1)	5163(1)	48(1)
C(5)	8802(2)	1739(1)	4891(1)	54(1)
C(6)	9257(2)	1315(1)	5222(1)	51(1)
C(7)	9648(2)	1399(1)	5853(1)	36(1)
C(8)	10184(2)	1008(1)	6246(1)	34(1)
C(9)	10326(3)	446(1)	6010(2)	54(1)
C(10)	10240(2)	3278(1)	6980(1)	42(1)
C(11)	9657(3)	3521(1)	7451(2)	53(1)
C(12)	10058(3)	3973(1)	7762(2)	73(1)
C(13)	10981(3)	4181(1)	7614(2)	78(1)
C(14)	11539(3)	3937(1)	7149(2)	65(1)
C(15)	11189(3)	3485(1)	6824(2)	50(1)
C(16)	8627(3)	3318(1)	7613(2)	65(1)
C(17)	7807(3)	3657(2)	7299(2)	92(2)
C(18)	8476(3)	3290(2)	8337(2)	85(1)
C(19)	11833(3)	3227(1)	6309(2)	60(1)
C(20)	12904(3)	3111(2)	6551(2)	83(1)
C(21)	11869(3)	3590(2)	5709(2)	90(1)

C(22)	11127(2)	846(1)	7233(1)	31(1)
C(23)	10637(2)	560(1)	7718(1)	35(1)
C(24)	11232(2)	259(1)	8143(1)	44(1)
C(25)	12263(2)	242(1)	8105(2)	50(1)
C(26)	12735(2)	528(1)	7628(1)	48(1)
C(27)	12177(2)	832(1)	7180(1)	38(1)
C(28)	9499(2)	581(1)	7787(1)	37(1)
C(29)	8988(3)	71(1)	7542(2)	64(1)
C(30)	9229(2)	695(1)	8477(1)	44(1)
C(31)	12716(2)	1127(1)	6649(2)	54(1)
C(32)	13601(2)	1464(1)	6899(2)	66(1)
C(33)	13093(3)	735(2)	6151(2)	91(1)
C(34)	5216(2)	1901(1)	8678(2)	53(1)
C(35)	6341(2)	1914(1)	8764(1)	36(1)
C(36)	6825(2)	2283(1)	9217(1)	35(1)
C(37)	6317(2)	2624(1)	9633(2)	50(1)
C(38)	6849(3)	2922(1)	10088(2)	56(1)
C(39)	7881(2)	2865(1)	10131(1)	48(1)
C(40)	8381(2)	2525(1)	9724(1)	34(1)
C(41)	9426(2)	2376(1)	9773(1)	35(1)
C(42)	10114(2)	2627(1)	10281(1)	47(1)
C(43)	6563(2)	1186(1)	8038(1)	34(1)
C(44)	6545(2)	1268(1)	7363(1)	42(1)
C(45)	6209(2)	853(1)	6968(2)	56(1)
C(46)	5890(3)	371(2)	7231(2)	67(1)
C(47)	5911(2)	291(1)	7881(2)	57(1)
C(48)	6247(2)	698(1)	8306(2)	42(1)
C(49)	6882(2)	1799(1)	7077(2)	54(1)
C(50)	7101(3)	1759(2)	6355(2)	81(1)
C(51)	6117(3)	2250(2)	7165(2)	69(1)
C(52)	6254(3)	598(1)	9031(2)	57(1)
C(53)	5163(3)	536(2)	9263(2)	105(2)
C(54)	6865(3)	101(2)	9227(2)	72(1)
C(55)	10674(2)	1756(1)	9442(1)	32(1)
C(56)	10832(2)	1360(1)	9921(1)	40(1)

C(57)	11726(3)	1075(1)	9922(2)	54(1)
C(58)	12455(2)	1177(1)	9483(2)	57(1)
C(59)	12308(2)	1584(1)	9033(2)	52(1)
C(60)	11421(2)	1881(1)	8998(1)	38(1)
C(61)	10042(3)	1232(1)	10419(1)	49(1)
C(62)	9504(3)	707(2)	10284(2)	87(1)
C(63)	10529(3)	1223(2)	11116(2)	91(2)
C(64)	11262(2)	2334(1)	8525(1)	41(1)
C(65)	11643(3)	2869(1)	8794(2)	73(1)
C(66)	11754(2)	2229(1)	7876(2)	58(1)
O(1S)	10374(4)	806(2)	3792(2)	150(2)
C(1S)	12150(6)	425(4)	4274(3)	237(4)
C(2S)	11457(5)	903(3)	3959(5)	289(4)
C(3S)	9702(7)	1157(3)	3305(3)	197(4)
C(4S)	8708(7)	908(3)	3420(4)	232(4)

Table B.11 Crystal data and structure refinement for [(^{iPr}PDI)Fe(CH_2CMe_3)][BPh_4]

Identification code	amt26	
Empirical formula	C71 H81.50 B F1.50 Fe N3	
Formula weight	1072.05	
Temperature	173(2) K	
Wavelength	0.71073 Å	
Crystal system	Monoclinic	
Space group	P2(1)/c	
Unit cell dimensions	a = 21.3132(7) Å	α= 90°.
	b = 12.8607(4) Å	β= 106.4620(10)°.
	c = 25.0256(9) Å	γ = 90°.
Volume	6578.4(4) $Å^3$	
Z	4	
Density (calculated)	1.082 Mg/m^3	
Absorption coefficient	0.274 mm^{-1}	
F(000)	2292	
Crystal size	0.60 x 0.20 x 0.10 mm^3	
Theta range for data collection	1.87 to 26.37°.	

Index ranges	-26<=h<=26, -16<=k<=16, -31<=l<=31
Reflections collected	56100
Independent reflections	13452 [R(int) = 0.0433]
Completeness to theta = 26.37°	100.0 %
Absorption correction	Semi-empirical from equivalents
Max. and min. transmission	0.9732 and 0.8530
Refinement method	Full-matrix least-squares on F^2
Data / restraints / parameters	13452 / 201 / 774
Goodness-of-fit on F^2	1.017
Final R indices [I>2sigma(I)]	R1 = 0.0487, wR2 = 0.1338
R indices (all data)	R1 = 0.0737, wR2 = 0.1453
Largest diff. peak and hole	0.342 and -0.506 e.$Å^{-3}$

	x	y	z	U(eq)
Fe(1)	2275(1)	9026(1)	2792(1)	31(1)
N(1)	2584(1)	10673(1)	2822(1)	28(1)
N(2)	2922(1)	9149(1)	2294(1)	26(1)
N(3)	2158(1)	7579(1)	2274(1)	30(1)
C(1)	3383(1)	11918(2)	2632(1)	46(1)
C(2)	3048(1)	10898(1)	2609(1)	30(1)
C(3)	3245(1)	10035(1)	2288(1)	28(1)
C(4)	3696(1)	10133(2)	1984(1)	35(1)
C(5)	3805(1)	9282(2)	1687(1)	39(1)
C(6)	3471(1)	8363(2)	1696(1)	36(1)
C(7)	3019(1)	8332(2)	1998(1)	30(1)
C(8)	2583(1)	7434(2)	2004(1)	33(1)
C(9)	2653(1)	6485(2)	1684(1)	52(1)
C(10)	2297(1)	11446(1)	3101(1)	31(1)
C(11)	2588(1)	11706(1)	3658(1)	35(1)
C(12)	2251(1)	12399(2)	3907(1)	43(1)
C(13)	1648(1)	12785(2)	3616(1)	46(1)
C(14)	1370(1)	12506(2)	3072(1)	47(1)
C(15)	1685(1)	11829(2)	2800(1)	39(1)
C(16)	3238(1)	11270(2)	4007(1)	42(1)
C(17)	3178(1)	10768(2)	4544(1)	52(1)

C(18)	3764(1)	12114(2)	4155(1)	63(1)
C(19)	1361(3)	11450(6)	2210(3)	42(2)
C(20)	1614(2)	12164(4)	1820(2)	67(2)
C(21)	623(3)	11449(6)	2021(4)	67(2)
C(19')	1419(6)	11707(8)	2153(5)	40(3)
C(20')	1224(5)	12697(6)	1811(3)	70(3)
C(21')	828(9)	11028(12)	2068(6)	118(7)
C(22)	1683(1)	6795(2)	2289(1)	33(1)
C(23)	1858(1)	5912(2)	2621(1)	40(1)
C(24)	1351(1)	5230(2)	2638(1)	50(1)
C(25)	720(1)	5407(2)	2342(1)	52(1)
C(26)	558(1)	6277(2)	2016(1)	50(1)
C(27)	1033(1)	6998(2)	1983(1)	40(1)
C(28)	2554(1)	5643(2)	2944(1)	58(1)
C(29)	2759(1)	4586(2)	2760(2)	78(1)
C(30)	2642(2)	5644(2)	3575(2)	88(1)
C(31)	862(1)	7948(2)	1612(1)	57(1)
C(32)	917(2)	7686(3)	1033(2)	99(1)
C(33)	193(1)	8399(3)	1578(2)	84(1)
C(34)	2080(1)	8658(2)	3520(1)	41(1)
C(35)	1371(13)	8736(16)	3596(11)	48(5)
C(36)	814(12)	8230(30)	3152(16)	96(7)
C(37)	1440(16)	8290(30)	4173(14)	89(7)
C(38)	1214(15)	9889(16)	3617(13)	58(5)
C(35')	1443(6)	8729(7)	3670(4)	33(2)
C(36')	975(6)	7932(10)	3326(5)	65(3)
C(37')	1527(7)	8506(10)	4290(4)	57(2)
C(38')	1150(8)	9813(8)	3553(6)	58(3)
B(1)	4371(1)	4649(2)	1392(1)	28(1)
C(40)	4476(1)	4849(2)	2064(1)	30(1)
C(41)	4543(1)	5819(2)	2324(1)	39(1)
C(42)	4614(1)	5938(2)	2890(1)	51(1)
C(43)	4615(1)	5079(2)	3221(1)	51(1)
C(44)	4556(1)	4111(2)	2983(1)	46(1)
C(45)	4489(1)	4003(2)	2421(1)	38(1)

C(46)	3821(1)	3722(2)	1198(1)	32(1)
C(47)	3204(1)	3812(2)	1282(1)	43(1)
C(48)	2722(1)	3076(2)	1115(1)	56(1)
C(49)	2847(2)	2167(2)	872(1)	63(1)
C(50)	3450(2)	2023(2)	798(1)	61(1)
C(51)	3926(1)	2790(2)	954(1)	44(1)
C(52)	5048(1)	4254(1)	1265(1)	28(1)
C(53)	5562(1)	3758(2)	1651(1)	32(1)
C(54)	6079(1)	3296(2)	1504(1)	37(1)
C(55)	6109(1)	3329(2)	959(1)	35(1)
C(56)	5615(1)	3829(2)	567(1)	37(1)
C(57)	5100(1)	4279(2)	716(1)	36(1)
C(58)	4127(1)	5730(1)	1037(1)	28(1)
C(59)	4569(1)	6557(2)	1067(1)	33(1)
C(60)	4397(1)	7486(2)	780(1)	37(1)
C(61)	3767(1)	7629(2)	445(1)	38(1)
C(62)	3318(1)	6835(2)	394(1)	38(1)
C(63)	3498(1)	5912(2)	685(1)	33(1)
F(1)	1912(2)	-131(3)	1225(1)	157(1)
F(2)	6285(2)	15313(3)	5279(2)	94(1)
C(1S)	1765(3)	-179(3)	659(2)	104(1)
C(2S)	2192(3)	-578(3)	414(2)	113(1)
C(3S)	2023(3)	-615(4)	-129(2)	142(2)
C(4S)	1423(4)	-280(5)	-468(3)	160(3)
C(5S)	1000(4)	130(6)	-199(3)	180(3)
C(6S)	1154(3)	234(4)	388(3)	142(2)
C(7S)	5652(2)	15173(2)	5154(1)	57(1)
C(8S)	5424(2)	14256(2)	5299(1)	52(1)
C(9S)	4766(2)	14075(2)	5143(1)	54(1)

Table B.12 Crystal data and structure refinement for (^{iPr}PDI)Fe(NCO)

Identification code	amt30
Empirical formula	C34 H43 Fe N4 O
Formula weight	579.57

Temperature	173(2) K	
Wavelength	0.71073 Å	
Crystal system	Monoclinic	
Space group	P2(1)/c	
Unit cell dimensions	a = 8.7891(5) Å	α= 90°.
	b = 23.7440(15) Å	β= 110.457(3)°.
	c = 16.4556(9) Å	γ = 90°.
Volume	3217.5(3) $Å^3$	
Z	4	
Density (calculated)	1.196 Mg/m^3	
Absorption coefficient	0.500 mm^{-1}	
F(000)	1236	
Crystal size	0.35 x 0.15 x 0.05 mm^3	
Theta range for data collection	1.72 to 26.37°.	
Index ranges	-8<=h<=10, -29<=k<=28, -20<=l<=20	
Reflections collected	25140	
Independent reflections	6568 [R(int) = 0.0504]	
Completeness to theta = 26.37°	99.9 %	
Absorption correction	Semi-empirical from equivalents	
Max. and min. transmission	0.9755 and 0.8445	
Refinement method	Full-matrix least-squares on F^2	
Data / restraints / parameters	6568 / 9 / 439	
Goodness-of-fit on F^2	1.017	
Final R indices [I>2sigma(I)]	R1 = 0.0528, wR2 = 0.1295	
R indices (all data)	R1 = 0.0953, wR2 = 0.1559	
Largest diff. peak and hole	1.387 and -0.325 $e.Å^{-3}$	

	x	y	z	U(eq)
Fe(1)	6115(1)	3083(1)	2456(1)	32(1)
O(1)	10297(3)	3683(1)	4363(2)	88(1)
N(1)	5484(3)	3943(1)	2147(1)	29(1)
N(2)	4077(3)	3054(1)	1438(1)	30(1)
N(3)	5757(3)	2213(1)	2183(1)	28(1)
N(4)	8069(4)	3156(1)	3464(2)	62(1)

C(1)	3498(4)	4614(1)	1197(2)	44(1)
C(2)	4147(3)	4039(1)	1492(2)	29(1)
C(3)	3311(3)	3538(1)	1065(2)	29(1)
C(4)	1893(3)	3519(1)	348(2)	36(1)
C(5)	1240(4)	3007(1)	-5(2)	39(1)
C(6)	2056(3)	2511(1)	365(2)	35(1)
C(7)	3467(3)	2544(1)	1084(2)	28(1)
C(8)	4445(3)	2074(1)	1529(2)	29(1)
C(9)	3968(4)	1481(1)	1260(2)	40(1)
C(10)	6431(3)	4393(1)	2659(2)	32(1)
C(11)	7848(4)	4552(1)	2522(2)	39(1)
C(12)	8818(4)	4957(2)	3083(3)	51(1)
C(13)	8428(5)	5181(2)	3740(2)	53(1)
C(14)	7034(5)	5022(2)	3867(2)	50(1)
C(15)	5984(4)	4627(1)	3327(2)	38(1)
C(16)	8301(4)	4289(2)	1804(2)	56(1)
C(17)	10088(6)	4139(3)	2092(3)	104(2)
C(18)	7820(6)	4670(2)	1022(3)	89(2)
C(19)	4476(4)	4439(2)	3484(2)	47(1)
C(20)	4876(5)	3986(2)	4183(3)	74(1)
C(21)	3557(5)	4929(2)	3699(2)	68(1)
C(22)	6818(3)	1778(1)	2666(2)	30(1)
C(23)	6478(4)	1503(1)	3335(2)	38(1)
C(24)	7507(4)	1069(2)	3762(2)	51(1)
C(25)	8817(4)	911(2)	3550(3)	55(1)
C(26)	9160(4)	1199(2)	2918(3)	55(1)
C(27)	8192(4)	1642(2)	2469(2)	44(1)
C(28)	5077(5)	1674(2)	3611(2)	53(1)
C(29)	4081(5)	1178(2)	3733(3)	71(1)
C(30)	5684(7)	2026(2)	4431(3)	87(2)
C(31)	8587(19)	1919(8)	1721(13)	55(4)
C(32)	8930(20)	1552(9)	1061(9)	103(5)
C(33)	9990(30)	2325(8)	2130(14)	145(9)
C(31')	8670(20)	2045(13)	1905(15)	59(6)
C(32')	8280(30)	1746(9)	1045(10)	82(5)

C(33')	10490(20)	2193(13)	2216(11)	107(9)
C(34)	9160(5)	3428(2)	3903(2)	60(1)

Table B.13 Crystal data and structure refinement for [(^{iPr}PDI)Fe(OEt_2)][$BArF_{24}$]

Identification code	amt31	
Empirical formula	C69 H65 B F24 Fe N3 O	
Formula weight	1474.90	
Temperature	293(2) K	
Wavelength	0.71073 Å	
Crystal system	Monoclinic	
Space group	P2(1)/c	
Unit cell dimensions	a = 17.6408(6) Å	α= 90°.
	b = 18.4423(6) Å	β= 104.481(2)°.
	c = 22.4263(7) Å	γ = 90°.
Volume	7064.3(4) $Å^3$	
Z	4	
Density (calculated)	1.387 Mg/m^3	
Absorption coefficient	0.320 mm^{-1}	
F(000)	3020	
Crystal size	0.45 x 0.30 x 0.15 mm^3	
Theta range for data collection	1.62 to 26.37°.	
Index ranges	-21<=h<=22, -23<=k<=22, -28<=l<=28	
Reflections collected	54965	
Independent reflections	14407 [R(int) = 0.0461]	
Completeness to theta = 26.37°	100.0 %	
Absorption correction	Semi-empirical from equivalents	
Max. and min. transmission	0.9535 and 0.8692	
Refinement method	Full-matrix least-squares on F^2	
Data / restraints / parameters	14407 / 867 / 1131	
Goodness-of-fit on F^2	1.097	
Final R indices [I>2sigma(I)]	R1 = 0.0625, wR2 = 0.1853	
R indices (all data)	R1 = 0.1033, wR2 = 0.2054	
Largest diff. peak and hole	1.414 and -0.810 $e.Å^{-3}$	

	x	y	z	U(eq)
Fe(1)	3366(1)	1566(1)	4379(1)	38(1)
O(1)	3154(1)	492(1)	4379(1)	51(1)
N(1)	3178(1)	1863(1)	3445(1)	34(1)
N(2)	2781(1)	2468(1)	4331(1)	34(1)
N(3)	3674(2)	1935(1)	5297(1)	37(1)
C(1)	2427(2)	2681(2)	2639(2)	54(1)
C(2)	2698(2)	2405(2)	3283(1)	38(1)
C(3)	2470(2)	2773(2)	3778(1)	36(1)
C(4)	2022(2)	3394(2)	3741(2)	45(1)
C(5)	1919(2)	3709(2)	4267(2)	45(1)
C(6)	2307(2)	3433(2)	4834(2)	41(1)
C(7)	2746(2)	2811(2)	4858(1)	34(1)
C(8)	3252(2)	2487(2)	5402(1)	38(1)
C(9)	3285(2)	2800(2)	6026(2)	53(1)
C(10)	3500(2)	1498(2)	3000(1)	38(1)
C(11)	3125(2)	892(2)	2673(1)	43(1)
C(12)	3499(2)	547(2)	2276(2)	58(1)
C(13)	4218(2)	767(2)	2220(2)	61(1)
C(14)	4576(2)	1344(3)	2547(2)	60(1)
C(15)	4230(2)	1730(2)	2941(2)	49(1)
C(16)	2337(2)	630(2)	2732(2)	52(1)
C(17)	2295(3)	-193(2)	2757(2)	79(1)
C(18)	1669(2)	886(3)	2208(2)	83(2)
C(19)	4654(2)	2374(2)	3289(2)	64(1)
C(20)	4797(3)	2955(3)	2860(2)	82(1)
C(21)	5429(3)	2144(3)	3720(3)	111(2)
C(22)	4265(2)	1634(2)	5794(2)	42(1)
C(23)	5027(2)	1920(2)	5900(2)	52(1)
C(24)	5597(2)	1625(3)	6368(2)	66(1)
C(25)	5443(3)	1072(3)	6735(2)	69(1)
C(26)	4701(3)	788(2)	6616(2)	62(1)
C(27)	4097(2)	1048(2)	6141(2)	48(1)

C(28)	5226(2)	2531(3)	5525(2)	66(1)
C(29)	6009(3)	2442(4)	5373(2)	97(2)
C(30)	5203(4)	3253(3)	5829(3)	119(2)
C(31)	3301(2)	722(2)	6042(2)	56(1)
C(32)	2879(3)	996(3)	6505(2)	87(2)
C(33)	3320(3)	-103(2)	6058(2)	86(1)
C(34)	3798(3)	-3(2)	4378(2)	72(1)
C(35)	4492(2)	444(3)	4346(2)	77(1)
C(36)	2438(2)	135(2)	4395(2)	66(1)
C(37)	1816(2)	683(3)	4355(2)	80(1)
B(1)	1268(2)	6011(2)	3552(2)	35(1)
C(44)	-874(2)	7431(2)	4228(2)	51(1)
F(1)	-1022(1)	7788(2)	4682(1)	98(1)
F(2)	-1259(1)	7731(2)	3715(1)	93(1)
F(3)	-1247(2)	6801(2)	4226(2)	103(1)
C(45)	1925(10)	8127(9)	5033(6)	76(7)
F(4)	1688(4)	8468(10)	5475(6)	99(6)
F(5)	2549(5)	7807(5)	5338(6)	91(4)
F(6)	2175(14)	8591(10)	4690(8)	187(10)
C(45')	1873(9)	8227(8)	4987(8)	93(9)
F(4')	2419(7)	8402(8)	4731(7)	116(6)
F(5')	2226(18)	7916(14)	5499(9)	236(14)
F(6')	1592(6)	8872(7)	5034(15)	162(9)
C(52)	2707(3)	7433(3)	2197(2)	88(2)
F(7)	2837(2)	8101(2)	2481(2)	163(2)
F(8)	2713(2)	7638(3)	1664(2)	163(2)
F(9)	3339(2)	7140(2)	2499(2)	141(2)
C(53)	-139(8)	7011(6)	1421(6)	71(6)
F(10)	-190(7)	7639(4)	1147(5)	117(5)
F(11)	-770(3)	6946(6)	1637(3)	83(3)
F(12)	-211(4)	6514(4)	995(3)	84(2)
C(53')	-88(14)	7049(10)	1505(11)	62(11)
F(10')	-568(12)	7440(30)	1732(8)	155(11)
F(11')	-71(14)	7406(19)	1007(9)	142(11)
F(12')	-476(17)	6443(10)	1335(19)	166(15)

C(60)	-66(3)	3908(2)	2181(2)	64(1)
F(13)	606(12)	3696(19)	2069(15)	108(13)
F(14)	-520(11)	3338(9)	2156(10)	55(7)
F(15)	-409(17)	4329(12)	1702(8)	73(8)
F(13')	548(13)	3477(18)	2208(14)	130(14)
F(14')	-721(11)	3519(10)	2028(13)	66(5)
F(15')	-140(18)	4345(16)	1710(9)	146(15)
F(13")	577(14)	3896(17)	1983(17)	82(7)
F(14")	-140(20)	3205(8)	2248(14)	146(17)
F(15")	-511(19)	4242(15)	1695(7)	89(12)
C(61)	-621(11)	4290(11)	4198(11)	79(12)
F(16)	-177(17)	3904(19)	4652(17)	93(7)
F(17)	-1255(14)	3890(20)	3996(13)	91(6)
F(18)	-850(20)	4834(13)	4497(14)	65(5)
C(61')	-640(8)	4269(8)	4226(5)	43(7)
F(16')	-147(12)	4014(18)	4724(11)	87(6)
F(17')	-1160(16)	3755(18)	4047(11)	95(6)
F(18')	-1000(20)	4819(11)	4413(16)	79(6)
C(68)	3780(8)	4620(8)	3604(7)	72(5)
F(19)	4200(14)	4076(11)	3909(5)	155(7)
F(20)	4294(11)	5051(8)	3454(13)	149(8)
F(21)	3417(8)	4327(10)	3083(6)	104(5)
C(68')	3821(8)	4716(9)	3502(8)	62(7)
F(19')	4528(6)	4595(19)	3828(8)	132(10)
F(20')	3878(15)	5134(9)	3051(9)	113(6)
F(21')	3544(14)	4104(11)	3265(14)	116(9)
C(69)	3300(8)	5309(7)	5526(8)	86(9)
F(22)	3765(10)	4761(7)	5746(5)	117(5)
F(23)	2734(5)	5224(17)	5813(5)	147(8)
F(24)	3717(13)	5878(7)	5769(3)	109(5)
C(69')	3253(7)	5358(9)	5574(6)	62(8)
F(22')	3956(6)	5129(19)	5841(6)	158(9)
F(23')	2797(10)	4905(9)	5765(7)	123(7)
F(24')	3131(19)	5978(6)	5799(4)	124(6)
C(38)	981(2)	6643(2)	3955(1)	35(1)

C(39)	1514(2)	7137(2)	4302(2)	44(1)
C(40)	1289(2)	7695(2)	4627(2)	53(1)
C(41)	506(2)	7796(2)	4611(2)	50(1)
C(42)	-27(2)	7334(2)	4261(1)	40(1)
C(43)	201(2)	6775(2)	3940(1)	36(1)
C(46)	1309(2)	6418(2)	2915(1)	35(1)
C(47)	1979(2)	6728(2)	2810(2)	44(1)
C(48)	1981(2)	7114(2)	2282(2)	50(1)
C(49)	1298(2)	7207(2)	1832(2)	48(1)
C(50)	624(2)	6926(2)	1929(2)	45(1)
C(51)	626(2)	6545(2)	2455(2)	40(1)
C(54)	664(2)	5326(2)	3416(1)	33(1)
C(55)	542(2)	4916(2)	2877(1)	39(1)
C(56)	45(2)	4322(2)	2770(2)	43(1)
C(57)	-355(2)	4106(2)	3196(1)	40(1)
C(58)	-229(2)	4495(2)	3735(1)	36(1)
C(59)	270(2)	5081(2)	3844(1)	35(1)
C(62)	2110(2)	5669(2)	3924(1)	36(1)
C(63)	2605(2)	5330(2)	3613(2)	43(1)
C(64)	3302(2)	5011(2)	3921(2)	49(1)
C(65)	3531(2)	5011(2)	4552(2)	54(1)
C(66)	3052(2)	5329(2)	4869(2)	49(1)
C(67)	2352(2)	5647(2)	4561(2)	41(1)

Table B.14 Crystal data and structure refinement for [(^{iPr}PDI)Fe(CO)$_2$][BArF$_{24}$]

Identification code	amt32	
Empirical formula	C67 H55 B F24 Fe N3 O2	
Formula weight	1456.80	
Temperature	293(2) K	
Wavelength	0.71073 Å	
Crystal system	Monoclinic	
Space group	P2(1)/c	
Unit cell dimensions	a = 17.4932(11) Å	α= 90°.

	b = 18.0250(11) Å	β= 106.010(3)°.
	c = 22.4714(13) Å	γ = 90°.
Volume	6810.7(7) Å^3	
Z	4	
Density (calculated)	1.421 Mg/m^3	
Absorption coefficient	0.332 mm^{-1}	
F(000)	2964	
Crystal size	0.40 x 0.25 x 0.05 mm^3	
Theta range for data collection	1.66 to 26.37°.	
Index ranges	-21<=h<=20, -22<=k<=22, -28<=l<=27	
Reflections collected	56881	
Independent reflections	13914 [R(int) = 0.0388]	
Completeness to theta = 26.37°	99.9 %	
Absorption correction	Semi-empirical from equivalents	
Max. and min. transmission	0.9836 and 0.8785	
Refinement method	Full-matrix least-squares on F^2	
Data / restraints / parameters	13914 / 396 / 1069	
Goodness-of-fit on F^2	1.059	
Final R indices [I>2sigma(I)]	R1 = 0.0588, wR2 = 0.1577	
R indices (all data)	R1 = 0.0855, wR2 = 0.1731	
Largest diff. peak and hole	0.934 and -0.602 e.Å^{-3}	

	x	y	z	U(eq)
B(1)	8799(2)	3979(2)	1453(1)	25(1)
C(36)	9396(2)	4695(2)	1576(1)	25(1)
C(37)	9774(2)	4939(2)	1140(1)	27(1)
C(38)	10258(2)	5560(2)	1229(1)	31(1)
C(39)	10381(2)	5979(2)	1767(1)	32(1)
C(40)	10002(2)	5760(2)	2198(1)	31(1)
C(41)	9516(2)	5136(2)	2103(1)	28(1)
C(42)	8788(2)	3600(2)	2118(1)	26(1)
C(43)	9499(2)	3521(2)	2583(1)	30(1)
C(44)	9536(2)	3180(2)	3141(1)	34(1)
C(45)	8856(2)	2897(2)	3258(1)	36(1)

C(46)	8156(2)	2949(2)	2802(1)	37(1)
C(47)	8121(2)	3295(2)	2240(1)	32(1)
C(48)	7934(2)	4300(2)	1065(1)	25(1)
C(49)	7433(2)	4665(2)	1354(1)	31(1)
C(50)	6724(2)	4993(2)	1019(2)	35(1)
C(51)	6495(2)	4974(2)	384(2)	38(1)
C(52)	6978(2)	4624(2)	87(1)	34(1)
C(53)	7688(2)	4298(2)	418(1)	29(1)
C(54)	9104(2)	3308(2)	1086(1)	25(1)
C(55)	8577(2)	2770(2)	769(1)	34(1)
C(56)	8819(2)	2180(2)	475(2)	43(1)
C(57)	9604(2)	2093(2)	486(2)	41(1)
C(58)	10145(2)	2609(2)	807(1)	33(1)
C(59)	9896(2)	3202(2)	1099(1)	27(1)
C(60)	10627(2)	5791(2)	736(2)	45(1)
F(1)	11191(2)	6282(2)	917(1)	94(1)
F(2)	10092(2)	6073(2)	248(1)	83(1)
F(3)	10935(2)	5228(1)	505(1)	63(1)
C(61)	10120(5)	6195(3)	2787(3)	31(3)
F(4)	9451(7)	6466(11)	2840(6)	89(4)
F(5)	10386(6)	5774(5)	3278(4)	60(2)
F(6)	10632(10)	6726(7)	2844(6)	97(4)
C(61')	10087(12)	6222(11)	2760(10)	102(15)
F(4')	10761(8)	6595(13)	2936(11)	69(6)
F(5')	9560(13)	6755(17)	2682(13)	83(6)
F(6')	10040(30)	5846(14)	3250(9)	114(11)
C(62)	10280(12)	3128(8)	3581(8)	50(10)
F(7)	10592(12)	3783(7)	3779(15)	119(7)
F(8)	10294(13)	2760(20)	4084(10)	135(9)
F(9)	10835(13)	2840(20)	3370(7)	142(9)
C(62')	10337(8)	3129(6)	3644(6)	49(6)
F(7')	10408(7)	3644(7)	4069(6)	93(4)
F(8')	10420(7)	2502(4)	3943(5)	70(3)
F(9')	10952(5)	3183(8)	3423(4)	87(4)
C(63)	7425(3)	2610(3)	2896(2)	62(1)

F(10)	7444(2)	2505(2)	3469(1)	91(1)
F(11)	7317(2)	1898(2)	2659(2)	121(1)
F(12)	6774(2)	2906(2)	2592(2)	114(1)
C(64)	6188(7)	5355(7)	1379(6)	54(6)
F(13)	5573(11)	5680(18)	1012(5)	154(8)
F(14)	6584(7)	5841(7)	1765(7)	89(4)
F(15)	5934(12)	4900(8)	1726(11)	108(5)
C(64')	6239(9)	5408(9)	1339(7)	56(8)
F(13')	5919(11)	6009(5)	1038(6)	78(4)
F(14')	6604(9)	5670(12)	1883(6)	89(5)
F(15')	5644(11)	5031(10)	1424(13)	97(6)
C(65)	6719(9)	4644(8)	-559(9)	70(10)
F(16)	7292(6)	4670(20)	-832(6)	196(14)
F(17)	6265(12)	5200(7)	-815(4)	93(5)
F(18)	6272(16)	4085(8)	-806(4)	118(8)
C(65')	6769(5)	4583(6)	-621(4)	41(4)
F(16')	6021(4)	4704(12)	-886(3)	117(5)
F(17')	6941(9)	3953(3)	-830(2)	86(3)
F(18')	7157(7)	5068(4)	-844(4)	93(4)
C(66)	8211(11)	1588(9)	245(9)	83(8)
F(19)	7780(8)	1371(7)	601(7)	104(4)
F(20)	8514(6)	965(7)	100(12)	140(11)
F(21)	7684(12)	1831(11)	-254(6)	133(8)
C(66')	8217(6)	1636(6)	84(6)	50(3)
F(19')	8116(10)	1090(7)	428(4)	131(7)
F(20')	8418(4)	1369(5)	-392(3)	74(3)
F(21')	7530(6)	1924(7)	-160(6)	97(4)
C(67)	10998(2)	2532(2)	834(2)	44(1)
F(22)	11399(2)	3180(2)	941(2)	99(1)
F(23)	11398(2)	2133(2)	1297(1)	89(1)
F(24)	11139(2)	2280(2)	336(1)	79(1)
Fe(1)	3525(1)	3273(1)	4425(1)	27(1)
O(1)	4792(2)	4364(2)	4524(1)	65(1)
O(2)	2298(2)	4385(2)	4428(1)	57(1)
N(1)	3253(1)	3080(1)	3521(1)	27(1)

N(2)	2881(1)	2428(1)	4367(1)	26(1)
N(3)	3764(2)	2978(1)	5308(1)	28(1)
C(1)	2410(2)	2340(2)	2657(1)	41(1)
C(2)	2745(2)	2558(2)	3318(1)	30(1)
C(3)	2502(2)	2160(2)	3803(1)	29(1)
C(4)	1990(2)	1563(2)	3750(2)	35(1)
C(5)	1876(2)	1256(2)	4277(2)	38(1)
C(6)	2289(2)	1518(2)	4856(2)	34(1)
C(7)	2800(2)	2112(2)	4891(1)	29(1)
C(8)	3331(2)	2457(2)	5437(1)	30(1)
C(9)	3352(2)	2197(2)	6072(2)	41(1)
C(10)	3570(2)	3493(2)	3090(1)	30(1)
C(11)	4314(2)	3284(2)	3026(1)	35(1)
C(12)	4619(2)	3687(2)	2615(2)	43(1)
C(13)	4199(2)	4278(2)	2291(2)	45(1)
C(14)	3477(2)	4476(2)	2365(1)	40(1)
C(15)	3143(2)	4099(2)	2772(1)	34(1)
C(16)	4774(2)	2624(2)	3362(2)	43(1)
C(17)	5604(2)	2845(3)	3746(2)	59(1)
C(18)	4826(3)	2012(2)	2909(2)	60(1)
C(19)	2354(2)	4342(2)	2849(2)	39(1)
C(20)	2395(3)	5131(2)	3111(2)	56(1)
C(21)	1689(2)	4289(2)	2247(2)	58(1)
C(22)	4383(2)	3321(2)	5796(1)	34(1)
C(23)	4201(2)	3913(2)	6128(2)	40(1)
C(24)	4830(3)	4224(2)	6580(2)	55(1)
C(25)	5582(3)	3951(3)	6695(2)	69(1)
C(26)	5747(2)	3373(3)	6356(2)	61(1)
C(27)	5157(2)	3044(2)	5891(2)	45(1)
C(28)	3375(2)	4230(2)	6018(2)	44(1)
C(29)	3080(3)	4146(3)	6600(2)	75(1)
C(30)	3351(3)	5034(2)	5807(2)	71(1)
C(31)	5337(2)	2393(3)	5528(2)	57(1)
C(32)	5232(4)	1663(3)	5814(3)	91(2)
C(33)	6158(3)	2431(3)	5424(2)	80(2)

C(34)	4313(2)	3936(2)	4485(1)	40(1)
C(35)	2782(2)	3973(2)	4424(1)	37(1)

Table B.15 Crystal data and structure refinement for (^{Et}(4-^{t}Bu)PDI)Fe(NO)

Identification code	amt33	
Empirical formula	C33 H43 Fe N4 O	
Formula weight	567.56	
Temperature	173(2) K	
Wavelength	0.71073 Å	
Crystal system	Monoclinic	
Space group	P2(1)/c	
Unit cell dimensions	a = 11.0312(10) Å	α= 90°.
	b = 12.4914(10) Å	β= 95.202(4)°.
	c = 21.767(2) Å	γ = 90°.
Volume	2987.0(5) Å^3	
Z	4	
Density (calculated)	1.262 Mg/m^3	
Absorption coefficient	0.537 mm^{-1}	
F(000)	1212	
Crystal size	0.40 x 0.20 x 0.05 mm^3	
Theta range for data collection	1.88 to 28.28°.	
Index ranges	-14<=h<=14, -16<=k<=16, -29<=l<=28	
Reflections collected	27665	
Independent reflections	7374 [R(int) = 0.0343]	
Completeness to theta = 28.28°	99.2 %	
Absorption correction	Semi-empirical from equivalents	
Max. and min. transmission	0.9737 and 0.8140	
Refinement method	Full-matrix least-squares on F^2	
Data / restraints / parameters	7374 / 0 / 425	
Goodness-of-fit on F^2	1.019	
Final R indices [I>2sigma(I)]	R1 = 0.0350, wR2 = 0.0825	
R indices (all data)	R1 = 0.0566, wR2 = 0.0931	
Largest diff. peak and hole	0.329 and -0.298 e.Å^{-3}	

	x	y	z	U(eq)
Fe(1)	1422(1)	8072(1)	1551(1)	21(1)
O(1)	3138(2)	7162(1)	2449(1)	68(1)
N(1)	1195(1)	9655(1)	1596(1)	21(1)
N(2)	-293(1)	8200(1)	1482(1)	20(1)
N(3)	930(1)	6823(1)	1027(1)	20(1)
N(4)	2460(1)	7600(1)	2075(1)	34(1)
C(1)	-199(2)	11112(1)	1878(1)	28(1)
C(2)	86(1)	9993(1)	1687(1)	21(1)
C(3)	-818(1)	9175(1)	1570(1)	20(1)
C(4)	-2071(1)	9293(1)	1492(1)	22(1)
C(5)	-2819(1)	8438(1)	1278(1)	22(1)
C(6)	-2244(1)	7513(1)	1102(1)	22(1)
C(7)	-986(1)	7412(1)	1188(1)	20(1)
C(8)	-245(1)	6589(1)	965(1)	21(1)
C(9)	-777(2)	5599(1)	666(1)	30(1)
C(10)	2184(1)	10405(1)	1640(1)	21(1)
C(11)	2799(2)	10662(1)	2211(1)	27(1)
C(12)	3777(2)	11367(2)	2213(1)	34(1)
C(13)	4136(2)	11799(2)	1681(1)	35(1)
C(14)	3523(2)	11533(2)	1124(1)	29(1)
C(15)	2551(1)	10821(1)	1092(1)	23(1)
C(16)	2439(2)	10198(2)	2804(1)	39(1)
C(17)	3482(2)	9669(2)	3193(1)	52(1)
C(18)	1920(2)	10524(2)	472(1)	29(1)
C(19)	860(2)	11249(2)	266(1)	44(1)
C(20)	1809(1)	6079(1)	829(1)	21(1)
C(21)	2161(2)	5182(1)	1183(1)	26(1)
C(22)	3072(2)	4535(2)	978(1)	34(1)
C(23)	3599(2)	4764(2)	446(1)	34(1)
C(24)	3246(2)	5658(2)	106(1)	29(1)
C(25)	2351(1)	6333(1)	290(1)	24(1)
C(26)	1615(2)	4901(2)	1772(1)	35(1)

C(27)	1083(2)	3776(2)	1775(1)	47(1)
C(28)	1950(2)	7318(2)	-69(1)	42(1)
C(29)	2730(2)	7716(2)	-543(1)	63(1)
C(30)	-4200(1)	8575(1)	1213(1)	25(1)
C(31)	-4558(2)	9400(2)	710(1)	37(1)
C(32)	-4618(2)	8973(2)	1825(1)	31(1)
C(33)	-4861(2)	7534(2)	1040(1)	34(1)

Table B.16 Crystal data and structure refinement for (^{iPr}PDI)Fe(NO)$_2$

Empirical formula	C34 H45 Cl2 Fe N5 O2	
Formula weight	682.50	
Temperature	173(2) K	
Wavelength	0.71073 Å	
Crystal system	Monoclinic	
Space group	P2(1)/c	
Unit cell dimensions	a = 9.9830(8) Å	α= 90°.
	b = 13.3090(10) Å	β= 100.421(3)°.
	c = 27.244(2) Å	γ = 90°.
Volume	3560.1(5) Å^3	
Z	4	
Density (calculated)	1.273 Mg/m^3	
Absorption coefficient	0.610 mm^{-1}	
F(000)	1440	
Crystal size	0.40 x 0.20 x 0.05 mm^3	
Theta range for data collection	1.71 to 28.28°.	
Index ranges	-13<=h<=13, -17<=k<=16, -36<=l<=36	
Reflections collected	66653	
Independent reflections	8833 [R(int) = 0.0313]	
Completeness to theta = 28.28°	99.9 %	
Absorption correction	Semi-empirical from equivalents	
Max. and min. transmission	0.9701 and 0.7925	
Refinement method	Full-matrix least-squares on F^2	
Data / restraints / parameters	8833 / 3 / 490	

Goodness-of-fit on F^2	1.037
Final R indices [I>2sigma(I)]	R1 = 0.0455, wR2 = 0.1136
R indices (all data)	R1 = 0.0597, wR2 = 0.1255
Largest diff. peak and hole	1.430 and -1.404 e.$Å^{-3}$

	x	y	z	U(eq)
Fe(1)	7949(1)	7631(1)	1751(1)	29(1)
N(4)	7196(9)	8549(4)	1994(2)	53(2)
O(1)	6784(14)	9291(7)	2155(2)	111(4)
N(4')	6863(18)	8297(18)	2045(7)	27(5)
O(1')	6236(16)	8922(18)	2251(8)	37(6)
N(5)	9471(2)	7923(2)	1643(1)	44(1)
O(2)	10558(2)	8263(2)	1606(1)	75(1)
N(1)	8843(2)	6795(1)	3278(1)	26(1)
N(2)	7773(2)	6233(1)	2050(1)	22(1)
N(3)	6769(2)	6903(1)	1175(1)	23(1)
C(1)	10541(2)	6883(2)	2724(1)	39(1)
C(2)	9204(2)	6604(1)	2864(1)	25(1)
C(3)	8260(2)	5936(1)	2519(1)	25(1)
C(4)	7941(2)	5002(2)	2696(1)	34(1)
C(5)	7136(2)	4345(2)	2383(1)	39(1)
C(6)	6637(2)	4642(2)	1897(1)	33(1)
C(7)	6955(2)	5590(1)	1745(1)	25(1)
C(8)	6427(2)	5991(1)	1243(1)	25(1)
C(9)	5562(2)	5342(2)	864(1)	35(1)
C(10)	9784(2)	7330(1)	3645(1)	26(1)
C(11)	9719(2)	8379(2)	3666(1)	29(1)
C(12)	10651(2)	8865(2)	4031(1)	37(1)
C(13)	11608(2)	8335(2)	4360(1)	40(1)
C(14)	11640(2)	7298(2)	4337(1)	35(1)
C(15)	10720(2)	6771(1)	3984(1)	28(1)
C(16)	8663(2)	8952(2)	3302(1)	34(1)
C(17')	7280(9)	8827(7)	3435(4)	42(2)
C(18')	9007(13)	10069(7)	3296(6)	64(3)

C(17)	7430(15)	9250(20)	3530(5)	74(5)
C(18)	9188(15)	9844(17)	3056(10)	100(7)
C(19)	10677(2)	5634(2)	3981(1)	33(1)
C(20)	11996(3)	5129(2)	4223(1)	57(1)
C(21)	9496(3)	5280(2)	4219(1)	53(1)
C(22)	6345(2)	7402(1)	702(1)	24(1)
C(23)	7087(2)	7264(2)	319(1)	28(1)
C(24)	6698(3)	7821(2)	-117(1)	38(1)
C(25)	5623(3)	8484(2)	-167(1)	45(1)
C(26)	4906(2)	8600(2)	213(1)	39(1)
C(27)	5237(2)	8063(2)	656(1)	29(1)
C(28)	8278(2)	6544(2)	363(1)	33(1)
C(29)	8063(3)	5770(2)	-57(1)	45(1)
C(30)	9610(3)	7099(2)	372(1)	59(1)
C(31)	4389(2)	8162(2)	1061(1)	39(1)
C(32)	3071(3)	7560(3)	918(1)	68(1)
C(33)	4091(3)	9251(2)	1170(1)	58(1)
Cl(1)	5586(1)	1788(1)	2641(1)	98(1)
Cl(2)	5724(1)	1963(1)	1587(1)	63(1)
C(1S)	4897(3)	1409(2)	2035(1)	66(1)

Table B.17 Crystal data and structure refinement for [(^{Me}PDI)Fe](μ-N_2)[Mo(N(Ar)^{t}Bu)$_3$]

Identification code	amt36	
Empirical formula	C66 H93 Fe Mo N8	
Formula weight	1150.27	
Temperature	173(2) K	
Wavelength	0.71073 Å	
Crystal system	Monoclinic	
Space group	P2(1)/c	
Unit cell dimensions	a = 18.4051(11) Å	α= 90°.
	b = 19.5349(8) Å	β= 110.994(2)°.
	c = 19.2228(11) Å	γ = 90°.

Volume	6452.6(6) $Å^3$
Z	4
Density (calculated)	1.184 Mg/m^3
Absorption coefficient	0.463 mm^{-1}
F(000)	2452
Crystal size	0.35 x 0.20 x 0.05 mm^3
Theta range for data collection	1.58 to 24.71°.
Index ranges	-21<=h<=21, -22<=k<=22, -22<=l<=22
Reflections collected	45724
Independent reflections	11004 [R(int) = 0.0811]
Completeness to theta = 24.71°	100.0 %
Absorption correction	Semi-empirical from equivalents
Max. and min. transmission	0.9772 and 0.8548
Refinement method	Full-matrix least-squares on F^2
Data / restraints / parameters	11004 / 0 / 701
Goodness-of-fit on F^2	0.999
Final R indices [I>2sigma(I)]	R1 = 0.0456, wR2 = 0.0967
R indices (all data)	R1 = 0.0989, wR2 = 0.1215
Largest diff. peak and hole	0.531 and -0.372 $e.Å^{-3}$

	x	y	z	U(eq)
Mo(1)	2785(1)	6905(1)	8005(1)	26(1)
Fe(1)	4381(1)	8964(1)	8480(1)	29(1)
N(1)	3608(2)	9844(2)	8006(2)	34(1)
N(2)	4953(2)	9784(1)	9030(2)	29(1)
N(3)	5617(2)	8686(2)	8862(2)	31(1)
N(4)	3776(2)	8171(2)	8285(2)	30(1)
N(5)	3376(2)	7667(2)	8177(2)	26(1)
N(6)	3326(2)	6339(2)	7497(2)	28(1)
N(7)	2931(2)	6636(2)	9034(2)	32(1)
N(8)	1746(2)	7225(2)	7367(2)	37(1)
C(1)	3336(3)	11042(2)	8269(3)	55(1)
C(2)	3820(3)	10400(2)	8406(2)	35(1)
C(3)	4577(3)	10394(2)	8969(2)	31(1)

C(4)	4952(3)	10956(2)	9377(2)	38(1)
C(5)	5720(3)	10910(2)	9832(2)	39(1)
C(6)	6119(3)	10314(2)	9837(2)	36(1)
C(7)	5725(2)	9758(2)	9421(2)	28(1)
C(8)	6089(2)	9132(2)	9318(2)	32(1)
C(9)	6948(3)	9049(2)	9658(3)	44(1)
C(10)	2892(3)	9863(2)	7382(2)	39(1)
C(11)	2186(3)	9810(2)	7479(3)	51(1)
C(12)	1510(3)	9885(3)	6863(3)	69(2)
C(13)	1539(4)	9990(3)	6162(3)	72(2)
C(14)	2240(4)	10013(2)	6079(3)	60(2)
C(15)	2935(3)	9953(2)	6673(3)	46(1)
C(16)	2153(3)	9673(3)	8235(3)	70(2)
C(17)	3696(3)	9991(3)	6569(3)	59(2)
C(18)	5984(2)	8084(2)	8704(2)	33(1)
C(19)	6096(3)	8054(2)	8035(2)	41(1)
C(20)	6508(3)	7501(2)	7913(3)	50(1)
C(21)	6792(3)	6991(2)	8435(3)	51(1)
C(22)	6643(2)	7015(2)	9078(3)	40(1)
C(23)	6237(2)	7558(2)	9232(2)	34(1)
C(24)	5812(3)	8613(2)	7465(3)	64(2)
C(25)	6074(3)	7575(2)	9940(3)	47(1)
C(26)	2798(2)	5863(2)	7001(2)	31(1)
C(27)	2630(3)	5245(2)	7267(2)	38(1)
C(28)	2107(3)	4784(2)	6797(3)	48(1)
C(29)	1756(3)	4957(2)	6054(3)	51(1)
C(30)	1911(3)	5565(3)	5774(2)	47(1)
C(31)	2439(3)	6010(2)	6253(2)	40(1)
C(32)	1952(4)	4108(2)	7095(3)	71(2)
C(33)	1515(3)	5739(3)	4956(3)	75(2)
C(34)	4117(2)	6386(2)	7463(2)	28(1)
C(35)	4157(3)	6962(2)	6935(2)	43(1)
C(36)	4690(2)	6541(2)	8238(2)	37(1)
C(37)	4350(3)	5709(2)	7205(3)	43(1)
C(38)	2865(3)	5908(2)	9097(2)	35(1)

C(39)	3517(3)	5489(2)	9284(2)	38(1)
C(40)	3454(3)	4783(2)	9334(3)	50(1)
C(41)	2727(4)	4505(3)	9198(3)	58(2)
C(42)	2067(4)	4900(3)	9014(3)	57(2)
C(43)	2146(3)	5613(2)	8965(2)	46(1)
C(44)	4169(4)	4340(2)	9525(3)	75(2)
C(45)	1282(4)	4586(3)	8879(3)	86(2)
C(46)	3219(3)	7029(2)	9749(2)	37(1)
C(47)	2790(3)	7706(2)	9611(3)	49(1)
C(48)	4088(3)	7151(2)	9988(2)	42(1)
C(49)	3042(4)	6651(3)	10361(3)	73(2)
C(50)	1168(3)	6801(2)	7483(3)	44(1)
C(51)	900(3)	6213(3)	7082(3)	52(1)
C(52)	342(3)	5804(3)	7206(3)	66(2)
C(53)	51(3)	6000(3)	7744(4)	77(2)
C(54)	318(3)	6580(3)	8171(3)	71(2)
C(55)	860(3)	6974(3)	8025(3)	55(1)
C(56)	39(4)	5170(3)	6737(4)	96(2)
C(57)	4(4)	6779(4)	8769(4)	112(3)
C(58)	1437(3)	7772(2)	6790(3)	51(1)
C(59)	1018(4)	7449(3)	6029(3)	88(2)
C(60)	872(3)	8231(3)	6994(4)	85(2)
C(61)	2114(3)	8187(2)	6763(3)	51(1)
C(1S)	8884(7)	7846(7)	9730(6)	196(6)
C(2S)	8841(5)	8131(6)	10397(8)	182(5)
C(3S)	8533(5)	7634(5)	10808(6)	133(4)
C(4S)	8479(6)	7967(6)	11498(8)	189(6)
C(5S)	8221(6)	7502(5)	11938(6)	184(6)

Table B.18 Crystal data and structure refinement for [(^{iPr}PDI)Fe(NO)][Na-C]

Identification code	amt38
Empirical formula	C51 H79 Fe N4 Na O8
Formula weight	955.02

Temperature	173(2) K	
Wavelength	0.71073 Å	
Crystal system	Monoclinic	
Space group	P2(1)/c	
Unit cell dimensions	a = 12.820(2) Å	α= 90°.
	b = 25.002(4) Å	β= 119.680(9)°.
	c = 18.422(3) Å	γ = 90°.
Volume	5130.0(14) $Å^3$	
Z	4	
Density (calculated)	1.237 Mg/m^3	
Absorption coefficient	0.357 mm^{-1}	
F(000)	2056	
Crystal size	0.60 x 0.30 x 0.03 mm^3	
Theta range for data collection	1.63 to 24.71°.	
Index ranges	-13<=h<=15, -29<=k<=29, -21<=l<=14	
Reflections collected	34902	
Independent reflections	8606 [R(int) = 0.0676]	
Completeness to theta = 24.71°	98.5 %	
Absorption correction	Semi-empirical from equivalents	
Max. and min. transmission	0.9894 and 0.8143	
Refinement method	Full-matrix least-squares on F^2	
Data / restraints / parameters	8606 / 0 / 642	
Goodness-of-fit on F^2	1.017	
Final R indices [I>2sigma(I)]	R1 = 0.0459, wR2 = 0.0958	
R indices (all data)	R1 = 0.0954, wR2 = 0.1182	
Largest diff. peak and hole	0.398 and -0.288 $e.Å^{-3}$	

	x	y	z	U(eq)
Fe(1)	4633(1)	3712(1)	2186(1)	21(1)
O(1)	6441(2)	4327(1)	3487(2)	57(1)
N(1)	5643(2)	3203(1)	2092(2)	23(1)
N(2)	3507(2)	3295(1)	1344(2)	24(1)
N(3)	3214(2)	4065(1)	1999(2)	23(1)
N(4)	5660(2)	4077(1)	2933(2)	30(1)

C(1)	5832(3)	2381(1)	1371(2)	38(1)
C(2)	5123(3)	2809(1)	1508(2)	25(1)
C(3)	3872(3)	2852(1)	1066(2)	25(1)
C(4)	3014(3)	2540(1)	418(2)	30(1)
C(5)	1809(3)	2666(1)	67(2)	35(1)
C(6)	1432(3)	3098(1)	358(2)	33(1)
C(7)	2288(3)	3415(1)	1008(2)	25(1)
C(8)	2138(3)	3862(1)	1398(2)	25(1)
C(9)	948(3)	4092(1)	1212(2)	37(1)
C(10)	6933(3)	3229(1)	2586(2)	22(1)
C(11)	7520(3)	2996(1)	3379(2)	27(1)
C(12)	8749(3)	3076(1)	3869(2)	34(1)
C(13)	9385(3)	3379(1)	3596(2)	35(1)
C(14)	8795(3)	3598(1)	2808(2)	32(1)
C(15)	7569(3)	3528(1)	2285(2)	23(1)
C(16)	6841(3)	2673(1)	3713(2)	31(1)
C(17)	6979(4)	2917(2)	4515(2)	50(1)
C(18)	7229(4)	2090(2)	3849(3)	59(1)
C(19)	6941(3)	3784(1)	1425(2)	29(1)
C(20)	7466(4)	3596(2)	881(2)	46(1)
C(21)	6958(4)	4386(1)	1480(2)	52(1)
C(22)	3210(3)	4540(1)	2427(2)	24(1)
C(23)	3049(3)	5038(1)	2031(2)	25(1)
C(24)	3070(3)	5496(1)	2467(2)	31(1)
C(25)	3249(3)	5468(1)	3267(2)	35(1)
C(26)	3416(3)	4981(1)	3647(2)	36(1)
C(27)	3400(3)	4509(1)	3245(2)	28(1)
C(28)	2918(3)	5085(1)	1168(2)	32(1)
C(29)	1883(3)	5445(1)	584(2)	42(1)
C(30)	4096(3)	5277(2)	1234(2)	44(1)
C(31)	3563(3)	3977(1)	3678(2)	36(1)
C(32)	2468(4)	3840(2)	3772(3)	52(1)
C(33)	4705(4)	3964(2)	4534(2)	52(1)
Na(1)	1451(1)	1359(1)	2494(1)	31(1)
O(2)	3544(2)	1525(1)	3629(2)	61(1)

O(3)	2284(3)	2230(1)	2337(2)	62(1)
O(4)	-117(2)	2103(1)	1866(2)	56(1)
O(5)	315(3)	1471(1)	3230(2)	53(1)
O(6)	2081(3)	715(1)	3688(2)	55(1)
C(34)	3877(4)	2079(2)	3701(3)	79(2)
C(35)	3549(5)	2280(2)	2878(4)	90(2)
C(36)	1615(4)	2668(2)	2322(3)	61(1)
C(37)	364(5)	2564(2)	1679(3)	71(1)
C(38)	-592(4)	2222(2)	2403(4)	77(2)
C(39)	-807(4)	1725(2)	2721(3)	67(1)
C(40)	216(5)	987(2)	3556(3)	69(1)
C(41)	1440(6)	785(2)	4137(3)	78(2)
C(42)	3349(5)	732(2)	4207(3)	73(2)
C(43)	3828(4)	1282(2)	4393(3)	75(2)
O(7)	2164(2)	1015(1)	1623(2)	48(1)
C(44)	2808(4)	526(2)	1769(3)	52(1)
C(45)	3614(4)	571(2)	1389(3)	51(1)
C(46)	3660(5)	1153(2)	1266(3)	68(1)
C(47)	2419(5)	1329(2)	1076(3)	67(1)
O(8)	-275(11)	771(6)	1676(7)	35(3)
C(48)	-996(13)	916(8)	828(12)	49(4)
C(49)	-790(14)	529(5)	306(6)	64(4)
C(50)	-690(20)	39(8)	835(16)	87(8)
C(51)	-197(18)	212(8)	1693(12)	82(8)
O(8')	-150(20)	788(11)	1637(16)	90(9)
C(48')	-830(30)	962(18)	770(20)	132(16)
C(49')	-1390(20)	423(8)	352(9)	59(5)
C(50')	-500(30)	2(16)	810(20)	79(11)
C(51')	-153(18)	213(11)	1705(11)	29(8)

Table B.19 Crystal data and structure refinement for [(^{Et}PDI)Fe(NO)(THF)][$BArF_{24}$]

Identification code	amt29
Empirical formula	C65 H55 B F24 Fe N4 O2

Formula weight	1446.79	
Temperature	173(2) K	
Wavelength	0.71073 Å	
Crystal system	Monoclinic	
Space group	C2/c	
Unit cell dimensions	a = 18.1216(5) Å	α= 90°.
	b = 18.1680(5) Å	β= 97.5470(10)°.
	c = 40.1862(12) Å	γ = 90°.
Volume	13116.0(6) $Å^3$	
Z	8	
Density (calculated)	1.465 Mg/m^3	
Absorption coefficient	0.345 mm^{-1}	
F(000)	5888	
Crystal size	0.25 x 0.15 x 0.10 mm^3	
Theta range for data collection	1.59 to 23.82°.	
Index ranges	-20<=h<=19, -20<=k<=20, -45<=l<=45	
Reflections collected	36690	
Independent reflections	10097 [R(int) = 0.0540]	
Completeness to theta = 23.82°	100.0 %	
Absorption correction	Semi-empirical from equivalents	
Max. and min. transmission	0.9663 and 0.9187	
Refinement method	Full-matrix least-squares on F^2	
Data / restraints / parameters	10097 / 496 / 1104	
Goodness-of-fit on F^2	1.019	
Final R indices [I>2sigma(I)]	R1 = 0.0551, wR2 = 0.1355	
R indices (all data)	R1 = 0.0954, wR2 = 0.1608	
Largest diff. peak and hole	0.937 and -0.414 $e.Å^{-3}$	

	x	y	z	U(eq)
Fe(1)	7540(1)	1991(1)	11343(1)	39(1)
O(1)	8225(1)	3312(1)	11529(1)	68(1)
O(2)	6409(1)	1966(1)	11327(1)	57(1)
N(1)	7521(1)	2063(1)	10852(1)	38(1)
N(2)	8455(1)	1630(1)	11299(1)	38(1)
N(3)	7748(2)	1435(2)	11768(1)	46(1)

N(4)	7757(2)	2858(2)	11463(1)	49(1)
C(1)	8299(2)	2040(2)	10385(1)	58(1)
C(2)	8158(2)	1948(2)	10740(1)	41(1)
C(3)	8725(2)	1682(2)	10997(1)	40(1)
C(4)	9436(2)	1441(2)	10964(1)	49(1)
C(5)	9866(2)	1128(2)	11237(1)	55(1)
C(6)	9587(2)	1070(2)	11539(1)	51(1)
C(7)	8878(2)	1311(2)	11567(1)	44(1)
C(8)	8445(2)	1227(2)	11843(1)	48(1)
C(9)	8775(2)	905(2)	12172(1)	66(1)
C(10)	6872(2)	2275(2)	10622(1)	40(1)
C(11)	6431(2)	1712(2)	10463(1)	45(1)
C(12)	5772(2)	1915(2)	10268(1)	53(1)
C(13)	5558(2)	2636(2)	10232(1)	57(1)
C(14)	6009(2)	3177(2)	10376(1)	59(1)
C(15)	6690(2)	3018(2)	10575(1)	51(1)
C(16)	6677(2)	921(2)	10500(1)	64(1)
C(17)	6179(4)	364(3)	10359(2)	163(3)
C(18)	7193(6)	3675(5)	10734(3)	93(4)
C(19)	7545(4)	4043(4)	10447(2)	82(2)
C(18')	7194(8)	3589(7)	10686(3)	33(3)
C(19')	6935(10)	4201(9)	10933(4)	127(7)
C(20)	7221(2)	1256(2)	11996(1)	53(1)
C(21)	6976(4)	1790(3)	12200(1)	110(2)
C(22)	6430(4)	1576(4)	12400(1)	145(2)
C(23)	6168(3)	887(4)	12399(1)	109(2)
C(24)	6413(2)	370(3)	12196(1)	78(1)
C(25)	6944(2)	541(2)	11986(1)	54(1)
C(26)	7467(9)	2514(5)	12226(3)	196(7)
C(26')	7001(5)	2602(5)	12206(2)	46(3)
C(27)	7571(5)	3006(6)	12508(2)	109(4)
C(27')	7709(6)	2679(6)	12403(4)	81(5)
C(28)	7212(2)	-38(2)	11759(1)	74(1)
C(29)	6711(4)	-598(3)	11640(2)	168(3)
C(30)	5915(2)	1349(3)	11278(1)	76(1)

C(31)	5171(3)	1644(4)	11146(2)	131(2)
C(32)	5191(5)	2285(7)	11365(3)	114(6)
C(32')	5191(4)	2470(5)	11162(3)	137(5)
C(33)	5946(3)	2628(3)	11354(1)	102(2)
C(40)	5660(3)	6532(4)	7978(2)	65(3)
F(1)	5476(2)	7162(2)	7845(1)	84(2)
F(2)	5036(3)	6197(3)	8000(1)	141(2)
F(3)	6013(4)	6213(3)	7754(1)	129(3)
C(40')	5635(5)	6537(5)	7984(3)	53(4)
F(1')	5083(4)	7004(6)	7947(2)	156(5)
F(2')	5366(5)	5872(3)	7929(2)	86(3)
F(3')	5965(4)	6630(6)	7714(2)	121(4)
C(41)	6561(2)	5537(2)	9108(1)	71(1)
F(4)	5878(2)	5385(2)	9168(1)	116(1)
F(5)	6802(2)	4885(1)	8998(1)	98(1)
F(6)	6988(2)	5656(2)	9385(1)	132(1)
C(48)	9678(2)	7231(2)	7983(1)	46(1)
F(7)	9477(1)	7852(1)	7816(1)	67(1)
F(8)	9397(1)	6679(1)	7791(1)	69(1)
F(9)	10413(1)	7188(1)	7993(1)	70(1)
C(49)	10060(4)	6483(4)	9172(2)	55(3)
F(10)	9938(4)	5766(3)	9162(2)	80(2)
F(11)	10785(3)	6537(4)	9175(2)	97(2)
F(12)	9923(4)	6674(5)	9475(1)	131(3)
C(49')	10061(4)	6452(5)	9189(2)	58(4)
F(10')	9791(5)	5807(4)	9250(2)	116(3)
F(11')	10759(3)	6350(5)	9144(2)	86(2)
F(12')	10086(4)	6832(4)	9468(2)	88(3)
C(56)	9105(3)	9394(3)	9721(1)	47(2)
F(13)	9674(2)	8961(2)	9804(1)	110(2)
F(14)	9004(2)	9814(2)	9977(1)	93(1)
F(15)	9304(2)	9832(2)	9497(1)	79(1)
C(56')	9050(7)	9304(7)	9784(3)	77(7)
F(13')	9603(5)	9338(10)	9605(3)	194(8)
F(14')	9336(4)	9035(5)	10080(2)	77(3)

F(15')	8919(7)	9978(5)	9877(4)	138(7)
C(57)	6594(5)	8354(4)	9844(2)	66(4)
F(16)	5965(4)	8721(4)	9757(2)	95(3)
F(17)	6371(4)	7655(3)	9835(2)	72(2)
F(18)	6744(5)	8539(6)	10161(2)	140(3)
C(57')	6548(4)	8386(5)	9848(2)	78(4)
F(16')	6164(4)	7778(4)	9775(2)	132(3)
F(17')	6747(4)	8378(5)	10177(1)	106(3)
F(18')	6072(4)	8915(4)	9769(2)	123(3)
C(64)	8510(5)	10208(4)	8135(2)	54(3)
F(19)	9036(3)	10329(3)	8383(1)	81(2)
F(20)	8840(4)	9861(4)	7905(2)	108(2)
F(21)	8321(3)	10851(3)	8010(2)	88(2)
C(64')	8393(5)	10209(4)	8055(2)	53(3)
F(19')	8656(5)	10731(4)	8254(2)	164(3)
F(20')	8153(3)	10508(3)	7765(2)	116(2)
F(21')	8962(3)	9812(3)	7991(2)	81(2)
C(65)	5802(2)	9871(2)	8272(1)	60(1)
F(22)	5612(1)	10107(2)	8562(1)	104(1)
F(23)	5656(1)	10419(1)	8059(1)	95(1)
F(24)	5320(1)	9337(1)	8170(1)	79(1)
C(34)	7092(2)	7278(2)	8671(1)	31(1)
C(35)	6626(2)	7188(2)	8368(1)	33(1)
C(36)	6144(2)	6596(2)	8309(1)	38(1)
C(37)	6108(2)	6064(2)	8549(1)	44(1)
C(38)	6569(2)	6129(2)	8849(1)	45(1)
C(39)	7053(2)	6720(2)	8906(1)	39(1)
C(42)	8502(2)	7569(2)	8689(1)	31(1)
C(43)	8758(2)	7547(2)	8376(1)	33(1)
C(44)	9430(2)	7217(2)	8323(1)	35(1)
C(45)	9865(2)	6875(2)	8584(1)	40(1)
C(46)	9617(2)	6863(2)	8897(1)	37(1)
C(47)	8957(2)	7206(2)	8946(1)	34(1)
C(50)	7737(2)	8250(2)	9134(1)	29(1)
C(51)	8358(2)	8648(2)	9280(1)	36(1)

C(52)	8395(2)	8957(2)	9599(1)	40(1)
C(53)	7825(2)	8870(2)	9787(1)	45(1)
C(54)	7205(2)	8477(2)	9650(1)	45(1)
C(55)	7165(2)	8183(2)	9329(1)	37(1)
C(58)	7498(2)	8673(2)	8515(1)	31(1)
C(59)	8023(2)	9108(2)	8386(1)	36(1)
C(60)	7844(2)	9770(2)	8220(1)	44(1)
C(61)	7124(2)	10024(2)	8177(1)	44(1)
C(62)	6587(2)	9609(2)	8303(1)	41(1)
C(63)	6774(2)	8952(2)	8470(1)	38(1)
B(1)	7708(2)	7942(2)	8749(1)	32(1)

Table B.20 Crystal data and structure refinement for (^{iPr}PDI)Fe(NO)(Py)

Identification code	amt40	
Empirical formula	C44 H53 F Fe N5 O	
Formula weight	742.76	
Temperature	173(2) K	
Wavelength	0.71073 Å	
Crystal system	Triclinic	
Space group	P-1	
Unit cell dimensions	a = 9.0172(6) Å	α= 70.383(3)°.
	b = 13.1118(9) Å	β= 81.498(4)°.
	c = 18.9981(13) Å	γ = 71.412(4)°.
Volume	2003.3(2) Å^3	
Z	2	
Density (calculated)	1.231 Mg/m^3	
Absorption coefficient	0.420 mm^{-1}	
F(000)	790	
Crystal size	0.35 x 0.15 x 0.05 mm^3	
Theta range for data collection	1.75 to 26.37°.	
Index ranges	-11<=h<=11, -16<=k<=16, -23<=l<=23	
Reflections collected	29355	
Independent reflections	8120 [R(int) = 0.0389]	
Completeness to theta = 26.37°	99.0 %	

Absorption correction	Semi-empirical from equivalents
Max. and min. transmission	0.9793 and 0.8668
Refinement method	Full-matrix least-squares on F^2
Data / restraints / parameters	8120 / 63 / 487
Goodness-of-fit on F^2	1.028
Final R indices [I>2sigma(I)]	R1 = 0.0458, wR2 = 0.1061
R indices (all data)	R1 = 0.0765, wR2 = 0.1231
Largest diff. peak and hole	1.679 and -0.349 e.$Å^{-3}$

	x	y	z	U(eq)
Fe(1)	6226(1)	2731(1)	2148(1)	22(1)
O(1)	8886(3)	1717(2)	3015(1)	56(1)
N(1)	5467(2)	4456(2)	2200(1)	20(1)
N(2)	4852(2)	3608(2)	1300(1)	20(1)
N(3)	6368(2)	1553(2)	1577(1)	23(1)
N(4)	7941(3)	2201(2)	2572(1)	31(1)
N(5)	4795(2)	2119(2)	3028(1)	24(1)
C(1)	4112(3)	6460(2)	1525(2)	29(1)
C(2)	4575(3)	5203(2)	1669(1)	22(1)
C(3)	4116(3)	4744(2)	1171(1)	20(1)
C(4)	3085(3)	5353(2)	598(1)	25(1)
C(5)	2756(3)	4808(2)	158(1)	28(1)
C(6)	3487(3)	3664(2)	285(1)	27(1)
C(7)	4541(3)	3081(2)	847(1)	22(1)
C(8)	5480(3)	1914(2)	1005(1)	24(1)
C(9)	5458(4)	1229(2)	514(2)	36(1)
C(10)	6064(3)	4847(2)	2691(1)	21(1)
C(11)	7489(3)	5113(2)	2500(1)	23(1)
C(12)	8032(3)	5484(2)	2989(1)	28(1)
C(13)	7195(3)	5620(2)	3632(1)	32(1)
C(14)	5803(3)	5343(2)	3817(1)	30(1)
C(15)	5222(3)	4931(2)	3365(1)	23(1)
C(16)	8434(3)	5022(2)	1781(1)	29(1)
C(17)	10049(3)	4180(2)	1935(2)	43(1)

C(18)	8593(3)	6176(2)	1282(2)	35(1)
C(19)	3713(3)	4592(2)	3597(1)	30(1)
C(20)	2280(3)	5575(3)	3305(2)	50(1)
C(21)	3508(4)	4096(3)	4443(2)	41(1)
C(22)	7484(3)	454(2)	1731(1)	25(1)
C(23)	7039(3)	-514(2)	2154(2)	29(1)
C(24)	8174(3)	-1554(2)	2302(2)	34(1)
C(25)	9702(3)	-1645(2)	2043(2)	39(1)
C(26)	10127(3)	-684(2)	1630(2)	38(1)
C(27)	9038(3)	383(2)	1467(2)	31(1)
C(28)	5379(3)	-481(2)	2468(2)	37(1)
C(29)	5311(4)	-856(3)	3323(2)	51(1)
C(30)	4707(4)	-1212(3)	2202(2)	56(1)
C(31)	9541(3)	1415(2)	987(2)	43(1)
C(32)	9779(5)	1446(3)	166(2)	63(1)
C(33)	10999(4)	1482(3)	1268(3)	69(1)
C(34)	3330(3)	2164(2)	2928(2)	31(1)
C(35)	2309(3)	1831(2)	3512(2)	39(1)
C(36)	2788(4)	1430(2)	4230(2)	42(1)
C(37)	4287(4)	1372(2)	4342(2)	38(1)
C(38)	5252(3)	1717(2)	3735(1)	31(1)
C(1S)	11416(5)	-1496(3)	4843(2)	71(1)
C(2S)	11371(4)	-2577(3)	5203(2)	66(1)
C(3S)	10511(5)	-3023(3)	4906(2)	67(1)
C(4S)	9752(5)	-2366(3)	4274(2)	63(1)
C(5S)	9794(4)	-1287(3)	3916(2)	53(1)
C(6S)	10642(4)	-840(3)	4204(2)	59(1)
F(1)	12399(7)	-1127(4)	5019(3)	108(2)
F(1')	9169(7)	-2946(5)	4094(3)	91(2)

Table B.21 Crystal data and structure refinement for (TRPY)FeR_2

Identification code	amt42
Empirical formula	C23 H33 Fe N3 Si2

Formula weight	463.55	
Temperature	173(2) K	
Wavelength	0.71073 Å	
Crystal system	Monoclinic	
Space group	C2/c	
Unit cell dimensions	a = 16.1666(10) Å	α= 90°.
	b = 9.6372(6) Å	β= 91.543(2)°.
	c = 15.9377(12) Å	γ = 90°.
Volume	2482.2(3) $Å^3$	
Z	4	
Density (calculated)	1.240 Mg/m^3	
Absorption coefficient	0.718 mm^{-1}	
F(000)	984	
Crystal size	0.60 x 0.40 x 0.10 mm^3	
Theta range for data collection	2.46 to 28.30°.	
Index ranges	-21<=h<=19, -12<=k<=9, -19<=l<=21	
Reflections collected	10728	
Independent reflections	3054 [R(int) = 0.0201]	
Completeness to theta = 28.30°	99.0 %	
Absorption correction	Semi-empirical from equivalents	
Max. and min. transmission	0.9317 and 0.6727	
Refinement method	Full-matrix least-squares on F^2	
Data / restraints / parameters	3054 / 0 / 166	
Goodness-of-fit on F^2	1.011	
Final R indices [I>2sigma(I)]	R1 = 0.0270, wR2 = 0.0681	
R indices (all data)	R1 = 0.0351, wR2 = 0.0741	
Largest diff. peak and hole	0.332 and -0.223 $e.Å^{-3}$	

	x	y	z	U(eq)
Fe(1)	5000	2336(1)	2500	24(1)
Si(1)	5710(1)	2233(1)	555(1)	30(1)
N(1)	3809(1)	2896(1)	1971(1)	30(1)
N(2)	5000	4427(2)	2500	28(1)
C(1)	3233(1)	1976(2)	1693(1)	35(1)

C(2)	2475(1)	2371(2)	1367(1)	44(1)
C(3)	2294(1)	3778(2)	1324(1)	50(1)
C(4)	2871(1)	4730(2)	1601(1)	44(1)
C(5)	3637(1)	4268(2)	1923(1)	32(1)
C(6)	4315(1)	5153(1)	2221(1)	32(1)
C(7)	4303(1)	6594(2)	2230(1)	41(1)
C(8)	5000	7322(2)	2500	46(1)
C(9)	4746(1)	2911(2)	19(1)	48(1)
C(10)	6268(1)	1173(2)	-248(1)	46(1)
C(11)	6401(1)	3741(2)	821(1)	48(1)
C(12)	5467(1)	1231(2)	1503(1)	29(1)

Table B.22 Crystal data and structure refinement for [(^{iPr}PDI)Fe(NO)][$BArF_{24}$]

Identification code	amt44	
Empirical formula	C72 H63 B F24 Fe N4 O	
Formula weight	1522.92	
Temperature	173(2) K	
Wavelength	0.71073 Å	
Crystal system	Monoclinic	
Space group	P2(1)/n	
Unit cell dimensions	a = 11.7959(9) Å	α= 90°.
	b = 17.6165(13) Å	β= 92.630(2)°.
	c = 33.471(3) Å	γ = 90°.
Volume	6948.1(9) $Å^3$	
Z	4	
Density (calculated)	1.456 Mg/m^3	
Absorption coefficient	0.329 mm^{-1}	
F(000)	3112	
Crystal size	0.40 x 0.15 x 0.03 mm^3	
Theta range for data collection	1.68 to 23.82°.	
Index ranges	-13<=h<=13, -13<=k<=20, -34<=l<=38	
Reflections collected	32871	
Independent reflections	10650 [R(int) = 0.0609]	

Completeness to theta = 23.82°	99.9 %
Absorption correction	Semi-empirical from equivalents
Max. and min. transmission	0.9918 and 0.8797
Refinement method	Full-matrix least-squares on F^2
Data / restraints / parameters	10650 / 104 / 1002
Goodness-of-fit on F^2	1.018
Final R indices [I>2sigma(I)]	R1 = 0.0561, wR2 = 0.1353
R indices (all data)	R1 = 0.1147, wR2 = 0.1657
Largest diff. peak and hole	0.638 and -0.503 e.$Å^{-3}$

	x	y	z	U(eq)
Fe(1)	4795(1)	7405(1)	3867(1)	29(1)
O(1)	4178(4)	7672(3)	3063(1)	93(2)
N(1)	6436(3)	7466(2)	3836(1)	28(1)
N(2)	5220(3)	7654(2)	4396(1)	28(1)
N(3)	3310(3)	7471(2)	4098(1)	28(1)
N(4)	4428(3)	7524(2)	3397(1)	47(1)
C(1)	8289(4)	7672(3)	4203(1)	48(1)
C(2)	7032(4)	7605(2)	4165(1)	32(1)
C(3)	6330(4)	7728(2)	4507(1)	34(1)
C(4)	6669(4)	7906(3)	4897(1)	43(1)
C(5)	5831(4)	8013(3)	5173(1)	46(1)
C(6)	4705(4)	7936(3)	5058(1)	40(1)
C(7)	4408(4)	7747(2)	4666(1)	30(1)
C(8)	3287(4)	7627(2)	4479(1)	31(1)
C(9)	2244(4)	7697(3)	4712(1)	47(1)
C(10)	6959(3)	7418(2)	3453(1)	28(1)
C(11)	7210(4)	8098(2)	3257(1)	33(1)
C(12)	7613(4)	8030(3)	2873(1)	36(1)
C(13)	7745(4)	7336(3)	2699(1)	39(1)
C(14)	7501(4)	6674(3)	2899(1)	37(1)
C(15)	7097(3)	6701(2)	3284(1)	31(1)
C(16)	7034(4)	8878(2)	3443(1)	41(1)
C(17)	6094(5)	9320(3)	3226(2)	80(2)

C(18)	8107(6)	9332(4)	3471(2)	94(2)
C(19)	6831(4)	5983(3)	3513(2)	45(1)
C(20)	7912(6)	5662(4)	3714(2)	97(2)
C(21)	6245(5)	5376(3)	3259(2)	78(2)
C(22)	2268(3)	7359(2)	3860(1)	29(1)
C(23)	1882(4)	6612(2)	3801(1)	33(1)
C(24)	919(4)	6509(3)	3558(2)	45(1)
C(25)	351(4)	7121(3)	3379(2)	45(1)
C(26)	759(4)	7844(3)	3439(1)	40(1)
C(27)	1725(4)	7986(2)	3680(1)	31(1)
C(28)	2512(4)	5943(3)	3989(2)	47(1)
C(29)	1752(6)	5281(4)	4082(2)	101(3)
C(30)	3487(9)	5707(5)	3746(3)	190(6)
C(31)	2147(4)	8792(2)	3746(1)	40(1)
C(32)	1312(5)	9255(3)	3983(2)	55(1)
C(33)	2358(5)	9192(3)	3355(2)	58(2)
B(1)	8206(4)	7311(3)	1295(1)	24(1)
C(40)	10772(4)	6028(3)	2376(1)	41(1)
F(1)	11668(2)	6119(2)	2626(1)	63(1)
F(2)	9959(3)	5752(2)	2596(1)	66(1)
F(3)	11021(3)	5492(2)	2120(1)	75(1)
F(4)	11133(4)	9295(2)	1897(1)	115(2)
F(5)	12031(3)	8790(2)	2384(1)	84(1)
F(6)	10369(3)	9194(2)	2461(1)	107(2)
F(7)	10528(3)	8894(2)	-30(1)	67(1)
F(8)	11369(2)	8684(2)	543(1)	76(1)
F(9)	10656(2)	9780(2)	407(1)	65(1)
F(10)	5534(3)	9385(2)	598(1)	90(1)
F(11)	6456(3)	9932(2)	160(1)	101(1)
F(12)	5755(3)	8833(2)	55(1)	109(2)
F(13)	4864(3)	9284(2)	1717(1)	84(1)
F(14)	6190(3)	9344(2)	2161(1)	65(1)
F(15)	4588(3)	8902(2)	2311(1)	81(1)
F(16)	4670(3)	5622(2)	1748(1)	84(1)
F(17)	5683(4)	5640(2)	2265(1)	97(1)

F(18)	4087(4)	6188(2)	2255(2)	165(3)
C(64)	6319(16)	5302(10)	366(5)	37(7)
F(19)	6199(16)	4564(7)	391(9)	83(6)
F(20)	6320(30)	5430(20)	-18(4)	126(14)
F(21)	5369(12)	5557(19)	495(11)	141(14)
C(64')	6294(13)	5369(8)	332(4)	54(6)
F(19')	5547(12)	5088(12)	571(3)	98(7)
F(20')	6479(7)	4856(14)	61(7)	132(10)
F(21')	5741(8)	5910(6)	150(5)	75(4)
C(65)	10423(15)	5072(9)	719(4)	41(6)
F(22)	10991(13)	5052(10)	1069(4)	72(5)
F(23)	11124(9)	5382(6)	470(5)	76(6)
F(24)	10314(10)	4368(7)	597(6)	81(6)
C(65')	10342(17)	5011(10)	696(4)	47(7)
F(22')	11254(8)	5344(7)	863(7)	74(6)
F(23')	10610(16)	4913(17)	322(3)	123(10)
F(24')	10250(12)	4343(8)	856(8)	110(8)
C(34)	9230(3)	7359(2)	1640(1)	26(1)
C(35)	9599(3)	6716(2)	1858(1)	26(1)
C(36)	10406(4)	6750(2)	2169(1)	28(1)
C(37)	10882(4)	7432(3)	2287(1)	38(1)
C(38)	10522(4)	8082(2)	2083(1)	38(1)
C(39)	9724(4)	8043(2)	1770(1)	33(1)
C(41)	11010(6)	8837(3)	2206(2)	63(2)
C(42)	8272(3)	8011(2)	965(1)	24(1)
C(43)	9303(4)	8247(2)	821(1)	29(1)
C(44)	9366(4)	8795(2)	522(1)	35(1)
C(45)	8392(4)	9137(3)	363(1)	39(1)
C(46)	7356(4)	8913(2)	499(1)	34(1)
C(47)	7301(4)	8346(2)	790(1)	30(1)
C(48)	10472(4)	9028(3)	364(2)	53(2)
C(49)	6296(5)	9261(3)	329(2)	54(1)
C(50)	7049(3)	7367(2)	1544(1)	26(1)
C(51)	6643(4)	8063(2)	1673(1)	30(1)
C(52)	5717(4)	8129(2)	1913(1)	34(1)

C(53)	5147(4)	7489(3)	2035(1)	37(1)
C(54)	5537(4)	6784(3)	1919(1)	37(1)
C(55)	6459(4)	6729(2)	1675(1)	31(1)
C(56)	5336(4)	8909(3)	2025(2)	47(1)
C(57)	4973(5)	6081(3)	2048(2)	56(2)
C(58)	8259(3)	6533(2)	1026(1)	22(1)
C(59)	7309(3)	6262(2)	807(1)	29(1)
C(60)	7347(4)	5622(2)	564(1)	32(1)
C(61)	8344(4)	5223(2)	531(1)	34(1)
C(62)	9313(4)	5484(2)	739(1)	29(1)
C(63)	9260(3)	6123(2)	979(1)	26(1)
C(1S)	3533(5)	6653(4)	858(2)	78(2)
C(2S)	2839(5)	6624(4)	1172(2)	75(2)
C(3S)	2540(5)	7279(4)	1355(2)	72(2)
C(4S)	2945(6)	7955(4)	1234(2)	78(2)
C(5S)	3650(5)	7990(3)	923(2)	75(2)
C(6S)	3947(5)	7327(4)	738(2)	77(2)
C(7S)	4629(4)	7353(3)	437(2)	57(2)

Table B.23 Crystal data and structure refinement for (^{iPr}PDI)Fe(NTMS)

Identification code	amt46	
Empirical formula	C36 H52 Fe N4 Si	
Formula weight	624.76	
Temperature	173(2) K	
Wavelength	0.71073 Å	
Crystal system	Monoclinic	
Space group	C2/m	
Unit cell dimensions	a = 26.4230(18) Å	α= 90°.
	b = 14.0146(9) Å	β= 112.679(2)°.
	c = 23.2578(16) Å	γ = 90°.
Volume	7946.6(9) Å^3	
Z	8	
Density (calculated)	1.044 Mg/m^3	

Absorption coefficient	0.435 mm^{-1}
F(000)	2688
Crystal size	0.60 x 0.40 x 0.08 mm^3
Theta range for data collection	1.57 to 27.48°.
Index ranges	-34<=h<=34, -17<=k<=18, -24<=l<=30
Reflections collected	33845
Independent reflections	9416 [R(int) = 0.0285]
Completeness to theta = 27.48°	99.1 %
Absorption correction	Semi-empirical from equivalents
Max. and min. transmission	0.9681 and 0.7802
Refinement method	Full-matrix least-squares on F^2
Data / restraints / parameters	9416 / 19 / 445
Goodness-of-fit on F^2	1.094
Final R indices [I>2sigma(I)]	R1 = 0.0550, wR2 = 0.1481
R indices (all data)	R1 = 0.0786, wR2 = 0.1593
Largest diff. peak and hole	0.856 and -0.652 e.$Å^{-3}$

	x	y	z	U(eq)
Fe(2)	607(1)	5000	3821(1)	29(1)
Si(2)	1901(1)	5000	3821(1)	52(1)
N(7)	1269(2)	5000	3854(4)	56(2)
C(43)	2454(3)	5000	4646(4)	85(3)
C(44)	2029(2)	3857(4)	3509(3)	83(2)
Si(2')	1704(1)	5000	3394(1)	42(1)
N(7')	1170(3)	5000	3620(4)	51(2)
C(43')	1479(4)	5000	2535(4)	132(6)
C(44')	2169(4)	3963(8)	3662(7)	212(6)
N(5)	441(1)	3601(1)	3814(1)	27(1)
N(6)	-24(1)	5000	4029(1)	21(1)
C(26)	-145(1)	2354(1)	4015(1)	42(1)
C(27)	29(1)	3355(1)	3974(1)	26(1)
C(28)	-253(1)	4154(1)	4100(1)	22(1)
C(29)	-712(1)	4143(1)	4252(1)	27(1)
C(30)	-937(1)	5000	4341(1)	30(1)

C(31)	751(1)	2851(1)	3671(1)	32(1)
C(32)	1138(1)	2340(2)	4160(1)	38(1)
C(33)	1423(1)	1618(2)	3998(1)	45(1)
C(34)	1326(1)	1408(2)	3393(1)	45(1)
C(35)	945(1)	1929(2)	2918(1)	44(1)
C(36)	649(1)	2661(1)	3049(1)	35(1)
C(37)	1253(1)	2545(2)	4836(1)	53(1)
C(38)	1262(1)	1645(2)	5213(1)	80(1)
C(39)	1771(1)	3133(3)	5122(2)	85(1)
C(40)	216(1)	3208(2)	2522(1)	45(1)
C(41)	-351(1)	2763(2)	2367(2)	73(1)
C(42)	336(1)	3265(3)	1932(2)	110(1)
Fe(1)	2442(1)	0	969(1)	25(1)
Si(1)	1204(1)	0	1109(1)	36(1)
N(1)	2219(1)	0	56(1)	28(1)
N(2)	3126(1)	0	891(1)	25(1)
N(3)	2948(1)	0	1848(1)	26(1)
N(4)	1820(1)	0	1029(1)	41(1)
C(1)	2515(1)	0	-848(2)	47(1)
C(2)	2615(1)	0	-163(1)	31(1)
C(3)	3151(1)	0	316(1)	30(1)
C(4)	3659(1)	0	258(2)	38(1)
C(5)	4128(1)	0	781(2)	41(1)
C(6)	4109(1)	0	1374(1)	35(1)
C(7)	3600(1)	0	1421(1)	29(1)
C(8)	3482(1)	0	1968(1)	29(1)
C(9)	3921(1)	0	2609(1)	40(1)
C(10)	1657(1)	0	-371(1)	32(1)
C(11)	1398(1)	875(2)	-559(1)	41(1)
C(12)	1718(1)	1815(2)	-380(1)	58(1)
C(13)	1571(2)	2404(3)	68(2)	123(1)
C(14)	1705(1)	2396(3)	-922(2)	85(1)
C(15)	839(1)	860(2)	-928(1)	58(1)
C(16)	563(1)	0	-1107(2)	64(1)
C(17)	2794(1)	0	2378(1)	28(1)

C(18)	2731(1)	873(2)	2632(1)	32(1)
C(19)	2606(1)	854(2)	3161(1)	39(1)
C(20)	2550(1)	0	3429(1)	40(1)
C(21)	2790(1)	1815(2)	2343(1)	44(1)
C(22)	3220(1)	2453(2)	2811(2)	79(1)
C(23)	2243(1)	2336(2)	2058(2)	68(1)
C(24)	1295(1)	0	1943(1)	40(1)
C(25)	775(1)	1064(2)	750(1)	67(1)